



## Durham E-Theses

---

# *Digital fault mapping and spatial attribute analysis of basement-influenced oblique extension in Passive margin settings*

Wilson, Robert W.

### How to cite:

---

Wilson, Robert W. (2006) *Digital fault mapping and spatial attribute analysis of basement-influenced oblique extension in Passive margin settings*, Durham theses, Durham University. Available at Durham E-Theses Online: <http://etheses.dur.ac.uk/2685/>

### Use policy

---

The full-text may be used and/or reproduced, and given to third parties in any format or medium, without prior permission or charge, for personal research or study, educational, or not-for-profit purposes provided that:

- a full bibliographic reference is made to the original source
- a [link](#) is made to the metadata record in Durham E-Theses
- the full-text is not changed in any way

The full-text must not be sold in any format or medium without the formal permission of the copyright holders.

Please consult the [full Durham E-Theses policy](#) for further details.

---

Academic Support Office, Durham University, University Office, Old Elvet, Durham DH1 3HP  
e-mail: [e-theses.admin@dur.ac.uk](mailto:e-theses.admin@dur.ac.uk) Tel: +44 0191 334 6107  
<http://etheses.dur.ac.uk>

# **Digital fault mapping and spatial attribute analysis of basement-influenced oblique extension in Passive margin settings**

by

**Robert W. Wilson**

**The copyright of this thesis rests with the  
author or the university to which it was  
submitted. No quotation from it, or  
information derived from it may be published  
without the prior written consent of the author  
or university, and any information derived  
from it should be acknowledged.**

**A thesis submitted in partial fulfilment of the degree of Doctor of Philosophy at the  
Department of Earth Sciences, University of Durham.**

**2006**



## **Declaration**

No part of this thesis has been previously submitted for a degree at this, or any other university. The work described in this thesis is entirely that of the author, except where reference is made to previously published work.

Robert W. Wilson

Department of Earth Sciences,  
University of Durham  
January 2006

**© Robert W. Wilson**

**The copyright of this thesis rests with the author. No quotation or data from it should be published in any format, including electronic and the Internet, without the author's prior written consent. All information derived from this thesis must be acknowledged appropriately.**

## **Abstract.**

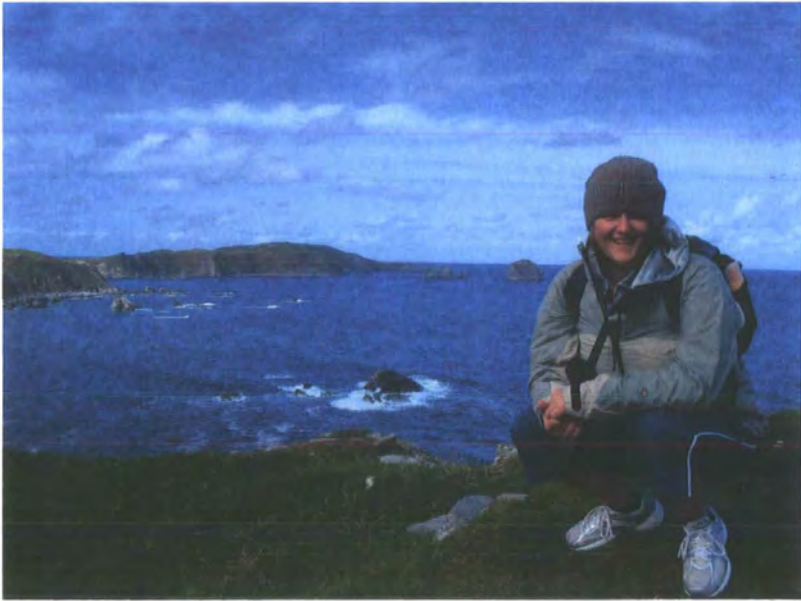
Oblique extension and passive margin segmentation may be attributed to the influence of basement structures. Pre-existing fabrics exert a strong control on the overall rift geometry in extensional settings, and can lead to the development of complex fault patterns, obliquely extending segments, deformation partitioning and transfer zones. In offshore settings, the nature of basement structure cannot easily be determined from seismic data, and onshore studies are increasingly used to assess basement controls.

A digital mapping methodology GAVA (Geospatial Acquisition Visualisation and Analysis) has been developed to integrate regional- to outcrop-scale data. Digital field mapping methods using DGPS, Laser-Range-finder and field-GIS are used to map faults to a dm- to m-scale accuracy by collecting spatial co-ordinates on a handheld computer whilst traversing along or across the exposed fault systems. Benefits of digital mapping include: more rapid data collection and analysis; all data geospatially located and stored in a digital database; GIS-based analysis and visualisation techniques; digital data format enables direct comparison with fault arrays interpreted from seismic data.

The GAVA workflow has been used to investigate three case studies on the North Atlantic Passive Margin: 1) NW Scotland; 2) Lofoten, NW Norway; and 3) Davis Strait, West Greenland. Each case study combines regional onshore and offshore mapping, using remote sensing and seismic interpretation, with detailed outcrop mapping of onshore fault exposures. Fault attributes (e.g. fault orientation, kinematics, fault linkage, fault-rock, overprinting relationships) observed at individual localities were collected in a GIS database. Kinematic fault analysis was carried out using strain inversion techniques at various scales. Spatial analysis was carried out using ArcGIS to identify relationships between various structures, while 3-D models were constructed in order to visualise these relationships over several orders of magnitude.

Results show that the complexity of rifted margins may be linked to changes in the obliquity of pre-existing structures relative to the regional extension vector. However, direct reactivation of structures need not always occur. The influence of pre-existing structures may also lead to localized variations in stress/strain orientations, which if analyzed in isolation can indicate extension non-parallel to regional stresses. Therefore, spatial analysis and studies across a range of scales is essential when analyzing such zones. Digital (GIS) mapping methods are an ideal way to carry out such studies, although further development of analysis and visualisation tools for geosciences is required in the field of GIS.

For Penny,



## Acknowledgements

Throughout my studies there have been a multitude of people who have contributed to my research and my life as a whole. Within the limited space available here it is not possible to list everybody, so I apologise now if you're not mentioned by name.

First I would like to thank my supervisors Ken McCaffrey and Bob Holdsworth, for their continued belief in me and my abilities, and giving me the chance to do a PhD in Durham. Thanks also to Jonny Imber who has acted as virtually a 3<sup>rd</sup> supervisor to my studies over the years.

This research has resulted from a NERC Ocean Margins LINK project (NER/T/S/2000/01018) co-funded by BP and Statoil (UK) Ltd., and associated tied studentship (NER/S/S/2001/06740). As my PhD was part of a broader project I would also like to thank all other members of the research team (including Jonny Imber, Richard Jones, Richard England, Phil Clegg, Lorrain Beacom and Katherine Alsop) for their help and advice throughout my four years of study.

During studies I have worked with various external co-workers who also deserve a mention. Thanks to the many members of GEUS who helped organise and run the 2003 field season in West Greenland, and in particular to Knud Eric Klint and Jeroen van Gool for including me in their field research team. Thanks to David Roberts, John Dehls and Bart Hendriks at NGU for their help and advice on my work in Lofoten and Møre-Trøndelag, and also tracking down many maps and papers of Norway for me.

Recognition must also be paid to Statoil (UK) and BP (Norway) for their financial backing of the LINK project and their contributions towards fieldwork in Greenland. Thanks to Robert Hunsdale for arranging and supervising my placement with Statoil in Stavanger, and a special thanks to Tony Doré for his direct and indirect support at various stages, and for suggesting Lofoten as a mapping area! Thanks also to Alastair Welbon and Tormod Henningsen for releasing the seismic data used in the Lofoten Study. I must also acknowledge the supplemental financial support towards my research from various groups through the award of research grants: the Geological Society of London's Annie Greenly award, the American Association of Petroleum Geologists Grants-in-Aid award, and the Edinburgh Geological Society's Mykura fund.

All my friends at Durham deserve a mention, though am not going to attempt to name them all! Thanks to Nic for his help and advice on all things to do with transtension and for also being one of my best friends at Durham. A big thank you must go to all other members of the RRG group (Ken, Jonny, Phil, Shaz, Nic, Bones, Adam, Nicola, Fabio, oh and Bob!) for helping to make the office a cheerful and friendly environment. Thanks also to my team mates in Geology 5-a-side team (Gary, Dougal, Rich, Nic, Colin, Darren, Tom, Chris, Ken and Mike) for some good games of football.

A huge thank you to my Mum and Dad for their help, support and encouragement at various times over the years, and for always being on hand to listen to my problems on the phone-a-moan hotline! Thanks also to Joan & Andy for their support during my long writing up stages.

However, I save the biggest thank you until last, to the person who has given me the support, encouragement and love needed for me to complete my work - thank you Penny!

## Contents

TITLE	i
COPYRIGHT	ii
ABSTRACT	iii
ACKNOWLEDGEMENTS	v
CONTENTS	vi
LIST OF TABLES AND FIGURES	xiii
<b>CHAPTER 1</b>	
<b>1. BASEMENT-INFLUENCED OBLIQUE EXTENSION IN PASSIVE MARGIN SETTINGS</b>	<b>1</b>
1.1. Introduction	1
1.2. Aims of research and areas studied	2
1.2.1. <i>Research Aims</i>	2
1.2.2. <i>Location of research areas</i>	3
1.3. Thesis outline	4
1.4. Basement inheritance and reactivation	5
1.4.1. <i>Basement inheritance vs. reactivation</i>	5
1.4.1.1. <i>What defines reactivation?</i>	6
1.4.2. <i>Mechanics of oblique reactivation during extension</i>	8
1.4.2.1. <i>Initiation of fracturing and reactivation</i>	8
1.4.2.2. <i>Continued activity on faults</i>	10
1.4.2.3. <i>Changes to the stress field</i>	10
1.5. Oblique extension and transtension	11
1.5.1. <i>Definitions of oblique extension and transtension</i>	11
1.5.2. <i>Principals of transtension</i>	12
1.5.2.1. <i>Transtension: 2-D vs. 3-D strain</i>	12
1.5.2.2. <i>Wrench dominated and extension dominated transtension</i>	13
1.5.3. <i>Faulting and deformation associated with transtension</i>	13
1.5.3.1. <i>Faulting under 2-D and 3-D strain</i>	13
1.5.3.2. <i>Fault patterns in transtension</i>	14
1.5.3.3. <i>Multimodal faulting: polyphase deformation and 3D strain</i>	15
1.5.4. <i>Spatial variations and deformation partitioning</i>	16
1.6. Fault and fracture classification and kinematic indicators	17
1.6.1. <i>Introduction</i>	17
1.6.2. <i>Fault classification</i>	18
1.6.2.1. <i>Andersonian "dynamic" classification of faults</i>	18
1.6.2.2. <i>Geometric/ kinematic classification of faults</i>	18
1.6.3. <i>Kinematic indicators and interpretation</i>	19



1.6.3.1.	<i>Brittle shear sense indicators</i>	19
1.6.3.1.1.	Slickenside striations	20
1.6.3.1.2.	Shear sense structures involving secondary fractures	20
1.7.	<b>Structural analysis of fault movements: Fault Kinematics and Palaeostress</b>	<b>21</b>
1.7.1.	<b><i>Stress vs. strain</i></b>	<b>21</b>
1.7.1.1.	<i>Coaxial vs. non-coaxial deformation</i>	22
1.7.2.	<b><i>Kinematic inversion to determine palaeostress</i></b>	<b>23</b>
1.7.2.1.	<i>Inversion procedures</i>	24
1.7.2.2.	<i>Analysis methods</i>	25
1.7.3.	<b><i>Palaeostress applications and their limitations</i></b>	<b>26</b>

## CHAPTER 2

2.	<b>DIGITAL GEOLOGICAL MAPPING – AN OVERVIEW OF DIGITAL MAPPING METHODS IN GEOSCIENCES.</b>	<b>41</b>
2.1.	<b>Introduction</b>	<b>41</b>
2.2.	<b>An overview of computer based mapping and GIS in Geosciences</b>	<b>42</b>
2.2.1.	<i>Introduction</i>	42
2.2.2.	<i>What is a GIS?</i>	43
2.2.3.	<b><i>GIS activities in geosciences</i></b>	<b>44</b>
2.2.3.1.	<i>Data Organisation</i>	45
2.2.3.2.	<i>Visualisation</i>	45
2.2.3.3.	<i>Spatial Query</i>	46
2.2.3.4.	<i>Data Combination and Integration</i>	47
2.2.3.5.	<i>Spatial Analysis</i>	47
2.2.3.6.	<i>Prediction</i>	47
2.3.	<b>What is digital geological mapping?</b>	<b>47</b>
2.3.1.	<b><i>Digital vs. Traditional mapping methods</i></b>	<b>48</b>
2.3.1.1.	<i>Traditional geological mapping</i>	48
2.3.1.2.	<i>Digital geological field mapping</i>	50
2.3.1.2.1.	Digital geological mapping	51
2.3.1.2.2.	Digital geological survey	52
2.3.2.	<b><i>Digital mapping Hardware and software</i></b>	<b>53</b>
2.3.2.1.	<i>Spatial location devices</i>	55
2.3.2.1.1.	GPS units	55
2.3.2.1.2.	Laser scanners and laser rangefinders	58
2.3.2.2.	<i>Data recording device</i>	58
2.3.2.3.	<i>Field-based software tools</i>	59
2.3.3.	<b><i>Cost vs. accuracy vs. mobility</i></b>	<b>60</b>
2.3.3.1.	<i>Cost, accuracy and mobility</i>	60
2.3.3.2.	<i>Testing GPS accuracy and precision</i>	61
2.4.	<b>GAVA workflow</b>	<b>62</b>
2.4.1.	<b><i>Introduction</i></b>	<b>62</b>
2.4.2.	<b><i>Preparation</i></b>	<b>63</b>
2.4.2.1.	<i>Creating the digital database – choosing formats and creating files</i>	63

<b>2.4.3.</b>	<b><i>Acquisition</i></b>	<b>65</b>
2.4.3.1.	<i>Integration of regional to outcrop data in a digital database</i>	65
<b>2.4.4.</b>	<b><i>Post-processing and analysis</i></b>	<b>66</b>
2.4.4.1.	<i>Post-processing data</i>	66
2.4.4.2.	<i>Visualisation I – 2-D maps and 2.5-D/ 3-D models</i>	66
2.4.4.3.	<i>Spatial and geostatistical analysis in GIS</i>	67
2.4.4.4.	<i>Data export to third party software</i>	68
<b>2.4.5.</b>	<b><i>3-D geological modelling</i></b>	<b>68</b>
2.4.5.1.	<i>Visualisation II – 3-D models</i>	68
2.4.5.2.	<i>Animations and video</i>	68
2.4.5.3.	<i>Publication and data archiving</i>	69
<b>2.5.</b>	<b>Testing the workflow</b>	<b>69</b>

## **CHAPTER 3 (CASE STUDY 1)**

<b>3.</b>	<b>THE VARYING BRITTLE FAULT STRUCTURES OF THE SCOTTISH NORTH COAST – EVIDENCE FOR BASEMENT INFLUENCED EXTENSION IN THE WEST ORKNEY BASIN AND IMPLICATIONS FOR THE ATLANTIC MARGIN</b>	<b>83</b>
	<b>ABSTRACT</b>	<b>83</b>
<b>3.1.</b>	<b>Introduction</b>	<b>83</b>
<b>3.2.</b>	<b>Geological setting</b>	<b>85</b>
3.2.1.	<i>Structure of the northwest UK Continental Shelf</i>	85
3.2.2.	<i>The West Orkney Basin</i>	86
3.2.3.	<i>Pre-Devonian basement structures</i>	87
<b>3.3.</b>	<b>Data acquisition methods</b>	<b>88</b>
3.3.1.	<i>Digital mapping and the GIS database</i>	88
3.3.2.	<i>Regional-scale structures</i>	88
3.3.3.	<i>Outcrop-scale structures</i>	89
3.3.4.	<i>3D structural models and visualisation</i>	90
<b>3.4.</b>	<b>Regional fault analysis</b>	<b>90</b>
3.4.1.	<i>Lineament patterns</i>	90
3.4.2.	<i>Regional 3-D models</i>	92
<b>3.5.</b>	<b>Outcrop scale structural analysis</b>	<b>93</b>
3.5.1.	<i>Kirtomy Bay</i>	93
3.5.1.1.	<i>Structure of Kirtomy bay micro-basin from 3-D models</i>	94
3.5.2.	<i>Glaisgo</i>	95
3.5.3.	<i>Coldbackie (Watch Hill)</i>	95
3.5.4.	<i>Durness</i>	96
3.5.5.	<i>Fault geometries and kinematics</i>	98
3.5.5.1.	<i>Kinematic analysis</i>	98
<b>3.6.</b>	<b>Discussion</b>	<b>99</b>
3.6.1.	<i>Fault patterns vs. Basement trends</i>	99
3.6.1.1.	<i>Fault patterns in Lewisian Foreland</i>	99
3.6.1.2.	<i>Fault patterns in Caledonian basement</i>	100
3.6.1.3.	<i>Reactivation of basement structures onshore</i>	101

3.6.2.	<i>Age relationships of sediments and structures</i>	103
3.6.2.1.	<i>Faults in Lewisian Foreland</i>	103
3.6.2.2.	<i>Faulting in Caledonian basement</i>	104
3.6.3.	<i>Linking onshore and offshore – indirect evidence for a North Coast transfer zone</i>	105
3.6.3.1.	<i>Origins of this transfer zone</i>	107
3.6.4.	<i>How does the structure of the North Coast relate to the present day NE Atlantic margin?</i>	108
3.7.	<b>Conclusions</b>	109

## CHAPTER 4 (CASE STUDY 2)

4.	<b>BASEMENT CONTROL ON FAULTING PATTERNS, TRANSTENSION AND STRUCTURAL SEGMENTATION OF THE LOFOTEN RIDGE, NORWEGIAN MARGIN: USING DIGITAL MAPPING TO LINK ONSHORE AND OFFSHORE GEOLOGY</b>	127
	ABSTRACT	127
4.1.	<b>Introduction</b>	127
4.2.	<b>Regional setting</b>	129
4.2.1.	<i>The Lofoten-Vesterålen margin</i>	129
4.2.2.	<i>The Lofoten-Vesterålen archipelago</i>	131
4.3.	<b>The fault architectures of the Lofoten-Vesterålen region</b>	133
4.3.1.	<i>GIS database</i>	133
4.3.2.	<i>Onshore ('surface') dataset</i>	134
4.3.3.	<i>Offshore ('subsurface') dataset</i>	136
4.3.4.	<i>Building 3D Models</i>	136
4.4.	<b>Regional structural analysis</b>	137
4.4.1.	<i>Onshore surface analysis</i>	137
4.4.1.1.	<i>Lineament populations</i>	137
4.4.1.2.	<i>Lineament domains</i>	137
4.4.1.3.	<i>Regional onshore models</i>	138
4.4.2.	<i>Offshore subsurface analysis</i>	139
4.4.2.1.	<i>Offshore Central Lofoten and the Havbåen sub-Basin</i>	139
4.4.2.2.	<i>Offshore North Lofoten</i>	139
4.5.	<b>Field data analysis</b>	140
4.5.1.	<i>Fault populations</i>	140
4.5.2.	<i>Fault interaction</i>	141
4.5.3.	<i>Spatial characteristics of faults and fractures</i>	142
4.5.3.1.	<i>Spatial analysis</i>	142
4.5.3.2.	<i>Fracture spacing analysis</i>	142
4.5.4.	<i>Kinematic analysis</i>	144
4.5.4.1.	<i>Inversion procedures</i>	144
4.5.4.2.	<i>Inversion results</i>	145
4.5.4.3.	<i>Transtension and the effects of fault obliquity in the NLD</i>	145
4.6.	<b>Discussion</b>	146
4.6.1.	<i>Regional vs. field measurements of onshore faults</i>	146
4.6.2.	<i>Complex faulting – oblique extension in North Lofoten</i>	147

4.6.3.	<i>Fault interaction and implications for stress inversion</i>	148
4.6.4.	<i>Fracture spacing and origins</i>	148
4.6.5.	<i>Segmentation of the LVA</i>	150
4.6.6.	<i>Transtensional model for the LVA</i>	150
4.6.7.	<i>The control of pre-existing structures on ridge development and segmentation</i>	151
4.6.7.1.	<i>Ridge development</i>	151
4.6.7.2.	<i>Transfer zones and segmentation</i>	154
4.7.	<b>Conclusions and Implications for future exploration on the Norwegian margin</b>	155

## CHAPTER 5 (CASE STUDY 3)

5.	<b>TRANSTENSION, BASEMENT REACTIVATION AND TRANSFORM FAULT DEVELOPMENT IN THE DAVIS STRAIT, WEST GREENLAND: LINKING ONSHORE STRUCTURES WITH OFFSHORE</b>	176
	<b>ABSTRACT</b>	176
5.1.	<b>Introduction</b>	176
5.2.	<b>Regional geological setting</b>	178
5.2.1.	<i>Tectonic margin</i>	178
5.2.2.	<b>Onshore basement structure and the Nagssugtoqidian Orogenic Belt</b>	180
5.3.	<b>Structural data acquisition</b>	182
5.3.1.	<i>Regional structural data</i>	182
5.3.2.	<i>Outcrop-scale structural data</i>	183
5.3.3.	<i>Areas and localities studied</i>	183
5.4.	<b>Regional fault populations</b>	184
5.4.1.	<i>Regional lineament trends</i>	184
5.4.2.	<i>Nordre Strømfjord region (Areas 1-3)</i>	185
5.4.3.	<i>Nordre Isortoq region (Area 4)</i>	185
5.5.	<b>Outcrop-scale fault populations</b>	186
5.5.1.	<i>Outcrops and exposure</i>	186
5.5.2.	<i>Measurements and determinations</i>	186
5.5.3.	<i>Age relationships</i>	187
5.5.4.	<i>Kinematic analysis</i>	189
5.5.4.1.	<i>Analysis method</i>	189
5.5.4.2.	<i>Inversion results</i>	189
5.6.	<b>Discussion</b>	190
5.6.1.	<b>Onshore structural framework (outcrop to basin scale)</b>	190
5.6.1.1.	<i>Fault patterns and Palaeostress</i>	190
5.6.1.2.	<i>Spatial and Temporal Variations</i>	190
5.6.1.3.	<i>Onshore-offshore correlations in the Sisimiut Basin</i>	192
5.6.2.	<b>The Davis Strait Transform and the Ungava fault zone (basin to margin scale)</b>	193
5.6.2.1.	<i>Transtension vs. wrench systems</i>	193
5.6.2.2.	<i>Basement influence in the Davis Strait region</i>	195
5.7.	<b>Conclusions</b>	196

## CHAPTER 6

<b>6.</b>	<b>DISCUSSION AND CONCLUSIONS</b>	<b>216</b>
<b>6.1.</b>	<b>Introduction</b>	<b>216</b>
<b>6.2.</b>	<b>Basement influence in extensional settings</b>	<b>217</b>
<b>6.2.1.</b>	<b><i>Reactivation of pre-existing fabrics</i></b>	<b>217</b>
<b>6.2.1.1.</b>	<i>Pervasive and discrete structures</i>	217
<b>6.2.1.2.</b>	<i>Basement reactivation vs. basement influence</i>	218
<b>6.2.2.</b>	<b><i>Orthogonal vs. oblique extension</i></b>	<b>219</b>
<b>6.3.</b>	<b>Determining stress and strain from fault slip analysis in complex fault zones</b>	<b>220</b>
<b>6.3.1.</b>	<b><i>Kinematic vs. Dynamic analysis</i></b>	<b>219</b>
<b>6.3.2.</b>	<b><i>Can palaeostress inversion give reasonable results in complex fault zones?</i></b>	<b>220</b>
<b>6.3.2.1.</b>	<i>Problems and limitations of palaeostress analysis</i>	221
<b>6.3.2.2.</b>	<i>Methods applied in this study</i>	224
<b>6.4.</b>	<b>The effects of basement on the structure and geometry of passive margins</b>	<b>225</b>
<b>6.4.1.</b>	<b><i>Margin segmentation</i></b>	<b>225</b>
<b>6.4.2.</b>	<b><i>Orthogonal and oblique margins</i></b>	<b>226</b>
<b>6.4.2.1.</b>	<i>Variations in structure and style</i>	226
<b>6.4.2.2.</b>	<i>Wide and narrow margins</i>	226
<b>6.4.3.</b>	<b><i>Oblique margins, transfer zones and transform faults – is there a link?</i></b>	<b>228</b>
<b>6.5.</b>	<b>Digital mapping methods: a review</b>	<b>229</b>
<b>6.5.1.</b>	<b><i>Have digital methods helped the project</i></b>	<b>229</b>
<b>6.5.1.1.</b>	<i>Data acquisition time</i>	229
<b>6.5.1.2.</b>	<i>Data management and sorting</i>	229
<b>6.5.1.3.</b>	<i>Spatial analysis</i>	229
<b>6.5.2.</b>	<b><i>Problems encountered during mapping and possible solutions</i></b>	<b>230</b>
<b>6.6.</b>	<b>Future trends in digital field mapping</b>	<b>231</b>
<b>6.6.1.</b>	<b><i>Multi-user mapping and telecommunications</i></b>	<b>231</b>
<b>6.6.2.</b>	<b><i>Future hardware and software tools</i></b>	<b>232</b>
<b>6.6.2.1.</b>	<i>All-in-one systems</i>	232
<b>6.6.2.2.</b>	<i>Voice recognition for hands free data collection</i>	232
<b>6.6.2.3.</b>	<i>Real time data analysis and 3-D visualisation: Field-GSIS</i>	233
<b>6.6.2.4.</b>	<i>Wearable computers and augmented reality</i>	233

## APPENDICES 241

APPENDIX 1: Digital Geological Mapping (DGM) hardware and software tools used 242

APPENDIX 2: Testing GPS accuracy 245

APPENDIX 3: Lists of project datasets and metadata files 250

<b>APPENDIX 4: Results of kinematic inversion (paleaostress) analysis</b>	<b>257</b>
<b>APPENDIX 5: Fracture spacing images and analysis</b>	<b>263</b>
<b>APPENDIX 6: 3D visualisation of ArcScene™ and GoCAD™ models (on DVD)</b>	
<b>APPENDIX 7: Other published articles by the author resulting from this study (on DVD)</b>	
<b>REFERENCES</b>	<b>267</b>

## Tables and Figures

### **CHAPTER 1**

Figure 1.1. ....	27
Figure 1.2. ....	28
Figure 1.3. ....	29
Figure 1.4. ....	30
Figure 1.5. ....	31
Figure 1.6. ....	32
Figure 1.7. ....	33
Figure 1.8. ....	34
Figure 1.9. ....	35
Figure 1.10. ....	36
Figure 1.11. ....	37
Figure 1.12. ....	38
Figure 1.13. ....	39
Figure 1.14. ....	40

### **CHAPTER 2**

Table 2.1. ....	70
Table 2.2. ....	70
Table 2.3. ....	71
Table 2.4. ....	71
Table 2.5. ....	72
Table 2.6. ....	73
Figure 2.1. ....	74
Figure 2.2. ....	75
Figure 2.3. ....	76
Figure 2.4. ....	77
Figure 2.5. ....	78
Figure 2.6. ....	78
Figure 2.7. ....	79
Figure 2.8. ....	80
Figure 2.9. ....	81
Figure 2.10. ....	82

### **CHAPTER 3**

Figure 3.1. ....	111
Figure 3.2. ....	112
Figure 3.3. ....	113
Figure 3.4. ....	114
Figure 3.5. ....	115
Figure 3.6. ....	116

Figure 3.7. ....	117
Figure 3.8. ....	119
Figure 3.9. ....	120
Figure 3.10. ....	122
Figure 3.11. ....	123
Figure 3.12. ....	124
Figure 3.13. ....	125
Figure 3.14. ....	126

**CHAPTER 4**

Table 4.1. ....	157
Table 4.2. ....	158
Table 4.3. ....	158
Figure 4.1. ....	159
Figure 4.2. ....	160
Figure 4.3. ....	161
Figure 4.4. ....	162
Figure 4.5. ....	163
Figure 4.6. ....	164
Figure 4.7. ....	165
Figure 4.8. ....	166
Figure 4.9. ....	168
Figure 4.10. ....	169
Figure 4.11. ....	170
Figure 4.12. ....	171
Figure 4.13. ....	172
Figure 4.14. ....	173
Figure 4.15. ....	174
Figure 4.16. ....	175

**CHAPTER 5**

Table 5.1. ....	198
Table 5.2. ....	199
Figure 5.1. ....	200
Figure 5.2. ....	201
Figure 5.3. ....	202
Figure 5.4. ....	203
Figure 5.5. ....	204
Figure 5.6. ....	205
Figure 5.7. ....	207
Figure 5.8. ....	208
Figure 5.9. ....	209



Figure 5.10. ....	210
Figure 5.11. ....	211
Figure 5.12. ....	212
Figure 5.13. ....	214
Figure 5.14. ....	215

## **CHAPTER 6**

Figure 6.1. ....	235
Figure 6.2. ....	236
Figure 6.3. ....	237
Figure 6.4. ....	238
Figure 6.5. ....	239
Figure 6.6. ....	240

## 1. Basement-influenced oblique extension in Passive Margin settings

### 1.1. Introduction

Passive margins constitute about 50% (c.  $45 \times 10^3$  km: inc. North and South Atlantic margins and Australian margins) of the overall length of present day continental margins (Gallagher and Brown, 1997) and represents the transition between the relatively simple tectonic setting of the ocean basins and the more complex continental regions. Most passive margins develop in two main stages: *rifting* and *drifting* (Withjack et al., 1998). The early stages of passive margin development are generally thought of as being akin to intra-continental rifting (e.g. East African Rift, Rhine Graben Rift, Baikal Rift). It is at this stage that pre-existing structures in continental basement are most likely to influence margin development by influencing the geometry and location of the rift system (Rosendahl, 1987; Morley et al., 1990, 2004; Clemens et al., 1997). The later, *drifting*, stage of margin development is associated with the onset of sea-floor spreading which can lead to a complex relationship of extensional and compressional (e.g. ridge-push) forces and further reactivation of pre-existing structures (Withjack et al., 1998; Imber et al., 2005). Oblique extension is likely, and plays an important role, in most continental rifts and passive margins settings for two main reasons: (1) Obliquely divergent displacements are an inevitable consequence of plate motions on a sphere (Dewey, 1975); (2) continental basement commonly contains pre-existing structures (e.g. faults or fabrics) many of which are likely to be oriented oblique to later extension episodes. Reactivation leads to plate margins that vary along-strike (Dewey et al., 1998).

Inherited weaknesses in basement may be a fundamental control on continental margin development (Dunbar and Sawyer, 1989; Davidson, 1997). Continental basement can have both pervasive and discrete weaknesses, both of which can influence later extensional systems (Morley et al., 2004). Pre-existing fabrics exert a strong control on the overall rift geometry in extensional settings, and can lead to the development of complex fault patterns, obliquely extending segments, deformation partitioning, and transfer zones (Morley 1990, 2004; Nelson et al. 1992; Clemson et al. 1997; Ebinger et al. 1999; Meisling et al., 2001; Paton & Underhill 2004, De Paola et al. 2005; Wilson et al. 2006). Most passive margins (and continental rifts) are segmented along strike into



## *Chapter 1 - Introduction*

zones characterized by a constancy in structural style (e.g. Francheteau and Le Pichon, 1972; Rosendahl, 1987; Morley et al., 1990; Doré et al., 1997; Clemson et al., 1997; Song et al., 2001). This margin segmentation has also been attributed to the influence of basement structure (e.g. Davison, 1997; Clemsen et al., 1997; Meisling et al., 2001).

Basement-influenced deformation can have important implications on basin and reservoir geometry, and can lead to the development of non-plane strain deformation, non-textbook fault geometries and complex reservoirs. Therefore understanding these effects has important implications for hydrocarbon exploration. One of the main problems when trying to analyse the effects of basement when studying offshore basins is that the structure of basement rocks beneath basins can generally not be seen in seismic data. Potential field-data (e.g. airborne gravity and magnetic surveys) may often be used to distinguish major regional variations in basement terrane (e.g. Doré et al., 1997; Olesen et al., 1997, 2002), however these still cannot easily distinguish pervasive fabrics or discrete structures in areas of similar basement terrane. Therefore, where possible, onshore studies are commonly used as this allows direct analysis of basement structures and their relationship with faulting and basin geometry. A further benefit of onshore studies is that kinematic indicators associated with faulting can be obtained, which are often not clear in seismic interpretations. A distinct problem when using onshore studies to develop offshore models however is that onshore data are generally not in a geospatially referenced digital format that is comparable to offshore data. This often leads to 2-D maps of structures being used to analyse what are essentially 3-D (4-D) relationships, which can lead to misinterpretations of structural similarities (Roberts and Holdsworth, 1999). Therefore there is a need for better integrated onshore and offshore data, which requires onshore data to be both in a digital format and geospatially correct.

### **1.2. Aims of research and areas studied**

#### ***1.2.1. Research Aims***

The main aims of this research are to investigate the role played by basement structures in the development of fault patterns on passive margins, with particular attention paid to

## *Chapter 1 - Introduction*

zones of obliquity. This requires an integrated onshore-offshore approach that allows the analysis of basement hosted faults and fractures and fault kinematics onshore and also offshore fault and basin development. Therefore this thesis generally has two key themes; 1) the development of onshore digital datasets that can be integrated with offshore models; and 2) the structural and kinematic analysis of fault patterns in basement-influenced passive margin areas. The first of these themes requires new digital mapping methods to be developed and established to enable geospatially correct digital data to be collected both at a regional and at an outcrop scale. The latter theme is more in fitting with classic geological research, however, where possible the benefits of having geospatial digital datasets are utilised in order to carryout various analyses.

### ***1.2.2. Location of research areas***

The three case study areas analysed during this research are all located on continental margins of the North Atlantic region (Fig. 1.1). Case study 1 looks at the basement structures in Northern Scotland and their structural implications for the margin to the west and northwest of the UK (Fig. 1.1). Case study two also looks at basement structures in the NE Atlantic, but further north, in the Lofoten-Vesterålen segment of the Norwegian Margin (Fig. 1.1). Case study three, on the other hand looks at the influence of basement structures on the West Greenland margin (Fig. 1.1). All three studies are predominantly concerned with the interpretation and analysis of fault and basement structures onshore, however efforts are made to link these onshore structures with those offshore.

The North Atlantic basement terranes in their present configuration were derived from three Precambrian continents; Laurentia, Baltica and Gondwana, which were brought together through the Appalachian/ Caledonian and Hercynian/ Variscan orogenies (Fig. 1.2). Over time, repeated tectonic episodes impart a fabric on the crust and lithosphere by juxtaposing blocks with different properties and boundary orientations. The rheology or mechanical behaviour of these blocks within the crust can control the rate of subsidence and geometry of subsequent (i.e. upper Palaeozoic, Mesozoic and Cenozoic) phases of basin evolution. In case study 1 (Northern Scotland),

## *Chapter 1 - Introduction*

and to a lesser extent case study 2 (Lofoten-Vesterålen), both Precambrian (Archaean and Palaeoproterozoic) and Caledonian basement structural terranes are apparent, whereas in case study 3 (West Greenland) only Precambrian terranes are present.

### **1.3. Thesis outline**

In **chapter 1** a brief overview of basement inheritance and its influence in extensional and passive margin settings is presented. The principles of transtension and the deformation patterns associated with oblique divergence are also reviewed. So too are some of the principal methods of collecting and analysing structural field data applied in this study.

**Chapter 2** contains a detailed overview of the use of digital fieldwork technologies, their increasing use in geological research and an analysis of the benefits of such methods compared to traditional geological mapping techniques. An outline of the digital methods developed and applied during this study is also presented.

**Chapters 3, 4 and 5** are three separate case study chapters investigating the influence of basement in three Passive margin settings in the Northern Atlantic (Figs. 1.1 & 1.3). In each study data analysis is primarily based on onshore studies of fault patterns in basement rocks at both regional and outcrop scales, however attempts are also made to link these structures with offshore structures in sedimentary basins.

**Chapter 3** (case study 1) contains a study of the basement-influence on post-Caledonian (Devonian/ Mesozoic) extension in Northern Scotland and the West Orkney Basin (Figs. 1.1 & 1.3), and the variations in faulting in different basement terranes.

**Chapter 4** (case study 2) studies the role played by oblique-basement structures in the segmentation of the Lofoten Ridge (NW Norway; Figs. 1.1 & 1.3), with implications for segmentation of the Norwegian margin as a whole.

**Chapter 5** (case study 3) studies the effects of intense basement fabrics on extension in the Davis Strait, West Greenland (Fig. 1.1), the role played by oblique-basement structures in the development of the Ungava transform fault.

**Chapter 6** summarises and discusses the main implications of the thesis in a broader context and a comparison between the structural style exhibited and effects of basement in each case study is assessed. An overall discussion of the usability and viability of digital mapping methods, with a review of the problems encountered during this research project. This section also includes a short note on the future of digital geological mapping.

#### **1.4. Basement inheritance and reactivation**

##### ***1.4.1. Basement inheritance vs. reactivation***

The term ‘basement’ has a range of meanings depending on the area of research being carried out. In offshore seismic studies ‘basement’ is usually used to describe “all non-prospective rocks which lie below prospective strata”, while in onshore studies the term basement is used to describe deformed crystalline metamorphic and plutonic rocks (often of Precambrian age, though not necessarily) that underlie sedimentary cover sequences (Allaby and Allaby, 1996). It is in this latter context that basement is referred to in this study. As crystalline basement of the continental crust preserves evidence of past deformation events, it is generally considered as being heterogeneous in structure. These heterogeneities are likely to affect later deformation processes as they lead to variations in mechanical strength and rheological behaviour of the rock (e.g. fault zone weakening; Holdsworth et al., 2001b). Peacock and Sanderson (1992) define three different types of anisotropy in rocks: (1) layering (e.g. bedding), (2) continuous (pervasive) anisotropy (e.g. foliation, shear zones, etc.), and (3) discrete planes of weakness (e.g. faults, cleavage planes, etc.). A number of studies have shown how such heterogeneities can influence fault geometries and strain reorientation during deformation (Donath 1961; Peacock and Sanderson, 1992). The influence of pre-existing basement structures, which includes reactivation, may more generally termed basement inheritance.

Basement inheritance is a widely accepted phenomenon in structural and tectonic geology, and is commonly cited in a range of tectonic systems. These include: continental rifted and passive margins (e.g. Doré et al., 1997; Clemson et al., 1997; Song et al., 2001); basin formation (e.g. Cooper and Williams, 1989; Coward, 1994); orogenic

and collision zones (e.g. Tavarnelli et al., 2004); strike-slip systems (e.g. the Great Glen Fault; Rogers et al., 1989; Holdsworth et al., 2001a); magmatic systems (e.g. Hutton, 1988). Furthermore, the influence of pre-existing structures has been suggested at plate scales (e.g. Sykes, 1978; Daily et al., 1989; Snyder et al., 1997; Oldow, 2003), regional scales (Doré et al., 1997; Pinheiro and Holdsworth, 1997; Paton and Underhill, 2004; De Paola et al., 2005b), outcrop scales (e.g. Laubach and Marshak, 1987; Beacom et al., 2001), grain scales (Hippler and Knipe, 1990; Lloyd and Knipe, 1992).

Factors which are generally believed to control basement inheritance are: mechanical rock strength and strength anisotropies (Morley et al., 2004); fault zone weakening (Holdsworth et al., 2001b); bulk properties (e.g. density) of basement terranes; and orientation of stresses relative to pre-existing structures (Dewey, 2002; De Paola et al., 2005b); however, other factors are also likely. Continental basement can have pervasive and discrete weaknesses, both of which can influence (and be reactivate) later extensional systems. Morley et al. (2004) describe how varying pervasivity (i.e. length and spacing) and strength of the weaknesses can affect later fault patterns (Fig. 1.4).

Signatures of basement inheritance include: (1) reactivation of pre-existing structures; (2) structural variations consistent with variations in basement terrane; (3) similarity of trend / orientation of structures of different age; (4) non-plane strain deformation, inc. transtension and transpression; (5) complex fault and fracture patterns; (6) overprinting structures. With the exception of reactivation most of the above list are all an indirect consequence of basement-influence, and may be attributable to alternative models therefore careful analysis is required when defining basement-influenced deformation.

#### 1.4.1.1. *What defines reactivation?*

In ancient settings, reactivation is defined as '*the accommodation of geologically separable displacement events (at intervals >1Ma) along pre-existing structures*' (Holdsworth et al. 1997). The time scales are important because shorter time intervals (< 1 Ma) may relate to recurrent movements within the seismic cycle (Wallace, 1984). In neotectonic environments, where dating of deformation can be more precise (e.g.

Stewart and Hancock, 1994), the time interval between recognisable reactivation events may be less (Muir Wood and Mallard, 1992; Holdsworth et al., 1997). Long periods of quiescence on some faults and shear zones possible indicate extinction or dormant behaviour until the appropriate stress regime develops (Muir Wood and Mallard, 1992).

Two types of reactivation have been identified (Holdsworth et al., 1997):

- a) Geometric reactivation – where reactivated structures display *different* senses of relative displacement for successive events.
- b) Kinematic reactivation – where reactivated structures display *similar* senses of relative displacement for successive events.

Stratigraphic, structural, kinematic, geochronological and neotectonic criteria (Fig. 1.5) are all considered reliable criteria for identifying reactivation (Holdsworth et al., 1997). The unequivocal use of geometric similarity as a criteria for identifying reactivation (e.g. by Sonder, 1956; Donath, 1962; O'Driscoll, 1980; Sutton and Watson, 1986) is not reliable (Holdsworth et al., 1997; Roberts and Holdsworth, 1999). Geometric similarities however, are especially common in structural interpretations of seismic data from offshore sedimentary basins (e.g. Brewer and Smythe, 1984; Gage and Doré, 1986; Bartholomew et al., 1993; Lee and Hwang, 1993; Doré et al., 1997). In many cases the linking of older onshore (basement) structures and younger structures offshore is based solely on geometric similarity (e.g. Enfield and Coward, 1987; Coward et al., 1989; Doré et al., 1997; Roberts and Holdsworth, 1999). Where possible, several different criteria should be used to define reactivation with increased certainty.

Similarities in trend of structures alone does not imply reactivation (i.e. geometric similarity; Holdsworth et al., 1997; Roberts and Holdsworth, 1999) for example in the north coast of Scotland a number of studies have discussed how Caledonian structures have been reactivated during later extensional events (Brewer and Smythe, 1984; Enfield & Coward, 1987), and part of this reasoning is that brittle faults trend parallel to basement fabrics. However onshore studies show that steep brittle faults demonstrably cut the moderately dipping Caledonian fabrics (Holdsworth et al., 1989) thus implying that reactivation is not a controlling factor (this example is discussed further in Chapter 3).



### 1.4.2. *Mechanics of oblique reactivation during extension*

There are three main factors that must be considered when assessing fabric (i.e. foliation, cleavage, faults, etc.) reactivation: (a) strength of the fabric relative to the intact rock; (b) the geometry of the fabric relative to the stress field; and (c) the sense of slip once the fabric becomes activated (Morley et al., 2004). The activation of fabrics during rifting can also be split into three stages: (1) the initial fracturing of the intact rock during the early stages of rifting; (2) subsequent activation of the established fault and fracture network; and (3) changes to the stress field (magnitude or orientation, at local or regional scales) during the evolution of the rift system.

#### 1.4.2.1. *Initiation of fracturing and reactivation*

The development of early stage rift faults can be characterised as a competition between the development of new optimally aligned fractures within isotropic rock and reactivation of pre-existing non-optimally aligned fractures following strength anisotropies (Fig. 1.6; Yin and Ranalli, 1992; Nieto-Samianiego and Alaniz-Alvarez, 1997; Morley et al., 2004). For a new fault to form at an ideal orientation to the principal stresses, the isotropic cohesive shear strength of the country rock ( $C$ ) must be overcome. The presence of discrete fabrics or pervasive strength anisotropies effects rock strength, reducing the cohesive shear strength ( $C_1$ ) relative to the isotropic rock strength ( $C$ ) (Ranalli and Yin, 1990). The differences in cohesive shear strength of a rock (i.e. between  $C$  and  $C_1$ ) can be considerable. Sibson (1977) show that the cohesive shear strength of an intact rock may be the order of 100 bar, whilst that of a cemented fault zone tends not to exceed 10 bar.

Jaeger and Crook (1967) show that the cohesive shear strength can also be defined as a variable ( $\Delta C$ ) that changes according to the angle between the strength anisotropy and the maximum principal stress ( $\theta_{re}$ )

$$C_1 = \Delta C \cos 2(\delta_{re} - \theta_{re}) \quad (1.1.)$$

where  $\delta_{re}$  is defined as the angle of shear failure relative to  $\sigma_1$  (typically about  $30^\circ$ ). The cohesive strength is least when  $\delta_{re} = \theta_{re}$ , and has a maximum value when the plane of anisotropy is at  $90^\circ$  to this.

## Chapter 1 - Introduction

The frictional behaviour of course has a significant controlling factor in the reactivation of faults (Fig. 1.6; Sibson, 1977). In a rock with fluid pressure,  $P_f$ , the effective principal stresses are:

$$\sigma_1' = (\sigma_1 - P_f) > \sigma_2' = (\sigma_2 - P_f) > \sigma_3' = (\sigma_3 - P_f) \quad (1.2.)$$

Sibson (1977, 1985, and 1995) shows the conditions for frictional reactivation of an existing cohesionless fault (i.e.  $C_1 = 0$ ) may be represented by Amonton's Law:

$$\tau = \sigma_{ne} \tan \phi \quad (1.3.)$$

where  $\tau$  and  $\sigma_{ne}$  are the shear and effective normal stress respectively acting on the potential fracture plane, and  $\phi$  is the angle of sliding friction on that plane (Fig. 1.6). The relationship between the angle of sliding friction and the coefficient of friction ( $\mu$ ) is given by:

$$\mu = \tan \phi \quad (1.4.)$$

which means *equation 1.3.* can be re-written as:

$$\tau = \mu \sigma_{ne} = \mu_s (\sigma_{ne} - P_f) \quad (1.5.)$$

where  $\mu_s$  is the static coefficient of friction. The frictional behaviour for a rock with strength anisotropy may therefore be described by the Coulomb-Navier shear failure criteria (Ranalli and Yin, 1990):

$$\tau = C_1 + \mu_2 \sigma_{ne} \quad (1.6.)$$

Figure 1.6 shows the effects of varying the strength anisotropy on the likelihood of fault reactivation relative to the development of new faults based on *equations 1.1.* and *1.6.*

1.4.2.2. *Continued activity on faults*

Once active faults are established extensively within a rock volume the Coulomb-Navier failure criteria is replaced by a sliding friction criteria (equivalent to Amonton's Law, *eq. 1.3.*), as the cohesive shear strength of the rock no longer applies. Byerlee (1978) found through a series of low temperature experiments that the static coefficient of friction ( $\mu_s$ ) is largely independent of rock type and falls generally in the range  $0.6 < \mu_s < 0.85$  (the value 0.7 is used in Fig. 1.6). Sliding friction is controlled by the ratio and magnitude of shear stress to normal stress, and is applicable under moderate to high normal stress conditions (Byerlee, 1978). Under this latter friction criterion those faults closest in orientation to the mechanically ideal orientation for the prevailing stress field will be favoured. This switch in failure criteria suggests that reactivation of basement structures is more likely early in a rifts evolution, with newly formed more optimally oriented faults becoming more dominant as the rift evolves; however in zones where non-optimally oriented (i.e. reactivated) faults predominate, continued activity on these structures is likely (Morley et al., 2004).

A limitation of the theory and equations outlined above is the fact that they are inherently based on 2-dimensional frameworks and assume an Andersonian stress system (Ranalli and Yin, 1990). Furthermore, angles referred to in *equation 1.1.* are measured relative to  $\sigma_1$  (and on the  $\sigma_1\sigma_3$  plane), which in the case of normal and reverse faults corresponds to angles of dip rather than trend/ orientation of a structure. However the overall principals of reactivation outlined above still apply to reactivation of obliquely trending structures too.

1.4.2.3. *Changes to the stress field*

The variation in magnitude of the intermediate principal stress ( $\sigma_2$ ) also has an important effect on active fracture orientations (Jaeger and Cook, 1967; Reches, 1978; Angelier et al., 1982; Krantz, 1988) and the orientation of maximum shear stress, which controls the sense of slip (Bott, 1959). The range of optimal strike directions for faults may be defined by the ratio of the intermediate stress to the other principal stresses ( $R$ ) (Bott, 1959):

$$R = \frac{\sigma_2 - \sigma_3}{\sigma_1 - \sigma_3} \quad (1.7.)$$

Triaxial tests also suggest that  $\sigma_2$  has a significant effect on rock strength (Chang and Haimson, 2000), with the lowest strength values when  $\sigma_2 = \sigma_3$ , and increases as  $\sigma_2$  increases. Morley *et al.* (2004) integrated the above principals of fault/ fabric reactivation in to a software program (FAST; Jones *et al.*, 2000) to predict the likelihood of fault and fracture reactivation. Their results showed that when  $\sigma_2 \approx \sigma_3$  and the rock is isotropic, then any strike orientation is possible. As the magnitude of  $\sigma_2$  increases with respect to  $\sigma_3$  so the range of anisotropy orientations likely to be reactivated increases. As  $\sigma_2$  approaches  $\sigma_1$  (i.e. moving towards strike-slip stress regime) the number of fault orientations likely to reactivate increases.

### 1.5. Oblique extension and transtension

Tectonic margins (be they plate margins or deformation zone boundaries) often follow zones of inherently weak fabric (e.g. NE Atlantic, Doré *et al.*, 1997), marking zones of repeated reactivation during successive crustal strains (Holdsworth *et al.*, 1997). With this in mind it is likely that many of these margins may be, or have segments that are, non-orthogonal to the regional extension direction during subsequent deformation events, leading to zones of oblique divergence. It has been estimated that about 50% of the modern divergent plate boundaries are significantly oblique (Woodcock, 1986), and it is likely that ancient tectonic margins had a similar character. Transtension is the state of strain resulting from a divergent displacement applied oblique to the boundaries of a deformation zone (Harland, 1971; Dewey *et al.*, 1998). Transtensional strains may arise as the consequence of the obliquity between regional (or local) strain fields and pre-existing rock anisotropies as layering, foliations, old fractures and faults, etc. (Holdsworth *et al.*, 1997), therefore they are an important factor to consider when analysing the basement-influence in extensional margins.

#### 1.5.1. Definitions of oblique extension and transtension

Dewey (2002) defines transtension as oblique extension which combines coaxial orthogonal extension and non-coaxial deformation zone parallel shear (Fig. 1.7a; see

section 1.7.1.1. for more detailed definitions of coaxial and non-coaxial deformation). Morley et al. (2004) are in agreement with this but draw a distinction between oblique extension and transtension; defining oblique extension as normal (extensional) faults that strike non-orthogonal to (i.e. as a result of the reactivation of pre-existing structures) within an Andersonian (coaxial) stress regime (i.e.  $\sigma_1$  vertical  $>$   $\sigma_2 \geq \sigma_3$ ), and transtension as a form of strike-slip deformation (i.e. intermediate principal stress,  $\sigma_2$ , is vertical) with an added component of orthogonal extension (Fig. 1.7b; Sanderson and Marchini, 1984; Dewey et al., 1998). However, Dewey (2002) suggest that the principles of transtension hold true for all forms of extension between the two end member states of purely extensional (pure shear) and purely strike-slip (simple shear) deformation (Fig. 1.8). Furthermore, there appears to be little difference between Morley et al.'s (2004) definition of oblique extension and 'extension dominated transtension' of Tikoff and Teyssier (1994), Dewey (2002) and De Paola *et al.* (2005). Therefore, in this study the terms 'oblique extension' and 'transtension' may be used interchangeably, however the former is generally used for describing geometric relationships, while the latter is used when kinematics are constrained.

## 1.5.2. Principles of transtension

### 1.5.2.1. Transtension: 2-D vs. 3-D strain

Transtension can be described qualitatively as being equivalent to the contemporaneous action of a "wrench" simple shear and an "extensional" pure shear, oriented respectively parallel and orthogonal to the boundary (Fig. 1.7b; Sanderson and Marchini, 1984; Fossen and Tikoff, 1993; Dewey et al., 1998).

Transtensional infinitesimal strain will occur when the bulk displacement is at an oblique angle  $\alpha$  to the deformation zone boundary faults (i.e.  $0^\circ < \alpha < 90^\circ$ ) (Fig. 1.8a). When the divergence angle  $\alpha$  is perpendicular ( $\alpha = 90^\circ$ ) or parallel ( $\alpha = 0^\circ$ ) to the boundary fault, we have pure shear coaxial extension (Fig. 1.8b) and non-coaxial wrench simple shear (Fig. 1.9c), respectively. These represent end-member strain states for transtension and both are considered in the present analysis to lead to plane strain (2-D) deformation (Figs. 1.8b-c). When the divergence vector is at an oblique angle, non-coaxial 3-D strain is always developed (Fig. 1.8a).

**1.5.2.2. Wrench dominated and extension dominated transtension**

Transtensional (and transpressional) strains are characterised by complex relationships between finite and infinitesimal strain ( $\equiv$  stress) axes. In transtensional zones with low to high angles of divergence ( $20^\circ < \alpha < 90^\circ$ ), where  $\alpha$  is the angle between regional displacement and boundary faults (McCoss, 1986; Dewey et al., 1998; De Paola et al., 2005a), the axes of infinitesimal ( $z_i$ ) and finite shortening ( $Z_i$ ) should always be coincident and vertical; this is identical to the case of orthogonal extension ( $\alpha = 90^\circ$ ) (extension-dominated transtension; EDTT); Fig. 1.8d). However, at low angles of divergence ( $\alpha < 20^\circ$ ), the infinitesimal axis  $z_i$  is horizontal, with the finite axis ( $Z_i$ ) eventually swapping orientation with the vertical intermediate finite axis  $Y_i$  with increasing amounts of finite strain (wrench-dominated transtension; WDTT); Fig. 1.8d). The threshold angle  $\alpha$  between wrench- and extension-dominated transtension has been termed the critical angle of displacement  $\alpha_{crit}$  (Smith and Durney, 1992). For an ideal incompressible material (with a Poisson's ratio of 0.5) this angle ( $\alpha_{crit}$ ) is  $20^\circ$  (McCoss, 1986). Teysier and Tikoff (1999) however, show that this angle may increase if there is a positive volume change (e.g. dyke emplacement) during deformation, and thus widening the zone of WDTT. De Paola et al. (2005) then took this further by taking into account for the Poisson's effect (i.e. variation in Poisson's ratio for different rocks). For most rock lithologies a  $\alpha_{crit}$  angle of between  $30^\circ$  and  $40^\circ$  is most appropriate (De Paola et al., 2005a), this is also consistent with observations made during analogue modelling of oblique extension (Withjack and Jamison, 1986).

**1.5.3. Faulting and deformation associated with transtension**

**1.5.3.1. Faulting under 2-D and 3-D strain**

The Andersonian theory of faulting, based on the Coulomb-Navier criterion (eq. 1.6.), predicts the development of a conjugate set of faults, which intersect parallel to the intermediate stress axis and have no slip component in the direction of this axis (Anderson, 1951). The symmetry of the system reflects the symmetry of the stress/infinitesimal strain tensor and the angle between the conjugate sets is a function of the internal friction coefficient  $\mu_i$  (eq. 1.4.; Fig. 1.9a). The Andersonian faulting model is associated with plane strain deformations since it implies no strain along the

intermediate axis and does not allow oblique-slip during faulting (Fig. 1.9a) since one of the three principal stresses is constrained to be normal to the earth surface, a surface where  $\tau = 0$ , i.e. it is a principal stress plane. Bott (1959) suggests therefore that oblique faulting occurs in cases where oblique-slip on reactivated pre-existing planes is realized under the influence of a reoriented stress system.

The Andersonian model cannot explain transtensional deformations since the latter is associated with a 3-D strain field. The slip model proposed by Reches (1978, 1983b) demonstrated that three sets of faults are necessary and sufficient to accommodate three-dimensional strain. If however, a specified rotation field is applied to the model in addition to a specified strain field, four sets of faults are necessary and are sufficient to accommodate the eight independent components of both tensors (Fig. 1.9b; Reches, 1978).

#### 1.5.3.2. *Fault patterns in transtension*

Dewey (2002) studied in detail the patterns of structures associated with the different states of transtensional deformation, and thus only a brief outline is given here. In Purely orthogonal extension zones fault patterns generally follow the Andersonian fault model (Anderson, 1951). In pure strike-slip systems, where the regional transport direction is parallel to the deformation zone, normal faults should develop at  $45^\circ$  to the deformation zone (i.e. simple shear; Fig. 1.8c; Wilcox et al., 1973). However, if the regional transport direction is oblique to the deformation zone (i.e. transtension; Fig. 1.9b) the orientation of normal faults may vary.

Following Withjack and Jamison (1986) there is a predictable relationship between the orientation of normal faults (assuming they form normal to the infinitesimal horizontal maximum extension strain axis,  $\beta_x$ ) and the overall system, which varies according to the angles made by the regional extension vector and the deformation zone boundary ( $\alpha$ ):

$$\beta_x = 90^\circ - 0.5 \tan^{-1} (\cot \alpha) \quad (1.8.)$$

which in terms of fault orientation relative to the deformation zone boundary ( $F_{\text{angle}}$ ) can be re-written as:

$$F_{\text{angle}} = 90 - \beta_x = 0.5 \tan^{-1} (\cot \alpha) \quad (1.9.)$$

Figure 1.10 shows a series of 2-D fracture maps showing how  $\alpha$  and  $\beta_x$  angles vary with increasing obliquity, based on analogue models of Withjack and Jamison (1986) and Clifton et al. (2000). These models highlight a marked change from simple coaxial to complex non-coaxial deformation with increasing obliquity. As transtensional deformation is non-coaxial, fault patterns associated with 3-D strain are also likely to develop (Reches, 1978; De Paola et al., 2005a).

#### 1.5.3.3. *Multimodal faulting: polyphase deformation and 3D strain*

Multiple fault orientations are common in many geological settings (e.g. Krantz, 1988, 1989; Nieto-Samaniego and Alvarez, 1997; Sagy et al., 2003). There are 5 known mechanisms to develop such patterns are:

- a) There are more than two sets of faults, because there have been two or more deformation events, separated in time, each with differently oriented stress axes, i.e. polyphase deformation. This explanation is linked to the Anderson's application of the Coulomb-Navier behaviour (*eq. 1.6.*) that precludes the simultaneous development of more than two conjugate sets of fault under a fixed stress field (Fig. 1.9a). Strain fields associated with this faulting criterion are inevitably plane strain.
- b) Wrench/ strike-slip faults often develop multiple fault orientations during simple shear. Reidel shear fractures, and antithetic/ synthetic fractures may develop in conjunction with a through going major fault (Logan et al., 1992).
- c) Reactivation of non-interacting faults according to the Bott (1959) model can account for different fault orientations. This model can also explain the mechanics of oblique-slip faulting, not allowed by the Anderson model.
- d) Multiple fault patterns are simultaneously developed as a response to an applied 3-D strain field (Fig. 1.9b; Reches, 1978 and 1983). In this case it has been demonstrated



that the symmetry of the fault pattern can be orthorhombic and be directly associated to the symmetry of the strain tensor. Under 3-D strain fields, six or eight sets of faults, depending on the presence or absence of rotational components, are necessary to accommodate the imposed deformation.

- e) The interacting block model (Nieto-Samaniego and Alaniz-Alvarez, 1995 and 1997) has been proposed to explain multiple fault patterns as the result of simultaneous and interacting reactivation between pre-existing faults. A fault pattern formed during a single deformation event of sliding on pre-existing planes has no restrictions regarding symmetry, number of slickenline sets, number of faults, or orientation of the faults (Nieto-Samaniego and Alvarez, 1997). As the number of phases of faulting increases, lower symmetry is expected. In this last case, a quantitative analysis of stress/strain axes direction is difficult since the pattern of deformation does not necessarily reflect the symmetry of the stress/strain tensor (Nieto-Samaniego, 1999).

During a bulk homogeneous transtensional deformation, case C seems to be the most likely kinematic solution which will govern the development of faulting patterns under infinitesimal strain fields. As finite strains accumulate, however, case B and particularly case D could increasingly become important. The Andersonian faulting patterns predicted by case A, in theory, should not develop. However, this observation seems to be at odds with worldwide evidence that both Andersonian faulting patterns and oblique displacements, are often associated, although they must operate at different scales.

#### ***1.5.4. Spatial variations and deformation partitioning***

A commonly recognised feature of transtensional systems is the partitioning of oblique rifting into contemporaneous domains of wrench- and extension-dominated transtension (e.g. Titus et al., 2002; Oldow, 2003; De Paola et al., 2005b). Strain partitioning has been described by Tikoff and Teyssier (1994) as an inevitable consequence during 3-D deformations, reflecting the complex relationships that exist between infinitesimal and finite strains. During wrench-dominated transtension ( $\alpha < 20^\circ$ ) the infinitesimal strain axes have an orientation consistent with strike-slip faulting, e.g.  $\lambda_H > \lambda_V > \lambda_h$ , but at the same time, the component of extensional pure shear intrinsic in the bulk transtensional

deformation ( $\lambda_v \equiv \lambda_2 < 1$ ), tends to build up and to be increasingly recorded as finite strain cumulates. If deformation reaches high values of finite strain, normal faulting can develop. The former fault pattern, made of sub-parallel strike-slip and normal faults, will continue to be active during deformation since they are favourably oriented to contemporaneously accommodate the wrench and extensional components of deformation (Tikoff and Teyssier, 1994, Dewey, 2002). These authors predict that the same mechanism should operate in the case of extension-dominated transtension ( $20^\circ < \alpha < 90^\circ$ ), where normal faulting in response to infinitesimal strains should pre-date strike-slip faulting developed in response to finite strains.

In most cases, strain partitioning is not simply an intrinsic consequence of finite 3-D deformations, but is induced by the presence of one or more pre-existing surfaces or zones of weakness along which a component of wrench simple shear can be preferentially accommodated. Such pre-existing weaknesses might include faults, shear zones, lithological boundaries and/or rheological anisotropies.

## **1.6. Fault and fracture classification and kinematic indicators**

### **1.6.1. Introduction**

A fracture is a brittle rupture within a (rock) material. Fractures form on all scales in the upper crust, from microfractures to continental scale fault zones, e.g. San Andreas Fault. The mesoscopic and megascopic scale structures are ultimately dependent on the nature of microscopic fractures. In fracture mechanics literature mesoscopic fractures are subdivided into three types based on the relative displacement of the material on either side of the fracture (Fig. 1.11; Twiss and Moore, 1992).

- a) Mode I – tensile opening, no shear (tension fractures)
- b) Mode II – in-plane shear (shear fractures)
- c) Mode III – anti-plane shear (shear fractures)

Joints and veins are examples of Mode I fractures, while shear fractures are examples of Mode II or Mode III fractures. A fault is a fracture that shows shear parallel to the rupture wall. This can occur by shear fracture (i.e. mode II/ III fractures) or by reactivation of tensile (mode I) fractures.

Tension fractures form perpendicular to the minimum principal stress ( $\sigma_3$ ) and parallel to the maximum principal stress ( $\sigma_1$ ), therefore strain is uniaxial. Shear fractures form in confined compression at angles of less than  $45^\circ$  to the maximum compressive stress ( $\sigma_1$ ). If the state of stress is biaxial, the shear fractures are parallel to the intermediate stress ( $\sigma_2$ ) and form a conjugate pair of planes at angles of less than  $45^\circ$  either side of the  $\sigma_1\sigma_2$  plane (Hancock, 1985).

### 1.6.2. Fault classification

There are many fault classification schemes based on the geometry and direction of slip on the fault. This can lead to a mixture of terminologies and descriptions used. In McClay (1987) two separate classification schemes are referred to: a) *Anderson's Dynamic Classification* which relates to the stress systems responsible for the faulting; and (b) a simple *Geometric Classification*.

#### 1.6.2.1. Andersonian "dynamic" classification of faults

Anderson's (1951) dynamic classification of faults is based on the assumption that one principal stress must be normal to the earth's surface, i.e. vertical (Fig. 1.12a). Using this classification faults are referred to as either: Normal faults ( $\sigma_1$  vertical), Wrench/ Strike-slip faults ( $\sigma_2$  vertical), or Reverse faults ( $\sigma_3$  vertical) (Fig. 1.12a).

#### 1.6.2.2. Geometric/ kinematic classification of faults

This classification is based upon the sense of movement and direction of slip across a fault plane, and leads to the following 5 classes (Fig. 1.12b):

- 1) *Normal faults/ Extension* – e.g. dip-slip normal faults and extensional faults
- 2) *Reverse faults/ Shortening* – e.g. dip-slip reverse, and thrust faults
- 3) *Strike-slip faults* – e.g. wrench faults, also transcurrent and transform faults
- 4) *Oblique-slip faults* – e.g. a combination of dip-slip and strike-slip
- 5) *Rotational faults*

McClay (1987) prefers the term *extension fault* over the more commonly used *normal fault* as it refers to the effect of the fault on the surrounding strata. However, in

## Chapter 1 - Introduction

this study, field work has been carried out predominantly in areas of crystalline basement with few stratigraphic markers. Therefore, the term *normal fault* is preferred in this study as it refers to a kinematic framework (i.e. hanging-wall down), rather than a stratigraphic one. The term *extensional fault* is generally reserved for describing faults and fault systems in a tectonic sense.

The term strike-slip fault is reasonably universal, and is therefore used throughout. However in some cases more specific terminologies are used, such as: *wrench faults* where a system of associated strike-slip faults is apparent (i.e. a system of Riedel shears and/or synthetic and antithetic strike-slip faults); *transform faults* for strike-slip faults which cut the whole lithosphere (Gilliland and Meyer, 1976; Woodcock 1986, 1994; Sylvester, 1988); and *transcurrent faults* for those which cut continental basement and sedimentary cover, but do not cut the entire lithosphere (Moody and Hill, 1956; Freund, 1974; Sylvester, 1988).

Oblique-slip faults are often referred to in this study as they are a common feature of oblique (non-plane strain) deformation zones. However these are generally linked to one of the above principal terminologies (e.g. *sinistral normal* oblique-slip fault). Rotational faults are generally difficult to identify in the field, and have therefore not been referred to in this study. Figure 1.12 shows an overall review of the terms used in this study and the fault types they refer to.

### **1.6.3. Kinematic indicators and interpretation**

#### **1.6.3.1. Brittle shear sense indicators**

The determination of the direction and sense of movement on faults is a basic requirement during brittle tectonic analysis. A range of minor structures can be employed as kinematic indicators to determine the sense of movement across faults and shear zones, particularly when the sense of slip cannot be determined by offset geological structures (a common problem in basement rocks). Brittle shear sense indicators fall into two categories: 1) slickenside striations; and 2) shear sense structures involving secondary fractures.

1.6.3.1.1. Slickenside striations

Several types of lineation may be observed on fault surfaces. Their morphologies and causes can be varied, but are usually dependent on lithology. Slickenside lineations/striations form parallel to the direction of displacement on a fault. Figure 1.13 illustrates several different types of slickenside lineation with sense of movement interpreted where possible.

Striations (fault striae) occur when fragments of rock or mineral grains scratch grooves into the fault surface (Fig. 1.13a). The end of the resultant striation (termed prod-, tool- and plough- mark by Tjia, 1971, Hancock, 1985, and Petit, 1987, respectively) points towards the movement of the missing wall. Mineral streaks may also develop as a result of smearing out mineral grains during fault movement; this semi-ductile deformation is more likely to occur at higher temperatures.

Slickenfibres are crystal lineations, generally of quartz or calcite, which grow as a result of dilation or opening during fault movement and are generally oriented sub-parallel to relative fault movements (Fig. 1.13b). Because the crystals grow at a low angle to the fault surface and tend to break off either along the fibres or at high angles to them, such fault surfaces tend to have a stepped texture (Fig. 1.13b) and when rubbed by the hand the surface feels smoothest in direction of motion of the missing block.

However in many cases striations may only yield information regarding the orientation, but not sense, of movement, and therefore other shear sense indicators must be sought.

1.6.3.1.2. Shear sense structures involving secondary fractures

Recognising fault and fracture patterns related to different fault movements allows for kinematic reconstructions both in remote sensing and in field observations. Early laboratory investigations on fracture development during shear (e.g. Cloos, 1955; Byerlee et al., 1978) reveal that a repeatable fabric could be produced under a wide range of confining pressures, strain rates and material types. R, R', P and T fractures (Fig. 1.14a) are the most abundant elements developing during shear (Logan et al., 1992). This fabric array seems to be self similar over a wide range of scales, from

microscopic to outcrop, and even regional scales, and in a wide range of materials. These fabrics provide a very useful instrument for determining shear sense in rocks at both outcrop and regional scales.

During brittle faulting, minor secondary fractures can develop at low- to moderate-angles to the fault. These secondary fractures may be either tensile or shear fractures. Generally tensile secondary structures are non-striated and may be mineralised, while secondary shear fractures are striated. The nomenclature adopted in this study is that of Petit (1987) and is based mainly on Riedel-type terminology. Three main types of fracture can be identified:

- 1) T-fractures: These are tensile fractures and thus unstriated. They develop at angles between  $30^{\circ}$  and  $90^{\circ}$  to the mean shear plane, and may be open or mineralised. They may also be straight or crescentic, with the horns of the crescents pointing in the direction of the missing block (Fig. 1.14; Petit, 1987).
- 2) R-fractures: Two types of extensional "R" (Riedel) fractures may be present. R-fractures form at low-angles ( $10^{\circ}$ - $20^{\circ}$ ) to the mean fault plane and synthetic to the main fault. R'-fractures form at high-angles ( $70^{\circ}$ - $90^{\circ}$ ) to the mean fault plane and are antithetic (Fig. 1.14a; Twiss and Moores, 1992). Petit (1987) describe a number of fault surface characteristics associated with R-fractures (Fig. 1.14b).
- 3) P-fractures: These form in response to contraction and are synthetic to the main fault, forming at low angles ( $10^{\circ}$ - $20^{\circ}$ ) to the mean fault plane (Fig. 1.14; Twiss and Moores, 1992; Petit, 1987).

## **1.7. Structural analysis of fault movements: Fault Kinematics and Palaeostress**

### **1.7.1. Stress vs. strain**

Stress and strain are fundamental concepts in structural geology, so clarity is needed in their discussion (Peacock & Marrett, 2000). Strain describes the deformation of a (rock) body in terms of its final shape relative to its initial shape. Stress describes the forces acting on every point of this body. Providing high enough stresses, rocks will eventually accommodate to these stresses by deforming. In general, *strain is a measurable parameter* for both ancient zones (e.g. orogens, basins, etc.), by means of structural geological analysis methods, and for active deformation zones, by means of geological

## *Chapter 1 - Introduction*

and geodetic techniques (e.g. GPS tracking). *Stress* on the other hand, *can only be deduced*, and special care has to be paid to consider the local situations and to estimate the deformational system in terms of coaxiality. This means that one has to assume a parallelism between the principal strain axis and the principal stress axis (Twiss and Moore, 1992). Knowledge about the palaeostress field that was active during the development of the investigated tectonic feature can give crucial information about the kinematic history of an area. However, when studying ancient tectonic settings it is strain that can be measured through the analysis of the deformed rock.

Over the years two different ways of viewing the deformation of geological structures have developed (see discussions of Pollard, 2000, and Peacock & Marrett, 1999, 2000). One view is that the stresses are an independent variable, acting on geological structures, whose deformation is the dependent material response to the applied stresses (e.g. Pollard et al., 1999). Another view treats the material displacements as the independent parameter, causing stresses to build up in structures, making them the dependent material response to strain (e.g. Tikoff and Wojtal, 1999).

If stress does control the resultant deformation it is important to understand how stresses are oriented at different points in space (Tikoff and Wojtal, 1999), this leads to the construction of stress maps (e.g. Zoback et al., 1989; Sperner et al., 2003). However, a problem with such regional stress maps is that stress distributions are likely to be modified by pre-existing structures, leading to localised variations that diverge significantly from regional patterns (Tikoff and Wojtal, 1999). Areas controlled by pre-existing structures are also likely to lead to non-coaxial deformation. Therefore a detailed understanding of pre-existing and basement structures is essential when assessing the apparent stresses of an area. It is also in these areas of non-coaxial deformation that the distinction between “control by stress and control by displacements” is likely to be resolved (Tikoff and Wojtal, 1999).

### *1.7.1.1. Coaxial vs. non-coaxial deformation*

In kinematic (strain) analysis, it is important to distinguish between coaxial and non-coaxial deformation (also see *section 1.5*). This distinction has significant implications

for whether one infers that stresses or displacements control deformation. If the infinitesimal strain (or stretching) axes ( $x_i$ ) are parallel to the finite strain axes ( $X_i$ ), then deformation is coaxial (Means, 1976; Tikoff and Wojtal, 1999). In coaxial deformation the principal movement directions are parallel to both the infinitesimal and finite strain axes.

Non-coaxiality refers to a lack of parallelism between the principal infinitesimal strain axes ( $x_i$ ) and finite strain axes ( $X_i$ ) (Means et al., 1980; Tikoff and Wojtal, 1999). For non-coaxial deformations, the principal movement directions are neither parallel to the infinitesimal or finite strain axes, furthermore, due to the effects of simple shear there is also a component of rotation. Non-coaxial deformations are often associated with material anisotropy and basement reactivation (e.g. De Paola et al., 2005b).

### ***1.7.2. Kinematic inversion to determine palaeostress***

Kinematic (strain) inversion analysis, more commonly termed paleostress analysis, is used to determine the local and/or regional stress field at the time of deformation. As the analysis of fault-slip data yields information concerning the orientation of the strain tensor, the calculated axes are referred to using infinitesimal/ finite strain nomenclature rather than principal stresses. These axes are then compared to other local and regional structures in order to assess their likely correspondence to regional stresses at the time of deformation.

Palaeostress inversion techniques have been used by various workers for nearly 40 years (see Angelier, 1994, and Ramsay and Lisle, 2000, for an exhaustive review). Stress inversion procedures rely on Bott's (1959) assumption that slip on a plane occurs in the direction of the maximum resolved shear stress. Inversely, the stress state that produced the brittle microstructures can be partially reconstructed knowing the direction and sense of slip on variably oriented fault planes. The slip direction on the fault plane is inferred from slickenlines and fault striae. The data used for the inversion are the strike and dip of the fault plane, the orientation of the slip line and the shear sense on the fault plane. The inversion of fault-slip data gives the four parameters of the reduced stress tensor: the principal stress axes  $\sigma_1$  (maximum compression),  $\sigma_2$  (intermediate



compression),  $\sigma_3$  (minimum compression) and the Stress Ratio,  $R = (\sigma_2 - \sigma_3)/(\sigma_1 - \sigma_3)$  (eq. 1.7). The comparison between strain axes, reconstructed from structures measured in the field, and stress axes, derived from stress inversion, is approximately valid only if we assume: 1) low strain intensity (i.e. the finite strain observed  $\approx$  infinitesimal strain); and 2) that significant rotations during progressive deformation are absent. Under these conditions, stress axes can be considered to approximately correspond to the strain axes as follows:  $\sigma_1 \equiv \lambda_3$ ;  $\sigma_2 \equiv \lambda_2$ ;  $\sigma_3 \equiv \lambda_1$ . Note, however, that this approach is only reasonable in regions where bulk finite strain – or more correctly, finite *non-coaxial* strains – are reasonably low, so that the misorientation between finite and infinitesimal strain axes is limited.

#### 1.7.2.1. Inversion procedures

Geologists and geophysicists have developed a number of methods to compute the stresses from an observed fault slip pattern. Each method makes certain assumptions and uses a particular guiding principle. The main principles are:

1. Minimizing the difference between the observed slip direction and the direction of maximum resolved shear stress in the fault plane produced by the regional stresses. The assumption is that the fault should slip in the direction of the maximum resolved shear stress, all other things being equal. Applying this principle leads to a set of non-linear equations which have been solved in a number of methods. Different methods of solving these equations have been developed by Angelier (1984), Etchecopar et al. (1981), Delvaux (2003) and others.
2. Minimizing the variation in the resolved shear stress on the fault plane in the slip direction. The method assumes that the shear stress for slip on the faults in the area should be approximately the same for all faults that slip under similar conditions of depth and regional stress state. Variations in rock type and fault geometry will cause deviations from this ideal. This principle has the advantage of leading to a set of linear equations. Michael (1984) developed this method.

3. Minimizing the difference between the principal stresses to cause slip on a fault and the regional principal stresses. To calculate the stress to cause slip requires that a slip failure criterion be known. The simplest assumption is a linear Mohr-Coulomb-type slip relation with zero cohesion, characteristic of friction on faults at shallow depths. This method was developed by Reches (1987) and leads to a set of linear equations. The assumption of zero cohesion is not critical, since only the stress ratios, not the absolute stresses themselves, can be determined.

*1.7.2.2. Analysis methods*

My Fault™ stereonet software, produced by Pangaea Scientific Ltd., was used for kinematic inversion analysis. This program offers a number of different methods of stress inversion based on various published works (e.g. Arthaud, 1969; Angelier, 1984; Michael, 1984; Reches, 1987; Sperner et al., 1993), thus allowing comparison of different analysis methods. Fault data was exported from the GIS database as ASCII files and imported into MyFault™ for data analysis.

The main procedure applied throughout this research was to invert a population of faults (be they bulk data, pre-sorted data, or locality data). Those faults with misfit angles greater than 40° were then rejected and the inversion procedure rerun (see methods of Titus et al., 2002). This process was repeated until a group of faults with a homogeneous solution was found. A minimum of 5 faults were considered the minimum number required for a valid interpretation (Titus et al., 2002), however a cut off of 10% of the original population was also applied. The rejected data were then rerun through the program in an attempt to derive multiple 'palaeostress' vectors. A similar iterative approach has been applied in the past by Titus et al. (2002). This procedure was generally repeated for various inversion methods (i.e. Angelier, 1984; Michael, 1984; Reches, 1987) to test the consistency of the results.

This procedure was applied both to the bulk data set for each study area, individual fault systems (sorted by geometry) for each area, and to fault populations from individual localities. This was done to test the consistency of the results and also in an attempt to identify local variations in stress/ strain in relationship to basement

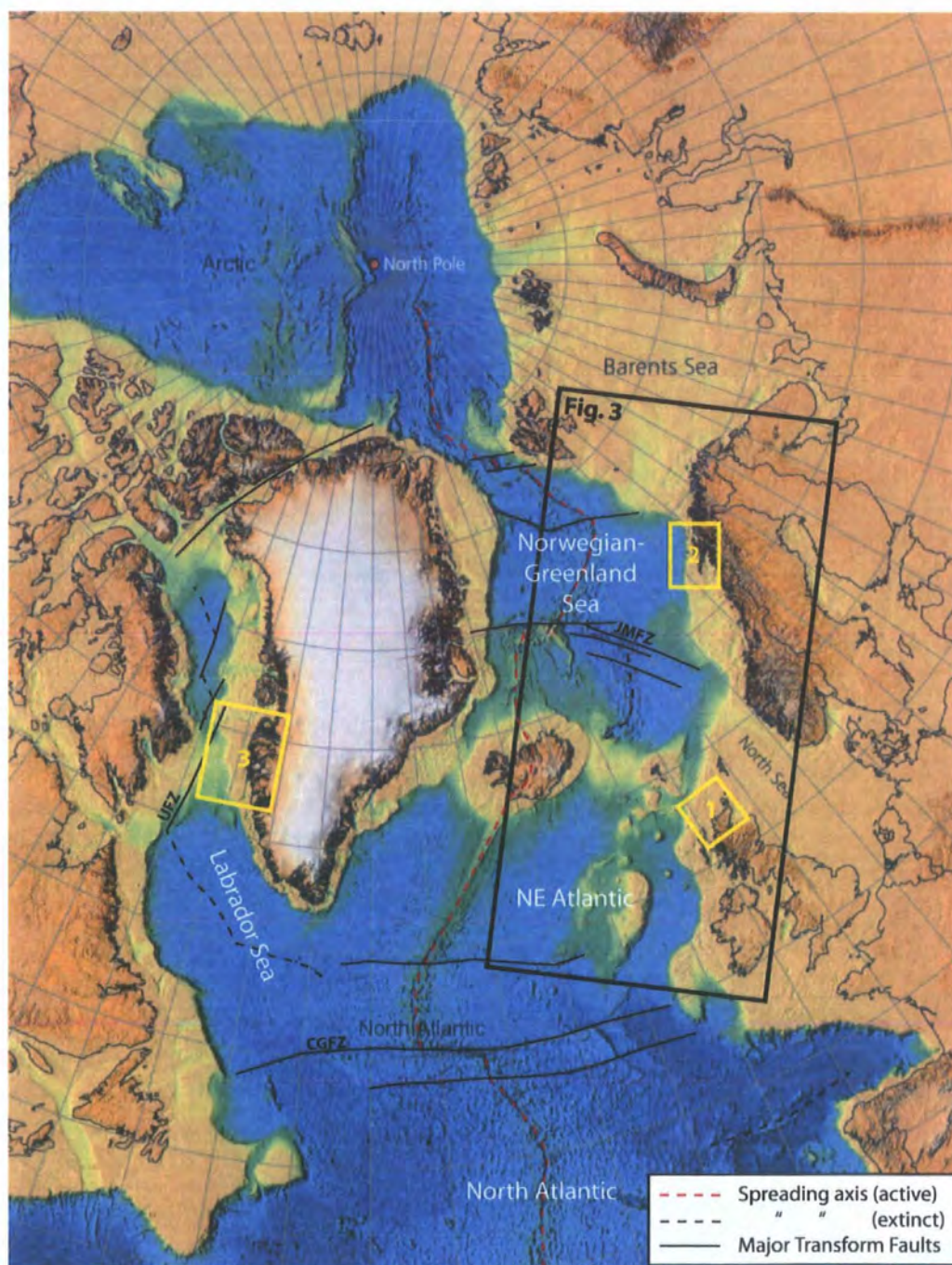
structures. In some cases manual sorting procedures are also applied (i.e. sorting into various fault systems, or the removal of faults that appear to violate the assumptions of stress inversion)

### **1.7.3. Palaeostress applications and their limitations**

Some authors have questioned the validity of palaeostress inversion through the analysis of brittle micro-structures (faults and fractures) as they argue that kinematic indicators are strain markers and thus do not relate to stress (e.g. Twiss and Unruh, 1998; Tikoff and Wojtal, 1999). Others have outlined a number of inherent limitations on stress inversion procedures (Dupin et al., 1993; Pollard et al, 1993; Cashman and Ellis, 1994; Nieto-Samaniego and Alaniz-Alvarez, 1997; Maerten 2000) which question the validity of the results. The following list outlines some the main factors that effect validity of inversion methods:

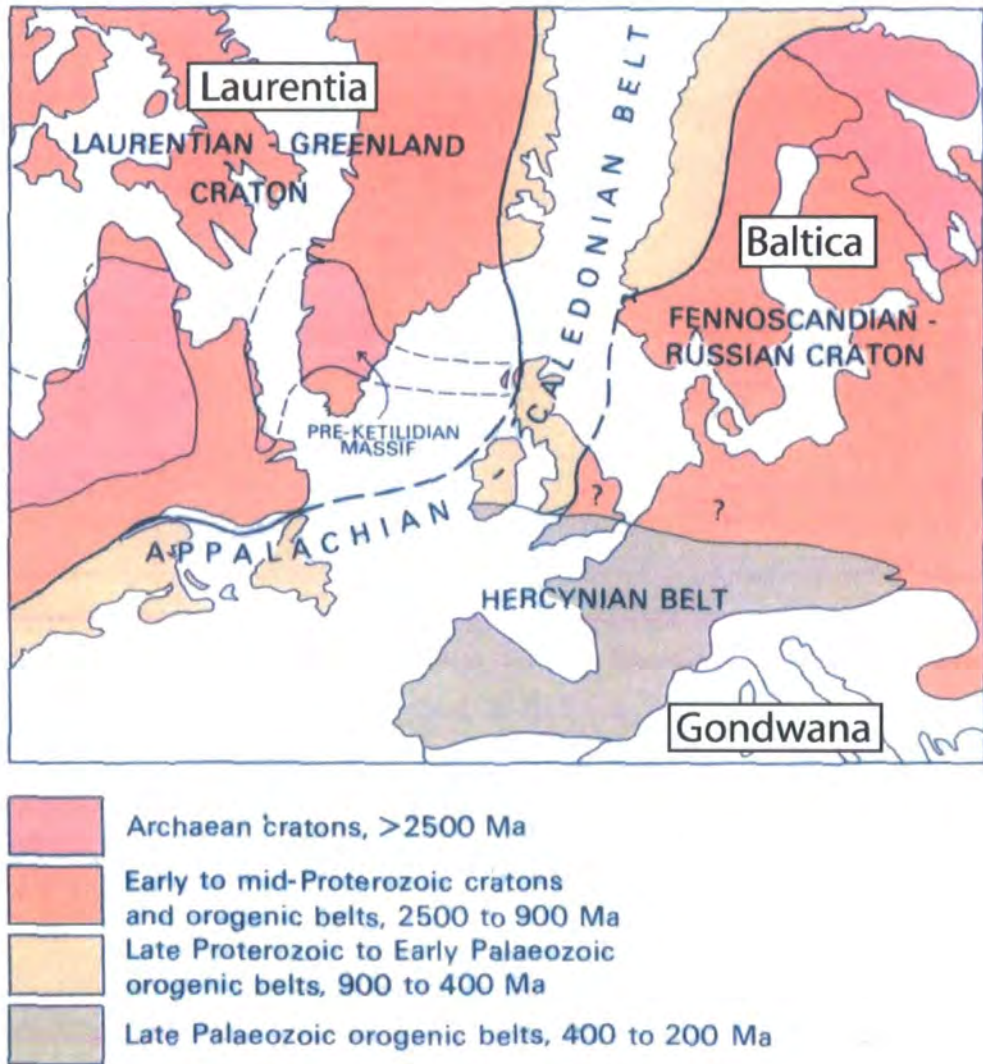
- a) Non-coaxial deformation
- b) 3-D strain
- c) Fault interaction – leading to slip non-parallel to regional shear stress
- d) Rock anisotropy – leading to local stress variations
- e) Mixing polyphase deformation events

As the areas studied in this research are all located in basement terranes (i.e. with many pre-existing structures) in zones of oblique divergence (leading to complex faulting, transtension, 3-D strain, etc), each of these factors may affect the validity of kinematic inversion in this study. Therefore, each of these limiting factors has been considered at every stage of the data collection and analysis process (i.e. detailed analysis of structures during fieldwork, data sorting, analysis procedures, etc). Furthermore, the results of the stress inversions are *never* used in isolation, as they are always verified using deductions concerning strain that are based on structural observations made in the field. A side issue of this research is therefore to test the usability and reliability of palaeostress analysis in areas of deformation that may violate a number of the main assumptions of inversion, and also asses the use of GIS in overcoming some of these problems (see chapter 6).



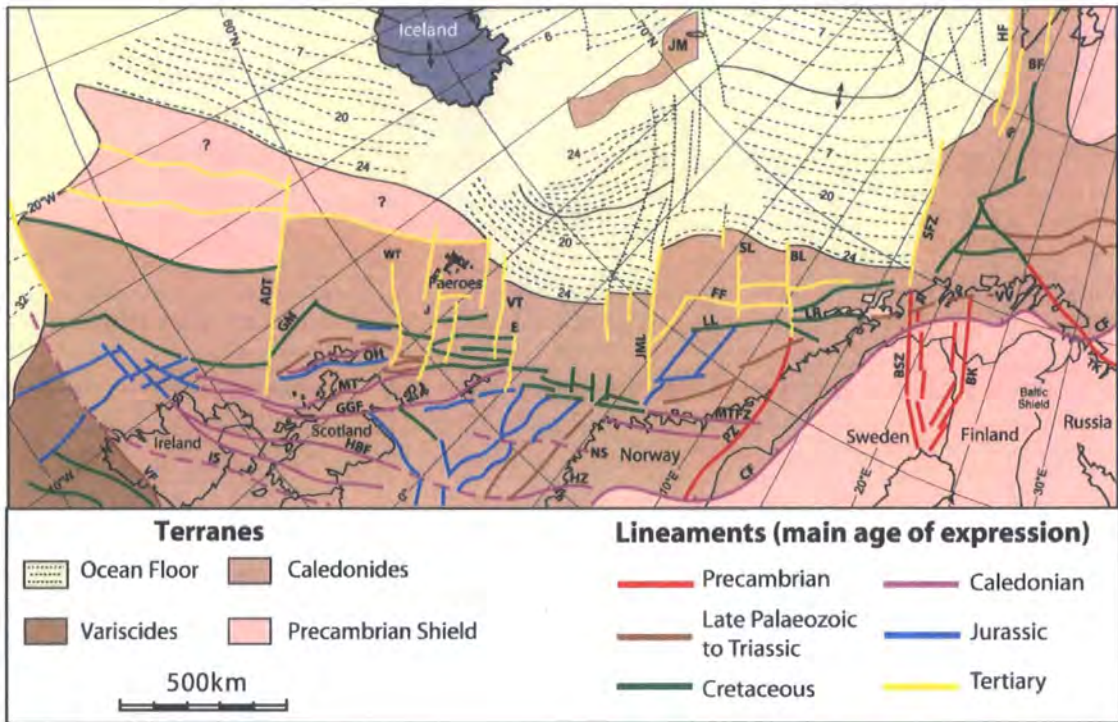
**Figure 1.1.**

The North Atlantic Passive Margin (after Lundin and Doré, 2005). Also highlighted location of case studies (yellow): 1 = case study 1 (Northern Scotland and West Orkney Basin); 2 = case study 2 (Lofoten-Vesterålen Archipelago, Norway); 3 = case study 3 (Davis Strait, West Greenland).



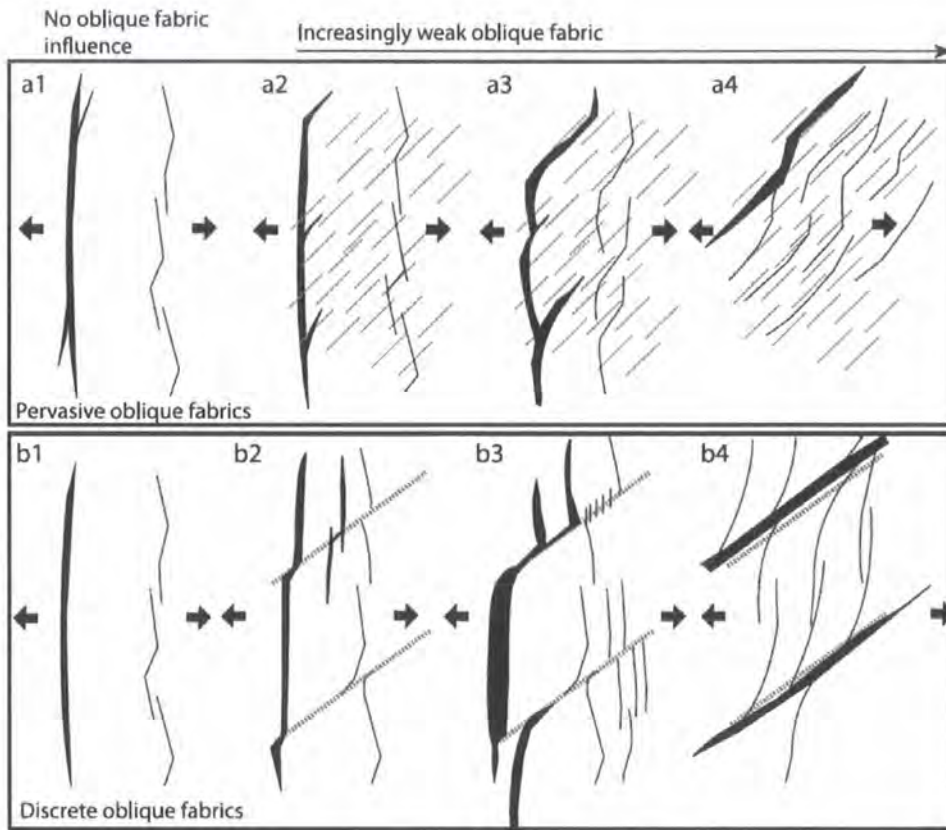
**Figure 1.2.**

Permian pre-drift reconstruction of the North Atlantic region, outlining main orogenic belts and basement cratons (after Anderton et al., 1979, and Stoker et al., 1993).



**Figure 1.3.**

Basement terranes and lineaments of the NW European Atlantic Margin. Lineaments are coloured according to their main observed age of expression (Dore et al., 1999). Abbreviations: ADT, Anton Dohrn Lineament; BF, Billefjorden Fault Zone; BK, Bothnian-Kvaenangen Fault Complex; BL, Bivrost Lineament; BSZ, Bothnian-Senja Shear Zone; E, Erlend Transfer; FF, Fles Fault Zone; GGF, Great Glen Fault; GM, Geikie Margin; HBF, Highland Boundary Fault; HF, Hornsund Fault Zone; IS, Iapetus Suture; J, Judd Lineament; JM, Jan Mayen; JML, Jan Mayen Lineament; LL, Lofoten Lineament; LR, Lofoten Ridge; MTL, Møre-Trøndelag Lineament; MTFZ, Møre-Trøndelag Fault Zone; MT, Moine Thrust; OH, Outer Hebrides Fault; SFZ, Senja Fracture Zone; SL, Surt Lineament; VT, Victory Lineament; WT, Wyville-Thomson Lineament..



**Figure 1.4.**

Schematic diagrams (plan view) showing how extensional fault patterns may change depending on the type of pre-existing strength anisotropy (pervasive or discrete) and relative weakness of the strength anisotropy (from Morley et al., 2004).

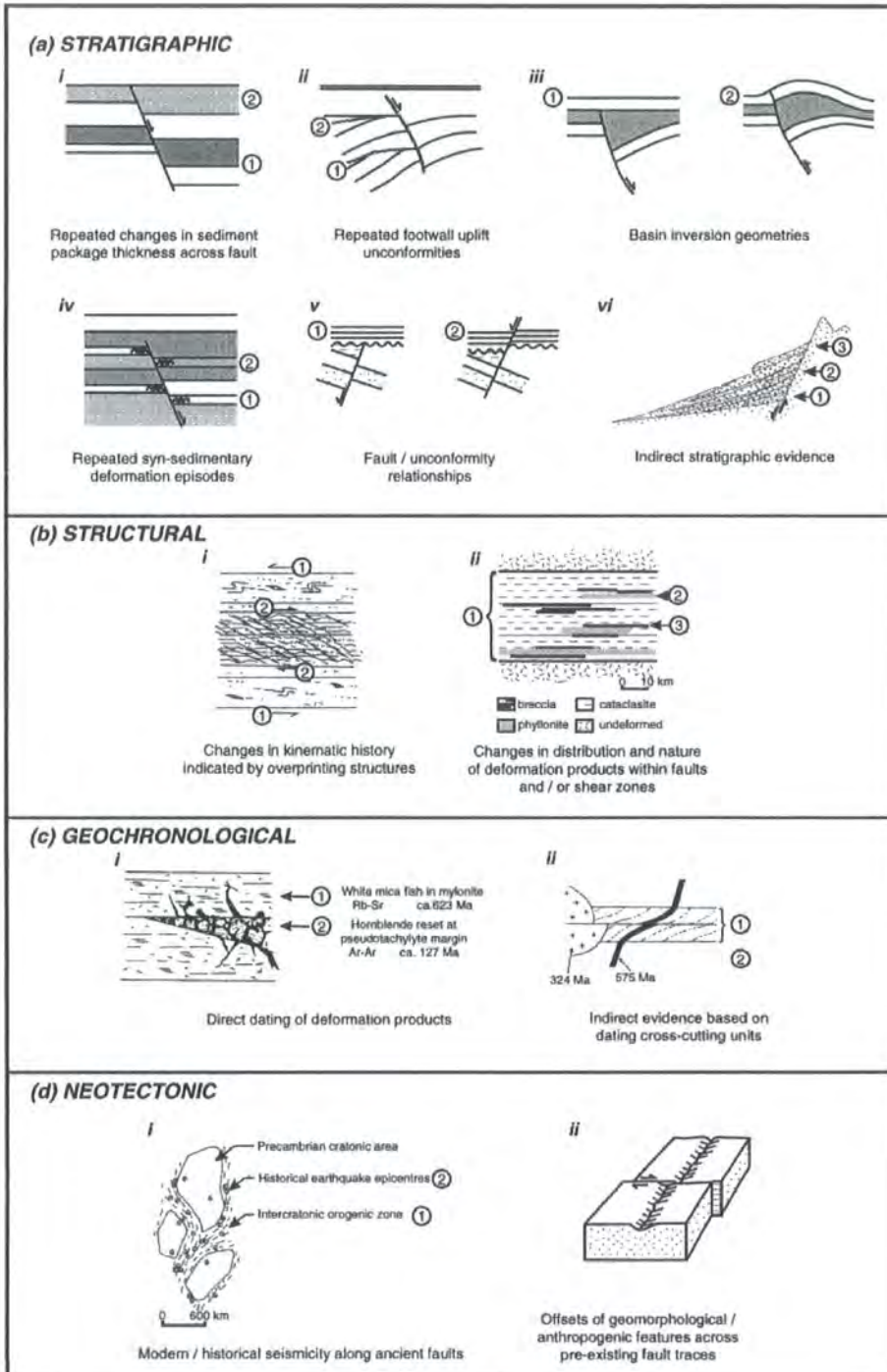
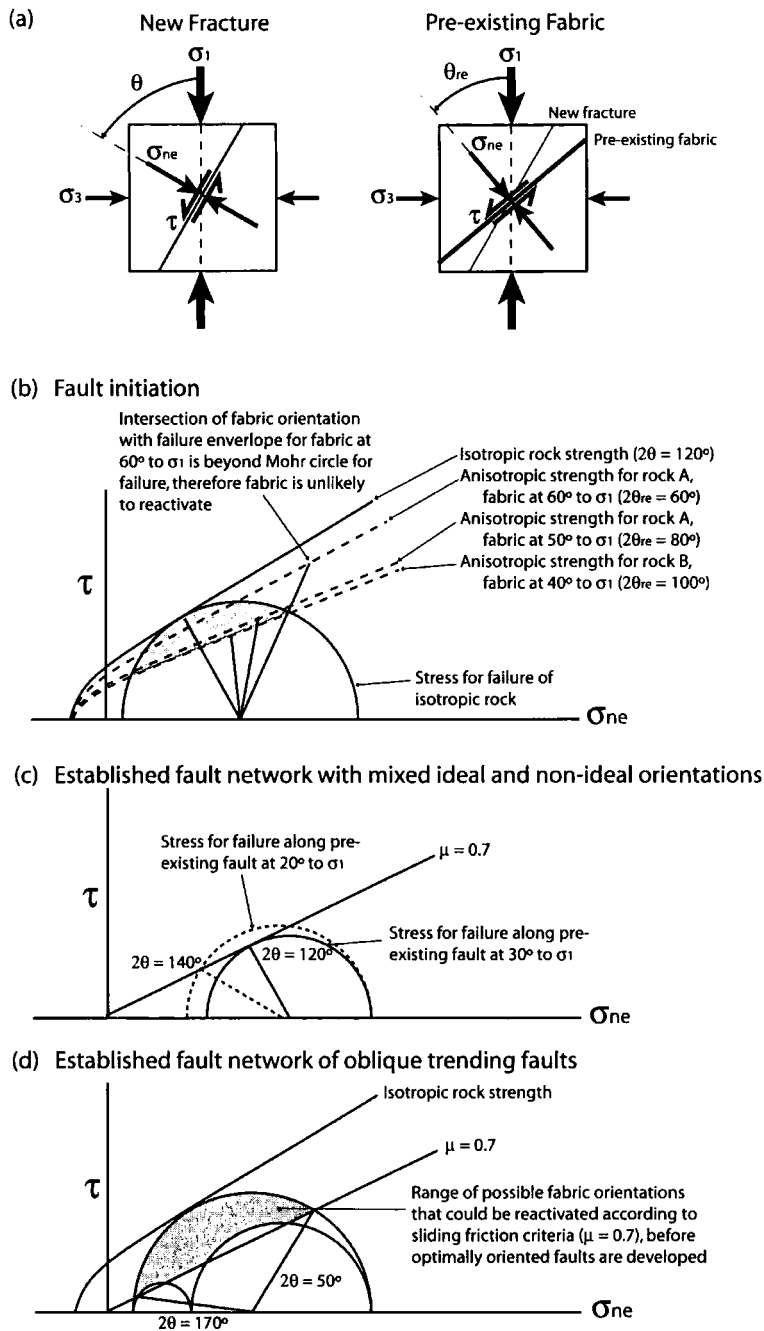


Figure 1.5.

Criteria for identifying reactivation (from Holdsworth et al., 1997).

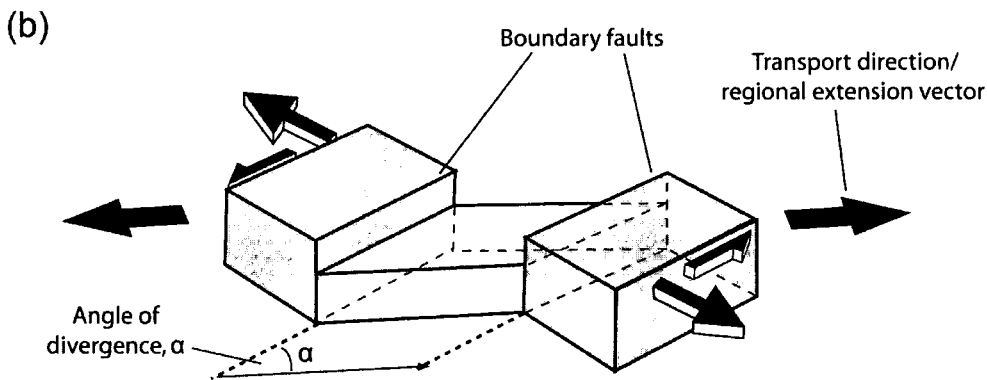
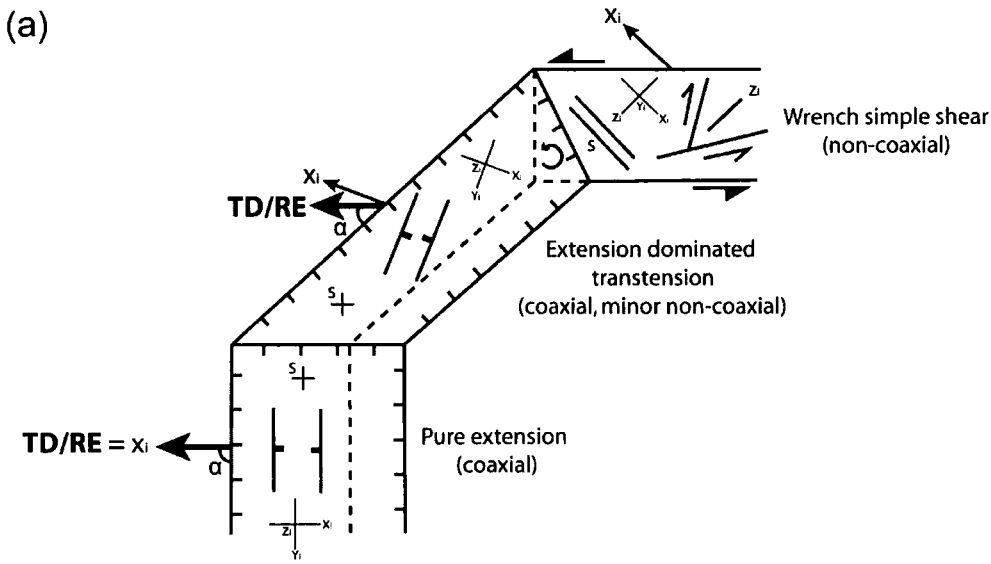


Chapter 1 - Introduction



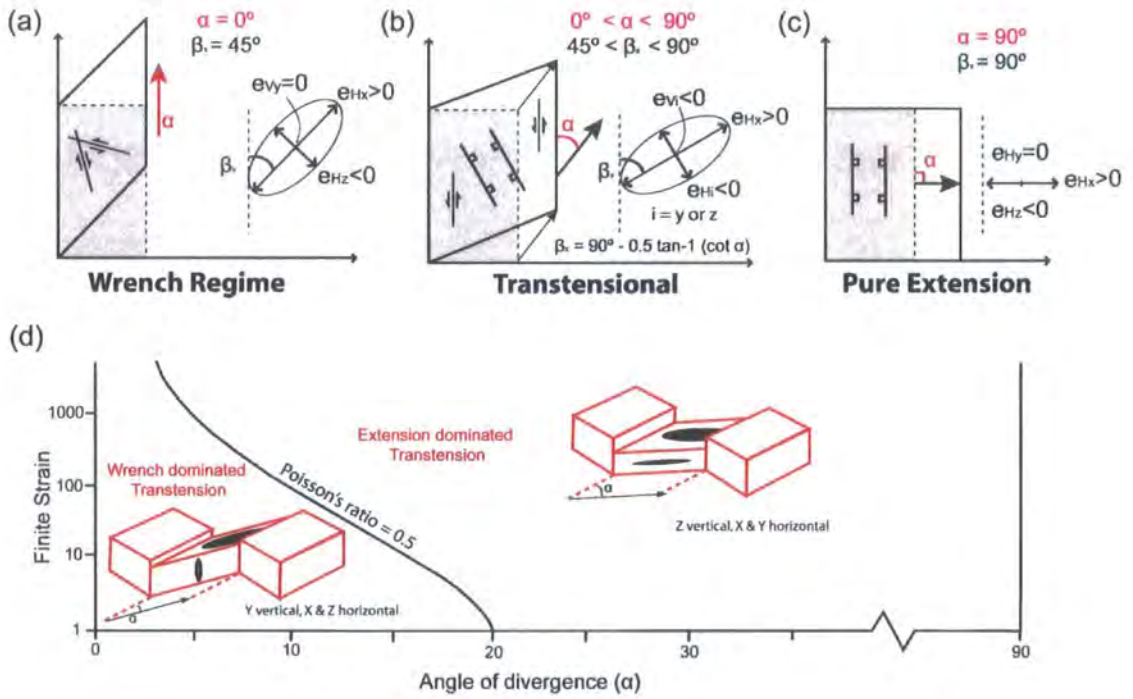
**Figure 1.6.**

(a) Geometric relationships in physical space between the principal stresses, orientation of the fracture plane, and the surface stress components for new fractures and pre-existing planes of weakness. (b) – (d) idealised Mohr circles illustrating interplay between initiation of new optimally oriented fractures, activation of oblique fabrics due to strength anisotropy and the activation of cohesionless faults of optimal and non-optimal orientations (from Morley et al., 2004).



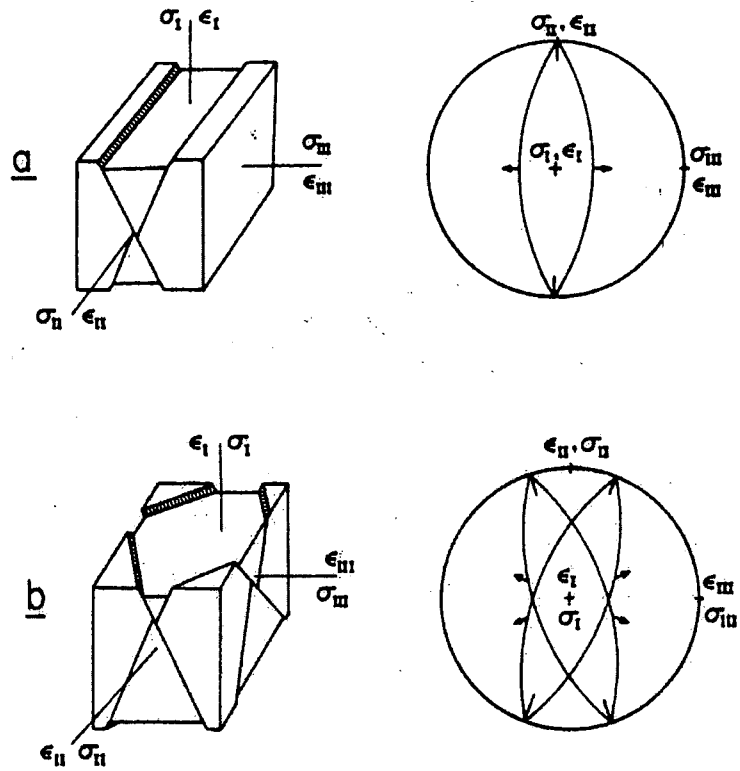
**Figure 1.7.**

(a) Schematic plan view diagram showing an example of transension (in this example extension-dominated transtension) in an increasingly oblique margin [after Dewey, 2002]. TD/RE = transport direction/ regional extension direction. (b) Simplified 3D cartoon model showing basic principles of Transension, i.e. “wrench” simple shear plus a component of “extensional” pure shear (after Sanderson and Marchini, 1984; Fossen and Tikoff, 1993; Dewey et al., 1998).



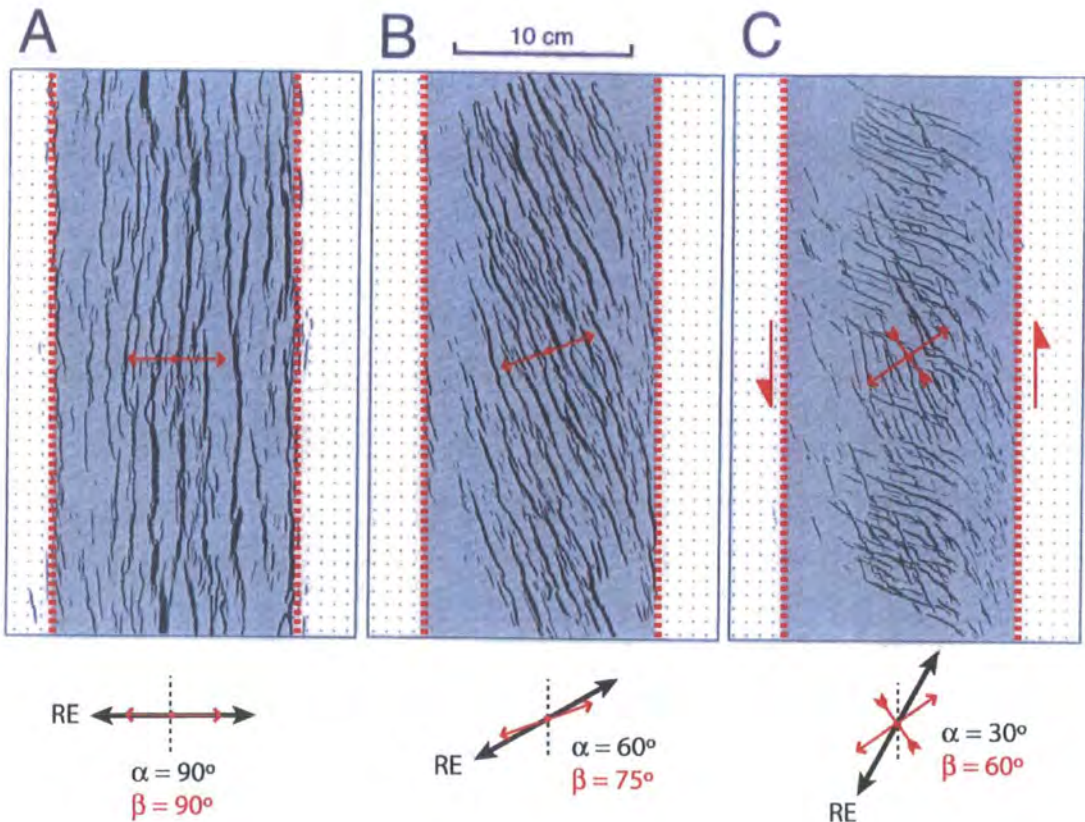
**Figure 1.8.**

Schematic 2D block diagrams outlining the basic relationship between  $\alpha$ ,  $\beta_x$  and infinitesimal strain axis ( $x$ ,  $y$ ,  $z$ ) for (a) pure strike-slip systems (simple shear), (b) pure extensional systems (pure shear), and (c) transension (after De Paola *et al.*, 2005). (d) Cartoon graph showing angle of divergence,  $\alpha$ , vs. horizontal finite strain. Solid curved line highlights the angle  $\alpha_{crit}$  which marks the transition from wrench dominated to extension dominated transension (modified from Teyssier and Tikoff, 1999).



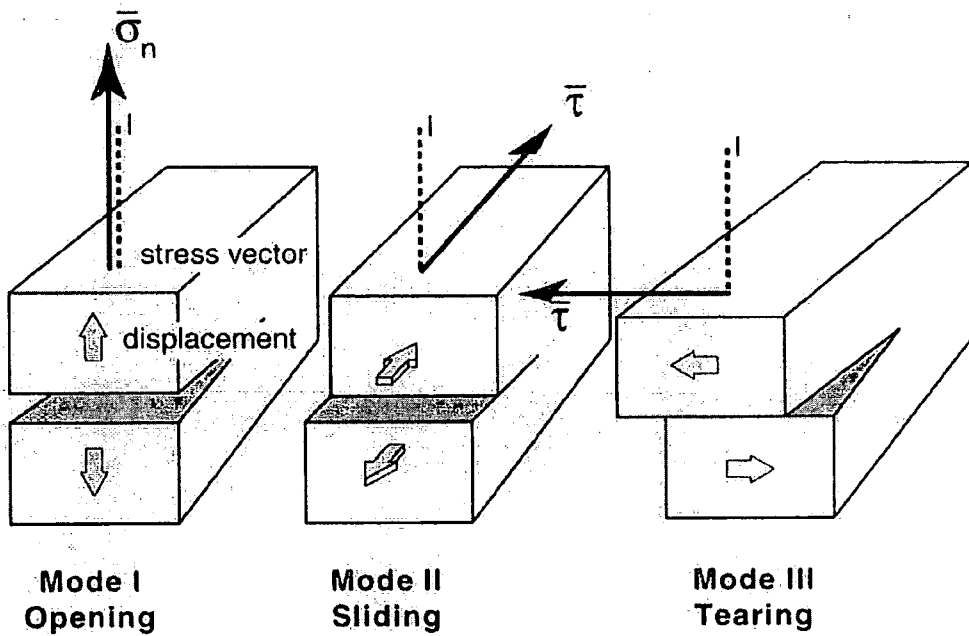
**Figure 1.9.**

(a) Andersonian fault system and relative symmetry of the associated stress and strain tensor (after Reches, 1983).  $\epsilon_1$ ,  $\epsilon_2$  and  $\epsilon_3$  are the infinitesimal strain axes. (b) Orthorhombic fault systems composed by four fault sets and four sets of slickenlines. Four sets of faults are necessary to accommodate three-dimensional strain (after Reches, 1983).



**Figure 1.10.**

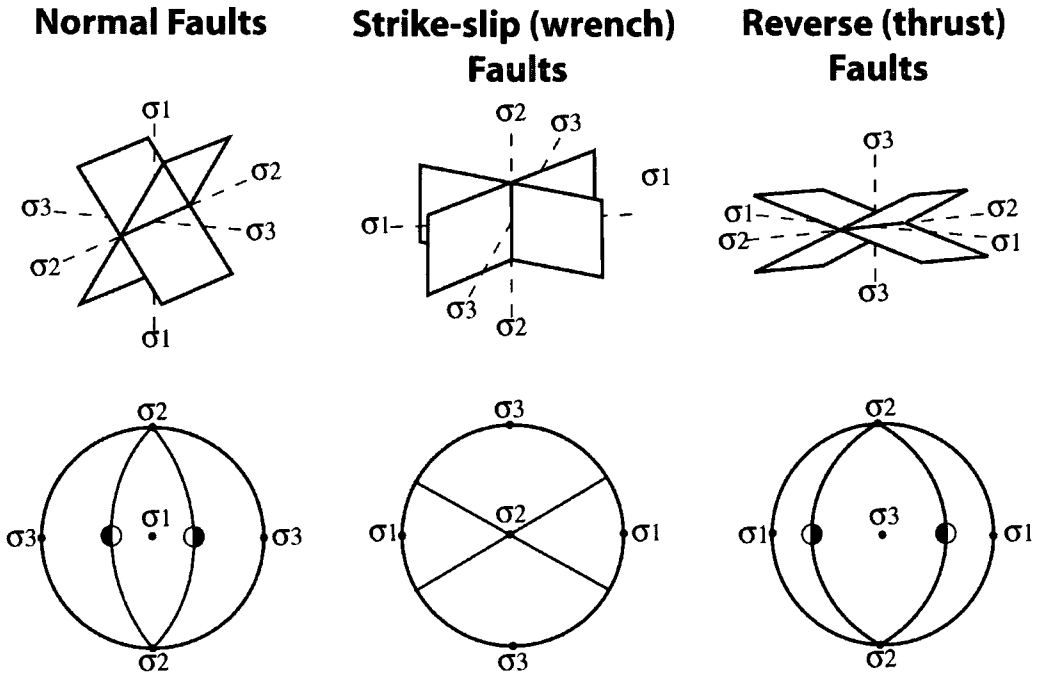
Fault patterns for different angles of obliquity, showing variations in angles of  $\alpha$  and  $\beta$  with increasing obliquity ( $\alpha$  = angle between regional displacement and the deformation zone boundary;  $\beta$  = angle between infinitesimal horizontal maximum extension strain axis and the deformation zone boundary). Deformation zone boundary outlined by dashed red lines. Images are based on results of analogue modelling by Withjack and Jamison (1986) and Clifton et al. (2000).



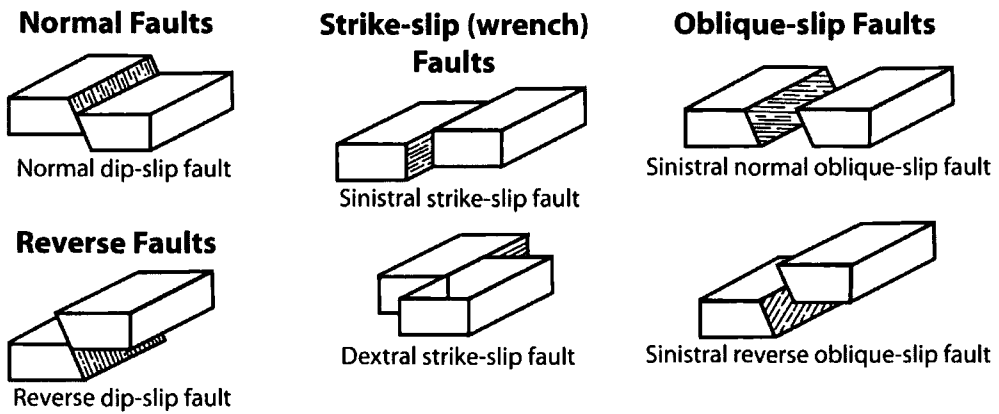
**Figure 1.11.**

Distinction of fracture types based on the relative displacement of the material either side of the fracture. Mode I fractures are tensile opening with no shear. Modes II and III fractures are shear fractures (in-plane and anti-plane shear respectively).

**(a) Andersonian Fault Classification**

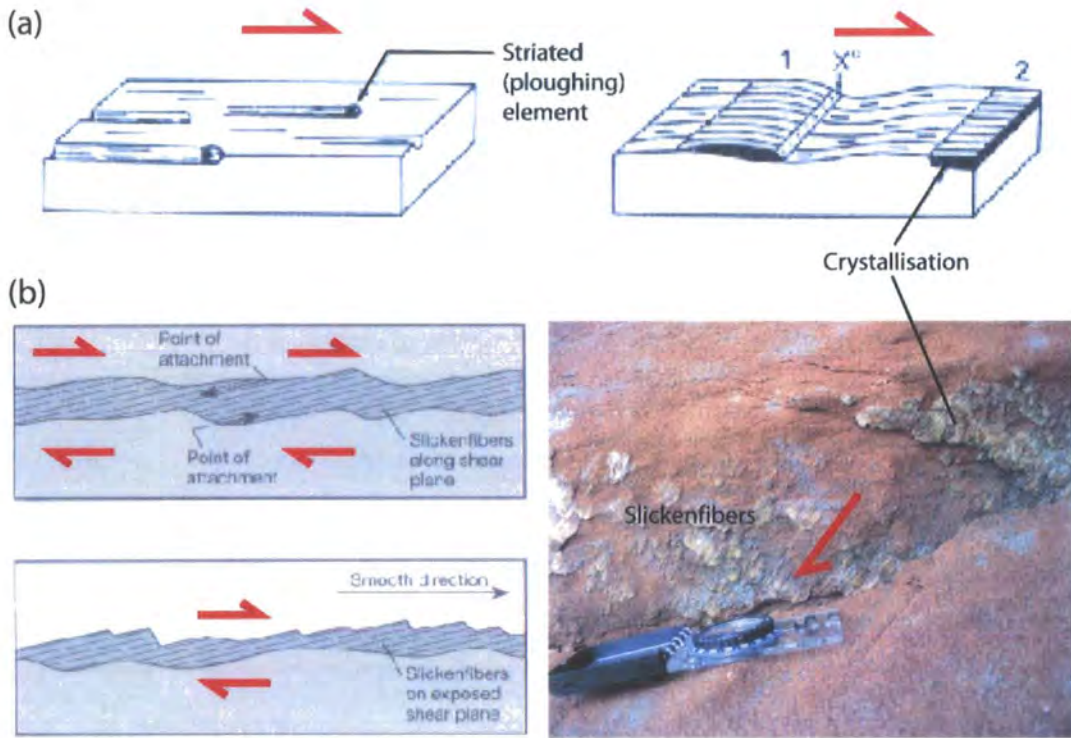


**(b) Geometric/ kinematic Fault Classification**



**Figure 1.12.**

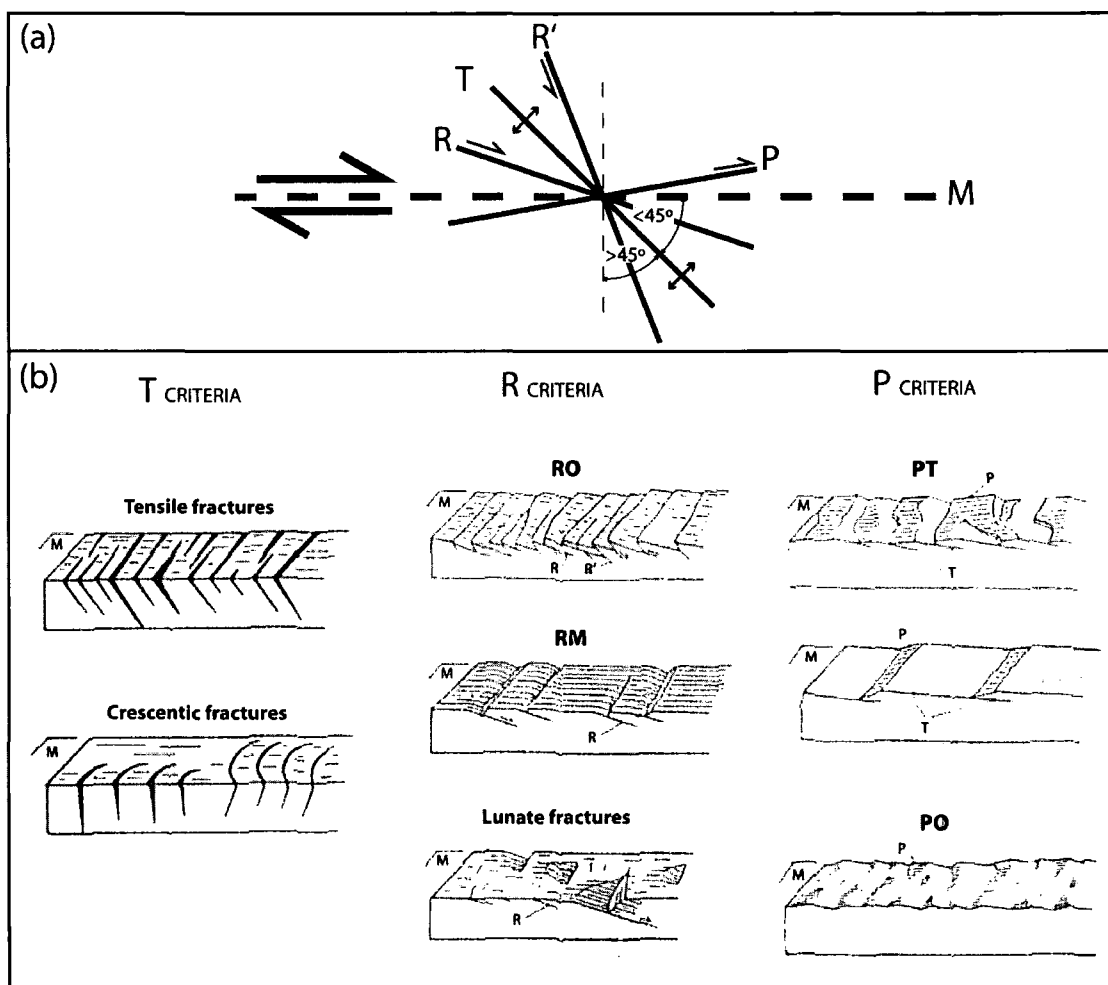
(a) Dynamic/ Andersonian fault classification; (b) Geometric and kinematic fault classification (from McClay, 1987).



**Figure 1.13.**

(a) Slickenside striations: striations (grooves) produced due to fragments of rock or mineral grains on the fault surface, and crystallisation on the lee side of irregularities on the fault surface forming overlapping sheets of fibrous mineralization (slickenfibres) (from Petit, 1987). (b) Development of stepped slickenfibres on a fault plane (from Twiss and Moore, 1992). Plus field photo showing an example of stepped slickenfibres (dextral oblique-slip fault).





**Figure 1.14.**

Shear sense criteria from secondary structures. (a) Orientation of secondary structures relative to main fault plane (M). R and R' correspond to synthetic and antithetic Riedel shears, T to tensile fractures and P to synthetic shears associated with dextral shear. (b) Block diagrams showing relationship between secondary structures and sense of shear on a brittle fault (after Petit, 1987). All movements are dextral.

## 2. Digital Geological Mapping – an overview of digital mapping methods in geosciences.

### 2.1. Introduction

Some 200 years ago the pioneering work of William Smith created a “Map that changed the world” (Fig. 2.1; Smith 1815; Winchester, 2001) when he compiled the first geological map of England. The methods used in constructing this map (i.e. pens, pencils and paper maps) have changed little in the two centuries that have followed. However, over the past decade a number of major advancements have been made in the way geological maps may be constructed, i.e. the development of digital mapping methods. In the geosciences, as in all scientific disciplines, digital methods are increasingly used for data management, analysis and visualisation; however these activities generally take place back in the laboratory and are not used routinely in the field. For example, there are ongoing British Geological Survey programs to ‘digitise’ existing maps at a range of scales combined also with a move towards 3-D digital data, i.e. the DigMap and 3DVF programmes respectively (Giles and Bain, 1995; Becken and Green, 2000; Hutson, 2005). Furthermore, most geoscientists already ‘digitise’ their field data when data are typed into spreadsheets or databases and maps are drawn on cartographic or graphic packages in the office or laboratory. We view these ‘digitising processes’ as a *secondary* form of digital mapping, which offers only a limited number of benefits to geological research compared to *primary* digital field data acquisition, which is the main focus of this chapter.

Technological advances have increasingly made digital field data acquisition a practical alternative to paper-based fieldwork methods in recent years (Struik *et al.* 1991, Schetselaar 1995, Brodaric 1997, Pundt & Brinkkotter-Runde 2000, Edmondo, 2002; Golledge, 2004; Wilson *et al.*, 2005). Pioneers have claimed that digital methods can improve the quality and efficiency of field data collection (Pundt & Brinkkötter-Runde 2000; Kramer, 2000; Brimhall and Vanegas, 2001; McCaffrey *et al.* 2003, 2005; Jones *et al.* 2004; Clegg *et al.* 2005) because they; 1) are potentially more accurate than traditional methods, 2) streamline the workflow from data acquisition-to-final product, 3) allow better visualisation of data in 2-D and 3-D, 4) enable data to be stored directly

## Chapter 2 – Digital mapping

into a well organised digital database, and 5) yield further insights because of the enhanced ability to perform geospatial analysis in addition to more traditional geometrical or temporal analysis of geological architectures.

Digital mapping and digital field-data acquisition methods are evolving rapidly through a challenging transition and development phase from traditional paper based methods to digital equivalents. Digital field mapping techniques were first discussed by Struik et al. (1991), and have since become well used by many geologists in North America, a fact outlined by a number of papers on digital fieldwork methods presented at most years USGS annual Digital Mapping Techniques conference, which has been running since 1997 (Soller, 1997). However, digital mapping methods are still not fully established in standard geological research practice, particularly in the European sector (Jackson and Asch, 2002). This slow transition from paper based to digital mapping methods are likely to be due to the following issues:

- (1) A fear that traditional geological mapping skills will be lost,
- (2) Belief that digital media cannot replace the versatility of pencils, paper and notebook
- (3) Cost of mapping equipment
- (4) New methods require geologists to spend time learning new skills
- (5) Unclear which workflows are most efficient

In this chapter each of these issues is addressed and a review of the overall digital workflow applied during research is presented.

### **2.2. An overview of computer based mapping and GIS in Geosciences**

#### **2.2.1. Introduction**

It was in the 1960s that the computer first became an option for geologic work (Berry, 2000), an early example being Sampson *et al.* (1966). It was also at this time that the earliest Geographic Information Systems were beginning to develop, firstly with the Canadian Geographic Information System at the Canadian Land Inventory in 1963, and later with the establishment of ESRI, at the Harvard Lab (Longley et al., 2001). By the early 1970s, there were about 450 references of computer use in geosciences (Hruska

## *Chapter 2 – Digital mapping*

and Burke, 1971). It was at this time that computer mapping really began, with the automated map drafting process (Rhind, 1971; Hutchison, 1973; Steinitz, 1976). It was soon realised that computer mapping was a far more efficient way to make maps as it allowed small changes to be made to maps without having to redraft the entire map-sheet. Some of the earliest geological surveys to apply computer methods for both mapping and data archiving were the Canadian (Hruska and Burk, 1971; Hutchison, 1973, 1974), British (BGS; Bickermore and Kelk, 1972; Rhind, 1973), Denmark/Greenland (GEUS; Platou, 1971; Dawes, 1987) and some sectors of the USGS (e.g. Kansas Geological Survey; Sorenson and Buchanan, 1990).

The next big step in the computer based geological mapping came in the early 1990s with the integration of GIS into the mapping process. In 1981, ESRI released the first commercial GIS (Geographic information system) software system; however, it was not until the early 1990s that this technology established a significant presence in geoscience research (Bonham-Carter, 1992, 2000). At this time GIS were generally designed to process and handle 2-D data, however, as geological data is inherently 3-D (or 4-D) in character, geologists realised that 3-D GIS or 'GSIS' (Geo-scientific information system; Jones et al., 2004) were required. This led to a distinct class of GIS software being developed to handle 3-D geological data (Turner, 1992, 2000; Houlding, 1994), however, such software is generally not suitable for handling detailed attribute data, and thus has not replaced standard GIS packages. It was at a similar time that the concept of digital field mapping was first considered a possibility (e.g. Struik et al., 1991; Brodarik, 1993). First developed as a means of streamlining the process of data collection to map production (Struik et al., 1991), digital field mapping is now used to collect geospatially located, highly accurate 3-D digital outcrop data using high precision DGPS and laser scanning devices (McCaffrey et al., 2005; Trinks et al., 2005).

### **2.2.2. *What is a GIS?***

Geographic information systems (GIS) are used to input, store, retrieve, manipulate, analyse and visualise geographically referenced or geospatial data (Longley et al., 2001). In a GIS, information is generally displayed as a series of layers that can be

superimposed, with each layer comprising separate data types (Fig. 2.2). These layers may be in raster (e.g. Tiff, JPEG, MrSID) or vector (point, line, polygon) data format.

GIS has evolved from its original guise as a computer mapping system and is now defined as ‘an information management system for organising, visualising and analysing spatially-oriented data’ (Coburn & Yarus 2000). At the roots of a GIS are three main types of computer software (Bonham-Carter, 2000): computer-aided design (CAD); image processing (IP) systems; and database management systems (DBMS). GIS combines the functionality of these three types of software. CAD systems (e.g. AutoCAD™) handle vector data, consisting of point, line and polygon graphical objects. IP systems (e.g. Photoshop™, Illustrator™, etc.) were designed for enhancing, visualising and analysing raster data. The third key component to a GIS is the DBMS, which are not specifically designed for spatial analysis, but for organising and searching attribute data. GIS now combines digital database, spatial analysis and multi-dimensional mapping capabilities which means that is a powerful tool for the geoscientist. GIS are used in a large number of applications that deal with spatial data, including social and economic planning, marketing, facilities management, environmental and resource assessment (Rhind, 1992; Longley *et al.*, 2001).

A form of GIS has evolved in recent years in order to meet the requirements of field-based GIS users also. Field-GIS systems are designed to be used on handheld computers for field mapping and outcrop data query (Edmondo, 2002). Both ‘in-house’ and commercial field-GIS systems have been developed; examples of these systems include FieldLog, GeoMapper, ArcPad™ and MapIT (Brodaric, 1997, 2004; Brimhall and Vanegas, 2001; Edmondo, 2002; Clegg *et al.*, 2006).

### **2.2.3. GIS activities in geosciences**

The use of GIS has proven useful in several geological disciplines including: hydrocarbon exploration, (Coburn and Yarus, 2000); mining and mineral exploration (Knox-Robinson and Gardoll, 1998); environmental assessments (Teso *et al.*, 1996); remote lineament analysis (Karpuz *et al.*, 1993; Gabrielsen *et al.*, 2002); and shear zone tectonics (Piazolo *et al.*, 2004). A brief discussion of the main GIS activities highlight many of the advantages of using GIS, as opposed to alternative software tools, to handle

## *Chapter 2 – Digital mapping*

and analyse geospatial data. Bonham-Carter (2000) defines six core GIS activities (summarised in Table 2.1), these are: (1) data organisation; (2) data visualisation (2D maps and 3D modelling); (3) data search and query; (4) data integration (combining multiple datasets); (5) data analysis (spatial and geostatistical analysis); (6) prediction and forward modelling. The sequence these activities are listed is also significant as these roughly follow the order in which they are undertaken within a project. Data base building, visualisation and data search are core activities central to all GIS projects, while integration, analysis and prediction are all important but are dependent on the aims of the project and resources available.

### *2.2.3.1. Data Organisation*

A spatial database lies at the heart of every GIS project, and the organisation of data according to a well documented data model is an essential step in the process. Spatial data are represented digitally both in vector (points, polylines, polygons) and raster forms (grid cells with values of continuous spatial variable).

GIS projects involve integration of data from a variety of sources: field data, lab based instrumental analysis (e.g. remote sensing or seismic interpretation), digitised paper maps, and information gathered from previously stored databases (e.g. Digimap, BGS digital database, Landmap). The database is the source of all subsequent GIS visualisation and analysis, and therefore it is essential that the final project goals are considered when first setting up a project database. Key factors to consider when setting up a database include: the map datum and coordinate systems; suitable data files and associated acquisition tables; types and volumes of data to be collected.

### *2.2.3.2. Visualisation*

In digital mapping, data are collected in either 2-D or 3-D mode (i.e. x.y. or x.y.z. location) and the data can be visualised using 2-D, 2.5-D or 3-D viewers. In a GIS, information is usually displayed as a series of layers that can be superimposed, with each comprising a single type of data. Typically this may comprise features or objects that have distinct shape and size, or field data that vary continuously over a surface (Longley et al., 2001). A key advantage of GIS-based mapping is that any number of different

## *Chapter 2 – Digital mapping*

types of data may be georeferenced and included in a separate layer of the database. Most desktop GIS programmes are specifically designed to deal with 2-D data, though some also have 3-D visualisation capabilities and modelling tools (e.g. ArcScene™ and ArcGIS™ 3D Analyst™). However, the functionality of these viewers may be somewhat limited when compared to more specialised 3-D GIS and GIS (GeoScientific Information System), such as Gocad™, Petrel™, and 3DMove™ (Mallet, 1992; Turner, 2000; McCaffrey et al., 2003, Jones et al., 2006).

In its simplest form of three-dimensional visualisation GIS data may be overlain, or ‘draped’, onto a digital terrain model (DTM), in the form of a surface fitted to a raster map of elevation values (e.g. Fig. 2.1b). This type of display has been referred to as a 2.5-D representation as they do not provide any direct information about the subsurface geology. (Longley et al., 2001; Jones et al., 2004). These data may then be displayed using a 3-D viewer that allows rotation to different vantage points as well as zoom and pan, and even simulate ‘fly-through’ animations. One particularly useful geological application of 2.5-D displays is to study the relationship of geological structures with topography (McCaffrey et al., 2003, 2005).

For fully 3D models (i.e. equivalent to seismic models offshore) structures must be projected into and out of the topographic surface and volumetric data visualised. Viewing geological data in 3-D helps geologists to visualise and analyse the three-dimensional nature of geological features (McCaffrey et al., 2003), however it is often the case that 3-D visualisation software are not as powerful at analysing attribute data. Furthermore, fully immersive software systems are now being developed which allow the user to see inside the 3D-model in a ‘virtual world’ (e.g. GeoProbe, Inside Reality™, Hydro VR; Hanley, 1999; Jones et al., 2006).

### *2.2.3.3. Spatial Query*

Spatial query can take two forms: an on-screen selection of a location (or area) to determine the characteristics from the database; or a search of the database for all those locations where a particular attribute (or combination of attributes) occurs. Whereas the visualisation function reveals patterns, spatial query is used to identify the specific

## Chapter 2 – Digital mapping

details about particular occurrences of spatial objects. This function is important for interrogating datasets, and the selected data can also be exported for further analysis.

### 2.2.3.4. *Data Combination and Integration*

The primary purpose of many GIS projects is to combine different map layers together in various ways for purposes of revealing or confirming spatial relationships in the data. The ability to combine map layers visually, or in spatial search operations, or to generate new layers by mathematical operations is the GIS equivalent of overlaying maps on a light table.

### 2.2.3.5. *Spatial Analysis*

Some well-known examples of spatial and geostatistical analysis include contouring methods, trend analysis, using variograms and spatial covariance diagrams, kriging and cokriging, spatial filtering, and fractal and multifractal analysis. Spatial analysis may also incorporate the attributes of adjacency and containment, the topological attributes of spatial objects. Spatial analysis in GIS is often exploratory in nature, seeking to uncover associations in the data that are otherwise unknown. This is useful when assessing geological field data as rock exposures are commonly discontinuous and thus extrapolation between outcrops is essential.

### 2.2.3.6. *Prediction*

The ultimate purpose of GIS may be to provide spatial predictions, which are often made to support decisions. Some good examples include oil, gas, and mineral exploration, landslide forecasting, and the assessment of the effect of disasters (Coburn & Yarus, 2000; Rosenberg, 2004). Decisions can be based on mathematical models of various types: spatial analysis tools; fuzzy membership functions, statistical regression, etc (e.g. McNoleg, 1996).

## 2.3. **What is digital geological mapping?**

Digital geological maps can be created in two main forms, (1) *primary mapping* and data capture (which includes fieldwork, remote sensing and aerial photograph analysis), and



## Chapter 2 – Digital mapping

(2) *secondary* mapping and digitization. *Secondary mapping* methods have been employed by many geological surveys to develop digital geological map databases (Jackson and Asch, 2002; Becken and Green, 2000). Both primary and secondary mapping are essential when carrying out geological studies of an area. However digitisation and analysis of existing data is well established in geological research, therefore the following sections shall concentrate on primary digital data capture, and more specifically digital field-base mapping.

### 2.3.1. Digital vs. Traditional mapping methods

#### 2.3.1.1. Traditional geological mapping

Traditional fieldwork methods are well covered in a number of publications (i.e. Barnes, 1981; Crompton, 1985; McClay, 1987; Barnes and Lisle, 2004) and are therefore only a brief overview is given here. Traditional field methods of geological mapping and data capture are generally paper-based activity using pencils, maps, field notebooks and compass-clinometers, and have remained virtually unchanged for almost 200 years (Smith 1815; Jones et al., 2004). One of the main reasons for this is that a field geologist generally work on foot and needs to carry their tools around with them, therefore equipment needs to be light weight, and due to the risk of loss or damage, also relatively cheap. Furthermore, the types of data collected can be quite varied and are not usually fully understood prior to embarking on a field expedition, therefore the mapping tools need to be relatively versatile.

The scientific aims of a study and the time available for fieldwork will generally determine the type of mapping carried out. Five main types of geological mapping are commonly identified (also see Table 2.2; Barnes, 1981; McClay, 1987; Jones et al., 2004):

- (1) *Reconnaissance mapping* typically covers a large area and is carried out in order to find out as much as possible about a poorly known region in a short period of time. This generally relates to mapping at 1:250 000 or smaller, and much of the work is likely to be done using *remote sensing* techniques, *photogeology*, *photogrammetry* and *'blind' spot sampling* (e.g. using a helicopter).

## Chapter 2 – Digital mapping

- (2) *Regional mapping* is typically carried out at 1:100 000 – 1:50 000 scale and are mapped onto appropriately scaled base maps or aerial photographs. Such mapping is generally the result of systematic programmes of field-based data gathering, fully supported by photogeological interpretation and integration of other datasets (e.g. sub-surface or geophysical datasets).
- (3) *Standard mapping* refers to normal UK practice and corresponds to BGS standard surveying and university undergraduate mapping projects. Mapping methods include *contact mapping* and *exposure mapping* (Barnes, 1981; McClay, 1987). This level of mapping is typically carried out at a scale of 1:25 000 – 1:10 000.
- (4) *Detailed mapping* generally refers to maps made at a scale of 1:10 000 or larger and in many cases they are produced to document key geological relationships in detail. These methods are essential for detailed structural studies in complexly deformed areas. Mapping methods can include *baseline mapping* and *survey-, grid-, planetable- and cairn-mapping* techniques (Barnes, 1981; McClay, 1987).
- (5) *Specialised mapping* refers to maps which are constructed for specific purposes and do not necessarily include all aspects of the observed geology. These include mine plans, geophysical/ geochemical/ geotechnical data maps, and can be at a variety of scales.

Both reconnaissance and regional scale mapping are already well established computer based processes, comprising remote sensing, aerial photograph analysis (*primary mapping*), and the digitisation and analysis of pre-existing map data (*secondary mapping*). Remote sensing may comprise the interpretation and analysis of a range of datasets derived from satellite data, e.g. Landsat and SPOT images, DTMs, geophysical data. Some basic methods for analysing remote sensing data are morphotectonics (analysing landforms and structures), terrain analysis and lineament mapping (Gabrielsen *et al.*, 2002 ; Cortés *et al.*, 2003). Generally, both reconnaissance- and regional-scale mapping should be carried out prior to fieldwork. However, post-

## Chapter 2 – Digital mapping

fieldwork analysis is also useful as a better understanding of regional structures is likely to be gained during the fieldwork.

Critical to all field-based data gathering and observational activities is the accurate positioning of the observed geological feature, and their spatial and temporal relationship with surrounding features. Furthermore, it is essential that all field maps and notebooks are legible for other readers, and that observed facts may be distinguished from inferences and interpretation (Ramsay and Huber, 1987). To build up an understanding of the area in question geologists are encouraged to interpret their observations and measurements as they map; however, this can lead to issues when analysing other people's data as it is often difficult to discern observational fact from interpretation. Jones et al. (2004) highlight a number of problems that can arise due to traditional field mapping methods, these include: (1) mixing observations with interpretations and priori assumptions; (2) slow and complex workflows from field mapping to published map production; (3) final map may result in loss of data and spatial precision (controlled by scale of published map); (4) final published map generally shows little information about data acquisition (i.e. uncertainty, acquisition method, etc). Digital mapping methods offer a solution to many of these problems.

A further issue regarding traditional methods is one of data management. Problems with the traditional methods arise when long-term data management and availability are considered as much of the raw map data is lost (McCaffrey et al., 2005). This issue is now recognised in NERC (National Environmental Research Council) policy with the requirement that all recipients of NERC grants provide copies of their datasets for the National Geosciences Data Centre (NGDC). Metadata is an essential part of these files (see *appendix 3* for metadata files associated with this project).

### 2.3.1.2. *Digital geological field mapping*

Recent innovations in computer and GPS (global positioning systems) technology have enabled the development of digital data capture and mapping in the field. McCaffrey et al. (2005) distinguish two distinct forms of digital field mapping: (a) *Digital Geological Mapping* (DGM); and (b) *Digital Geological Survey* (DGS) methods (Fig. 2.3). With geological mapping, the aim is to abstract information from a given location as a series

## Chapter 2 – Digital mapping

of symbols and colours plotted on a geological map at scales typically from 1:5,000 upwards. In contrast, geological survey or ‘plane tabling’ involves precise recording of topographic and geological information at scales less than 1:5,000 and with as little abstraction as possible. With digital geological mapping, the aim is to replace existing paper-based methods with an equivalent digital media (e.g. a handheld computer + GPS). Digital geological surveying has a similar aim, however, data acquisition occurs at a much higher spatial resolution (mm to cm) using high precision DGPS and/or laser scanning equipment. The key difference is principally one of scale. For example, a digital geological survey will record an attribute such as bedding dip at centimetre or finer resolution continuously over an entire outcrop, whereas for geological mapping a single average dip value would be recorded. In this project only DGM methods are used; however, a brief overview to both mapping types is given below as an understanding of the entire digital field mapping spectrum is important.

### 2.3.1.2.1. Digital Geological Mapping

DGM is a methodology by which a geologist collects GPS-located field data in a digital format on a handheld computer or tablet PC. The method has been adapted from digital mapping and surveying techniques that are now widely used in construction, engineering and environmental industries. Early pioneers that have customised these techniques in an attempt to replace traditional paper-based methods with digital equivalents include Struik et al. (1991), Brodarik (1993, 1997), Schetselaar (1995), Briner et al. (1999), Kramer (2000), Pundt and Brinkkötter-Runde (2000), Xu et al. (2000), Maerten et al. (2001) and Brimhall and Vanegas (2001). Digital acquisition is gradually becoming more commonplace, particularly in North America, although European geological institutes have been slower to take up these new methods (Jackson & Asch, 2002)

DGM is a relatively cheap (i.e. a total budget of as little as £500 is needed; *see side note 1, page 14*; Wilson et al., 2005) and flexible system that is suitable for most mapping purposes (except perhaps highly detailed outcrop mapping which require cm-scale accuracy). The system involves three key components: (1) GPS or DGPS receiver; (2) handheld computer (i.e. pocket PC, PDA or tablet PC); and (3) field-GIS software (e.g. ArcPad™) (Figs. 2.3 and 2.4; Kramer, 2000; Edmondo, 2002; Jones et al., 2004).

## *Chapter 2 – Digital mapping*

Other optional tools include a good quality digital camera and a Laser rangefinder (for accurately locating features on a vertical profile) (Fig. 2.3). DGM methods bear a strong resemblance to traditional methods in that field data are stored in a ‘digital notebook’ (i.e. PDA) and on to digital base-maps and attribute tables in a field-GIS (Fig. 2.4). Table 2.3 outlines the data typically recorded using traditional mapping methods and their digital equivalent.

The key advantage of digital mapping over conventional paper-based mapping lies in the automatic recording of positional data for each observation, meaning that the geospatial context is maintained. Additional benefits include: the data is stored directly into existing databases; all files have an associated metadata file; and the opportunity to map at different scales and the ability to change this ‘on the fly’ whilst in the field. Furthermore, any number of different types of data may be georeferenced and included as a separate layer within the GIS project database. These can then be displayed and analysed in conjunction with newly acquired field data. By comparison, such disparate types of data would traditionally be spread widely between field notebook, paper maps, isolated files on a computer, boxes photographs, scientific journals and papers.

Localities and outcrop features are recorded as GPS located (x.y.z.) points in 3-D space, with all details being recorded in an attribute table (Table 2.3). Field sketches (drawn on handheld computer) and digital photos can also be hyperlinked to these ‘point’ files. Linear features on the Earth’s surface (such as faults and lithological contacts) are mapped as polylines, with line vertices recorded from GPS, while details about the feature (e.g. type of feature, certain or uncertain, length, orientation, comments, etc.) are stored in the attribute table. Area features (i.e. lithological units) generally filled in during post processing of the data, snapping polygon vertices to features mapped in the field.

### 2.3.1.2.2. Digital Geological Survey

DGS entails fine-scale (cm) digital acquisition using a variety of geomatic surveying equipment (Fig. 2.3; Clegg et al., 2005; McCaffrey et al., 2005). They provide 3-D coordinate data at fine (typically < 1 cm) resolution with either automatic attribute (e.g.

## Chapter 2 – Digital mapping

colour intensity) or user-enabled attribute (e.g. surface slope, bedding dip) recording. Although largely being developed for engineering use, these methods are now being adapted for geoscience data (Xu et al, 2004; Pringle et al 2004; Clegg et al., 2005; McCaffrey et al., 2005). Laser scanning or reflectorless surveying methods are best used on steep, vertical or overhanging sections whereas aerial photogrammetric methods are an appropriate method for beach or outcrop pavements. Kinematic or survey-grade GPS is used to geospatially reference all other methods or can be used as a stand-alone acquisition tool.

These survey data can be used to create virtual outcrop exposures, using 3-D data-point set (a 'point cloud') that may be meshed to form a 2½ -D outcrop surface (Clegg et al., 2005). Attributes such as bedding dip may be directly mapped on to this surface by using at sample locations or summarized on a contoured plot. Alternatively, the surface may be coloured from digital photographs to form a 2½-D photo-realistic outcrop image displayed on a computer monitor, from which detailed geological interpretations can be made in the laboratory in order to constrain the true 3-D spatial architecture of the outcrop (Clegg et al., 2005; Trinks et al., 2005).

### 2.3.2. *Digital mapping Hardware and software*

Field-mapping systems have been around for several years (Brodaric and Fyon, 1989; Kramer, 2000; Edmondo, 2002), however the choice of systems available is somewhat varied and controlled to a major extent by user preferences and project aims (Edmondo, 2002). Many of the hardware and software tools needed for digital mapping have already been discussed in previous sections; however this section is aimed as a review, and more specifically a list of the tools used during the course of this project (see *appendix 1* for full list of hardware and software tools used during research). The essential hardware tools for digital field mapping are a *spatial location device* (i.e. GPS, laser rangefinder, etc.) and a *data recording device* (e.g. PDA, tablet PC), other items include a digital camera, extra memory (memory cards), back-up power (batteries) and, of course, a compass-clinometer.

**SIDE NOTE 1 - Digital field mapping on a shoestring!**

Many people may be put off trying out new digital methods, as they can be seen as an expensive alternative to traditional “map, compass and notebook methods”. However this is no longer the case. The recent increase in popularity of Pocket PCs and GPS systems means that prices are becoming more and more affordable. With a little shopping around it is now quite easy to set your self up with the vital equipment needed for digital field mapping with a budget of under £500!



The essential items required for a digital mapping exercise are: a **Handheld computer/ PDA** to record data, a **GPS/DGPS** unit for accurate positioning in ‘real-time’, a **data cable** to connect GPS to PDA, **Field GIS software** (e.g. ArcPad 6; Edmondo 2002) and a **digital camera** to record observations (Wilson *et al.* 2005). Optional extras include: **Ruggedised PDA case** (the PDA is the most expensive item, therefore protecting it from adverse

weather conditions and general wear and tear is advisable), **data storage cards** (for hard back up of data). GIS software (such as ArcGIS™) is also required on a desktop/ laptop computer for post processing and data analysis. Table 1 shows a list of cost for these items, with some examples collected during a product search (\*prices correct as of 2/3/2005).

Equipment	Price	Examples*
Pocket PC/ PDA	From £150	Dell Axim X30 (£148 from <a href="http://www.dell.co.uk">www.dell.co.uk</a> ), HP IPAQ H5550 (£264.99 from <a href="http://www.amazon.co.uk">www.amazon.co.uk</a> )
Handheld GPS	From £75	Garmin geko 201 (£91.84; from <a href="http://www.gpsw.co.uk">www.gpsw.co.uk</a> ),
Ruggedised PDA case (optional)	~£50	Armor 3600 (\$99.95 from <a href="http://www.armorbyotter.com">www.armorbyotter.com</a> )
Data cable	~£15	PDA to Garmin GPS cable (£15.99 from <a href="http://www.expansys.com">www.expansys.com</a> )
Field mapping software (GIS)	£75	ArcPad 6 (£75, educational price, from <a href="http://www.esri.co.uk">www.esri.co.uk</a> )
Data storage card	~£10	Kingston 128MB CompactFlash Card (£8.39 from <a href="http://www.amazon.co.uk">www.amazon.co.uk</a> ),
Digital Camera	From £100	Canon Powershot A400 (£109.63 from <a href="http://www.amazon.co.uk">www.amazon.co.uk</a> )
	<b>£475</b>	<b>£498.85</b>

When choosing digital mapping tools it is generally a trade-off between data quality (i.e. accuracy), speed of data capture, and cost (Fig. 2.5). However a number of other factors also need considering when choosing the right equipment, these include: size, weight, battery life, processor power, connectivity, data display, ruggedness, and compatibility (Table 2.4; Edmondo, 2002).

In this study a total equipment budget of <£10,000 was set, and a key requirement is that the equipment was mobile and versatile enough to be handled by a single user (i.e. moderate to light weight, not too bulky). Furthermore, as mapping was to be carried

## Chapter 2 – Digital mapping

out at a range of scales (i.e.  $10^5 - 10^1$ ) meter/sub-meter real-time accuracy GPS accuracy was required. The following sections discuss the various hardware devices, their cost, speed of acquisition and use. Table 2.5 shows a number of scenarios, and lists which mapping system is most suitable (for full list of the equipment used in this project see *appendix 1*).

### 2.3.2.1. Spatial location devices

#### 2.3.2.1.1. GPS units

GPS units fall into three broad categories based on DGPS (differential correction) accuracy: (1) recreational-grade receivers that are accurate from 5 to 15 m; (2) mapping-grade receivers that are accurate to sub-meter scale; and (3) survey-grade receivers that have sub-cm accuracy.

Recreational-grade GPS (i.e. standard pocket-sized GPS used by hikers, etc.) are small and lightweight and are therefore useful in situations where weight is an issue (Table 2.5). However a downside to these units is that their accuracy is generally only about 5 to 15 m, and therefore is not suitable for detailed-mapping (i.e. 1:10 000 or larger scale).

Mapping-grade receivers generally fall in to the category of DGPS (differential GPS) and provide sub-meter accuracy through differential correction via signals from ground based radio beacons, or through WAAS (Wide Area Augmentation System; see *side note 2, page 56*). These units require an extra receiver (beacon receiver) to pick up these signals, thus making them heavier and more cumbersome than recreational-grade GPS.

Survey-grade receivers are only suitable for highly detailed and specialised mapping situations that require mm-scale accuracy (i.e. outcrop-modelling). The terrain and location of a mapping area have a major control on whether survey-grade mapping systems are suitable for a project as the equipment is very heavy and cumbersome, thus cannot be transported very far (Table 2.5). Furthermore, they require considerable post-processing, though field acquisition time is relatively fast. However, probably the most significant controlling factor when considering using these systems is cost! At about ~£20 000 they are far more expensive than other alternatives (Fig. 2.6).

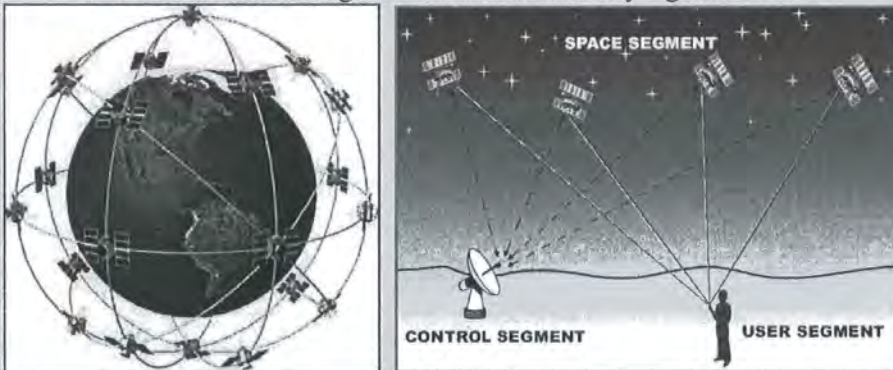


### **SIDE NOTE 2 - GPS and how it Works**

The Global Positioning System (GPS) is a navigation and precise-positioning tool. Developed by the US Department of Defence in 1973, GPS was originally designed to assist soldiers and military vehicles, planes, and ships in accurately determining their locations world-wide. Today, the uses of GPS have extended to include both the commercial and scientific worlds.

Three distinct parts make up the Global Positioning System. The *space segment* of the system consists of 24 satellites, orbiting 20,000 km above the Earth in 12-hour circular orbits. GPS satellites transmit two low power radio signals, designated L1 and L2. Civilian GPS uses the L1 frequency of 1575.42 MHz in the UHF band. The signals travel by line of sight, meaning they will pass through clouds, glass and plastic but will not go through most solid objects such as buildings and mountains. A GPS signal contains three different bits of information – a pseudorandom code, ephemeris data and almanac data. The pseudorandom code is simply an I.D. code that identifies which satellite is transmitting information. You can view this number on your GPS unit's satellite page, as it identifies which satellites it's receiving. Ephemeris data, which is constantly transmitted by each satellite, contains important information about the status of the satellite (healthy or unhealthy), current date and time. This part of the signal is essential for determining a position. The almanac data tells the GPS receiver where each GPS satellite should be at any time throughout the day. Each satellite transmits almanac data showing the orbital information for that satellite and for every other satellite in the system.

24 GPS satellites orbiting the Earth and the three key segments of GPS



The control segment tracks the satellites and provides them with corrected orbital and clock (time) information. There are five control stations located around the world – four unmanned monitoring stations and one master control station. All stations constantly receive satellite signals, however only the master control station corrects the satellite data and sends these corrected signals back to the satellites.

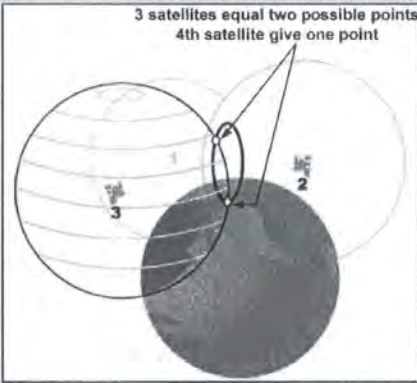
The user segment simply comprised the user and their GPS receiver! Users include pilots, boaters, hikers, military, in-car navigation, and of course Earth Scientists.

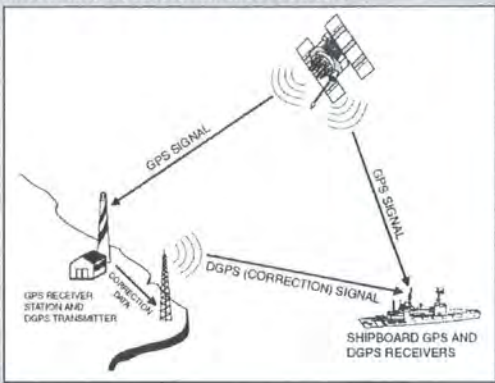
GPS satellites circle the earth twice a day in a very precise orbit and transmit signal information to earth. GPS receivers take this information and use triangulation (or trilateration) to calculate the user's exact location. Essentially, the GPS receiver compares the time a signal was transmitted by a satellite with the time it was received. The time difference tells the GPS receiver how far away the satellite is. Now, with distance measurements from a few more satellites, the receiver can determine the user's position.

A GPS receiver must be locked on to the signal of at least three satellites to calculate a 2D position (latitude and longitude) and track movement. With four or more satellites in view, the receiver can determine the user's 3D position (latitude, longitude and altitude). Once the user's position has been determined, the GPS unit can calculate other information, such as speed, bearing, track, trip distance, distance to destination, sunrise and sunset time and more.

**How DGPS works: Trilateration and differential corrections**

3 satellites equal two possible points  
4th satellite give one point





**Typical Sources of GPS Errors:**

- *Ionosphere and Troposphere* - As the satellite signal passes through the atmosphere it slows down.
- *Signal Multi-Path* - The satellite signal can be reflected off of objects such as tall buildings, mountains and other large rock surfaces. This causes the signal to increase its travel time.
- *Receiver Clock Errors* - The clock in a receiver is not an atomic clock as it is in the satellite and the built-in clock can generate small errors in timing.
- *Ephemeris Errors* - These are inaccuracies of the reported position of a satellite.
- *Low Number of Visible Satellites* - The fewer satellites signals the receiver receives will result in a less accurate location reading. Buildings, high terrain and trees are just some things that can block satellite signals.
- *Bad Satellite Geometry* - Bad satellite geometry exists when the satellites are located either in a line or are closely grouped together.
- *Intentional degradation of the satellite signal* - Selective Availability (SA) is an intentional degradation of the signal once imposed by the U.S. Department of Defence. The US government turned off SA in May 2000.

**Differential corrections – ways to improve accuracy:**

Differential GPS (DGPS) is a way of improving the accuracy of GPS. Data from a receiver at a known stationary location (base or reference) is used to correct the data received from a receiver at an unknown location (rover). These corrections can be applied in real time or by post processing.

- *Real-Time Corrections* - base station and rover communication
- *Real-Time Corrections* - WAAS/EGNOS, satellite subscription service, radio beacon signals
- *Post-Processing Corrections* - Base stations record corrections and then upload the files for storage onto large capacity servers. Public and private agencies distribute this information electronically.

In this study a combination of recreational and mapping grade GPS/DGPS were used. A backpack-mounted DGPS (either a Trimble AG122 or Ashtech Promark II) was the preferred spatial location device as it provides sub-meter accuracy. However a recreational GPS (e.g. Garmin Geko 201) was also kept in reserve should the DGPS unit fail. A select few localities were also georeferenced to a higher precision using survey and post-processing techniques in order to establish ground control points for detailed (i.e. sub-meter scale) outcrop mapping using field photographs (i.e. equivalent to

## *Chapter 2 – Digital mapping*

traditional cairn mapping methods) and a laser rangefinder (see below). However, this was not done on a widespread basis as data acquisition time was slow (i.e. 30 minutes per GPS point; plus post-processing time).

### *2.3.2.1.2. Laser scanners and laser rangefinders*

Laser rangefinders and terrestrial laser scanners (also known as LiDAR – Light Detecting And Ranging) are used to collect geospatial data from vertical/ sub-vertical sections that are inaccessible for GPS mapping (Xu et al., 2001; Clegg et al., 2005; Trinks et al., 2005). Laser scanners collect highly accurate (mm-scale) outcrop data but (like survey-grade real-time kinematic GPS) are very expensive (Tables 2.5 and 2.6), and therefore were not used during this research project. Laser rangefinders on the other hand are much cheaper (though accuracy is less, ~30 cm), and can be used to measure the location of individual observations and structural measurements relative to the instrument (which should be GPS located). A MDL LaserAce 300 laser-ranging device was used for recording vertical profile data during this research project.

### *2.3.2.2. Data recording device*

There are a number of different forms of data recording device, and the decision as to which option to choose is controlled by specific mapping scenario (which again links back to key factors such as mobility, accuracy, data memory, etc.; see Table 2.5). The three alternative devices considered here are: (1) a handheld computer or PDA (personal digital assistant); (2) a tablet PC; and (3) a laptop computer suitable for fieldwork.

For basic mapping probably the most suitable device is a PDA (Fig. 2.4; Golledge, 2004; Wilson et al., 2005). These are small lightweight and also relatively cheap to buy (i.e. prices range from £150 - £500). They also have relatively long battery lives (i.e. ~8hrs on full use) suitable for a standard day's field mapping. These units do not have the full software capabilities of a desktop/laptop computer, and require specialised mobile software, e.g. Windows<sup>®</sup> CE. Therefore, for data processing, a desktop/ laptop computer is also required.

A step up from PDAs are tablet PCs (Kramer, 2000; Clegg et al., 2006). These provide the user a far bigger display, and also usually have much larger processing and

## *Chapter 2 – Digital mapping*

memory capabilities. Tablet PCs also run standard desktop software systems (e.g. Windows<sup>®</sup> XP) therefore providing the user with a much wider range of software tools and capabilities, and the ability to process data while in the field. Tablet PCs usually work on a touch-screen interface, thus allowing the user to create hand-drawn digital sketches in the field; however, a down side of this is that text input is also touch-screen based. Tablet PCs are usually a lot more expensive than PDAs (e.g. equivalent in price to laptop computers).

Alternatively, Laptops computers may also be developed for fieldwork (e.g. Black and Walker, 2001). The benefit of using a laptop in the field is that it provides the user with the full range of desktop capabilities. Furthermore, the user interface is a standard keyboard and mouse, rather than touch-screen display that is more common for PDAs and tablet PCs. A major draw back to using laptop computers in the field is their size, weight and toughness. However, recent advances in the mobile capabilities of laptop computers (e.g. significant decreases in size and weight, and the energy saving capabilities of Intel<sup>®</sup> Centrino™ processors) mean that laptop computers may also be a viable option for fieldwork.

Ruggedised versions of all these units are also available, but at an extra expense (can add 50% to the total cost of the unit, e.g. a ruggedised PDA may cost ~£1000, whereas a standard PDA costs no more than £500), alternatively ruggedised cases may be purchased to fit most standard PDAs and tablet PCs at far less expense (though as these encompass the unit, they may hamper connectivity to other devices, so care must be taken when choosing the right case).

A PDA (HP Jornada 540 – later replaced by a Compaq Ipaq 3835), running Windows<sup>®</sup> CE, and a ruggedised case was the preferred choice of device for this research project. This decision was made on the basis of size, weight, compatibility (i.e. windows based media) and overall cost of unit. A laptop computer was also used while in the field for data processing and back-up, but not for direct data acquisition.

### *2.3.2.3. Field-based software tools*

~~Various software tools are now available for digital field mapping. Field-GIS systems designed specifically for use with GPS link-up include: ArcPad™ (ESRI; Edmondo,~~

## Chapter 2 – Digital mapping

2002; Haugerud and Thoms, 2004), TerraSync™ (Trimble), FieldLog (Brodaric, 1997, 2004), GeoMapper (Brimhall and Vanegas, 2001), MapIT (Clegg et al., 2006). Some of these systems are suitable for running on Windows® CE (i.e. on a PDA) while others are not, therefore decisions regarding hardware should be made in conjunction with software preferences.

The preferred choice of software for this project was ESRI's ArcPad (Fig. 2.4). This was in part because ArcPad has been designed to work seamlessly with ArcGIS™ desktop, our preferred GIS system. Furthermore, ESRI software provides educational discounts, thus making it the cheapest system available for academic research.

As ArcPad uses the same file systems as ArcGIS™ desktop it allows a similar layer based display. Geo-registered images of shaded topography, orthophotographs, and remote sensing images can be displayed on the screen as background information, while the current GPS location is displayed with a point symbol. Spatial information can be input as vector data to the ArcPad project by either tracing features on the screen that are visible on the displayed images, or by “walking out” the features using the active GPS function (either by continuous GPS data streaming, or user defined GPS vertices). Furthermore, the user can create personalised geological mapping applets and data entry forms (see *appendix 3*; Haugerud and Thoms, 2004) which give a pick lists of data attributes, allowing user input of attributes such as rock type, strike and dip, descriptions, etc., and thus build the GIS database in the field (Fig. 2.4). As with desktop GIS these attributes can be displayed on the screen with unique symbols for better visualisation of the map as it is being built. Finally, at the end of a field day, the fully attributed data can be directly downloaded into ArcGIS™ without the need to hand-enter field notes and other descriptions.

### **2.3.3. Cost vs. accuracy vs. mobility**

#### **2.3.3.1. Cost, accuracy and mobility**

In any field data capture project there is fundamental trade-off between the data quality/accuracy, the speed of capture and the overall cost of the system (Fig. 2.5). Figure 2.6 shows how GPS accuracy is closely linked to the cost of the unit, fitting an apparently logarithmic relationship between cost and accuracy. Those units that plot below this line

forfeit either on real-time accuracy, speed of data capture, or mobility to account for the cheaper cost. While those that plot above this line are those that offer extra features at an extra cost (i.e. all in one units, ruggedised casings, etc.).

### 2.3.3.2. Testing GPS accuracy and precision

Table 2.6 shows the results of an assessment of the precision, or error, of various GPS units (McCaffrey et al., 2005). The test comprised the collection of a stream of GPS data from a specific locality and analysing the variability of the GPS points at this locality. The results of this test suggest that recreational-grade GPS (i.e. Garmin III+) have a horizontal precision (hp) of about 3 m, while mapping-grade units (e.g. CSI GBX Pro or Promark II) have a hp of 0.3-0.5 m, and survey systems (e.g. real-time kinematic, RTK, GPS) have a hp of 0.001 m (1 mm). Unusually, the results of this test suggest that a recreational-grade GPS with WAAS enabled (e.g. Garmin Geko 201) has a similar precision to mapping-grade units.

This test gives an estimate of the precision of the GPS unit, but does not necessarily depict the unit's accuracy. Therefore, a further independent test of GPS accuracy was also carried out to assess the repeatability of each system (i.e. consistency of GPS location when repeatedly returning to the same site). Over a 50 day period, GPS readings for various GPS units (e.g. Trimble AG122, Trimble GeoExplorer, Garmin Geko 201) were repeatedly recorded (2-5 points per day) at a surveyed locality point (using a survey-grade, mm accuracy, RTK GPS). During acquisition various metadata attributes (e.g. weather conditions, number of satellites, time and date, PDOP – Position Dilution of Precision) were recorded in order to assess the effects of these variables on GPS location.

Figures 2.7 and 2.8 show a qualitative assessment of the results of this experiment, while a more quantitative analysis is given in *appendix 2*. As Figure 2.7 shows, each GPS unit forms its own distinct cluster, with the cluster size giving an indication of the GPS accuracy. The Trimble AG122 appears to have the tightest distribution of points (RMS\_error = 0.46 m; see *appendix 2*), while the Trimble Geoexplorer and Garmin Geko are somewhat less (RMS\_error of 1.67 m and 2.31 m respectively). Note both the Garmin Geko (collected using waypoint collection on GPS

## *Chapter 2 – Digital mapping*

unit) and the Trimble Geoexplorer points cluster around a centre point that is near coincident with the survey site; however the points of the Trimble AG122 backpack appear offset to the west by about 0.5 meters (Fig. 2.7). This is because the beacon receiver on the backpack is mounted over the right shoulder of the user, and therefore if the user stands directly over the survey point the beacon is offset to the right (note that the user faced the same direction – south – every time a reading was taken). The results of this analysis of the Garmin Geko (WAAS enabled) are in contrast to those of the previous test, as here the recreational-grade GPS underperforms considerably compared to the mapping-grade units. A further variation which cannot be explained as yet is the apparent elongate, N-S, distribution of Trimble Geoexplorer points (Fig. 2.7).

Figure 2.8 show a series of plots outlining variations in attributes for each locality for the Trimble AG122. These suggest that there is a strong correlation between PDOP and the number of satellites available. Furthermore, those points with lower PDOP (i.e. better accuracy) lie closer to the survey site than those with higher PDOP, which may suggest that the although the beacon receiver is mounted off-centre, a further factor is also causing this offset of the GPS localities. A more fundamental variation can be seen in the variations in location on a day by day basis. On any given day the GPS localities have a very close relationship (tight cluster), however, from one day to the next the location of these clusters may vary. Highlighted in Figure 2.8 are three main clusters showing how the preferred location of the GPS appears to have wandered with time. These results all suggest that although GPS localities may be highly precise during any one measurement (i.e. 0.3 m) their accuracy/ repeatability on a day by day/ month by month basis may be somewhat less (i.e. ~1 m).

### **2.4. GAVA workflow**

#### **2.4.1. Introduction**

The case studies carried out during the course of this research comprise regional to outcrop studies onshore, and also the integration of offshore datasets. In order to implement these digital mapping techniques into an overall project, a suitable workflow is required. Such a workflow has been developed during the course of this research. This workflow groups together a range of complimentary digital mapping methods, and is

collectively termed “GAVA” (*Geospatial Acquisition, Visualisation & Analysis*) (Clegg et al., 2005; Wilson et al., 2005; Jones et al., 2006). This integrates field- and laboratory-based digital mapping methodologies and allows for continual data analysis and evaluation at every stage in the data gathering process. Figure 2.9 outlines the factors that make up the GAVA workflow.

### **2.4.2. Preparation**

#### **2.4.2.1. *Creating the digital database – choosing formats and creating files***

A key part of digital mapping is pre-fieldwork preparation and setting up the digital database. As the field data are added directly to the database during digital field mapping, the database needs to be prepared prior to fieldwork. The initial databases should include point and polyline files and associated attribute tables for all features that are planned to be mapped (e.g. faults, lithologies, sample sites), and also the georeferencing of all base-maps and images (i.e. aerial photographs) required to aid field mapping. Furthermore, data input-forms, dropdown menus, and associated applets can also be created to enable more efficient field-data entry. These pre-created menus also enable data to be recorded in a consistent format which is essential for data analysis (e.g. BGS Lexicon of Named rock units; Becken & Green; 2004). This is in contrast to traditional paper-based methods which require little pre-fieldwork preparation and the database is generally built after the data is collected.

Creating database files prior to fieldwork generally requires some knowledge of the study area and the type of structures that are to be mapped. It is possible to create data files in the field; however for a well structured database it is best to create the files prior to fieldwork. This is also better policy in terms of logistical expense as costly fieldwork time is spent mapping structures and recording data, rather than managing files.



### **SIDE NOTE 3 - Map datums and coordinate systems**

#### ***What is a Datum?***

The earth's surface is not perfectly round, but shaped as an ellipsoid. Datums were developed to accurately map topographic differences in the earth's surface based on an ellipsoid. A datum is a set of parameters defining a coordinate system, and a set of control points whose geometric relationships are known, either through measurement or calculation. Every map that shows a geographic coordinate system such as UTM or Latitude and Longitude with any precision will also list the datum used on the map.

The Global Positioning System uses an earth centred datum called the World Geodetic System 1984 or WGS 84. WGS 84 was adopted as a world standard from a datum called the North American Datum of 1983 or NAD 83. For all practical purposes there is no difference between WGS 84 and NAD 83.

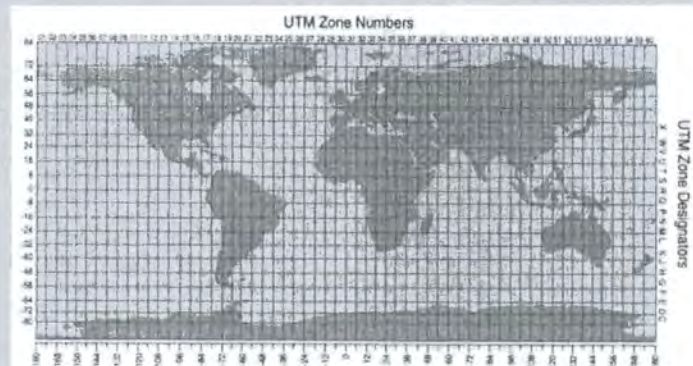
#### ***Coordinate systems:***

There are two types of coordinate systems: geographic and projected. Geographic coordinate systems use latitude and longitude coordinates on a spherical model of the earth's surface. Projected coordinate systems use a mathematical conversion to transform latitude and longitude coordinates that fall on the earth's three-dimensional surface to a two-dimensional surface.



*Geographic* - Latitude-Longitude is a coordinate system that treats the globe as if it were a sphere or spheroid. The sphere is divided into 360 equal parts called degrees. Each degree can be further subdivided into 60 minutes, each composed of 60 seconds. The standard origin is where the Greenwich Prime Meridian meets the Equator.

*Projected* - Universal Transverse Mercator (UTM) is not a true map projection, but a coordinate system that divides the globe into sixty zones, each spanning six degrees of longitude.



The map projection used on Ordnance Survey Great Britain maps is known as the British National Grid. The Transverse Mercator easting and northing axes are given a false origin (map datum: OSGB1936) just south-west of the Scilly Isles to ensure that all coordinates in Britain are positive. The false origin is 400 km west and 100 km north of the true origin on the central meridian at 49° N 2° W.

Due to errors in projection the safest policy when collecting digital field data worldwide is to use WGS 84, and either Geographic or UTM projections. Furthermore, this policy also allow better integration of onshore and offshore data.

## *Chapter 2 – Digital mapping*

Choosing the right map projection and map datum is one of the most important decisions to be made when handling digital map data as mixing data with different map projections can be a major source of error. Most GIS systems (such as ArcGIS™) have the ability to handle and present a variety of different map projections and coordinate systems, and convert maps on the fly. However, small errors (i.e. a few meters) can arise when converting from geographic to projected coordinate systems (see *side note 3, page 24*, for definitions). Geographic coordinate systems are better suited when dealing with worldwide datasets, however as they are based on a spheroid, units are in degrees, which thus hinders measurements of distance and area. Projected coordinate systems divide the grids of equal area, thus enabling the mapper to analyse unit distances and areas better. However, projected grids only cover small areas of the Earth's surface (e.g. UTM zones), and thus regional studies may truncate a number of different zones.

In this study, the preferred coordinate systems were UTM zones for each area, based on the WGS 84 (World Geodetic System 1984) datum as this allows best integration of regional datasets and also onshore-offshore studies. The only exceptions to this were onshore studies in the UK which used the British National Grid coordinate system (OSGB 1936 map datum), for consistency with Ordnance Survey and BGS maps.

### **2.4.3. Acquisition**

#### *2.4.3.1. Integration of regional to outcrop data in a digital database*

As outlined in previous sections, there is a large range of different methods of digital data acquisition. As geoscientists often need to consider geological phenomena of a range of scales, from outcrop observations and measurements at a cm-scale, to regional structures that can span hundreds of kilometres, in most situations optimum results are obtained by combining more than one mapping method.

In this study we use mapping-grade DGPS field mapping methods (i.e. DGM), combined with lab based regional and reconnaissance mapping (i.e. remote sensing, aerial photograph, DTM and geophysical map analysis), see Figures 2.10a-d for an example of a multi-scalar project datasets. Table 2.2 gives a summary of various forms of mapping at different scales and the digital mapping methods applied in their

## *Chapter 2 – Digital mapping*

construction. These multi-scalar onshore models are then combined with offshore seismic interpretation models to develop fully onshore-offshore models for each case study.

### **2.4.4. *Post-processing and analysis***

#### **2.4.4.1. *Post-processing data***

With the exception of survey methods, digitally mapped datasets require far less post-fieldwork processing (prior to analysis and interpretation) compared to traditional paper based mapping techniques as all the data has been digitised and sorted while in the field (i.e. no need for digitising field-slips or typing up field notes). It should be noted that some post-fieldwork analysis may also be carried out at the end of each field day on a laptop computer at base camp. This may include downloading and hyper-linking photographs, or digitising polygon files from field data.

#### **2.4.4.2. *Visualisation I – 2-D maps and 2.5-D/ 3-D models***

Digital field mapping techniques generally entail the collection of point and line data (i.e. the equivalent to uncoloured field-slips), and to complete the geological map, polygons depicting lithological and/ or structural units are required. These can easily be created by GIS from the field data, and where there is no field data available some manual extrapolation is required (though aerial photographs and other base maps can be used to aid this process. As with traditional field mapping methods (i.e. solid/ dashed lines), some sort of distinction between observed and extrapolated structures should be made (either through attribute entry, or the use of separate files).

ArcGIS suite has a number of different viewers: ArcMap for viewing 2-D data (it is in this interface that all data analysis and data processing occurs); ArcScene for simple 3-D visualisation (but only has limited data analysis capabilities); and ArcGlobe, which allows data to be viewed in a global context at a variety of scales. The final 2-D map can be viewed alongside other layers within the ArcMap, or viewed as a 2.5-D model (i.e. map draped over topographic model) in ArcScene (e.g. Fig. 2.10e).

3-D visualisation and analysis functionality is limited in standard desktop GIS programmes (i.e. ArcScene); therefore data often requires export to a 3-D GIS or GSIS

## Chapter 2 – Digital mapping

(GeoScientific Information System), such as Gocad™ or Petrel™, for 3-D modelling and analysis. Such modelling and analysis may include extrapolation of surfaces into and out of an outcrop/ topographic surface through point or lineament traces, thus depicting the 3-D structure of an outcrop (e.g. Trinks et al., 2005; Wilson et al., 2005). These 3-D models may then be re-imported to ArcGIS if required.

### 2.4.4.3. *Spatial and geostatistical analysis in GIS*

As map data depict the spatial distribution of features, one of the most useful functions that can be carried out in GIS is spatial analysis. Most geologists carry out very simple spatial analyses when analysing maps, however these are often based simply on visual observations (e.g. noting that there are more features of one type in area A than area B), and do not entail any systematic or quantitative analysis. Spatial analysis in GIS can help derive new information from mapped data, analyse spatial relationships, and build spatial models through integrated data analysis. Both spatial location and attribute data can be analysed. Most desktop GIS provide a rich set of tools to perform cell-based (raster) analysis, and also analysis of vector data. This latter case may include the generation of density maps from point and line features, distance analysis, trend analysis and attribute variations (Fig. 2.10f). Multivariate statistical analysis allows for the exploration of relationships between many different types of attributes. Cell-based analysis may use neighbourhood functions to create output values for each cell location based on the value for the location and the values identified in a specified neighbourhood. The neighbourhood can be of two types, moving or a search radius. More advanced analyses are also possible e.g. simultaneously execute Boolean queries and algebraic calculations on multiple inputs. It should be noted that a limited number of spatial analysis functions can also be carried out in the field (i.e. spatial query), though as yet this functionality is relatively poor.

There are two main groupings of interpolation techniques: deterministic and geostatistical. Deterministic interpolation techniques create surfaces from measured points, based on either the extent of similarity (Inverse Distance Weighted) or the degree of smoothing (Radial Basis Functions). Geostatistical interpolation techniques (kriging) utilize the statistical properties of the measured points. Geostatistical techniques quantify

the spatial autocorrelation among measured points and account for the spatial configuration of the sample points around the prediction location. The most common output for these spatial analyses are raster maps highlighting various distributions of objects and features; however, GIS tools also enable spatial statistics and statistical analysis to be carried out, thus leading to more quantitative analysis for data.

There are also a limited number of geological analysis tools designed for ArcGIS which may be implemented, these include rose diagram tools and stereonet plotting tools such as GIS-Stereoplot (Knox-Robinson and Gardoll, 1998). GIS-Stereoplot enables stereonets to be drawn within the GIS environment and interactive spatial query and selection to be carried out on both maps and stereonet. The benefits of this GIS tool have also been discussed by Piazzolo et al. (2004).

#### *2.4.4.4. Data export to third party software*

As GIS is not commonly used by all geologists, there is a need to export selected datasets to other software programs to carry out more specialised geological analysis (e.g. kinematic inversion using MyFault™ software). Generally data is exported as ASCII format, which can then be imported into most other software tools. Depending on the type of data being analysed the resultant calculations may then be re-imported to the GIS project, or added as a new attribute to existing datasets for spatial analysis.

### **2.4.5. 3-D geological modelling**

#### *2.4.5.1. Visualisation II – 3-D models*

In the previous section, visualisation techniques were used to aid data analysis and interpretation, however, here the aim is to produce a final model (or models) that help depict the 3-D relationship between structures, plus the results and findings of the overall study. As the final datasets are usually relatively large, relatively fast/ high powered computers with good visualisation cards are required to handle the data.

#### *2.4.5.2. Animations and video*

As not all users have access to the 3-D visualisation software needed to visualise the raw data-files, alternative visualisation methods need to be set up to allow third parties to

## Chapter 2 – Digital mapping

view the final model, without need of access to the raw data files. These may include 3-D images (e.g. VRML files), which can be viewed using suitable free software (such as GLview), which allow the viewer to zoom, pan and rotate the model, but cannot select or remove features. ArcExplorer is a GIS tool that allows third parties to view, zoom, select, and pan on 2-D ArcGIS projects, but does not allow the viewer to edit the data, however, no 3-D equivalent is available as yet. Alternatively 3-D fly-through animations/ movies (e.g. avi files) showing both 2-D and 3-D models from various angles, at different scales, and with different layers active may be created, and sound may also be included. Animations of this type have been created for various projects and models constructed during this project are included in *appendix 6* (on CD/DVD).

### 2.4.5.3. *Publication and data archiving*

There are various options available for publication of digital map products. These include: upload onto web-based GIS database (e.g. ArcIMS) for online access (reference); submit to online mapping journals (e.g. Journal of Maps; Smith, 2005); incorporation into scientific publications. Furthermore, data archiving of both data files and associated metadata should also be undertaken. For NERC grants holders this comprises uploading files onto the National Geosciences Data Centre (NGDC).

## 2.5. **Testing the workflow**

The following chapters present three case studies (looking a basement-influenced extension in the North Atlantic) in which the GAVA workflow has been implemented in various forms. A discussion of the benefits and problems encountered when applying these digital mapping methods during these studies, and discussion of the future trends of digital mapping generally is also given.

## Chapter 2 – Digital mapping

GIS Activity	Description
Data organisation	Data collection, data acquisition and digitisation, data compilation and editing, database construction and management
Data visualisation	Interactive display and interrogation of geospatial data in 2-D and 3-D displays
Data search and data query	Interactive search for attributes or spatial location
Data integration	Combine and overlay maps in raster and vector format; generate new layers from integrated files
Data analysis	Transformations and measurements of objects on data layers to characterise and extract meaning
Data prediction for decision support	Simple or complex analysis for prediction using data driven methods; decision support based on GIS interpretation and modelling

**Table 2.1**

Core GIS activities and a brief description (after Bonham-Carter, 2000)

Mapping type	Reconnaissance	Regional	Standard*	Detailed	Specialised
<b>Map scale</b>	1:250 000 or smaller	1:100 000 to 1:50 000	1:25 000 to 1:10 000	1:10 000 or larger	Various
<b>Traditional methods</b>	Remote sensing, photogeology, blind-spot sampling	Aerial photograph analysis, traverse mapping on appropriate field slips	Contact mapping and exposure mapping on 1:10 000 field slips	Baseline mapping, planetable and cairn mapping	e.g. detailed data sampling, structural & stratigraphic logs, sub-surface mapping (e.g. mine plans)
<b>Geospatial abstraction</b>	Very high implicit in sampling strategy prior to fieldwork	High in field and also during cartography	Medium levels of abstraction in the field; captures some outcrop structure	Very little abstraction; can capture the entire outcrop	Dependent on scale of mapping.
<b>Typical wavelength of structures</b>	>10 <sup>5</sup> m	10 <sup>2</sup> - 10 <sup>5</sup> m	10 <sup>2</sup> - 10 <sup>4</sup> m	10 <sup>-3</sup> - 10 <sup>3</sup> m	Various
<b>Digital equivalents</b>	Remote sensing, digital aerial photography, GPS-referenced locality mapping	Digital elevation models, digitised maps, DGM, GPS-referenced data collection	Digital elevation models, aerial photogrammetry, digitised maps, DGM, GPS-referenced data collection	Aerial and outcrop photogrammetry, DGM, DGS, real-time kinematic GPS mapping, Laser Scanning	Photographic logs, DGM, DGS, Laser Scanning

\*this refers to normal UK practice, which corresponds to BGS standard surveying and university undergraduate projects.

**Table 2.2**

Summary table of geological mapping at various scales, traditional methods and their digital equivalents (adapted from McCaffrey et al., 2005).

## Chapter 2 – Digital mapping

Field data	Example	Traditional media	Digital alternative
Mapping on a Field slip	1:10,000 base map	Paper map	Drawing GPS located polylines* on digital topography or aerial photograph on a PDA
Metadata	Date, weather, location	Paper Notebook	Database on PDA
Observation	Grain size, texture, mineralogy, geometry,	Paper notebook	GPS located point* plus database entry on PDA
Locality	Grid reference	Paper notebook	GPS located point* plus database entry on PDA
Sketches	Outcrop interpretation	Paper notebook or art-book	Digital sketching on PDA/ tablet PC (with/ without field photograph)
Photograph	Outcrop image	Transparency, print	Digital photograph hyperlinked to locality point*
Section logging	Sedimentary log	Logging sheets	A digital logging template on PDA (with/ without field photograph)

\*i.e. shapefiles

**Table 2.3**

Typical field data types and their digital alternatives (after McCaffrey et al., 2005).

Requirements	Determining factor
Size, mobility	Proximity to mapping area, transportation, carrying capability
Weight	Physical carrying restrictions
Battery life and battery type	Operating time, cost, added weight
Processor and data storage	Amount and type of background data and data to be captured, cost
GPS accuracy	Scale of mapping, cost
Connectivity	number of peripheral devices (e.g. GPS, laser rangefinder)
Display	Readability in bright- and poor-light conditions, display size
Ruggedness	Environment (tropical/ desert), cost
Compatibility	Preferred data formats and user systems (e.g. Windows software)
Cost	Budget

**Table 2.4**

Factors to be considered when choosing the right field-mapping systems (after Edmondo, 2001)



Chapter 2 – Digital mapping

	Requirements	Mapping scenario	Spatial location device (i.e. GPS)	Computer
Accuracy	Centimetre	Detailed mapping and Survey	Survey grade DGPS, Laser scanner	Specialist mapping system, Laptop PC
	Sub-meter	Detailed and standard mapping	Backpack DGPS, Laser rangefinder	Tablet PC, PDA
	>1 meter	Regional and reconnaissance mapping	Handheld GPS	PDA
Datasets	Large data set	Advanced project, detailed mapping and specialised applications	Survey grade DGPS or Backpack DGPS, Laser scanner	Specialist mapping system, Tablet PC, Laptop PC
	Moderate dataset	Detailed and standard mapping	Handheld GPS or backpack DGPS	Tablet PC, PDA
	Small dataset	Regional and reconnaissance mapping and sampling	Handheld GPS or backpack DGPS	PDA
Battery life	Long life	Inaccessible power supply for long periods	Handheld GPS	PDA
	Moderate life	Mapping for long periods, intermittent access to power supply	Backpack DGPS, Laser rangefinder	Tablet PC, PDA
	Short life	Nearby power supply	Survey grade DGPS	Laptop PC
Weight	Heavy (weight not an issue)	Survey site, close to infrastructure	Survey grade DGPS, Laser scanner	Specialist mapping system, Laptop PC
	Moderate (weight of moderate concern)	Detailed and standard mapping	Backpack DGPS, Laser rangefinder	Tablet PC
	Light (weight of high concern)	Regional and reconnaissance mapping	Handheld GPS	PDA
Cost	>£10,000	Cost not an issue, industry research	Survey grade DGPS, Laser scanner	Specialist mapping system, Laptop PC
	£500 - £10,000	Standard mapping, reasonable funds available	Backpack DGPS, Laser rangefinder	Tablet PC
	<£500	Very tight budget, e.g. undergraduate field mapping	Handheld GPS	PDA

**Table 2.5**

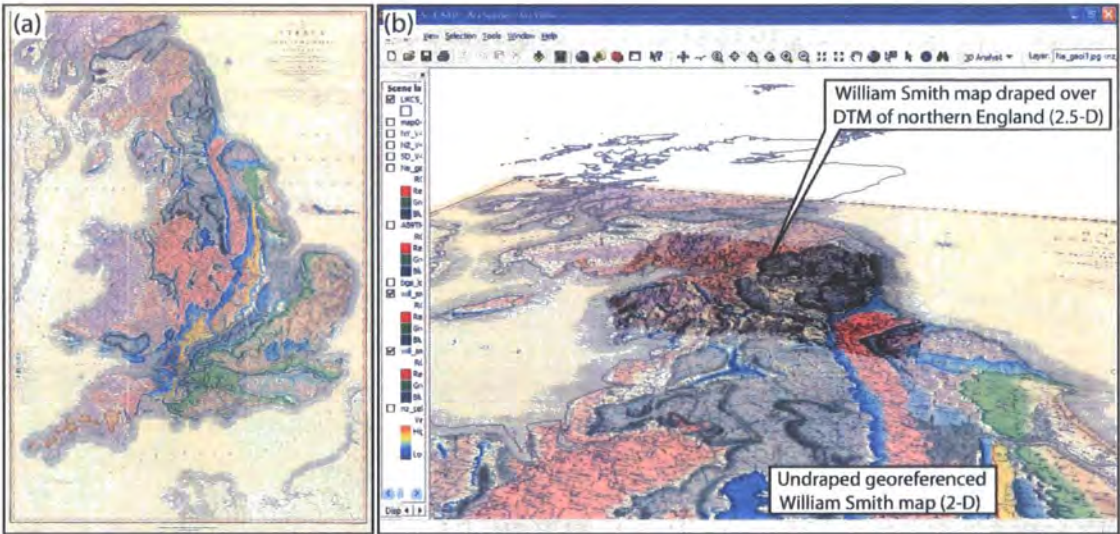
Scenarios, requirements, and hardware recommendations for digital field data-capture (after Edmondo, 2002)

	GPS units for DGM					GPS units for DGS	
	Garmin III+ handheld	Garmin Geko 201	CSI GBX PRO	Trimble Geoplotter XM	Promark 2 (roving)	Promark 2 (Survey Mode)	Trimble 5700/5800
<b>Instrument details</b>							
DGPS correction	N/A	WAAS enabled	Beacon	WAAS	WAAS	L1-carrier wave	L1 & L2 carrier wave + RTK
Real/time or post process	N/A	N/A	Real time	Real time	Real time	Post-process	Post-process
<b>Precision tests</b>							
No. of positional fixes	101	99	108	56	107	N/A	N/A
Horizontal Sd (m)	3.419	0.16	0.359	0.41	0.358	0.001*	0.001*
Vertical Sd (m)	3.778	0.74	0.683	0.48	0.517	0.003*	0.002*
PDOP during test	1.9	1.5	2.7	2.3	3.6	<4	<4
<b>Operational</b>							
Time for position	2min	2min	45s	2min	150s	c. 30 mins	c 10mins/ 1s for RTK
Bulk (size/weight)	Low	Low	Intermediate	Intermediate	Low	High	High
Accuracy	3-5m	1-3m	0.5-1m	0.5-3m	0.5-3m	1-10mm	1-10mm
Purpose	DGM > 100m scale	DGM > 10 m scale	DGM > 10 m scale	DGM > 10 m scale	DGM > 10 m scale	DGS sub-cm scale	DGS sub-cm scale
Cost	c. £200	c.£120	c. £1,800	c.£5,000	c. £4,000	c. £4,000	c. £25,000

\*after post-processing

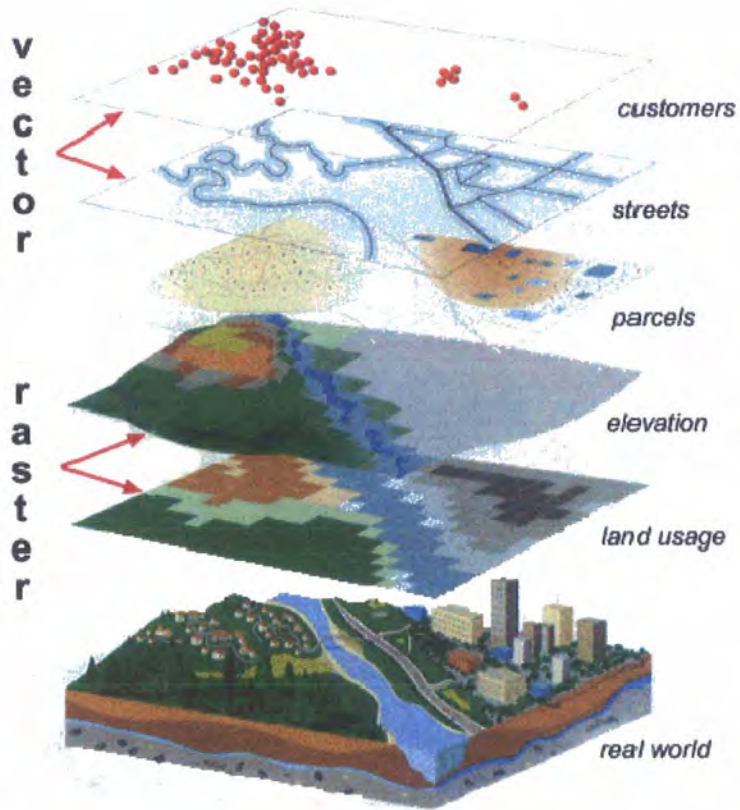
**Table 2.6**

Various GPS units, their use, calculated precision and predicted performance in the field (McCaffrey et al., 2005)

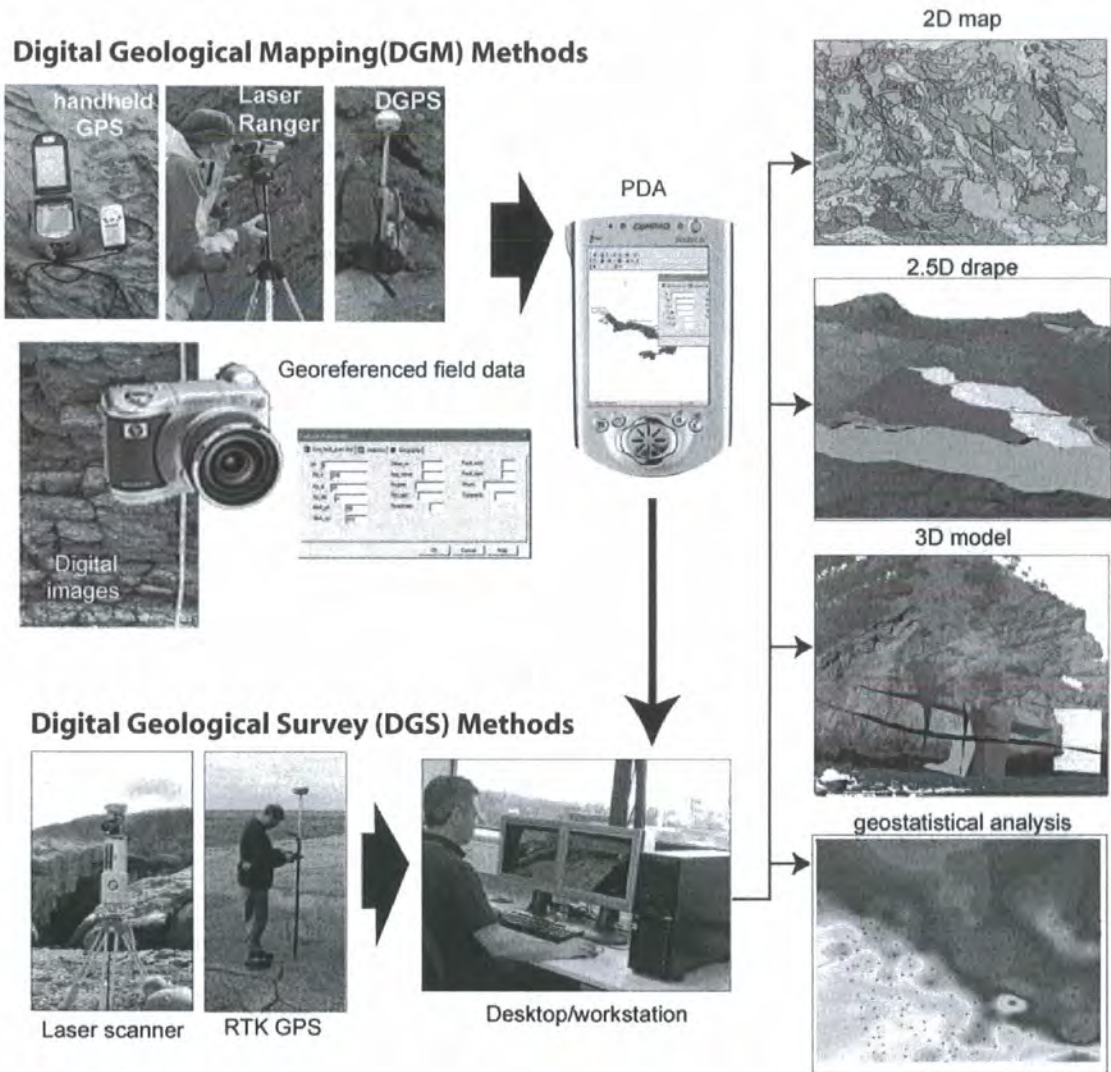


**Figure 2.1.**

(a) “The map that changed the world”, William Smith’s (1815) map of the geology (‘strata’) of England and Wales. (b) 2.5-D/ 3-D visualisation in its simplest form, ArcScene model of William Smith map draped over DEM for Northern England (also see animation 1 in *appendix 6* for a ‘fly-through’ animation of this model).

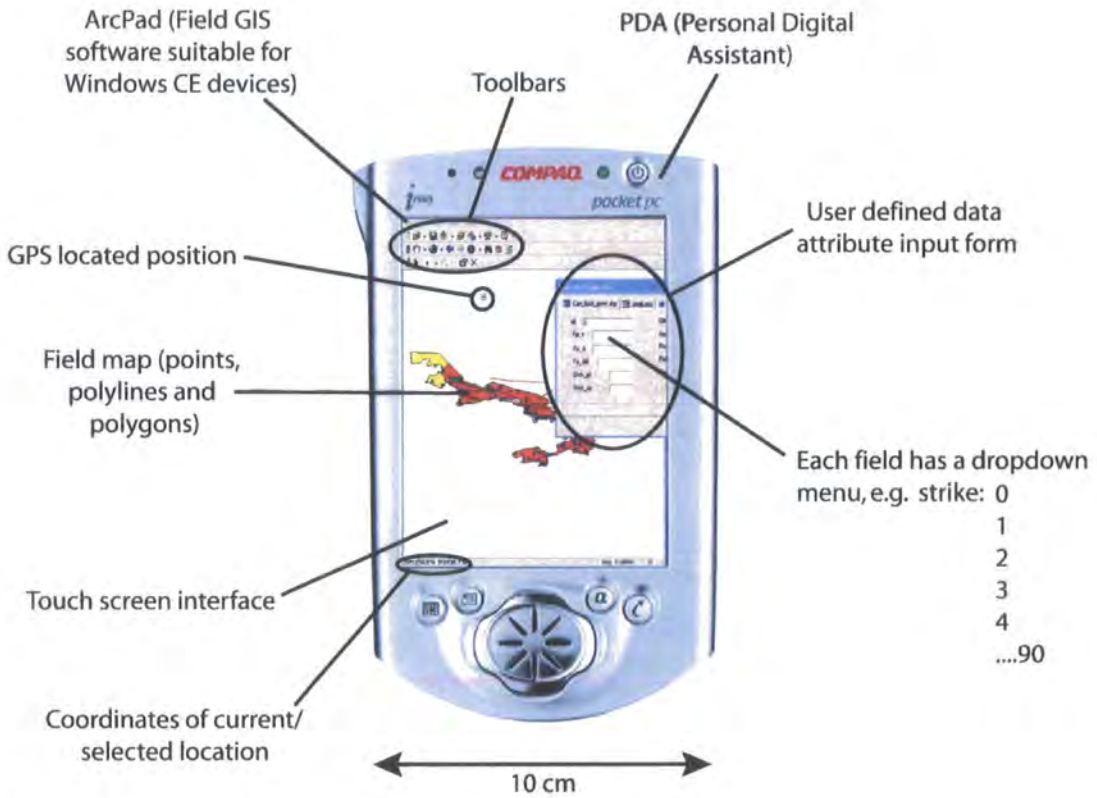


**Figure 2.2.**  
The concept of GIS layers (taken from ESRI website)



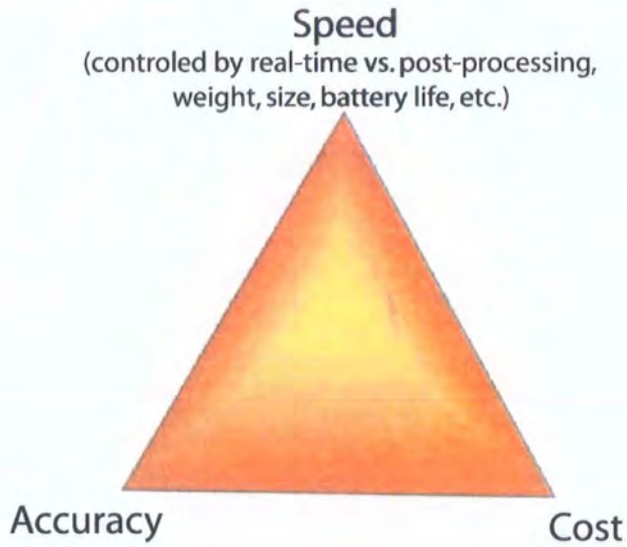
**Figure 2.3.**

Principal workflows of digital fieldwork, outlining DGM and DGS as separate entities (McCaffrey et al., 2005).

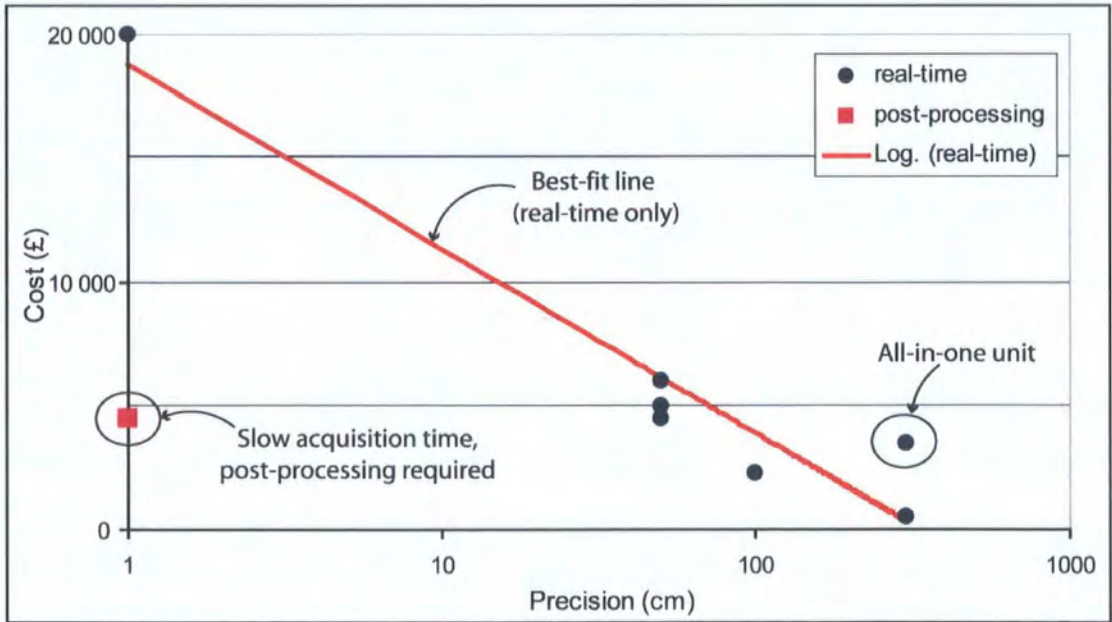


**Figure 2.4.**

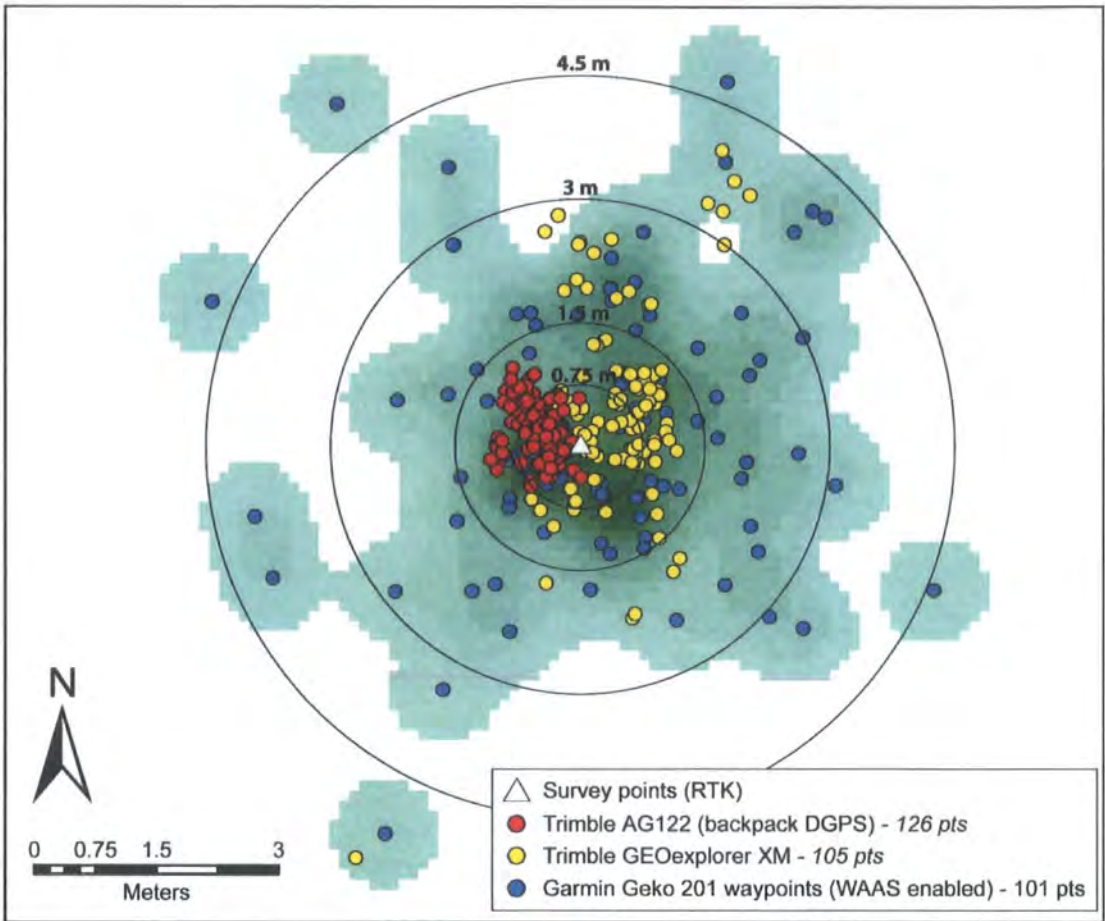
Example of field-GIS software (ArcPad™) on a PDA running Windows CE. Data attribute input forms are created prior to fieldwork using (ArcPad Application Builder), though simple versions may also be created on-the-fly in the field. Polygons are created from point and polyline data on laptop/ desktop computer at field base camp/ office.



**Figure 2.5.**  
Relationship between data accuracy, speed of data capture, and cost of digital mapping systems.



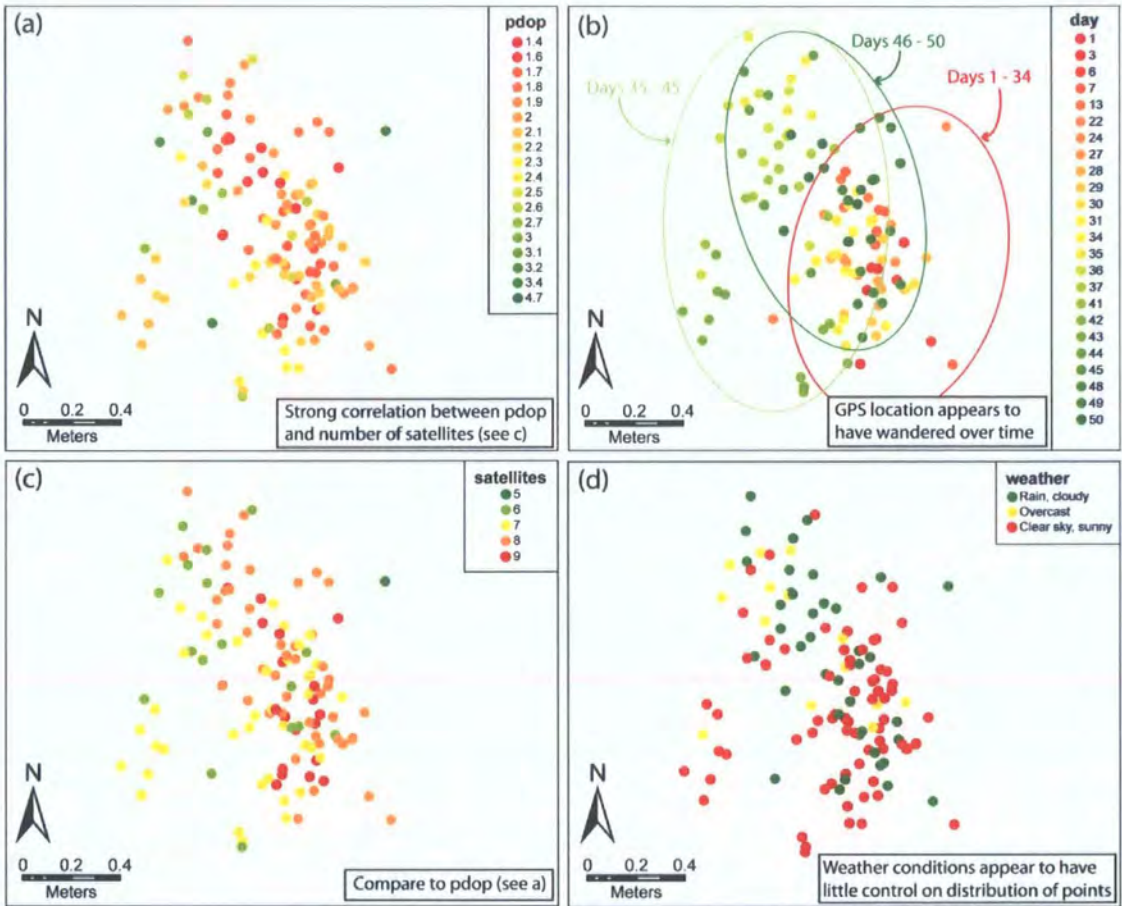
**Figure 2.6.**  
Log-linear graph showing GPS precision vs. cost (note prices cost of include PDA where appropriate).



**Figure 2.7.**

Field test of GPS repeatability (accuracy). White triangle shows survey point (surveyed using RTK DGPS). Green raster cloud show a density map for distribution of waypoints collected using Garmin Geko 201. Note, Trimble AG122 point cluster offset ~0.5 m west of survey point due to beacon receiver being mounted on right shoulder of user (i.e. not directly over survey point on which the user stands; user always facing south!). Map projection: British National Grid.





**Figure 2.8.**

Comparing metadata attributes with GPS precision. (a) Variations in pdop (Position Dilution of Precision), (b) temporal variations, (c) number of satellites, and (d) weather conditions. Data points collected using Trimble AG 122 backpack DGPS. Map projection: British National Grid.

Chapter 2 – Digital mapping

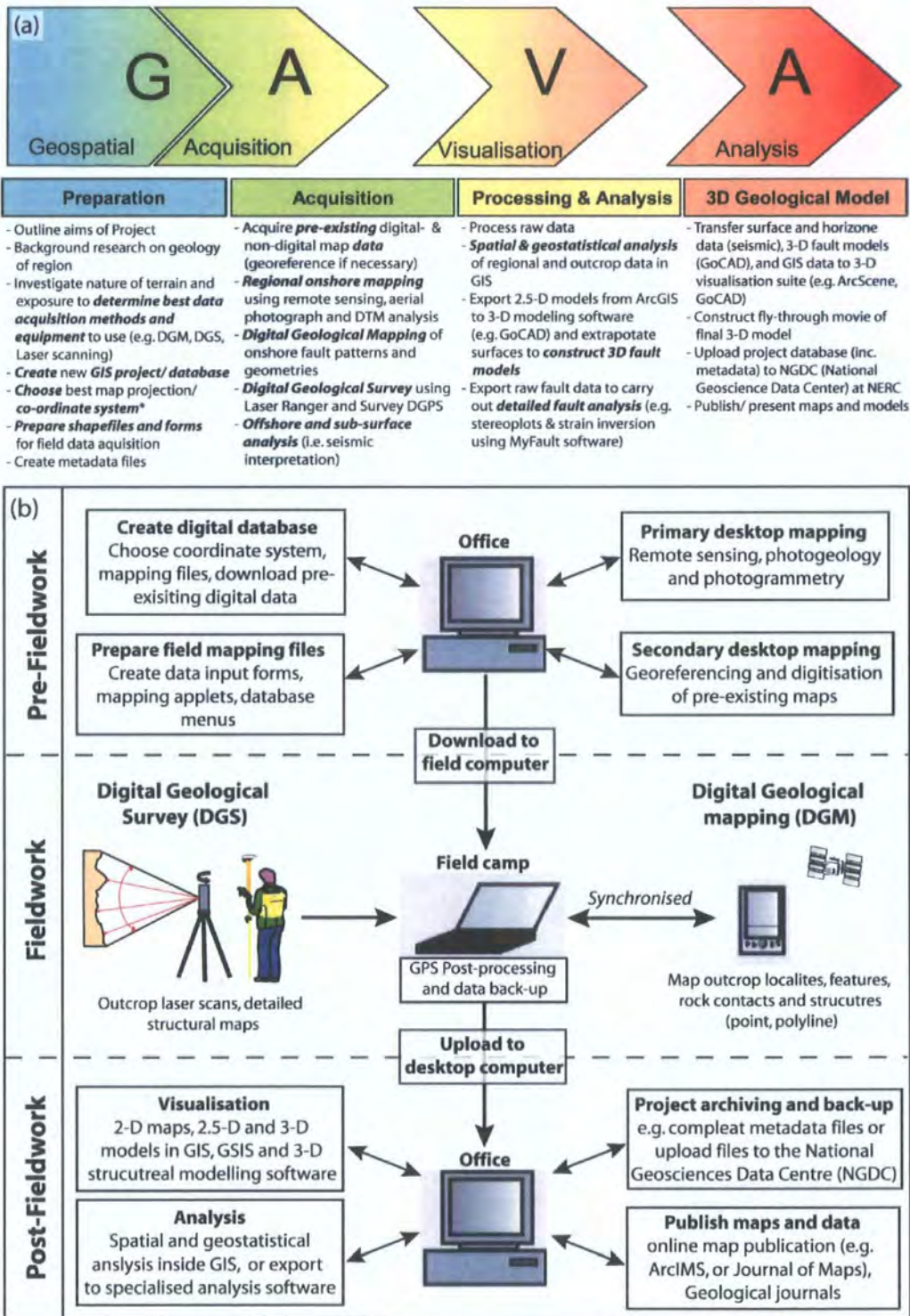
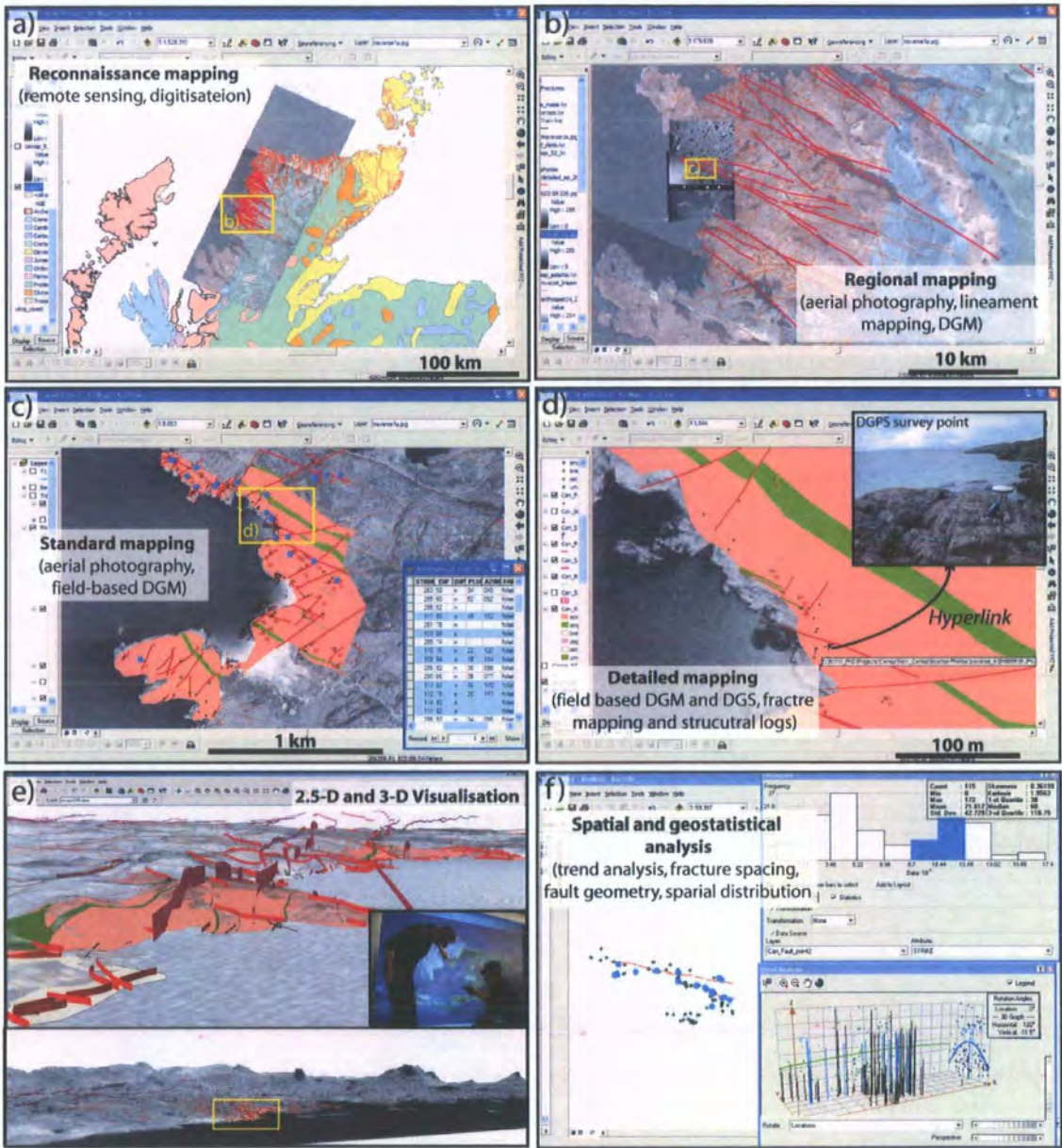


Figure 2.9.

(a) Basic summary of GAVA workflow. (b) Schematic diagram showing key stages of digital mapping and database development (modified from Jones et al., 2004).



**Figure 2.10.**

Example of a multi-scale digital dataset constructed using GAVA workflow. (a) Reconnaissance maps comprising remote sensing data and digitisation of pre-existing data. (b) Regional maps constructed from aerial photograph analysis and digital field sampling. (c) Field-based digital geological mapping and attribute collection. (d) Detailed digital field mapping using survey-grade GPS and planetable mapping methods. (e) 2-D and 3-D visualisation of digital map data. (f) Spatial and geostatistical analysis of attribute data.

### **3. Digital mapping and visualisation of brittle fault patterns along the Scottish North Coast – basement-influenced extension, and implications for the NE Atlantic Margin**

**Abstract:** The structural configuration of the northwest UK Continental Shelf is considered to have been influenced by the strongly anisotropic basement rocks that underlie the region. The North Coast of Scotland has been well cited in the past as an area of basement-influenced faulting and basin development. However recent studies have cast some doubt on these models, therefore this study presents a re-examination of the post-Caledonian structures along the north coast of Scotland and their relationship with local and regional basement structures. Regional studies show that variations in post-Caledonian fault patterns correlate with changes in basement structure. Detailed outcrop studies however, show that basement-fault reactivation is not apparent in most areas, though complex fault patterns may be a result of 3-D strain developed as a result of basement influence. Onshore – offshore fault linkage is demonstrable in the eastern part of the study area (e.g. at Strathy), however further west this is less clear. A prominent ESE-WNW trending strike-slip fault parallel to the coast can be traced onshore and appears to act as a barrier to the onshore propagation of offshore faults. This fault and the complex fault patterns developed along the north coast appear to make up a sinistral transfer zone that was active during Devonian and/or Permian-Triassic times. This transfer may also have affected later extensional tectonics in the Mesozoic and Cenozoic further offshore on the UK Continental shelf (i.e. development of Ymir Ridge).

#### **3.1. Introduction**

The present-day structural configuration of the NE Atlantic margin is considered to have been influenced by an inherited NE-trending basement grain (Stoker *et al.*, 1993). Pre-existing basement structures are well known to strongly influence the location and architecture of sedimentary basins and rift systems on passive margins (Johnson & Dingwall, 1981; Bartholomew *et al.*, 1993; Clemson *et al.*, 1997; Paton & Underhill, 2004), leading to the development of complex fault patterns, obliquely extending segments, deformation partitioning, and transfer zones (Daley *et al.*, 1989; Morley *et al.*, 1990, 2004; Nelson *et al.*, 1992; Ebinger *et al.*, 1999; De Paola *et al.*, 2005). Structural trends on the NE Atlantic margin follow two distinct trends: 1) NE-

SW; and 2) NW-SE to ESE-WNW (Fig. 3.1; see also fig. 1 of Doré *et al.* 1997), both of which are similar to structural trends in basement exposures onshore (i.e. Proterozoic and Caledonian structures respectively).

Perhaps one of the most cited areas for basement influenced extension and basin development around the British Isles is the north coast of Scotland (Brewer & Smythe, 1984; Enfield & Coward, 1987; Laubach & Marshak, 1987; Stein 1988; Coward *et al.*, 1989; Stein & Blundell, 1990; Snyder, 1990). The West Orkney Basin lies off the north coast of Sutherland and Caithness, and overlies Lewisian and Caledonian basement terranes, exposed onshore. Extensional faulting that led to the development of the basin has been linked to the apparent reactivation of Caledonian thrust faults in basement (Enfield & Coward, 1987; Coward *et al.*, 1989). Furthermore, NW-SE trending Laxfordian fabrics appear to be reactivated as cross-faults and transfer faults to these NE-SW trending extensional faults (Laubach & Marshak, 1987; Stein 1988; Coward *et al.*, 1989). However, recent studies have cast some doubt on these basement reactivation models in the West Orkney Basin and along the Scottish north coast (Beacom, 1999; Roberts & Holdsworth, 1999).

In this study we attempt to carryout a reappraise the influence of basement structures on later brittle fault patterns along the Scottish North Coast. We approach this task predominantly from an onshore perspective, looking at brittle fault patterns and structures at regional to outcrop scales. This onshore approach enables us to carryout a direct comparison between faults and pre-existing structures in basement. Onshore observations are then compared to offshore stratigraphic and fault models for the West Orkney Basin. To aid these studies, new digital mapping methodologies are applied (Jones *et al.*, 2004; McCaffrey *et al.*, 2005), thus allowing integration and analysis of multiple data types in a single GIS (Geographic Information System) project. This digital approach also allows spatial variations to be analysed using GIS-based tools. Furthermore, 3D modelling and visualisation of digital datasets is also used to help understand and interpret complex structural relationships between basement and cover at a variety of scales.

Fault patterns in both Lewisian and Caledonian basement and red-bed sedimentary infills are assessed from regional to outcrop scales. Detailed outcrop-scale studies of basement faulting for Durness (GR: 240400 967900), Skerray (265800 963900), Glaisgo (271400 963600) and Kirtomy (274200 964100) are all presented. Red-bed outliers at Coldbackie Bay (261000 960300), nr Tongue, (i.e. the

Watch Hill outlier; Holdsworth et al., 2001) and Kirtomy are also studied, as these are believed to be onshore continuations of offshore basins (Coward et al., 1989). Fault patterns in Devonian Old Red Sandstone sequences are also assessed at Portskerra (287100 966100).

## **3.2. Geological setting**

### **3.2.1. Structure of the northwest UK Continental Shelf**

Northern Scotland has a complex structural history and a tectonic framework that reflects the strong anisotropic nature of the pre-Devonian basement rocks of the area (Stoker *et al.*, 1993). These basement structures formed during Archaean/Proterozoic and Caledonian tectonism, and have exerted a significant control on basin development at many stages in the margins history. The main rift systems of the margin trend NE-SW and less dominantly N-S to NNE-SSW, parallel to Caledonian basement trends, and have subsidiary ESE-WNW to NW-SW fault systems controlled by lateral structures formed parallel to the Caledonian Thrust transport direction (Butler and Coward, 1984; Coward et al., 1987). These rift systems record multiple episodes of rifting from Devonian to Palaeocene times (Doré et al. 1997). In the shelf areas west and northwest of the UK at least 6 main phases of rifting have been described: 1) Devono-Carboniferous, 2) Permo-Triassic, 3) Middle Jurassic, 4) Late Jurassic, 5) Cretaceous, and 6) Palaeocene (Kimbell *et al.*, 2005, and references therein).

The majority of lineaments trending NW-SE to ESE-WNW appear to have acted as transfer zones within these rift systems during the evolution of the margin (Rumph *et al.*, 1993; Doré *et al.*, 1997; Kimbell *et al.*, 2005). Some have been interpreted as having a pre-Caledonian history (e.g. the Anton Dohrn Lineament in the Hatton–Rockall area, Fig. 3.1, Dickin, 1992), while others may have originated during the development of separate post-Caledonian extensional basins controlled by Caledonian trends (Rumph *et al.*, 1993). In some cases these continental lineaments/transfer zones pass laterally into oceanic transform faults, although this is not always true (Lister *et al.*, 1986).

~~A major ESE-WNW lineament off NW Scotland is the Wyville-Thomson~~  
Lineament complex (WTL; which includes the Wyville-Thomson, Ymir, Bill Bailey and other minor ridges; Fig. 3.1) which can be traced from the ocean-continent boundary to the West Orkney Basin (Kimbell *et al.*, 2005). This lineament complex

marks a major dextral offset between the North Rockall Basin and the basins to the northeast, and is believed to have acted as a transfer zone during Mesozoic and Cenozoic times (Kimbell *et al.*, 2005; Johnson *et al.*, 2005).

### 3.2.2. *The West Orkney Basin*

The West Orkney Basin lies off the Scottish North Coast and to the west of Orkney Islands (Fig. 3.2). This basin consists of a series of half-graben sub-basins formed preferentially by reactivation of easterly dipping Caledonian thrusts, such as the Outer Isles, Moine, Naver, and Swordly thrusts (Brewer & Smythe, 1984; Coward *et al.*, 1987, 1989; Snyder, 1990; Stoker *et al.*, 1993). The sub-basins contain westerly dipping sediments which form wedge-shaped packages indicative of syn-depositional tectonism (Kirton & Hitchen, 1987). The age of the sediments making up the basin is somewhat contentious, with both Devonian (Enfield & Coward, 1987; Coward *et al.*, 1989) and Permian-Triassic (Kirton & Hitchen, 1987; Stoker *et al.*, 1993) ages being assigned.

Fault patterns within the West Orkney Basin are dominantly NNE-SSW trending normal faults with associated ESE-WNW trending transfer faults (Fig. 3.2; Enfield & Coward, 1987; Coward *et al.*, 1989). Enfield & Coward (1987) used the 'bow and arrow' method to suggest that the regional extension vector, that led to the development of faults in the basin, was oriented NW-SE. Coward *et al.*, (1989) also noted that total fault throws die out rapidly to the south near the Scottish north coast, which lead to the suggestion that extension was transferred westwards to the North Minch Basin (however, further questions are raised regarding the presence of Devonian sediments in this basin also; Stein 1988).

A number of these extensional faults have been linked at depth to low angle east-dipping detachments comparable to Caledonian thrusts (Brewer & Smythe, 1984; Snyder, 1990). This led to an interpretation that the West Orkney Basin formed by reactivation and extensional collapse of Caledonian structures (Enfield & Coward, 1987; Norton *et al.*, 1987; Coward *et al.*, 1989), in fitting with the Devonian orogenic collapse models of McClay *et al.* (1986). However, this model has more recently been questioned (Roberts & Holdsworth, 1999) due to the presence of apparently thick Permian-Triassic sediments offshore (Stoker *et al.*, 1993) and also because onshore extensions of offshore faults noticeably cut basement structures at high angles in many areas (Holdsworth, 1989).

### 3.2.3. *Pre-Devonian basement structures*

'Basement' rocks of the region encompass all pre-Devonian strata and can be divided into two major basement terranes, separated by the Moine Thrust Zone (Fig. 3.2): the Lewisian-Foreland terrane (to the west) and the Caledonian terrane (to the east) (Stoker *et al.*, 1993). These two terranes show markedly different pre-Devonian tectonostratigraphic histories.

The Lewisian-Foreland terrane consists predominantly of metamorphic rocks of the Lewisian Complex locally overlain by Torridonian (Upper Proterozoic) arkosic sandstones, grits and conglomerates, and Cambro-Ordovician shelf sediments (Peach *et al.* 1907). The Lewisian Complex consists of orthogneisses, acid to ultrabasic intrusives, and metasediments, and is a residual fragment of the Laurentian-Greenland continental craton (Bridgewater *et al.*, 1973; Park and Tarney, 1987; Park, 1991). The main structural trends in the Lewisian are ESE-WNW to NW-SE, marked by the Scourie dyke suite (of early Proterozoic age) and a series Laxfordian shear zones (Fig. 3.2a; Park and Tarney, 1987; Park, 1991; Kinney *et al.*, 2005).

The Lewisian Complex is unconformably overlain by mid- to late Proterozoic Torridonian, and Cambro-Ordovician sediments; in places the latter oversteps the Torridonian to rest directly on the Lewisian. These sediments have not been subjected to any severe metamorphism or deformation, except within the Moine thrust zone. The Torridonian predominantly consists of fluvial sandstones and conglomerates, while the later Cambro-Ordovician succession comprise of shallow marine quartzites and carbonates of the Lower Cambrian Eribole Sandstones and Cambrian to Lower Ordovician Durness Group respectively (Johnstone & Mykura, 1989). These sediments are generally horizontal to sub-horizontally bedded.

The Moine thrust zone forms an important tectonic boundary separating the Lewisian Foreland and Caledonian basement terranes (Fig. 3.2). With the exception of a few Caledonian thrusts and imbricate zones, the Lewisian Foreland terrane is relatively undeformed compared to rocks in the hangingwall. East of the Moine Thrust lies the Caledonian basement terrane, part of the Appalachian-Caledonian orogenic belt (Anderton *et al.*, 1979). The Moine metasediments (Moine Supergroup), found in the hanging wall of the Moine Thrust, carry a strong *c.* N-S trending Caledonian tectonic fabric developed parallel to bedding. The fabric generally dips eastwards at about 15° close to the Moine Thrust, but steepens to near



vertical as you move eastwards (Barr et al., 1986). Further east, in Caithness and Orkney, Moine rocks are overlain by Devonian Old Red Sandstones of the Orcadian Basin (Johnstone & Mykura, 1989; Seranne, 1992; Friend et al., 2000). The eastern boundary to the Moinian rocks of the Scottish north coast is the Great Glen–Walls Boundary transcurrent fault system, which also marks a transition to the Dalradian basement units of the Grampian Highlands (Fig. 3.2).

### **3.3. Data acquisition methods**

#### **3.3.1. Digital mapping and the GIS database**

Digital mapping technologies are changing the way geologists create maps in the field. Digital field mapping tools and software can now link the field geologist to digital versions of pre-existing maps and ortho-photographs, while providing full edit, point/ line/ area creation, and data attribute recording capabilities (Kramer, 2001; Jones *et al.*, 2004; McCaffrey *et al.*, 2005). Laser range-finding devices and Global Positioning System (GPS) receivers also enable accurate and versatile tools for locating geological features in the field. These digital mapping methods form part of a new in-house mapping methodology, 'GAVA' (Geospatial Acquisition, Visualization & Analysis; Clegg *et al.*, 2005; Wilson *et al.*, 2005; McCaffrey *et al.*, 2005) which integrates field- and laboratory-based digital mapping methodologies.

In this study we compiled remote sensing and field datasets in a single GIS database using the ArcGIS™ suite (Figs. 3.3 and 3.4). The methods for acquiring each of these data formats are described in the following sections.

#### **3.3.2. Regional-scale structures**

*Regional-scale structures* in our digital database were compiled from two main sources: 1) digitization of pre-existing geological maps; and 2) new interpretations of remote sensing imagery, particularly lineament analysis. Basement fabrics and lithologies were mapped from previously published geological maps for Sutherland, Caithness and Orkney. Brittle fault structures were interpreted from satellite images using lineament mapping methods (Sabins, 1987; Gabrielsen *et al.*, 2002; Cortés *et al.*, 2003), inside ArcGIS™, at a variety of scales (1:100 000 and 1:10 000). Panchromatic Landsat and SPOT images (15m pixel resolution), and orthorectified aerial photographs (1-2m pixel resolution) covering much of the Scottish north coast. Attribute data (i.e. trend; length; offset; comments) were also recorded and stored in

the GIS database. After interpretation, lineaments were then compared to a DTM (Digital Terrain Model) and refined using GIS analysis. Particular care was taken to avoid the inclusion of basement fabrics in the lineament database. This was confirmed by studying pre-existing geological maps during lineament analysis, and was additionally checked during fieldwork.

These lineament maps were analysed using various spatial analysis tools inside ArcGIS™. These include lineament density maps (constructed by counting total line length within a moving 10km search window for each 10° lineament trend), and rose diagram maps plotted in a similar way (Fig. 3.4). Using overlay maps and selection tools in ArcGIS™ the distribution of various lineament trends could then be compared to basement rock lithologies and structures.

### **3.3.3. Outcrop-scale structures**

*Outcrop-scale structures* and data were recorded using both digital mapping and digital survey methods (see McCaffrey *et al.*, 2005) in order to build both detailed data attribute files and 3D geometric models. Digital reconnaissance mapping and data attribute collection, using a hand-held computer (HP/ Compaq Ipaq PDA) connected to a differential-GPS receiver (Trimble™ AG122), was used to collect a geological overview and detailed structural database for each locality, while a laser rangefinder (MDL LaserAce 300) was used to record detailed geometries of outcrop data in 3D (Fig. 3.3; Xu *et al.*, 2000; Wilson *et al.*, 2005). The former stores the geospatial data directly in the GIS database, while in the latter, data are recorded as a x.y.z. point-cloud which then requires post processing and conversion to linear and/or planar data using a suitable 3D modelling system (i.e. GoCAD™).

Fault attribute data were plotted on stereonet both inside ArcView™ (see stereoplotting tools of Knox-Robinson and Gardoll, 1998) for spatial analysis, and exported to other stereonet software for more quantitative geometric and kinematic analysis. My Fault™ stereonet software, produced by Pangaea Scientific Ltd., was used for kinematic analysis (i.e. palaeostress analysis), using the inversion method outlined by Michael (1984). Our procedure was to invert a population of faults from a single locality. Those faults with misfit angles greater than 45° were then rejected and the inversion procedure rerun. This process was repeated until a group of faults with a homogeneous solution was found. The rejected data were then rerun through

the program in an attempt to derive multiple 'palaeostress' vectors. A similar iterative approach has been applied by Titus *et al.* (2002).

#### **3.3.4. 3D structural models and visualisation**

As all the data collected are in a digital format they can be incorporated into geospatially correct 3D models that can be viewed at a range of scales (i.e. regional to outcrop scale).

Regional models are based predominantly on raster images (e.g. SPOT/ Landsat images, aerial photographs, and geological maps) draped over a Digital Terrain Model (DTM) for the Northern Highlands. This type of model can be easily constructed in ArcScene (ArcGIS™) and helps to visualise the overall relationship between geological structures and topography (McCaffrey *et al.*, 2003), however, such models only show features on the Earth's surface and are thus often referred to as 2.5-D representations (Longley *et al.*, 2001; Jones *et al.*, 2004), rather than true 3-D models. Therefore, 3-D structural modelling has also been carried out in GoCAD™ for both regional and outcrop scale data. Regional scale modelling follows a similar technique to that described above, i.e. 2-D structures draped over a DEM, however by using geological modelling tools such as GoCAD™ linear structures (such as faults and bedding planes) can be projected into the subsurface based on their intersection with topography (providing topographic relief is sufficient to generate a reasonable 2.5-D trace). Outcrop scale models are built using two key methods: 1) building linear and planar structures from laser ranger point cloud data, and: 2) by using attribute data (e.g. strike and dip) collected in the field to project 1-D (point) and 2-D (polyline) structures into 3-D (planes). A detailed outcrop model for Kirtomy Bay has been constructed using both these methods.

As part of the GoCAD™ project, offshore data from the West Orkney Basin (including in house reinterpretations of BIRPS, GRID and MOIST data carried out by J. Imber and R.W. England) were also incorporated in the model in an attempt to distinguish onshore and offshore relationships.

### **3.4. Regional fault analysis**

#### **3.4.1. Lineament patterns**

A total of more than 2300 lineaments were picked from Landsat and Spot images, and almost 2800 from aerial photographs, for the Northern Highlands and Scottish

North Coast respectively (Fig. 3.4). Cross-referencing with published BGS maps, and ground truthing, during fieldwork, suggest that almost all lineaments picked correspond to moderate/ steeply- dipping (i.e.  $>45^\circ$ ) brittle faults. The trends of these regional faults (lineaments) vary markedly from west to east, with the main changes appearing to correlate with variations in host rock/ basement terrane (Fig. 3.4a).

Statistical analysis of both lineament length and lineament orientation was carried out for the Lewisian Foreland and Caledonian basement terranes (Fig. 3.5). In the Lewisian Foreland terrane; three dominant lineament orientations are apparent NE-SW, E-W and ESE-WNW; while the length of lineaments varies from 167 m to 21 km with a mean length of 1912 m (Fig. 3.5a). In the Caledonian basement terrane dominant lineament trends are less clear, while lineament lengths vary from 283 m to 41 km and a mean length of 3431 m (Fig. 3.5b).

Many lineaments appear to trend parallel to basement trends in the Lewisian Foreland (i.e. ESE-WNW), of which a reasonable number appear to correspond to brittle faults (compare to BGS map sheets for Stoer, Assynt, Cape Wrath and Loch Eribol), some of which cross-cut the Moine Thrust. In the Caledonian terrane these lineaments appear far more discrete (Fig. 3.4a), though still mark zones of significant displacement, which may suggest either reactivation or strain localisation.

Similar variations in lineament pattern can be seen in lineaments derived from aerial photograph analysis, with NE-SW and ESE-WNW trends predominating in the west, and more variable trends further east (Fig. 3.4c). However, in these eastern (Caledonian) areas, a number of discrete lineament systems can be identified. One such system is an E-W trending set of lineaments, with NE-SW and ESE-WNW splay faults and secondary structures, running inland from Torrisdale Bay and south of Kirtomy (Fig. 3.4c). The orientation of secondary structures associated with this E-W system suggests an en echelon array consistent with sinistral shear. Furthermore, offsets on basement structures also suggest sinistral and/ or normal movements on associated NE-SW trending splay faults. This system may also link up with a set of ESE-WNW trending lineaments running through Skerry and offshore south of Eilean Nan Ron (Fig. 3.4c).

Another pronounced system of Caledonian hosted lineaments trend N-S to NNW-SSE, however these generally trend parallel to basement fabrics trends (i.e. at Glaisgo, Kirtomy and Strathy Point), and often these have NE-SW trending subsets, suggesting possible dextral shear (e.g. Strathy Bay Fault; Fig. 3.4c). An exception to

this is the NNW-SSE trending lineaments near Coldbackie which appear to cut low angle Caledonian structures and show little evidence lateral shear (i.e. no secondary structures).

### **3.4.2. Regional 3-D models**

3D visualisation of lineament data in conjunction with satellite images and geological map data draped over a DTM clearly highlights some of the most prominent fault zones along the north coast and their interaction with topography. For example, the E-W fault system south of Kirtomy (described above) marks a prominent valley orthogonal to basement trends, and is clearly therefore a major structure of the area. Attempts have been made to extrapolate lineaments into the subsurface, however this was only successful for a limited number of faults as topographic relief is not very high relative to lineament length in many cases (good interaction with topography is essential for this method).

Offshore data from the West Orkney Basin have also been incorporated in to these models (Fig. 3.6). These include seismic horizon maps for top basement/ lower Devonian and top middle-Devonian, plus fault sticks and surfaces for major faults. Viewing onshore and offshore structures together clearly show that there are marked contrasts in fault orientation and geometry between the two areas. Offshore faults are generally oriented NNE-SSW and dipping moderately ( $40^{\circ}$ - $60^{\circ}$ ) to the east, onshore faults on the other hand are oriented in a more N-S to NNW-SSE orientation, and dip far more steeply ( $>75^{\circ}$ ). Our regional 3D models also highlight the difficulties of linking onshore and offshore faults along the north coast

Major onshore structures such as the Moine, Naver and Swordly thrusts can potentially be identified (though in the latter case the dip of the structure is far shallower than that seen onshore) however these appear to lie west of the location predicted by simple offshore continuation of onshore structures. This implies that either the structures are non-linear (i.e. curve along strike) or are offset by unidentified structures in the near offshore. As there is a distinct lack of data in the near offshore, it is unclear which of these solutions is more likely.

### 3.5. Outcrop scale structural analysis

#### 3.5.1. Kirtomy Bay

Kirtomy Bay is a prominent sedimentary (red bed) outlier surrounded by sub-vertical Moine basement rocks. The overall geometry of this outlier is one of a sedimentary half-graben (Enfield and Coward, 1987; Coward *et al.*, 1989) with a NNW-SSE bounding fault at the basin's western margin (Fig. 3.7). The basement fabric of the underlying basement is dominated by NNW-SSE trending sub-vertical mylonites and blastomylonites, showing sub-horizontal dextral shear fabrics. Brittle (dextral strike-slip) faults appear to reactivate these basement fabrics (Figs. 3.8 and 3.9a), with small (2-5 mm wide) cataclastic shear bands and fracture zones trending parallel to ductile basement structures. The bounding fault of the basin appears to be one such basement reactivated fault (Fig. 3.7). A second system of faults and fractures, oriented ENE-WSW, also cut these basement fabrics at high angles (Figs. 3.7b and 3.8).

Exposures of breccio-conglomerate can be found directly adjacent to the basin-bounding fault, unconformably overlying basement rocks in its hangingwall (Figs. 3.7b and 3.9a). Clasts within the breccio-conglomerate vary in size from ~2 m to 2-3 cm, and show well rounded to sub-angular shape. Lithologically the clasts appear to be derived from Moine basement rocks of both local and more distant exposures. As with the sediments of the overall basin these conglomeritic rocks have a distinct red colour, indicating sub-aerial deposition, in possibly an alluvial system. The presence of a series of medium grained (2-5 mm) deep red arkosic sandstone units (e.g. Fig. 3.9c) within the sequence of deposits suggests that input of material may have been episodic or pulsed. Imbrication of clasts suggests transport from the SW (though as the exposure was within a few meters of the fault scarp, this may not indicate anything about the regional transport direction). Further away from the basin margin sediments become finer and more sandstone (arkosic arenite) dominated. The geometry (strike and dip) of bedding also changes away from the basin margin (Figs. 3.7c-d), with the strike of the beds changing from margin parallel (NNW-SSE) to NE-SW, a shallowing of dip is also apparent. Intra-basin sandstone units appear relatively unstructured, with alternating units appearing to vary only in degree of cementation.

Movement indicators (i.e. slickenlines) could not be identified on the main bounding fault; however a number of fault patterns within its hanging wall may be

used to infer the overall movement and kinematics of the fault. ENE-WSW trending faults form a small graben in the hanging wall of the NNW-SSE bounding fault (Fig. 3.7). Basin margin conglomerate appears also to infill this graben (Figs. 3.7b, d), and breccio-conglomerate can also be seen infilling faults and fractures in basement (Fig. 3.9b). Kinematic indicators on these ENE-WSW faults suggest dip-slip normal movements. Furthermore, a complex system of faults and fractures cut the conglomerates units adjacent to the basin-bounding fault. These faults resemble a flower structure in appearance (Fig. 3.9c), dominated by a sub-vertical NNW-SSE trending fault (i.e. sub-parallel to the bounding fault). Slip movements on faults associated with this structure show a mixture of dip-slip normal and dextral oblique- and strike-slip (Fig. 3.9c-e). These all suggest a dextral-oblique movement sense on the master fault (also identified by Coward et al., 1989).

Faults away from the basin margin (i.e. in the intra-basin sandstone sequences) appear fewer, and far less complex. Dominant fault trends within the basin are ENE-WSW, with NNW-SSE subsets, and generally show normal oblique-slip and dextral oblique-/ strike-slip movements respectively (Figs. 3.8 and 3.9f-h).

#### *3.5.1.1. Structure of Kirtomy bay micro-basin from 3-D models*

A detailed 3-D model of the Kirtomy Bay basin has been created in GoCAD from aerial photographs, detailed DEM's (~5m resolution), digital field data, and laser ranger outcrop data. These clearly show that the overall structure of the basin is a sediment filled half-graben, bound by a steep basement fault (Fig. 3.7d).

Fault surfaces and bedding planes have been constructed from x.y.z. point data (recorded using a laser ranger and DGPS) using structural modelling tools in GoCAD™ (Fig. 3.7e). The accuracy and geometry of these surfaces has been confirmed and further constrained by incorporating outcrop data (i.e. bedding of fault measurements) into the model (Fig. 3.7f). Field measurements appear to correspond well with structures mapped in using Laser ranger techniques. The resultant bedding plane models clearly highlight a distinct hangingwall syncline plunging moderately to the west-northwest (Fig. 3.7d). Hanging wall synclines have been modelled in the past as a result of continued drag on the bounding fault, though this effect may also be a result of differential compaction within the basin (Thompson and Underhill, 1993). The former of these two explanations would also be consistent with the observed dextral shear along the bounding fault, and is therefore favored.

Also apparent from 3-D models is the onlapping of intra-basin sandstones on to the steeply dipping breccio-conglomerate adjacent to the fault scarp. This would suggest that initially, sediment input into the basin was slower than fault movement at the margin. This may explain why the conglomerates appear far more fractured than the sandstone units.

### **3.5.2. *Glaisgo***

Basement fabrics at Glaisgo are sub-vertical bands of orthogneiss, trending NW-SE (Fig. 3.8). Fault patterns in this area fall into two main categories. The first are a system of major NE-SW trending faults, which correspond to the system of splay faults off the E-W trending lineament observed in aerial photograph analysis. These faults exhibit both sinistral strike-slip and normal dip-slip movements; however the latter appear to be dominant and also more recent movements (Fig. 3.10a). The scale of these faults appears to be in the order of 10's to 100's of meters in length (traceable in aerial photographs and to a lesser extent in the field), and show possible displacements in the order of meters – dm (however marker units are uncertain).

At the outcrop scale a second system of faults and fractures is apparent which are shown in Figure 3.10b. These second order faults and fractures are classified as such because their length and movement are only in the order of meters/ cm respectively. As Figures 3.8 and 3.10b show, two dominant fault orientations at Glaisgo trending NNE-SSW and ENE-WSW, which appear to be a conjugate set exhibiting dextral and sinistral movements respectively. A system of tensile fractures filled with calcite which range in orientation from NNE-SSW to ENE-WSW, however mean trend is NE-SW (Fig. 3.10b), consistent with normal fault trends. Both major and minor faults at Glaisgo are therefore indicative of NW-SE extension (sub-parallel to basement fabric); however, minor faults also suggest a wrench system (i.e. intermediate principal stress is vertical).

### **3.5.3. *Coldbackie (Watch Hill)***

Coldbackie Bay, like Kirtomy, is a red bed outlier bound to the west by a faulted half graben structure, overlying Moine basement (Fig. 3.11a). As extensive mapping of the area has recently been carried out by Holdsworth et al. (1997; 2001) and, given the lack of extensive exposure inland, studies here concentrated predominantly on the nature of the basement cover interface and kinematics of faulting in the area.



Therefore field mapping was limited to the well exposed coastal areas in Coldbackie Bay, and with only limited study of inland areas.

The basin bounding fault (Watch Hill Fault) is exposed about half way up Cnoc na Fhreicheadain (Watch Hill; GR: 261100 959800), however, no kinematic indicators are apparent as the surface is covered by a thick layer of well cemented-breccia (Fig. 3.11b). This breccia layer does not bear any structures that suggest it is a fault-breccia, and a number of large elongate lithoclasts can be seen lying parallel to the fault scarp (inset Fig. 3.11b), thus suggesting gravity may have controlled their deposition. Therefore a possible origin for this breccia layer is that of a scree deposit along an exposed scarp.

The basement rocks in this area are predominantly Moine mylonites, though reworked Lewisian exposures can also be found, that dip shallowly ( $<30^\circ$ ) to the SE. Faults and fractures cutting these basement rocks are generally NW-SE trending, east dipping normal faults (Figs. 3.8 and 3.11c, d), though some strike-slip movements are also apparent. Some of these faults appear to form small half-graben structures, which are infilled by sub-horizontal conglomerate layers (Fig. 3.11e, f). Unlike the conglomerates at Kirtomy, these deposits show virtually no sign of deformation (e.g. faults and fractures). Basement exposures also show evidence for low-angle, late Caledonian brittle faults and fold structures. These have been attributed to late Caledonian extensional detachments (Holdsworth et al., 2001), and thus care was taken not to confuse the kinematic indicators of these structures with those of steep brittle faults of the area.

#### **3.5.4. Durness**

The basement rocks exposed at Durness show the most varied structure of all the localities studied as they comprise four different units: Lewisian Basement, Moine Supergroup, Torridonian sandstones, and Cambro-Ordovician sediments. The oldest rocks are Laxfordian migmatic, mafic and acid gneisses of the Lewisian basement (Watson, 1983). A pervasive steeply dipping foliation striking NW-SE dominates these rocks, while abundant pegmatite veining can be seen running parallel to and cross-cutting these fabrics. Mylonitised Lewisian and Moine rocks are also exposed in the Durness region in Caledonian inliers at Faraid Head and Sango Bay, fabrics in these units generally dip moderately ( $30-50^\circ$ ) towards the east and southeast.

Torridonian and Cambro-Ordovician sequences are generally sub-horizontal to shallowly dipping units.

Lewisian hosted faults and fractures trend NE-SW, NW-SE, and to a lesser extent N-S (see Loch Uamh Dhadaid and Sangobeg faults in Fig. 3.8). NE-SW faults show strike-slip/ oblique-slip slickenlines, post-dated by dip-slip slickenlines development. NW-SE faults also show this apparent strike-slip post-dated by dip-slip relationship. Faults hosted by Moine and reworked Lewisian basement rocks on Faraid Head and in Sango Bay inliers (Fig. 3.8) generally trend N-S to NE-SW and ESE-WNW (e.g. Figs. 3.12d, e). Movements recorded on NE-SW trending faults are dominantly dip-slip extension, while on ESW-WSW faults both strike-slip and dip-slip slickenlines were observed. Faults and fractures cutting Cambrian quartzites and piperock (Eribole formation) generally trend NE-SW, and show dip-slip extensional movements (recorded at Sango Bay and Sangobeg, Figs. 3.8 and 3.12b). While the Durness limestone contains NE-SW and ESE-WNW trending faults and fractures (Smoo Cave, Fig. 3.8).

Major NE-SW and ESE-WNW trending fault scarps showing evidence for significant extensional displacements can be found at the eastern end of Sango Bay (Sango Bay Fault; GR. 241050 967500) and Creag Thairbhe (Faraid Head fault; GR. 240550 968540) respectively (Figs. 3.12a-d). Collectively these and associated extensional faults (e.g. Fig. 3.12e) have led to the down-throwing of rocks of the Moine thrust zone in the Durness and Faraid Head inliers (Beacom 1999).

Faulting in all units is characterised by red-orange haematite staining, brecciation and evidence for calcite veining. However a number of faults also show evidence for clastic sediment infill (Figs. 3.12c, d). Infill consists of poorly sorted angular to sub-rounded clasts of mylonitised and unmylonitised gneiss (characteristic of Moine and Lewisian basement rocks), clasts of Torridonian and Cambrian sandstones, and angular clasts of Durness limestone, supported in an Fe-oxide rich matrix of calcite and quartz. Patterns within the matrix of the breccia suggest that fluids mobilised the sediment prior to lithification. These sedimentary breccias are veined by calcite and cut by younger fractures showing dip-slip slickenfibers. The fault scarps of both the Sango Bay and Faraid Head faults show good examples of sediment breccia infill (Fig. 3.12d). Furthermore, infill on the Faraid Head Fault suggests more than one infill event as sediments can be seen to infill fractures cutting earlier infill material.

On the east side of Faraid Head (GR. 239279 970667) a small (~1m wide) lamprophyre dyke appears to have intruded along a pre-existing NW-SE trending fault (Fig. 3.12f). The pre-existing fault adjacent to the dyke margin shows evidence for strike-slip movements, while calcite-filled fractures cutting the dyke also trending NW-SE show both strike-slip and dip slip movements.

### **3.5.5. *Fault geometries and kinematics***

During fieldwork, over 900 mesoscale (cm-dm scale) faults and fractures, and associated slip-striae have been recorded. Figure 3.8 shows stereoplots of faults and associated slickenlines for each field locality. Fault orientations identified at outcrop appear to be in agreement with those interpreted from lineament analysis (compare Figs. 3.5 and 3.8), however no simple systematic patterns seems to be apparent based on either location or host rock lithology. The dominant fault orientation appears to be NNE-SSW to NE-SW in Durness, and to a lesser extent Glaisgo and Kirtomy, while Coldbackie is dominated by NW-SE oriented faults, and Skerray and Portskerra show predominantly ENE-WSW oriented faults (Fig. 3.8). Furthermore, with the exception of Kirtomy Bay (where reactivation of basement is clearly identified), there appears to be little correlation between dominant fault orientation and the geometry of basement structures and fabrics (Fig. 3.8), at least in terms of reactivation.

#### **3.5.5.1. *Kinematic analysis***

Kinematic analysis (i.e. palaeostress inversion) was carried out on fault populations from each mapping locality, the results of which are presented in Figure 3.13 (and also *appendix 4*). Although fault patterns and geometries appear to vary at each locality, the apparent stress tensors for each appear far more consistent. Fault populations for each locality all reveal an ENE-WSW to NW-SE tensile stress tensor, with in some cases an added component of NE-SW compressive stress (e.g. Glaisgo; Fig. 3.13). The only exception to this is the fault population collected at Coldbackie Bay, which fit a NE-SW extension direction. These palaeostress results are all in fitting with the more qualitative analysis for the development of faults at each locality, as described above.

## **3.6. Discussion**

### **3.6.1. *Fault patterns vs. Basement trends***

As Figure 3.4 shows, brittle fault patterns vary markedly along the Scottish North Coast. West of the Moine Thrust (i.e. Lewisian Foreland) fault patterns are dominated by NE-SW and ESE-WNW trends, while to the east (i.e. Caledonian basement) structural trends appear more variable; though east of Strathy N-S trends appear to dominate (Fig. 3.4).

#### *3.6.1.1. Fault patterns in Lewisian Foreland*

Laubach & Marshak (1987) previously mapped the onshore fault patterns west of the Moine Thrust and defined a similar system of faults to those of this study; i.e. a dominant set of NE-SW-trending, NW-dipping faults, and an orthogonal set of NW-SE to ESE-WNW trending faults. The authors suggested that these fault sets developed during a single phase of deformation and that the latter formed in the hanging wall of the NE-SW sets in order to accommodate differential extension along these faults. However, Beacom (1999) highlights the fact that although in the Durness area NW-SE faults appear to terminate against NE-SW faults, further west in Cape Wrath the reverse appears true. This mutual cross cutting relationship between fault sets and the mixture of both strike-slip and dip-slip faulting on both systems suggest that a more complex relationship is likely.

Multimodal fault patterns and mutually cross-cutting relationships are a likely consequence of 3-D strain (Reches, 1983; Nieto-Samaniego and Alaniz-Alvarez, 1997; Healy et al., 2005). Similar 3-D strain patterns have been observed in other areas of the Lewisian Foreland (Gairloch and Clachtoll; Beacom et al., 1999; Gruinard Bay; Healy et al., 2005), although different ages are assigned in each case (Torridonian and Triassic respectively).

Beacom (1999) observed that the fault systems recognised in Durness and Cape Wrath are comparable to the extensional fault configurations defined by Etheridge (1986) and Destro (1995). Etheridge (1986) suggested that normal faults and transfer faults form in most extensional systems and that the geometric interaction of these structures often results in complex fault systems. Destro (1995) made a further distinction, recognising two different types of cross-faults that link extensional fault systems: transfer faults and release faults. Transfer faults connect distinct normal faults and fault zones and predominantly show sub-horizontal displacements. Release faults on the other hand are associated with individual normal faults, and are a necessary requirement to accommodate varying vertical

displacements along the fault. Release faults form in the hangingwall of major normal faults and generally have oblique-slip movements sub-orthogonal to the major fault. Beacom (1999) noted that NE-SW faults terminated against a major ESE-WNW fault at Port Odhar (Cape Wrath) and suggested that this fault acted as a transfer fault that was subsequently reactivated as a release fault (i.e. strike-slip followed by dip-slip movements). The Faraid Head fault is believed to be a continuation of this same fault (Fig. 3.14). In the Durness area, NE-SW faults appear to be the major fault set, with ESE-WNW trending release faults forming in the hangingwall of these structures, as observed by Laubach & Marshak (1987). However such models do not explain the apparent strike-slip movements on all faults (only ESE-WNW transfer faults).

An alternative to the release fault and transfer fault scenarios described by Beacom (1999) is that deformation is transtensional, and a combination of both wrench- and extension- dominated transtension is present (Dewey, 2002; De Paola et al., 2005). Lewisian basement fabrics have a NW-SE to ESE-WNW preferred fabric orientation. This basement anisotropy is therefore sub-parallel to the regional extension direction calculated from palaeostress analysis (Fig. 3.13) and inferred from offshore fault patterns (Coward et al., 1989). Therefore if the faults in this area formed due to basement controlled transtension, structures should appear wrench dominated (Dewey, 2002; De Paola et al., 2005). However, once faults are established, and levels of finite strain are high enough, a change from wrench dominated to extension dominated deformation (i.e. switching of y and z axis) is predicted (Tikoff and Teyssier, 1994). This would explain why we appear to see dip-slip movements post-dating strike-slip and oblique-slip movements on most faults.

#### *3.6.1.2. Fault patterns in Caledonian basement*

The fault patterns east of the Moine Thrust appear somewhat varied compared to those in the west. ESE-WNW trending structures appear far more discrete east of the Moine Thrust (i.e. less dominant, only a few major faults; Fig. 3.4a), though a number of major regional faults can be recognised (e.g. the Loch Shin Fault). A prominent ESE-WNW to E-W trending fault can also be traced onshore through Bettyhill on the north coast, and appears to exhibit sinistral strike-slip movements (Fig. 3.14). c. N-S trending faults appear to vary in trend from NNW-SSE to N-S across the region, and a number of which correspond to sediment filled half-grabens

(e.g. at Coldbackie, Kirtomy and Strathy). Fault movements on the basin bounding fault at Kirtomy (and possibly also Strathy) appear to correspond to outcrop-scale dextral-transension (i.e. a combination of both strike-slip and normal faults) due to the oblique reactivation of basement anisotropy. Within the basin (away from the margin) far more simple NE-SW normal faults are apparent. A WNW-plunging hangingwall syncline, fold axis oblique to bounding fault, can be seen in 3-D models of the kirtomy micro-basin (Fig. 3.7); however the origins of this hangingwall syncline are unclear. Fold closure would be consistent with the dextral shear structures observed along the basin-bounding fault, and folds of this type are common in transtensional systems (Schreurs and Colletta, 1998; De Paola et al., 2005b), however, formation due to inversion events documented further east in mid-Devonian strata in Caithness (Coward et al., 1989; Serrane 1992) cannot be ruled out.

The fault patterns and kinematics observed at Coldbackie appear at odds with those at each of the other localities. This would suggest that these structures either: (a) developed during a separate geological event, (b) reflect a localised variation in the regional stress, or (c) have undergone subsequent deformation after their development (e.g. later rotation of the faults). There is little evidence to suggest the latter, which therefore implies either an age difference, or stress variations are the cause.

### *3.6.1.3. Reactivation of basement structures onshore*

Basement reactivation onshore along the Scottish north coast appears far less prevalent than is suggested by the literature for offshore models (e.g. Brewer and Smythe, 1984; Enfield and Coward, 1987; Coward et al., 1989; Snyder, 1990). With the exception of the bounding fault of the Kirtomy Bay micro-basin (Figs. 3.7 and 3.9), very little evidence for basement reactivation can be observed in the areas and outcrops studied.

Basement reactivation is highly apparent at Kirtomy Bay, though only in the vicinity of the basin bounding fault. The basement rocks at Kirtomy (in the hangingwall of the Swordly Thrust; Burns et al., 2004) appear to have a unique character within the Moine group in that they exhibit steeply dipping dextral shear structures (including asymmetric boudins and cm-scale kink-bands), which appear out of character with the general SE-NW compressional structures of the



Calidonides. This suggests that this area may have undergone localised ductile reactivation late in the Caledonian Orogeny, or alternatively marks a zone of complexity within the compressional system. This irregularity of basement structures in the Kirtomy area may be the reason basement reactivation is apparent at Kirtomy, but not in much of the rest of the Caledonian sequences.

Around Glaisgo (and west of Kirtomy) basement fabrics appear to trend in a NW-SE orientation, which is sub-parallel to the inferred regional extension (Coward et al., 1989; and this study). In this area faults and fractures appear to cut these basement fabrics at high angles (Fig. 3.10), and no evidence for basement reactivation can be seen.

Although faults appear to strike sub-parallel to basement trends in the Coldbackie Bay area, this concordance is purely based on similarity of trend. Steep brittle faults clearly cross-cut more moderately dipping Moine basement fabrics, and this appears true for most faults in the Tongue area (Holdsworth, 1989).

In the Durness region both Laubach and Marshak (1987) and Beacom (1999) suggest that although NE-SW trending faults lie parallel to Caledonian trends, basement reactivation is not apparent. However, Hippler and Knipe (1990) suggest that the pre-existing grain and sub-grain fabrics in mylonitised Cambrian quartzites of the Sango Bay outlier appear to influence fracture location during cataclasis. Beacom (1999) proposed that the lack of reactivation of Lewisian fabrics may be a consequence of widespread pegmatite veining in the area.

Later reactivation of faults at Durness however cannot be ruled out. Fault offsets inferred from the variations in rock type within the footwall and hangingwall of faults at Durness suggest that total displacements on these faults was relatively high (i.e. > 1km). As this offset cannot now be seen this suggests that significant erosion of the footwall blocks must have taken place since displacement. However, sediment infill has also been observed along these same faults (Fig. 3.12; Beacom 1999), which suggests that faulting took place at or near the surface. Therefore either active erosion was occurring during faulting, and infill marks the last stages of this deformation, or sediments infill marks renewed activity on faults after erosion of the footwall blocks.

### ***3.6.2. Age relationships of sediments and structures***

#### ***3.6.2.1. Faults in Lewisian Foreland***

ESE-WNW and NE-SW faults at Durness have mutually cross-cutting relationships at both outcrop and regional scale. Furthermore, fault characteristics (e.g. infill, fault rock, veining, etc) and kinematics are comparable on each system, thus suggesting faults were active contemporaneously. Both ESE-WNW and NE-SW faults clearly breach Caledonian structures (inc. Moine thrust) resulting in the downthrow, and current location of, Caledonian basement outliers at Faraid Head and Sango Bay. This proves a post-Caledonian age for these faults (Hippler and Knipe, 1990; Beacom 1999), however further age constraints are difficult to establish. Sediment infill along both ESE-WNW and NE-SW faults at Faraid Head and Sango Bay (Figs. 3.12c, d) have a distinctive red colour that resembles ORS deposits further east, which may suggest a Devonian age for faults. Mesozoic ages have also been suggested based on correlations with offshore faults in the Minch and Outer Isles Basins (Steel and Wilson, 1975; Laubach and Marshak, 1987; Stein, 1989).

The lamprophyre dyke observed to have intruded along a pre-existing NW-SE trending fault on Faraid Head is highly fractured by calcite filled veins running parallel to the dyke trend (Fig. 3.12f). Faults and fractures cutting the dyke show evidence for both strike-slip and dip-slip normal fault movements. Both calcite veining and normal faults predict an extension direction consistent with that predicted by dyke opening, and thus may suggest that this phase of deformation was coincident with emplacement. Due to the highly fractured and fluidised nature of the dyke exposure, dating has not been attempted on samples taken from the outcrop. However, two phases of lamprophyre dyke emplacement have been identified from past studies in the Northern Highlands (Speight and Mitchell, 1979). Canning et al. (1998) describe an extensive suite of late Caledonian lamprophyre dykes injected during a pulse of post-orogenic magmatism dated at  $400 \pm 10$  Ma (Rock et al., 1988), spanning from the Northern Highlands down and as far as the Lake District in Northern England. Emplacement of these dykes has been linked also to sinistral transtension along the Southern Uplands, Highland Boundary and Great Glen Faults (Soper and Woodcock, 2003). An extensive suite of Permo-Carboniferous lamprophyre dykes is also well documented for much of the Northern Highlands and Orkney (Speight and Mitchell, 1979; Rock, 1983; Baxter and Mitchell, 1984; Baxter, 1987). Baxter and Mitchell (1984) reported late Permian ages ( $249-268 \pm 4$  Ma) for dykes east of Tongue. Due to its altered state, it is unclear to which suite of dykes the Faraid Head Lamprophyre is likely to be associated. However, as the dyke appears to



exploit a pre-existing fault that also cuts Caledonian basement fabrics, the age of the fault may therefore be described as post-Caledonian and pre-Permian, therefore placing it in the Devonian or early Permian age bracket.

#### *3.6.2.2. Faulting in Caledonian basement*

From lineament analysis and regional geology maps in the area around Bettyhill, Glaisgo and Kirtomy it appears that a major sinistral strike-slip fault runs onshore in a *c.* E-W orientation, and that the surrounding faults (including the NNW-SSE trending Kirtomy fault and NE-SW trending normal faults at Glaisgo) are all associated with this system (Fig. 3.14). Furthermore, kinematic analysis at various localities suggests that most faults are consistent with a regional NW-SE extension direction (see also palaeostress plots in Fig. 3.13), thus suggesting these faults may all be contemporaneous. The only exception to this are faults at Coldbackie/ Watch Hill which indicate a NE-SW extension direction (Fig. 3.13). This may suggest that faulting at Coldbackie is of a different age to these other systems, or alternatively that these faults have been rotated due to continued sinistral shear along ESE-WNW and E-W faults to the north. There is little field evidence to support this latter scenario, and therefore it is unlikely.

The age of the red bed outliers near Tongue (which includes the Coldbackie/ Watch Hill outlier) and Kirtomy are of some debate in the literature. Some works favour a Permo-Triassic age (McIntyre et al., 1956; Johnstone and Mykura, 1989; Carter et al., 1995), whilst others prefer an older Devonian (Old Red Sandstone, ORS) age (Geikie, 1878; Crampton and Curruthers, 1914; Blackbourn, 1981a, b; O'Reilly, 1983). Detailed discussions of the evidence for and against these hypotheses are given in Blackbourn (1981a, b), O'Reilly (1983), Johnstone and Mykura (1989) and Holdsworth et al. (2001). Most onshore indicators appear to favour a Devonian (ORS) age for the outliers (Holdsworth et al., 2001). This is based on the fact that these outliers are very similar in facies, colour and tectonic style to ORS deposits further east near the margin of the Orcadian Basin (Caithness and Orkney, Fig. 3.2). Sediments at Kirtomy strongly resemble those seen in the Devonian basin sediments east of Strathy (Fig. 3.14; Johnstone and Mykura, 1989), both in lithology and basin geometry, which suggests that these are of similar age. Furthermore, similar fining up sequences to those seen Lower and Middle ORS deposits from much of the Northern Highlands (Read et al., 1925) have been

identified at Coldbackie/ Watch Hill (Blackbourn, 1981b); however, much of this evidence is somewhat inconclusive.

The only absolute ages that have been acquired (using fission-track analysis of zircons and apatites collected from the Watch Hill outlier) for these outliers support a Permian-Triassic age (Carter et al., 1995). Therefore, assuming no resetting of the systems after deposition, the results of fission-track analysis (favouring Permian-Triassic sediments) appear at odds with bulk of the more qualitative geological evidence (which suggest Devonian ORS). A possible explanation for this may be that the upper, syenite bearing sequences of the Watch Hill outlier (Holdsworth et al., 2001) are of the younger Permian-Triassic age, while the lower sequences are of ORS. This may account for the lack of deformation seen in the conglomerates at Coldbackie. However, to test this theory, further analysis would be necessary.

It should be noted that there is a similar debate regarding the age of sediment deposits offshore in the West Orkney Basin. Enfield & Coward (1987) proposed that the Permian-Triassic sediments at, or near, the sea bed only form a thin veneer capping a predominantly Old Red Sandstone basin succession. However Kirten and Hitchen (1987) proposed that in the deepest parts of the basin (i.e. adjacent to the bounding faults) up to 8000m of syn-rift Permian-Triassic strata may be preserved. The deepest well drilled in the basin (202/19-1; see fig. 31 of Stoker et al., 1993, for location) favours this latter scenario, showing 2931 m- thick sequence of Permian-Triassic New Red Sandstones and evaporites (Stoker et al., 1993). However, this well does not preclude the presence of Devonian sediments in the deepest parts of the basin, just that the basin comprises significant amounts of younger sediment infill. Offshore models also suggest that Devonian strata thicken towards the south-east (and associated thinning of Permian-Triassic) where extensive Old Red Sandstone deposits of the Orcadian Basin can be seen (Friend et al., 2000).

### ***3.6.3. Linking onshore and offshore – indirect evidence for a North Coast transfer zone***

In the eastern part of the West Orkney Basin a number of faults appear to be traceable from onshore to offshore (Fig. 3.14). These include the Strathy Head Fault which bounds a moderately sized Devonian outlier (Johnstone and Mykura, 1989) which can be easily distinguished in offshore data. A reasonable link may also be

made between the Kirtomy Bay micro-basin and a similar sediment filled half-graben, picked in seismic, that formed in the hangingwall of the Swordly Thrust (MOIST: Brewer and Smythe, 1984; DRUM: Snyder 1990; Stoker et al., 1993). However, the onshore continuation of this sedimentary outlier is somewhat limited and appears to die out against a splay-fault from the *c.* E-W trending fault system running onshore from Bettyhill (Fig. 3.14). Further west a number of other reactivated Caledonian structures can be seen in seismic section (e.g. Naver and Moine Thrusts) with extensive sedimentary deposits in their hangingwall, however, no evidence can be found for these onshore. Onshore the Naver Thrust runs west of Bettyhill (and Glaisgo) in a NNW-SSE orientation. However, offshore corresponding structures identified as the Naver Thrust (Snyder 1990; Stoker et al., 1993) appear to be some 10 km further west than would be expected by extrapolating onshore geometries offshore. This offset may be a consequence of the offshore continuation of the sinistral strike-slip fault running through Bettyhill westward into Torrisdale Bay (Fig. 15a, c). However, sinistral offsets of the Swordly Thrust on this fault appear only to be in the order of 1-2 km, thus implying that offset on this strike-slip fault increases westwards. A similar left lateral offset of the Moine Thrust is also apparent further west. These apparent left lateral offsets of basement structures, taken with the observation that offshore structures do not appear to continue onshore, suggests a E-W or ESE-WNW (i.e. coast parallel) fault somewhere off the north coast. Such a structure has been suggested in the past by other authors (e.g. Coward et al., 1989; Stein & Blundell, 1990).

Coward et al. (1989) noted that fault throws on major faults within the West Orkney basin die out very rapidly close to the north coast, furthermore, fault throws suggested from sedimentary basins onshore (e.g. at Kirtomy Bay) are relatively small compared to those offshore. Therefore, they suggested that extension within the West Orkney Basin was likely to have been transferred westwards in to the North Minch Basin. Old Red Sandstone sequences have not been identified in the Minch Basin (Brewer & Smythe; 1984; Stein 1988; Stein & Blundell, 1990), therefore, if the main extension within the West Orkney Basin were of Devonian age (as proposed by Coward et al., 1989), then this model appears unlikely, however a Permian-Triassic extension (Stoker et al., 1993; Friend et al., 2000) would be consistent with this transfer model.

Figure 3.14 shows the structures and kinematics along the Scottish north coast may all correlate with an ESE-WNW transfer zone. Beacom (1999; after Holdsworth & Strachan, 1996) also suggested that the ESE-WNW faults bounding the Faraid Head outlier form part of an ESE-WNW trending fault zone (Fig. 3.14). With the exception of Coldbackie, all localities analysed in this study indicate NW-SE extension, which is consistent with offshore structures (Fig. 3.13). Many localities also show evidence for both strike-slip and dip-slip normal faulting, and 3-D strain, which are all a likely consequence of deformation within a transfer zone. An explanation for the irregularity at Coldbackie may be that it lies south of the proposed transfer zone and thus did not develop during the same tectonic event (or alternatively local stresses were different south of the transfer zone).

Other evidence for a major ESE-WNW trending structure running near-shore to the Scottish north coast may come from palaeocurrent directions in sedimentary outliers near Tongue (Holdsworth et al., 2001). Cross-bedding, clast imbrication and channel orientation in the Watch Hill conglomerates and sandstones indicate a palaeocurrent towards the NNW, while the presence of syenite bearing units, in the upper sequences of these deposits, suggest that they are likely to be sourced from the Ben Stumanadh and/or Ben Loyal intrusions to the south (Hingham, 1977; O'Reilly, 1983; Holdsworth et al., 2001). However, sediments on the Roan Islands further north do not show this southerly sediment source. Instead deposits are consistent with deposition in a braided river system dominated by longitudinal bars, and was draining an area to the west and northwest (Blackbourn, 1981a; also refer to fig. 31 of Holdsworth et al. 2001). As Figure 3.14 shows, the Roan Islands lie to the north of a series of E-W trending faults on the mainland, and thus are likely to fall within the proposed NCTZ which may have channelled sediments along its length (hence the east-southeasterly palaeocurrent direction).

#### *3.6.3.1. Origins of this transfer zone.*

Transfer zones are often attributed to the reactivation of basement structures (Morley et al., 1990, 2004). As the proposed North Coast Transfer Zone runs in an ESE-WNW orientation, this may imply that reactivation of Laxfordian structures within the Lewisian basement terrane may be a potential origin; however the lack of evidence for reactivation at Durness (Beacom, 1999; and this study) make this an unlikely model. Alternatively, these pre-existing basement structures may impede

lateral (in this case to the south) fault propagation within the West Orkney Basin, which could thus lead to the development of this transform. As offshore faults appear to be traceable onshore in the east (i.e. at Strathy) where basement structures are sub-parallel to fault trends (and thus favourable for fault propagation), but not further west, where basement structures (i.e. Moine Thrust Zone and Laxfordian structures) are more oblique to fault trends, this would appear consistent with this model.

#### ***3.6.4. How does the structure of the North Coast relate to the present day NE Atlantic margin?***

The North Coast Transfer Zone proposed in this study may be traced westward along strike where it appears to coincide with the Ymir Ridge, which makes up the southern unit of the Wyville-Thomson Lineament complex (WTL; Fig. 3.1). This lineament complex is believed to have acted as a major transfer zone during Mesozoic times, separating basins with differing polarities (Lister *et al.*, 1986). Gravity imaging (Fig. 3.1) and sediment thickness models (Kimbell *et al.*, 2005) suggest that there is a major dextral offset across the WTL the North Rockhall Basin and the basins to the northeast. This is consistent with the apparent right-lateral step marked by the West Orkney Basin on the Scottish north coast (Fig. 3.2). Furthermore, evidence for sinistral strike-slip faulting and associated folding in Cenozoic times along the Ymir and Wyville-Thomson Ridge (Johnson *et al.*, 2005) suggesting that the WTL acted as a transfer zone at this time also.

It should be noted however, that the Wyville-Thomson Ridge can also be traced eastwards and corresponds well with the southern margin of the North Rona Basin, but does not appear to correlate with any structures in the West Orkney Basin (Figs. 3.1 and 3.2). This may suggest that the Wyville-Thomson Ridge first developed as a transfer zone in the Permian-Triassic separating the east-dipping Outer Isles Basin and west-dipping North Rona Basin (Kirten and Hitchen, 1987), and post-dates the initial development of the West Orkney Basin.

This correlation between the structure of the Scottish North Coast and the geometry of the continental margin is somewhat qualitative as no direct links such as reactivation of onshore structures has been identified, although offshore studies in the Outer Isles Basin and NW of the Hebrides may reveal a more direct link. However recent studies have shown that margin segmentation, such as the

development of the WTL, may result from variations in the obliquity of pre-existing structures (see *Chapter 4*), but does not necessarily require their reactivation.

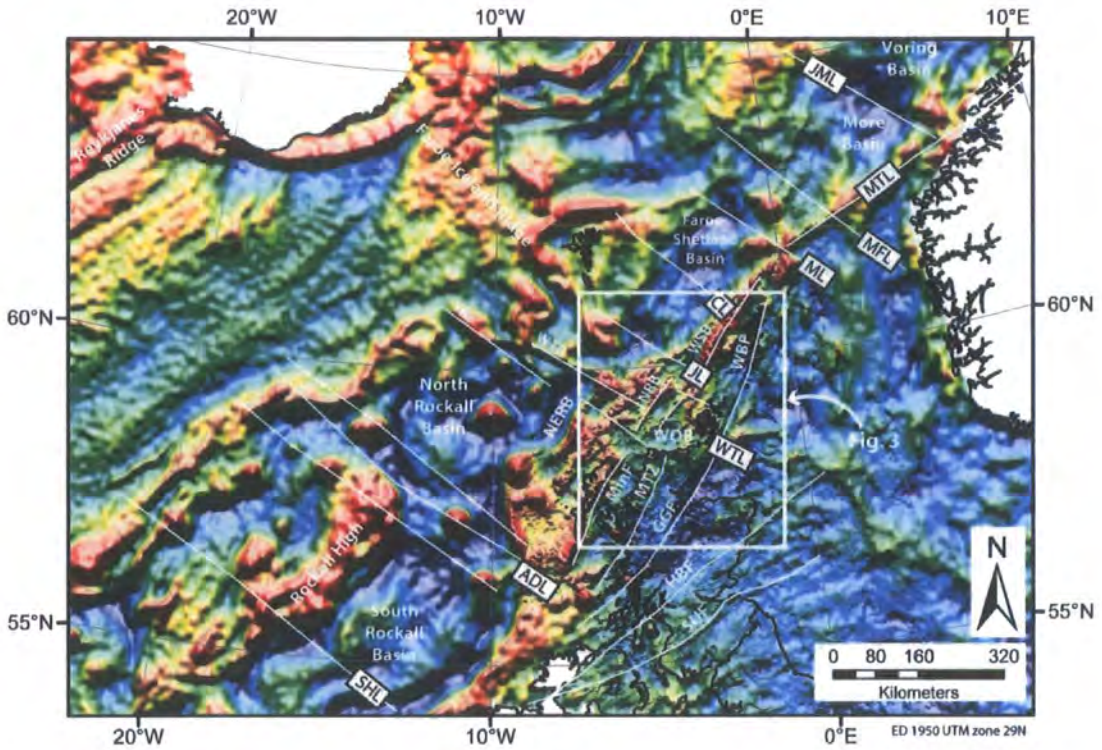
### **3.7. Conclusions**

The aim of this paper was to reassess the influence played by pre-existing basement structures on fault patterns and development along the Scottish north coast. At a regional scale onshore (i.e. using SPOT images), late brittle faults appear to show a strong correlation with variations in basement structure and many lineaments can be seen to lie parallel to basement trends (Fig. 3.4). Therefore regional scale analysis suggests that basement influence is likely. However more detailed studies (i.e. aerial photographs and outcrop studies) show that in many cases these similarities are simply based on trend alone and that reactivation is not evident (i.e. steep brittle faults cutting shallowly dipping Caledonian fabrics; Holdsworth, 1989).

Detailed fault analysis at various localities along the north coast show that fault patterns vary significantly from area to area. Outcrop scale analysis suggests that with the exception of Kirtomy Bay, basement reactivation is not apparent. Nevertheless, the orientation of basement fabrics may influence fault patterns at some scales (e.g. secondary strike-slip faults at Glaisgo may be a consequence of extension parallel to basement fabric). Although fault patterns appear to vary considerably, all localities (with the exception of Coldbackie) appear consistent with a NW-SE regional extension (Fig. 3.13), which has also been modelled from offshore structures in the West Orkney Basin (Coward et al., 1989).

As all onshore data have been compiled using digital mapping techniques (McCaffrey et al., 2005), 3-D digital models have been created and integrated with offshore seismic data for the West Orkney Basin. Attempts have been made to link onshore and offshore structures. However, it appears difficult to correlate onshore and offshore structures in the west (i.e. offshore structures appear to lie west of their predicted location based on extrapolation of onshore structures), however further east onshore-offshore links can be easily made (e.g. basin-bounding faults at Kirtomy Bay and Strathy). This lack of linkage between onshore and offshore may be a consequence of a major sinistral strike-slip fault running ESE-WNW near the Scottish North Coast. Such a structure may be traced onshore in the vicinity of Bettyhill (mid-way along the north coast; Fig. 3.14), and appears to mark the southern boundary of the Kirtomy micro-basin (though terminates against the Strathy

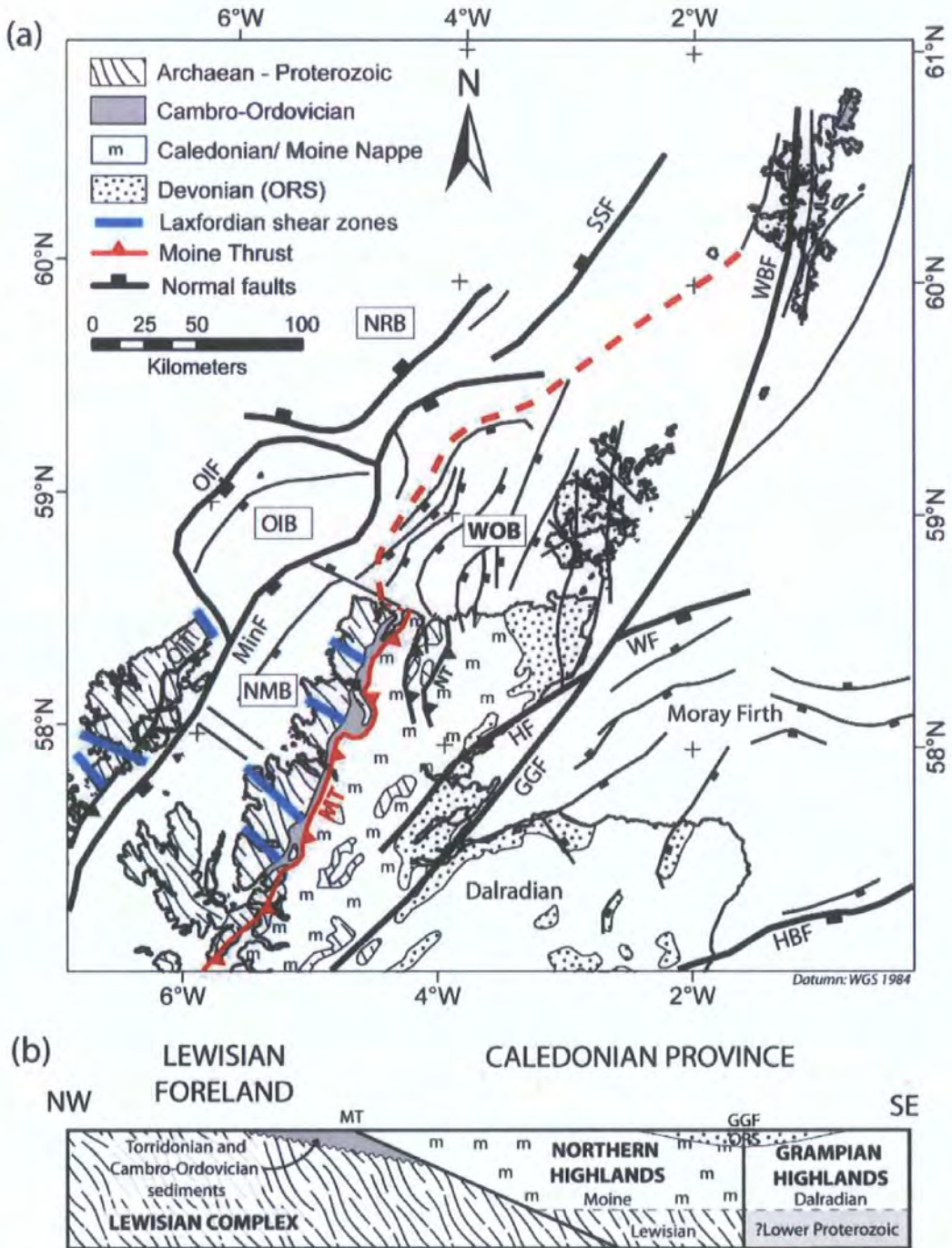
Head Fault; Fig. 3.14). This structure, along with complex fault geometries (associated with 3D strain) at Durness, may make up a regional transfer zone running along the Scottish North Coast. A similar structure has also been proposed in previous studies by Coward et al. (1989), Beacom (1999) and (Holdsworth et al., 2001). This structure appears to have marked a significant structure in the development of the West Orkney Basin (during Devonian and / or Permian-Triassic times) and may also be associated with later extensional tectonics in the Mesozoic and Cenozoic through linkage with the Ymir Ridge and Wyville-Thompson Lineament complex further west (Johnson et al., 2005), though this last statement requires further investigation.



**Figure 3.1.**

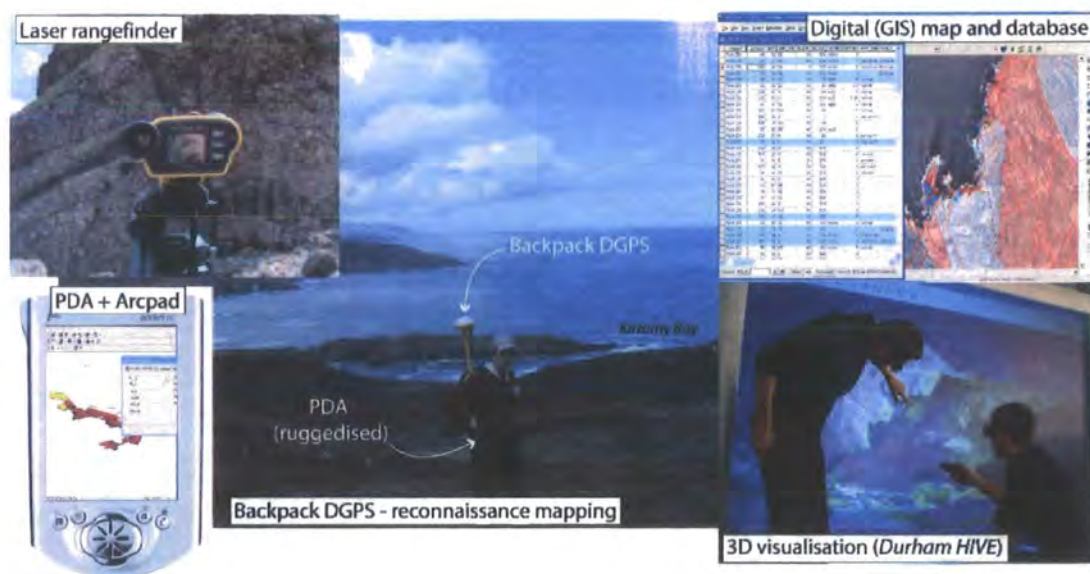
Image of gravity variations across the NE Atlantic (modified from Kimbell et al., 2005). Major basement fault and lineaments segmenting margin are highlighted. Abbreviations: ADL, Anton Dohrn Lineament; CL, Clair Lineament; GGF, Great Glen Fault; HBF, Highland Boundary Fault; JL, Judd Lineament; JML, Jan Mayen Lineament; MFL, Marflo Lineament; MinF, Minch Fault; ML, Magnus Lineament; MTL, Møre-Trøndelag Lineament; MTFZ, Møre-Trøndelag Fault Zone; MTZ, Moine Thrust Zone; NERB, North-east Rockall Basin; NRB, North Rona Basin; SHL, South Hatton Lineament; SUF, Southern Uplands Fault; WBF, Walls Boundary Fault; WOB, West Orkney Basin; WSB, West Shetland Basin; WTL, Wyville-Thomson Lineament Complex; WTR, Wyville-Thomson Ridge; YR, Ymir Ridge.





**Figure 3.2.**

(a) Map of the main structural features of Northern Scotland (after Coward *et al.*, 1989 and Seranne, 1992). (b) Simplified cross-section showing basement terranes across the Northern Scottish Highlands (from Stoker *et al.*, 1993). Abbreviations (see also Fig. 3.1): HF, Helmsdale Fault; MT, Moine Thrust; OIF, Outer Isles Fault; OIT, Outer Isles Thrust; NMB, North Minch Basin; NS, Naver Thrust; ORS, Old Red Sandstone; OIB, Outer Isles Basin; SSF, Shetland Spine Fault; WF, Wick Fault.



**Figure 3.3.**

Building the digital database – principal hardware and software tools used as part of the GAVA (Geospatial acquisition, visualisation and analysis) workflow.

**Figure 3.4.** (overleaf)

(a) Lineaments and basement geology map of Northern Highlands of Scotland. Lineaments interpreted from panchromatic SPOT images at 1:100,000 scale, basement geology data derived from published 1:250 000 solid geology maps of Sutherland, Caithness, and Orkney (BGS map sheets). Offshore faults from Coward et al. (1989). (b) Rose diagram map (5 km grid squares) and lineaments derived from SPOT images for area outlined in (a). See text for spatial analysis method. (c) Lineaments derived from aerial photograph analysis (picked at 1:10 000 scale), plus rose diagrams for each area mapped. Outlined in blue is mean basement trend for area, while outer circle on rose diagrams corresponds to 20% of data.

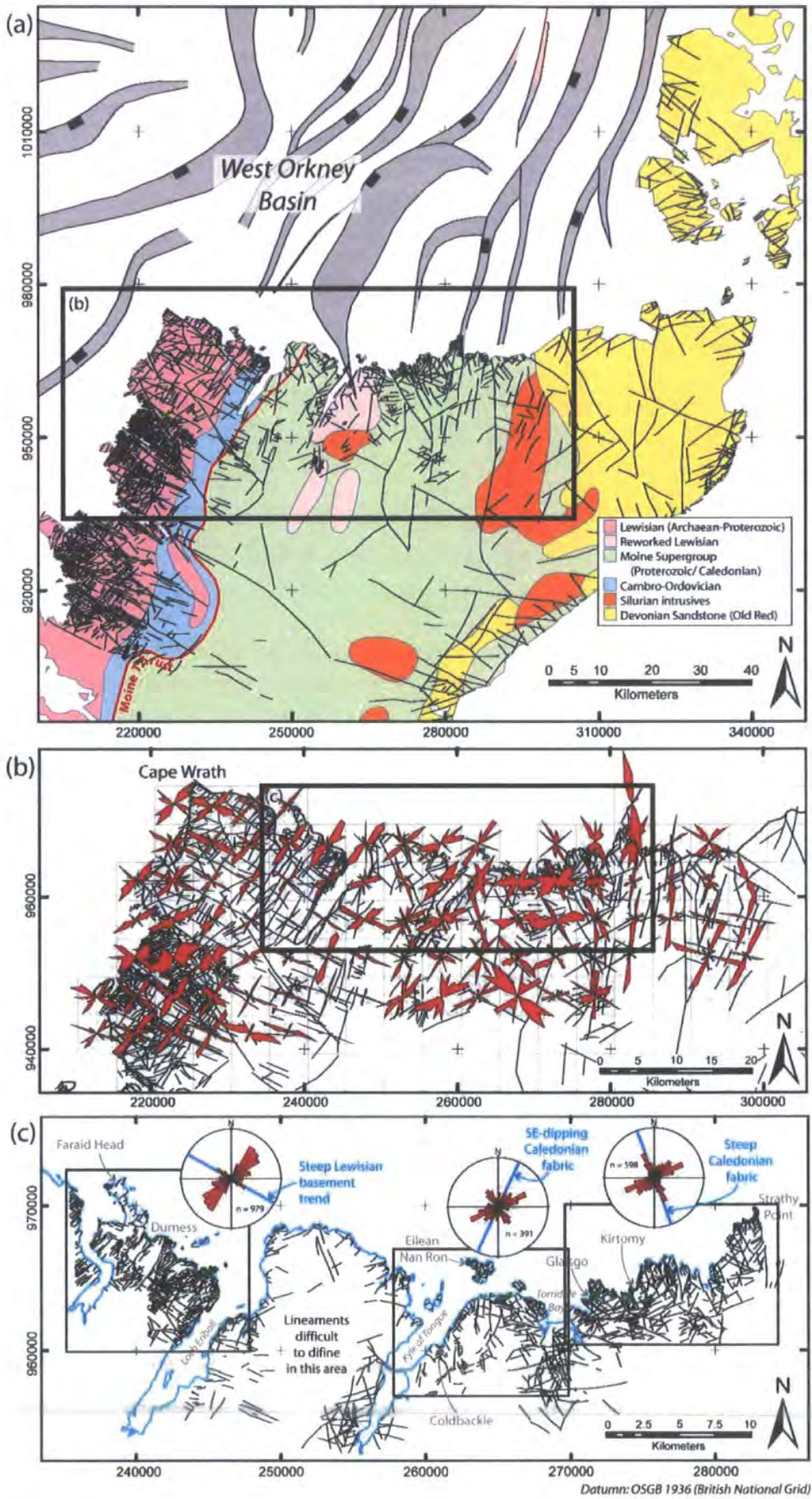
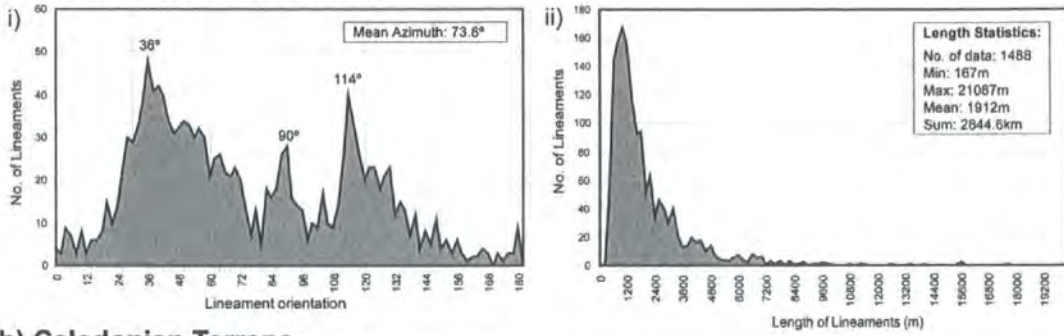


Figure 3.4.

(a) Lewisian Foreland Terrane



(b) Caledonian Terrane

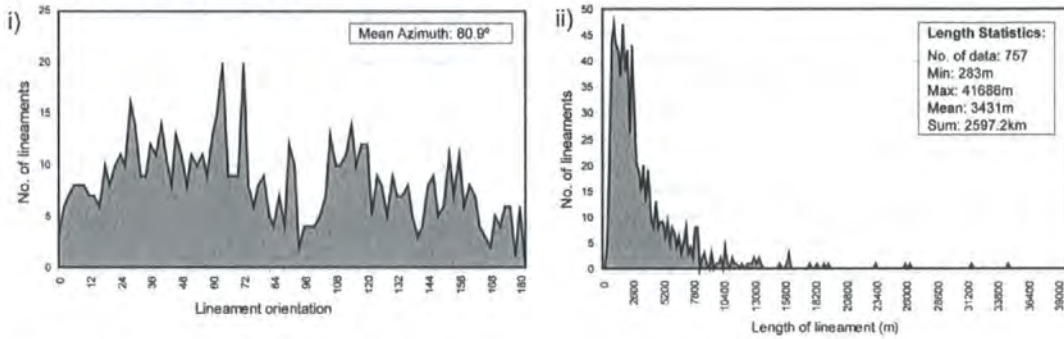
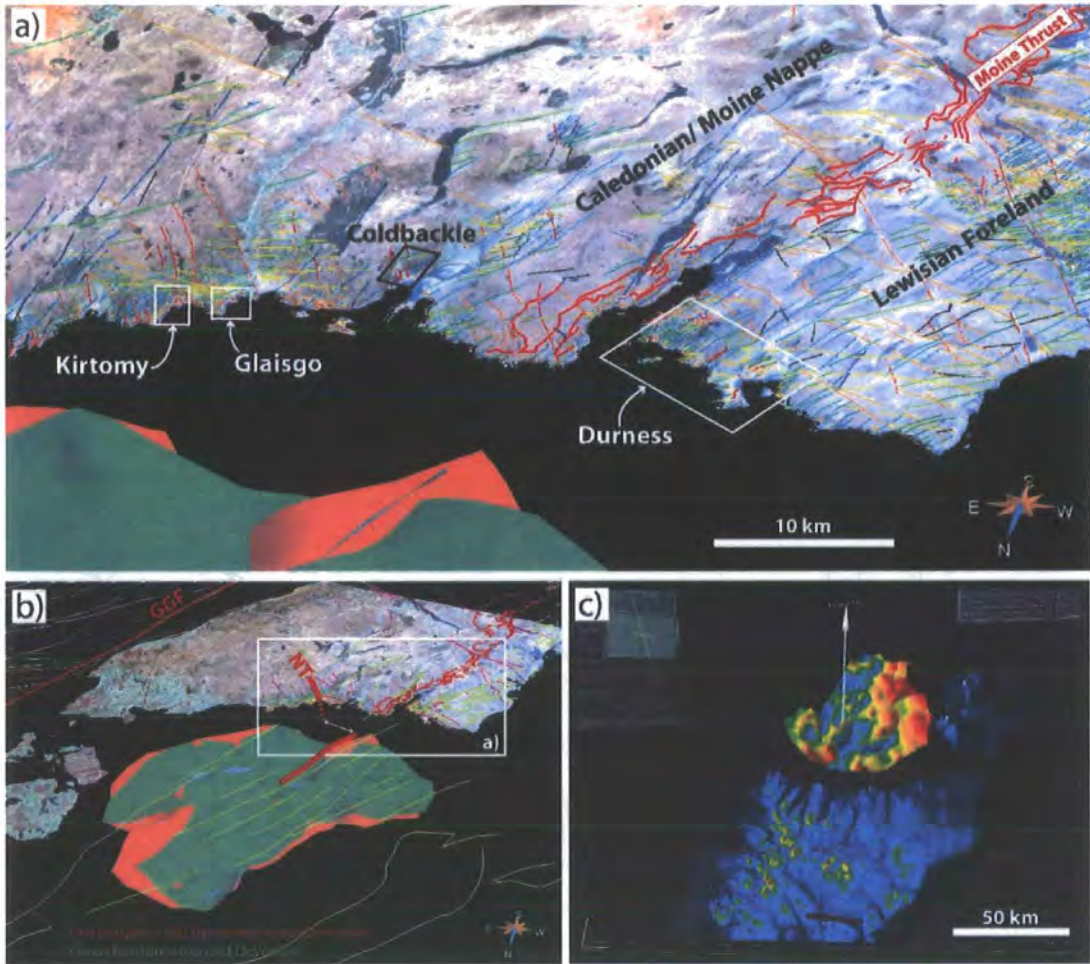


Figure 3.5.

(a) Histogram showing: i) orientation, and ii) length of lineaments hosted by Lewisian Foreland Terrane. (b) Similar plots for lineaments hosted by Caledonian Terrane. Data analysed refers only to lineaments derived from SPOT image analysis.



**Figure 3.6.**

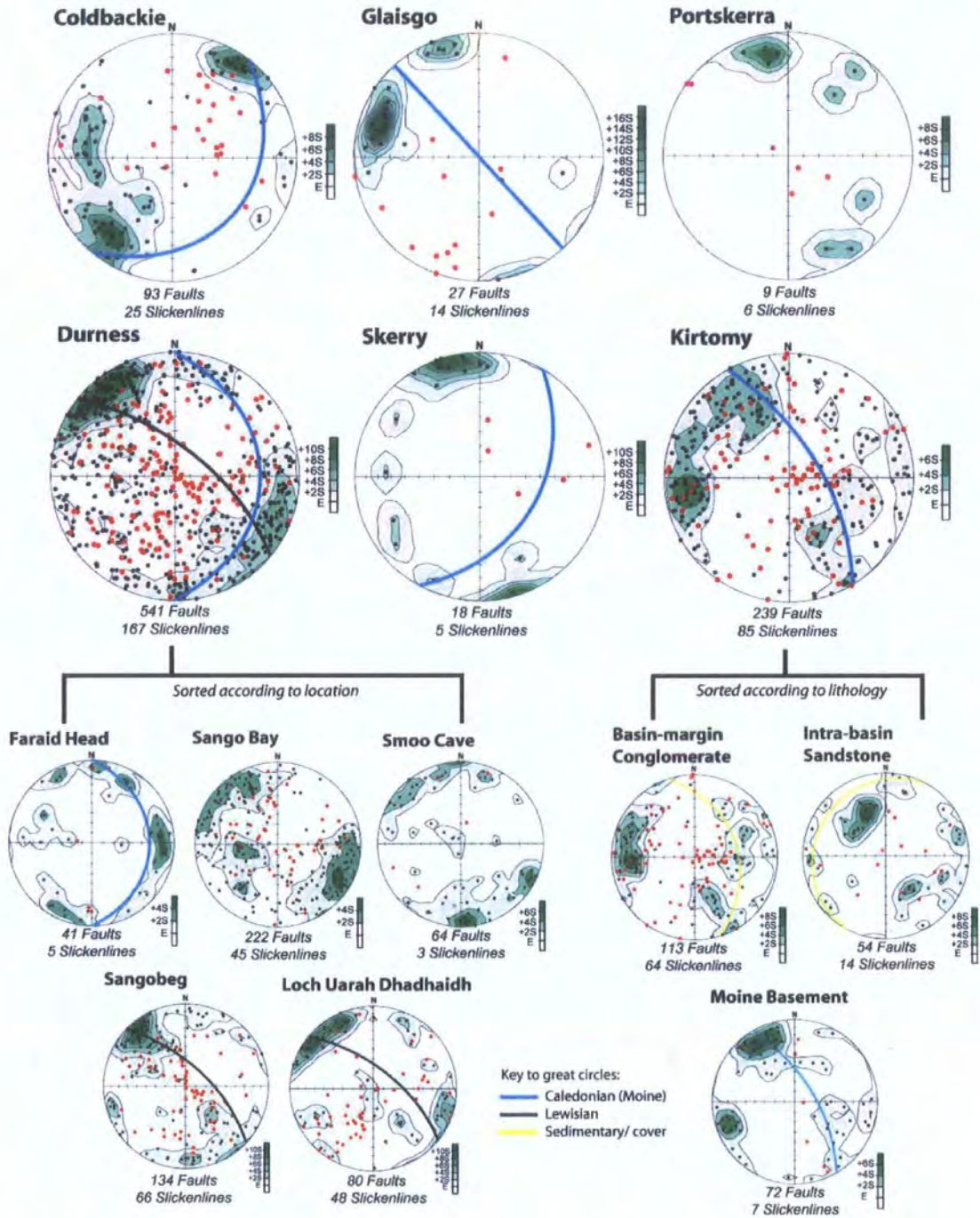
(a) 3D structural model (constructed in GoCAD™) of the Scottish North Coast showing a colour Landsat image, lineaments data, and main Caledonian fault structures (e.g. Moine Thrust Zone) draped over a Digital Terrain Model (DTM), viewed from NNW. Key field localities are also highlighted. (b) Same model viewed at a regional scale showing offshore structures (offshore fault lineaments derived from 1:250,000 scale geological maps produced by the British Geological Survey). Horizon data for top basement/ lower Devonian and top mid-Devonian stratigraphic reflectors picked from BIRPS (GRID) seismic profiles. Also outlined is the offset between onshore and offshore coverage of the Naver Thrust (NT). (c) Onshore-offshore models viewed using Schlumberger's fully immersive Inside Reality™ software.



Figure 3.7. (caption overleaf)

**Figure 3.7.**

(a) Panoramic photo of the Kirtomy Bay micro-Basin (looking SW). (b) View of basin bounding fault, looking north, showing basement parallel faults and also orthogonal faults. (c) View looking east across the sedimentary basin, showing gradual change in strike of sedimentary strata. (d) 3D digital model (viewed in GoCAD) of Kirtomy Bay, showing bounding faults and outcrop bedding data (small circular surfaces). (e) and (f) show simplified structure and style of micro-basin, highlighting hangingwall syncline (see also inset stereonet) and apparent fault closure to both west and south.



**Figure 3.8.**

Equal-area lower-hemisphere stereonet projections for each locality (see Fig. 3.4) showing poles to fault planes (contoured) and associated slickenlines. Also shown is mean orientation (great circles) of basement fabric at each locality (where no data is given structures are either irregular or sub-horizontal). Durness data are further subdivided into sub-localities (see Fig. 3.12); while Kirtomy data are also sorted according to lithology (i.e. faults in Moine basement, basin-margin conglomerate, and intra-basin sandstone). Great circles define mean geometry of basement/ host rock in area (blue = Caledonian; Black = Lewisian; yellow = sedimentary).



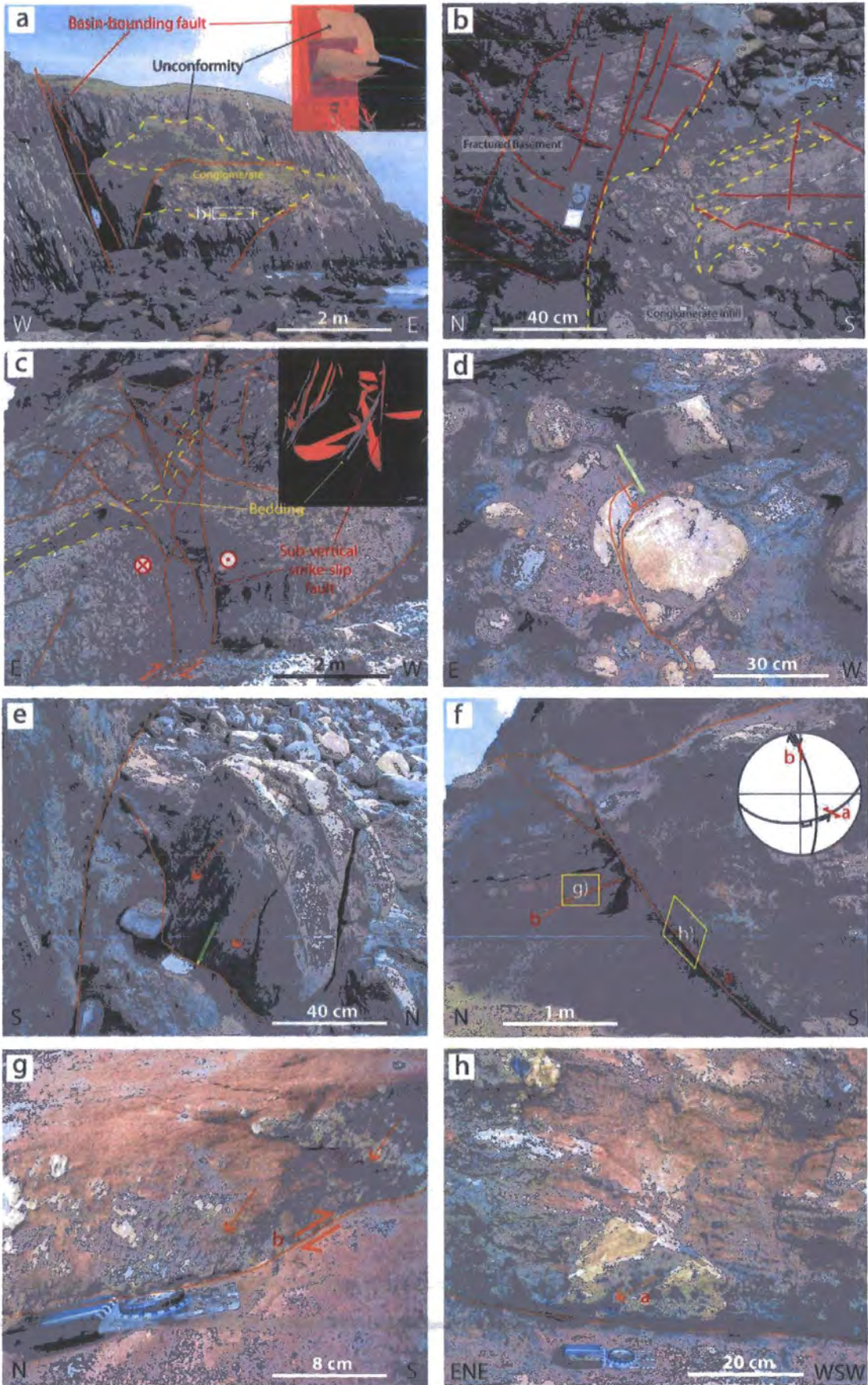


Figure 3.9. (caption overleaf)

**Figure 3.9.**

Field photos showing main structures observed at Kirtomy. (a) Breccio-conglomerate unconformity in hangingwall of basin bounding fault. Conglomerate is cut by, but also infills ENE-WSW trending graben faults. Inset shows 3-D GoCAD model of this structure, constructed from DGPS outcrop and laser ranger data. (b) Breccio-conglomerate infill of faults and fractures in basement at unconformity (for location see fig. a). (c) Highly fractured conglomerate units adjacent to bounding fault. Dextral strike-slip fault zone trending parallel to bounding fault, plus associated normal faults, note similarity to strike-slip follower structure. Inset shows 3-D GoCAD model of this fault complex created from outcrop data collected using laser ranger. (d) and (e) Dip-slip normal offsets in faults cutting conglomerate, trending N-S and ENE-WSW respectively. (f) Faults cutting intra-basin sandstone. Inset stereonet shows geometry of faults (marked a & b in photo) and associated slip-striae. (g) Dextral oblique-slip slickenfiber growth on footwall fault (fault b in fig. f). (h) 2 cm thick zone of euhedral calcite crystals overprinted by oblique-slip (sinistral) normal slickenlines on ENE-WSW fault (fault a in fig. f)

**Figure 3.10. (overleaf)**

Fault structures observed at Glaisgo. (a) Major NE-SW trending normal faults showing dip-slip extensional movements. (b) Secondary fault and fracture trends (photo in plan view) cutting alternating bands of augen gneiss and more mylonitic basement; inset shows a simplified plot of fracture trends. Conjugate faults and tensile fractures are consistent with NW-SE tension and NE-SW contraction.

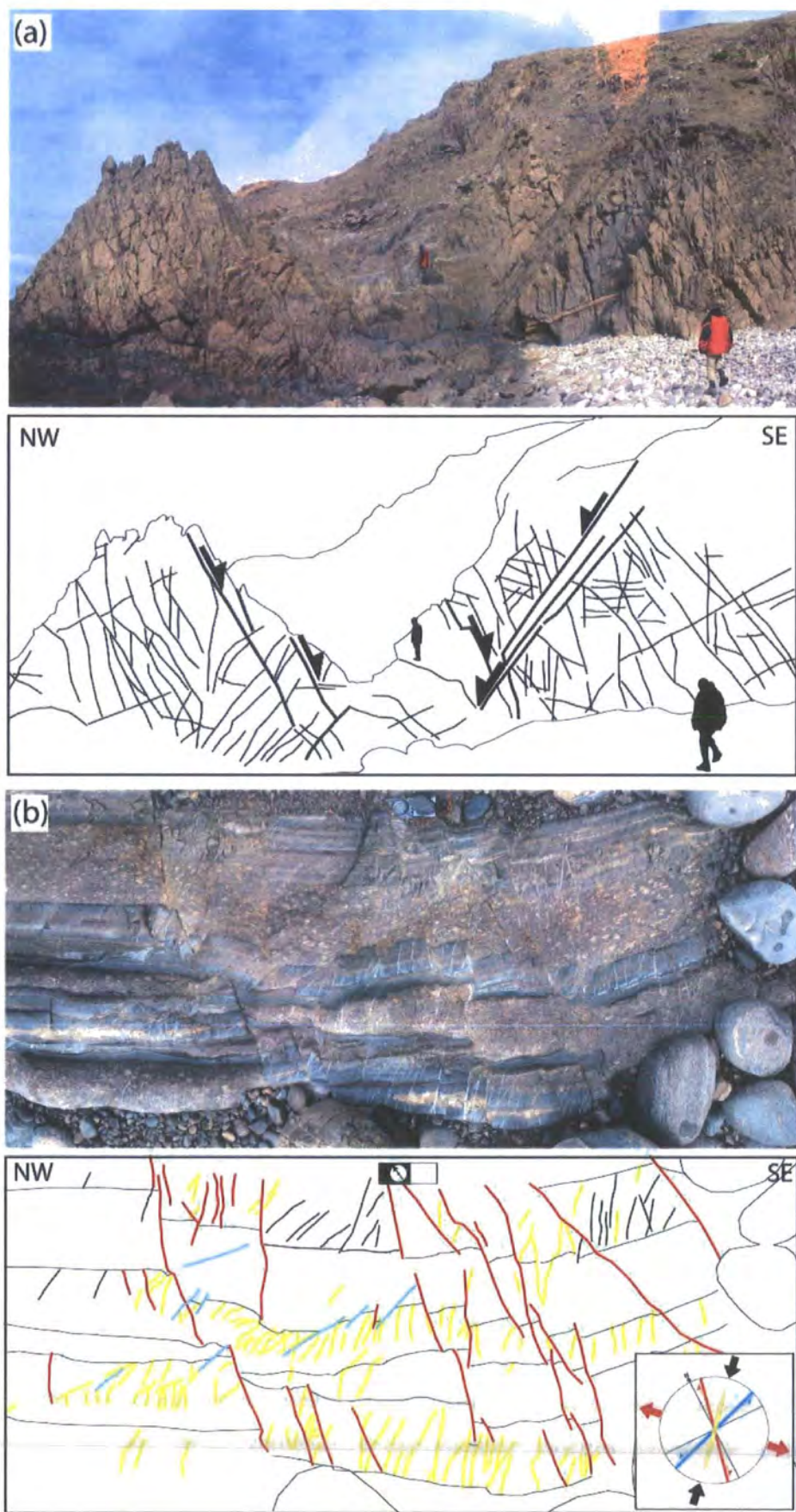
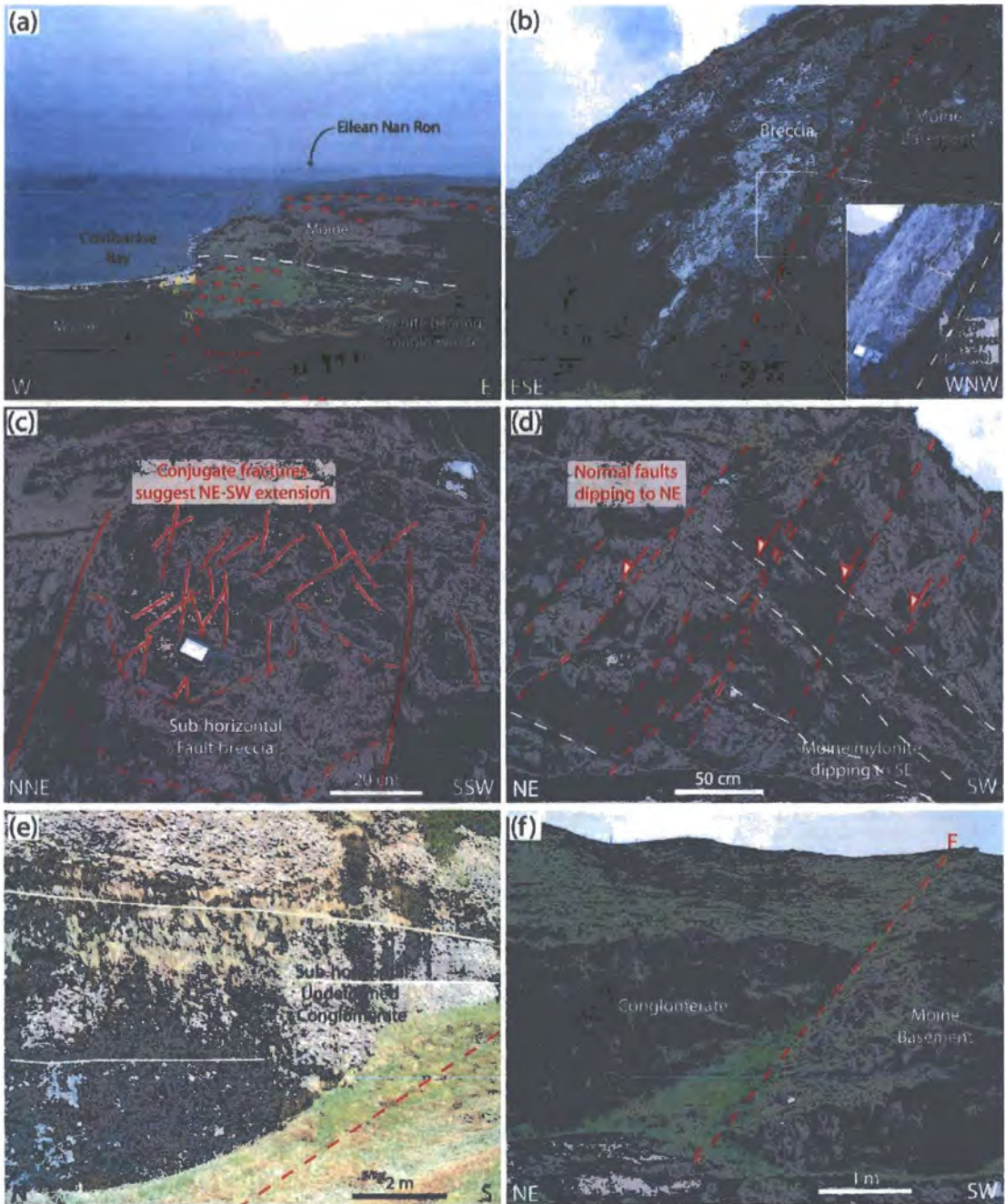
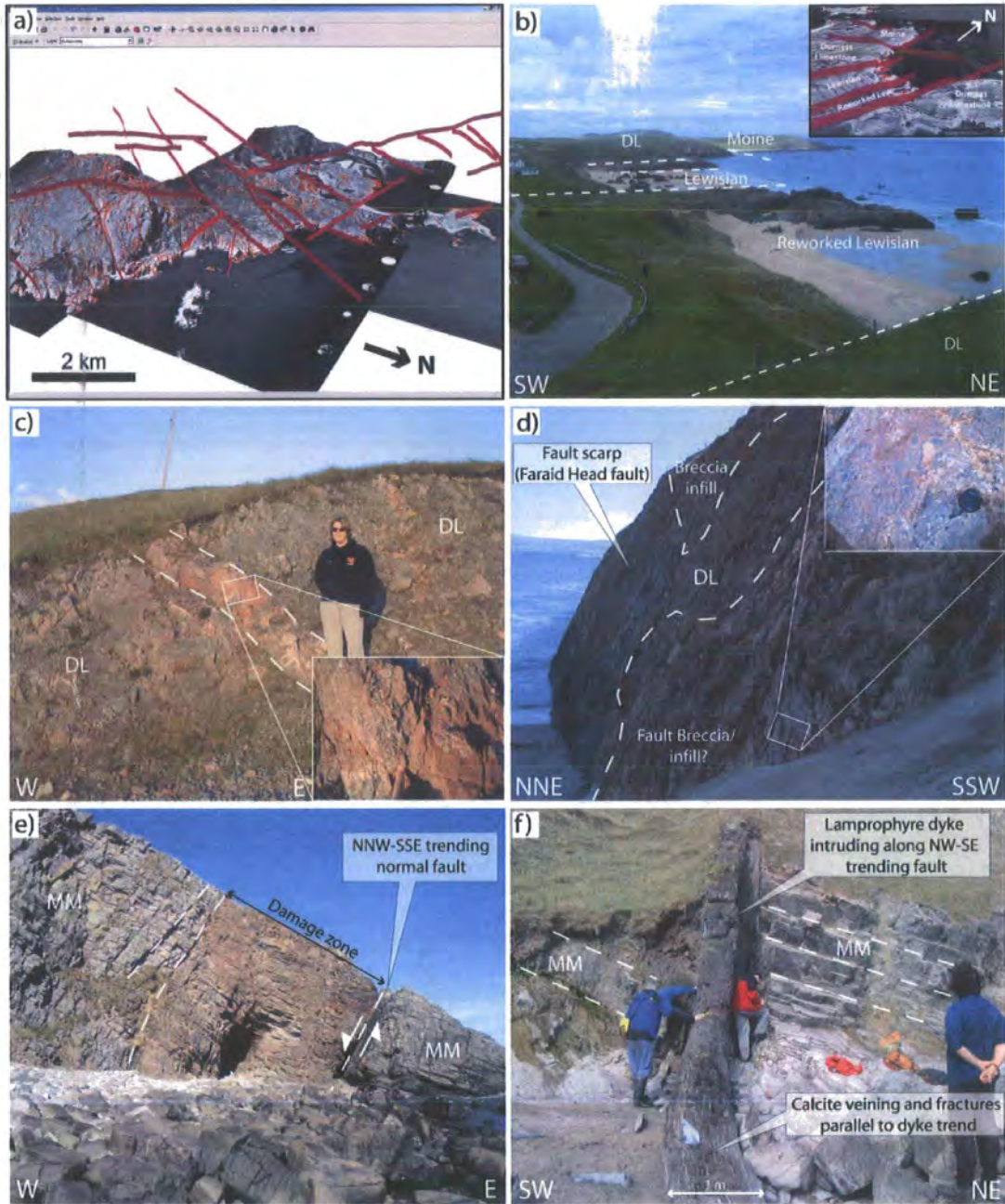


Figure 3.10.



**Figure 3.11.**

(a) View of Coldbackie/ Watch Hill outlier, looking north from west slope of Cnoc an Fhreiceadain (Watch Hill). (b) Fault breccia along N-S trending section of Watch Hill fault marking west border of sedimentary outlier. (c) Conjugate fractures cutting basement rocks, plus also sub-horizontal fault breccia below unconformity, likely associated with extensional collapse structures seen locally (Holdsworth et al., 2001). (d) NW-SE trending normal faults cutting basement rocks. (e) Sub-horizontal syenite-bearing conglomerate units (Holdsworth et al., 2001), showing little evidence of deformation. (f) NW-SE trending half-graben filled with near horizontal conglomerate strata (late syn- or post-tectonic?).



**Figure 3.12.**

(a) 3-D model showing the multi-modal fault patterns at Durness. (b) View of Sango Bay inlier bound by steep NNE-SSW trending normal faults, looking NW towards Faraid Head; inset shows similar view in 3-D model. (c) Clastic sediment infill along a NNE-SSW trending fault cutting Durness limestone exposures adjacent to the Sango Bay Fault (which also shows evidence of infill); inset shows close up view of Fe-rich infill material. (d) ESE-WNW trending fault scarp (Faraid Head Fault) bordering the Faraid head inlier, also showing infill breccia (however lower down the scarp it is less clear if breccia is infill or fault rock). (e) N-S trending normal fault/ fault zone cutting low-angle Moine mylonites on Faraid Head. (f) Small (1 m wide) Lamprophyre dyke intruding along pre-existing NW-SE trending strike-slip fault (Faraid Head). See Fig (a) for location of each photo.

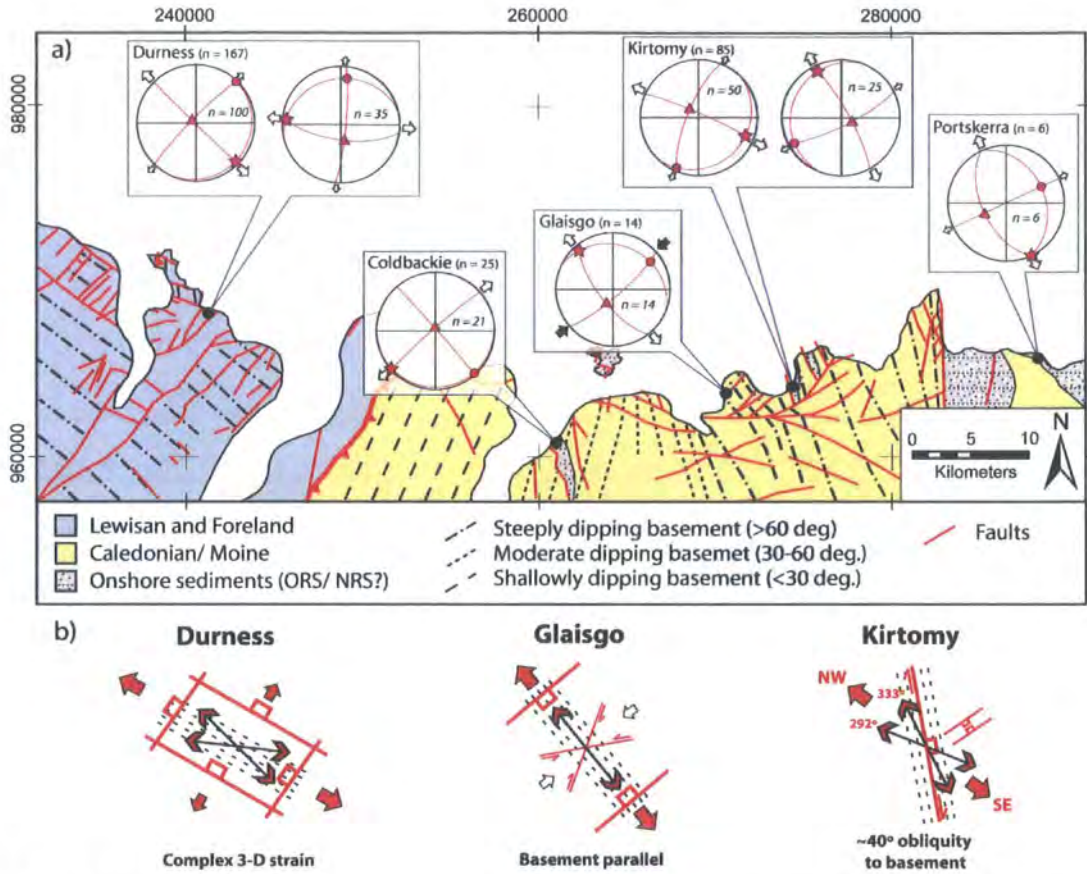


Figure 3.13

(a) Simplified basement structure map overlain by stereonets showing results of kinematic/palaeostress inversion for data at each locality. (b) Summary diagrams showing main fault trends and apparent regional extension axis at different localities.

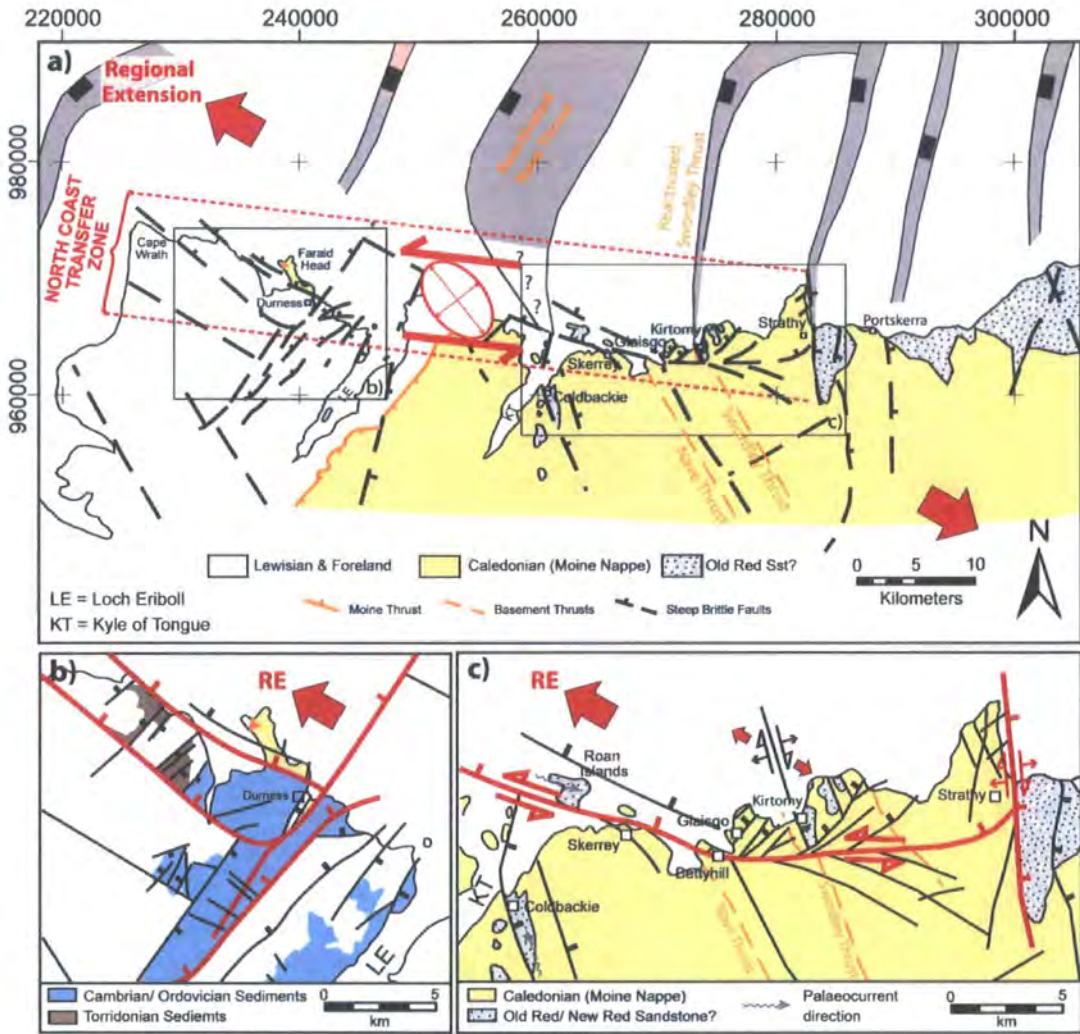


Figure 3.14.

(a) Regional structure of the North Coast Transfer Zone. (b) Multimodal extensional faulting in the Durness/ Cape Wrath region (Lewisian Foreland). (c) Onshore propagation of sinistral strike-slip fault transfer fault nr. Bettyhill, and terminating against the Strathy Head Fault. West of Strathy all onshore propagating normal faults of the WOB terminate against the transfer fault.

#### **4. Basement control on faulting patterns, transtension and structural segmentation of the Lofoten Ridge, Norwegian Margin: using digital mapping to link onshore and offshore geology**

**Abstract:** An integrated onshore–offshore study involving regional to outcrop scale fault analysis is used to develop a consistent structural model for transtension along the Lofoten ridge. The Lofoten-Vesterålen archipelago (LVA) is a segmented basement high showing distinct lateral variations in trend, deformational style, and structural complexity. This study investigates whether segmentation can be linked to differences in the obliquity of pre-existing structures relative to plate movement vectors. Regional analysis of fault lineament patterns using Geographic Information Systems (GIS) reveals that the LVA can be sub-divided into a series of distinct lineament domains. These domains are closely coincident with changes in ridge trend, and variations in structure within offshore models derived from seismic reflection studies. Digital field mapping and spatial analysis of faulting in the North Lofoten, which is highly oblique to the regional structural trend, reveal that faulting is dominated by transtensional dip-slip and oblique-slip movements associated with NW–SE extension. The overall change in fault orientation, fault geometry and deformation style are consistent with models for transtension where the ridge-bounding structure becomes increasingly oblique to regional extension. Ridge trend may be controlled by basement structures (e.g. Devonian detachments), or alternatively buoyancy effects of Precambrian granitic plutons in North Lofoten.

##### **4.1. Introduction**

Most passive margins are segmented along strike, giving rise to discrete zones characterized by constancy in structural style (e.g. Francheteau and Le Pichon, 1972; Doré et al., 1997; Clemson et al., 1997; Song et al., 2001). This segmentation is also seen in continental rifts that are the precursor to these passive margins (e.g. Rosendahl, 1987; Morley et al., 1990). The boundaries between margin/ rift segments are generally believed to exhibit a variety of structural styles ranging from transfer faults (Gibbs, 1984) and accommodation zones (Bosworth et al., 1986) to transform faults. The origins of this segmentation and segment boundary zones are



often attributed to the influence of basement structure (e.g. Davison, 1997; Clemens et al., 1997). One possibility is that such segmentation reflects along-strike changes in the orientation of pre-existing structures in the underlying continental basement. A corollary of this model is that if such pre-existing structures undergo reactivation then they will often be significantly oblique to the direction of regional extension. This leads to the development of zones of oblique extension or transtension (Fig. 4.1a) (Withjack and Jamison, 1986; Tikoff and Teyssier, 1994; Dewey, 2002; Morley et al., 2004; De Paola et al., 2005a, 2005b) on what would otherwise be a simple extensional margin.

Transtensional strains are characterized by complex relationships between finite and infinitesimal strain axes that critically depend on the angle  $\alpha$  between the regional displacement and the deformation zone boundary faults. In extension-dominated transtension ( $20^\circ < \alpha < 90^\circ$ ) the axes of infinitesimal ( $z$ ) and finite shortening ( $Z'$ ) should always be coincident and vertical, which is comparable to the case of orthogonal extension ( $\alpha = 90^\circ$ ) (Figs. 4.1a, b) (McCoss, 1986; Dewey et al., 1998; De Paola et al., 2005a). However, at low angles of divergence ( $\alpha < 20^\circ$ ), the infinitesimal axis  $z$  is horizontal, with the finite axis ( $Z'$ ) eventually swapping orientation with the vertical intermediate finite axis  $Y'$  with increasing amounts of finite strain ('wrench-dominated transtension'; Figs. 4.1a, b). It is not surprising, therefore, that both field- and laboratory-based studies of deformation styles in oblique and transtensional settings have shown that these zones exhibit more complex fault patterns than those traditionally associated with orthogonal rifting (e.g. Withjack and Jamison, 1986; Schreurs and Colletta, 1998; Clifton et al., 2000; McClay, 2002; Dewey, 2002; De Paola et al., 2005a). Furthermore, the presence of pre-existing structures lying at an oblique angle to imposed opening vectors may commonly lead to the partitioning of oblique rifting into contemporaneous domains of wrench- and extension-dominated transtension (Titus et al., 2002; Oldow, 2003; De Paola et al., 2005b).

The Norwegian continental margin is a well documented example of a segmented passive margin (Doré et al., 1997; Tsikalas et al., 2001; Olesen et al., 2002; Mosar, 2003). This segmentation is generally defined by the presence of a series of NW–SE-trending transfer zones (Figs. 4.2a, b) (Blystad et al., 1995; Olesen et al., 1997, 2002; Brekke, 2000; Tsikalas et al., 2001). These transfer zones are

believed to reflect major basement structures at depth (Strömberg, 1976; Mjelde et al., 2003). This appears to be true for the largest transfer zones (e.g. Jan Mayen, Bivrost, Senja Fracture Zones), which we term here first-order transfer zones. However, others are simply inferred across areas of changing fault trend, fault polarity or basin geometry (e.g. Mosken, Jannegga and Vesterålen transfer zones) (Tsikalas et al., 2001), and in many cases no attributable basement structure is observed. These we term second-order transfer zones. In this paper, we investigate the hypothesis that it is the orientation of individual segments and their basement-influenced bounding faults relative to the regional extension vector that controls fault complexity and the development of second-order transfer structures.

The Lofoten Ridge (Fig. 4.2b) is a basement ridge showing distinct lateral variations in trend, and provides a good opportunity to compare fault architectures found in crystalline basement onshore (Tveten and Zwaan, 1993; Løseth and Tveten, 1996; Olesen et al., 1997; Klein et al., 1999; Steltenpohl et al., 2004), with those developed in sedimentary basins offshore (Mokhtari and Pegrum, 1992; Løseth and Tveten, 1996; Tsikalas et al., 2001). The Lofoten Ridge has been strongly affected by tectonic activity during the Late Mesozoic extension prior to the separation of Norway and Greenland and, given its curved geometry, is an ideal location to look for evidence of basement-influenced oblique extension. The area is also an excellent analogue for offshore basement fault blocks beneath the Norwegian and other passive margins.

In the present study, we apply new digital mapping workflows (Jones et al., 2004; Wilson et al., 2005; McCaffrey et al., 2005) to construct a structural database for both onshore and offshore structures on the Lofoten-Vesterålen archipelago (LVA; Fig. 4.2c). All data are stored digitally in a Geographic Information System (GIS) database that facilitates the interpretation of multiple/integrated datasets (e.g. seismic data, remote sensing, field mapping; Jones et al., 2004; Piazzolo et al., 2004). It also provides an ability to analyze structures spatially across a wide range of scales.

## **4.2. Regional setting**

### **4.2.1. The Lofoten-Vesterålen margin**

Past studies (Talwani and Eldholm, 1977; Olesen et al., 1997; Doré et al., 1999; Brekke, 2000; Mosar, 2003) have shown that the Norwegian continental margin can

be divided into a series of segments (Møre, Vøring, Lofoten-Vesterålen and Western Barents Sea Margins; Fig. 4.2). The Lofoten-Vesterålen margin segment lies between the Bivrost and Senja Fracture Zones (Fig. 4.2) (Eldholm et al., 1979; Tsikalas et al., 2001). Compared to its neighboring margin segments, the Lofoten-Vesterålen Margin has a relatively narrow continental shelf and steep slope. Seismic and geophysical studies in this segment show a rift complex of margin-parallel basement ridges and shallow Mesozoic basins (Mokhtari and Pegrum, 1992; Løseth and Tveten, 1996; Olesen et al., 1997, 2002; Tsikalas et al., 2001). Tsikalas et al. (2001) further sub-divide the margin into a series of intra-margin segments (the Lofoten, Vesterålen, and Andøya segments) based on changes in fault polarity and intensity. These intra-margin segments are thought to be separated by transfer zones (Jannegga, Vesterålen; Figs. 4.2. b, c), also identified by Olesen et al. (1997, 2002).

The Norwegian margin has a prolonged Paleozoic to Cenozoic history of intermittent extension and basin formation dating from the Devonian post-orogenic (i.e. post-Scandian) collapse of the Caledonide Orogeny (Fossen and Dunlop, 1998; Doré et al., 1999; Fossen, 2000). Regional extension episodes have been documented in the Devono-Carboniferous, Permian, through the Late Jurassic to Early Cretaceous, and in Late Cretaceous to Early Cenozoic times (Blystad et al., 1995; Lundin and Doré, 1997; Brekke, 2000). The last extensional event is considered to have culminated in continental break-up and massive igneous activity at the Paleocene–Eocene transition, ~55Ma (Eldholm et al., 1989; Skogseid et al., 1992, 2000; Eide, 2002; Ren et al., 2003).

Late Jurassic–Early Cretaceous rifting is the dominant tectonic episode that gave rise to the prominent NE–SW-trending structures on the margin (Blystad et al., 1995; Doré et al., 1999; Brekke, 2000, Tsikalas et al., 2001). There are two dominant NE-SW-oriented ridges on the Lofoten-Vesterålen margin: the Lofoten Ridge and the Utrøst Ridge (Fig. 4.2b). On the Vøring margin, to the south, Doré et al. (1999) and Lundin and Doré (1997) have divided this Late Jurassic–Early Cretaceous episode into two separate tectonic events, but the lack of reliable pre-Cretaceous data does not allow this distinction to be made on the Lofoten-Vesterålen margin (Tsikalas et al., 2001). Extensive syn-rift thickening of Lower Cretaceous sequences is apparent along faults bordering the western flank of the Lofoten ridge, indicating that tectonism was active until about Hauterivian time, ~130Ma (Doré et al., 1999; Tsikalas et al., 2001)

#### 4.2.2. *The Lofoten-Vesterålen archipelago*

The inner-Lofoten-Vesterålen margin is dominated by the Lofoten Ridge, which can be split into three sections (north, central and south) showing variations in trend (Fig. 4.2b). With the exception of a few small islands (e.g. Røst and Værøy), the south Lofoten Ridge lies below sea level (Fig. 4.2b), whereas the central and north Lofoten Ridge make up part of the Lofoten-Vesterålen archipelago (LVA) (Fig. 4.2c). Collectively, the ridge marks a prominent NE-SW trending horst, bound on both sides by deep sedimentary basins (Vestfjorden and Ribban Basins) (Mokhtari and Pegrum, 1992; Blystad et al., 1995; Løseth and Tveten, 1996). The archipelago is composed mainly of high-grade metamorphic Precambrian rocks (with ages in the range 2.7 to 1.1 Ga) (Griffin et al., 1978) which have undergone a multistage exhumation history (Griffin et al., 1978; Hendriks, 2003). The exposed rocks are mainly migmatitic gneisses that were metamorphosed to amphibolite and granulite facies, and extensively intruded by mangeritic and charnockitic plutons (Griffin et al., 1978; Corfu, 2004a). U-Pb dating of these plutons suggest that the main phase of emplacement was between 1800-1790 Ma (Corfu, 2004a) and make up the bulk of the rocks exposed in north Lofoten (i.e. on Austvågøya and Vestvågøya) (Tveten, 1978; Corfu, 2004a). Unlike other exposures of the Western Gneiss Region, the Caledonian fabrics are only weakly developed in these basement rocks of the LVA (Griffen et al., 1978; Tull et al., 1985; Steltenpohl et al., 2004). This has been attributed to the lack of fluids in the dry granulite facies basement in the area (Bartley, 1982; Olesen et al., 1997). Separating these Precambrian basement terranes from the Caledonian nappe sequences to the east are a series of steeply dipping brittle-ductile to cataclastic faults called the Vestfjorden-Vanna fault complex (Fig. 4.2 b, c) (Andresen and Forslund, 1987; Olesen et al., 1997). This fault zone has been attributed to Late Jurassic–Early Cretaceous age movements (Andresen and Forslund, 1987), although older Permian movements have also been suggested (Olesen et al., 1997; Steltenpohl et al., 2004).

A large fault defines the western flank of the Lofoten Ridge (the West Lofoten Border Fault - WLBF (Løseth and Tveten, 1996) Fig. 4.2), and also forms the major bounding fault to the Ribban Basin offshore. This basin is sub-divided into the Skomvær and Havbåen Sub-basins (Fig. 4.2c) (Mokhtari and Pegrum, 1992; Olesen et al., 1997; Tsikalas et al., 2001). In places, the WLBF has a cumulative throw to the W or NW in excess of 3 km (Tsikalas et al., 2001). Traced northwards,

the WLBF changes orientation from a NNE–SSW-trend to NE–SW/ ENE–WSW trend between Moskenesøya and Vestvågøya (Fig. 4.2c), and this is reflected in the overall trend of the Lofoten Ridge footwall. This change is coincident with an apparent change in fault polarity within the Ribban Basin from dominantly NW-dipping in the south to dominantly SE-dipping in the north (Tsikalas et al., 2001). It also coincides with the diminishing significance of the Eastern Lofoten Border Fault (ELBF; Fig. 4.2c) northwards. These observations have led to a transfer zone being inferred through the area (Fig. 4.2), the Jannegga transfer zone of Tsikalas et al. (2001). Olesen et al. (2002) on the other hand, place this transfer further NE (between Vestvågøya and Austvågøya) and term it the Melbu transfer.

Another major transfer zone has been inferred to run through Vesterålen (Olesen et al., 1997, 2002; Tsikalas et al., 2001). However, apart from a few discrete NW–SE trending strike-slip faults running across Vesterålen that may be associated with this transfer structure, no major transverse fault is apparent. The transfer zone is instead characterized by an apparent regional barrier to the propagation of NE–SW faults (Olesen et al., 1997). This region has been described as a ‘twist zone’ by Olesen et al. (1997, 2002), and is more comparable to the ‘transfer zones’ described by Morley et al. (1990). Also coincident with this inferred transfer zone on Vesterålen is a steep magnetic gradient oriented NNW–SSE with a positive anomaly to the west and a negative anomaly to the east. This boundary has been attributed to the prograde metamorphic transition from amphibolite-facies migmatites in the east to granulite-facies rocks in the west (Griffin et al., 1978; Olesen et al., 1991). However, Corfu (2004b) has proposed alternatively that this gradient marks a major Caledonian tectonic boundary on Vesterålen.

All transfer zones that have been inferred in the region (Fig. 4.2) are based on changes in fault polarity and sediment thickness offshore (Tsikalas et al., 2001), and variation in crustal structure onshore (Løseth and Tveten, 1996; Olesen et al., 1997, 2002). All follow a preferred NNW-SSE to NW-SE orientation, which is thought to reflect the influence of Proterozoic shear zones within the basement (e.g. the Bothnian-Senja Fault Zone, Fig. 4.2b) (Henkel, 1991; Lundin and Doré, 1997; Olesen et al., 1997; Fichler et al., 1999). These transfers have also been speculatively linked to fracture zones far offshore that supposedly offset early magnetic anomalies generated during sea-floor spreading (Lister et al., 1991; Tsikalas et al., 2001),

although the results of new aeromagnetic surveys now question the existence of these oceanic fracture zones (Olesen et al., 2005).

Apatite fission-track (AFT) data, radiometric dating and onshore analysis all suggest that the basement rocks of Lofoten and Vesterålen experienced similar post-Caledonian histories until the Late Paleozoic (Hames and Anderson, 1996; Klein et al., 1999). Subsequently, these two areas appear to have undergone differential vertical movements (Hendriks and Andriessen, 2002). Again segmentation is apparent, with different cooling and denudation histories found throughout the archipelago. AFT analysis in Central and North Lofoten and Vesterålen suggest that outer-Vesterålen (i.e. Langøya) was exhumed (based on cooling ages) in Permian-Triassic times, whereas analyses in North Lofoten (and possibly also inner Vesterålen) suggest Jurassic-Cretaceous denudation ages (Hendriks and Andriessen, 2002; Hendriks, 2003), at a time when Langøya was subsiding and covered by sediments (Davidsen, 2000). Central Lofoten shows evidence for cooling in Mid Cretaceous times (Hendriks and Andriessen, 2002). Hendriks and Andriessen (2002) proposed that the transfer zones have in some way accommodated these differential vertical movements, although the precise mechanism to account for such movements is not explained.

### **4.3. The fault architectures of the Lofoten-Vesterålen region**

#### **4.3.1. GIS database**

In any study where both onshore and offshore fault data are examined at a range of scales it will be advantageous to use a Geographic Information System (GIS). GIS is an information system used to input, store, retrieve, manipulate, analyze and visualize geographically referenced geospatial data (Longley et al., 2001). GIS has already proven useful in several geological disciplines including: hydrocarbon exploration, (Coburn and Yarus, 2000); mining and mineral exploration (Knox-Robinson and Gardoll, 1998); environmental assessments (Teso et al., 1996); remote lineament analysis (Karpuz et al., 1993; Gabrielsen et al., 2002); and shear zone tectonics (Piazolo et al., 2004). In this study we compiled offshore seismic reflection, remote sensing and field datasets in a single GIS database using the ArcGIS™ suite (see *appendix 3* for full list of database files and coverages).

The benefits of this digital approach are: 1) all data are geospatially located in a consistent coordinate system (in this study all data are assigned WGS 84 UTM

Zone 33); 2) data can be analyzed across a range of scales (i.e. regional- to outcrop-scale data may be viewed, analyzed and stored together: Jones et al., 2006a); 3) raw (primary) data are easily distinguished from secondary data and interpretations (Jones et al., 2004); 4) better integration of data from different sources is possible, including collation of both onshore and offshore data into a single data-model; and 5) powerful analysis and visualization techniques can be employed using a range of software packages such as GoCAD™, Traptester, Petrel, 3D Move, Inside Reality, etc. (McCaffrey et al., 2003; Hodgetts et al., 2004; Jones et al., 2004; Wilson et al., 2005). This digital workflow forms part of a new in-house mapping methodology, 'GAVA' (Geospatial Acquisition, Visualization & Analysis) (Clegg et al., 2005; Wilson et al., 2005; McCaffrey et al., 2005) which integrates field- and laboratory-based digital mapping methodologies and allows for continual data analysis and evaluation at every stage in the data gathering process

#### **4.3.2. Onshore ('surface') dataset**

*Regional-scale structures* in our digital database were compiled from two main sources: 1) digitization of pre-existing geological maps; and 2) new interpretations of remote sensing imagery, particularly lineament analysis. Fault structures at this scale were interpreted from Landsat TM6 (Thematic Mapper) data. The application of lineament analysis for the interpretation of geological structures is a well established method that has been widely applied in Norway (e.g. Gabrielsen and Ramberg, 1979; Karpuz et al., 1993, 1995; Braathen and Gabrielsen, 1998; Gabrielsen et al., 2002). Gabrielsen et al. (2002) recently produced an onshore lineament map for the whole of Norway at 1:750,000 scale (data available from [www.ngu.no](http://www.ngu.no)). Following their methodology, lineaments were picked from Landsat images along the LVA at a scale of 1:100,000. Attribute data (i.e. trend; length; offset; comments) were also recorded and stored in the GIS database. After interpretation, lineaments were then compared to a DTM (Digital Terrain Model) and refined using GIS analysis. Particular care was taken to avoid the inclusion of basement fabrics in the lineament database. This was confirmed by studying pre-existing geological maps during lineament analysis, and was additionally checked during fieldwork.

*Outcrop-scale structures* were collected using some of the new digital geological techniques outlined by McCaffrey et al. (2005). Digital methods are becoming a

common means of field data acquisition (Maerten et al., 2001; Hodgetts et al., 2004; Jones et al., 2004; Clegg et al., 2005). This is in part because the equipment and software required now meet the needs of the field geologist (e.g. portability, accuracy, versatility, cost, etc.; Edmondo, 2002; Wilson et al., 2005), but also because it is becoming increasingly recognized that having precise geospatially located field data enables efficient 3D visualization and analysis in ways that are not possible with data collected using traditional paper-based notebook collection methods (McCaffrey et al., 2005). Gathering outcrop data in digital format (compatible with standard software used in the hydrocarbon industry) is a prerequisite for efficient comparison between onshore and offshore data. Digital data acquisition is also a key component in the construction of virtual outcrop models for use as reservoir analogues (Pringle et al., 2004; Jones et al., 2006b).

The equipment used for data capture during geological fieldwork in Lofoten comprised the following: (1) a hand-held computer (HP Jornada PDA) equipped with mobile GIS Software; (2) a backpack mounted Differential Global Positioning Satellite receiver (Trimble™ AG122); (3) a laser rangefinder (MDL LaserAce 300); and (4) a digital camera (Wilson et al., 2005). Field data were recorded in the form of 3D shapefiles (containing x.y.z. position), using ArcPad™ (version 6), a mobile GIS software suitable for running on Windows CE devices (Edmondo, 2002). Outcrop data (e.g. fault measurements and lithological data) were stored in point shapefiles, while linear features in map view (e.g. fault trace, traverse line, etc.) were recorded as polylines. These were supplemented by georeferenced outcrop photos and field sketches, both in a digital format. Structures exposed in vertical outcrops (i.e. road cuts) were recorded using a combination of digital photography and 3D outcrop data capture using a laser ranger (recording x.y.z. point-cloud data for outcrop surfaces and fault traces; Xu et al., 2000).

Field mapping was concentrated on Lofoten's northernmost island, Austvågøya, (Fig. 4.2c). The fjords of Raftsundet and Øksfjorden are conspicuous topographic/ bathymetric lineaments cutting across the islands of Austvågøya and Hinnøya. These lineaments are believed to represent major NNE-SSW trending faults that continue to the southwest beneath the Vestfjorden Basin. To the northeast these lineaments die out rapidly in a zone of apparently complex faulting. For this reason, and also because of the excellent exposure on Austvågøya, the rocks around Raftsundet were chosen for detailed field data analysis.



#### 4.3.3. *Offshore ('subsurface') dataset*

During the development of our regional structural database a number of regional offshore fault maps were digitized, including: Mokhtari and Pegrum (1992); Blystad et al. (1995); Løseth and Tveten (1996); Olesen et al. (1997, 2002); and Tsikalas et al. (2001). However, some inconsistencies were found between these data sets (i.e. trends of faults, fault linkage, etc.) and consequently twenty-four 2D seismic lines (data coverage approx. 100 km x 75 km) were studied for an area west of the Lofoten ridge (refer to Fig. 4.6 showing location of survey area).

Seismic interpretation was carried out using GeoFrame IESX™ before exporting fault and horizon data to TrapTester™ to construct a 3D structural model of the area. Five prominent reflectors were mapped, and have been correlated with the intra-Mesozoic, Base Cretaceous, intra-Lower Cretaceous, Aptian and Albian horizons mapped by Tsikalas et al. (2001) in the Ribban Basin. Larger faults have been linked with some confidence based on mapped variations in fault throw, and the resulting fault polygon maps have been exported to GIS for comparison with onshore structures, while geometries have been analysed in TrapTester™.

#### 4.3.4. *Building 3D Models*

3D models provide a powerful tool for regional-scale structural investigations. Simple models for the Lofoten ridge were first constructed in ArcGIS™, by overlaying Landsat images for the LVA region onto a DTM of the area. These models can be viewed from different vantage points, zoomed to different scales, and simulated 'fly-through' animations created. This is particularly useful for studying the relationship between structures and topography. Bedrock maps, gravity maps and magnetic maps were also draped onto the DTM for similar studies. These simple models have been described as '2.5-D' representations (Longley et al., 2001; Jones et al., 2004) as they do not provide any direct information about the subsurface geology. For a fully 3D model (i.e. equivalent to seismic models offshore) structures must be projected into and out of the topographic surface. For this type of analysis, more specific 3D modelling software is required. Following structural interpretations in GoCAD™, regional 3D fault models were then re-imported into ArcGIS (ArcScene) for integration with field GIS data and offshore fault and horizon models. For fly-through animations of these models see *appendix 6*.

#### 4.4. Regional structural analysis

##### 4.4.1. Onshore surface analysis

###### 4.4.1.1. Lineament populations:

Along the Lofoten-Vesterålen archipelago, good exposures in crystalline basement and the strong topographic relief permit the ground-truthing of lineaments that were mapped using Landsat TM data. The region appears highly faulted and fractured, as indicated by the dense set of over 2000 lineaments identified from the remote sensed data (Gabrielsen et al., 2002 and this study). These regional lineament maps show the Lofoten Ridge to have 2 dominant lineament trends, NNE–SSW ( $020^{\circ}$ – $040^{\circ}$ ) and ENE–WSW ( $070^{\circ}$ – $090^{\circ}$ ) (Fig. 4.3), with subsidiary NW–SE, NE–SW and E–W trends. Central Lofoten (i.e. Flakstadøya and Moskenesøya; Fig. 4.2c) and outer-Vesterålen both show dominant N–S and NNE–SSW oriented lineament suites, while an ENE–WSW-trending lineament suite can be seen in North Lofoten (Vestvagøya and Austvagøya; Fig. 4.2c) running east towards Ofotfjorden (Fig. 4.3a). Other systems include a NW–SE-trending suite on Vesterålen (Fig. 4.3a). Field reconnaissance of the area has confirmed that most of these lineaments correspond to major fault structures (see Fig. 4.8). In some cases the structures themselves cannot be directly identified as they lie at the bottom of fjords or vegetated valleys (e.g. Raftsundet; see Fig. 4.8). However, the intensity of fracturing in adjacent areas of exposed rock is consistent with their location close to major fault structures.

###### 4.4.1.2. Lineament domains:

Spatial analysis tools in ArcGIS have been used to quantitatively analyze these lineament patterns in more detail. Lineament density maps were made by counting the total number and total length of lineaments within a moving  $1 \text{ km}^2$  search window. These maps highlight the dominant lineament in different parts of the LVA. Directional analysis was also carried out using rose diagram plotting tools in ArcView. Having gridded the area into  $10 \text{ km} \times 10 \text{ km}$  cells, rose diagrams were plotted for each cell (Fig. 4.3b). This spatial analysis reveals that the LVA can be sub-divided into a series of distinct lineament domains: 1) Central Lofoten (CLD); 2) North Lofoten (NLD); 3) Lødigen (LødD); 4) Hinnøya (HinD); and 5) Langøya (LangD); Fig. 4.4a and Table 4.1). In all 5 domains, a dominant lineament trend is NNE-SSW to NE-SW, with some domains also showing a second dominant trend: ENE-WSW in North Lofoten, and NW-SE on Hinnøya. These domains are

coincident with changes in ridge trend, and with previously documented variations in regional gravity and magnetics, denudation ages and offshore fault patterns (Fig. 4.4b, c) (Tsikalas et al., 2001; Hendriks and Andriessen, 2002; Olesen et al., 2002). Gravity highs appear associated with areas showing a single preferred lineament trend (i.e. Central Lofoten and Langøya domains; Fig. 4.4b; also refer to fig. 10 of Olesen et al., 2002), while magnetic highs can be seen along the entire Lofoten Ridge (i.e. below CLD and NLD) and on Langøya (Fig. 4.4c).

#### 4.4.1.3. Regional onshore models:

3D fault models have been created for these lineament maps using structural modeling tools in GoCAD™. By overlaying Landsat lineament interpretations (in vector form) over a DTM, the lineaments then take on a 2.5D configuration (a curved line in 3D space). If there is sufficient interaction between topography and the lineament trace – the considerable topographic relief of Lofoten is perfect for this – then best-fit surfaces can be constructed along each lineament, thus producing a representative fault plane (see Fig. 4.5). Not only does this method provide a model to help visualize the 3D structure of the region, but also, as a consequence of the method, strike and dip of these regional fault surfaces can be calculated. These faults can then be compared to the equivalent geometries interpreted from offshore seismic data and to field data (Fig. 4.5).

3D fault models were created using this method over a 1250 km<sup>2</sup> (i.e. 25 km x 50 km) area in North Lofoten (Figs. 4.2. b and 4). Like the rest of the NLD, lineament orientations in this area have two distinct preferred orientations, NNE–SSW/ NE–SW (~035°) and ENE–WSW/ E–W (~080°). The resulting 3D model for these structures displays a rhombic fault block pattern (Fig. 4.5), while the poles to planes of these regional structures appear to cluster in a bimodal distribution (Fig. 4.5f). Due to the lineament picking method favoring straighter lines (i.e. the picker is nearly always biased towards drawing straighter lines, particularly across areas of uncertainty – such as hill slopes in shadow or less distinct lineament trace), the faults may appear steeper than they really are (i.e. a straighter line equates to a steeper structure), which may account for the apparent clustering around the vertical dip.

#### 4.4.2. Offshore subsurface analysis

A map of fault structures previously identified by Tsikalas et al. (2001), together with similar structural trends identified in this study are shown in Figure 4.4. Figure 4.6 shows line interpretations of a series of NW–SE trending seismic profiles across the Ribban Basin (Havbåen sub-Basin), while Figure 4.7 shows an overall 3D model of the area derived from these interpretations (constructed using Traptester, ArcGIS and ArcScene). Both these figures highlight a distinct change in basin geometry and structure between the offshore areas of Central Lofoten and North Lofoten.

##### 4.4.2.1. Offshore Central Lofoten and the Havbåen sub-Basin:

Offshore Central Lofoten is characterized by a single major NNE–SSW- to NE–SW-trending border fault (parallel to the ridge trend) bounding a large depocenter (the Havbåen sub-Basin; Figs. 4.6. and 4.7. a). Syn-rift thickening of Upper Jurassic and Lower Cretaceous sequences is apparent along the WLBF in this area, while most Middle Cretaceous sediment infilling the Havbåen sub-Basin appears to be associated with thermal subsidence, thickening towards the centre of the basin. Intra-Lower Cretaceous and Middle Cretaceous hangingwall sequences dip away from the WLBF before shallowing to horizontal through a hangingwall syncline (Fig. 4.6). This geometry resembles a similar compaction-related geometry discussed by Thompson and Underhill (1993) for faulting in the Moray Firth. These structures are interpreted to form in response to differential compaction as a consequence of varying hangingwall and footwall lithologies together with a buttressing effect created by the underlying rigid footwall.

##### 4.4.2.2. Offshore North Lofoten:

The North Lofoten ridge trends ENE–WSW. Here the WLBF appears to bend round into a NE–SW to ENE–WSW orientation, with a number of NNE–SSW-trending faults splaying off it (green faults in Figs. 4.6. and 4.7.). As these ‘splay faults’ are oriented counter-clockwise of the main border fault, this resembles an en-echelon style fault geometry from which a component of sinistral shear could be inferred along the WLBF in this area. Throws on the WLBF and associated faults are reduced compared to those seen to the south, and there is also significantly less thermal subsidence and infilling. Furthermore, in the northern part of this area, sedimentary sequences appear to have been uplifted and eroded (Tsikalas et al., 2001). This is

likely to have occurred at the same time as the sediments that covered Vesterålen were eroded away (Dalland, 1981; Løseth and Tveten, 1996).

Also characteristic of this area are a number of major NNE–SSW-trending, east-dipping faults located farther offshore (yellow faults in Figs. 4.6 and 4.7). These faults show extensive syn-rift thickening of hangingwall sequences of Late Jurassic to Mid Cretaceous (Aptian) age (Fig. 4.6).

It is important to note that there are no distinct structures marking the position of the Jannegga transfer zone (see Fig. 4.6), and that this zone simply marks the transition between two fault systems with differing trends. A field outcrop analysis was undertaken in order to investigate further the complex faulting patterns in the NLD. The mapping area chosen for detailed field analysis is highlighted in Figures 4.4 and 4.5.

## **4.5. Field data analysis**

### **4.5.1. Fault populations**

During fieldwork, 666 mesoscale (cm-dm scale) faults and fractures and associated slip-striae have been measured at over 20 localities across NE Austvågøya. More than 60% of the faults measured exhibit good kinematic indicators, in the form of slickenlines and striated coatings (Fig. 4.8f). Kinematic indicators such as Reidel shears were used to infer shear direction and shear sense on each fault plane (Petit, 1987).

Almost all exposures in the mapping area were in charnockites (orthopyroxene granite) and mangerites (orthopyroxene monzonite) of the Raftsund pluton. These rocks exhibit a weak E–W trending fabric; however in many places basement fabrics were indiscernible. Best fresh exposures of fault surfaces were found on road cut sections and shorelines, however due to the dramatic topography of the area many fault cores can also be easily traced up mountainsides (Fig. 4.8d). Fault exposures varied from large solitary faults in a relatively undeformed country rock (Fig. 4.8c), to fault zones of highly fractured rock. Fault rocks observed were generally cataclastic (i.e. breccia and cataclasite; Fig. 4.8e) and little evidence for fluids was observed (only example of mineralization was found at locality L07 in the hanging wall of the Ingelsfjorden fault, in the form of epidotic slickenfibers).

When plotted stereographically, three main fault clusters are apparent (Fig. 4.9ai), with strike orientations that closely match the data derived from lineament analysis (Fig. 4.5f). These clusters reflect 2 distinct fault geometries: 1) NNE–SSW to NE–SW trending faults, dipping NW and SE (*System 1*; Fig. 4.9b); and 2) ENE–WSW to E–W trending faults dipping mainly to the north (*System 2*; Fig. 4.9c). These fault geometries are matched by similar fracture/ joint trends (i.e. surfaces with no clear evidence for slip; Fig. 4.9aiii). Note that only ENE–WSW and E–W trending surfaces showed plumose markings characteristic of joints (Fig. 4.8). Plots of slip striae (Fig. 4.9aii) show that all fault orientations are dominated by dip-slip or oblique-slip normal fault movements. However, a small number of strike-slip movements were also observed (Figs. 4.9biii and ciii), and some faults exhibit multiple slip-striae. Strike-slip striae on System 1 (NNE–SSW oriented) faults appear to indicate a dextral shear sense; while on System 2 (ENE–WSW oriented) faults, sinistral shear is apparent.

Both cross-cutting relationships and slickenline patterns have been analyzed to determine a temporal succession of fault movements. No conclusive and consistent sense of cross-cutting relationships between faults has been observed, with examples of system 1 faults cross-cutting system 2 faults and vice versa in a single area of exposure. In many cases, multiple slickenlines on a single fault surface can be attributed to fault interaction rather than reactivation (see below), although strike-slip striae appear to consistently post-date dip-slip striae on some NNE–SSW-trending (system 1) fault surfaces.

#### **4.5.2. Fault interaction**

As there are multiple fault orientations, and the spacing between faults is small (generally <2 m) some interaction between structures is likely. As the stereonets in Fig. 4.9a show, the mean slickenline orientation lies parallel to the intersection between mean fault planes. This may indicate that fault interaction has occurred during fault-slip. A number of direct examples of fault interaction are observed at outcrop (e.g. Figs. 4.10. a, b) and are comparable with the relationships described for the interacting block model of Nieto-Samaniego and Alaniz-Alvarez (1997). This reinforces the hypothesis that the polymodal fault sets observed, developed during the same phase of extension.

### 4.5.3. Spatial characteristics of faults and fractures

#### 4.5.3.1. Spatial analysis:

A spatial analysis of fault geometry and slickenline data was carried out in ArcView using an interactive GIS-stereonet program provided by Knox-Robinson and Gardoll (1998). Figure 4.11 shows a summary map, and associated stereonets, for fault populations for localities in the area of Raftsundet. Localities were chosen in order to analyze the variations in faulting both parallel and perpendicular to the major lineament structures, but were also controlled by outcrop distribution and ease of access. Fault geometries at outcrop generally reflect regional lineament trends. However, in many cases, the main lineament trend for a locality is often the secondary fault system at outcrop (i.e. *system 2* may be the major lineament trend, but *system 1* faults may predominate at outcrop, or vice versa). In addition to analyzing each locality individually, fault geometries were also analyzed with respect to increasing distance from inferred major structures (such as Raftsundet). However, no distinct patterns of spatial distribution were observed.

#### 4.5.3.2. Fracture spacing analysis:

A series of cross-sectional fracture maps were created at various localities from photographic mosaics georeferenced using the laser ranger. These fracture maps enable the analysis of fracture attributes both in one-dimensional (1-D; i.e. fracture spacing) and two-dimensional (2-D; i.e. connectivity, density) sampling methods (Gillespie et al., 1993; Beacom et al., 2001; McCaffrey et al., 2003b). In order to analyze the spacing and degree of clustering of faults/fractures in the area, line transects were made across each fracture map, recording the position of fractures along the sample line (Fig. 4.12.a). These line transect data were then analyzed using in-house software to calculate fracture spacing attributes (see Table 4.2 for summary of attributes calculated for each transect).

Gillespie *et al.* (1993, 1999) demonstrated that the fracture spacing population technique of Harris et al. (1991) is the only reliable method for characterizing the spatial attributes of fractures measured in 1-D samples. In this technique, the spacing between immediately adjacent fractures is plotted on a spacing vs. cumulative frequency graph (termed 'population plots' in McCaffrey et al., 2003b). By using a variation of logarithmic and linear axes, the data may plot as straight lines. The four most common distributions are normal, log-normal, negative

exponential and power-law (McCaffrey et al., 2003b). Different distributions have been found to correlate with different spacing characteristics. Distributions may be quantitatively compared by using distribution curves fitted using least squared regression analysis (see exponent column in Table 4.2; McCaffrey et al., 2003b).

In order to analyze these spacing data thoroughly, a number of other attributes were also calculated for each transect. Fracture density (FD), the number of fractures per meter (note that relative fracture density between lines may also be assessed using population plots; steeper lines equate with higher fracture density); mean fracture spacing (MFS; equivalent to  $1/\text{FD}$ ); standard deviation (SD); and the coefficient of variation ( $C_v$ ).  $C_v$  has been used (McCaffrey and Johnston, 1996; Beacom et al., 2001) as a numerical measure of clustering in 1D datasets.  $C_v$  is defined as the ratio of the standard deviation to the mean for a given attribute (Cox and Lewis, 1986), in this case fault spacing. If fractures are clustered then  $C_v > 1$ , and if anti-clustered then  $C_v < 1$ .  $C_v = 0$  means a regular spacing, while  $C_v = 1$  reflects a random distribution (McCaffrey and Johnston, 1996; Beacom et al., 2001).

Table 4.2 shows a summary of the data recorded for each transect line. Figure 4.12b shows plots of fracture density (FD) vs.  $C_v$ , illustrating that the fractures generally show a random to moderately clustered distribution ( $C_v \geq 1$ ), but that this variation is not dependent on FD. Almost all transect lines reveal a population plot of fracture spacing best-fitted by an exponential distribution, with higher exponent values in zones of increased FD. For a dataset best fitted by an exponential distribution, the mean and standard deviation values are expected to be similar. In a plot of mean fracture spacing (MFS) vs. standard deviation (SD) (Fig. 4.12c) we can see there is a good relationship between the two parameters, which is consistent with the exponential distributions observed in our population plots. Exponential distributions are characteristic of randomly-spaced fracture systems (Rives et al., 1992).

A simple spatial analysis of the data was also carried out by plotting FD,  $C_v$  and exponent of fracture spacing vs. distance from major fault structures (i.e. Raftsundet fault and Ingelsfjorden fault in Fig. 4.11). A small increase in fracture density and exponent values can be seen in the vicinity of the Raftsundet fault (Fig. 4.12d), but is not observed in  $C_v$  values. No discernable trends were observed for the spatial distribution on  $C_v$  values, or for any attributes relative to the Ingelsfjorden fault.



#### 4.5.4. Kinematic analysis

Kinematic analysis (strain inversion) was carried out using so-called 'paleostress analysis' techniques. The analysis of fault slip data yields information concerning the orientation of the strain tensor, and thus the calculated axes are referred to using infinitesimal/ finite strain nomenclature rather than principle stresses. The aims of our study here were: 1) to determine if all fault movements are compatible with a single strain field; and 2) to derive a 'palaeostress' tensor from the outcrop data that can be compared to regional fault patterns developed onshore and offshore. Kinematic inversion techniques have been extensively used by various workers for nearly 40 years (see Angelier, 1994, and Ramsay and Lisle, 2000, for an exhaustive review). The assumptions and methods of palaeostress have been discussed in detail in many other papers (Etchecopar et al., 1981; Angelier, 1984, 1994; Michael, 1984; Reches, 1987; Delvaux and Sperner, 2003) and are not discussed here.

##### 4.5.4.1. Inversion procedures:

In total 414 faults with good kinematic indicators were recorded (Fig. 4.9a), which can be used for kinematic inversion. My Fault™ stereonet software, produced by Pangaea Scientific Ltd., was used for kinematic analysis.

Two separate procedures for sorting the fault data into populations for inversion analysis have been applied during the present study. The first (*Procedure 1*) simply uses the entire unsorted dataset (i.e. all 414 fault and fault striae) while the second (*Procedure 2*) required manual sorting and separate analysis of the data into fault systems.

*Procedure 1:* After input of the raw data, data files were corrected to ensure that all striae lie perfectly on their respective fault planes (i.e. no angular mis-match). To do this, fault striae were rotated along the common plane containing the striae and the pole of the fault plane. Following this, the bulk fault population dataset was inverted. Those faults with high misfit angles ( $>40^\circ$ ) relative to the inversion result were then rejected and the inversion rerun. This procedure was repeated until a single group of faults with a homogeneous solution could be found. The rejected data were then rerun through the program in an attempt to derive multiple 'palaeostress' vectors. A similar iterative approach has been applied in the past by Titus et al. (2002). This procedure was then repeated for various inversion methods (i.e. Angelier, 1984; Michael, 1984; Reches, 1987) to test the consistency of the results.

*Procedure 2:* A potential risk when analyzing a bulk fault population dataset with uncertain age relationships is that the kinematic data being analyzed represent more than one phase of movement. This can result in the derived vectors reflecting a combination of the two or more phases and may not be geologically meaningful (Delvaux and Sperner, 2003). Fault data were separated according to fault geometry (i.e. fault systems 1 and 2; Fig. 4.9b, c), and any examples of structures associated with fault interaction were disregarded as this violates the basic assumptions of inversion methods (Nieto-Samaniego and Alaniz-Alvarez, 1997). As the data have already been sorted prior to analysis, the 'iterative' sorting approach, used during Procedure 1, was only required for the strike-slip fault set.

#### 4.5.4.2. *Inversion results:*

Bulk inversion of all fault data using the inversion method of Michael (1984) produced an apparent NW-SE-trending, maximum extension, infinitesimal strain axis ( $X_i \equiv \sigma_3$ ), 316/03, and sub-vertical infinitesimal minimum extension (or shortening) direction ( $Z_i \equiv \sigma_1$ ) (Fig. 4.13a). Similar values for ( $X_i$ ) were calculated using all other inversion methods (Fig. 4.13b).

Following *procedure 2*, three separate sets of 'palaeostress' axes can be derived, one for each fault system analyzed (i.e. system 1 dip-slip, system 2 dip-slip, and all strike-slip faults; Fig. 4.13c-e). Analysis of each fault system yield similarly oriented axes (of course for strike-slip faults the  $Y_i$  and  $Z_i$  axes are switched; i.e.  $Z_i$  is horizontal), although there is a 24° variation in the azimuth of the extensional axes ( $X_i$ ).

#### 4.5.4.3. *Transtension and the effects of fault obliquity in the NLD*

For a homogeneous transtension, the maximum principal extension axis ( $X_i$ ) should always lie in the horizontal plane during progressive deformation (Sanderson and Marchini, 1984; McCoss, 1986). Following Withjack and Jamison (1986) and De Paola et al. (2005a) there is a predictable relationship between the angles made by the regional (or in this case, domainal) extension vector ( $\alpha$ ) and the infinitesimal horizontal maximum extension strain axis ( $\beta$ ) measured relative to the deformation zone boundary (Fig. 4.14a) according to the equation (shown graphically in Fig. 4.14b):

$$\beta_x = 90^\circ - 0.5 \tan^{-1} (\cot \alpha) \quad (4.1)$$

From the stress inversions carried out under procedure 2 for system 1 faults,  $\beta_x = 84^\circ$  (measured between the maximum principal extension axis and the main fault trend; Fig. 4.14c) which corresponds to  $\alpha = 78^\circ$ , and a local inferred extension vector of  $312^\circ$  (Fig. 4.14c). As  $\beta_x \approx \alpha$ , this suggests that system 1 faults are mainly accommodating a component of orthogonal extension. However for system 2 faults,  $\beta_x = 71^\circ$ , corresponding to an angle  $\alpha = 52^\circ$ , which also yields a local inferred extension vector of  $312^\circ$  (Fig. 4.14c). This is consistent with the sinistral oblique-slip directions generally associated with these faults (e.g. Fig. 4.13d). Thus, the extension directions, determined through a separate inversion analysis for each fault system, show distinctly different orientations (i.e. system 1 = WNW–ESE extension, system 2 = NNW–SSE extension). However, by applying *equation 4.1*. to these results, an exactly coincident regional extension vector is obtained (system 1 =  $312^\circ$ , system 2 =  $312^\circ$ ), which is very similar to that calculated for the strike-slip faults ( $318^\circ$ ) and the bulk dataset analyzed using procedure 1 ( $316^\circ$ ). Therefore bulk regional extension for the NLD can be estimated as NW–SE (Fig. 4.14d). This faulting pattern suggests a combination of reactivation of pre-existing structures - e.g. joints and fractures (system 2, and possibly system 1) and the development of new faults (system 1) as a result of the imposed strain, without larger-scale domainal partitioning of the bulk strain. Also, the consistency in the apparent regional extension vector for each fault system lends further support to field observations that the faults analyzed are contemporaneous.

## 4.6. Discussion

### 4.6.1. Regional vs. field measurements of onshore faults

Regional fault models derived from lineament analysis for the NLD show a rhombic fault block pattern (Fig. 4.5), with the poles to planes of these regional faults clustering in a bimodal distribution (i.e. near vertical dips; Fig. 4.5f). However, field observations suggest that many of these regional faults have a shallower dip than those suggested by our 3-D model. For example, Figure 4.8d shows three large fault traces identified in the field which dip at  $\sim 60\text{--}65^\circ$  north. These faults were also recognized from lineaments on the Landsat image and in the GoCAD model, these

planes dip at  $>80^\circ$ . Studies of outcrop scale faults would also suggest that the dominant fault dip is closer to  $\sim 70^\circ$  (Fig. 4.9) than vertical as predicted by regional models (Fig. 4.5f). Therefore, it would appear that a limitation of this method of fitting best-fit planes through lineament traces can lead to an oversteepening of the fault plane by  $\sim 10\text{--}15^\circ$ . Hence, any regional fault dipping at  $>75^\circ$  is likely to appear near vertical in this model. Consequently, we interpret the derived lineament data as masking a polymodal fracture distribution which we relate to 3D deformation, rather than 2D plane strain (see below and Oertel, 1965, Reches, 1978, and Krantz, 1989).

#### 4.6.2. *Complex faulting – oblique extension in North Lofoten*

Figure 4.15a shows a summary of the regional onshore structures along the Lofoten ridge. It is dominated by two dominant lineament trends (NNE–SSW and ENE–WSW), while the overall ridge trend is ENE–WSW. Comparison with fault traces in experimental clay models of oblique extension (Withjack and Jamison, 1986, Clifton et al., 2000) suggest that the fault patterns are similar to those in models where  $\alpha \leq 30^\circ$ , which would suggest a regional WNW–ESE extension direction. This oblique extension is consistent with offshore fault patterns which show an en echelon style set of faults splaying off the NE–SW to ENE–WSW-trending WLBF, suggesting a component of sinistral shear on the border fault. The kinematic inversion analysis of outcrop-scale faults within the NLD suggests a NW–SE ( $\sim 320^\circ$ ) extension. If we use the ridge trend in this domain ( $085^\circ\text{--}265^\circ$ ) to define regional-scale orientation of the deformation zone boundary faults, then  $\beta = 55^\circ$  for the NLD. By applying equation 4.1., we obtain an angle  $\alpha = 20^\circ$ , and a regional extension vector (RE) oriented  $285^\circ$  (Table 4.3). Importantly, this direction corresponds well with extension directions documented along other parts of the Norwegian margin during the Early Cretaceous (e.g. Mosar et al., 2002).

Significantly, rift systems that undergo extension oblique to the basin bounding faults commonly show complex multi-modal fault patterns (e.g. Withjack and Jamison, 1986; Clifton et al., 2000; Dewey, 2002; De Paola et al., 2005a, 2005b). Both regional and outcrop studies in northern Lofoten have revealed an apparent polymodal fault geometry, i.e. fault patterns dominated by more than two distinct fault sets (Fig. 4.9a).

#### **4.6.3. Fault interaction and implications for stress inversion**

Methods for determining the regional stress tensor from populations of faults with slickenlines have been around for nearly 40 years (Arthaud, 1969; Etchecopar et al., 1981; Angelier, 1984, 1994; Michael, 1984; Reches, 1987; Delvaux and Sperner, 2003). In recent years, a number of studies have examined the limitations of these methods (Pollard et al., 1993; Cashman and Ellis, 1994; Nieto-Samaniego and Alaniz-Alvarez, 1997; Maerten, 2000). Slickenlines are kinematic indicators (slip-vectors), and when these are used to interpret the regional stress field a number of assumptions have to be made. One of the most important assumptions is that the slickenlines are produced by the general stress tensor, implying that faults do not interact and that the stress field is not significantly perturbed after fault slip. *Pollard et al.* (1993) discuss how interaction between pre-existing planes can lead to stress field perturbations of up to 40° in orientation when the density of fault planes is high. Interacting fault movements on pre-existing planes can lead to multiple slickenline sets forming under a single regional stress field (e.g. Cashman and Ellis, 1994).

In some areas of North Lofoten there is strong evidence to suggest that fault interaction has played a significant role in the development of faults. The mean slickenline orientation lies parallel to the intersection of two of the major fault systems (e.g. Fig. 4.9a) and several examples of fault interaction have been recognized at outcrop (e.g. Fig. 4.10). Nieto-Samaniego and Alaniz-Alvarez (1997) have suggested that fault systems controlled by fault block interaction may not be suitable for palaeostress analysis as a number of basic assumptions of these methods are violated. However, given the large number of data collected in the present study and the seeming consistency of the palaeostress analysis results, we feel that, in this case, a valid result has been obtained. One reason for this is that using a GIS for data management allowed efficient, quantitative filtering of all data points that do not meet certain geospatial or geological criteria. For example, all faults showing outcrop evidence for 'fault interaction' were removed from the analysis.

#### **4.6.4. Fracture spacing and origins**

Fault spacing at localities across the mapping area (Fig. 4.11) is consistently described by a negative exponential distribution with slightly higher exponents closer to the Raftsundet fault (Fig. 4.12d). Exponent values range from 0.0007 to 0.0030, and when compared to past studies in mature basement deformation zones (with

highly focused deformation and evidence of reactivation) such as the Møre-Trøndelag Fault Zone (Sleight, 2001; McCaffrey et al., 2003b), these values fall in the range for background and minor faults (Fig. 4.12d). This, combined with the generally random fracture spacing and only relatively low levels of clustering, suggests that although the rocks of North Lofoten are ancient Precambrian basement, brittle deformation appears to be relatively immature. This apparent immaturity is consistent with two other field observations in Lofoten: a) the fact that we see little evidence for reactivation of earlier brittle fault sets; and b) there is little evidence for widespread localization of displacement along specific fault structures in onshore exposures.

In regions located well away from larger-scale faults, the majority of fractures in exposed basement lack slickenlines and have the appearance of joints (Fig. 4.8g). In some examples, these surfaces carry ornamentations that closely resemble plumose markings (Fig. 4.8g) (Hodgson, 1961). When plotted on a stereonet, poles to these joint planes display three distinct clusters of similar orientations to those recognized for poles to faults with slickenlines (Fig. 4.9a). This leads us to propose that the main transtensional fracture sets observed in the field in the NLD may represent reactivated joints. Rives et al. (1992) have shown that for joints where there is a low fracture density and little interaction, the spacing distribution is likely to be exponential. Collectively, the field observations, orientation data and spacing distribution data suggest, therefore, that the fractures in the NLD are formed due to the reactivation of pre-existing joint sets in basement.

The age of these joints is unknown at present. However, at locality L03 (GR: 499621 7591288 – UTM zone 33N) a lamprophyre dyke trending parallel (084/82S) to system 2 faults was observed (Fig. 4.8h). Brittle faults at, and near, the margin of this dyke show evidence for sinistral strike-slip movements, while an earlier prominent set of tensile (mode 1) fractures, i.e. joints, trend parallel to the dyke and the associated faults (including the joint with the plumose markings shown in Fig. 4.8g). The age of the dyke is unknown, but we suggest that it may have been emplaced synchronous with joint formation in these basement rocks. We can speculate that the dyke may possibly be anything from Late Paleozoic to Early Mesozoic in age (Færseth et al., 1976), but an even older age of intrusion cannot be entirely ruled out.

#### 4.6.5. *Segmentation of the LVA*

Detailed onshore lineament studies have revealed that the LVA can be divided into a series of distinct lineament domains (Fig. 4.5 and Table 4.1). These variations are coincident with changes in ridge trend and physiography (i.e. landscape, topography, etc). In Central Lofoten (i.e. CLD) the trend of the ridge is NNE-SSW, whereas in the North Lofoten (i.e. NLD) the ridge becomes ENE-WSW-trending, and is also much broader. These changes onshore are coincident with important structural changes offshore. The WLBF bounding the CLD is a single, major, NNE-SSW-trending fault with ~3 km throw (Fig. 4.6), whereas in the NLD the WLBF is indistinct, and appears to bend round into a more ENE-WSW trend with a series of NNE-SSW-trending, west-dipping, splay-faults, with lesser throw (Fig. 4.6). Also in the offshore NLD there is a change in fault polarity, as east-dipping faults appear to take up a larger proportion of the Cretaceous extension, and seem to have stayed active until Aptian times.

Structural segmentation of the Lofoten-Vesterålen region was previously identified by Løseth and Tveten (1996), Olesen et al. (1997, 2002) and Tsikalas et al. (2001) based on changes in fault polarity and sediment thickness offshore, and crustal structure (derived from potential field data) onshore. Hendriks and Andriessen (2002) then discussed this further using fission track data to identify ridge domains with different denudation histories. A number of rift segments and transfer zones have been proposed (see Fig. 4.2), but there are disagreements concerning the exact position and orientation of these structures (e.g. Tsikalas et al., 2001; Olesen et al., 2002). Table 4.1 shows a correlation between lineament domains identified in this study to those in previous studies, together with the transfer zones that are believed to separate these domains.

#### 4.6.6. *Transtensional model for the LVA*

Onshore, variations in the dominant lineament/fracture trends along the Lofoten ridge can be explained using a model for oblique extension/ transtension along the LVA that develops due to the changing trend of the deforming zone and zone boundary structures with respect to the regional extension vector (Fig. 4.15). In this model there are three distinct deformation zones. In Central Lofoten there is a zone of orthogonal extension ( $\alpha = 90^\circ$ ) (zone A), passing northwards into two zones of transtension (B and C). Zone B corresponds to an angle  $\alpha$  of  $\sim 35^\circ$ , which is close to

the transition between extension-dominated and wrench-dominated transtension (shown as  $20^\circ$  in Fig. 4.1, but is generally ranges from  $30^\circ$ - $40^\circ$  for most rocks, see De Paola et al., 2005a) while zone C lies just within the wrench-dominated field (horizontal z-axis) with  $\alpha \sim 20^\circ$  (Fig. 4.15). Analogue models for increasingly oblique extension show that fault orientation will change with respect to the angle of obliquity,  $\alpha$  (Fig. 4.15c, Table 4.3) (Withjack and Jamison, 1986; Clifton et al., 2000). The fracture patterns predicted by these models show similar trends to those observed in lineament patterns for each domain along the Lofoten ridge (Figs. 4.4 and 4.15a).

The model for increasingly oblique transtension northwards along the Lofoten ridge is also consistent with offshore structural changes. Each zone is predicted to exhibit different faulting patterns and degrees of vertical shortening. In zone A, the shortening axis is vertical predicting a significant amount of vertical thinning and rift-related subsidence. In Zones B and C smaller amounts of vertical thinning and rift-related subsidence are predicted. Our observations offshore suggest that in the Central Lofoten domain the WLBF has a large throw, with a deep sedimentary basin developed in its hanging wall. Along strike in the region offshore from the NLD, the fault throws are reduced and the basins are markedly shallower or even absent.

In our model, the boundaries between each domain may have started off trending roughly N-S (perhaps controlled by pre-existing Permian extensional structures; Steltenpohl et al., 2004) and highly oblique to the regional extension. As extension continued these boundaries are likely to have rotated counter-clockwise to lie parallel to the NNW-SSE-trending transfer zones inferred by Tsikalas et al. (2001) and others (Figs. 4.2 and 4.15).

#### ***4.6.7. The control of pre-existing structures on ridge development and segmentation***

##### ***4.6.7.1. Ridge development:***

Prior to assessing ridge segmentation, we first consider factors that may have controlled the position of the Lofoten ridge. Geophysical studies (Sellevoll, 1983; Olesen et al., 1997, 2002) in central and northern Norway show the Lofoten ridge to be associated with strong magnetic and gravimetric anomalies (Figs. 4.4b, c). The positive gravity anomaly beneath the south and central Lofoten Ridge (Fig. 4.4b) are



believed to reflect a shallow Moho discontinuity and uplifted high grade rocks of intermediate density (Sellevoll, 1983; Olesen et al., 2002). This exhumation of rocks from the deep crust has led some authors to describe Lofoten as a ‘core complex’ (Hames and Anderson, 1996). However no such anomaly exists beneath north Lofoten. This further substantiates our offshore analysis that shows that greater extension has occurred in south and central Lofoten, although does not explain the oblique development of more northern areas of the Lofoten Ridge. The entire Lofoten Ridge is marked by a strong positive magnetic anomaly, which is likely to reflect the presence of granulite facies basement rocks at or near the surface, while the lows mark areas of thicker sedimentary sequences (i.e. greater depth to top-basement) within the basins (Fig. 4.4c). Having said this, it should be noted that a distinct E–W trending magnetic gradient (magnetic high in north, and low in south; Fig. 4.4c) can be traced westward from Hadsselfjoden (and the E–W trending ‘zone C’ of our transtension model – Fig. 4.15).

The South and Central Lofoten Ridges have similar geophysical characteristics to most other NE–SW trending basement highs on the Norwegian margin (e.g. Utgard High, Utrøst Ridge), and are therefore likely to have originated during simple orthogonal extension. However the prominent structure of the oblique trending North Lofoten Ridge needs some further explanation. Oblique extension is generally associated with the reactivation or control of pre-existing structures (Holdsworth et al., 1997). No distinct fabrics (e.g. shear zones, strong foliation, etc.) were observed within the basement rocks studied that could account for the north Lofoten ridge trend. A few discreet E–W trending joints and dykes were recorded that appear to be reactivated by faults at outcrop; however these are not intense enough to account for the overall change in ridge trend.

Olesen et al. (2002) proposed a model in which the border faults to the North Lofoten Ridge reactivate ‘spoon-shaped’ Devonian detachments (Fig. 4.16a; also see fig. 16 of Olesen et al., 2002). Field observations of these low-angle, Devonian, detachment structures have been made in Hinnøya (Løseth and Tveten, 1996) and northern Austvågøya (this study). A small increase in fracture densities around these Devonian structures may suggest that they have played a role in the development of later (Mesozoic) fault patterns observed at outcrop in this study. However, such low-angle structures are only likely to have a limited effect on the location and

orientation of steeply-dipping Mesozoic basin bounding extensional structures, and therefore further structural influence is required.

Recent Apatite fission-track (AFT) studies suggest that the LVA has undergone differential block uplift in post-Caledonian times (Fig. 4.16b). Hendriks and Andriessen (2002) document different AFT ages for different parts of the LVA indicating differential vertical movements across the area. The oldest cooling/denudation ages are observed on Langøya, which indicate uplift/exhumation during the Permian/Triassic, while evidence for Jurassic/Cretaceous sediments found on Andøya (Dalland, 1981) and in Sortlundsundet (Davidsen, 2000) suggest subsidence at this time. North Lofoten on the other hand shows evidence for cooling/denudation from Mid Jurassic to Early Cretaceous. It is possible that the earlier exhumed Langøya block acted as a barrier to the developing WLBF and that as a result extension was transferred eastwards from the Lofoten ridge towards the already established (Olesen et al., 1997) Vestfjorden-Vanna fault complex (Fig. 4.16c). The apparent younging in denudation age from NE to SW along the Lofoten Ridge may be explained due to the SLD undergoing greater extension uplift and erosion, exposing rocks exhumed from deeper in the crust, and which therefore passed through the apatite partial annealing zone later (see fig. 11 in Redfield et al., 2005).

The rocks of the north Lofoten ridge are dominated by anorthosite-mangerite-charnockite-granite (AMCG) suite of plutons (Fig. 4.16c) (Griffin et al., 1978; Corfu, 2004a) dating from ~1.8 Ga. The basement rocks on south Lofoten on the other hand are dominantly older Archaean/Palaeoproterozoic gneisses (Tveten, 1978; Corfu, 2004a). Granites typically have lower densities than the surrounding basement rocks, which can lead to a buoyancy effect as the granites as they move towards equilibrium with the surrounding basement (Bott, 1967). This basement buoyancy effect has been used to explain the tectonic stability and/ or uplift of areas underlain by granites (Bott, 1967; Donato et al., 1983). In addition, it has been suggested that this stability is most effective during times of extension (Bott et al., 1978). It is possible that the AMCG suite may have controlled the trend and development of the North Lofoten Ridge in this manner (Fig. 4.16c). Furthermore, as these granites are of Precambrian age, this buoyancy effect may also account for the trends of the 'spoon-shaped' Devonian detachments described by Olesen et al. (2002), and also the apparent elevated nature of the Lofoten Ridge through time (Sherlock, 2001).

Another possibility is that this oblique trend of the north Lofoten Ridge simply reflects a relay/ accommodation zone where extensional strain is transferred from the WLBF/ Lofoten ridge to the Vestfjorden-Vanna fault complex in the east (Fig. 4.16d). However one or more of the above structures are also likely to have had an influence on the location of this relay zone.

#### *4.6.7.2. Transfer zones and segmentation:*

The transtensional domainal model proposed here requires that the Lofoten ridge and associated offshore basins are segmented. This view seems to fit well with the view that the Norwegian Margin is segmented by a series of transfer zones (Lundin and Dore, 1997; Olesen et al., 1997, 2002; Tsikalas et al., 2001). The Bivrost, Vesterålen and Senja transfer zones have been attributed to the influence of deep seated basement structures at depth (Olesen et al., 2002; Mjelde et al., 2003). Known examples of such structures include the Bothnian-Kvænangen and the Bothnian-Senja fault complexes (Fig. 4.2). Other similar trending basement shear zones have been suggested to explain Lofoten's transfer zones (Mosken, Jennegga). However, our study and those of other workers (e.g. Tveten and Zwaan, 1993; Løseth and Tveten, 1996) have not been able to identify regional scale transfer faults (and associated shear zones) separating each domain. The domain boundaries appear instead to be zones of 'soft linkage' between areas characterized by different fault geometries that are related to variations in the angle of divergence between ridge border faults and regional extension. Therefore, these second-order transfer zones appear controlled by ridge trend, rather than vice versa. However, the relationship between first-order transfer structures appears less clear.

Corfu (2004b) proposed that a major Caledonian tectonic boundary occurs on Vesterålen marked by a sharp NNW–SSE-trending, magnetic gradient (Figs. 4.4c and Fig. 4.16d). This boundary has also been attributed to the prograde metamorphic transition from amphibolite-facies migmatites in the east to granulite-facies rocks in the west (Griffin et al., 1978; Olesen et al., 1991). This boundary may have some influence upon the apparent lack of fault linkage across the Vesterålen transfer zone (Løseth and Tveten, 1996; Olesen et al., 1997), but is unlikely to have had a significant effect on the trend of the Lofoten ridge unless a major component of dextral shear and fault block rotation was invoked, for which there is no evidence.

#### **4.7. Conclusions and Implications for future exploration on the Norwegian margin**

Through an integrated onshore, offshore and regional to outcrop-scale fault study we present a consistent structural model for transtension along the Lofoten ridge. The LVA can be divided into a series of distinct lineament domains reflecting varying fault patterns. In North Lofoten, there is evidence that the fault systems have formed due to reactivation of pre-existing joints. Fault-slip inversions suggest an ESE-directed regional vector of extension, consistent with Late Jurassic to Early Cretaceous rifting documented elsewhere along the Norwegian Margin (Mosar et al., 2002). Variations in onshore lineament patterns and topography are matched by offshore changes in basin depth and fault geometry. Basin geometry and fault complexity appear to be controlled by variations in the orientation of the basin bounding structures, with deep basins and simple faulting typical of areas where the ridge/ border fault is normal to extension, and complex faulting and less subsidence in more oblique settings. The changes in fault orientation, fault geometry and inferred extension directions for each domain in the Lofoten are consistent with transtensional models where the ridge-bounding structure becomes increasingly oblique to extension (Fig. 4.15) (Withjack and Jamison, 1986; Clifton et al., 2000; Dewey, 2002, De Paola et al., 2005b). No major discrete basement structures (such as basement shear zones) occur onshore separating segment domains which are instead interpreted as zones of 'soft linkage'.

Regional changes in depth to Moho show that the Surt, Bivrost and Vesteralen transfer zones are all deep seated structures (Olesen et al., 2002; Mjelde et al., 2003), and are therefore termed first-order transfer zones. However, the transfer zones that segment the Lofoten Ridge (Mosken and Jennegga transfer zones; Fig. 4.2) do not show this deep seated character and appear to represent regions of 'soft linkage' between structures. These zones also appear to be associated with changes in ridge trend and are thus attributed to changes in deformation style between zones of differing margin obliquity.

A number of recent studies of basement ridge structures on the Norwegian margin have shown that ridge trend relative to the regional stress vector plays an important role in the complexity of basins and potential reservoir plays (e.g. Gernigon et al., 2003; Ren et al., 2003; Imber et al., 2005). Many of these studies attribute these complex reservoirs to later reactivation of rift systems (e.g. Imber et

al., 2005). Our study broadly confirms this suggestion and additionally illustrates that these zones of complexity can form early in the development of rifted margin due to variations in initial rift trend that may be themselves controlled by features originating in the deeper basement such as the AMCG Pluton suite and/or Devonian detachment structures.

Lineament Domain	Margin segment <sup>c</sup>	Transfer Zones	Comments
<b>Langøya (LangD)</b>	Andoya Segment		<b>Lineaments:</b> N-S, NE-SW, ENE-WSW, NW-SE <b>Bounding fault:</b> No apparent bounding fault structure <b>Uplift (denudation):</b> Permo-Triassic <sup>b</sup> (covered by sediments in Mid Jurassic/ Early Cretaceous)
<b>Hinnøya (HinD)</b>	Andoya Segment		<b>Lineaments:</b> NE-SW, NW-SE, NNW-SSE <b>Uplift (denudation):</b> possibly Early Cretaceous (Hendriks, 2003)
<b>Lødingen (LøD)</b>	Andoya Segment		<b>Lineaments:</b> NNE-SSW, ENE-WSW/ E-W Major NE-SW-trending regional fault - Storvatnet Fault (part of the Vestfjorden-Vanna Fault Complex)
		Vesterålen TZ <sup>a,b</sup>	NNW-SSE trending magnetic anomaly Zone acts as barrier between NE-SW-trending faults
<b>North Lofoten (NLD)</b>	Vesterålen Segment		<b>Lineaments:</b> NNE-SSW, ENE-WSW/ E-W <b>Bounding fault:</b> ENE-WSW <b>Uplift (denudation):</b> Mid Jurassic/ Early Cretaceous <sup>b</sup>
		Jannegga TZ <sup>c</sup> or Melbu TZ <sup>a</sup>	Apparent gravity and magnetic anomaly Marked by change in fault polarity offshore
<b>Central Lofoten (CLD)</b>	Lofoten Segment		<b>Lineaments:</b> N-S, NNE-SSW, NE-SW, NW-SE <b>Bounding fault:</b> NNE-SSW <b>Uplift (denudation):</b> Early Cretaceous <sup>b</sup>
		Mosken TZ <sup>a</sup>	Coincident with NW-SE trending gravity and magnetic anomaly Left-lateral offset on ridge trend

<sup>a</sup>Olesen *et al.* (2002), <sup>b</sup>Hendriks and Andriessen (2002), <sup>c</sup>Tsikalas *et al.* (2001)

**Table 4.1.**

Summary of correlations between lineament domains identified in this study with those of previous works (Tsikalas *et al.*, 2001<sup>c</sup>; Hendriks and Andriessen, 2002<sup>b</sup>). Also listed are the transfer zones that divide these domains (Tsikalas *et al.*, 2001<sup>c</sup>; Olesen *et al.*, 2002<sup>a</sup>).

Locality	Transect line	Trend, degrees	Transect length, m	N	Sp	Exponent	MFS	SD	FD	Cv
L09	3000a	159	76.93	227	EXP	0.0026	0.34	0.35	2.95	1.20
L09	3000b	147	78.23	166	EXP/PL	0.0014	0.47	0.64	2.12	1.44
L09	3001a	162	80.71	160	EXP	0.0017	0.50	0.53	1.98	1.04
L09	3001b	145	56.14	93	EXP	0.0014	0.60	0.63	1.66	1.08
L08	3002	131	75.04	145	EXP	0.0014	0.52	0.64	1.93	1.29
L06	3004a	142	86.98	195	EXP	0.0020	0.45	0.45	2.24	1.09
L06	3004b	155	75.79	111	EXP	0.0010	0.68	0.93	1.46	1.37
L05	3006	20	80.15	69	EXP	0.0008	1.16	1.18	0.86	1.05
L05	3008	72	40	54	EXP	0.0011	0.74	0.81	1.35	1.15
L04	3009	77	61.4	62	EXP	0.0011	0.99	0.82	1.01	0.86
L04	3010	74	28.58	38	EXP/LN	0.0016	0.75	0.80	1.33	1.21
L03	3011	125	104.65	104	EXP	0.0007	1.01	1.29	0.99	1.36
L10	3101	8	95.67	166	EXP/PL	0.0012	0.58	0.75	1.74	1.27
L10	3102	177	40.81	91	EXP	0.0020	0.45	0.46	2.23	1.01
L12	3103	25	58.98	90	EXP	0.0013	0.66	0.71	1.53	1.10
L11	3104	173	50.21	229	EXP/PL	0.0030	0.22	0.29	4.56	1.33
L13	3105	29	33.58	69	EXP	0.0029	0.49	0.31	2.06	0.65
L13	3106	31	21.59	31	EXP	0.0013	0.70	0.66	1.44	0.97
L15	3110	9	21.89	23	EXP	0.0008	0.95	1.01	1.05	1.06

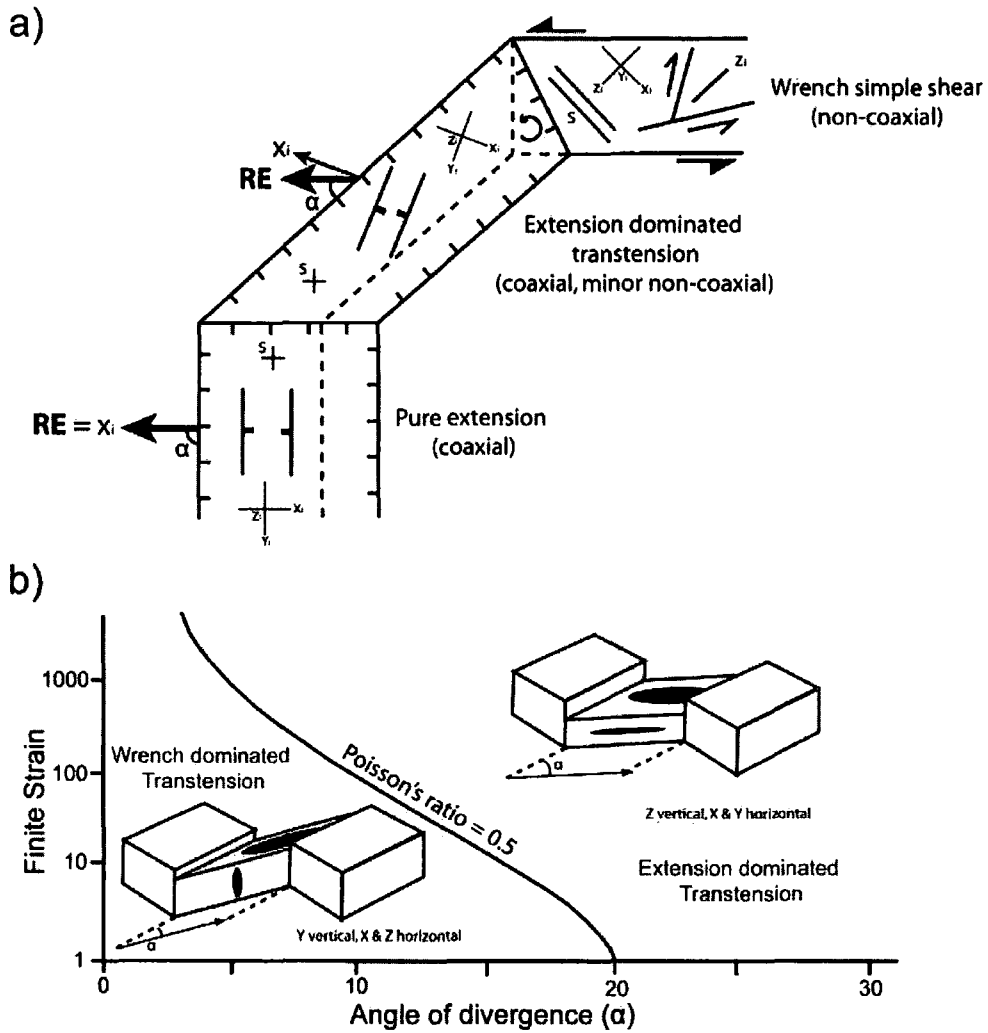
Abbreviations: N - number of fractures; Sp - spacing distribution; MFS - mean fracture spacing; SD - standard deviation; FD - fracture density; Cv - coefficient of variation

**Table 4.2.** Summary of fracture spacing data acquired through photographic fracture traverse analysis.

Deformation zone (& trend)	Deformation type	$\beta$	$\alpha$	Faults predicted by <i>Withjack and Jamison (1986)</i>		Apparent strain axis
				Fault type	Trend relative to the deformation zone boundary	
A (015)	Pure extension (coaxial)	90	90	Normal	0 (015)	285
B (070)	EDTT (Coaxial + non-coaxial)	62.5	35	Sinistral SS, Dextral SS, Normal	0° counter-clockwise (070), 60° counter-clockwise (010), 26° counter-clockwise (044)	312.5
C (085)	WDTT (non-coaxial)	55	20	Sinistral SS, Dextral SS	6° counter-clockwise (079), 66° counter-clockwise (019)	320

**Table 4.3.**

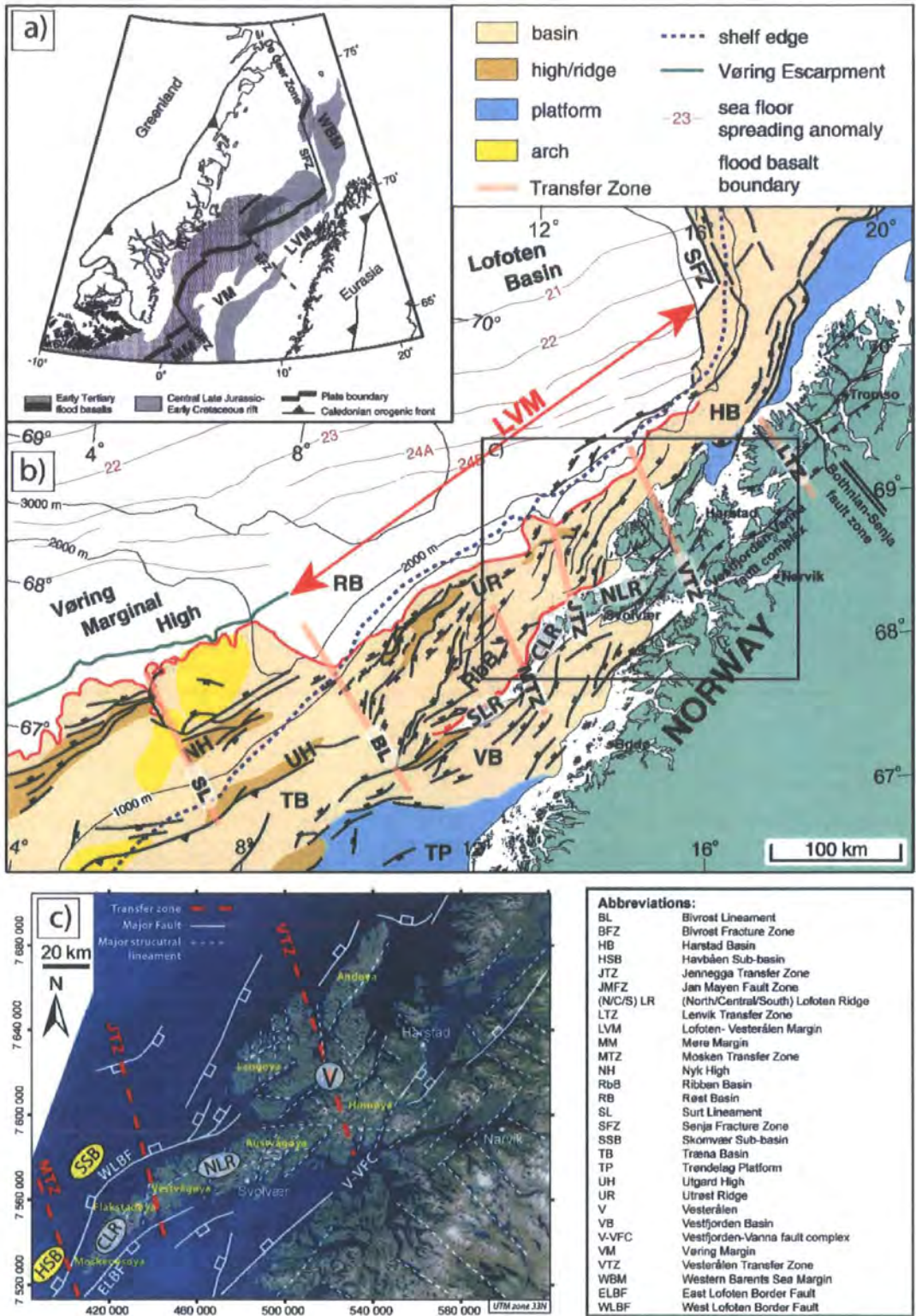
Table summarising the predicted orientations of faults based on fault models of Withjack and Jamison (1986) for segmented transtension model for the Lofoten Ridge (see Fig. 4.16). Regional extension is taken to be 285-105, calculated by applying *equation 4.1.* to mean 'palaeostress' vector determined through kinematic analysis (i.e. in deformation zone C).



**Figure 4.1.**

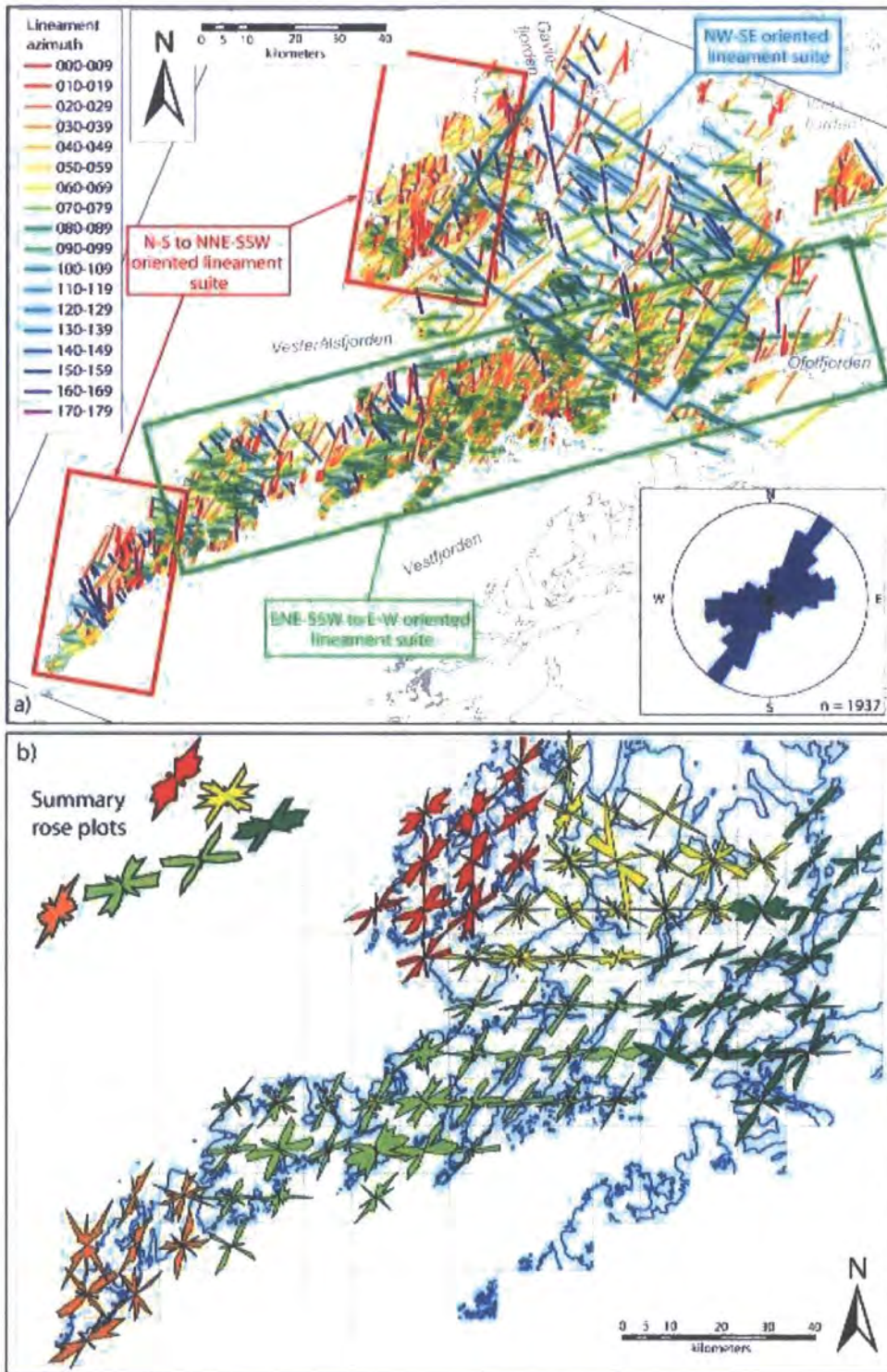
(a) Schematic plan view diagram showing an example of transtension (in this example extension dominated transtension) in an increasingly oblique margin (after Dewey, 2002). RE = regional extension direction. (b) Cartoon graph showing angle of divergence,  $\alpha$ , vs. horizontal finite strain. Solid curved line highlights the angle  $\alpha_{crit}$  which marks the transition from wrench dominated to extension dominated transtension (modified from Teysier and Tikoff, 1999).





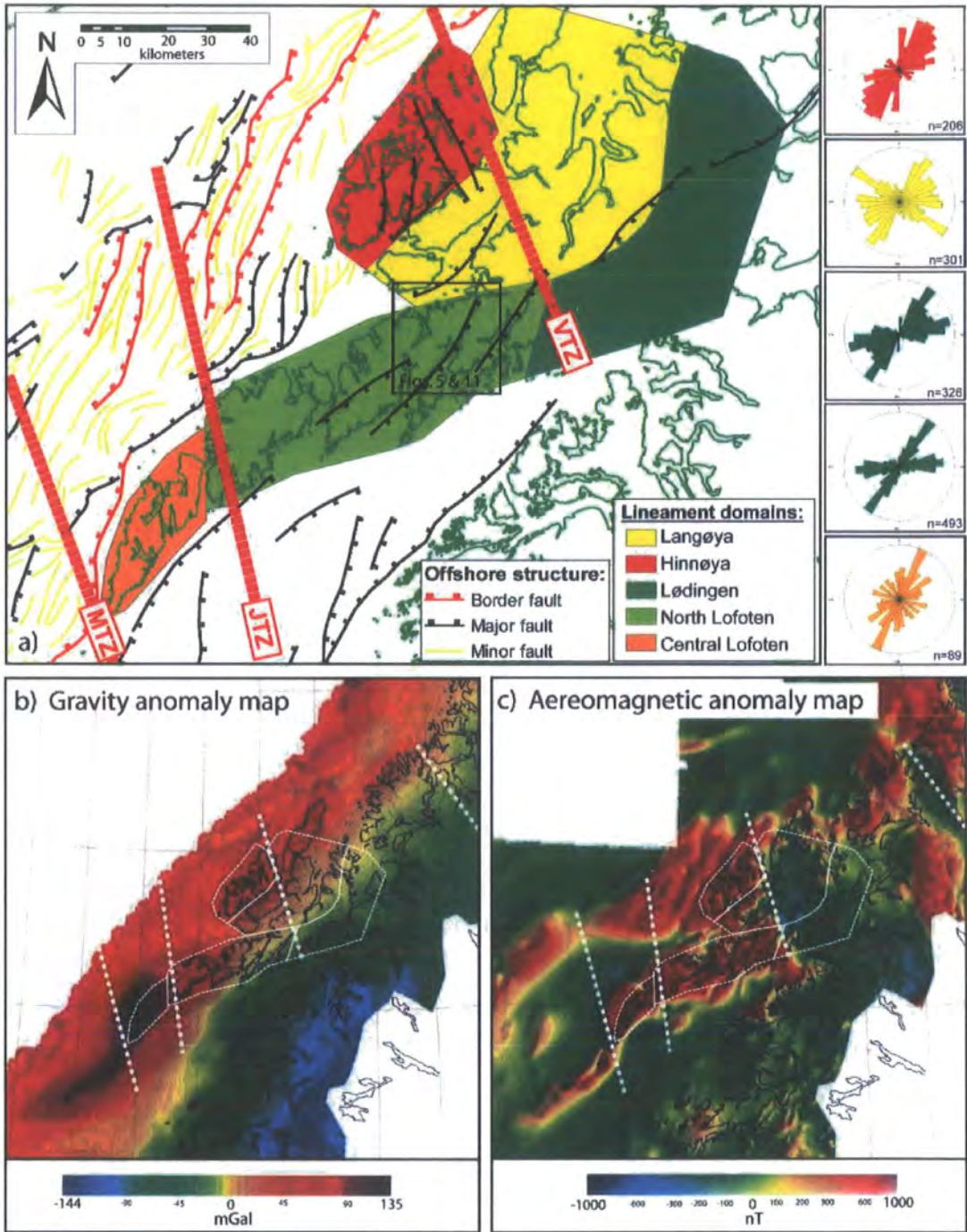
**Figure 4.2.**

(a) Simplified tectonic map of Norwegian – Greenland plate margins, about 2 My after break-up of Eurasia and Greenland (from Tsikalas et al., 2001). (b) Tectono-magmatic map of the Lofoten-Vesterålen Margin (modified from Tsikalas et al., 2001). (c) Landsat image of the Lofoten-Vesterålen archipelago. Highlighted in red are the transfer zones proposed in past studies (Olesen et al., 1997, 2002; Tsikalas et al., 2001).



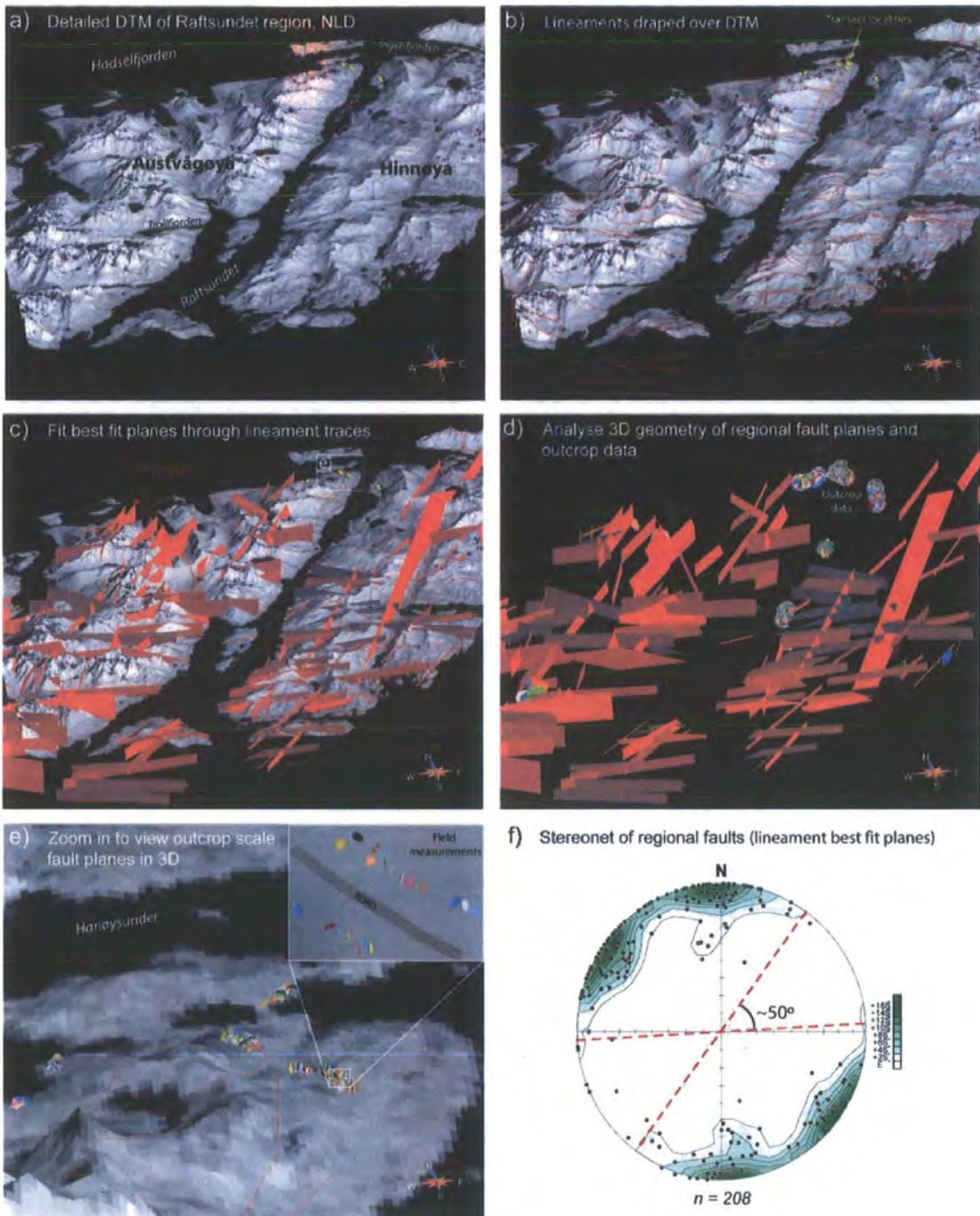
**Figure 4.3.**

Regional lineament analysis of satellite data for the LVA. (a) Landsat TM image with structural lineaments mapped at 1:100,000 scale, plus a rose diagram highlighting dominant lineament trends. (b) Rose diagram map for lineaments shown in (a). Map grided in to 10 x 10 km squares, with corresponding rose diagrams plotted for each square. Plots coloured according to similarities in trend. Plots in top left show summary plots for changes in lineament trend along the ridge.



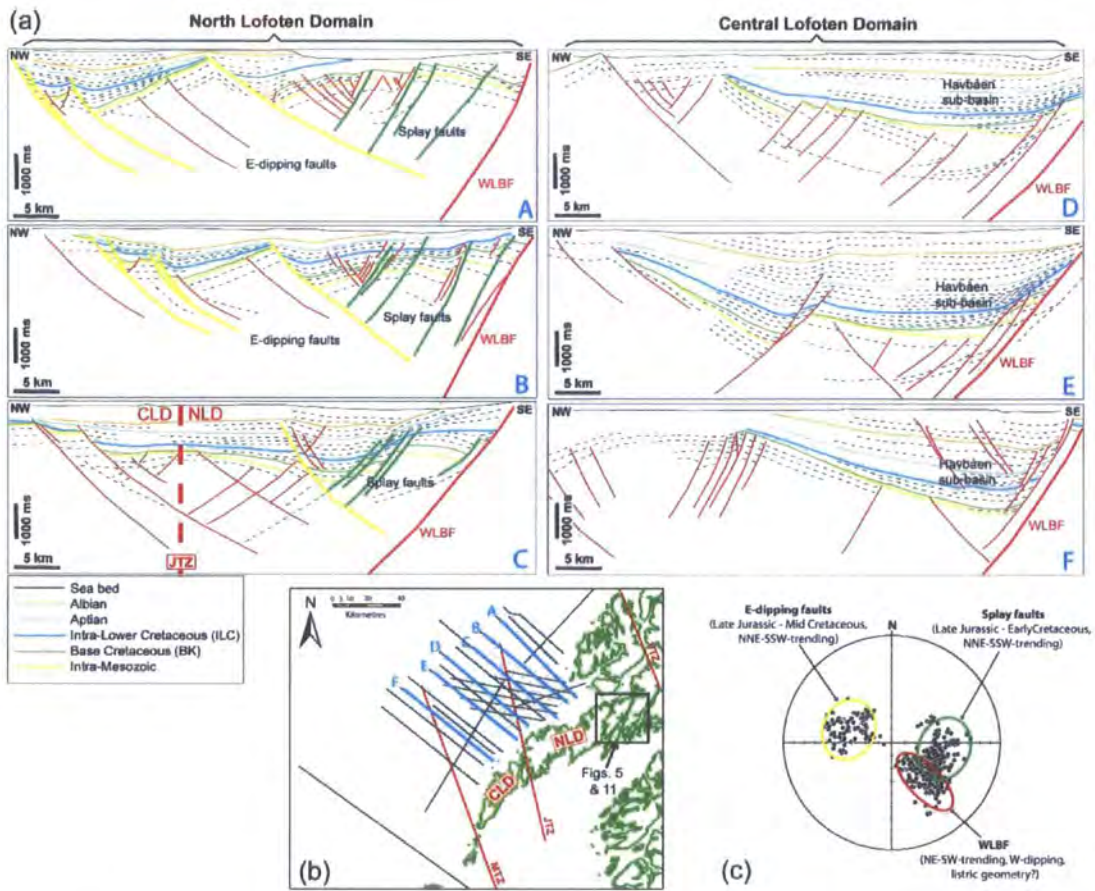
**Figure 4.4.**

(a) Lineament domains identified for the LVA, with rose diagrams highlighting dominant trends in each domain. Offshore fault structures taken from Tsikalas et al. (2001). (b) Gravity and (c) aereomagnetic maps for the Lofoten-Vesterålen Margin (maps published by the Geological Survey of Norway; Dalsegg et al., 1992; Blokkum et al., 1992). Lineament domains are outlined with solid white lines, transfer zones of Tsikalas et al. (2001) are shown as dashed lines.



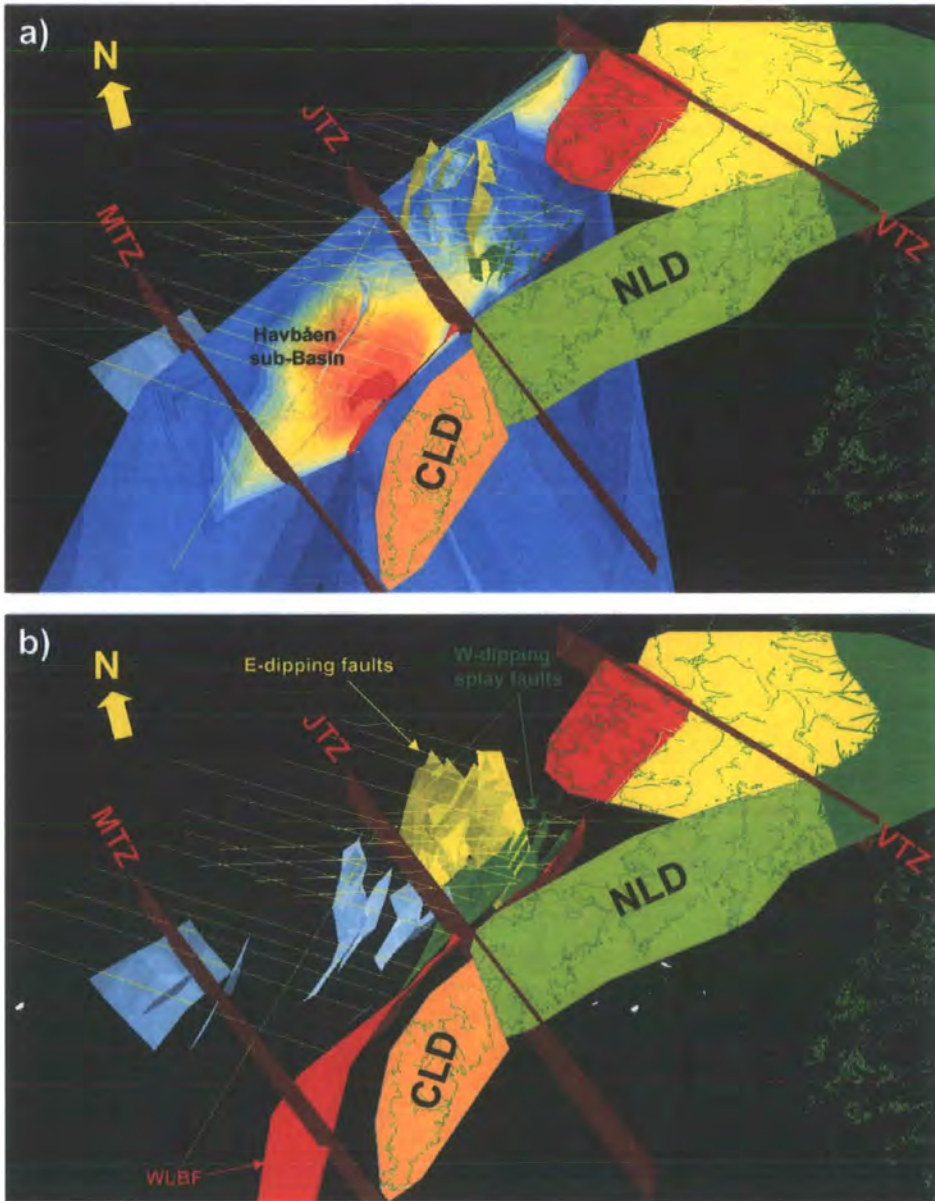
**Figure 4.5.**

(a) 2.5-D model of the Raftsundet region, Austvågøya, N. Lofoten, comprising a Landsat image draped over DTM. (b) Lineaments (vector data) imported from ArcGIS, and draped over DTM. (c) Best-fit planes fitted through 3-D lineament traces to produce a 3-D fault model. (d) Regional and outcrop scale fault planes analyzed in same 3-D model. (e) Fault planes at outcrop, fault geometries recorded as point data in the field using digital mapping methods. (f) Equal-area lower-hemisphere stereonet of regional fault planes derived from best-fit planes through 3-D lineament traces. All models are constructed using Gocad™.



**Figure 4.6.**

(a) A series of interpreted seismic profiles, trending NW–SE, across the Ribban Basin. Profiles highlight changes in basin geometry and fault style between North Lofoten and Central Lofoten. (b) Base-map showing location of seismic lines used in this study relative to Lofoten coastline and “transfer zones”. (c) Stereonet (poles to planes) of faults picked in seismic (dips calculated using an interval velocity of 3000 m/s; readings taken every 1 km).



**Figure 4.7.**

Seismic horizons and fault surfaces imported into onshore-offshore 3D model in ArcGIS (ArcScene). **(a)** Base Cretaceous horizon map showing a large depocenter (the Havbåen sub-basin) offshore Central Lofoten, and no basin apparent in North Lofoten. **(b)** Fault model showing distinct change in geometry from South to North Lofoten (Red = WLBF, green = splaying faults, yellow = low-angle E-dipping faults, blue = other minor faults). Also shown are onshore lineament domains (coloured polygons) and NNW-SSE-trending transfer zones (red planes).

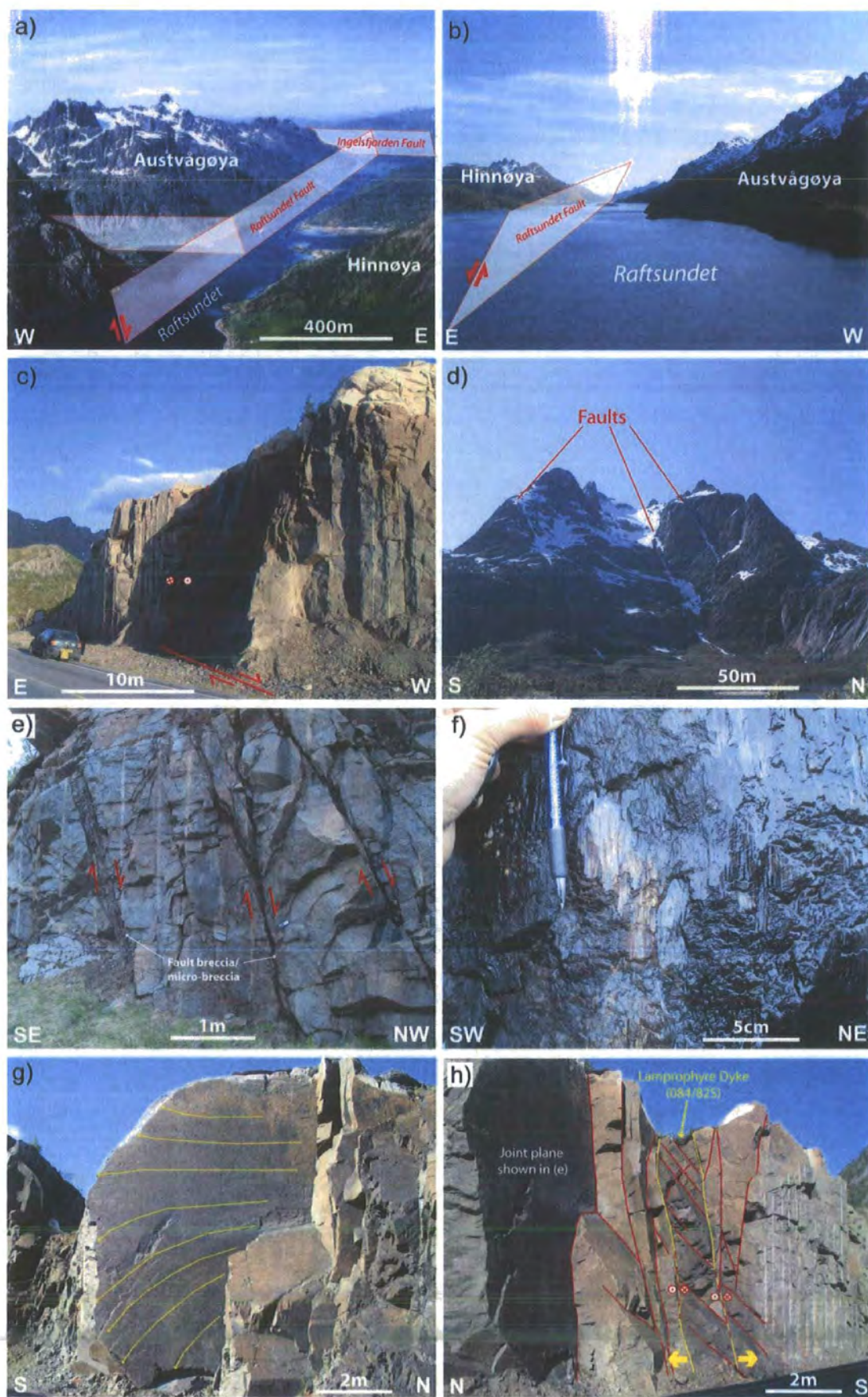


Figure 4.8. (caption overleaf)

**Figure 4.8.**

Photographs showing regional to outcrop scale structures seen in Lofoten. (a) & (b) Raftsundet, believed to mark the trace of a major SE-dipping fault (based on topographic contrasts either side of fjord, and also dominant dip direction of outcrop-scale faults – see Fig. 4.9); (c) Typical exposure of fault surface away from major lineaments (i.e. Raftsundet), example shown is a N–S trending dextral strike-slip fault; (d) Lineaments picked from Landsat images are easily identifiable in the field; (e) NW-dipping system 1 faults containing fault breccias; (f) dip-slip extensional slickenlines (striae) on system 1 faults; (g) E–W trending joint with ornamentations that closely resemble plumose markings (Hodgson, 1961); (h) Lamprophyre dyke trending parallel to system 2 faults and joints shown in (g).



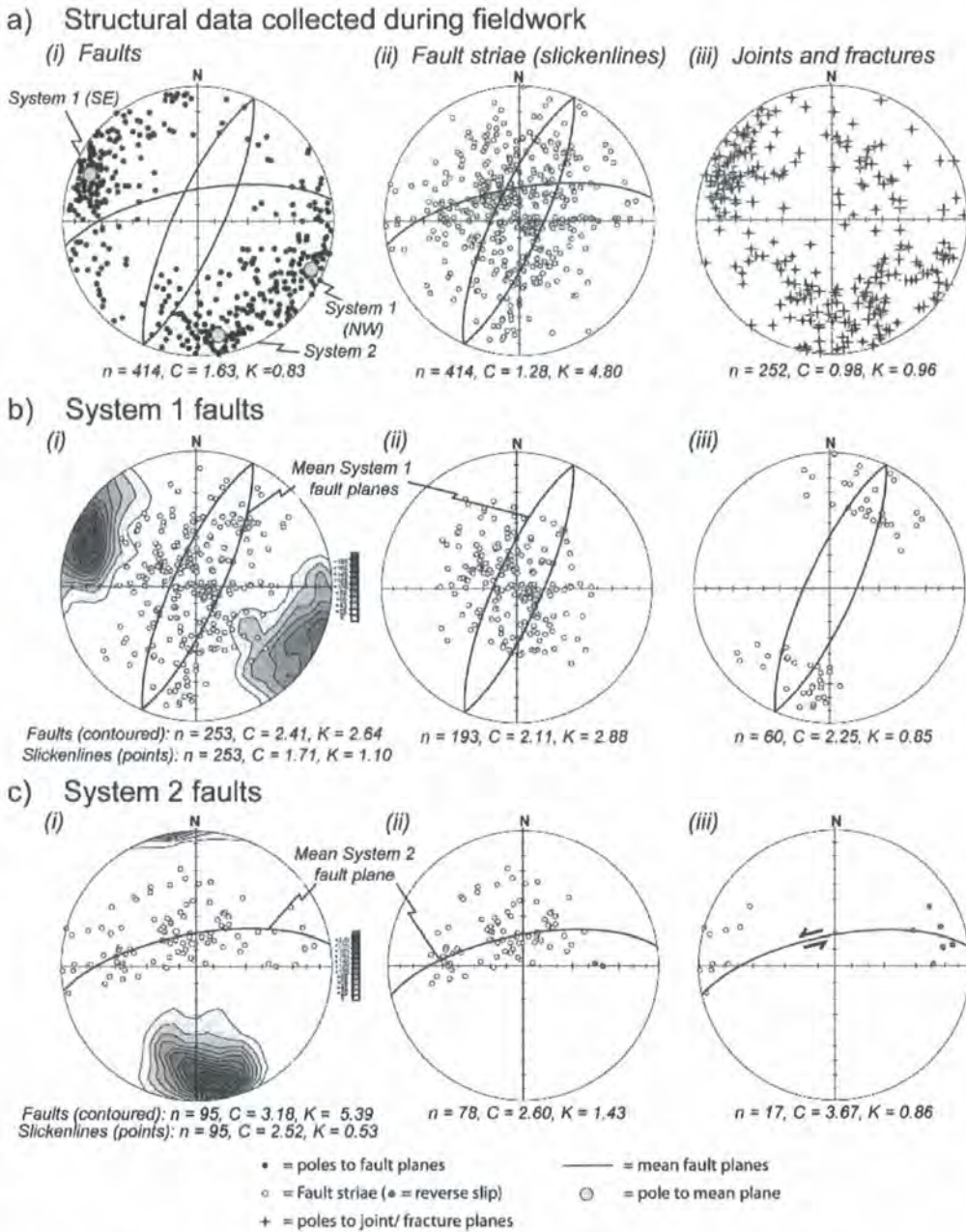
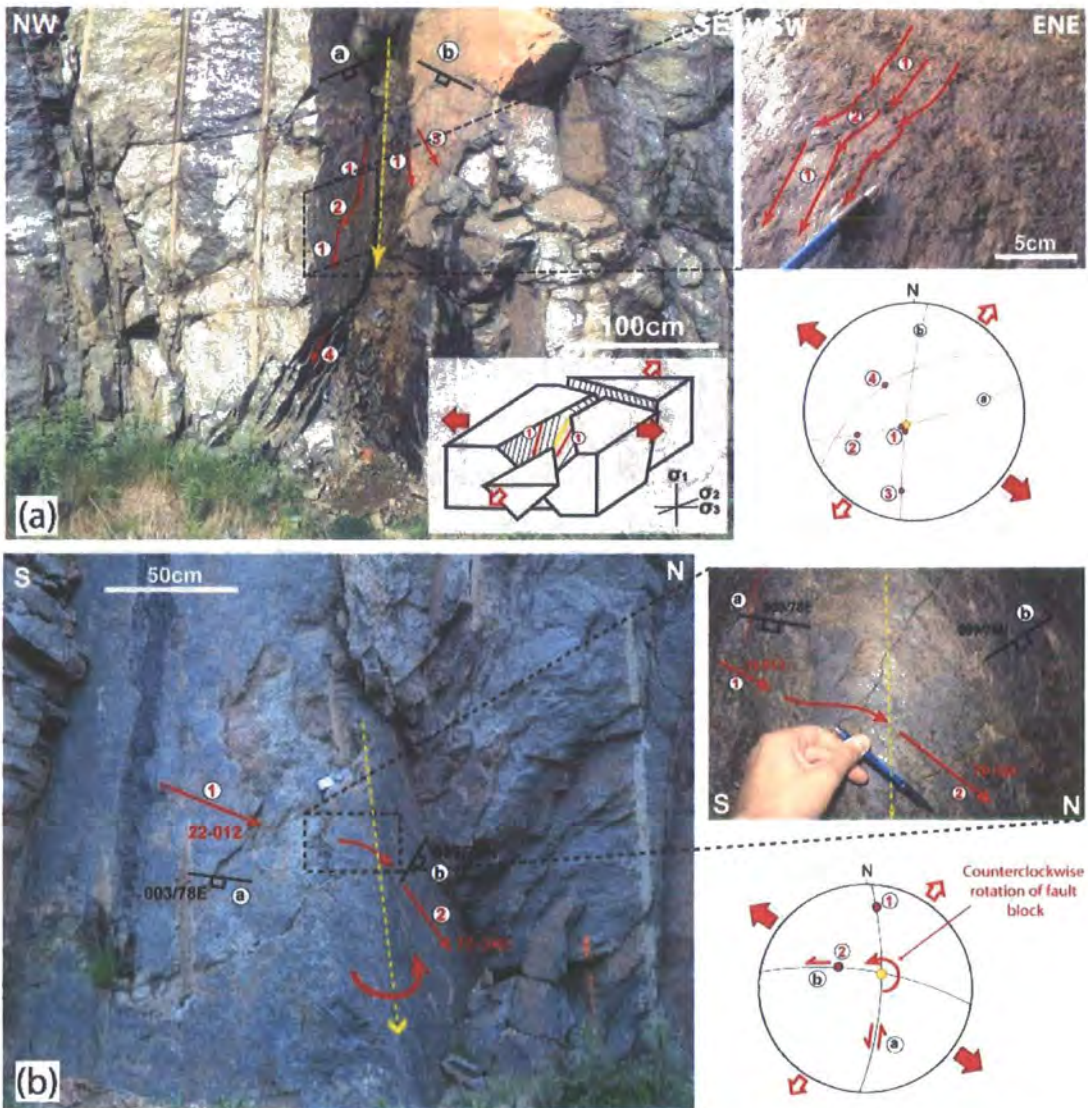


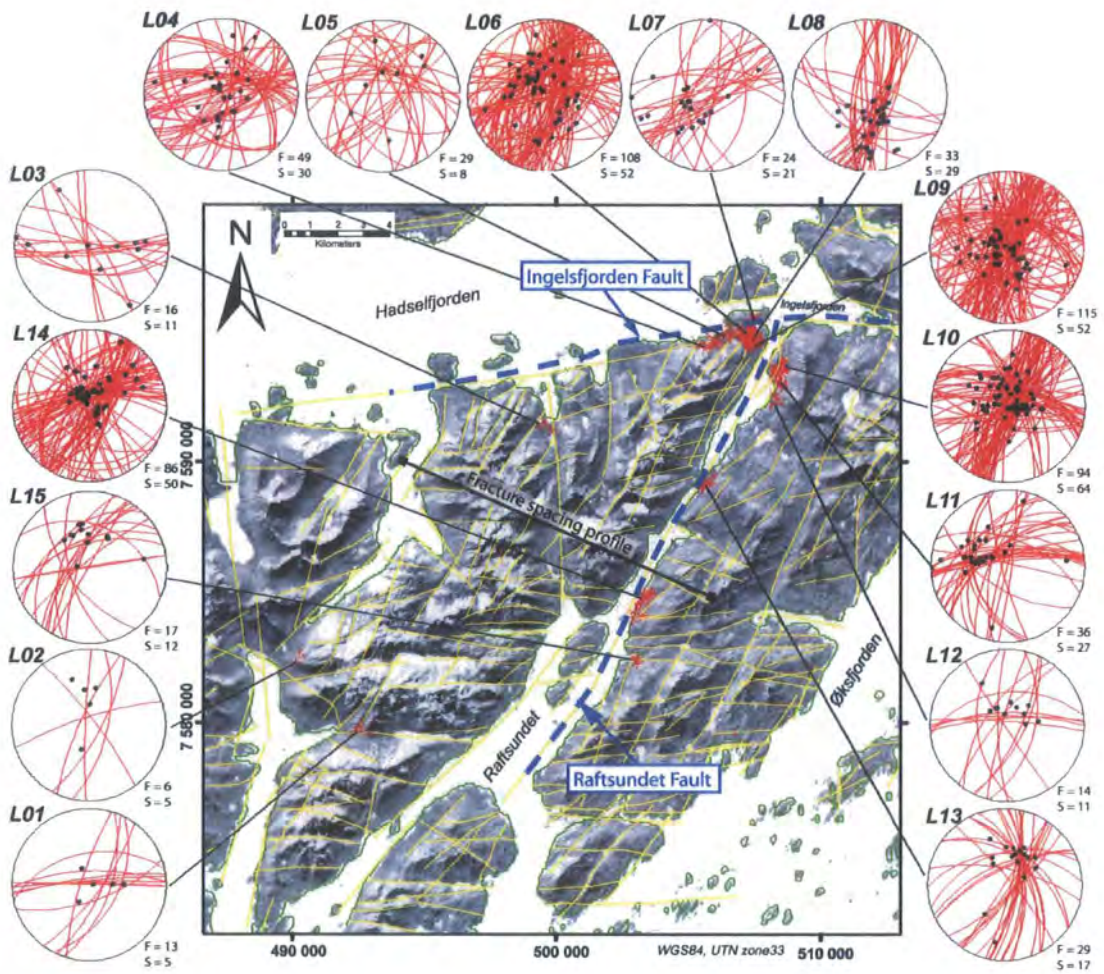
Figure 4.9.

Equal-area lower-hemisphere stereonets of structural data from Austvågøya, N. Lofoten. (a) *i*) poles to planes for all fault recorded in the field, *ii*) slickenline lineations on these faults, and *iii*) poles to planes for joints and fractures. (b) Stereonets for system 1 faults (NNE–SSW/ NE–SW-trending) showing: *i*) contours of poles to planes, plus all associated slickenlines (points), *ii*) dip-slip slickenlines, and *iii*) strike-slip slickenlines. (c) Stereonets for system 2 faults (ENE–WSW-trending) showing: *i*) contours of poles to planes, plus all associated slickenlines (points), *ii*) dip-slip & oblique-slip slickenlines, and *iii*) strike-slip slickenlines. Data included on each plot are: number of data (*n*) and eigenvector ratios reflecting ‘strength’ (*C*) and ‘shape’ (*K*) of preferred orientation.



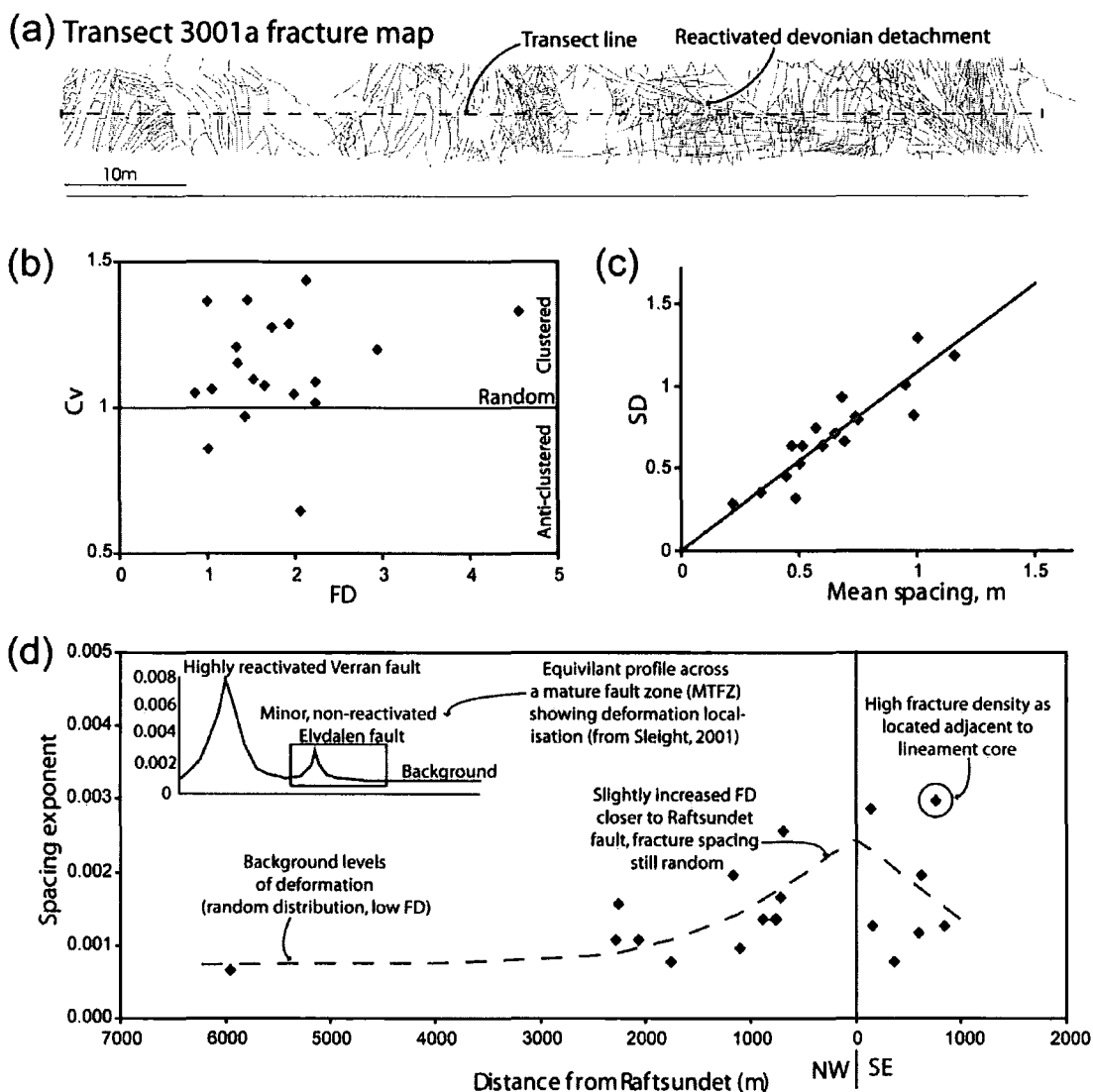
**Figure 4.10.**

(a) Field example of fault interaction, at Locality L06 (G.R.: 507134 7595034), showing intersecting faults with slickenlines parallel to intersection line (highlighted in yellow). (i, ii, iii) Outcrop photos showing intersecting fault and corresponding slickenlines at various scales. Also note the stepwise/ curved slip movements on the fault. (iv) stereonet of faults and slickenlines measured at outcrop (v) interacting block model (Nieto-Samaniego and Alaniz-Alvarez, 1997). (b) Second example of complex fault interaction, also at Locality L06 (G.R.: 507166 7594937), where continuous set of slickenlines can be traced round a 90° bend, from intersecting fault surfaces. A N–S trending fault (fault a) shows sinistral strike-slip movements. These then bend round into an E–W trending fault (fault b) with sinistral oblique-slip. This complex interaction is indicative of counter-clockwise rotation during fault movement.



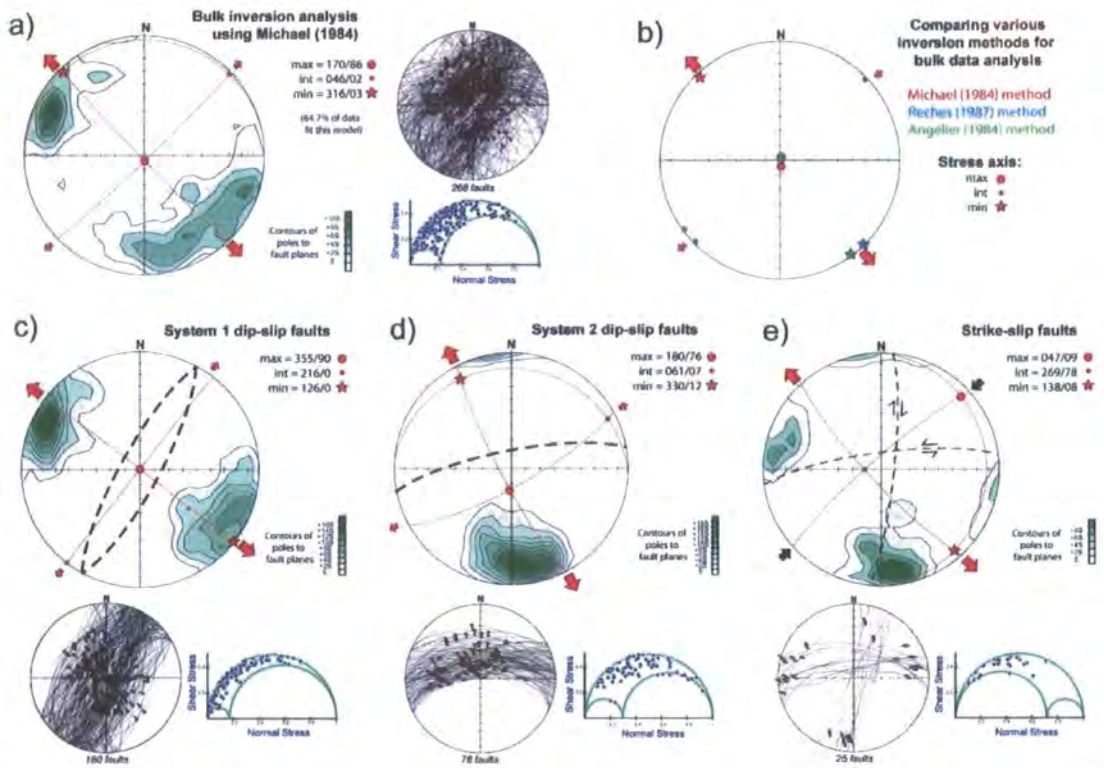
**Figure 4.11.**

ArcGIS map showing location of fault populations and traverse sites, surrounded by individual stereonets for each locality. Stereonets plotted using GIS Stereoplot (Knox-Robinson and Gardoll, 1998) for ArcView 3.x. Black line shows basic trend of fracture spacing profile shown in Figure 4.12d.



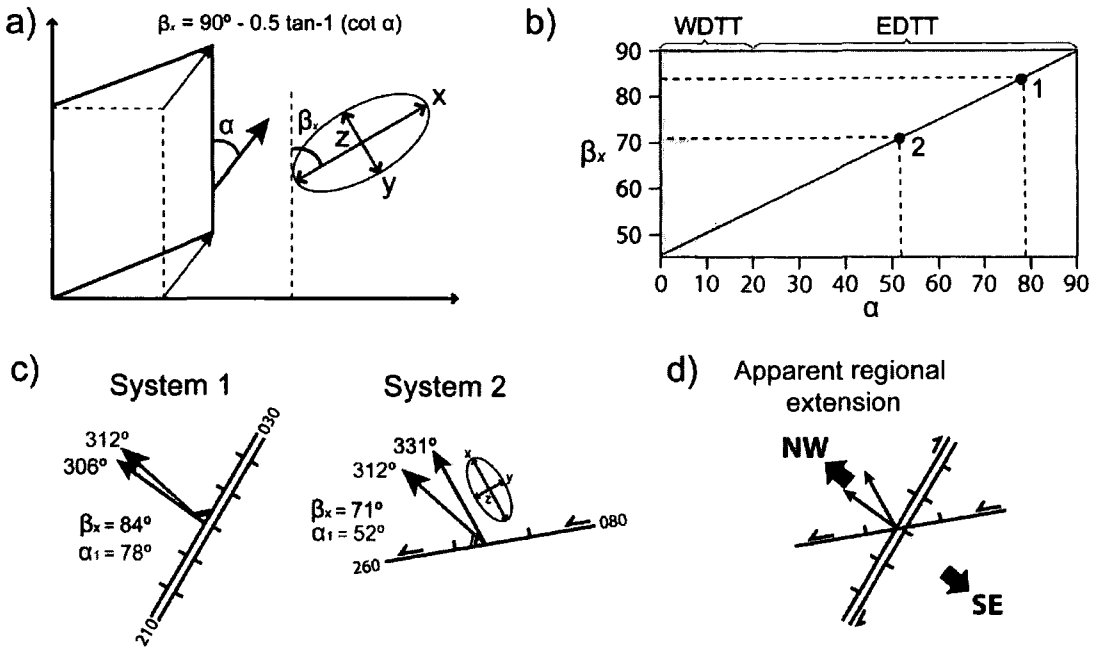
**Figure 4.12.**

(a) Example transect fracture map (for Transect 03001a, locality L09). (b) Plot of fault density vs.  $C_v$  values for fracture spacing, reflecting a random to mildly clustered distribution. (c) Plot of mean spacing vs. standard deviation for fracture spacing. Close correlation between the two shows that most data is consistent with an exponential spacing distribution. (d) A plot of the spacing exponent (acquired by plotting spacing data on population plots) vs. distance to the Raftsundet fault (Fig. 4.11), showing a slight increase towards the fault. This is also matched by a similar increase in FD.



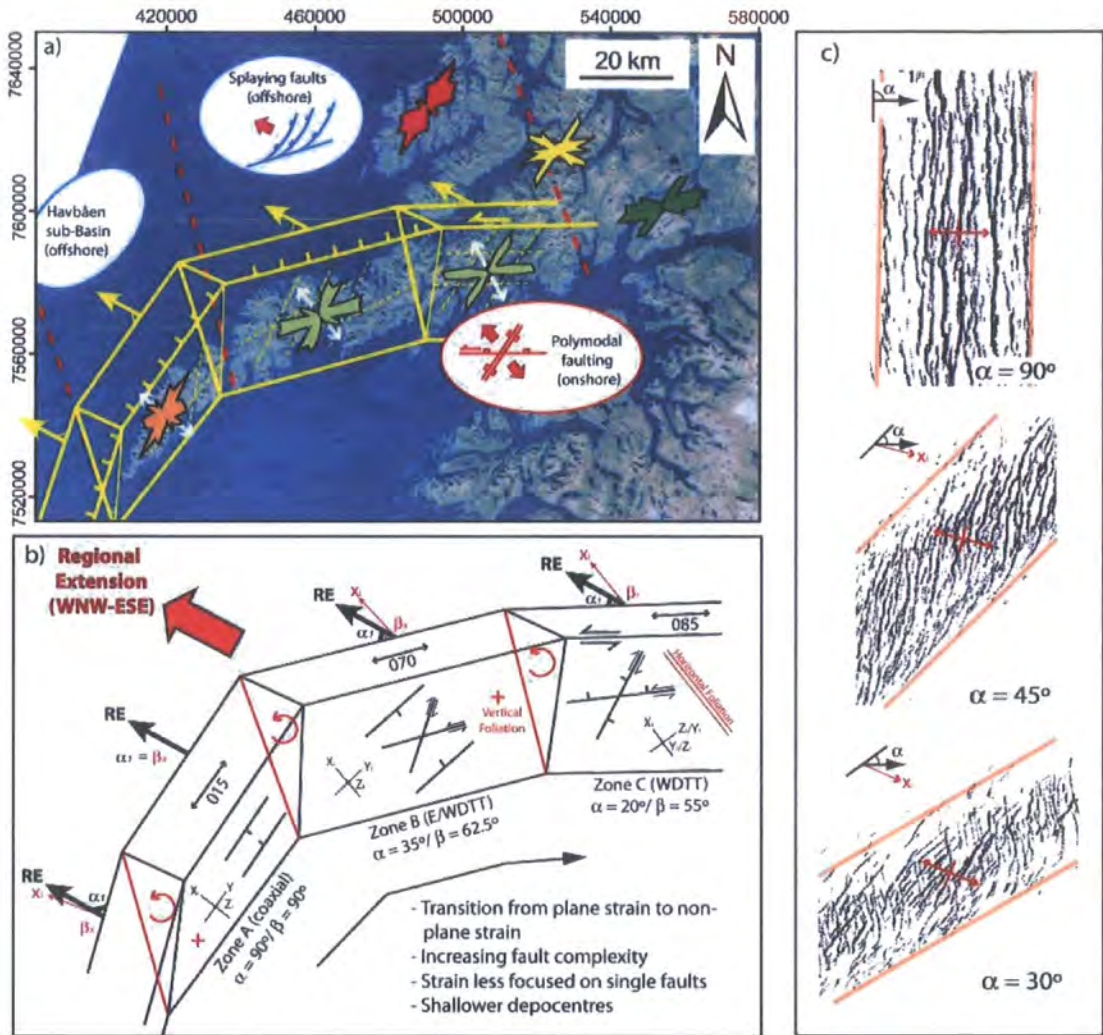
**Figure 4.13.**

Kinematic inversion analysis. (a) Stereonet showing results of inversion analysis for bulk data (after 6 iterations) using the Michael (1984) method, plus stereonet of raw data and corresponding three-dimensional Mohr circle. (b) Stereonet showing similar stress vectors for bulk analysis of data using 3 alternate inversion methods (Michael, 1984; Angelier, 1984; Reches, 1987). (c) Inversion analysis for system 1 dip-slip faults, (d) for system 2 dip-slip faults, and (e) strike-slip faults, using Michael (1984) method. (c) - (e) also include stereonets of raw data and corresponding three-dimensional Mohr circles.



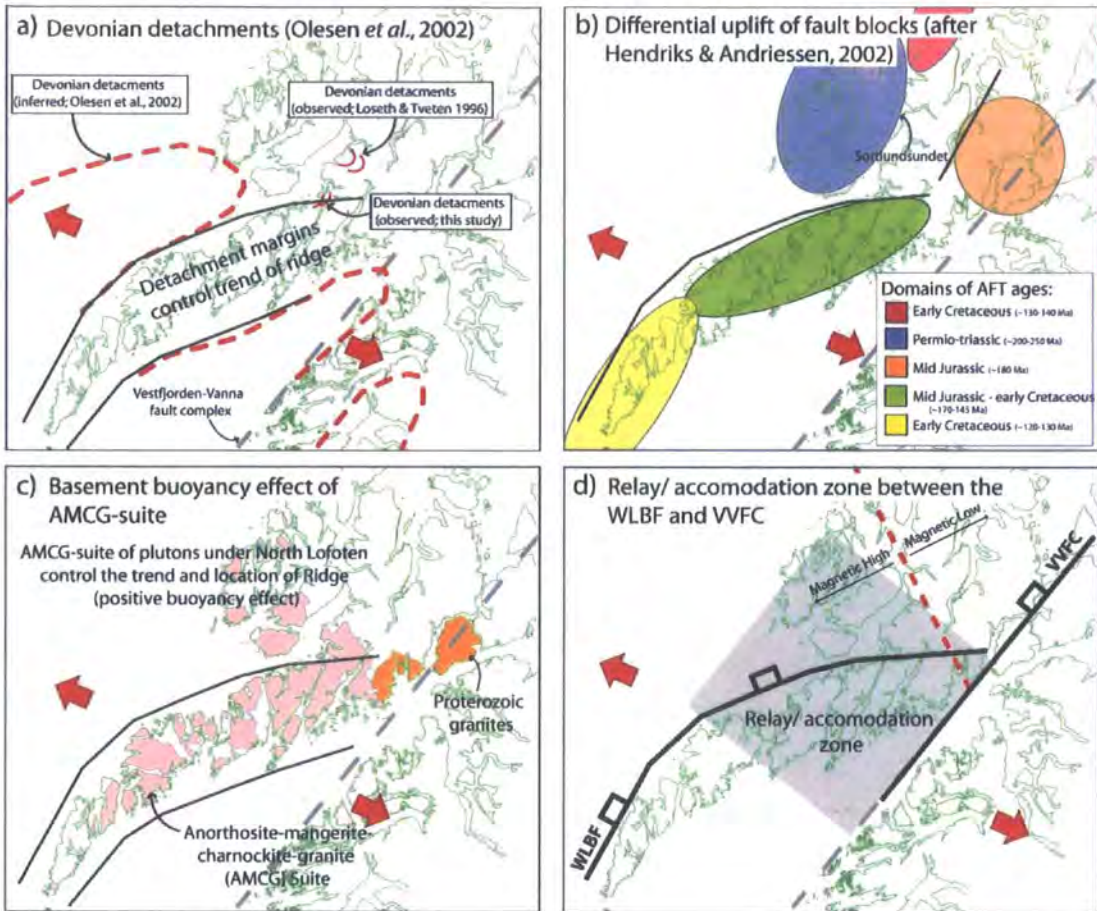
**Figure 4.14.**

(a) Simplified box model summarizing relationship between  $\alpha$  and  $\beta_x$  and the relative to the deformation boundary. (b)  $\alpha$  vs.  $\beta_x$  plot corresponding to solution of *equation 4.1*. (from De Paola et al., 2005a). Points 1 & 2 correspond to  $\alpha$  and  $\beta_x$  angles for systems 1 & 2 faults respectively (calculated by assuming fault strike corresponds to deformation zone boundary). (c) Summary diagrams showing  $\alpha$  and  $\beta_x$  angles for fault system 1 and system 2, and apparent extension vector after applying correction. (d) Both faults systems appear to have developed under a single phase of NW-SE extension.



**Figure 4.15.**

(a) Summary of observations made in this study, in fitting with a model for transtension in North Lofoten. Rose diagrams from Figure 4.3b. (b) Predicted deformation patterns and the effects of increasing obliquity along the Lofoten Ridge (based on models of Withjack and Jamison, 1986; Dewey, 2002). (c) Fault trace maps for various angles of divergence, highlighting the effects of increasing obliquity (i.e. decreasing  $\alpha$ ) on fault patterns; taken from results of experimental clay models by Clifton et al. (2000).



**Figure 4.16.**

Potential origins and controls on the development of the oblique trending Lofoten Ridge. (a) ‘spoon-shaped’ Devonian detachment faults may have controlled the trend of the northern part of the Lofoten Ridge (based on model of Olesen et al., 2002). (b) Differential uplift of fault blocks (after Hendriks and Andriessen, 2002). The earlier uplifted (Permo-Triassic) Outer Vesterålen Block (blue) may have acted as a barrier to later faults developing during the denudation of the Inner-Vesterålen and Lofoten (during Jurassic–Cretaceous times). Denudation ages from AFT studies by Hendriks (2004). (c) Basement buoyancy effect caused by the AMCG-suite underlying much of North Lofoten leads to oblique trend of ridge, i.e. similar to effect of granites under Mid North Sea High (Dunato et al., 1983). (d) Alternatively, the oblique trending North Lofoten Ridge may simply be a relay/accommodation zone between the West Lofoten Border Fault (WLBf) and the Vestfjorden-Vanna Fault Complex (VVFC). One or more of the above may have jointly influenced the development of this relay zone.



## **5. Transtension, basement reactivation and transform fault development in the Davis Strait, West Greenland: linking onshore structures with offshore**

**Abstract:** Transform fault zones are often characterised by significant transtensional strains and the sedimentary basins that develop in such settings are likely to exhibit complex fault patterns compared to the regions they offset. The origin and development of such structures is still not fully understood, nor is the role of pre-existing basement structures. The Davis Strait of West Greenland contains the Ungava fault zone, a transform fault zone separating the failed spreading centres of the Labrador Sea and Baffin Bay. Detailed onshore studies of fault patterns and kinematics, at regional to outcrop scales, have been used to analyse the spatial and temporal variations in fault development. These are compared to basement heterogeneities, and also the structural patterns developed offshore in the Davis Strait. Two main fault systems are apparent: 1) c. N-S trending normal faults, and 2) strike-slip faults with localised transpression. These conform to extension-dominated and wrench-dominated systems associated with the regional NNE-SSW trending Ungava fault zone in the David Strait. Extension-dominated faults appear to pre-date wrench-dominated strike-slip and reverse faults. This implies a counter-clockwise rotation of the stress field with time, consistent with fault patterns and magnetic anomalies observed in the Labrador Sea to the south. Our findings suggest that the pre-existing basement structures of the Palaeoproterozoic Nagsugtoqidian orogen have indirectly influenced the location and development of this transform, but direct reactivation is limited to localised areas (e.g. south Sisimiut Basin). At the basin scale, however, pre-existing basement fabrics do appear to define a number of distinct deformation zones.

### **5.1. Introduction**

Many basins develop in strike-slip settings (Harding, 1974, 1985; Mann et al., 1983; Christie-Blick and Biddle, 1985; Sylvester, 1988; Allen et al., 1998; Waldron, 2005), and include pull-apart basins formed at releasing bends (Mann et al., 1983) and larger-scale transtensional basins (Dewey, 2002). Such basins are often associated with

complex fault patterns that may comprise a variety of fault orientations and fault types (Fig. 5.1a; Dewey, 2002; De Paola et al., 2005b), and may be further complicated by the effects of rotation around a vertical axis (Waldron, 2005).

Normal faults formed within strike-slip systems are common in sedimentary basins, and generally develop in an en echelon arrangement. In pure strike-slip systems, where the regional transport direction is parallel to the deformation zone, normal faults should develop at 45° to the deformation zone (i.e. simple shear; Fig. 5.1; Wilcox et al., 1973). However, if the regional transport direction is oblique to the deformation zone (i.e. transtension; Fig. 5.1b) the orientation of normal faults may vary. Following Withjack and Jamison (1986) there is a predictable relationship between the orientation of normal faults (assuming they form normal to the infinitesimal horizontal maximum extension strain axis,  $\beta_x$ ) and the overall system, which varies according to the angles made by the regional extension vector and the deformation zone boundary ( $\alpha$ ) (Fig. 5.1b):

$$\beta_x = 90^\circ - 0.5 \tan^{-1} (\cot \alpha) \quad (5.1.)$$

which in terms of fault orientation relative to the deformation zone boundary ( $F_{\text{angle}}$ ) can be re-written as:

$$F_{\text{angle}} = 90 - \beta_x = 0.5 \tan^{-1} (\cot \alpha) \quad (5.2.)$$

Pre-existing fabrics and anisotropies may exert a strong control on the overall rift geometry in both strike-slip and extensional settings, and can lead to the development of complex fault patterns, obliquely extended segments, partitioned deformation, and transfer zones (Morley et al., 1990, 2004; Nelson et al., 1992; Clemson et al., 1997; Ebinger et al., 1999; Paton and Underhill, 2004, De Paola et al., 2005). Peacock and Sanderson (1992) define three different types of anisotropy in rocks: (1) layering (e.g. bedding), (2) continuous anisotropy (e.g. foliation, shear zones, etc.), and (3) discrete planes of weakness (e.g. faults, cleavage planes, etc.). A number of studies have shown how such heterogeneities can influence fault geometries and strain reorientation during

deformation (Donath 1961; Peacock and Sanderson, 1992). In transtension, the presence of pre-existing structures lying at an oblique angle to imposed opening vectors may commonly lead to the partitioning of oblique rifting into contemporaneous domains of wrench- and extension-dominated deformation (Oldow, 2003; De Paola et al., 2005). Furthermore, pre-existing basement structures have been linked to the initiation and development of transfer and transform fault systems in a number of settings (Le Pichon and Hayes, 1971; Rosendahl, 1987; Clemson et al., 1997).

The west Greenland margin contains a series of deep sedimentary basins (Fig. 5.2b) (Chalmers and Pulvertaft, 2001; Christiansen et al., 2002), a number of which lie in the vicinity of the Davis Strait transform fault system (known as the Ungava Fault Zone) that links the failed spreading centres of the Labrador Sea and Baffin Bay (Fig. 5.2; Chalmers et al., 1995; Chalmers and Pulvertaft, 2001). More detailed studies suggest that pre-existing structures may control the location and geometry of major bounding faults in some offshore sedimentary basins of the Davis Strait (e.g. Sisimiut Basin). Furthermore, basement fabrics of the Nagssugtoqidian orogen have also been proposed as a strong influence on the location and development of this transform system as a whole (Wilson et al., 2006).

The aims of this paper are twofold: 1) to investigate the variations in fault geometry and kinematics of outcrop to basin scale (meters – kilometres) structures onshore, and compare these structures offshore, and 2) use these findings to assess the spatial and temporal variations in faulting during the development of the Davis Strait transform. Particular attention is paid to the influence of pre-existing basement structures both at the basin and at the margin scale.

## **5.2. Regional geological setting**

### **5.2.1. Tectonic margin**

The margin of West Greenland (Fig. 5.2) formed by opening of the Labrador Sea – Davis Strait – Baffin Bay seaway in late Mesozoic – early Cenozoic time (Chalmers and Pulvertaft, 2001, and references therein). According to some authors, rifting and tectonic subsidence began in the Early Cretaceous, at the same time as sea-floor spreading in the North Atlantic south of the Charlie Gibbs Fracture zone (Chron 33, *c.* 81 Ma in the

Labrador Sea; Roest and Stivastava, 1989). However, Chalmers and Laursen (1995) and Chalmers and Pulvertaft (2001) suggest that sea-floor spreading did not start until Early Palaeocene (Chron 27). A distinct change in orientation of fracture zones associated with the opening of the Labrador Sea can be seen at ~Chron 24 (Roest and Stivastava, 1989; Chalmers and Pulvertaft, 2001; Lundin and Doré, 2005), suggesting two phases of opening. Sea-floor spreading appears to have ceased by the Oligocene (Chron 13).

The west Greenland margin can be split into three segments exhibiting distinctly different fault patterns and basin geometries (Fig. 5.2). In the Labrador Sea, to the south, and Baffin Bay, to the north, faulting appears to be dominated by NNW-SSE to NW-SE trending normal faults running near parallel to the margin. Between these two dominantly extensional margin segments is a more complex sinistral transform fault system, known as the Ungava fault system (Fig. 5.2; Chalmers et al., 1995), in the Davis Strait. This zone is coincident with the steep basement fabrics of the Nagssugtoqidian orogenic belt; however these faults cut basement fabrics at relatively high angles (Wilson et al. 2006). In this zone, faults dominantly trend N-S and NNE-SSW, with localized zones of basement-parallel faults (e.g. Nuussuaq basin, Chalmers et al., 1999; Sisimiut Basin, Wilson et al., 2006). Normal faults generally trend N-S, which is some 20–30° clockwise from those developed in the Labrador Sea and Baffin Bay (Fig. 5.2). The Ungava transform fault system appears to have developed numerous splays, with local restraining bends developing compressional structures such as positive flower structure known as the Ikermiut Fault Zone (Fig. 5.2; Chalmers et al., 1995).

The Sisimiut basin lies immediately west of the Nordre Strømfjord – Nordre Isortoq region onshore (Fig. 5.2). The northern parts of the Sisimiut Basin have been uplifted and eroded in relatively recent geological times (Chalmers, 2000), possibly as late as Miocene or even Pliocene times. The eastern border of the Sisimiut Basin is a major fault lying close to the coast and is bound to the west and northwest by the Ikermiut Fault Zone (Fig. 5.2; Chalmers et al., 1995; Chalmers and Pulvertaft, 2001). To the southeast of the Sisimiut Basin is the Nukik Platform, an area of shallow basement and volcanics. Separating the Sisimiut Basin from the Nukik Platform are a series of ENE-WSW and E-W trending faults that trend roughly parallel to fjords along the coast (e.g. the Nordre Isortoq Fjord; Fig. 5.3). It has been suggested that these faults reactivate

basement structures of the Central Nagssugtoqidian orogen (Wilson et al., 2006). These faults affect Mesozoic sediments and are overstepped by Palaeocene sediments, so that the latest significant movement on them must have been prior to the end of the Palaeocene. Associated with these faults are a series of thick prograding sediments known as the Nukik Fan (Henderson et al., 1981; Ottesen, 1991). The Late Cretaceous Nukik Fan is an example of a hanging-wall fan, where sand, or coarser sediment, have been deposited on the hanging-wall of either an active fault or fault escarpment.

### **5.2.2. Onshore basement structure and the Nagssugtoqidian Orogenic Belt**

Onshore exposures in central West Greenland, from Søndre Strømfjord in the south to Disko Bugt in the north, comprise high-grade gneisses of the Palaeoproterozoic Nagssugtoqidian orogen (Ramberg, 1949; van Gool et al., 2002; Fig. 5.3). The Nagssugtoqidian orogen is a 300km wide belt of predominantly Archaean orthogneisses, with minor supracrustal rocks and Palaeoproterozoic intrusives, which were re-worked during Palaeoproterozoic orogenesis (van Gool et al., 2002). This tectonic belt resulted from a continent-continent collision between the Archaean North Atlantic Craton to the south and an Archaean continental mass to the north (Karlsbeek et al. 1987; van Gool et al. 2002). Rocks within the orogen were metamorphosed to upper amphibolite to lower granulite facies conditions, while those in the southern foreland escaped the Nagssugtoqidian metamorphic overprint and preserve an Archaean granulite facies mineralogy (van Gool et al., 2002). These basement rocks form ENE-trending linear belts of steeply dipping gneisses, some of which are crustal-scale shear zones (i.e. the Nordre Strømfjord shear zone and Nordre Isortoq shear zone; Fig. 5.3), which alternate with zones dominated by kilometre-scale fold structures (van Gool et al., 2002). The Nagssugtoqidian orogen is divided into three tectonic segments: the southern, central and northern Nagssugtoqidian orogen (Fig. 5.3; Marker et al., 1995).

The *Northern Nagssugtoqidian orogen* (NNO) is characterised by a rather irregular pattern of magnetic anomalies with a predominantly E-W linear trend (Rasmussen and van Gool, 2000). These patterns generally represent large-scale fold structures and both shallow and steeply dipping shear zones (Fig. 5.4c) in Archaean gneisses. Palaeoproterozoic deformation and metamorphism diminishes gradually

northwards towards Disko Bay. The southern part of the NNO is dominated by the *Nordre Strømfjord shear zone* (NSSZ), which also marks the boundary between the NNO and central zone to the south. Bak et al. (1975) and Sorensen (1983) interpreted it as a crustal scale shear zone, with sinistral displacements of up to 120 km. The NSSZ has also been interpreted as a near vertical steep belt on the northern flank of a large monocline to the south, and has also been termed the *Nordre Strømfjord seep belt* (van Gool et al., 1996; Hanmer et al., 1997; Rasmussen and van Gool, 2000). Although this zone does not represent a major metamorphic boundary (i.e. suggesting that no major displacements occurred) there is good evidence for sinistral shear within, and on the margins of this zone, thus the term ‘shear zone’ is preferred (van Gool et al., 2002).

The *Central Nagssugtoqidian orogen* (CNO) contains three ENE–WNW-trending domains, each with a distinct structural character. These domains are the *CNO flat belt*, *Nordre Isortoq shear zone* (NISZ), and *southern CNO* (Fig. 5.3; van Gool et al., 1996; Rasmussen and van Gool, 2000). The CNO flat belt marks a large antiformal structure with open, upright folds between two the NSSZ and NISZ steep belts (van Gool et al., 2002). This belt contains mainly Archaean orthogneisses, Palaeoproterozoic supracrustals, and Palaeoproterozoic quartz-diorite to tonalitic intrusives (Kalsbeek et al., 1987; van Gool et al., 2002). The NISZ is a zone of steeply dipping and tightly folded gneisses consisting of interleaved orthogneisses and pelitic to quartzitic paragneisses, which define an area of low magnetic anomaly (Rasmussen and van Gool, 2000; van Gool et al., 2002). Within the belt, a number of smaller sinistral strike slip shear zones can be found. This zone forms a strong regional lineament that may be traced offshore into the southern margin of the Sisimiut Basin (Fig. 5.2).

The southern CNO is dominated by the Palaeoproterozoic Sisimiut charnockite suite and high grade granitoid gneisses in the east (Fig. 5.3; Kalsbeek and Nutman, 1996). The Ikertôq thrust zone (Korstgard et al., 1987), a 5 to 10 km wide strongly lineated zone, defines the southern boundary of the CNO, and forms a distinct lithological and metamorphic boundary (Grocott, 1979). In addition the CNO marks the southern limit of the Sisimiut charnockite suite, and the northern limit of the Kangâmiut dyke swarm.

The *Southern Nagssugtoqidian orogen* (SNO) and *Nagssugtoqidian front* are to be found south of the Ikertôq thrust zone (Fig. 5.3; Korstgard et al., 1987; van Gool et al., 2002). The SNO is made up of Archaean granulite gneisses reworked at amphibolite facies. A strong feature of the SNO, and Archaean foreland to the south, is the Kangâmiut dyke swarm. The *Nagssugtoqidian front* marks the southernmost boundary of the orogenic belt with Archaean foreland of the North Atlantic Craton to the south (Fig. 5.3).

### 5.3. Structural data acquisition

This study combines the analysis of a variety of data types (i.e. remotely sensed data, geophysical images, topographic data, field data) covering a range of scales. In order to handle this wide range of data types, and also to enable a geospatial analysis of all data have been compiled into a digital database using ArcGIS software. Geographic Information Systems (GIS) are becoming increasingly used in the construction and storage of geological databases (Rhind, 1992; Bonham-Carter, 2000; Jones et al., 2004), with the main functions being: (1) data organisation, (2) data visualisation, (3) data search, (4) data combination, (5) data analysis, and (6) data prediction and decision support (Bonham-Carter, 2000).

The overall workflow follows the digital field data acquisition, visualization and analysis methods outlined by McCaffrey et al. (2005), termed GAVA (Geospatial Acquisition, Visualisation and Analysis), which integrates field- and laboratory-based digital mapping methodologies and allows for continual data analysis and evaluation at every stage in the data gathering process.

#### 5.3.1. Regional structural data

Regional structures were studied by analysis of Landsat images, aeromagnetic anomaly maps (Rasmussen and van Gool, 2000; van Gool et al., 2002) and Digital Terrain Models (DTM). Structural lineament maps were constructed at a variety of scales (1:500 000, 1:100 000 and 1:20 000) through the analysis of Landsat data and aerial photographs inside ArcGIS. Attribute data (i.e. trend, length, offset, comments) were also recorded and stored in the GIS database. After interpretation, lineaments were then

compared to a DTM and refined using ArcGIS lineament analysis tools (e.g. density maps, trend analysis, and rose plotting tools).

Aeromagnetic anomaly maps from the region (Rasmussen and van Gool, 2000; van Gool et al., 2002) were studied together with pre-existing geological map data (Escher, 1995; Olesen, 1984; Henriksen et al., 2000) in order to assess the onshore variations in basement architecture and structural trends. Regional geophysical maps (Planke et al., 2004) were also used to identify major structural trends offshore in an attempt to identify basement structures in the Davis Strait.

### ***5.3.2. Outcrop-scale structural data***

Due to the isolated nature of the field localities, battery/ power supplies were limited, thus the use of computers (including pocket PCs used for digital data collection) in the field was restricted. Outcrop scale field data could only be recorded in a semi-digital format: i.e. using a pocket GPS to record data points as waypoints, while attribute data were recorded in conventional notebook format, and then transferred to a GIS file on return to the camp. Although this is not fully consistent with the 'GAVA' digital mapping methods described by McCaffrey et al. (2005), the resulting data files still have the necessary geospatial component.

Aerial photographs were used during field data acquisition, allowing ground-truthing and modifications of regional structures identified in pre-fieldwork analysis. Alongside reconnaissance mapping of the area, detailed fault populations (of at least 30 faults) were collected, recording geometry, kinematics and various other fault attributes for faults and fault zone observed (Table 5.1). The lithology and structure of were also extensively mapped in order to assess the relationships, if any, between basement rocks and later brittle fault patterns.

### ***5.3.3. Areas and localities studied***

The onshore research in this study lies entirely within the granulite facies orthogneisses of the Central Nagssugtoqidian orogenic belt (see above; Fig. 5.4; Marker et al., 1995; van Gool et al., 2002). Field data were collected from various localities in 4 mapping areas spanning from Inugsuk (on the border between the Northern and Central



Nagssugtoqidian Orogen) to Nordre Isortoq (Figs. 5.3 and 5.4). These mapping areas were chosen prior to fieldwork based on prior knowledge within GEUS and lab-based regional studies of Landsat and aerial photographs. A number of factors were considered when choosing these areas, including: the number and range of prominent lineament trends in the area; location with respect to regional structures (e.g. the Nordre Strømfjord and Nordre Isortoq Shear Zones); and accessibility.

The mapping areas typically cover 25 – 30 km<sup>2</sup> and each is marked by a distinct basement fabric/ geometry. Areas 2 and 4 are within the Nordre Strømfjord and Nordre Isortoq Shear Zones respectively (Fig. 5.4), and are thus characterized by steeply dipping belts of intense shear zone fabrics, trending *c.* ENE (065°) and *c.* E-W (085°). Area 1 lies to the north of the Nordre Strømfjord Shear Zone, while area 3 to the south (in the central-NO flat belt), and are characterised by less intense basement trends and foliation that dips at shallower angles.

## **5.4. Regional fault populations**

### **5.4.1. Regional lineament trends**

Landsat analysis of the region reveals that the onshore exposures to the east of the Davis Strait are cut by several distinct lineament sets (Fig. 5.4a; see also Wilson et al., 2006). Rose diagrams (Fig. 5.5) show that lineaments trending in almost all directions can be observed, but dominant lineament trends are N–S to NNE–SSW, ENE–WSW to ESE–WNW, and NW–SE (Figs. 5.4 and 5.5). ENE–WSW-trending lineaments appear to predominate; however as this trend is parallel to basement structures, this is not necessarily representative of the dominant fault trend. These lineament maps have been compared to existing onshore and offshore geology maps, and there is a strong correlation between lineaments and mapped fault trends. Lineament trends also appear to vary spatially (see below).

Lineament trends identified from aerial photographs (Fig. 5.4b) are similar with those identified from Landsat, with the dominant trends being N–S to NNE–SSW, ENE–WSW to ESE–WNW, and NNW–SSE (Fig. 5.5b). Areas that lie in the vicinity of *Nordre Strømfjord* and *Nordre Isortoq* were analysed in detail using aerial photographs at 1:20 000 scale (see below; Fig. 5.4b). During field data collection, many of the

lineaments identified from aerial photographs were analysed, and with the exception of a few basement parallel trends (which correspond to basement fabrics) ground-truthing confirmed that lineaments in these areas generally correspond to major faults or fault zones.

#### **5.4.2. Nordre Strømfjord region (Areas 1-3)**

Area 1 (Fig. 5.4b) is dominated by NNW-SSE, NNE-SSW and ENE-WSW (basement parallel) lineament trends (Fig. 5.5c). Major lineaments (i.e. longest and most prominent in map view) trend NNE-SSW. Similar trends can also be seen in area 2 (Fig. 5.4b), but there appears to be a stronger influence of N-S to NNE-SSW trends compared to area 1 (Fig. 5.5d). Again the largest lineaments in the area are NNW-SSE and NNE-SSW trending, with the latter appearing to cross cut all others (Fig. 5.4b).

South of the Nordre Strømfjord, in area 3 (Fig. 5.4b), lineament patterns appear to change markedly, with the main structural trends falling in a range from N-S to ENE-WSW (i.e. NNW-SSE trending structures, which predominate to the north, are sparse; Fig. 5.5e). A number of ESE-WNW trending lineaments are also apparent in this area, but which are not observed to the north. A number of major N-S to NNE-SSW trending lineaments can be identified in the coastal areas SW of area 3 (Fig. 5.4b), and may be traceable offshore.

#### **5.4.3. Nordre Isortoq region (Area 4)**

In area 4 (Fig. 5.4b) aerial photographs reveal a number of different fault trends, though similar to those seen further north (in areas 1-3). A distinct change in fault pattern can be identified north and south of an intense zone of steep basement fabrics associated with the Nordre Isortoq Shear Zone (Fig. 5.4b). North of this zone N-S and NNE-SSW trending faults predominant, while south of this steep belt, ENE-WSW, ESE-WNW, and N-S trends are more prominent (Figs. 5.4b and 5.5f). This switch is similar to the change observed between areas 2 and 3 (i.e. across the southern margin of the Nordre Strømfjord shear zone).

Crosscutting relationships for lineaments are difficult to discern in most areas. However in areas 1 and 2 NNE-SSW trending lineaments appear to crosscut all other

structures, and show sinistral offsets. A more detailed assessment of the age relationships between lineament trends is given in Wilson et al. (2006).

## **5.5. Outcrop-scale fault populations**

### **5.5.1. Outcrops and exposure**

Outcrops are generally well exposed, with the best exposure on the valley sides, where rock and cliff sections are common, and along coastal sections where several small bays outline primary structures in the rocks, such as fault and fracture zones (Figs. 5.4b and 5.6a-b). The rocks in the area are predominantly quartzo-feldspathic, pelitic and semi-pelitic gneisses metamorphosed to amphibolite facies during Nagssugtoqidian orogenics. The basement fabrics ENE-trending linear belts of steeply dipping gneisses (inc. the Nordre Strømfjord and Nordre Isortoq shear zones; Fig. 5.3 and 5.4), which alternate with zones dominated by kilometre-scale fold structures. Good fault exposures are generally found in coastal areas where tidal effects have lead to clean exposures; where as inland faults are generally marked by incisive gullies with only a limited number of fresh fault surfaces to be observed. Most fault rocks observed were either cataclasites or pseudotachylites, and there was little to no evidence of fluids and mineralization associated with faulting. The only exception to this was iron staining on faults cutting more pelitic (Fe-rich) units.

### **5.5.2. Measurements and determinations**

During fieldwork, over 1800 mesoscale (cm-dm scale) faults and fractures and associated slip-striae have been measured at over 20 localities. The distribution of all measured strikes for all faults and fractures in each mapping area are also shown in Fig. 5.5. Dominant fracture trends tend to range from N-S to NW-SE (Fig. 5.5), while various fault orientations and fault types were observed (Fig. 5.8). More than 40% of the faults measured exhibit good kinematic indicators, in the form of slickenlines and striated coatings (Fig. 5.8). In order to evaluate the palaeostress conditions from a fault population, it is important to also know the sense of slip on a large percentage of the faults (Angelier, 1985). In some localities, offsets on pre-existing structures (such as basement units and fabrics) could be used to identify the slip-sense on faults, but in most

cases the morphology of the fault surface and secondary structures, such as stepped slickenfibers and Riedel-type fracture development (Figs. 5.6 and 5.7) were used (Angelier, 1985, and Petit, 1987).

Dominant fault types were strike-slip faults (619), of which 54% are dextral and 46% sinistral (Fig. 5.8). Dextral faults generally trend NW-SE, ESE-WNW, and ENE-WSW (Figs. 5.6e, f and 5.7e, g), while sinistral faults trend from N-S to ENE-WSW (Figs. 5.6a-c and 5.7d). Normal faults trend N-S, NNW-SSE (Figs. 5.6g and 5.7f) and ENE-WSW (basement parallel, Fig. 5.6f), and a number of reverse faults, trending ENE-WSW, were also recorded (Figs. 5.6h and 5.7c, d). Figure 5.8 shows stereoplots for each of the fault types recorded.

A distinct change in dominant fault orientation can be seen across the Nordre Strømfjord (Fig. 5.9). In areas 1 and 2 (Fig. 5.4b) faults are dominated by *c.* N-S (i.e. NNW-SSW through to NNE-SSW; Fig. 5.5c, d) faults, while south of the fjord, in area 3 (Fig. 5.4b) NE-SW to E-W faults predominate (Fig. 5.5e). Furthermore, south of the fjord a number of fault populations recorded were dominated by reverse faults (e.g. Locality 202, Figs. 5.6h and 5.9); while north of the fjord, normal and strike-slip faults predominate. Similar patterns can also be seen in the Nordre Isortoq region, but at a slightly smaller scale. A prominent steep belt of the Nordre Isortoq shear zone cuts through the area covered by mapping area 4 (Fig. 5.10). A distinct change in fault pattern, fault geometry, and kinematics occurs across this zone (Figs. 5.5f and 5.10). North of this steep belt faults generally trend *c.* N-S and show strike-slip and normal movements, while south of the steep belt fault trends become *c.* E-W and exhibit strike-slip and reverse movements (Fig. 5.7).

### **5.5.3. Age relationships**

A younging table (Table 5.2) was constructed (using methodology of Potts and Reddy, 1999, 2000) in order to determine the relative age relationships of each fault set based on the field observations (e.g. crosscutting relationships and overprinting fault striae; Figs. 5.6 and 5.7). For the interpretation of age relationships faults have been categorised into seven distinct systems based on orientation and slip: ESE-WNW; NNE-SSW; NNW-SSE; N-S (strike-slip); N-S (normal); ENE-WSW (strike-slip); and ENE-WSW

(reverse). As discussed by Potts and Reddy (1999, 2000), the number different possible deformation histories,  $h_c$ , that can account for a given number of fault and fracture sets,  $n$ , is given by:

$$h_c = (n - 1) ! \quad (5.3.)$$

Thus for our seven fault sets,  $h_c = (6 \times 5 \times 4 \times 3 \times 2 \times 1) = 720$ . The number of different crosscutting relationships,  $p_c$ , needed to determine a complete fault history is:

$$p_c = n (n - 1) \quad (5.4.)$$

this corresponds to forty-two different crosscutting relationships for our seven fault sets.

Cross-cutting relationships and overprinting fault striae presented in Table 5.2 to determine relative age relationships suggest that both strike-slip and reverse movements post-date normal (dip-slip) movements. This observation can be made most evident by the observation of strike-slip movement's overprinting dip-slip moments on N-S trending faults. Basement parallel faults appear to have been active throughout the brittle deformation history, as mutual crosscutting relationships can be seen with all other fault systems (Table 5.2). However the age relationships for all other fault sets appears far less clear as mutual cross-cutting relationships appear to suggest that these systems were active contemporaneously. The observation that orientation and movement of strike-slip faults are consistent with shear fractures associated with a NNE-SSW sinistral wrench system (Wilson et al., 2006) also supports this apparent contemporaneous age relationship. Slip striae and pseudotachylite on the surfaces of reverse faults show little evidence for reworking, and a spatial and kinematic association with strike-slip movements is apparent. This may suggest that reverse fault movements were associated with strike-slip structures. However, strike-slip faults were noted to cross-cut these thrust faults at some localities (Fig. 5.7d).

#### 5.5.4. Kinematic analysis

##### 5.5.4.1. Analysis method

My Fault™ stereonet software, produced by Pangaea Scientific Ltd., was used for kinematic analysis, using the inversion method outlined by Michael (1984). Our procedure was to invert a population of faults from a single locality. Those faults with misfit angles greater than 45° were then rejected and the inversion procedure rerun (also see Titus et al., 2002). This process was repeated until a group of faults with a homogeneous solution was found. In all cases, a minimum of 7 faults were remaining at each locality (5 is considered the minimum number required). The disregarded data for each locality were then rerun through the inversion procedure to separate out multiple deformation events. In many cases, 10 out of 17 localities, a clear second set of stress axes could be derived from the data, but these were often only slight variations on the primary set, or represent a switching of one of the horizontal and the vertical axes (see Figs. 5.9 and 5.10; and also *appendix 4*)

##### 5.5.4.2. Inversion results

The results of kinematic analysis on faults at various localities (Figs. 5.9 and 5.10; and *appendix 4*) show that palaeostress tensors generally fit into two systems. One system, found at 10 localities, represents pure ENE–WSW (axes range from NE–SW to E–W) extension; while the other, found at 15 localities, exhibit a similar extension direction, but with an added component of perpendicular compression (SSE–NNW) (see Figs. 5.9 and 5.10). Two further localities (401 and 408; Fig. 5.10) also show solely compressional (SSE–NNW) stress tensors. These results, summarised in Fig. 5.11, clearly demonstrate that extension is predominantly ENE–WSW, and compression predominantly SSE–NNW (or sub-vertical in areas of pure extension). Fracture trends do not appear to match fault orientations (Fig. 5.5), and consistently trend in a NNW–SSE orientation. Assuming that the bulk of the fractures are mode I opening structures (i.e. tensile fractures and joints; Hancock, 1985), then these would also support a dominantly ENE–WSW extension vector, consistent with the results of palaeostress inversion (Fig. 5.11). The results at the outcrop scale (Fig. 5.11) are consistent with the results of bulk inversion of each of the various fault types recorded (Fig. 5.8b). However, by carrying

out a locality by locality assessment, spatial variations in the palaeostress tensors can also be assessed.

## 5.6. Discussion

### 5.6.1. Onshore structural framework (outcrop to basin scale)

#### 5.6.1.1. Fault patterns and Palaeostress

At least two distinct fault systems can be identified in the areas studied: 1) normal faults, and 2) strike-slip faults with associated subordinate reverse faults. Normal faults generally trend N-S to NNW-SSE (although a small number also reactivate ENE-WSW trending basement structures; Fig 8), and correspond to an ENE-WSW extension vector, which has also been identified by palaeostress analysis. Furthermore, the preferential alignment of tensile fractures across the region also suggest the same orientation of extension. The orientation of strike-slip faults is more diverse, but the geometry of these faults is consistent with synthetic and antithetic faults and Reidel-type shear fractures typical of a wrench zone (Fig. 5.1a). The orientation and movement sense on the faults are indicative of a NNE-SSW trending sinistral wrench system. The infinitesimal strain axes predicted by this system of faults (assuming simple shear, with axis at  $45^\circ$  to trend of wrench system; Fig. 5.1a) would therefore be NE-SW to ENE-WSW (c.  $055^\circ$ - $235^\circ$ ) extension ( $x_i$  - axis) and SE-NW to SSE-NNW (c.  $145^\circ$ - $325^\circ$ ) shortening ( $z_i$  - axis), which is consistent with the results of palaeostress analysis at various localities (Fig. 5.11). An equivalent NNE-SSW trending sinistral strike-slip system of course lies offshore in the Davis Strait (i.e. the Ungava fault zone), and thus these onshore fault patterns are likely to be associated with the development of this transform fault (Wilson et al., 2006).

#### 5.6.1.2. Spatial and Temporal Variations

Spatial variations in both fault geometry and kinematics appear to be coincident with variations in basement structure. Steep belts of both the Nordre Strømfjord and Nordre Isortoq shear zones mark a transition from dominantly c. N-S to NNE-SSW trends in the north, to predominantly NE-SW to ESE-WNW trends (Fig. 5.4b). Distinct zones of compressional structures (i.e. reverse faults; Figs. 5.6h and 5.7c) associated with strike-

slip palaeostress interpretations can be identified (Figs. 5.9 and 5.10). Furthermore, on the north side of these basement anisotropies fault patterns change markedly and appear to be dominated by strike-slip and extensional faults (Figs. 5.9 and 5.10). In these two areas no lithological similarities can be seen to account for these variations, therefore it is more likely that the controlling factor is basement structure (i.e. in both cases the change in patterns is coincident with a marked steepening and intensification of basement fabrics, with similar patterns developing in both cases). The presence of pre-existing structures lying at oblique angles to imposed opening vectors may commonly lead to the partitioning of transtensional deformation into zones of wrench- and extension-dominated deformation (Tikoff and Teyssier., 1994; Jones and Tanner, 1995; De Paola et al., 2005). However, this would require that faults developed during a single deformation event.

Cross-cutting relationships and apparent strike-slip reactivation of N-S trending Normal faults suggests that faults may have formed during more than one phase of deformation, with normal faults predating strike-slip and reverse faults (Table 5.2). This observation appears to be at odds with the spatial partitioning model outlined above, and would suggest that the zones of extension-dominated and wrench- dominated deformation mark a temporal transition.

Geoffroy et al. (1998) found similar strike-slip and extensional palaeostress axes for populations of Palaeocene faults cutting Palaeocene lavas on west Disko, which they attribute to regional stresses and not a secondary consequence of flexure in the area. Furthermore, they also suggest that *c.* NE-SW extension postdates *c.* E-W extension in the area. Locally transpressional structures associated with sinistral strike-slip movements on Ungava/ Ikermiut fault zone have been observed offshore (Chalmers et al., 1995; Chalmers and Pulvertaft, 2001) which are comparable to inversion structures formed at pre-existing releasing bends (Dooley et al., 1999). This transpression effects Eocene strata, and is therefore interpreted as a consequence of late Eocene deformation (Chalmers and Pulvertaft, 2001). Using these correlations with comparable regional structures (see also Wilson et al., 2006) we suggest at least two phases of deformation lead to the development of these faults: (1) oblique extension/ transtension; followed by



(2) regional sinistral strike-slip with localised transpression (Fig. 5.12). This would also imply a counter-clockwise rotation of the regional extension vector with time.

#### 5.6.1.3. Onshore-offshore correlations in the Sisimiut Basin

A strong structural link can be made between the Nordre Isortoq Shear Zone (onshore) and the south Sisimiut Basin border fault (offshore). Figure 5.12 highlights the strong correlation between this border fault and the offshore continuation of the shear zone, which has led to the interpretation that reactivation of steep basement fabrics have controlled the location and geometry of the southern margin of the Sisimiut Basin. In addition, further links can be made between this structural trend and the location of the Ikermiut fault zone (i.e. restraining bend/ right step in Ungava Fault Zone; Chalmers et al., 1995; Chalmers and Pulvertaft, 2001) in the central Davis Strait, and also the Sisimiut lineament to the west-southwest (Fig. 5.12). The Sisimiut lineament is a distinct NNE-SSW to NE-SW trending structural lineament that can be identified in bouguer gravity anomaly maps offshore, west of the Ungava fault zone (Fig. 5.12; Christiansen et al., 2002; Planke *et al.*, 2004). The *Sisimiut lineament–Ikermiut FZ–Nordre Isortoq Shear Zone line* (SL-IFZ-NISZ line; Fig. 5.3) defines a curved trace that fits well with the overall proposed trend of the Nagssugtoqidian orogenic belt offshore and may thus define a strong basement trend across the Davis Strait. As this basement trend appears to coincide with a number of important structures and deformation zones, this suggests that basement structure has a strong control both onshore and offshore.

Similarities can also be drawn between the spatial variation in dominant lineament trends onshore and the changes in trend of major border faults of the Sisimiut Basin offshore (Fig. 5.5a). Where the Sisimiut Basin border fault comes closest to the mainland (in the CNO flat belt) lineament trends are predominantly NNE-SSW trending, consistent with the major fault offshore (Fig. 5.5a). Further north the border fault curves round into a NNW-SSE to NW-SE orientation, this is matched by a general northward transition from predominantly NNE-SSW to NNW-SSE trending lineaments onshore (Fig. 5.4a), culminating in some major NW-SW trending fault controlled fjords in the NNO (see Fig. 5.4a and fig. 4 of Piazzolo et al. 2004). With the exception of the south Sisimiut Basin border fault (which reactivates basement fabrics) normal faults seen

offshore trend NNW-SSE and N-S, which are similar to those recorded onshore. These are post-dated by NNE-SSW strike-slip systems in the Ungava fault zone, which are again consistent with onshore structures.

## 5.6.2. *The Davis Strait Transform and the Ungava fault zone (basin to margin scale)*

### 5.6.2.1. *Transtension vs. wrench systems*

Field evidence appears to suggest that faults developed during two phases of deformation: 1) extensional/ transtensional, and 2) a sinistral wrench system, with localised transpression. This model also appears to fit for offshore fault structures in various parts of the Davis Strait. Experimental models of transtensional and oblique rift systems (Withjack and Jamison, 1986; Tron and Brun, 1991) show that there is a predictable relationship between the orientation of normal faults relative to the deformation zone boundary (see *equations 1 and 2*). It should be noted that the models of Tron and Brun (1991) appear to be more analogous to the fault systems of the Davis Strait, as they define a principal displacement zone (e.g. equivalent to the Ungava fault zone) rather than deformation zone boundaries (outlined in Withjack and Jamison, 1986).

If we assume the current trend of the Ungava fault zone as the principal displacement zone,  $\alpha$  and  $\beta_x$  angles can be calculated for various fault systems using *equation 1*. These can then be compared to regional extension vectors (i.e. inferred from structural trends and magnetic anomaly trends in the Labrador Sea), and also palaeostress calculations from field data.  $\beta_x$  angles for N-S trending normal faults relative to the Ungava fault zone are  $75^\circ$ , which corresponds to an angle  $\alpha$  of  $60^\circ$ , and an extension vector of 075-255 (Fig. 5.13a). This fits with the regional extension vectors inferred from similar age faults and pre-chron 24 magnetochrons in the Labrador Sea (Fig. 5.13a; Chalmers and Pulvertaft, 2001), and also with the results of palaeostress inversion onshore (this study). This consistency between predicted and observed fault models suggests that there was likely to be some form of NNE-SSW trending structure acting as the deformation boundary (or principal deformation zone) controlling normal fault geometries from very early in the margins history (e.g. a proto-Ungava fault zone).

Applying *equation 1* to strike-slip faults along the margin is far less simple. If we consider the Ungava fault zone as an ideal wrench system (simple shear,  $\alpha = 0$ ), then an  $\beta_x$  angle of  $45^\circ$ , and an infinitesimal strain axis ( $x_i$ ) of  $060^\circ$ - $240^\circ$ , is predicted. This is consistent with palaeostress interpretations (Figs. 5.11 and 5.13), and also extension implied from similar age structures in the Labrador Sea. However, this simple shear model implies a regional extension (transport) direction parallel to the Ungava fault zone (i.e.  $015^\circ$ - $195^\circ$ ), which is *not* consistent with structures in the Labrador Sea ( $055^\circ$ - $235^\circ$ ). The regional extension direction implied from younger extensional faulting and sea-floor spreading magnetochrons (i.e. post-chron 24) in the Labrador Sea is  $055^\circ$ - $235^\circ$  (Fig. 5.13b), which corresponds to an  $\alpha$  angle of  $40^\circ$ , and thus  $\beta_x$  of  $65^\circ$  (i.e.  $x_i = 080^\circ$ - $260^\circ$ ). These angles do not predict the observed wrench-dominated system (Fig. 5.13c). However, it has been shown that a positive volume change (i.e. such as magma injection during sea-floor spreading) can broaden the zone of wrench dominated transtension (WDTT; Fig. 5.13c; Teyssier and Tikoff, 1999). Therefore, although the apparent angle of divergence along the Ungava fault zone (as interpreted from structural trends in the Labrador Sea, Phase 2a; Fig. 5.13a) appears to be well within the EDTT domain, the transform can still be dominated by strike-slip structures due to the volume increase as a result of sea-floor spreading in the Labrador Sea. An alternative explanation for this paradox may be that the deformation was partitioned into wrench dominated movements along the Ungava fault system and more diffuse extension across the region (e.g. in the form of normal faulting and/ or tectonic subsidence). Similar examples of partitioned transtension have been presented in other areas by Dewey (2002), Oldow (2003) and De Paola et al. (2005b). As field observations clearly indicate extensional faults pre-dating strike-slip, this latter hypothesis seems less likely, or at least requires further investigation.

Analysis of fault patterns and magnetochrons in the Labrador Sea suggest a  $15$ - $20^\circ$  counter clockwise rotation in spreading axis during the early Eocene (chron 24.  $\sim 55.9$ - $53.3$  Ma; Fig. 5.13), as opening started between Greenland and Europe (Srivastava, 1978; Chalmers and Pulvertaft, 2001). However, this alone is not enough to account for the transition from an extension-dominated to wrench-dominated system in the Davis Strait (Fig. 5.13), and further explanation is needed (as outlined above). Other

factors that may contribute to the observed counter-clockwise rotation of the extensional axes with time may be the effect of bulk non-coaxial sinistral shear component of deformation (see fig. 1 of Waldron, 2005). Also, the onset of sea-floor spreading (chron 27) generates ridge push forces that could lead to the transition from extension-dominated to wrench-dominated transtension. To distinguish which of these effects may have played the dominant role in driving the transition from extension-dominated to wrench-dominated deformation requires better constraints on the timing of deformation (i.e. did WDTT begin at chron 27 or 24?).

*5.6.2.2. Basement influence in the Davis Strait region.*

The location of transform faults is often attributed to pre-existing basement structures (Le Pichon and Hayes, 1971; Rosendahl, 1987). Wilson et al. (2006) highlighted the apparent correlation between the location of the complex fault patterns of the Davis Strait and the Nagssugtoqidian orogenic belt, and suggested that this basement structure controlled the development of the transform. However, with the exception of the southern bounding fault to the Sisimiut Basin (Fig. 5.12) there is little evidence for direct reactivation of basement by later faults offshore east of the Ungava fault zone. By contrast, a number of faults can be seen oriented parallel to NE-SW trending fabrics, including the Sisimiut lineament on the western, Canadian side of the UFZ (Fig. 5.2).

From the fault patterns and data presented in this study, we suggest that the intense basement fabrics of the Nagssugtoqidian orogenic belt acted as a barrier to NNW-SSE faults propagating from the southeast in the Labrador Sea (Fig. 5.14). Due to the obliquity between the trend of the orogenic belt and the regional extension direction, a clockwise rotation, associated with dextral sense of shear along basement trends, may be predicted. This would therefore deflect the trend of the propagating rift system into a NNE-SSW orientation, returning to original NNW-SSE trends north of the orogenic belt (Fig. 5.14a). However only a limited amount of basement parallel faulting was observed in the field, which would suggest that this basement shear hypothesis is unlikely to be the main influence on deflecting the trend of the propagating ridge.

An alternative model is one that is analogous to cleavage refraction through layers of different rock strength and competency (see figs. 10.23 and 21.22-21.24 in

Ramsay and Huber, 2002). As basement anisotropies can have a strong effect on the mechanical properties of the rock, this would imply that rocks within the Nagssugtoqidian orogenic belt may have different overall rock strength to those outside. Bradshaw and Zoback (1988) highlight the fact that stress and strain can be refracted through different lithologies. Therefore, it is possible that the variations in mechanical properties of the different basement terranes lead to refraction of the orientation of the propagating ridge within the Davis Strait (Fig. 5.14a). Similar studies have been carried out at the outcrop scale by Peacock and Sanderson (1992) through analysing the effects of layering and anisotropy on fault orientations. In their studies they show that fault geometry varies with the orientation of layering relative to the stress field, and also that the geometry of faults in brittle layers (e.g. shale) varies markedly from those in less brittle layers (e.g. sandstone), due to the differences in mechanical properties of the layers.

### **5.7. Conclusions**

The Davis Strait has a distinctly different fault pattern compared with the extensional basins of Baffin Bay and the Labrador Sea to the north and south (Fig. 5.2), and is dominated by an extensional plate boundary transform fault zone. Outcrop to basin scale studies of fault patterns in onshore basement exposures reveal that two main fault systems are apparent: 1) a system of *c.* N-S trending normal faults, and 2) a system of strike-slip faults associated with a regional NNE-SSW trending wrench system. Reactivation of basement structures can be seen, however, these structures are generally localised to shear zones (e.g. Nordre Strømfjord and Nordre Isortoq shear zones) and do not appear to be a dominate fault system. Spatial analysis of fault patterns and kinematics suggest that intense basement fabrics of various shear zones within the Nagssugtoqidian orogenic belt have lead to strain localisation and/ or deformation partitioning onto zones of extension and wrench dominated transtension, with localised zones of reverse faulting. This onshore basement influence is matched directly by offshore structural variations (such as localised transpression in the Ikermiut fault zone). Along side spatial partitioning of transtension, there also appears to have been a temporal effect, with extension-dominated transtensional faults pre-dating wrench-

dominated faulting. This transition from extension-dominated to wrench-dominated faulting may be linked to a three potential factors: (1) onset of sea-floor spreading in the Labrador Sea (Palaeocene, chron 27), (2) a 15-20° counter-clockwise rotation of the spreading axis in the Labrador Sea during the early Eocene (chron 24; Chalmers and Pulvertaft, 2001), or (3) bulk non-coaxial sinistral shear (Waldron, 2005). However, to distinguish which of these is the dominant control requires better constraints on the timing of deformation.

The intense basement fabrics of the Nagssugtoqidian orogenic belt have also been linked to regional scale variations and the development of the Davis Strait Transform fault zone. 5.14 shows a summary cartoon outlining the development of the fault systems in the Davis Strait. Basement influence appears to have led to a change in trend of the rift system propagating from the southeast in the Davis Strait region. This may be the result of localised basement reactivation, or alternatively refraction of the stress field due to the effects of differing mechanical properties of rocks within the Nagssugtoqidian orogenic belt and those outside (Fig. 5.14a). Following the development of the rift system in the Davis Strait, a system of *c.*N-S trending normal faults develop oblique to rift (in an en echelon arrangement; Fig. 5.14b). This was followed by strike-slip movements associated with an overall sinistral wrench system of the Ungava fault zone (Fig. 5.14c), as a result of sea-floor spreading in the Labrador Sea. Had sea-floor spreading continued in the Labrador Sea, the structures of the Davis Strait would have likely evolved into a continent–ocean fracture zone similar to those seen in the equatorial Atlantic margins of Africa and South America (La Pichon and Hays, 1971; Davis et al., 2005).

*Chapter 5 – Basement influence in the Davis Strait*

<b>attribute</b>	<b>data type</b>	<b>data recorded</b>
x	text	easting (UTM zone 22)
y	text	northing (UTM zone 22)
z	text	height above sea level
Fault type	text	fracture/joint, normal, reverse, strike-slip
Fault geometry	numeric	strike and dip of fault plane
Fault striae	numeric	plunge and azimuth of striae
Movement sense	text	sense of slip on fault (also recorded if certain or uncertain)
Fault shape	text	planar, undulating, irregular
Fault surface	text	striated, smooth, rough
Fault rock	text	gouge, breccia, cataclasite, pseudotachylite, mica smears (also recorded sample ID if samples were taken)
Comments	text	other comments (e.g. infill, offset, x-cutting relationships)

**Table 5.1.**

Fault attributes collected at each locality as part of fault population dataset. Also stored in GIS database.

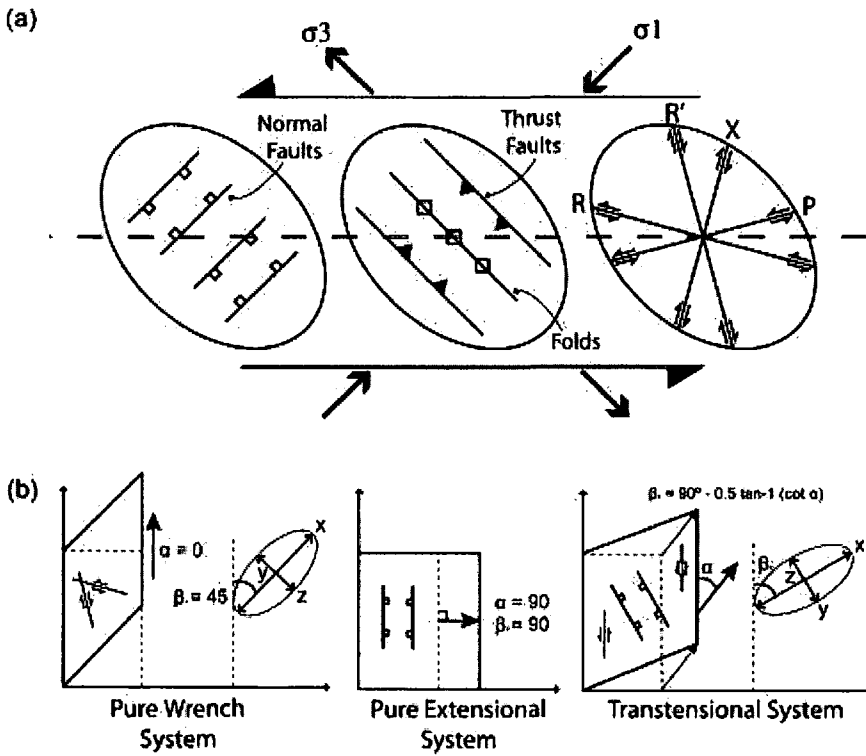
Chapter 5 – Basement influence in the Davis Strait

		Younger						
		ESE-WNW	NNE-SSW	NNW-SSE	N-S (strike-slip)	N-S (normal)	ENE-WSW (reverse)	ENE-WSW (strike-slip)
Older	ESE-WNW		✓	(not seen)	✓	(not seen)	✓	(not seen)
	NNE-SSW	(not seen)		(not seen)	✓	(not seen)	✓	✓
	NNW-SSE	(not seen)	✓		(not seen)	(not seen)	(not seen)	✓
	N-S (strike-slip)	✓ 7e	✓ 6c	✓		(not seen)	✓	✓
	N-S (normal)	✓	✓ 6a	✓	✓		✓	✓
	ENE-WSW (reverse)	✓	✓	(not seen)	✓ 7d	(not seen)		✓ 7d
	ENE-WSW (strike-slip)	✓	✓	✓	✓	✓	✓ 7c	

**Table 5.2.**

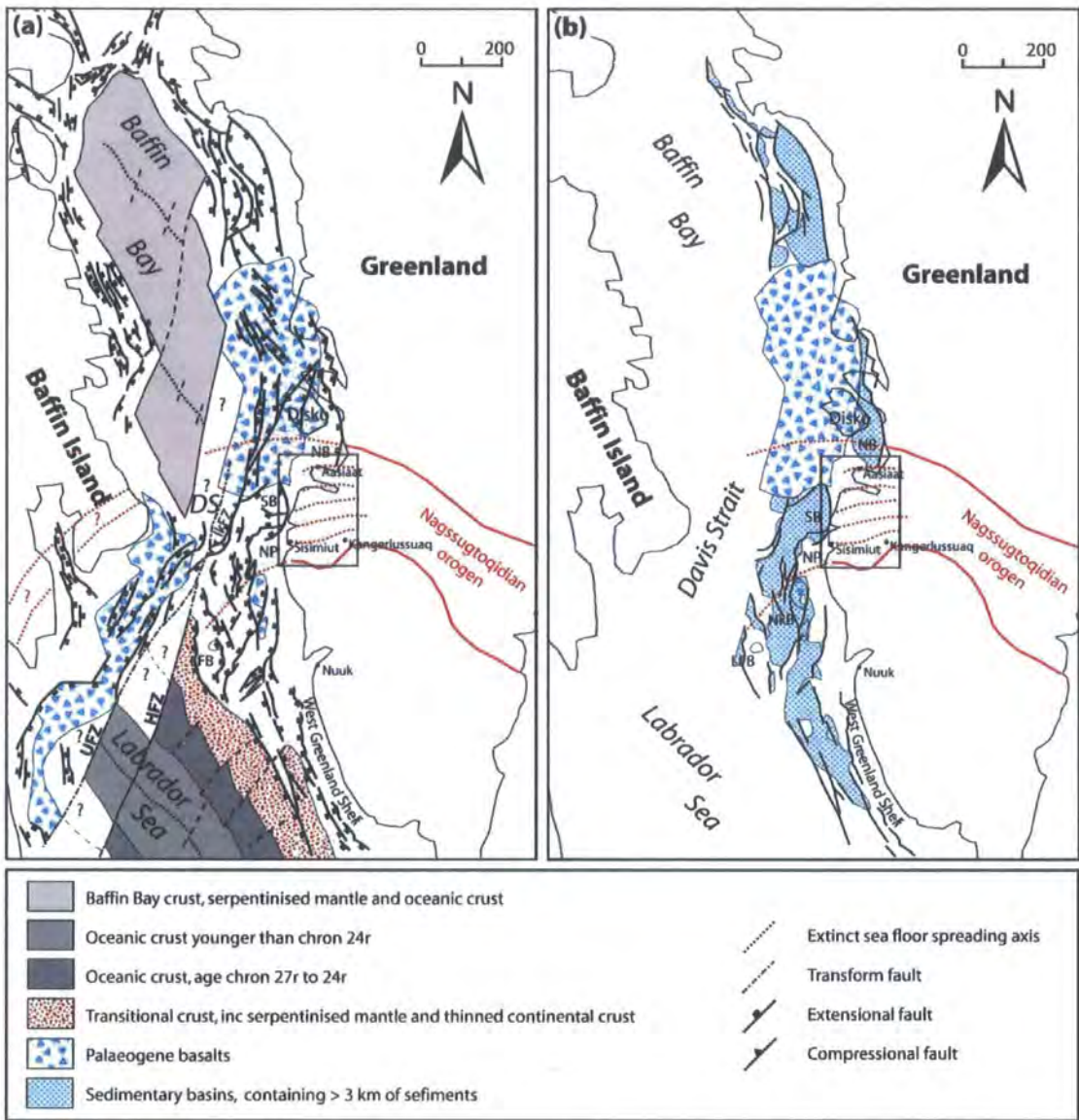
Younging table for fault sets observed in mapping areas 1-4 (Fig. 5.4b). Each cell in matrix represents a possible relative age for the seven fault sets identified. Numbers/ letters (*in italics*) refer to field observations shown in Figs. 5.6 and 5.7.





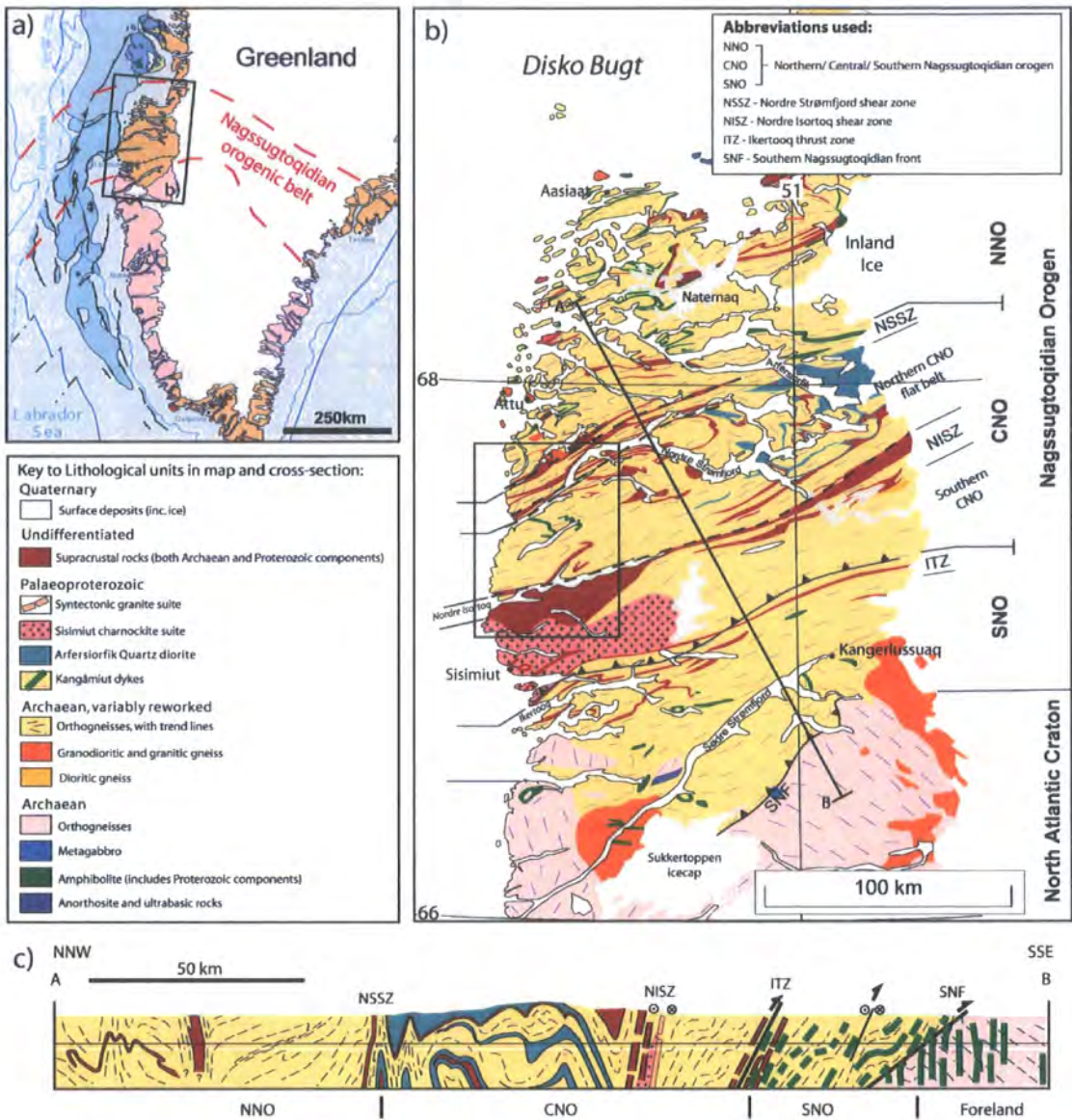
**Figure 5.1.**

(a) Diagram illustrating the structures that may develop due to incremental strain associated with simple-shear deformation in a sinistral strike-slip system (after Harding 1974; Sylvester, 1988).  
 (b) Schematic 2D block diagrams outlining the basic relationship between  $\alpha$ ,  $\beta_x$  and infinitesimal strain axis ( $x, y, z$ ) for pure strike-slip systems (simple shear), pure extensional systems (pure shear), and transtension (after De Paola *et al.*, 2005).



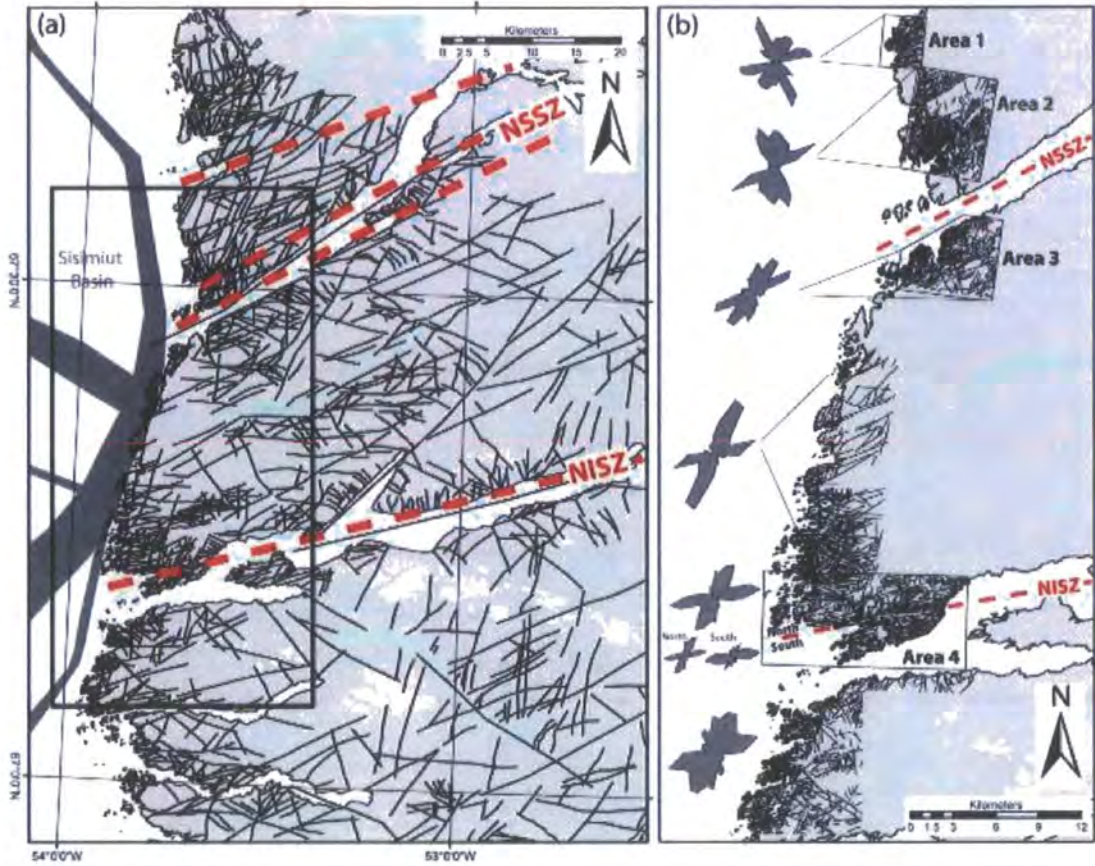
**Figure 5.2.**

Regional maps of the Labrador Sea – Davis Strait – Baffin Bay seaway highlighting: (a) tectonic structures; and (b) sedimentary basins and structural highs. DS = Davis Strait, HFZ = Hudson fault zone, IkFZ = Ikermiut fault zone, LFB = Lady Franklin basin, NB = Nuussuaq basin, NkB = Nuuk basin, NP = Nukik platform, SB = Sisimiut basin, UFZ = Ungava fault zone. Area outlined shows map coverage of Fig. 5.3.



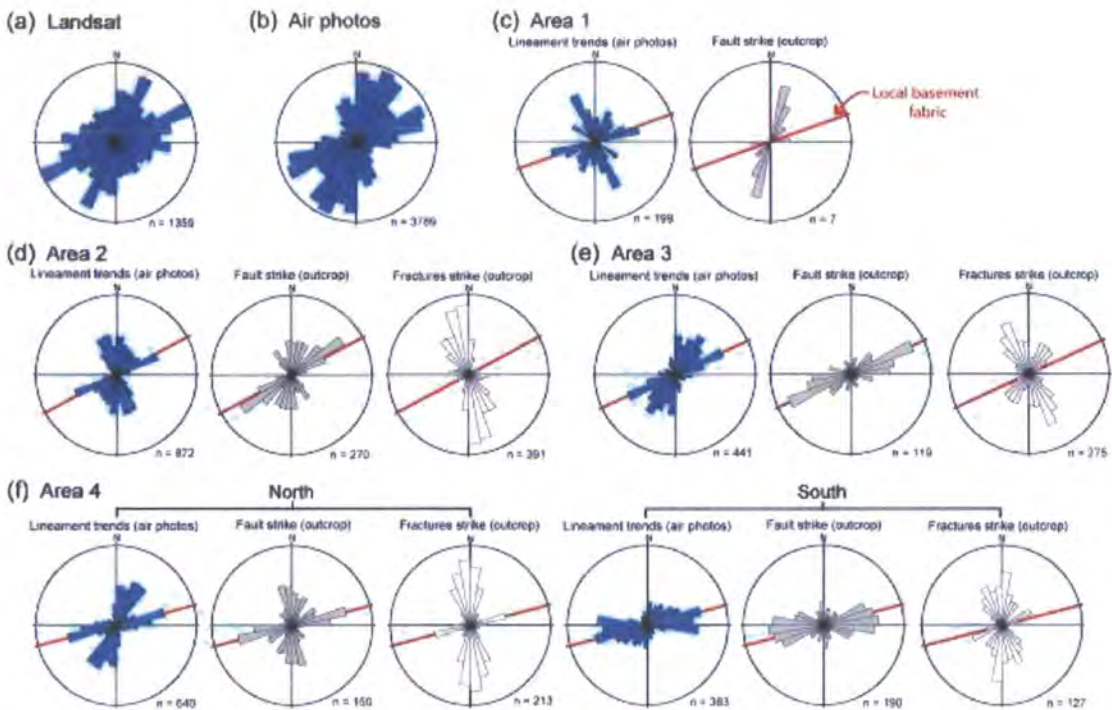
**Figure 5.3.**

(a) Generalised map of southern Greenland showing location of sedimentary basins offshore west Greenland (see Fig. 5.1b) relative to onshore basement terranes. (b) Geological map of the Nagssugtoqidian orogen (modified from van Gool et al. 2002). (c) Cross-section through Nagssugtoqidian orogen, line of section shown in (b) (after van Gool et al. 2002).



**Figure 5.4.**

- (a) Lineament map of CNO, lineaments picked from Landsat image at a scale of 1:100 000 scale.
- (b) Detailed lineament maps for selected areas picked from aerial photographs at a scale of 1:20 000 scale.



**Figure 5.5.**

Rose diagrams for lineaments (dark grey) picked from (a) Landsat, (b) aerial photographs, and (c)–(f) in areas 1, 2, 3 and 4 respectively. (c)–(f) also include rose diagrams for strike of faults (light grey) and fractures (white) measured at outcrop. Area 4 (f) is divided in to separate zones, *north* and *south* of the NISZ, shown in Fig. 5.5. Bold lines represent the local trend of basement fabrics.

Chapter 5 – Basement influence in the Davis Strait

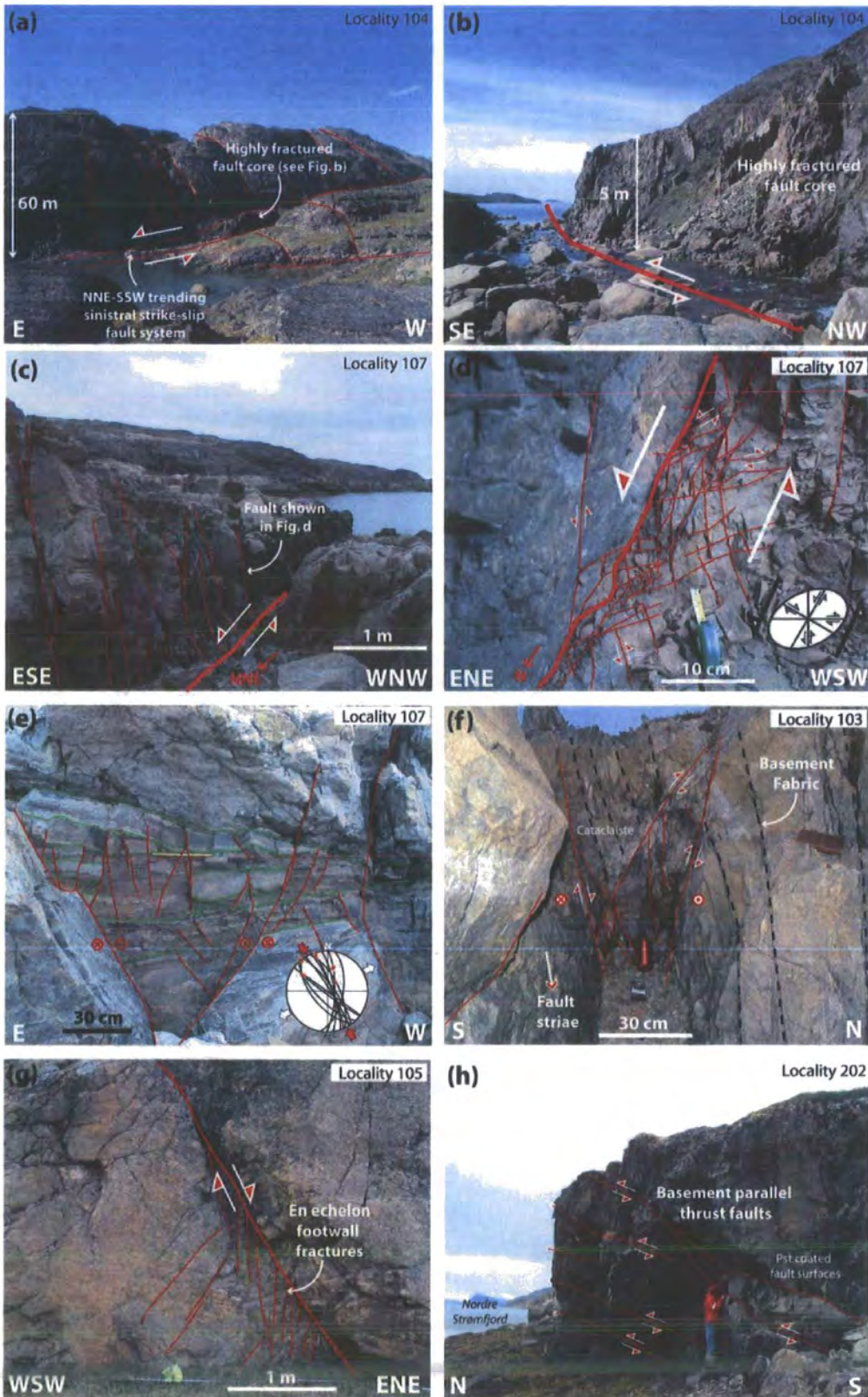


Figure 5.6. (caption overleaf)

**Figure 5.6.**

Photographs showing regional to outcrop scale structures seen in the Nordre Strømfjord region (areas 1-3). (a) Major NNE–SSW trending sinistral strike-slip fault, cross cutting all other fault systems (locality 104). (b) Zoom in of highly fractured NNE–SSW trending fault core shown in (a) (locality 104). (c) NNE–SSW trending sinistral strike-slip fault, and associated en echelon set of N–S trending faults (locality 107). (d) Zoom in of N–S trending sinistral strike-slip faults shown in (c) showing associated Riedel shear fractures (locality. 107). (e) NNW-SSE and N-S trending faults exhibiting strike-slip and oblique slip movements, indicative of ENE-WSW extension (also locality 107). (f) Normal fault core (cataclastic fault rock) trending parallel to basement (Locality 103). (g) NNW–SSW trending normal faults (locality 105). (h) Thrust faults on the south side of the Nordre Strømfjord (locality 202). For map view of localities see Fig. 5.9.

**Figure 5.7. (overleaf)**

Photographs showing regional to outcrop scale structures seen in the Nordre Isortoq area (area 4). (a) Prominent ENE–WSW to E–W trending valley, marking trend of Nordre Isortoq shear zone (NISZ), which marks a distinct boundary in basement structural trends. (b) Conjugate NNW–SSE to N–S trending faults and fractures on north side of NISZ, plus basement parallel (ENE–WSW) normal fault (locality 403). (c) ENE–WSW to ESE–WNW trending thrust faults, with component of dextral oblique-slip on south side of NISZ (locality 401). (d) N-S trending sinistral strike-slip fault/ fault zone crosscutting thrust faults outlined in c) (locality 401). (e) ESE–WNW trending dextral fault, characteristic of major faults on south side of NISZ (locality 402). (f) slip surface of dextral fault shown in e), sense of movement defined by PO slip criteria, plus further observations in the field (locality 402). (g) E–W trending vertical strike-slip fault showing fault striae and dextral Riedel shear fabrics (locality 405). (h) N–S trending normal fault exhibiting a polished surface with dip-slip striae (locality 409). See Petit (1987) for definitions of slip criteria. For map view of localities see Fig. 5.10.

Chapter 5 – Basement influence in the Davis Strait

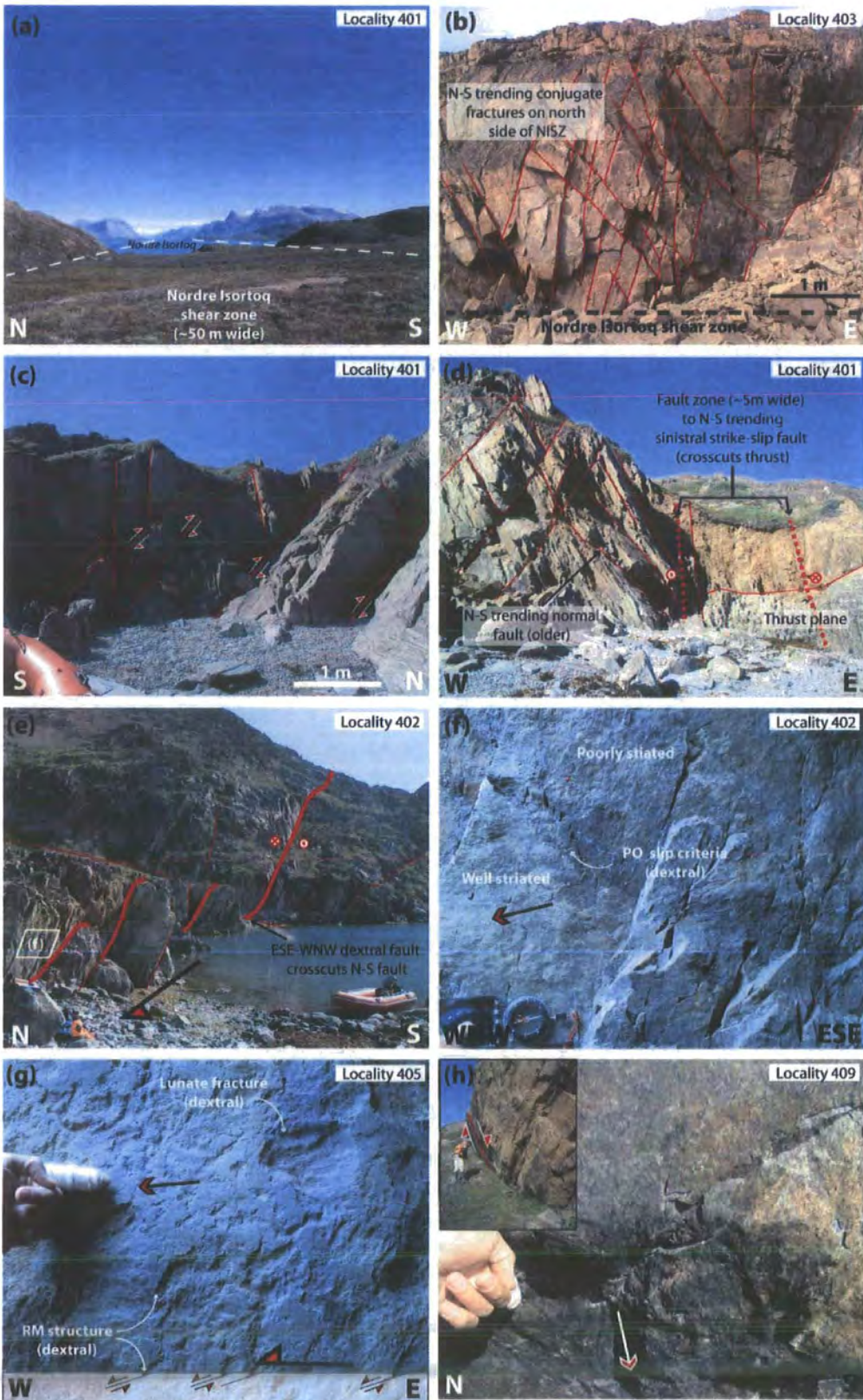
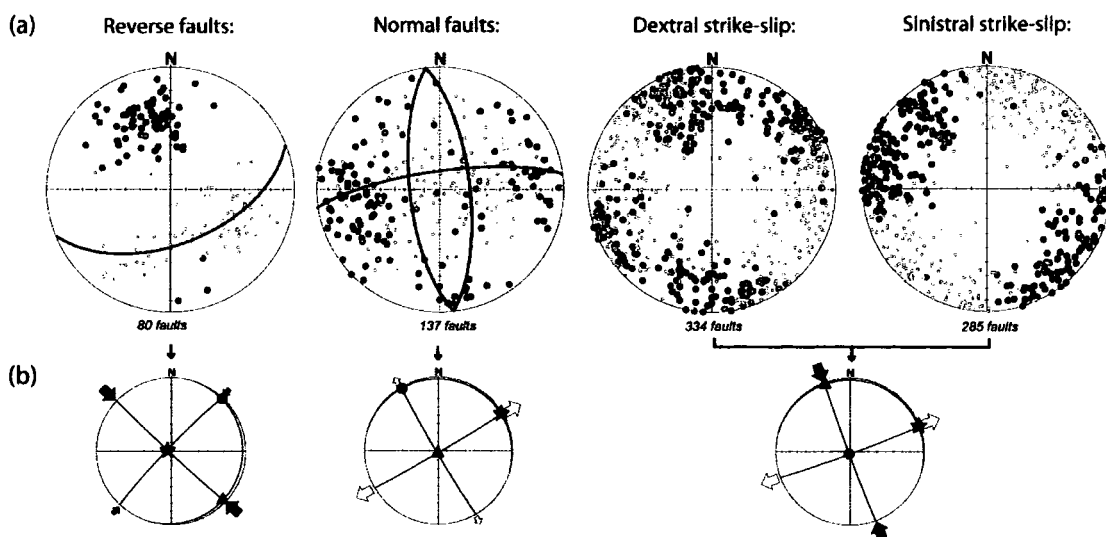


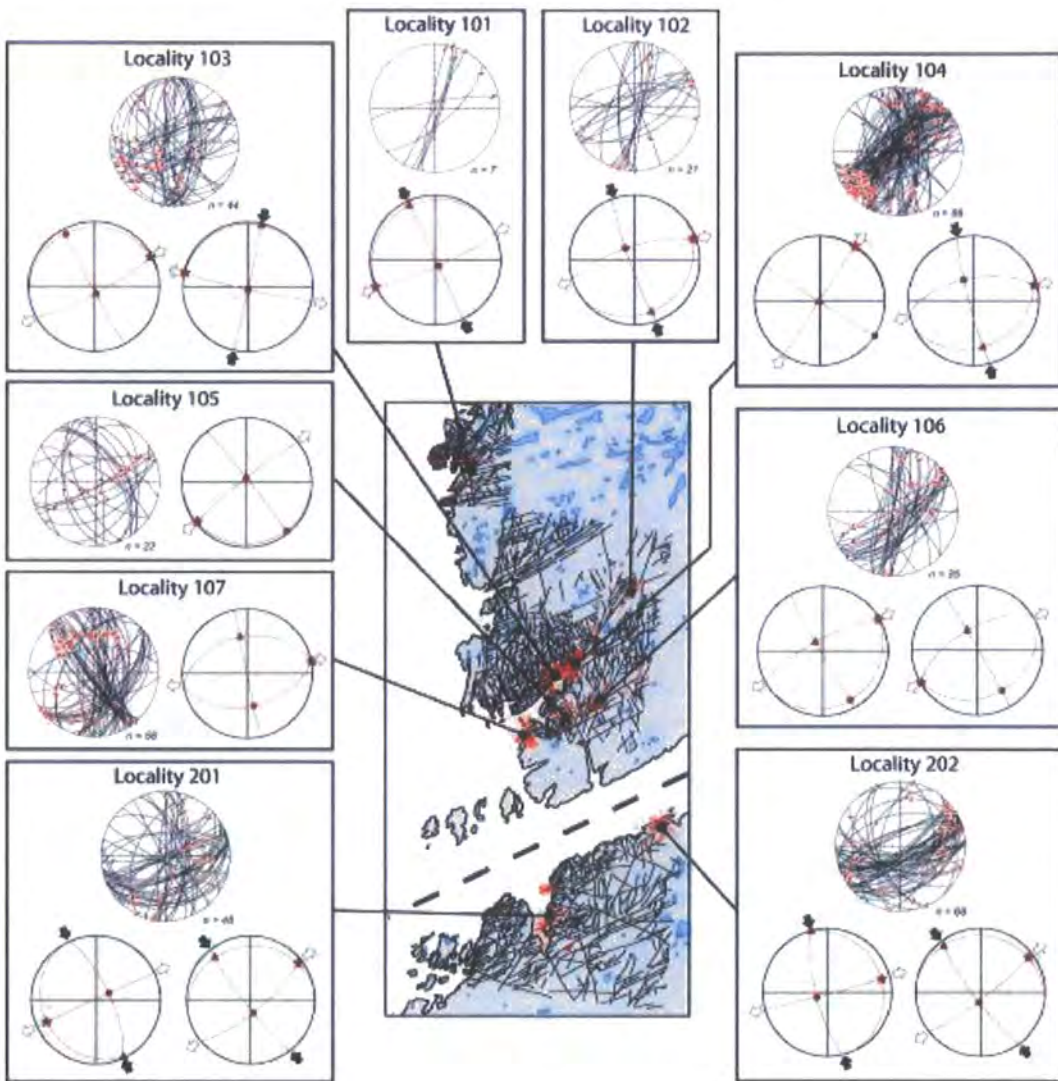
Figure 5.7.





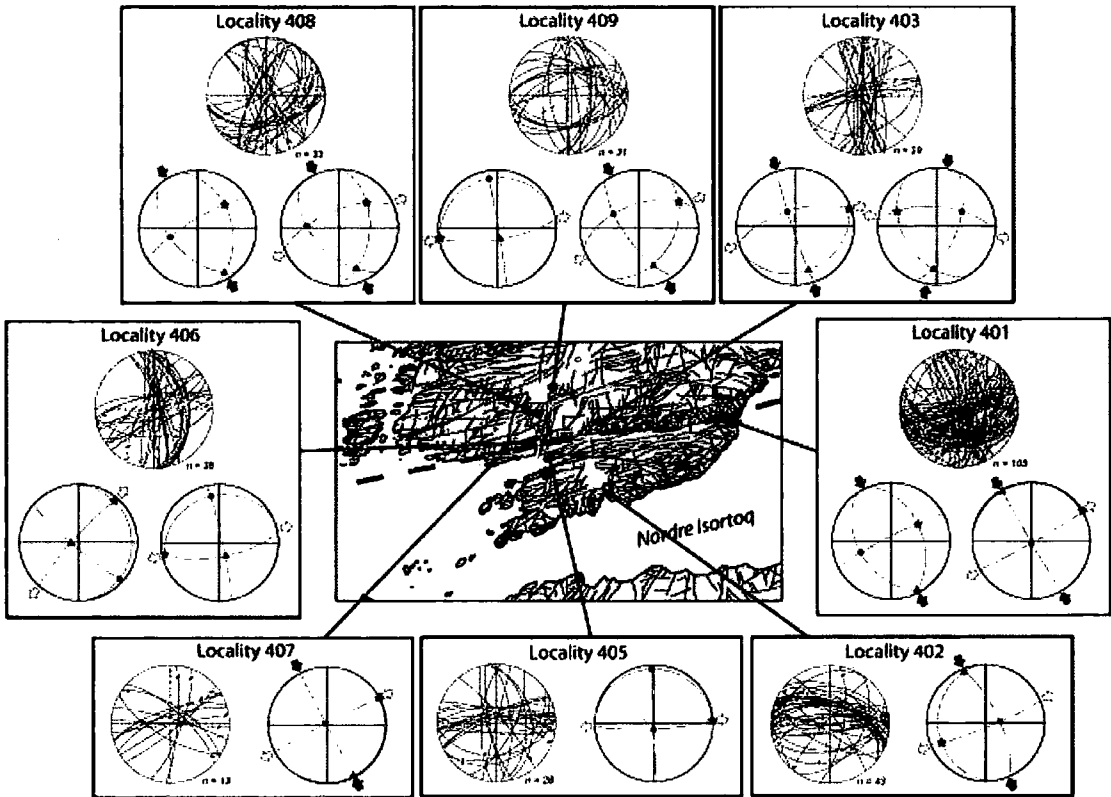
**Figure 5.8.**

(a) Lower hemisphere equal area stereonet showing faults and associated slip striae for Reverse, Normal and strike-slip faults. Solid black circles = poles to fault planes, open circles = slip striae. (b) Stress tensors for each fault system, using inversion method of Michael (1984). All strike-slip faults have been inverted together as a single population. Triangle =  $\sigma_1$ ; circle =  $\sigma_2$ ; star =  $\sigma_3$ .



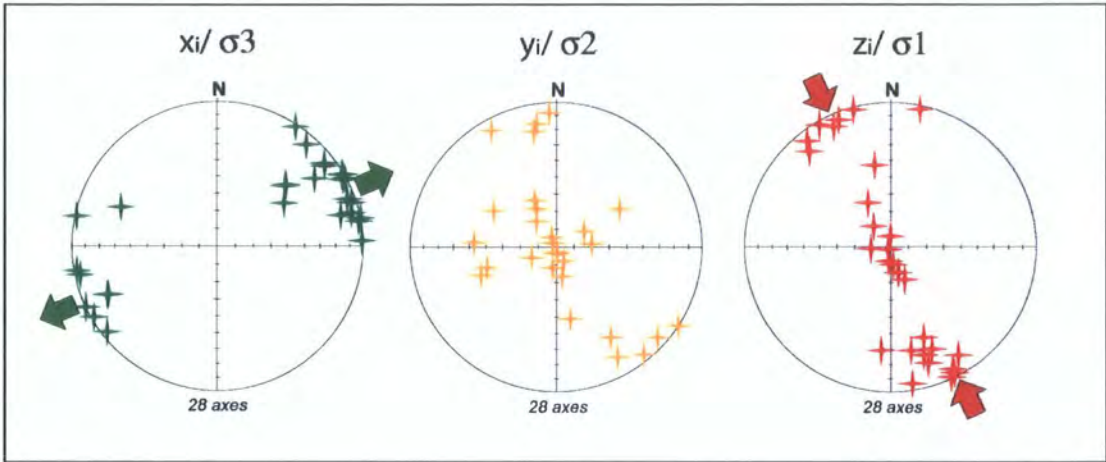
**Figure 5.9.**

Detailed lineament maps (derived from aerial photograph analysis) for areas 1-3 with superimposed stereonets showing fault geometries and apparent stress tensors at various localities. See *appendix 4* for further details about inversion applied at each locality. Triangle =  $\sigma_1$ ; circle =  $\sigma_2$ ; star =  $\sigma_3$ .



**Figure 5.10.**

Detailed lineament maps (derived from aerial photograph analysis) for area 4 with superimposed stereonets showing fault geometries and apparent stress tensors at various localities. See appendix 1 for further details about inversion applied at each locality. Triangle =  $\sigma_1$ ; circle =  $\sigma_2$ ; star =  $\sigma_3$ .



**Figure 5.11.**

Lower hemisphere stereonet solutions for palaeostress axes calculated from fault populations at each locality (see Figs. 5.10 and 5.11).

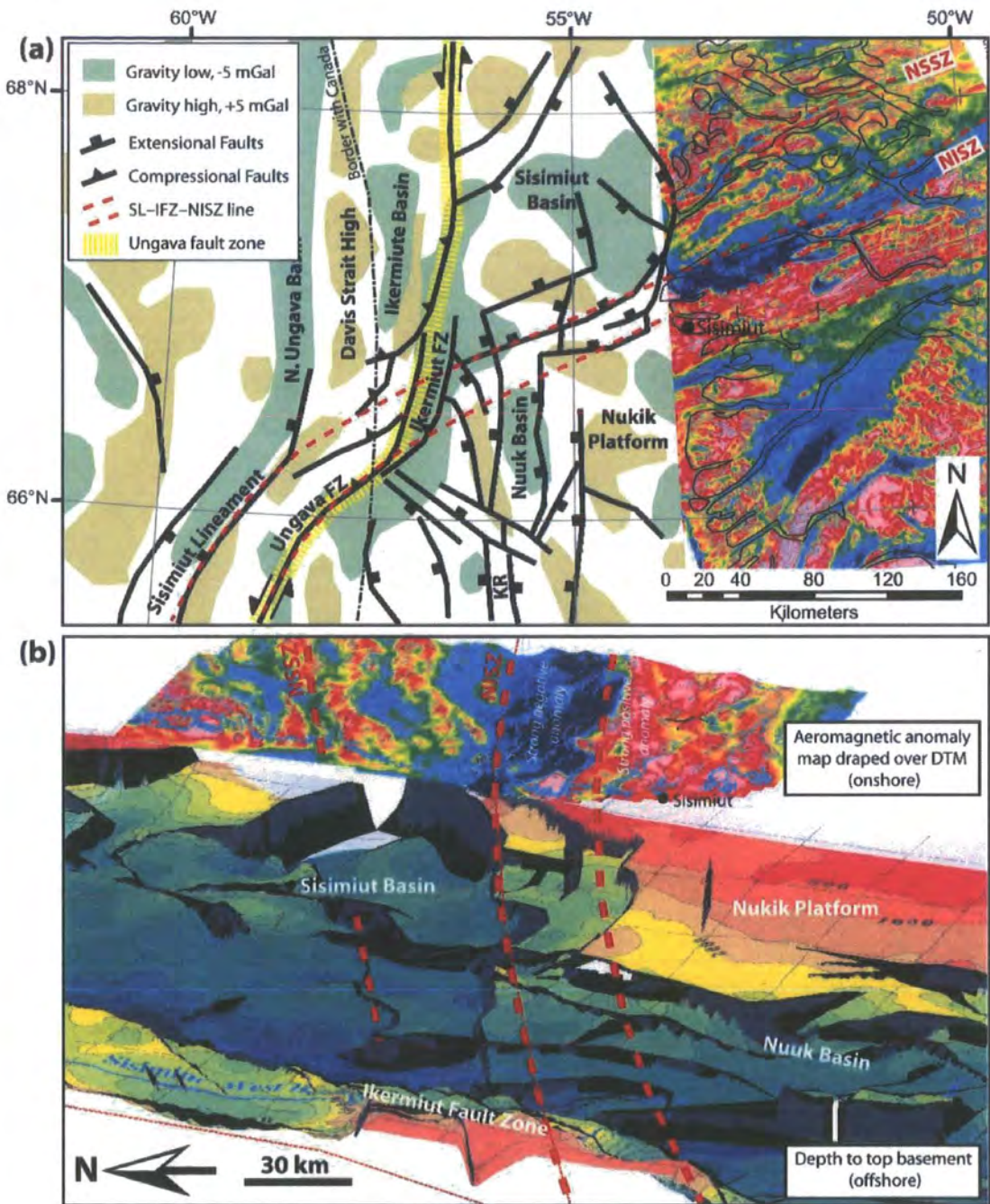


Figure 5.12. (caption overleaf)

**Figure 5.12.**

(a) Zoom in of Ikermiut Fault zone and south Sisimiut Basin highlighting apparent link between the Sisimiut lineament, Ikermiut FZ and Nordre Isortoq Shear Zone. Onshore basement trends outlined by aeromagnetic anomaly map (Rasmussen and van Gool, 2000; van Gool *et al.*, 2002), blue = negative anomalies, Red/ pink = positive anomalies. Offshore basin and basement structure represented by 100 km high-pass filtered Bouger gravity anomalies, structural highs outlined by +5mGal contour (brown), and sedimentary basins by -5mGal contour (green; contour data adapted from Planke *et al.*, 2004). Yellow dashed line marks trend of Ungava fault system. (b) 3D structural model in ArcScene (ArcGIS suite) showing correlation between onshore structures and those bordering the Sisimiut Basin.

**Figure 5.13. (overleaf)**

Summary diagram showing the relationship between the orientation of the Ungava fault zone, fault patterns (both onshore and offshore) in the Davis Strait, and regional stresses. (a) Phase 1 refers to the older N-S trending faults in the Davis Strait, while (b) phase 2 relates to younger strike-slip systems.  $\alpha$  and  $\beta_x$  angles are measured relative to the mean orientation of the Ungava fault zone (015°-195°). The regional extension vector (Reg V.) is inferred from fault trends in the Labrador Sea of similar age. Two sets of  $\alpha$  and  $\beta_x$  angles are given for phase 2 based on: a) manual calculations using equation, and b) assuming only simple shear. Compare  $\alpha$  and  $\beta_x$  angles to  $\sigma_3$  palaeostress axes calculated from field data (Figs. 5.10, 5.11 and 5.12). (c) Shows an  $\alpha$  vs.  $\beta_x$  plot corresponding to solution of equation 1 (from De Paola *et al.*, 2005). Highlighted in grey is the zone of wrench dominated transtension (WDTT; Tikoff and Teyssier, 1994; Teyssier and Tikoff, 1999; Dewey *et al.*, 2002; De Paola *et al.*, 2005b). An  $\alpha_{crit}$  (i.e.  $\alpha$  angle marking transition from WDTT to EDTT; McCoss, 1986) value of 30° is used as this is most representative of real rock values (De Paola *et al.*, 2005a) and in fitting with the results of analogue models (e.g. Withjack and Jamison, 1986). Points 1 & 2A correspond to  $\alpha$  and  $\beta_x$  angles calculated using *equation 1* for phases 1 & 2 respectively. Point 2b shows  $\alpha$  and  $\beta_x$  angles for phase two assuming only simple shear. (d) Schematic plot of  $\alpha$  vs. finite strain showing how a positive volume change (e.g. sea-floor spreading) can widen the zone of WDTT (after Teyssier and Tikoff, 1999). EDTT = extension dominated transtension; WDTT = wrench dominated transtension.

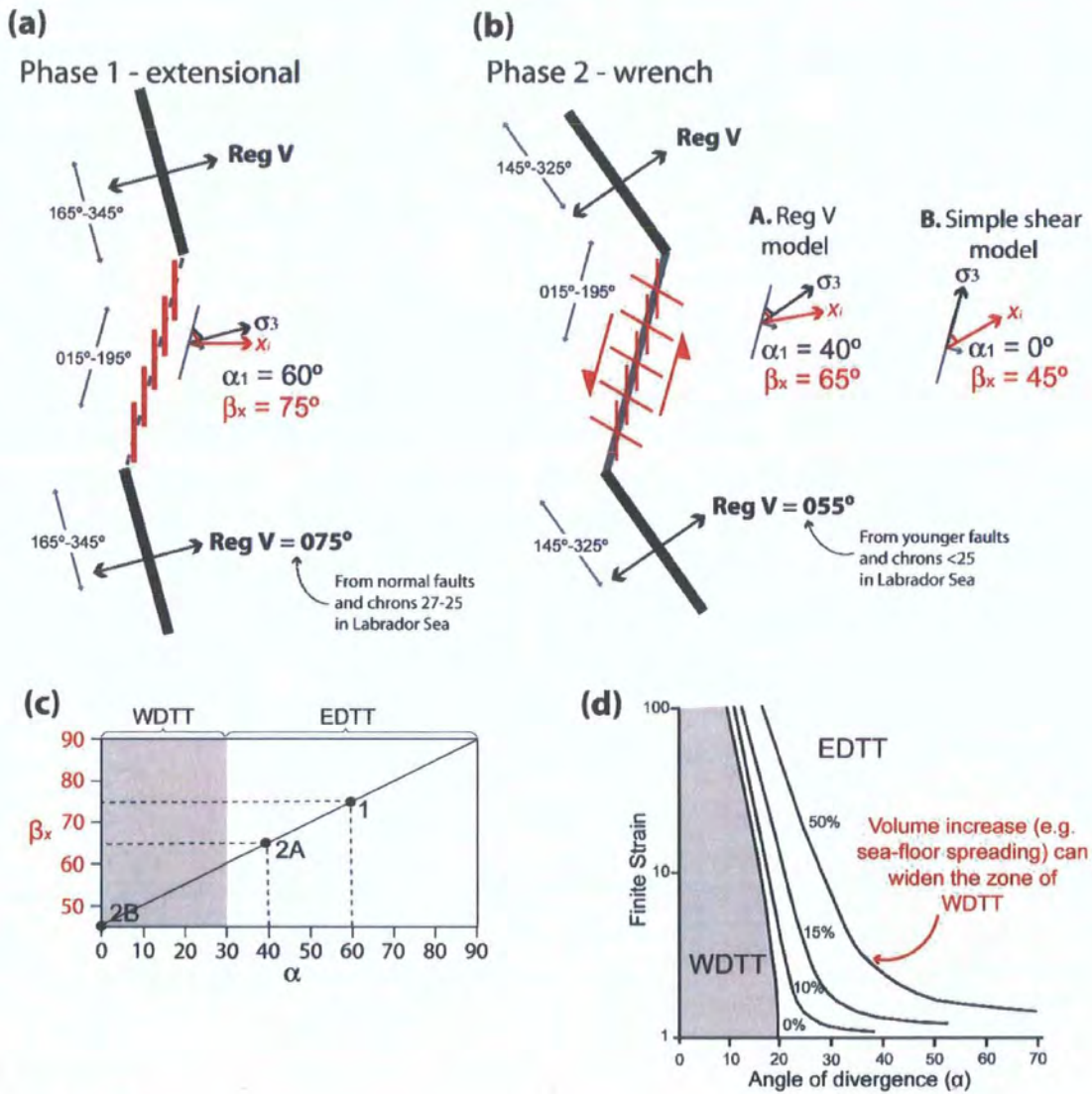
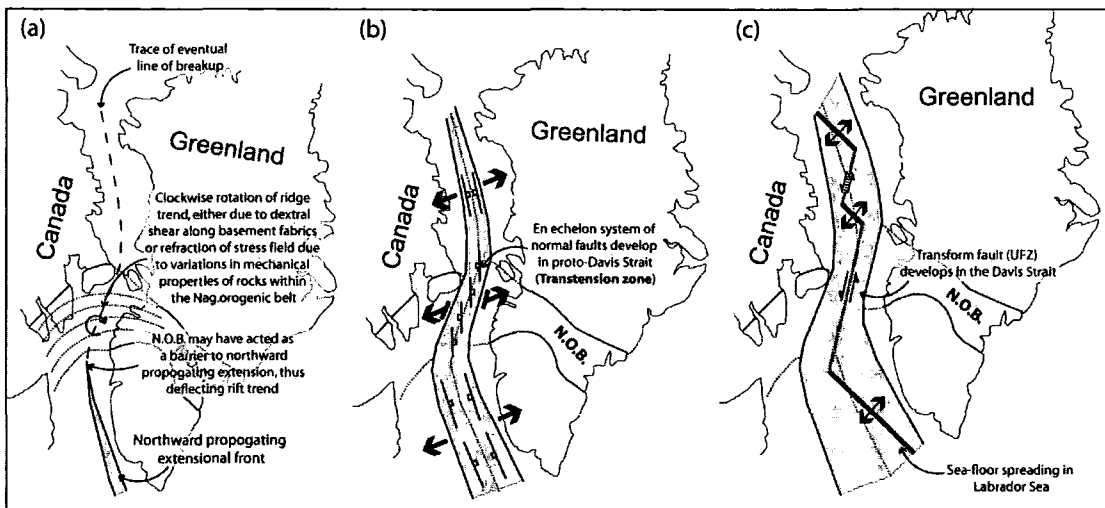


Figure 5.13.



**Figure 5.14.**

Cartoon summary of the opening of the Labrador Sea – Davis Strait – Baffin Bay seaway. (a) Northward propagating North Atlantic rift system deflected into NNE-SSW orientation in NOB due to: A. dextral shear and clockwise rotation as a result of obliquity between regional extension direction and basement structures; or B. refraction of fault orientation and stress field due to differences in mechanical properties of rocks within and rocks outside the Nagssugtoqidian orogenic belt (early – mid Cretaceous?). (b) ENE-WSW regional extension leads to a system of N-S trending en echelon extensional faults develop in transfer zone across proto-Davis Strait (late Cretaceous – Palaeocene extension). (c) Onset of sea-floor spreading in Labrador Sea and Baffin Bay, Transform fault develops in Davis Strait, deformation dominated by strike-slip structures (Eocene Transform system). NOB = Nagssugtoqidian Orogenic Belt.



## **6. Discussion, conclusions and the future of digital field mapping.**

### **6.1. Introduction**

The main aims of this research have been to investigate the role played by basement structures in the development of fault patterns on passive margins, with particular attention paid to zones of oblique divergence. To study structures in basement it is essential to analyse structures onshore because they cannot be easily distinguished and are usually inferred offshore. Thus, the second key component of this research was the development of onshore digital mapping techniques to create geospatially accurate onshore maps in a format that may be integrated with offshore data. This discussion is intended as a review of both these key themes.

First part of this chapter concentrates on the effects of pre-existing basement structures and oblique extension on passive margins. However, as the individual datasets have already been discussed in their corresponding chapters, this section is a more generic discussion of the controls on structural development, at both regional and outcrop scales, by pre-existing structures in basement and oblique extension. The findings of this study are then applied to passive margins more generally. This section also discusses the significance and validity of kinematic/ palaeostress analysis techniques applied in this study.

The latter part of this chapter is a review of the digital mapping techniques developed and applied in this study; containing a discussion of the usability of digital mapping methods, and some of the problems encountered during the course of the research. The benefits (if any) these techniques have brought to this study are also assessed. This section includes a discussion of the potential improvements that could be made to these methods, and the overall future of digital mapping as a field based technique.

## 6.2. Basement influence in extensional settings

### 6.2.1. Reactivation of pre-existing fabrics

#### 6.2.1.1. Pervasive and discrete structures

Pre-existing heterogeneities in the continental lithosphere are thought to influence markedly its response to subsequent deformation (Butler et al., 1997; Holdsworth et al., 2001b). Natural pre-existing basement fabrics fall into two main classes: pervasive and discrete (Peacock and Sanderson, 1992; Morley, 1999, 2004). Pervasive fabrics are present throughout a large volume of rock and impose strength anisotropy. Common examples of pervasive fabrics comprise metamorphic rock fabrics such as slaty cleavage, schistosity and foliation. Discrete fabrics are isolated planes or zones (e.g. fault planes or shear zones) which mark a contrast in strength or material behaviour with the surrounding rock volume.

Rocks that display pervasive fabrics do not usually display isotropic rock strength (Morley, 1999). Donath (1961) showed that fracture dip and orientation were strongly linked to cleavage orientation, however it was also noted that although the strike of fractures followed that of pre-existing structures, the dip of fractures did not. Furthermore, Youash (1969) demonstrate that the tensile strength of rocks loaded at 0-60° to pre-existing discontinuities is only ~25-75% that of samples loaded at 90°. As this study has concentrated on basement rocks, pervasive fabrics are common in all three case studies. For example on the Scottish North Coast (*Chapter 2*) reactivation of a steep basement fabrics created fault bound half-grabens, such as Kirtomy Bay.

Discrete planes or zones of weakness exert a local influence on fault patterns. Unlike pervasive fabrics which generally influence the majority of faults, discrete structures tend to produce trends that are atypical of the area. As discussed in chapter 1, during the early stages of deformation there are competing factors between the creation of new structures and the reactivation of pre-existing structures.

Reactivation of discrete structures is well documented (e.g. Grønlie and Roberts, 1989; Imber et al., 1997; Rogers et al., 1989; Holdsworth et al., 2001b), and a number of examples can be seen in each of the case studies presented here. For example, in North Lofoten (*Chapter 4*) pre-existing joint sets appear to be reactivated by later fault

movements. While the reactivation of discrete shear zones is also apparent in West Greenland (Chapter 5).

As well as being zones of active displacement, pre-existing discontinuities (both pervasive and discrete) can act to inhibit fracture propagation. If the frictional shear strength of the discontinuity is sufficiently low relative to the tensile strength of the surrounding material, or the strength contrast between two adjacent units, fracture trends may be diffracted, reoriented or terminated (Teufel and Clark, 1984; Peacock and Sanderson, 1992). Blanton (1982) showed that at low angles (30-60°) between the discontinuity and the trend of the propagating fracture, the fracture is likely to turn into the discontinuity, while at high angles the fracture is more likely to propagate across them. Good examples of this may be seen both in the North coast of Scotland (i.e. change in trend from NNE-SSW offshore faults to basement parallel, N-S, onshore) and on the Norwegian margin (i.e. change in trend of the Lofoten Ridge). Significant variations in strength anisotropy appears to have acted as a significant influence on the development of the Ungava fault zone, in the Davis Strait (West Greenland), where the anisotropic nature of the Nagssugtoqidian Orogenic belt appears to have diffracted the propagating rift trend, though not into an orientation parallel to basement fabrics.

#### 6.2.1.2. *Basement reactivation vs. basement influence*

In *Chapter 1* the concepts of basement reactivation and basement influence were introduced. The key difference between the two concepts is that the former is concerned with '*the accommodation of geologically separable displacement events along pre-existing structures*' (Holdsworth et al. 1997), while the latter relates to a much broader range of structures that differ from simple Andersonian, plane strain due to the effect of pre-existing basement structures and their relationship with regional stresses. Basement-influence may affect the location, trend, geometry, length, or deformation style.

Pervasive fabrics seem more likely to be associated with basement-influence tectonics, while discrete fabrics and zones of weakness are more susceptible to direct reactivation. This observation may be highlighted best by the West Greenland case study (*Chapter 5*) which shows at the plate margin scale that pervasive basement fabrics of the

Nagssugtoqidian Orogenic belt have diffracted the trend of the propagating rift into an orientation non-ideal to regional stresses. This may be attributed to the contrast in strength anisotropy of the rocks inside and outside of the orogenic belt. Within the orogenic belt a series of discrete vertical shear zones are apparent (e.g. the Nordre Strømfjord and Nordre Isortoq shear zones), these shear zones mark areas of localised basement reactivation, however the pervasive fabrics of most of the orogenic belt do not favour reactivation and are cut by faults at high angles to the fabric.

Another example of pervasive fabrics influencing fault patterns, but not direct reactivation is the observation that many faults may trend parallel to the basement fabrics, however the dip of these structures is somewhat different, e.g. late brittle faults trending parallel to, but cutting at high angles, the Caledonian fabrics of Northern Scotland (*Chapter 3*; Holdsworth, 1989; Roberts and Holdsworth, 1999).

### **6.2.2. *Orthogonal vs. oblique extension***

Where extension is orthogonal to rift trend, fault patterns are relatively simply, conforming to Andersonian, plane strain fault models (Anderson, 1951). In oblique extension, the trend of the deformation zone/ rift is oblique to the regional extension direction. In such settings both extension perpendicular and shear parallel to the rift contribute to deformation. The acute angle,  $\alpha$ , between the rift trend and the displacement is inversely related to the degree of obliquity, thus highly oblique rifts have low values of  $\alpha$  (Fig. 6.1; Withjack and Jamison, 1986). Deformations associated with obliquely divergent displacements are geometrically and kinematically controlled by the angle  $\alpha$  between the direction of divergence and the boundary faults orientation. This inevitably leads to a 3-D strain field and consequently, to complex and polymodal fault patterns, which may significantly deviate from the relatively simple Andersonian fault patterns developed under plane strain conditions.

Zones of oblique extension occur because fabrics within the crust are sufficiently weak in oblique directions to favour failure in a non-ideal orientation. Oblique faults can exhibit predominantly dip-slip or strike-slip motion depending upon the relative magnitude of the intermediate stress to the principal stresses (Bott, 1959) and the angle

of oblique extension. The reactivation of major pre-existing structures, which often lie at an oblique angle to regional displacements, often leads to strain partitioning of the bulk strain and development of kinematically and spatially distinct, contemporaneous structural domains (Dewey, 2002; Oldow, 2003; De Paola et al., 2005b). Larger displacements and thinner cover sequences are also thought to favour strain partitioning over distributed deformation (Schlische et al., 2002).

Experimental models (e.g. Withjack and Jamison, 1986; Tron and Brun, 1992; Clifton et al., 2000) provide some good examples of the differences between orthogonal and oblique extensional fault systems, how they evolve, and also highlight the fact that high angles of extension ( $\alpha < 30^\circ$ ) are required before deformation becomes wrench dominated (Fig. 6.1). Regional fault patterns along the Lofoten Ridge (*Chapter 4*) appear to closely fit these models. However, these models do not represent all styles of oblique extension nor the potential interaction and influence of pre-existing structures in the crust (Morley, 1999). This is because pre-existing fabrics imposed on the deforming material are not penetrative, but applied at the base of the model, consequently they reflect 2-D fabric, rather than 3-D fabrics seen in nature (however, this may be more indicative of basement vs. cover relationships).

Extensional fault systems commonly localise along pre-existing structures (weaknesses) oriented obliquely to regional extension directions. The analogue models shown in Figure 6.1 do not exhibit significant reactivation of the deformation boundary/velocity discontinuity representing the pre-existing structure, therefore are not representative of basement reactivation. For example, at Kirtomy Bay, on the Scottish north coast (*Chapter 3*), direct dextral oblique-/ strike-slip reactivation of pre-existing structures is apparent in an overall extensional basin, and the orientation of faults in the hanging wall do not match those predicted by these analogue models.

### **6.3. Determining stress and strain from fault slip analysis in complex fault zones**

#### **6.3.1. Kinematic vs. Dynamic analysis**

Marrett and Peacock (1999) describe two main forms of structural analysis: kinematic analysis and dynamic analysis. Kinematic analysis addresses the pattern of motion

and/or displacement within a material (e.g. translation, rotation, strain) that produces structures, without regard to associated stresses. Dynamic analysis concerns the pattern of forces within material (e.g. stress) and the relationship between strain and stress during the development of structures. Marrett and Peacock (1999) compared these analyses methods and concluded that kinematic analysis required fewer and more testable assumptions. A key question of course is ‘can you deduce dynamic information (stress) from kinematic data (strain)?’ Palaeostress inversion methods (e.g. Angelier, 1982, 1984; Michael, 1984; Reches, 1987) fall into the field of ‘dynamic analysis’ (Marrett and Allmendinger (1990), however, the field data used is kinematic (i.e. fault geometry and fault-slip).

Marrett and Allmendinger (1990), proposed a method of kinematic analysis of fault slip data, considering strain instead of stress. They argue that dynamic (stress) and kinematic (strain) analysis should be combined in the analysis of fault slip data. The uncertainty concerning the applicability of the basic assumptions of dynamic analysis on specific field data is thought to be reduced by their kinematic analysis, where the consistency of the assumptions can be tested in the field (Marrett and Allmendinger, 1990). Indeed, graphical determination of the kinematic axes of shortening and extension are basically an alternative representation of the field observation data, equivalent to fault plane solutions P and T axes. This would imply that kinematic analysis of fault slip data yield kinematic (strain) principal axes, in stead of stress axes.

### ***6.3.2. Can palaeostress inversion give reasonable results in complex fault zones?***

#### ***6.3.2.1. Problems and limitations of palaeostress analysis***

Some authors have questioned the validity of palaeostress inversion through the analysis of brittle micro-structures (faults and fault-striae) as they argue that kinematic indicators are strain markers and thus do not relate to stress (e.g. Twiss and Unruh, 1998; Tikoff and Wojtal, 1999). This is not a problem in areas of simple coaxial deformation; however this argument becomes valid for non-coaxial deformation. Tikoff and Wjordan (1999) question the practice of deducing information about stresses from deformed rocks. They argue that for non-coaxial deformation, such as simple shear, the principal

movement directions are parallel neither to the infinitesimal nor the finite strain axes. This is due to the interaction between rock anisotropy and minor perturbations in the principal movement directions. The velocity boundary conditions control the deformation, whereas the stresses adopt orientations and magnitudes to conform to these conditions.

A prerequisite for the deduction of stresses from strains following the constitutive equations is the isotropy of the deformed material. In non-isotropic rocks, analysis becomes much more complicated. Non-coaxial deformation due to these anisotropies can lead to contradicting results in the interpretation of palaeostress deformations. Reactivation is commonly observed in basement rocks due to the presence of pre-existing planes of weakness such as faults, foliation, cleavage and lithological contacts. Sliding along faults weakened during the faulting process is much easier. A major weakened fault in an advanced stage of growth slides under many stress fields, including those unfavourably oriented. Careful analysis is needed when assessing the results of stress inversion on reactivated faults (Nieto-Saminiego, 1999).

If there is kinematic interaction between planes, the assumption of fault independence is not satisfied (Nieto-Saminiego and Alaniz-Alvarez, 1997). In zones of complex, closely spaced faults with multiple orientations, the likelihood of fault interaction is high. Nieto-Saminiego (1999) states that as fault block interaction may lead to localised variations in stress (i.e. due to movements on adjacent faults) and slickenlines non-parallel to regional/ far-field stresses, such zones are not suitable for palaeostress inversion. Interacting fault movements on pre-existing planes can also lead to multiple slickenline sets forming under a single regional stress field (e.g. Cashman and Ellis, 1994).

Palaeostress reconstructions applied in many studies also have a further shortcoming in that in order to collect enough fault and striae orientations it is often necessary to include data from several locations. As there may have been localised variations in stress orientation during deformation, induced by basement anisotropy or fault interaction (e.g. Pollard et al., 1993), this may lead to a statistical error in the results obtained which is difficult to estimate. Pollard et al. (1993) discuss how

interaction between pre-existing planes can lead to stress field perturbations of up to 40° in orientation when the density of fault planes is high.

It has also been argued that kinematics may be scale dependent as larger faults often have smaller splays and secondary faults of varying orientation and the stresses one infers from these secondary structures will differ from that of the primary fault (Tikoff and Wjordan, 1999). Furthermore, due to strain partitioning, we cannot always reliably assume that infinitesimal strain or stress axes resolved in one part of a study area are parallel to regional transport directions, unless their relationship to the deformation patterns in adjacent crustal domains is also considered (De Paola, 2005).

Figure 6.2 shows two models which highlight why it is essential to compare local palaeostress data to regional structures in order to determine the overall tectonic system. For transtensional faulting stress tensors may remain generally homogeneous in terms of  $\sigma_3$  orientation despite a variety of fault slip patterns. Figure 6.2a shows the results of stress inversion for normal dip-slip, normal-dextral oblique-slip and pure strike-slip faulting, for a transtensional fault zone, and all indicate a consistent E-W direction of extension, though  $\sigma_2$  and  $\sigma_1$  axis may switch. In contrast, palaeostress analyses of normal dip-slip faults within a dextral pull-apart basin of a similarly orientated fault system reveal a NW-SE direction of extension, parallel to the trend of the major strike-slip fault (Fig. 6.2b); however regional extension is still E-W.

Stress permutations are common at local and regional scales (Angelier, 1994; Oldow, 2003; De Paola et al., 2005b), particularly in zones of transtension and 3-D strain. Extensional fault systems may have permutations that result in perpendicular systems of conjugate normal faults ( $\sigma_2/\sigma_3$  permutation; Fig. 6.3a), or in mixed conjugate sets of strike-slip and normal faults ( $\sigma_1/\sigma_2$  permutation; Fig. 6.3b). These permutations may be due to the effects of pre-existing structures (e.g. localised shortening in the vicinity of basement shear zones within the overall strike-slip system of West Greenland), deformation partitioning (e.g. De Paola et al., 2005b), levels of finite strain (e.g. transition from wrench dominated to extension dominated transtension with increased finite strain, as seen in North Lofoten), and stress ratios ( $R$ ). For pure extensional systems  $R = 0.5$ , and thus are unlikely to show stress permutations, while



multidirectional extensional systems (e.g. 3-D strain) have low values of  $R$ , and are thus prone to  $\sigma_2/\sigma_3$  permutations (e.g. Fig. 6.3a). Homogeneous transtensional systems (e.g. Sanderson and Marchini, 1984) are likely to have high values of  $R$ , and are thus prone to  $\sigma_1/\sigma_2$  permutations (Fig. 6.3b).

#### 6.3.2.2. *Methods applied in this study*

Despite all this opposition against the use of ‘dynamic’ palaeostress inversion analysis, these methods have proven to be valid and powerful over the years (e.g. Angelier, 1982, 1985, 1995; Michael, 1984; Delvaux and Sperner, 2003; Yamanji, 2003; De Paola et al., 2005a, b). In this study a combination of both fault kinematics and deduced stress (dynamic) analysis is used in order to define both local and regional tectonic regimes affecting the study areas. Furthermore, the results of the stress inversions are *never* used in isolation, as they are always verified using deductions concerning strain that are based on structural observations made in the field.

Throughout these studies a variety of analysis techniques have been used in each study to test both the consistency and reliability of the results. Bulk analysis of entire datasets, analysis of individual fault systems, and outcrop by outcrop studies were all carried out. Furthermore, inversion procedures of Angelier (1984), Michael (1984), Reches (1987) were all tested.

As all the data collected in this study are geospatially located and stored in an ArcGIS database, the data can be easily sorted both spatially and/ or by common attributes prior to analysis. This ability to sort the data in this way should help to overcome some of the issues outlined above. As discussed in sorting of the Lofoten dataset faults that clearly show violations of the assumptions of inversion analysis (e.g. fault interaction) may be filtered out of the analysis; other attributes may also be used to sort the datasets (e.g. fault rock type, mineralization, etc.). By analysing the spatial variations in palaeostress, localised variations and permutations may be assessed, either by their location, or their association with other structures (e.g. pre-existing faults and shear zones or basement terranes). For example, in West Greenland we see that in the vicinity of major shear zones local stress variations are apparent, thus highlighting the

importance of collecting data from a variety of areas to gain a true understanding of the regional stresses.

#### **6.4. The effects of basement on the structure and geometry of passive margins**

Inherited weakness in the basement may be a fundamental control on continental margin development (Dunbare and Sawyer, 1989; Stoker et al., 1993; Davison, 1997; Doré et al., 1997). Pre-existing structures may influence the structure of continental margins in a number of ways, these include: margin segmentation, orientation, geometry and structural style. In the following sections these effects are discussed further, using both examples from this study and other passive margins worldwide (e.g. Brazilian Margin).

##### **6.4.1. Margin segmentation**

Lateral segmentation is a common feature of both passive margins (Francheteau and Le Pichon, 1972; Doré et al., 1997; Clemson et al., 1997; Song et al., 2001; Tsikalas et al., 2001) and continental rifts systems (Rosendahl, 1987; Morley et al., 1990). The development of rift segments is characterised by punctuated, discontinuous zones of extension (i.e. rift segments). These segments may vary according to their mean orientation, dominant fault geometry (i.e. strike and dip), or dominant fault type. Rift segment boundaries are termed transfer zones, and may be in the form of discrete linking faults, or complex fault zones (Morley et al., 1990; Corti, 2004).

The origins of this segmentation and segment boundary zones are often attributed to the influence of basement structure (e.g. Davison, 1997; Clemens et al., 1997). Transfer zones have been associated with the direct reactivation of major basement structures at depth (Strömberg, 1976; Mjelde et al., 2003). This appears to be the case for the largest transfer zones (e.g. Jan Mayen, Bivrost, Senja Fracture Zones of the Norwegian Margin), which have been termed first-order transfer zones. However, as discussed in *Chapter 4*, transfer zones may also develop due to variations in trend and structure along a margin, with the transfer zone forming as a zone of linkage and mechanical interaction between adjacent rift segments. These have been termed second-order transfer zones, or accommodation zones (Bosworth et al., 1986).

## 6.4.2. Orthogonal and oblique margins

### 6.4.2.1. Variations in structure and style

Deformations associated with obliquely divergent displacements are geometrically and kinematically controlled by the angle  $\alpha$  between the direction of divergence and the boundary fault orientation (Withjack and Jamison, 1986; Clifton et al., 2000). The relationship between fault patterns and obliquity is discussed in *section 6.2.2.* and summarised in Figure 6.1. Rift segments at high angles to regional displacement (i.e. extension closer to orthogonal) favour fewer faults with large fault throw (i.e. deformation more focused along major faults), and also the location of depocentres. Rift segments that lie at relatively low-angles to the regional displacement direction will display lower throw (i.e. less subsidence) and a larger component of strike-slip motion. Furthermore, basins that do form in the hanging wall of these faults are likely to be shallow, have an asymmetric geometry, and may also show evidence of shortening (e.g. transtensional folds sub-parallel to extension; Schreurs & Colletta, 1998).

The Lofoten ridge is a perfect example of a ridge showing a distinct change in structure and style due to zones of orthogonal and oblique extension. Other examples include the moderately oblique Campos-Santos portion of the Brazilian Margin which appears to trend parallel to a major vertical strike-slip shear zone (the Alem Paraibá SZ), and associated thrust faults, onshore (Davison, 1997; Meisling et al., 2001)

### 6.4.2.2. Wide and narrow margins

Davison (1997) discuss the possible link between the width of passive margin segments and the presence of pre-existing structures. It is suggested that in areas of strong basement weakness, narrow margins are more likely, as deformation is likely to be focused along discrete deformation zones. This appears to be true for some oblique margin segments, but not all. An example of an exception to this rule is the Campos-Santos segment, which is an oblique margin segment trending parallel to basement structures onshore, but is also relatively wide.

The Lofoten case study (*Chapter 4*) appears to suggest a similar model to that of the Campos-Santos margin, with orthogonal segments showing more focused

## *Chapter 6 – Discussion and conclusions*

deformation (consistent with narrow margins) and oblique segments showing diffuse faulting over a wider area. This is interpreted as a being a consequence of 2-D vs. 3-D strain; with zones of 2-D/ plane strain showing more focused deformation along ideally oriented faults, and zones of 3-D/ non-plane strain showing more distributed deformation, and multimodal fault patterns.

Analogue models of oblique extension generally suggest that rift zones are relatively wide in orthogonal and moderately oblique zones of extension, and it is only at high angles of obliquity (i.e.  $\alpha < 30^\circ$ ) that the deformation zone begins to narrow (Fig. 6.1 Tron and Brun, 1992; Clifton et al., 2000), which is coincident with the transition from extension dominated to wrench dominated faulting. Therefore it may be reasonable to suggest that zones of extension dominated transtension are likely to be wider than wrench dominated zones. The narrow oblique-margins described by Davison (1997) are generally highly oblique and dominated by strike slip movements, a prime example being the Barreirinhas-Ceara-Potiguar Basins (Fig. 6.4).

The structural configuration of the Davis Strait of West Greenland is a likely precursor to the narrow margin of the Barreirinhas-Ceara-Potiguar Basins (Fig. 6.4). As sea-floor spreading ceased in the Labrador Sea before the Greenland and North American plates fully separated, the width of the Davis Strait margin cannot be determined. However, as the major through going faults are strike-slip and the extent of rift related normal faults appear to be relatively narrow, it may be logical to assume that the resultant margin would also have been narrow.

Another similarity between these two margins is that a distinct change in rift/margin trend is coincident with the intersection of a zone of intense basement structure. In *Chapter 5* the influence of the Nagssugtoqidian Orogenic belt on the trend of the northward propagating Labrador Sea rift is discussed. On the Brazilian margin (and also the conjugate margin of West Africa) an intense shear zone belt termed the Equatorial Shear Corridor (Fig. 6.4; Davison, 1997) appears to have acted in a similar way. This Shear zone acted as a distinct barrier to rifts propagating from the south, as extension to the south and north of this zone are separated by some 40 Ma, and the trend of the rift/margin varies markedly. Furthermore, these margin trends are oblique to basement

structures, and thus it is “basement-influence” rather than basement reactivation that is the major control.

### **6.4.3. Oblique margins, transfer zones and transform faults – is there a link?**

Figure 6.4 shows a basic map of the Atlantic, outlining the trend of the mid-Atlantic ridge, and the major transform faults offsetting it. Also highlighted are the main margins that run oblique to the trend of the ridge spreading centres Atlantic. Wilson and Williams (1979) discuss the relationship between margin segments of various orientation, basin axes and the presence of transform faults in the Atlantic. A strong correlation between oblique margin segments and the presence of major transform faults is apparent (Fig. 6.4). These transform faults accommodate a simple shear component of extension, while the spreading centres accommodate the pure shear that makes up the overall oblique ridge/ margin trend.

In some cases, continental lineaments and transfer zones pass laterally into oceanic transform faults; although this is not always true (Lister *et al.*, 1986). On the Lofoten Margin ‘secondary’ transfer zones are not linked to mid-ocean ridge transform faults; however further north and south (i.e. Senja and Jan Mayen fracture zones respectively), primary transfer zones separating major margin segments may be linked. On the West Greenland margin we see an example of an extensional transfer zone that evolved into a transform fault with the onset of sea-floor spreading in the Labrador Sea. The main contrasts between those that develop into transform faults and those that do not, appear to be the scale of the structure and whether it is lithospheric or crustal in nature. As only a limited number of examples have been analysed in this study this correlation needs further research (e.g. Barreirinhas-Ceara-Potiguar Basins – Guinea Basin margins and the Equatorial shear belt; Fig. 6.4)

## **6.5. Digital mapping methods: a review**

### ***6.5.1. Have digital methods helped the project***

Many users of digital mapping methods have claimed that digital methods can improve the quality and efficiency of field data collection (Pundt & Brinkkötter-Runde 2000; Kramer, 2000; Brimhall and Vanegas, 2001; McCaffrey et al. 2003, 2005; Jones et al 2004) in a number of ways. These include: 1) accurate geospatial data, 2) streamline the workflow from data acquisition-to-final product, 3) good visualisation of data and models, 4) data stored in a well organised digital database, and 5) data integration. The findings of this study are in agreement with these statements; however, further comments are required in certain areas.

#### *6.5.1.1. Data acquisition time*

Although the overall workflow from data acquisition to production is streamlined as a consequence of digital mapping, it should be noted that time spent in the field collecting data may increase. As a field mapper is required to assess the accuracy of the GPS this can result in time being lost in terms of analysing geological structures. The speed of data recording may also be slightly slower as the touch-screen interface of a PDA requires more care to be taken than writing notes in a notebook. A solution to this latter problem is hands free data recording (e.g. voice recognition, automatic measuring devices, etc.).

#### *6.5.1.2. Data management and sorting*

In terms of this study, possibly the most significant benefit of digital mapping process has been the GIS data management. The ability to sort data in terms of both attributes and spatial distribution have helped overcome some of the apparent problems previously identified in palaeostress analyses (e.g. localised variations, fault interaction, etc.)

#### *6.5.1.3. Spatial analysis*

The ability to accurately analyse the spatial distribution of structures has also contributed to the findings of this study. The ability to overlay various data layers within

GIS has allowed fast and easy correlation of various data sets (e.g. basement terranes, fault patterns, locality data), thus enabling spatial correspondences to be identified. Furthermore, the ability to visualise structures in three-dimensions has enabled a fully 3-D comparison between pre-existing structures and later fault patterns.

### **6.5.2. Problems encountered during mapping and possible solutions**

Various problems were encountered during mapping, some of which are generic, and others due to specific mapping situations. These include:

- *Accuracy of GPS* decreases dramatically when close to vertical outcrops as view of sky (and thus satellites) is impaired – a laser rangefinder may be used to locate outcrop localities on cliff sections, though locations require post processing and attributes are not stored directly into GIS.
- *Slower speed of data capture compared to traditional mapping methods* (see sections 6.2.2.2. for possible solutions).
- *Battery life and lack of power supply in remote areas* (e.g. West Greenland) – solutions may be to carry a generator (very heavy), carry a number of spare batteries (heavy), or solar panels to charge batteries (unreliable, requires consistently good weather, etc.).
- *Hardware problems*, such as poor screen visibility on some PDAs (i.e. Jornada 540) in daylight, no communication between GPS and PDA (check cables, connections and software interface settings, i.e. baud rate, etc.).
- *Equipment failure* - In case of equipment failure, it is advisable to carry back-up systems, such as a pocket GPS, spare PDA, and of course in a worst case scenario pencils, paper and notebook!
- *Damage due to poor weather conditions* – one PDA device was damaged (water damage resulting in loss of touch-screen functionality); however, a ruggedised case would have prevented this.
- *Inconsistencies in spatial location of map data files*: often due to differing coordinate systems and map datum (also check GPS settings).

## **6.6. Future trends in digital field mapping**

Since the concept of digital geological field mapping was first discussed (i.e. Struik et al., 1991), significant advances in hardware and software systems that are available have been made. Most of these advances have come in the area of data acquisition (e.g. GPS accuracy, size and weight of equipment); however data analysis and visualisation are still considered post-fieldwork processes. A key benefit of digital mapping over traditional methods is that they allowing the field geologist to analyse and visualise the data recorded while still at the outcrop, therefore future development needs to improve this aspect of the mapping process.

### **6.6.1. Multi-user mapping and telecommunications**

The mapping carried out in this study was relatively simple to set up as only a single user mapping system was needed (Fig. 6.5a). However, one of the key advantages of digital methods is that data may be easily integrated from a number of users (Fig. 6.5b). This requires standardised procedures and database formats to be established (e.g. BGS Lexicon of Named rock units; Becken & Green; 2004). Two examples of multi-user mapping are shown in Figure 6.5b & c.

Figure 6.5b shows simple communications for multi-user field mapping. Field data may be uploaded and integrated on a PC, at the field base camp, at the end of each days mapping. Prior to the following days work the updated files are then reloaded on to the field mapping device thus ensuring all mappers have up-to-date data files.

Figure 6.5c shows multi-user mapping system via wireless communication, enabling real-time data capture and integration, thus keeping all users fully up-to-date with all data acquired by the team. This telecommunications for real-time update and analysis of data to support problem solving and decision making has been termed ‘telegeoprocessing’ (Xue et al., 2002). This system may provide mappers with the ability to run iterative processing and interpretation via continuous feedback with co-workers in the office. This system may also enable non-field geologists (i.e. office based researchers) to view field exposures in real time – i.e. fieldwork equivalent to web-/ teleconferencing. Satellite communications technology combined with GRID (e.g.



[www.earthsystemgrid.org/](http://www.earthsystemgrid.org/)) facilities will bring supercomputing power to field geologists. Satellite communications will also allow access to online data (e.g. base maps, photos, articles etc.) while in the field. Casademont et al. (2004) give a review of the current availability suitable equipment for wireless field-mapping systems and highlight that many of the main system requirements are already readily available (e.g. smartphones/ PDA-smatphones). They then apply these systems to develop services such as remote access to extensive map databases using Hyper Text Transfer Protocol (HTTP), and virtual ‘real-time’ post-processing of DGPS signals via SMS messaging.

### **6.6.2. *Future hardware and software tools***

#### **6.6.2.1. *All-in-one systems***

Three-in-one systems (i.e. GPS, handheld computer and GIS) are already on the market in the form of Trimble’s Geoexplorer series, which have been tested during the course of this research. There are a number of PDA’s on the market that combine a number of systems, including: PDA (+ digital camera, + GPS, or + mobile phone). The benefit of these systems is that they are more compact and remove the need for connecting cables. Furthermore, by having multi-function devices data recording and sorting should become more streamlined and enable more field functionality (e.g. digital camera linked to GPS allows images to be geospatially referenced in the field, rather than during post-processing as currently required). However, a drawback of these systems encountered in this research is that as the system is all-in-one, if something goes wrong it is more difficult to fix/ replace the problem unit.

Currently laser rangefinder data needs post-processing (using trigonometry and input of GPS data) to enable real-world coordinates, however, if a GPS unit was also added to the laser ranger unit (two-in-one) true coordinates may be recorded and input directly into the GIS project.

#### **6.6.2.2. *Voice recognition for hands free data collection***

Voice recognition is a concept many researchers are considering. This would provide hands free data recording at the outcrop, thus allowing measurements to be taken and

recorded more quickly. However, voice recognition would lose the benefits of using dropdown tables to record consistent data formats.

Another way to speed up the process of recording field data would be digital tools for recording measured data (i.e. digital compass-clinometers, digital tape measures) which record the data directly into the computer. Such tools are currently being developed at the Massachusetts Institute of Technology (MIT) and at by other research institutes.

#### *6.6.2.3. Real time data analysis and 3-D visualisation: Field-GSIS*

Most geologists are encouraged to interpret their observations in the field and attempt to build up a 3-D/ 4-D model in their minds eye. Therefore, for a fully field-based digital mapping process the mapper need to be able to carry out a component of data analysis and visualisation in the field (i.e. to test models and visualise the 3-D nature of an outcrop). Having this functionality in the field requires improvements to the functionality of field-based GIS (i.e. suitable for running on a PDA) so that they have more of the functions of a desktop GIS or GSIS. The visual capabilities of field-based software tools also needs to be improved. ArcPad extensions have been developed to aid data acquisition and analysis in the field using ArcPad Application Builder (e.g. Haugerud and Thoms, 2004); however, these are still relatively simple compared to desktop PC capabilities. An alternative, to making major changes to field-based software, the development of smaller, lightweight ruggedised tablet PC's and laptops, could also provide the functionality of desktop systems in the field. As the desktop software would be of more use to a wider range of users, this latter case is probably a more likely development route.

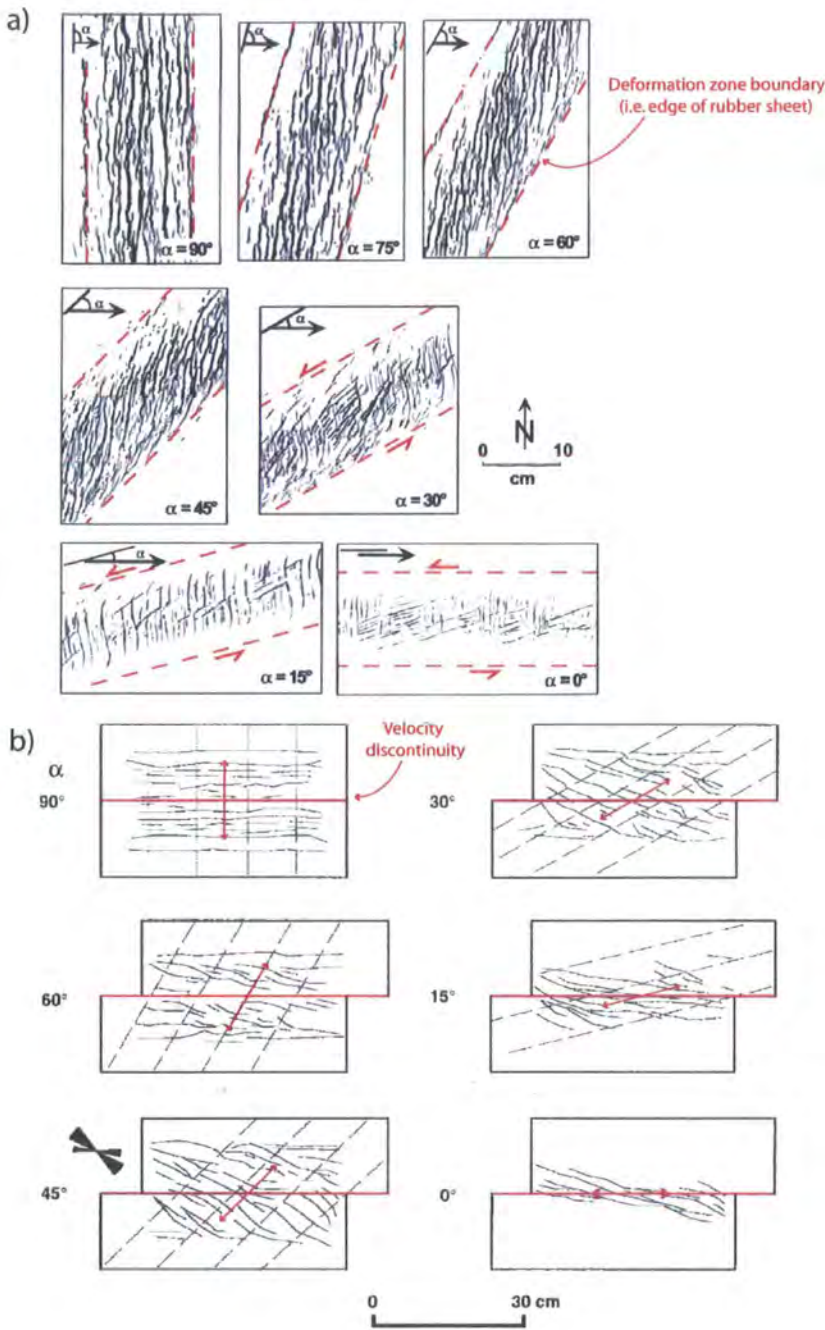
#### *6.6.2.4. Wearable computers and augmented reality.*

The possible application of wearable computers is discussed in Pundt and Brinkkötter-Runde (2000). Wearable computers offer many potential benefits (e.g. portability, hands-free use), however possible the most significant is in-the-field visualisation. Two types of display are potentially available for visualisation when using wearable

## *Chapter 6 – Discussion and conclusions*

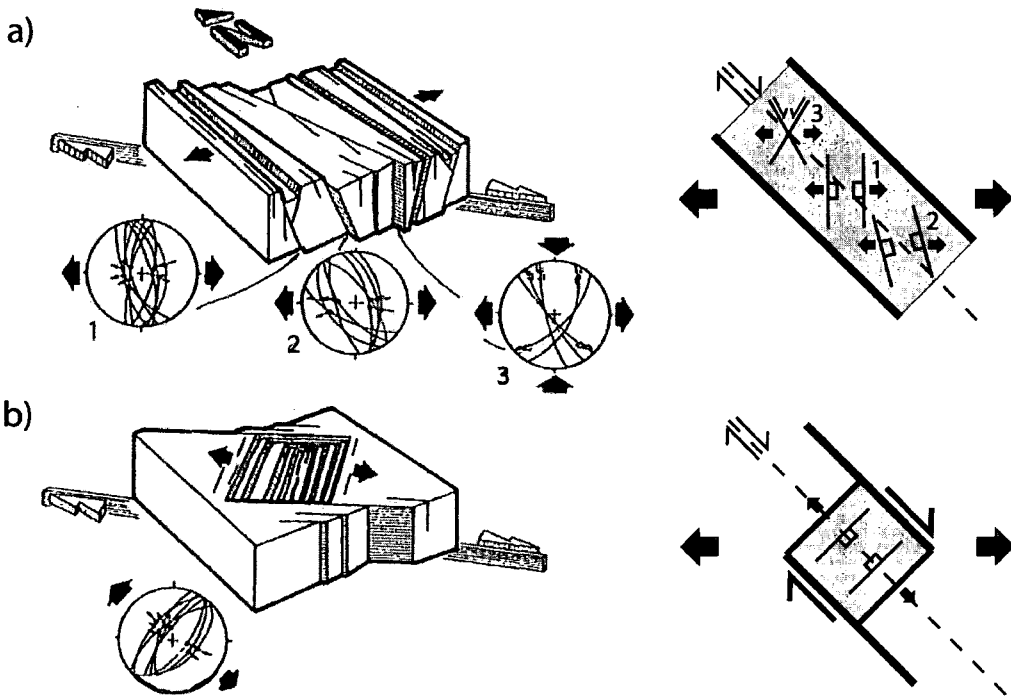
computers: 1) solid head-mounted display, without view of real world; and 2) augmented reality (i.e. the user sees a combination of real world view and a virtual computer generated scene; Fig.6.6). For fieldwork, the latter is the more suitable as it is essential to see the outcrop exposures while in the field, while the former may be more suitable for lab-based analyses.

Much technological research is currently being applied to developing robotic field equipment for Lunar and Martian research. An example of this is McGuire et al. (2005) and their work on the 'Cyborg Astrobiologist', a wearable computer and video camcorder system that is being used to test and train computer-vision systems to have some autonomous decision-making capabilities.



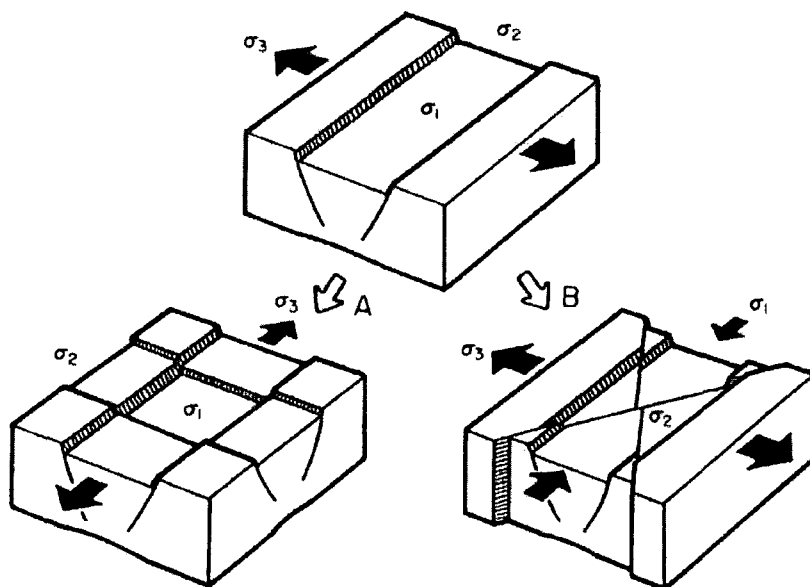
**Figure 6.1.**

Two examples of fault patterns developed during analogue modelling of oblique extension. a) Clifton et al. (2000) (after Withjack and Jamison, 1986). b) Tron and Brun (1991). Note, a) shows sinistral-oblique extension, while b) shows dextral-oblique extension.



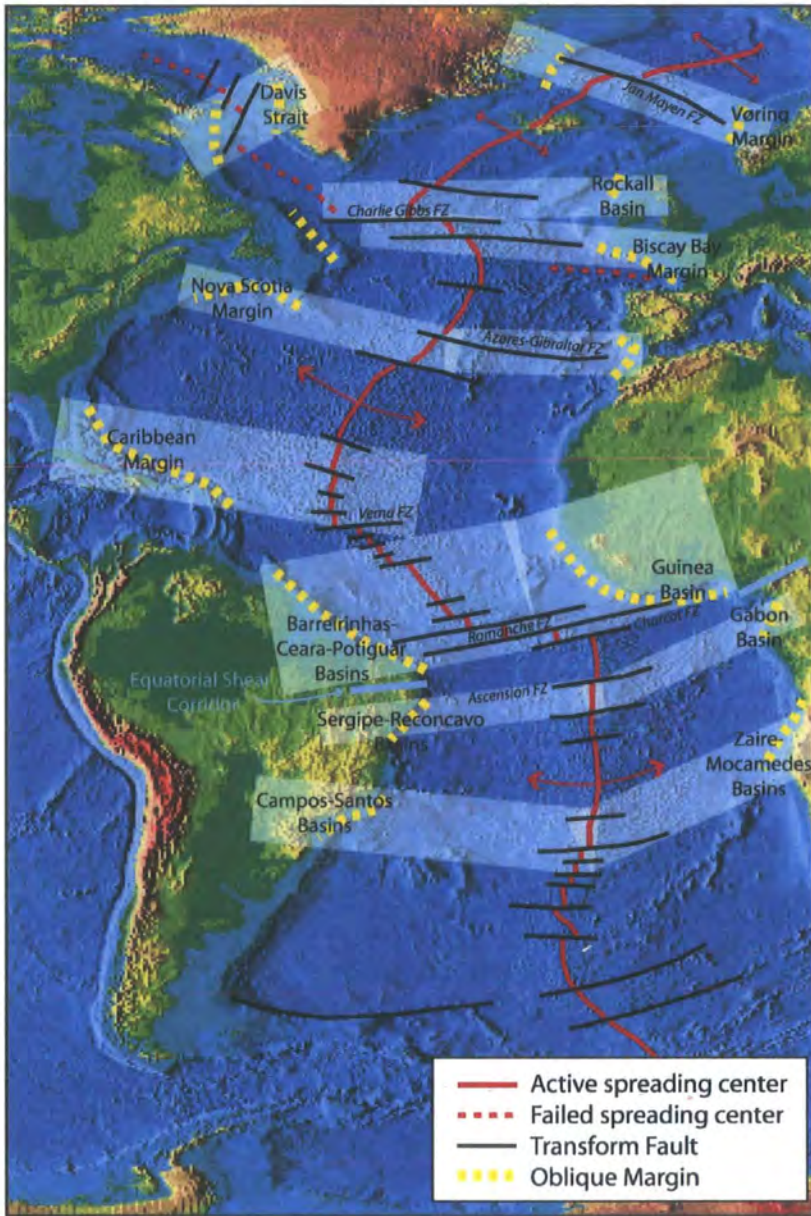
**Figure 6.2.**

Diagrammatic models of two distinctly different fault mechanisms induced by the same NW-SE dextral transcurrent fault. a) Transensional faulting. b) strike-slip pull apart. White arrows: strike-slip movement. Black arrows: localised extension. Red arrows: regional stresses (after Angelier, 1994).



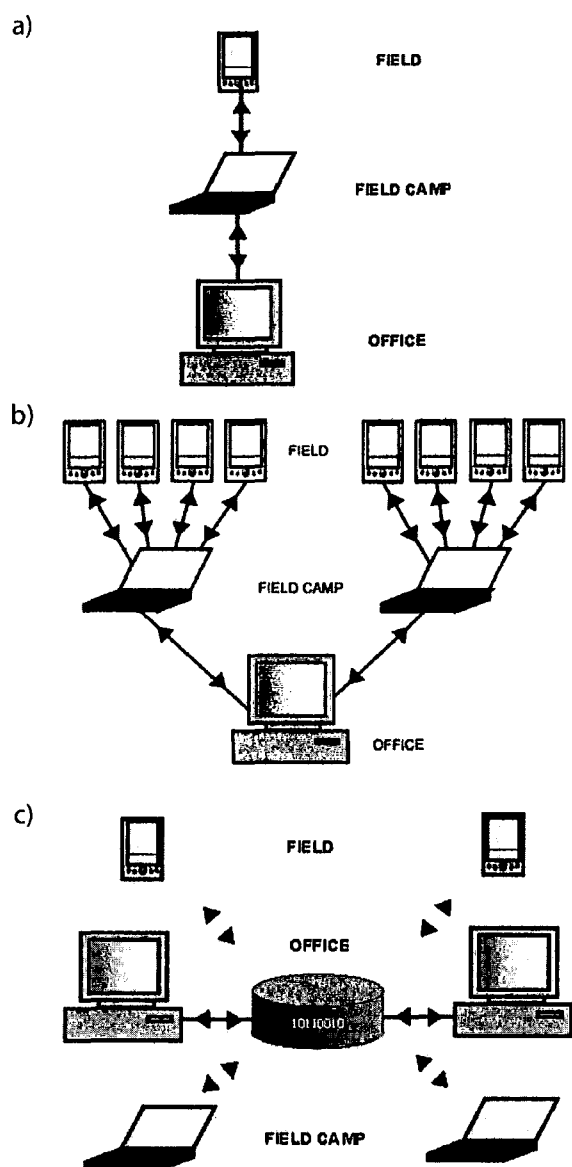
**Figure 6.3.**

Permutations between stress axes and rift opening. a)  $\sigma_2/\sigma_3$  permutation (perpendicular extension; b)  $\sigma_2/\sigma_3$  permutation (normal fault extension to strike-slip regime) (Angelier, 1994).



**Figure 6.4.**

A map of the Atlantic highlighting the trend of the mid-Atlantic ridge, and the major transform faults offsetting it. Also outlined are 6 major oblique margin segments, and apparent correlations between oblique margins, transform faults and major changes in ridge trend. This map is based on the map shown in Figure 6.1 of Wilson and Williams (1979).



**Figure 6.5.**

Digital field mapping PC configurations and data synchronisation. (a) single user (as applied in this study). (b) multi-user, allowing research teams to collect large datasets in a consistent format. (c) Multi-user via wireless communication, enabling continuous feedback and data updates while in the field. This latter example also enables field data to be processed (by supercomputers in office) and then viewed by mappers while still in the field. This system may also enable non-field geologists (i.e. office based researchers) to view field exposures in real time – i.e. fieldwork equivalent to web-/tele-conferencing!





**Figure 6.6.**

Future methods of field data capture. Wearable computers for synchronous outcrop and data visualisation (i.e. augmented reality).

**APPENDICES**

(ALSO REFER TO FILES IN ENCLOSED CD/DVD)

## APPENDIX 1 – DIGITAL MAPPING HARDWARE AND SOFTWARE.

### GPS receivers and spatial location devices used:

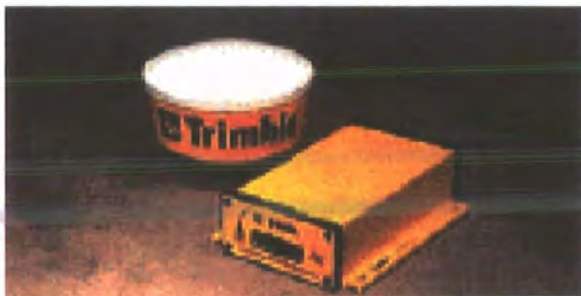
#### 1. *Ashtech Promark2 Survey and Navigational DGPS unit:*

- Dual mode: 'Survey' mode for mm precision, 'Navigational' mode for m precision real-time DGPS
- Accepts EGNOS/WAAS correction data in Nav. Mode
- Survey mode is slow (30 mins. per point) and requires post-processing
- Very light and portable
- Requires only AA batteries



#### 2. *Trimble AgGPS 122 back pack beacon DGPS*

- Combined 12 channel & beacon differential receiver
- Real-time corrections
- >0.5 m accuracy
- Heavier than *Ashtech Promark2* and requires 12 volt batteries



3. **Garmin Geko 201**

- Small pocket sized recreational GPS available
- Accepts WAAS correction data
- 12 channel receiver
- 5m accuracy
- Light weight and Waterproof
- Requires only AA batteries



4. **Laser Ace 300 laser rangefinder**

- Point and press data recording
- Digital compass
- PDA or data logger required to record data
- Data requires post processing and georeferencing
- Lightweight



**Data recording devices:**

1. **Jornada 548 PDA**

- 133 mhz 32-bit Hitachi processor, ,
- 64Mb RAM
- 12-bit colour LCD touch sensitive screen (poor for use outdoors!)



2. **Compaq iPAQ 3950 PDA**

- 400MHz Intel PXA250 processor
- 64Mb SDRAM
- 32Mb ROM
- 16bit touch sensitive transreflective screen (suitable for use in daylight)



**Other Hardware tools:**

1. **HP 912 digital camera**



- 2.24 megapixel,
- 3x optical plus 2x digital
- Pentax zoom lens with auto-focus

2. **Battery charger, solar panel, etc.**

3. **Memory Cards for data storage and back-up**

4. **Laptop computer**

**Software systems used:**

- **Ashtec Solutions** - GPS post processing and data creation software
- **ArcGIS 9.0** - Desktop GIS application
- **ArcPad 6** - FieldGIS suitable for PDAs running Windows CE
- **ArcPad Studio Application Builder 6** - Application builder for ArcPad
- **Erdas Imagine** - Image processing and interpretation software
- **GoCAD** - Reservoir modelling software
- **Geoframe** - Seismic interpretation and database creation
- **Traptester** - Fault analysis and fault seal analysis software

**APPENDIX 2 – GPS ACCURACY.**

**GPS horizontal accuracy.**

The first step in assessing the horizontal accuracy of the GPS results is to calculate the Root Mean Square (RMS) of the measured error for each point.

$$RMS\_Error = \sqrt{\frac{\sum_{i=1}^N Error_i^2}{N}}$$

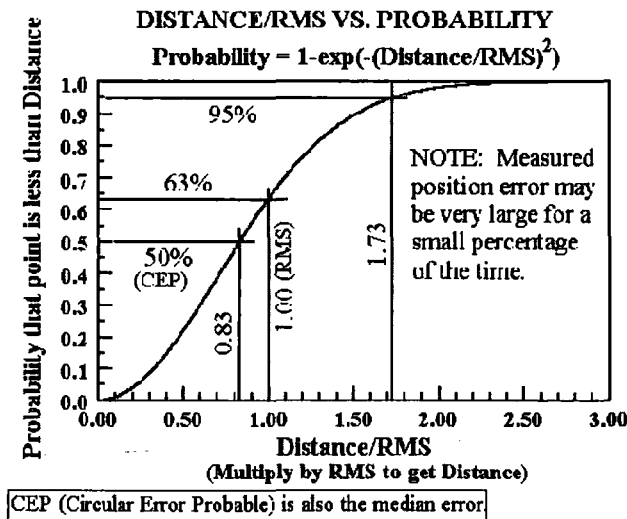
which may also be written as:

$$RMS\_Error = \sqrt{(Mean\_Error)^2 + (Standard\_Deviation\_of\_Error)^2}$$

The distribution of GPS fixes of a position may be approximated by a bivariate normal distribution with no correlation between the two variables. Sometimes this distribution has been inaccurately called "Gaussian"; but only a "slice" in any direction will indeed be a normal (Gaussian) distribution. For simplicity, one might assume the same variance in each direction (measurements show this is not quite actually true). With those approximating assumptions, the error distribution can be described by a very simple equation, which is known as a Weibull distribution with shape factor  $\beta = 2$  or Rayleigh distribution:

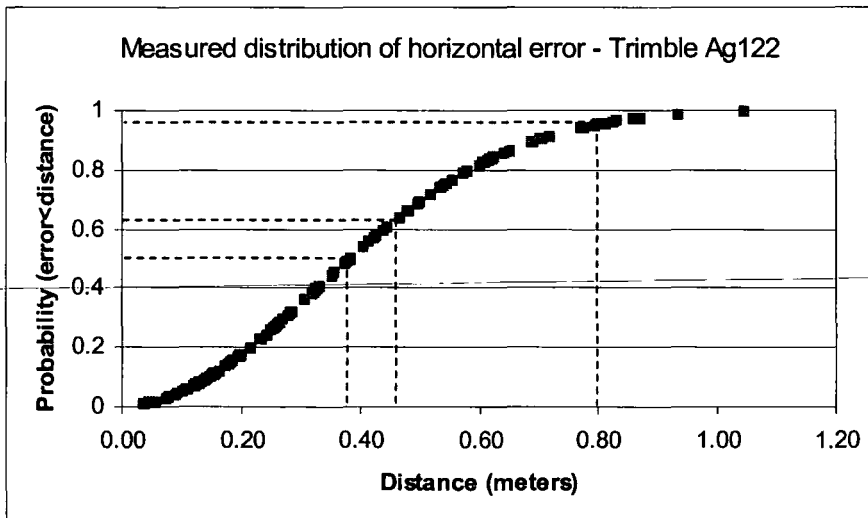
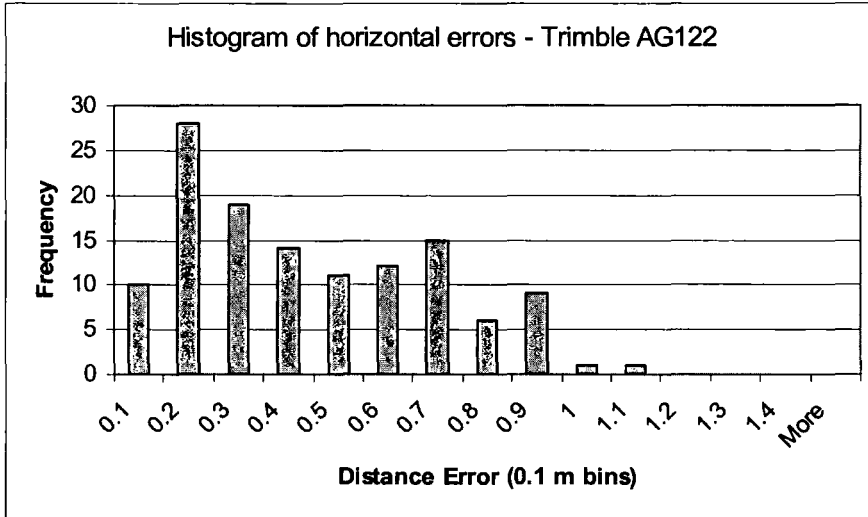
$$Probability(Error \leq Distance) = 1 - e^{- (Distance / RMS\_Error)^2}$$

The plot below is useful in relating the RMS error, the median (50% error bound or CEP error), and the 95% error bound ( $\Delta HPRE_{95}$ ) to the Rayleigh distribution used for modelling GPS error.



Appendix

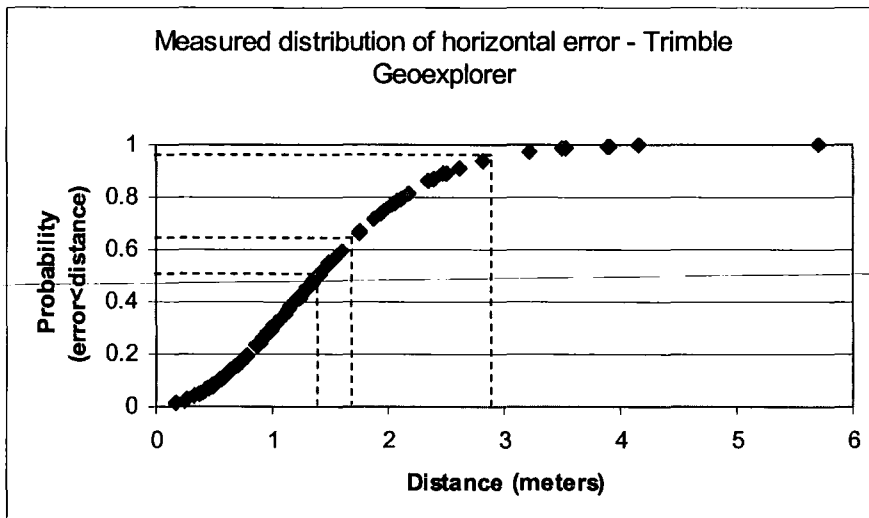
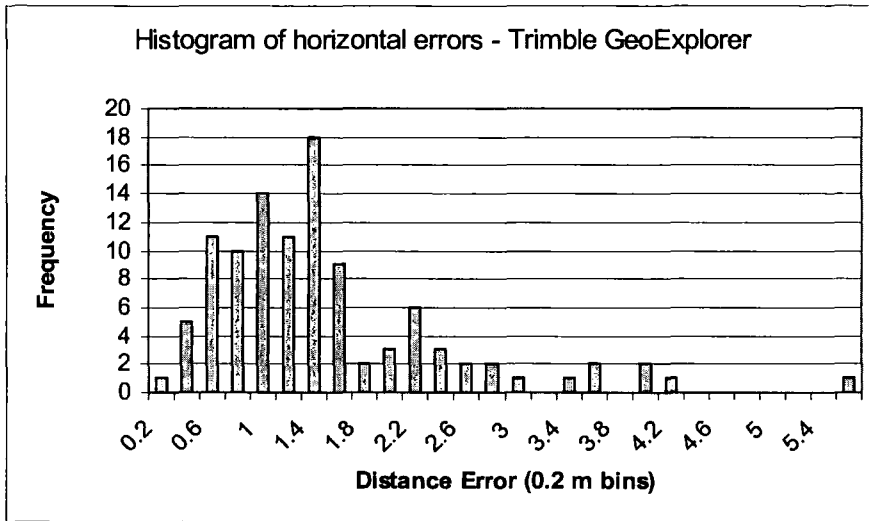
Trimble AG122



RMS = 0.464 m (63%)  
CEP/ Mean error = 0.393 m (50%)  
95% error = 0.8 m (95%)

Appendix

Trimble GeoExplorer XM

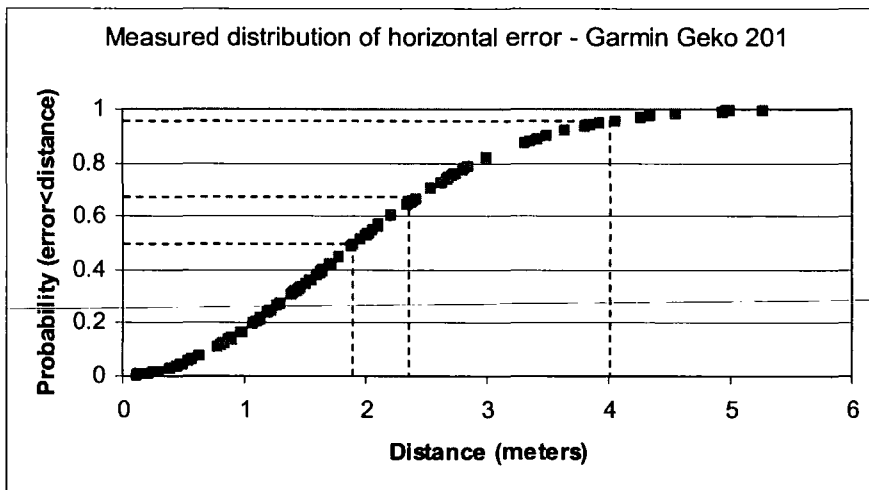
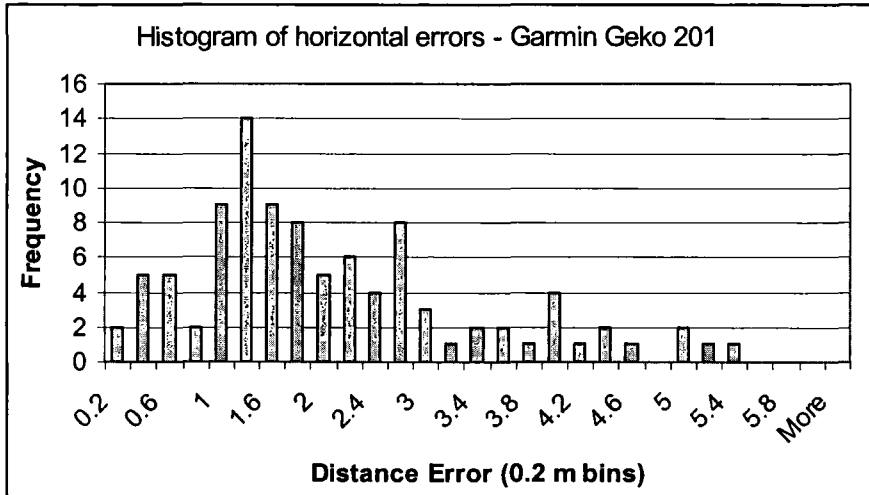


RMS = 1.672 m (63%)  
CEP/ Mean error = 1.388 m (50%)  
95% error = 2.9 m (95%)



Appendix

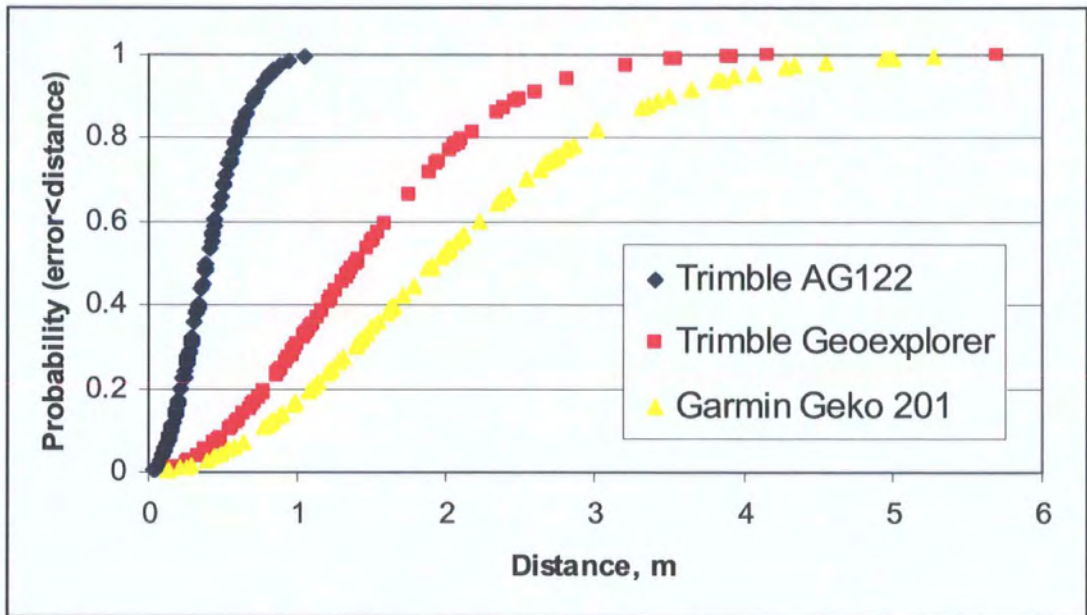
Garmin Geko 201



RMS = 2.31 m (63%)  
CEP/ Mean error = 1.948 m (50%)  
95% error = 4.05 m (95%)

Appendix

Comparison of each GPS:



### **APPENDIX 3 – PROJECT DATA FILES & METADATA.**

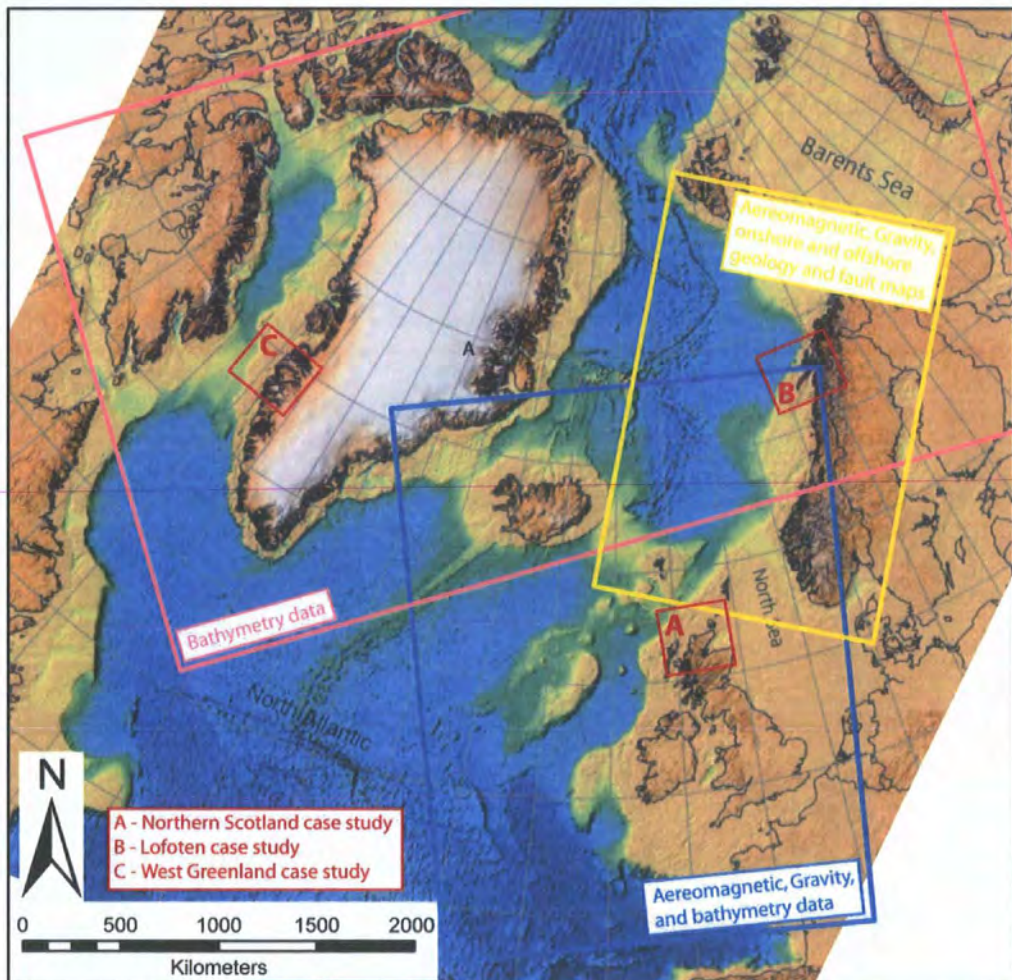
*Section 1 – Data coverage's for each project*

*Section 2 – List of digital data sources*

*Section 3 – Project metadata files (also see CD for full list of metadata files)*

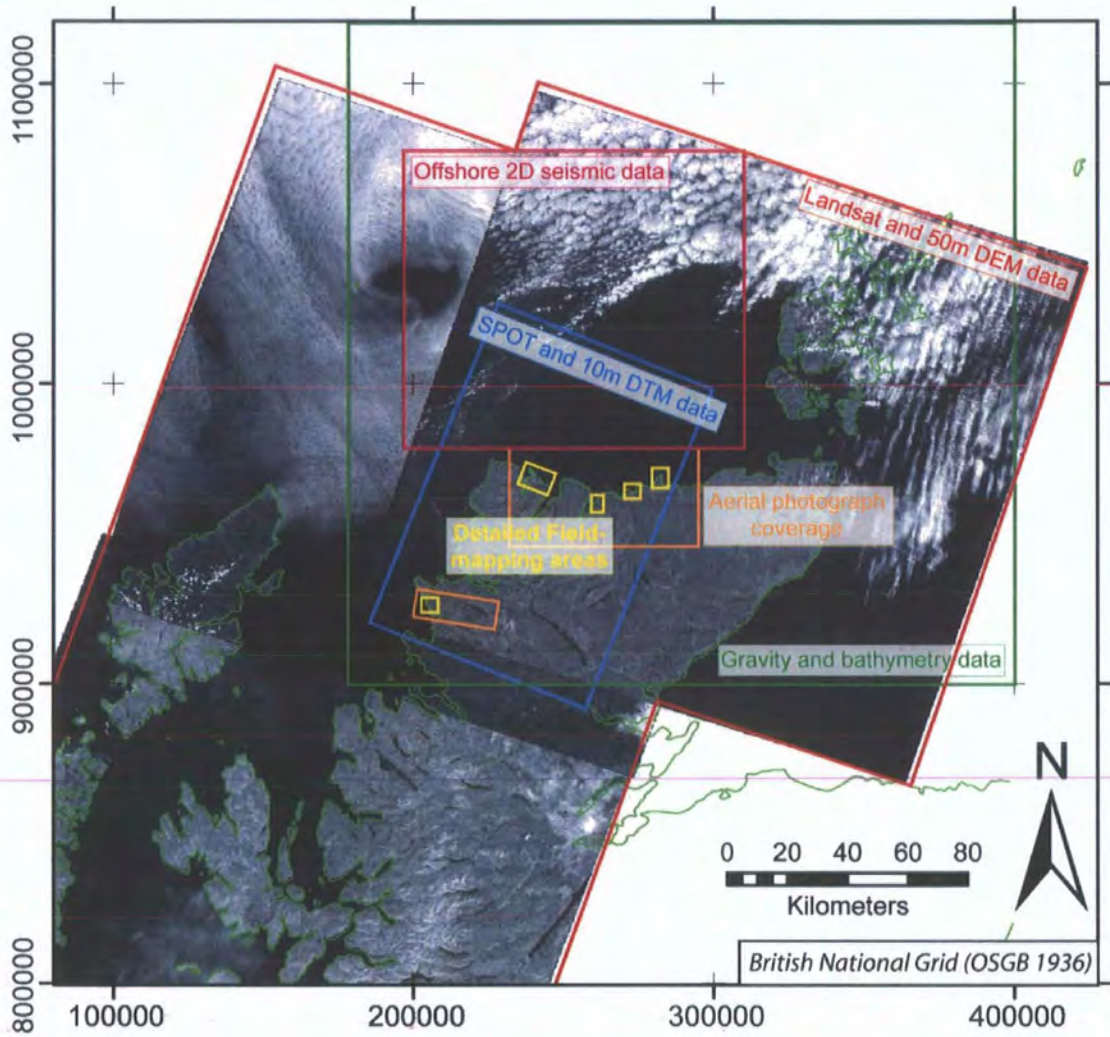
#### **Section 1**

##### **(a) North Atlantic data coverages**



Various regional datasets for the north Atlantic compiled from pre-existing datasets and public domain data.

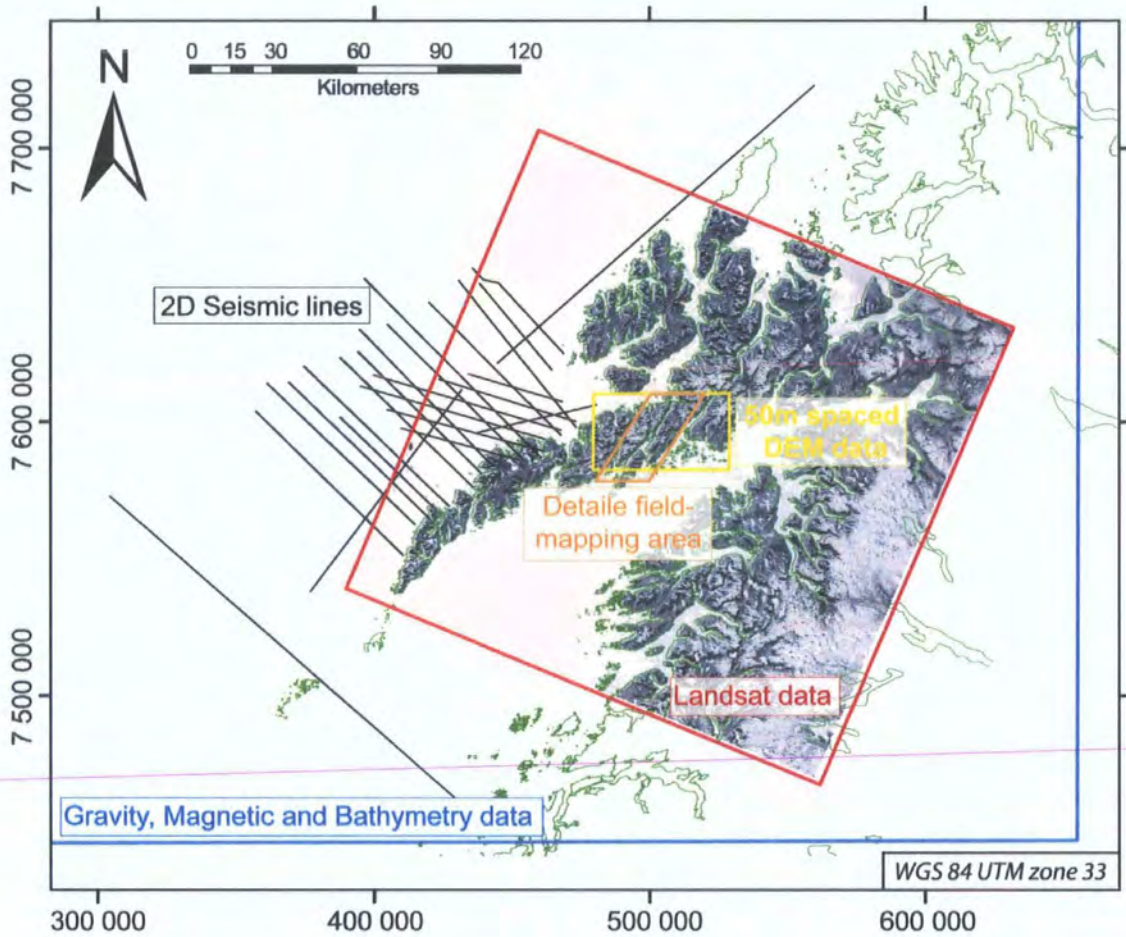
**(b) Scottish North Coast Project**



**Project database includes:**

- Landsat Images (image resolution 30 m)
- SPOT images (image resolution 10 m)
- DEM/DTM data at 50 m and 10 m resolution respectively
- Aerial Photographs of various areas (image resolution 1-2 m)
- Offshore -2D seismic data (BIRPS datasets)
- Digital field mapping at various localities

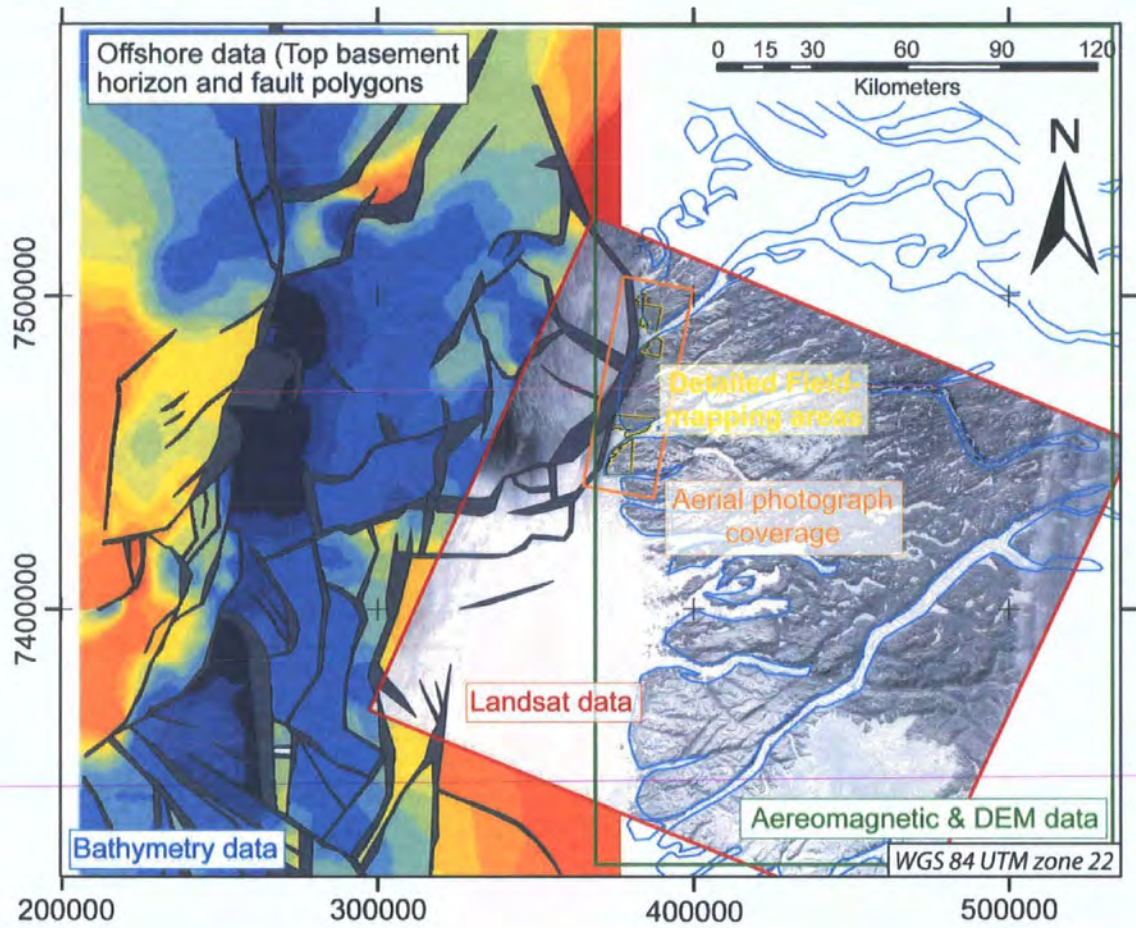
(c) Lofoten project dataset:



**Project database includes:**

- Regional Bathymetry data (1 km spacing)
- Gravity and aeromagnetic data
- Landsat Images (image resolution 30 m)
- DEM data (50 m resolution)
- Offshore -2D seismic data
- Digital field mapping at various localities

(d) West Greenland project dataset:



**Project database includes:**

- Regional Bathymetry data (1 km spacing)
- Aeromagnetic data
- Landsat Images (image resolution 30 m)
- DEM data (100 m resolution)
- Aerial Photographs of various areas (image resolution 1-2 m)
- Offshore data – horizon and fault polygon maps for top basement reflector
- Digital field mapping at various localities

## Appendix

### **Section 2 - Sources of digital data:**

#### ***Worldwide data:***

- *Landsat images – Global Land Cover Facility - Earth Science data interface, University of Maryland (<http://glcfapp.umiacs.umd.edu:8080/esdi/idex.jsp>) \**
- *Bathymetry – National Geophysical Data Center (NGDC) ([www.ngdc.noaa.gov/mgg/bathymetry/relief.html](http://www.ngdc.noaa.gov/mgg/bathymetry/relief.html)) \**

#### ***Scotland/ UK data:***

- *Digital base map and DEMs – EDINA Digimap (<http://edina.ac.uk/digimap/>) †*
- *Panchromatic Landsat and SPOT images – Landmap Project (Manchester University) ([www.landmap.ac.uk/](http://www.landmap.ac.uk/)) †*
- *Aerial photographs – RCAHMS ([www.rcahms.gov.uk/aerialphotography.html](http://www.rcahms.gov.uk/aerialphotography.html))*
- *Geological map data (non-digital) – BGS ([www.bgs.ac.uk](http://www.bgs.ac.uk))*

#### ***Norway data:***

- *Digital base maps and DEMs – Statens Kartverk ([www.statkart.no/](http://www.statkart.no/))*
- *Geological and geophysical maps – Geological Survey of Norway/ NGU ([www.ngu.no.](http://www.ngu.no.)) \**
- *Offshore seismic data – Statoil/ NPD*

#### ***Greenland data:***

- *Digital base maps and aerial photographs all supplied by GEUS ([www.GEUS.dk/geuspape-uk.htm](http://www.GEUS.dk/geuspape-uk.htm))*

*\* signifies free public domain data*

*† signifies free data through CHEST agreement (i.e. educational)*

**The following pages show example metadata files for datasets produced during this study, and stored in the Durham RRG – GAVA metadata database (copies shall also be stored in the National Geosciences Data Centre).**

Appendix

Durham RRG – GAVA metadata sheet

<i>Dataset Identifiers</i>		
<b>Dataset name</b>	Lofoten - Regional mapping study onshore	
<b>Geographic Region</b>	Lofoten Islands, NW Norway	
<b>Date established</b>	2003/06/01	
<b>Data collected by?</b>	Robert W. Wilson	
<i>Dataset Description</i>		
<b>Dataset type</b>	ArcGIS files: shapefiles (polylines); 1km and 30m DEM (GRID); Landsat TM images (tif). GoCAD files include: point (ps), line (pl), and surface (ts), raster (tif)	
<b>Derived from another dataset?</b>	Landsat images (also included in file)	
<b>Purpose of data collection</b>	PhD project	
<b>Equipment used</b>	ArcGIS and GoCAD <span style="float: right;">Completeness: 100%</span>	
<i>Geospatial</i>		
<b>Projection system</b>	WGS 1984 UTM zone 33N Ellipsoid (for projection): UTM Units x, y, z: meters	
<b>Scale or Spatial resolution</b>	1:100 000	
<b>Grid North or Magnetic North?</b>	Grid North	
<b>Positional Accuracy</b>	~30-50m (image/ DEM resolution)	
<b>Bounding coordinates of dataset</b>		
389085 West	North 7695615 South 7450800	East 649500
<i>IT summary for dataset</i>		
<b>Data format</b>	ArcGIS 3D-polyline shapefiles, raster images and TIN's; GoCad Project files	
<b>Where loaded?</b>	ISIS01/RRG/dgl3rww/Lofoten	
<b>Size (compressed/live)</b>	~1.75Gb	
<b>Initial Back-up information</b>	<b>Where?</b> RWW's personal Hard drive <b>When last back-up?</b> 01/08/2005	
<i>Data Attributes</i>		
<b>List attributes in data set and units</b>	LINEAMENTS = orientation (deg), length (m), offset (m), comments;	
<b>Dip and strike format</b>	dip-direction (azimuth) / dip	
<i>Other information</i>		
File contains all remote sensing data collected as part of RWW's PhD research (Durham), these include: all Landsat images (c/o Maryland website), Lineament maps (originals, plus analysis files), DEM's, and GoCad project files.		

**Metadata author** R.W.Wilson

Version: final



Appendix

**Durham RRG – GAVA metadata sheet**

<i>Dataset Identifiers</i>		
Dataset name	Lofoten – Detailed field-mapping study onshore (Raftsundet area)	
Geographic Region	Austvågøya, Lofoten, NW Norway	
Date established	2003/06/01	
Data collected by?	Robert W. Wilson	
<i>Dataset Description</i>		
Dataset type	ArcGIS files: shapefiles (polylines); 1km and 30m DEM (GRID); Landsat TM images (tif). GoCAD files include: point (ps), line (pl), and surface (ts), raster (tif)	
Derived from another dataset?		
Purpose of data collection	PhD project	
Equipment used	ArcGIS and GoCAD	Completeness: 90%
<i>Geospatial</i>		
Projection system	WGS 1984 UTM zone 33N	
Ellipsoid (for projection):	UTM	
Units x, y, z:	meters	
Scale or Spatial resolution	>1:5 000	
Grid North or Magnetic North?	Grid North	
Positional Accuracy	~1m (DGPS mapping using Ashtech Promark 2 and Garmin eTrex)	
	<b>Bounding coordinates of dataset</b>	
	North 7620000	
460000 West		East 540000
	South 7560000	
<i>IT summary for dataset</i>		
Data format	ArcGIS 3D-point and polyline shapefiles, field photographs (JPEG), fracture traverses (JGEG/ Excel spreadsheets), laser rangefinder outcrop data (ASCII files & GoCAD pointsets)	
Where loaded?	ISIS01/RRG/dgl3rww/Lofoten	
Size (compressed/live)	~3Gb	
Initial Back-up information	Where?	RWW's personal Hard drive
	When last back-up?	01/08/2005
<i>Data Attributes</i>		
List attributes in data set and units	See metadata for each shapefile.	
Dip and strike format	strike (= dip-direction - 90°) / dip / sense	
<i>Other information</i>		
File contains all field data collected as part of RWW's PhD research (Durham)		

Metadata author R. W. Wilson

Version: final

## **APPENDIX 4 – STRESS INVERSION ANALYSIS**

### **Inversion Procedures:**

#### ***Michael (1984) – Minimized Shear Stress Variation***

Slip on a fault surface occurs when the resolved shear stress on that surface exceeds the frictional resistance to slip. For a uniform regional state of stress, the direction of slip will depend upon the orientation of the fault and local factors such as frictional anisotropy. Thus the actual slip direction may not coincide with the maximum resolved shear stress. To estimate the regional stresses, Michael (1984) made the simplifying assumption that the magnitude of the slip stress on the fault is similar for all faults in the set at the time of slip. Thus, minimizing the variations in slip stress among the faults leads to an overdetermined set of linear equations. These equations are solved by the standard eigenvector method, giving the three principal stresses and their direction.

#### ***Angelier (1984) – Minimized Non-slip Shear Stress***

Slip on a fault surface occurs when the resolved shear stress on that surface exceeds the frictional resistance to slip. For a uniform regional state of stress, the direction of slip will depend upon the orientation of the fault and local factors such as frictional anisotropy. Thus the actual slip direction may not coincide with the maximum resolved shear stress. To estimate the regional stresses, Angelier (1984) examined a number of relations expressing the deviations between the maximum resolved shear stress on the fault plane and the actual slip direction, all of which lead to a non-linear minimization problem. Another approach giving a similar result minimizes the variations in the non-slip stress (the shear stress component in the fault plane normal to the slip direction) among the faults, leading to an overdetermined set of linear equations. These equations are solved by the standard least squares techniques, giving the three principal stresses and their direction.

#### ***Reches (1987) – Minimized Principal Stress Variation***

This method, developed by Reches (1987), assumes that the stress to cause fault slip obeys a Coulomb yield criterion,  $\tau = C + \mu \sigma$ , where  $\tau$  is the shear stress to cause slip,  $C$

## Appendix

is the cohesion stress,  $\mu$  is the friction coefficient and  $\sigma$  is the normal stress on the fault. From this relation, you can derive the principal stresses necessary for slip to occur. Assuming that all faults in the set were subject to the same regional stress state, then the principal stresses should be the same for all faults. Variations in material properties and other local effects will cause the actual stress state to vary between faults.

### **Analysis method:**

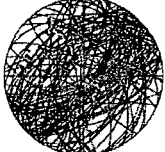
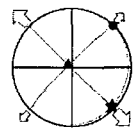
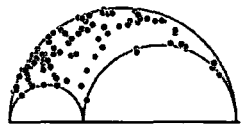
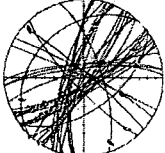
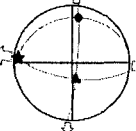
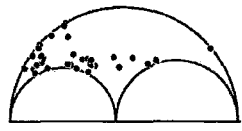
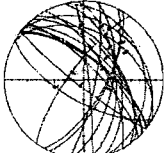
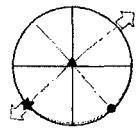
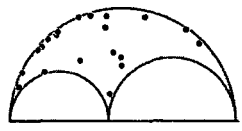
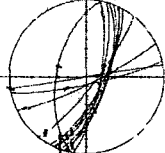
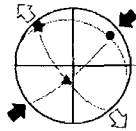
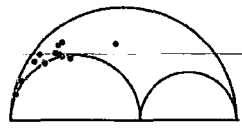

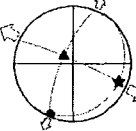
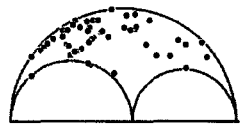

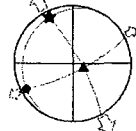
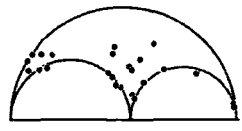
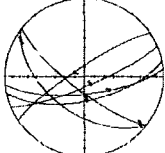
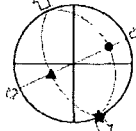
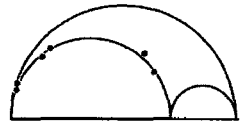
The tables below show the results of palaeostress analysis at each locality. The columns are defined as follows: *Loc.* is the locality number. *N, % tot.* shows the number of faults used in the inversion, and the percentage of the total original population. *Faults and Striae* show a lower hemisphere, equal area stereonet plot of faults (great circles) and slickenlines (points/ arrows). The *Stress tensor* column shows principle axes of the stress tensors plotted on equal area stereonets, triangle =  $\sigma_1$ ; circle =  $\sigma_2$ ; star =  $\sigma_3$ . The *Mohr Circle* column shows the upper half of three-dimensional Mohr circles with fault data given by small circles. *Principle axes* column lists the vectors (given as azimuth/ plunge) for each of the principle axes ( $\sigma_1$ ,  $\sigma_2$ ,  $\sigma_3$ ). The comments column lists other relevant data (i.e. R and MSS) derived from inversion, plus general descriptions of the apparent palaeostress. Abbreviations: R = Stress Ratio; MSS = Mean Shear Stress.

### **Results:**

The following tables show the results of palaeostress analysis on a locality by locality basis. All data presented in the following tables were calculated using inversion procedure of Michael (1984).

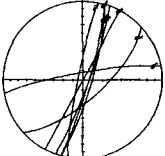
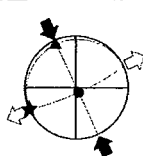
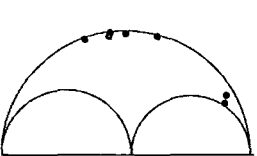
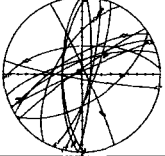
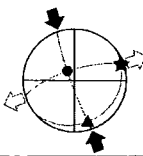
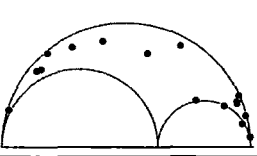
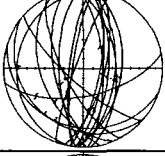
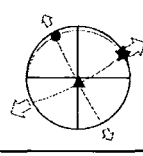
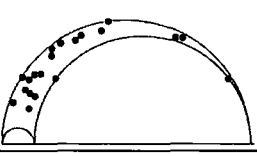
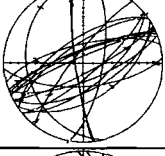
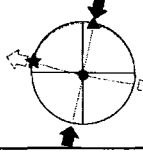
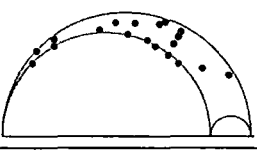
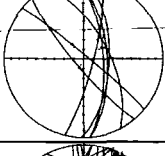
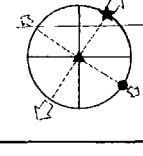
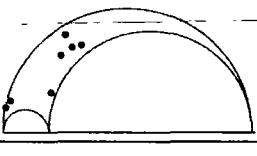
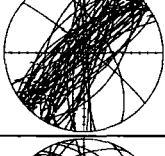
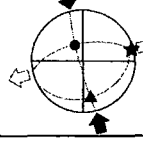
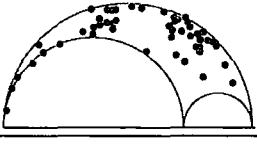
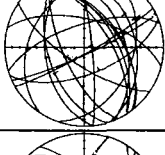
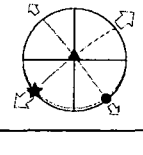
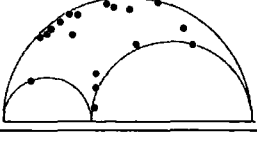
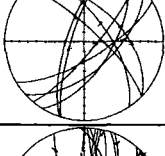
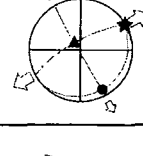
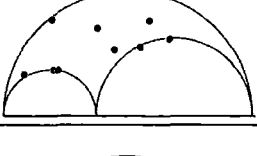
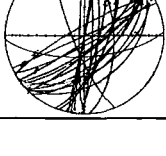
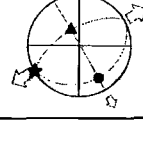
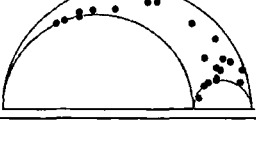
Appendix

**Scottish North Coast dataset:**

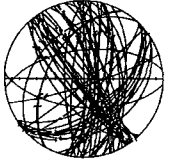
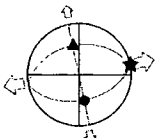

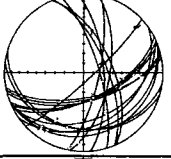
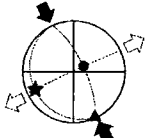
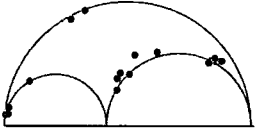
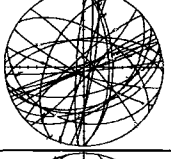
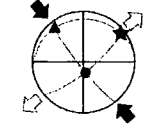
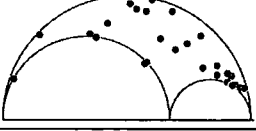
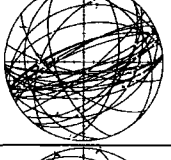
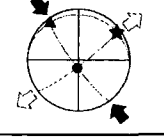
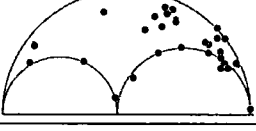
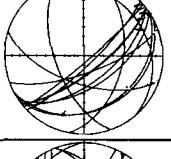
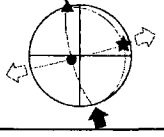

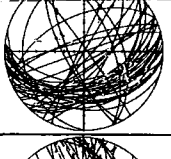
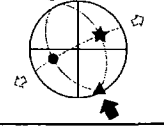
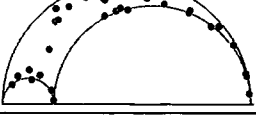
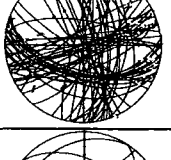
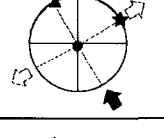
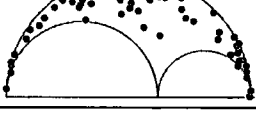
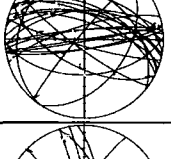
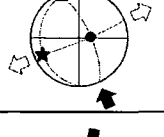

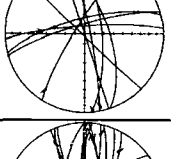
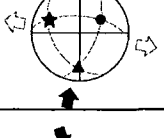
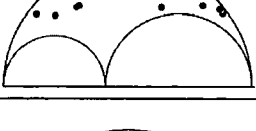
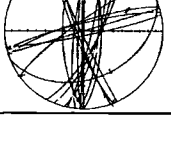
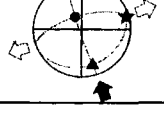

Loc	N, % tot.	Faults and striae	Stress Tensor	Mohr Circle	Principle axes	Comments
Durness_1	N = 100 60.0%				$\sigma_1 = 301/84$ $\sigma_2 = 044/01$ $\sigma_3 = 134/06$	R = 0.33 MSS = 0.310
Durness_2	N = 35 21.0%				$\sigma_1 = 168/67$ $\sigma_2 = 008/21$ $\sigma_3 = 275/07$	R = 0.47 MSS = 0.246
Coldbackie	N = 21 84.0%				$\sigma_1 = 342/86$ $\sigma_2 = 139/04$ $\sigma_3 = 229/02$	R = 0.44 MSS = 0.329
Skerryay	Too few fault striae observed to construct a viable interpretation!					
Glasgo	N = 14 100%				$\sigma_1 = 203/67$ $\sigma_2 = 53/21$ $\sigma_3 = 319/11$	R = 0.58 MSS = 0.256
Kirtomy_1	N = 50 58.8%				$\sigma_1 = 313/73$ $\sigma_2 = 204/06$ $\sigma_3 = 112/16$	R = 0.54 MSS = 0.363
Kirtomy_2	N = 25 29.4%				$\sigma_1 = 112/74$ $\sigma_2 = 241/10$ $\sigma_3 = 333/12$	R = 0.53 MSS = 0.208
Portskerra	N = 6 100%				$\sigma_1 = 245/56$ $\sigma_2 = 065/34$ $\sigma_3 = 155/0$	R = 0.71 MSS = 0.223

Appendix

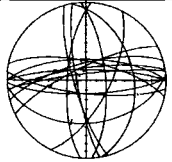
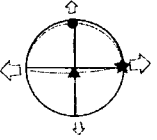
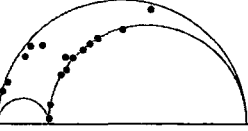
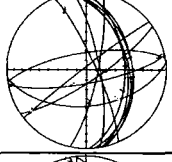
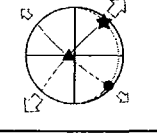
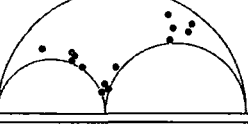
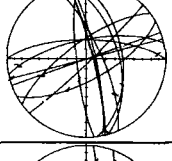
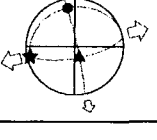
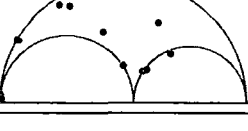
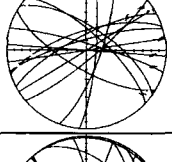
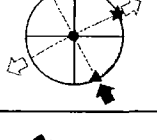
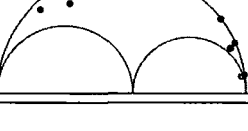
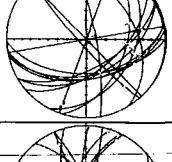
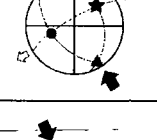

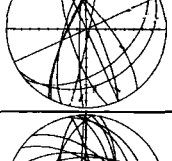
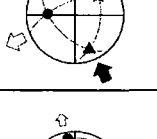
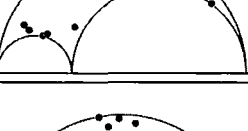
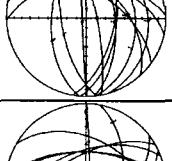
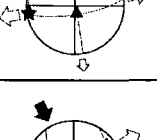

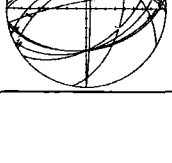
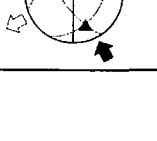
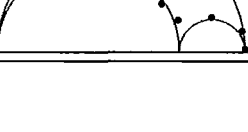
**West Greenland dataset:**

Loc	N, % tot.	Faults and striae	Stress Tensor	Mohr Circle	Principle axes	Comments
101	N = 7 100%				$\sigma_1 = 335/09$ $\sigma_2 = 152/81$ $\sigma_3 = 245/00$	R = 0.52 MSS = 0.407
102	N = 17 81.0%				$\sigma_1 = 162/17$ $\sigma_2 = 322/72$ $\sigma_3 = 070/06$	R = 0.63 MSS = 0.236
103	N = 20 45.5%				$\sigma_1 = 172/80$ $\sigma_2 = 331/09$ $\sigma_3 = 062/03$	R = 0.13 MSS = 0.315
103	N = 20 45.5%				$\sigma_1 = 012/03$ $\sigma_2 = 173/86$ $\sigma_3 = 282/01$	R = 0.84 MSS = 0.345
104	N = 7 8.0%				$\sigma_1 = 223/88$ $\sigma_2 = 123/00$ $\sigma_3 = 033/02$	R = 0.19 MSS = 0.255
104	N = 54 61.4%				$\sigma_1 = 169/28$ $\sigma_2 = 335/61$ $\sigma_3 = 076/06$	R = 0.72 MSS = 0.336
105	N = 18 81.8%				$\sigma_1 = 359/84$ $\sigma_2 = 141/05$ $\sigma_3 = 232/04$	R = 0.36 MSS = 0.334
106	N = 9 25.7%				$\sigma_1 = 321/75$ $\sigma_2 = 151/14$ $\sigma_3 = 060/02$	R = 0.37 MSS = 0.258
106	N = 26 74.3%				$\sigma_1 = 333/62$ $\sigma_2 = 149/28$ $\sigma_3 = 240/02$	R = 0.77 MSS = 0.182

Appendix

107	N = 58 100%				$\sigma_1 = 349/42$ $\sigma_2 = 169/48$ $\sigma_3 = 079/00$	R = 0.62 MSS = 0.238
201	N = 19 40.4%				$\sigma_1 = 155/01$ $\sigma_2 = 061/72$ $\sigma_3 = 246/18$	R = 0.42 MSS = 0.207
201	N = 28 59.6%				$\sigma_1 = 320/15$ $\sigma_2 = 169/73$ $\sigma_3 = 052/08$	R = 0.67 MSS = 0.162
202	N = 35 51.5%				$\sigma_1 = 322/08$ $\sigma_2 = 190/78$ $\sigma_3 = 053/09$	R = 0.46 MSS = 0.229
202	N = 13 19.1%				$\sigma_1 = 345/02$ $\sigma_2 = 246/75$ $\sigma_3 = 076/14$	R = 0.79 MSS = 0.199
401	N = 42 40.0%				$\sigma_1 = 153/06$ $\sigma_2 = 249/44$ $\sigma_3 = 057/45$	R = 0.21 MSS = 0.267
401	N = 63 60.0%				$\sigma_1 = 330/03$ $\sigma_2 = 175/87$ $\sigma_3 = 060/01$	R = 0.62 MSS = 0.237
402	N = 25 59.5%				$\sigma_1 = 338/06$ $\sigma_2 = 085/70$ $\sigma_3 = 246/19$	R = 0.73 MSS = 0.25
403	N = 9 31.0%				$\sigma_1 = 185/28$ $\sigma_2 = 059/48$ $\sigma_3 = 292/29$	R = 0.41 MSS = 0.322
403	N = 20 69.0%				$\sigma_1 = 163/23$ $\sigma_2 = 333/66$ $\sigma_3 = 072/04$	R = 0.8 MSS = 0.153

Appendix

405	N = 16 57.1%				$\sigma_1 = 187/82$ $\sigma_2 = 357/08$ $\sigma_3 = 088/01$	R = 0.21 MSS = 0.249
406	N = 14 38.9%				$\sigma_1 = 265/79$ $\sigma_2 = 132/07$ $\sigma_3 = 041/08$	R = 0.44 MSS = 0.213
406	N = 14 38.9%				$\sigma_1 = 157/70$ $\sigma_2 = 349/20$ $\sigma_3 = 258/04$	R = 0.54 MSS = 0.155
407	N = 13 100%				$\sigma_1 = 153/03$ $\sigma_2 = 316/87$ $\sigma_3 = 062/01$	R = 0.55 MSS = 0.291
408	N = 16 48.5%				$\sigma_1 = 148/13$ $\sigma_2 = 253/49$ $\sigma_3 = 048/38$	R = 0.45 MSS = 0.263
408	N = 12 36.4%				$\sigma_1 = 158/25$ $\sigma_2 = 273/43$ $\sigma_3 = 048/37$	R = 0.3 MSS = 0.252
409	N = 13 41.9%				$\sigma_1 = 164/75$ $\sigma_2 = 351/15$ $\sigma_3 = 260/02$	R = 0.27 MSS = 0.372
409	N = 13 41.9%				$\sigma_1 = 160/34$ $\sigma_2 = 300/49$ $\sigma_3 = 055/20$	R = 0.73 MSS = 0.199

## Appendix 5 - Fracture spacing images and analysis

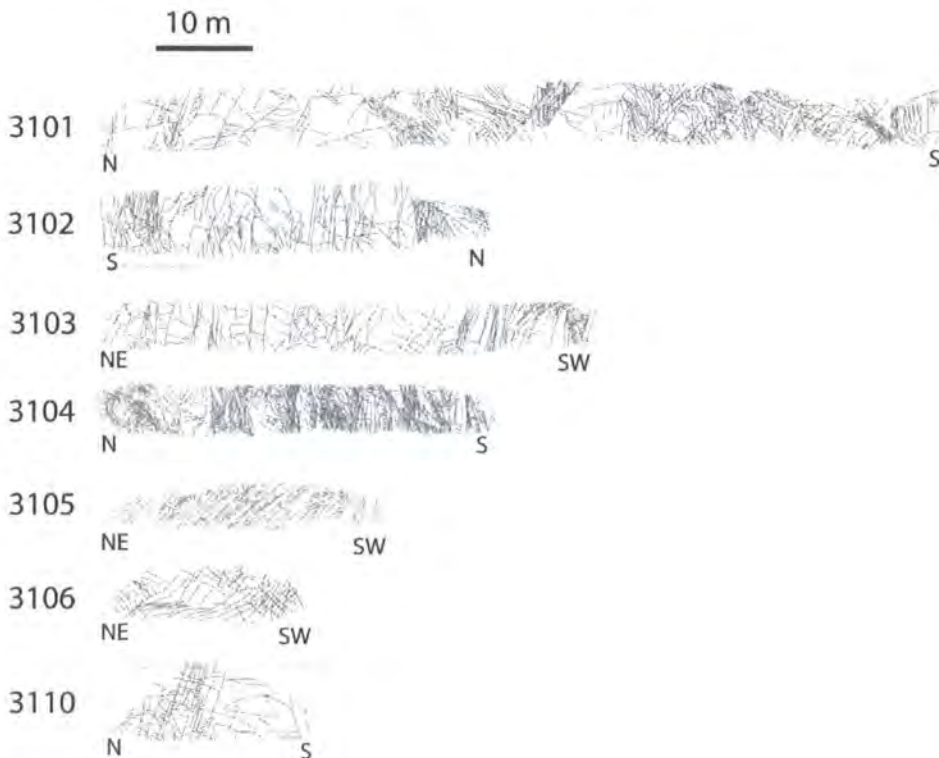
The Lofoten dataset includes a section on analysis of fracture spacing (see *section 4.5.3.2*). Here the method of analysis used is is

### ***Analysis method:***

- Step 1:** Photographic mosaics of key outcrops were recorded in the field, georeferenced using DGPS and Laser rangefinder.
- Step 2:** Mosaics were then imported into CorelDraw\* where images were analysed and 2-D fracture maps created (see below). Fracture maps were then exported as JPEG images.
- Step 3:** JPEGs were then imported into windows image analysis software, UTHSCSA ImageTool v.3 (<http://ddsdx.uthscsa.edu/>), where fracture spacing was measured along horizontal profiles. Results were then exported as ASCII data for import to Excel.
- Step 4:** Fracture Spacing analysis was carried out using FRACHARS v.2 script for Microsoft Excel, created by K. McCaffrey. See an example of the output data below.

\* (N.B. as most traverses profiles were in vertical section GIS was not suitable for mapping fractures in photo-mosaics)

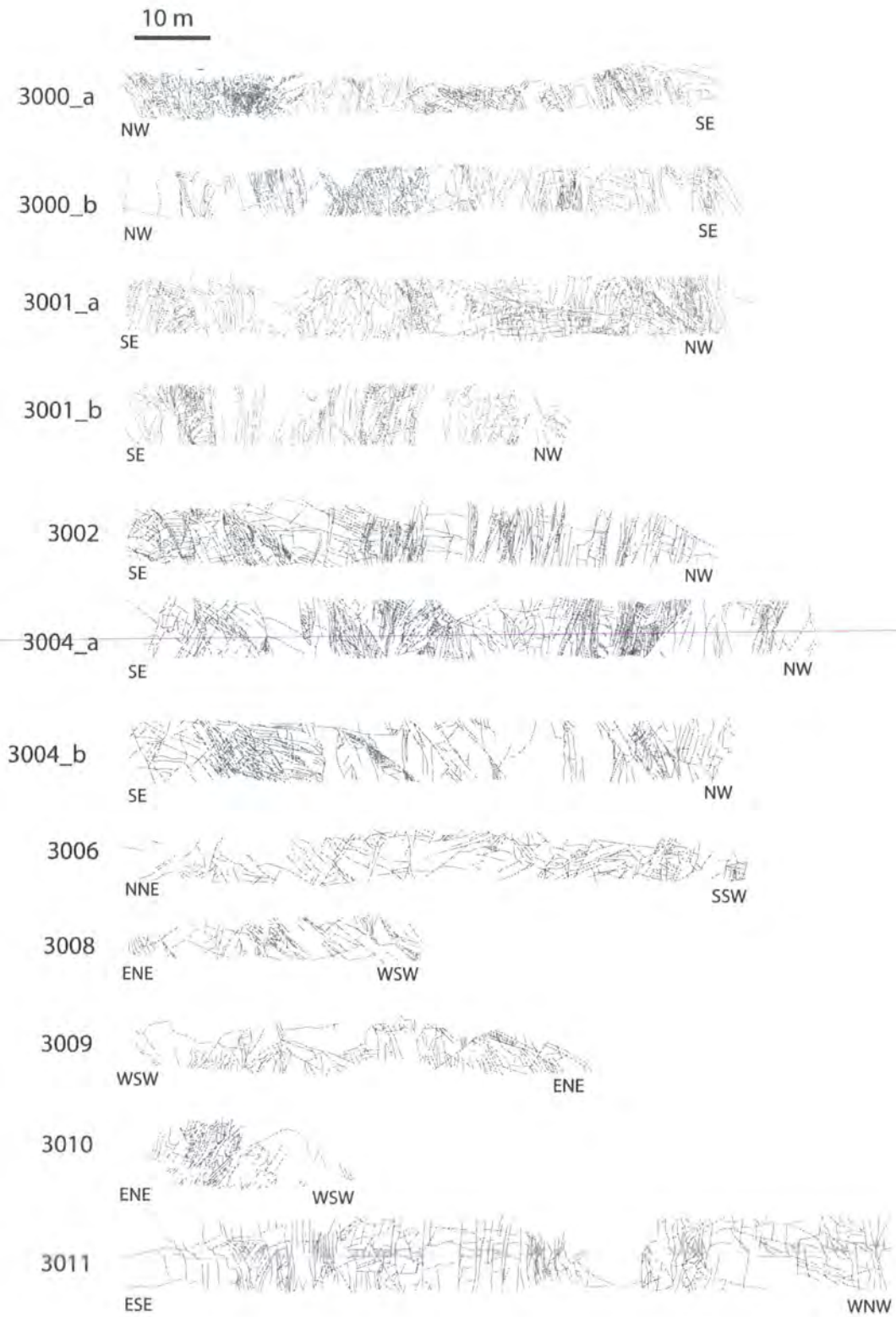
### Fracture spacing traverses - east of Raftsundet



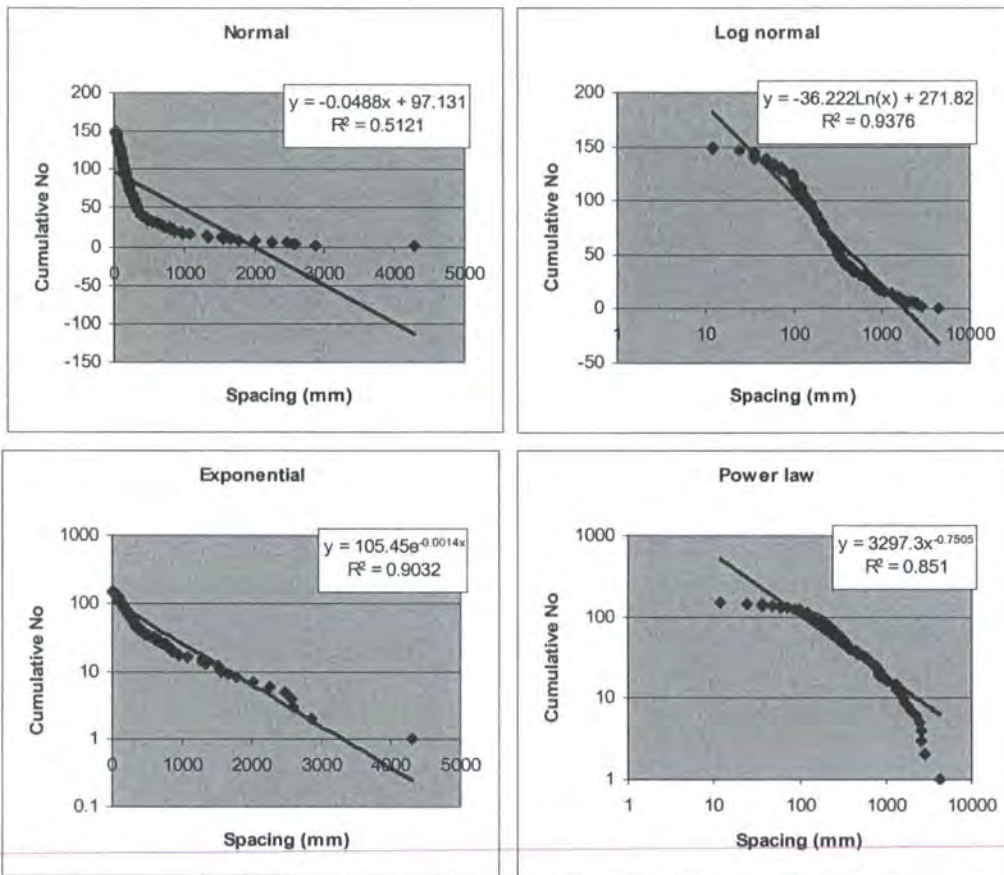


Appendix

Fracture spacing traverses - west of Raftsundet



## Appendix



Above: Example fracture spacing graphs (Trav 3000b) created using FRACHARS v.2.

Below: Table of results for

Transect line	Trend, degrees	Transect length, m	N	Sp	Exponent	MFS	SD	FD	Cv
3000a	159	76.93	227	EXP	0.0026	0.34	0.35	2.95	1.20
3000b	147	78.23	166	EXP/PL	0.0014	0.47	0.64	2.12	1.44
3001a	162	80.71	160	EXP	0.0017	0.50	0.53	1.98	1.04
3001b	145	56.14	93	EXP	0.0014	0.60	0.63	1.66	1.08
3002	131	75.04	145	EXP	0.0014	0.52	0.64	1.93	1.29
3004a	142	86.98	195	EXP	0.0020	0.45	0.45	2.24	1.09
3004b	155	75.79	111	EXP	0.0010	0.68	0.93	1.46	1.37
3006	20	80.15	69	EXP	0.0008	1.16	1.18	0.86	1.05
3008	72	40	54	EXP	0.0011	0.74	0.81	1.35	1.15
3009	77	61.4	62	EXP	0.0011	0.99	0.82	1.01	0.86
3010	74	28.58	38	EXP/LN	0.0016	0.75	0.80	1.33	1.21
3011	125	104.65	104	EXP	0.0007	1.01	1.29	0.99	1.36
3101	8	95.67	166	EXP/PL	0.0012	0.58	0.75	1.74	1.27
3102	177	40.81	91	EXP	0.0020	0.45	0.46	2.23	1.01
3103	25	58.98	90	EXP	0.0013	0.66	0.71	1.53	1.10
3104	173	50.21	229	EXP/PL	0.0030	0.22	0.29	4.56	1.33
3105	29	33.58	69	EXP	0.0029	0.49	0.31	2.06	0.65
3106	31	21.59	31	EXP	0.0013	0.70	0.66	1.44	0.97
3110	9	21.89	23	EXP	0.0008	0.95	1.01	1.05	1.06

Abbreviations: N - number of fractures; Sp - spacing distribution; MFS - mean fracture spacing; SD - standard deviation; FD - fracture density; Cv - coefficient of variation

## References

### References.

- Allaby, A. & Allaby, M. (1996) Oxford Concise Dictionary of Earth Sciences. Oxford University Press, 410 pp.
- Allen, M.B., MacDonald, D.I.M., Xun, Z., Vincent, S.J. & Brouet-Menzies, C. (1998) Transtensional deformation in the evolution of the Bohai Basin, northern China. In: Holdsworth, R.E., Strachan, R.A., Dewey, J.F. (Eds.), Continental transpressional and transtensional tectonics. Geological Society of London Special Publication 135, 215-229.
- Anderson, E.M. (1951) The dynamics of faulting, 2<sup>nd</sup> edition, Oliver and Boyd, Edinburgh.
- Anderton, R., Bridges, P.H., Leeder, M.R. & Shellwood, B.N. (1979) A dynamic stratigraphy of the British Isles: a study in crustal evolution. George Allen & Unwin, London.
- Andresen, A. and T. Forslund (1987), Post-Caledonian brittle faults in Troms: geometry, age and tectonic significance, paper presented at 'The Caledonian and Related Geology of Scandinavia' conference, Cardiff, Sept. 22-23.
- Angelier, J., Tarantola, A. & Valette, B. (1982) Inversion of field Data in fault tectonics to obtain the regional stress – 1. Single phase of fault populations: a new method of computing the stress tensor. *Geophysical Journal of the Royal Astronomical Society*, 69, 607-621.
- Angelier, J. (1984) Tectonic stress analysis of fault slip data sets. *Journal of Geophysical Research*, 89, 5835-5848.
- Angelier, J. (1985) Neogene palaeostress changes in the Basin and Range: a case study at Hoover Dam, Nevada-Arizona. *Geological Society of America Bulletin*, 96, 347-361.
- Angelier, J. (1994) Fault slip analysis and palaeostress reconstruction. In: Hancock, P.L. (Ed.), *Continental Deformation*, Pergamon Press, Oxford. 53-101.
- Arthaud, F. (1969) Méthode de détermination graphique des directions de raccourcissement, d'allongement et intermédiaire d'une population de failles. *Bulletin de la Société Géologique de France*, 7, 729-737.
- Bak, J., Korstgård, J.A. & Sørensen, K. (1975) A major shear zone within the Nagsugtoqidian of West Greenland. *Tectonophysics*, 27, 191-209.
- Barnes, J.W. (1981) *Basic Geological Mapping*. Geological Society of London Handbook Series, Open University Press, Milton Keynes.
- Barnes J.W. & Lisle, R.J. (2004) *Basic Geological Mapping*. Wiley, Chichester, 132 pp.

## References

- Barnes, R.P., Rock, N.M.S. & Gaskarth, J.W. (1986) Late Caledonian dyke-swarms in Southern Scotland: new field, petrological and geochemical data for the Wigtown Peninsula, Galloway. *Geological Journal*, 21, 101-125.
- Barr, D., Holdsworth, R.E. & Roberts, A.M. (1986) Caledonian ductile thrusting in a Precambrian metamorphic complex: The Moine of northwestern Scotland. *Bulletin of the Geological Society of America*, 97, 754-764.
- Bartholomew, M.J., Peters, J.M. & Powell, C.M. (1993) Regional structural evolution of the North Sea: oblique slip and reactivation of basement lineaments. In Parker, J.R. (Ed.), *Petroleum geology of Northwest Europe: Proceedings of the Forth Conference*, Geological Society, London, 1109-1122.
- Bartley, J.M. (1982), Limited basement involvement in Caledonian deformation, Hinnøy, North Norway, and tectonic implications, *Tectonophysics*, 83, 185-203.
- Baxter, A.N. (1987) Petrochemistry of late Palaeozoic alkali lamprophyre dykes from north Scotland. *Transactions of the Royal Society of Edinburgh, Earth Sciences*, 77, 267-277.
- Baxter, A.N. & Mitchell, J.G. (1984) Camptonite – monchiquite dyke swarms of Northern Scotland; age relationships and their implications. *Scottish Journal of Geology*, 20, 297-308.
- Beacom, L. (1999) The kinematic evolution of reactivated and non-activated faults in basement rocks, NW Scotland. Unpublished PhD thesis, Queen's University of Belfast, UK.
- Beacom, L.E., Anderson, T.B. & Holdsworth, R.E. (1999) Using basement-hosted clastic dykes as syn-rift palaeostress indicators: an example from the basal Stoer Group, northeast Scotland. *Geological Magazine*, 136, 301-310.
- Beacom, L.E., Holdsworth, R.E., McCaffrey, K.J.W. & Anderson, T.B. (2001) A quantitative study of the influence of Pre-existing compositional and fabric heterogeneities upon fracture zone development during basement reactivation. In: Holdsworth, R.E., Strachan, R.A., Magloughin, J.F. & Knipe, R.J. (Eds.), *The nature and tectonic significance of fault zone weakening*, Geological Society Special Publication 186, 195-211.
- Becken, K. & Green, C. (2000) DigMap: a digital geological map of the United Kingdom. *Earthwise*, 16, 8-9.
- Berry, J.K. (2000) Geographic Information System (GIS) technology: a brief history, trends, and probable future. In: Coburn, T.C. & Yarus, J.M. (Eds.), *Geographical information systems in petroleum exploration and development*. American Association of Petroleum Geologists Computer Applications in Geology 4, 9-16.
- Blackbourn, G.A. (1981a) Correlation of Old Red Sandstones (Devonian) outliers in the Northern Highlands of Scotland. *Geological Magazine*, 118, 409-414.

## References

- Blackbourn, G.A. (1981b) Probable Old Red Sandstone conglomerates around Tongue and adjacent areas, north Sutherland. *Scottish Journal of Geology*, 17, 103-118.
- Blanton, T.L. (1982) An experimental study of interaction between hydraulically-induced and pre-existing fractures. SPE/DOE pre-print 10847, Proceedings of the Unconventional Gas Recovery Symposium, Pittsburgh, 559-571.
- Blokkum, O., et al. (1992) Aeromagnetisk anomalikart Norge (aeromagnetic anomaly map of Norway), 1:1 million. Norges geologiske undersøkelse.
- Blundell, D.J., Hurich, C.A. & Smithson, S.B. (1985) A model for the MOIST seismic reflection profile, N Scotland. *Journal of the Geological Society (London)*, 142, 245-258.
- Blystad, P., Brekke, H., Færseth, R.B., Larsen, B.T., Skogseid, J. & Tørudbakken, B. (1995) Structural Elements of the Norwegian continental shelf II: The Norwegian Sea Region. NPD Bulletin, 8, Norwegian Petroleum Directorate, Stavanger.
- Bonham-Carter, G.F. (1992) "Applying GIS to geology". *Geotimes*, August 1992, 6-7.
- Bonham-Carter, G. (2000) An overview of GIS in the geosciences. In: Coburn, T.C. & Yarus, J.M. (Eds.), *Geographical information systems in petroleum exploration and development*. American Association of Petroleum Geologists Computer Applications in Geology, 4, 17-26.
- Bonini, M., Souriot, T., Boccaletti, M. & Brun, J.P. (1997) Successive orthogonal and oblique extension episodes in a rift zone: laboratory experiments with the application to the Ethiopian Rift. *Tectonics*, 16, 347-362.
- Bott, M.H.P. (1959) The mechanics of oblique slip faulting. *Geological Magazine*, 96, 109-117.
- Bott, M.H.P. (1967) Geophysical investigations of the Northern Pennine basement rocks. *Proceedings of the Yorkshire Geological Society*, 36, 139-168.
- Bott, M.H.P., Robinson, J. & Kohnstamm, M.M. (1978) Granite beneath Market Weighton, East Yorkshire. *Journal of the Geological Society (London)*, 135, 535-543.
- Bosworth, W., Lister, G.S., Etheridge, M.A. & Symonds, P.A. (1986) Comment and reply on 'Detachment faulting and the evolution of passive continental margins', *Geology*, 14, 890-892.
- Braathen, A. & Gabrielsen, R.H. (1998) Lineament architectures and fracture distribution in metamorphic and sedimentary rocks, with application to Norway. Norges Geologiske Undersøkelse report 98.043.
- Brekke, H. (2000) The tectonic evolution of the Norwegian Sea continental margin with emphasis on the Vøring and Møre basins. In: Nøttvedt, A. (Ed.), *Dynamics of the Norwegian Margin*, Geological Society Special Publication 167, 327-378.

## References

- Brewer, J.A. & Smythe, D.K. (1984) MOIST and the continuity of crustal reflector geometry along the Caledonian – Appalachian orogeny. *Journal of the Geological Society (London)*, 141, 105-120.
- Brimhall and Vanegas, (2001) Removing science workflow barriers to adoption of digital geological mapping by using the GeoMapper Universal Program and visual user interface. *Digital Mapping Techniques 2001, Workshop Proceedings, USGS, Open-File Report 01-223*.
- Briner, A.P., Kronenberg, H., Mazurek, M., Horn, H., Engi, M. & Peters, T. (1999) FieldBook and GeoDatabase – tools for field data acquisition and analysis. *Computers and Geosciences*, 25, 1101-1111.
- Bridgewater, D., Watson, J. & Windley, B.F. (1973) The Archaean craton of the North Atlantic region. *Philosophical Transactions of the Royal Society, London*, 273A, 493-512.
- Brodaric, B. & Fyon, J.A. (1989) OGS FieldLog: A microcomputer-based methodology to store, process and display map-related data. Ontario Geological Survey, open file report 5709, 77 pp.
- Brodaric, B. (1997) Field data capture and manipulation using GSC FIELDLOG v3.0. In: Stoller, D.R. (Ed.) *Proceedings of a Workshop on Digital Mapping Techniques: Methods for Geologic Map Capture, Management and Publication*. USGS, Open File report, 97-269, 77-81.
- Brodaric, B. (2004) The design of GSC FieldLog: ontology-based software for computer aided geological field mapping. *Computers and Geosciences*, 30, 5-20.
- Burns, I.M., Fowler, M.B., Strachan, R.A. & Greenwood, P.B. (2004) Geochemistry, petrogenesis and structural setting of the meta-igneous Strathy Complex: a unique basement block within the Scottish Caledonides? *Geological Magazine*, 141, 209-223.
- Butler, R.W.H. & Coward, M.P. (1984) Geological constraints, structural evolution and deep geology of the northwest Scottish Highlands. *Tectonics*, 3, 347-365.
- Byerlee, J. D. (1978) Friction of rocks. *Pure and Applied Geophysics* 116, 615-626.
- Canning, J.C., Henney, P.J., Morrison, M.A., Van Calsteren, P.W.C., Gaskarth, J.W. & Swarbrick, A. (1998) The Great Glen Fault: a major vertical lithospheric boundary. *Journal of the Geological Society (London)*, 155, 425-428.
- Carter, A., Bristow, C.S. & Hurford, A.J. (1995) The application of fission track analysis to the dating of barren sequences: examples from red beds in Scotland and Thailand. In: Duray, R.E. & Hailwood, E.A. (Eds.), *Non-biostratigraphic methods of dating and correlation*. Geological Society of London Special Publication 91, 41-56.

## References

- Casademont, J., Lopez-Aguilera, E., Paradells, J., Rojas, A., Calveras, A., Barceló, F. & Cotrina, J. (2004) Wireless technology applied to GIS. *Computers and Geosciences*, 30, 671-682.
- Cashman, P.H. & Ellis, M.A. (1994) Fault interaction may generate multiple slip vectors on a single fault surface, *Geology*, 22, 1123-1126.
- Chalmers, J.A. (1991) New evidence on the structure of the Labrador/ Greenland continental margin. *Journal of the Geological Society (London)*, 148, 899-908.
- Chalmers, J.A. (2000) Offshore evidence for Neogene uplift in central West Greenland. *Global and Planetary Change*, 24, 311-318.
- Chalmers, J.A. & Laursen, K.H. (1995) Labrador Sea: the extent of continental crust and the timing of the start of sea floor spreading. *Marine and Petroleum Geology*, 12, 205-217.
- Chalmers, J.A. & Pulvertaft, T.C.R. (2001) Development of the continental margins of the Labrador Sea: a review. In: Wilson, R.C.L., Whitmarsh, R.B., Taylor, B. & Froitzheim, N. (Eds.), *Non-volcanic rifting of continental margins: A comparison of evidence from land and sea*. Geological Society of London Special Publication 187, 77-105.
- Chalmers, J.A., Pulvertaft, T.C.R., Christiansen, F.G., Larsen, H.C., Laursen, K.H. & Ottesen, T.G. (1993) The southern West Greenland continental margin: rifting history, basin development, and petroleum potential. In: Parker, J.R. (Ed.) *Petroleum Geology of Northwest Europe: proceedings of the 4<sup>th</sup> Conference*. Geological Society, London, 915-931.
- Chalmers, J.A., Dahl-Jensen, T., Bate, K.J. & Whittaker, R.C. (1995) Geology and petroleum prospectivity of the region offshore southern West Greenland. *Rapport Grønlands Geological Undersøgelse* 165, 13-21.
- Chalmers, J.A., Pulvertaft, T.C.R., Marcussen, C. & Pedersen, A.K. (1999) New insight into the structure of the Nuussuaq Basin, central West Greenland. *Marine and Petroleum Geology*, 16, 199-224.
- Chang, C. & Haimson, B. (2000) True triaxial strength and deformation of the German Continental Deep Drilling Program (KTB) deep hole amphibolite. *Journal of Geophysical Research*, 105, 18,999-19,013.
- Christiansen, F.G., Olsen, J.C., Planke, S., Amundsen, H.E.F., Bojesen-Koefoed, J.A., Dalhoff, F., Myklebust, R., Nøhr-Hansen, H. & Sønderholm, M. (2002) West Greenland basin development – new evidence of old sediments. American Association of Petroleum Geologists Hedberg Conference, Stavanger, Norway, 8-11 September 2002.
- Christie-Blick, N. & Biddle, K.T. (1985) Deformation and basin formation along strike-slip faults. In: Biddle, K.T., Christie-Blick, N. (Eds.), *Strike-slip deformation,*

## References

- basin formation, and sedimentation. Society of Economic Palaeontologists and Mineralogists Special Publication 37, 1-34.
- Clegg, P., Bruciatelli, L., Domingos, F., Jones, R.R., De Donatis, M. & Wilson, R.W. (2006) Digital geological mapping with tablet PC and PDA: a comparison. Computers and Geosciences, in press.
- Clegg, P., Trinks, I., McCaffrey, K.J.W., Holdsworth, R.E., Jones, R.R., Hobbs, R. & Waggott, S. (2005) Towards the virtual outcrop. Geoscientist, Geological Society of London, 15/ 1.
- Clemson, J., Cartwright, J. & Booth, J. (1997) Structural segmentation and the influence of basement structure on the Namibian passive margin. Journal of the Geological Society (London), 154, 477-482.
- Clifton, A.E., Schlische, R.W., Withjack, M.O. & Ackermann, R.V. (2000) Influence on rift obliquity on fault-population systematics: results of experimental clay models. Journal of Structural Geology, 22, 1491-1509.
- Cloos, H. (1955) Experimental analysis of fracture patterns. Geological Society of America Bulletin, 66, 241-256.
- Coburn, T.C. and J.M. Yarus (2000), Geographical information systems in petroleum exploration and development. American Association of Petroleum Geologists Computer Applications in Geology No. 4, 315 pp.
- Cooper, M. A. & Williams, G. D. (Eds.) (1989) Inversion Tectonics. Geological Society London Special Publication 44.
- Corfu, F. (2004a), U-Pb age, setting and tectonic significance of the Anorthosite-Mangerite-Charnockite-Granite Suite, Lofoten-Vesterålen, Norway. Journal of Petrology, 45, 1799-1819.
- Corfu, F. (2004b), U-Pb geochronology of the Leknes Group: an exotic Early Caledonian metasedimentary assemblage stranded on Lofoten basement, northern Norway. Journal of the Geological Society (London) 161, 619-629.
- Cortés, A.L., Soriano, M.A., Maestro, A. & Casas, A.M. (2003) The role of tectonic inheritance in the development of recent fracture systems, Duero Basin, Spain. Int. J. Remote Sensing, 24, 4325-4345.
- Corti, G. (2004) Centrifuge modelling of the influence of crustal fabrics on the development of transfer zones: insights into the mechanics of continental rifting architecture. Tectonophysics, 384, 191-208.
- Coward, M.P. & Enfield, M.A. (1987) The structure of the West Orkney Basin and adjacent basins. In: Brooks, J. & Glennie, K. (Eds.), Petroleum Geology of North West Europe: proceedings from the 3<sup>rd</sup> Petroleum Geology Conference, Graham A. Titman., UK, 687-696.



## References

- Coward, M.P., Enfield, M.A. & Fischer, M.W. (1989) Devonian basins of Northern Scotland: extension and inversion related to Late Caledonian – Variscan tectonics. In: Cooper, M.A. & Williams, G.D. (Eds.), *Inversion Tectonics*, Geological Society of London Special Publication 44, 275-308.
- Coward, M.P. (1994) Inversion tectonics. In: Hancock, P.L. (Eds.), *Continental deformation*, Pergamon Press, Oxford. 289-304.
- Cox, D.R. & Lewis, P.A.W. (1966) *The statistical analysis of series of events*. Methuen & Co., London, 285 pp.
- Crampton, C.B. & Curruthers, R.G. (1914) *The geology of Caithness*. Memoir of the Geological Survey of Great Britain, Sheets 110 and 116, with parts of 109, 115 and 117 (Scotland).
- Crompton, R.R. (1985) *Geology in the Field*. Wiley, New York.
- Dalland, A. (1981) Mesozoic sedimentary succession at Andøy, Northern Norway, and relation to the structural development of the North Atlantic area, *Canadian Society of Petroleum Geologists Memoir*, 7, 563-584.
- Dalsegg, E. et al. (1992) Tyngdeanomalikart Norge (gravity anomaly map of Norway), 1:1 million, Norges geologiske undersøkelse og Statens kartverk.
- Daly, M.C., Chorowicz, J. & Fairhead, D. (1989) Rift basin evolution in Africa: the influence of reactivated steep basement shear zones. In: Cooper, M. A. & Williams, G. D. (Eds.), *Inversion Tectonics*. Geological Society London Special Publication 44, 309-334.
- Davidsen, B., Smelror, M. & Ottesen, D. (2001) Et nyoppdaget Mesozoisk basseng i Sortlandsundet, Vesterålen. Abstracts from NGF Vinterkonferanse, Oslo, Geonytt, 42-43.
- Davis, R.J., MacLeod, C.J., Morgan, R. & Briggs, S.E. (2005) Termination of a fossil continent-ocean fracture zone imaged with three-dimensional seismic data: The Chain Fracture Zone, eastern equatorial Atlantic. *Geology*, 33, 641-644. doi: 10.1130/G21530.1.
- Davison, I. (1997) Wide and narrow margins of the Brazilian South Atlantic, *Journal of the Geological Society (London)*, 154, 471-476.
- Dawes, P.R. (1987) Topographical and geological maps of Hall Land, northern Greenland: description of a computer-supported photogrammetrical research program for production of new maps, and the lower Palaeozoic and surficial geology. *Gronlands Geologiske Undersogelse, ITS Bulletin* 155.
- Delvaux, D. & Sperner, B. (2003) New aspects of tectonic stress inversion with reference to the TENSOR program. In: Nieuwland, D.A. (Ed.), *New Insights into Structural Interpretation and Modelling*. Geological Society Special Publication, 212, 75-100.

## References

- De Paola, N. (2005) The structural evolution of transtensional basins and rifted margin. Unpublished PhD thesis, Durham University, UK.
- De Paola, N., Holdsworth, R.E. & McCaffrey, K.J.W. (2005a) The influence of lithology and pre-existing structures on reservoir-scale faulting patterns in transtensional rift zones. *Journal of the Geological Society (London)*, 162, 471-480.
- De Paola, N., Holdsworth, R.E., McCaffrey, K.J.W. & Barchi, M.R. (2005b) Partitioned transtension: an alternative to basin inversion models. *Journal of Structural Geology*, 27, 607-625.
- Destro, N. (1995) Release fault: a variety of cross fault in linked extensional fault systems, in the Sergipe-Alagoas Basin, NE Brazil. *Journal of Structural Geology*, 17, 615-629.
- Dewey, J.F. (1975) Finite plate evolution: some implications for the evolution of rock masses at plate margins. *American Journal of Science*, 275-A, 260-284.
- Dewey, J.F., Holdsworth, R.E. & Strachan, R.A. (1998) Transpression and transtension zones. In: Holdsworth, R.E., Strachan R.A. & Dewey J.F. (Eds.), *Continental Transpressional and Transtensional Tectonics*. Geological Society of London, Special Publication 135, 1-14.
- Dewey, J.F., 2002. Transtension in Arcs and Orogens. *International Geology Review* 44, 402-439.
- Dickin, A.P. (1992) Evidence for an Early Proterozoic crustal province in the North Atlantic region. *Journal of the Geological Society (London)*, 149, 483-486.
- Donath, F.A. (1962) Analysis of basin-range structure, South-central Oregon. *Geological Society of America Bulletin*, 73, 1-16.
- Donato, J.A., Martindale, W. & Tully, M.C. (1983) Buried Granites within the Mid North Sea High, *Journal of the Geological Society (London)*, 140, 825-837.
- Dooley, T., McClay, K., Bonora, M., 1999. 4D evolution of segmented strike-slip fault systems: applications to NW Europe. In: Fleet, A.J., Boldy, S.A.R. (Eds.): *Petroleum geology of Northwest Europe, Proceedings of the Fifth Conference*, Geological Society, London, 215-225.
- Doré, A.G., Lundin, E.R., Fichler, C. & Olesen, O. (1997) Patterns of basement structure and reactivation along the NE Atlantic margin. *Journal of the Geological Society (London)*, 154, 85-92.
- Doré, A.G., Lundin, E.R., Jensen, L.N., Birkeland, Ø., Eliassen, P.E. & Fichler, C. (1999) Principal tectonic events in the evolution of the northwest European Atlantic margin. In: Fleet A.J. & Boldy, S.A.R. (Eds.), *Petroleum geology of Northwest Europe: Proceedings of the Fifth Conference*, Geological Society, London, 41-61.

## References

- Dunbar, J.A. & Sawyer, D.S. (1989) How pre-existing weaknesses control the style of continental break-up. *Journal of Geophysical Research*, 94, 7278-7292.
- Dupin J.-M., Sassi W., & Angelier J. (1993) Homogeneous stress hypothesis and actual fault slip: a distinct element analysis. *Journal of Structural Geology*, 15, 1033-1043.
- Ebinger, C.J., Jackson, J.A., Foster, A.N. & Hayward, N.J. (1999) Extensional basin geometry and elastic lithosphere. *Philos. Trans. R. Soc. Lond.*, A357, 741-765.
- Edmondo, G.P. (2002) Digital Geologic Field Mapping Using ArcPad. *Digital Mapping Techniques 2002, Workshop Proceedings, USGS, Open-File Report 02-370*, 129-134.
- Eide, E.A. (co-ord.) (2002), BATLAS – Mid Norway plate reconstruction atlas with global and Atlantic perspectives, Geological Survey of Norway, 75 pp.
- Eldholm, O., Sundvor, E. & Myhre, A. (1979) Continental margin off Lofoten-Vesterålen, Northern Norway. *Marine Geophysical Researches*, 4, 3-35.
- Eldholm, O., J. Thiede, and E. Taylor (1989), Evolution of the Vøring volcanic margin, *Proceedings of the Ocean Drilling Program, Scientific Results*, 104.
- Enfield, M.A. & Coward, M.P. (1987) The structure of the West Orkney Basin, northern Scotland. *Journal of the Geological Society (London)*, 144, 871-884.
- Escher, J.C. & Pulvertaft, T.C.R. (1995) Geological map of Greenland, 1:2 500 000. Copenhagen: Geological Survey of Greenland.
- Etchecopar, A., Vasseur, G. & Daignieres, M. (1981) An inverse problem in microtectonics for the determination of stress tensors from fault striation analysis. *Journal of Structural Geology*, 3, 51-65.
- Etheridge, M. A. (1986) On the reactivation of extensional fault systems. *Philosophical Transactions of the Royal Society of London* A317, 179-194.
- Færseth, R.B., Macintyre, R.M. & Naterstad, J. (1976) Mesozoic alkaline dykes in the Sunnhordland region, western Norway: ages, geochemistry and regional significance. *Lithos*, 9, 331-345.
- Fichler, C., Rundhovde, E., Olesen, O., Sæther, B.M., Rueslåtten, H., Lundin, E.R. & Doré, A.G. (1999) Regional tectonic interpretation of image enhanced gravity and magnetic data covering the mid-Norwegian Shelf and adjacent mainland. *Tectonophysics*, 306, 183-197.
- Fossen, H. (2000) Extensional tectonics in the Caledonides: synorogenic or postorogenic? *Tectonics*, 19, 213-224.
- Fossen, H. & Tikoff, B. (1993) The deformation matrix for simultaneous simple shearing, pure shearing and volume change and its application to transpression/transension tectonics. *Journal of Structural Geology*, 15, 413-422.

## References

- Fossen, H. & Dunlap, W.J. (1998) Timing and kinematics of Caledonian thrusting and extensional collapse, southern Norway: evidence from  $^{40}\text{Ar}/^{39}\text{Ar}$  thermochronology. *Journal of Structural Geology*, 20, 765-781.
- Friend, P.F., Williams, B.P.J., Ford, M. & Williams, E.A. (2000) Kinematics and dynamics of Old Red Sandstone basins. In: Friend, P.F. & Williams, B.P.J. (Eds.), *New Perspectives on the Old Red Sandstone*. Geological Society of London Special Publication 180, 29-60.
- Francheteau, J. & Le Pichon, X. (1972) Marginal fracture zones as structural framework of continental margins in South Atlantic Ocean. *American Association of Petroleum Geologists Bulletin*, 56, 991-1007.
- Freund, R. (1974) Kinematics of transform and transcurrent faults. *Tectonophysics*, 21, 93-134.
- Gallagher, K. & Brown, R. (1997) The onshore record of passive margin evolution. *Journal of the Geological Society (London)*, 154, 451-457.
- Gabrielsen, R. H. & Ramberg, I. B. (1979) Fracture patterns in Norway from Landsat imagery: results and potential use. In: *Proceedings of the Norwegian Sea Symposium*, Tromsø, Norway.
- Gabrielsen, R.H., Braathen, A., Dehls, J. & Roberts, D. (2002) Tectonic lineaments of Norway. *Norwegian Journal of Geology*, 82, 153-174.
- Gage, M.S. & Doré, A.G. (1986) A regional geological perspective of the Norwegian offshore exploration provinces. In: Spencer, A.M. et al. (Eds.), *Habitat of hydrocarbons on the Norwegian continental shelf*. Norwegian Petroleum Society, 21-38.
- Geikie, A. (1878) On the Old Red Sandstone of Western Europe. *Transactions of the Royal Society of Edinburgh*, 28, 345-452.
- Geoffroy, J., Gélard, J.P., Lepvrier, C. & Olivier, P. (1998) The coastal flexure of Disko (West Greenland), onshore expression of the 'oblique reflectors'. *Journal of the Geological Society (London)*, 155, 463-473.
- Gernigon, L., Ringenbach, J.C., Planke, S., Le Gall, B. & Jonquet-Kolstø, H. (2003) Extension, crustal structure and magmatism at the outer Vøring Basin, Norwegian margin. *Journal of the Geological Society (London)*, 160, 197-208.
- Gibbs, A.D. (1984) Structural evolution of extensional basin margins. *Journal of the Geological Society (London)* 141, 609-620.
- Giles, J.R.A. & Bain, K.A. (1995) The nature of data on a geological map. In: Giles, J.R.A. (Ed.) *Geological Data Management*, Geological Society Special Publication 97, 33-40.
- Gillespie, P.A., Howard, C., Walsh, J.J. & Watterson, J. (1993) Measurement and characterisation of spatial distributions of fractures. *Tectonophysics*, 226, 113-141.

## References

- Gillespie, P.A., Johnston, J.D., Loriga, M.A., McCaffrey, K.J.W., Walsh, J.J. & Watterson, J. (1999) Influence of layering on vein systematics in line samples. In: K.J.W. McCaffrey, L. Lonergan, and J.J. Wilkinson (Eds.) Fractures, fluid-flow and mineralization, Geological Society Special Publication 155, 35-56.
- Gilliland, W. N. & Meyer, G. P. (1976) Two classes of transform faults. Geological Society of America Bulletin, 87, 1127-1130.
- Golledge, N. (2004) Digital field survey technology: the future of BGS mapping? Earthwise, 20, 4-5.
- Graham, D.W., Larsen, L.M., Hanan, B.B., Storey, M., Pedersen, A.K. & Lupton, J.E., (1998) Helium isotope composition of the early Iceland mantle plume inferred from the Tertiary picrites of West Greenland. Earth and Planetary Science Letters 160, 241-255.
- Griffin, W.L., Taylor, P.N., Hakkinen, J.W., Heier, K.S., Iden, I.K., Krogh, E.J., Malm, O., Olsen, K.I., Ormaasen, D.E. & Tveten, E. (1978), Archaean and Proterozoic crustal evolution in Lofoten-Vesterålen, N Norway. Journal of the Geological Society (London) 135, 629-647.
- Grocott, J. (1979) Shape fabrics and superimposed simple shear strain in a Precambrian shear belt, West Greenland. Journal of the Geological Society (London) 136, 471-488.
- Grønlie, A. & Roberts, D. (1989) resurgent strike-slip development along the Hitra-Snåsa and Verran Faults, Møre-Trøndelag Fault Zone, Central Norway. Journal of Structural Geology, 11, 295-305.
- Hames, W.E. & A. Anderson (1996) Timing of Palaeozoic orogeny and extension in the continental shelf of north-central Norway as indicated by laser  $^{40}\text{Ar}/^{39}\text{Ar}$  muscovite dating. Geology, 24, 1005-1008.
- Hancock, P.L. (1985) Brittle microtectonics: principles and practice. Journal of Structural Geology, 7, 437-457.
- Hanley, S. (1999) Analysing real data in a virtual world. The Leading Edge, 710-712
- Hanmer, S., Mengel, F., Connelly, J. & van Gool, J. (1997) Significance of crustal-scale shear zones and syn-kinematic mafic dykes in the Nagssugtoqidian Orogen, SW Greenland: a re-examination. Journal of Structural Geology, 19, 59-75.
- Harding, T.P. (1974) Petroleum traps associated with wrench faults. American Association of Petroleum Geologists Bulletin, 58, 1290-1304.
- Harding, T.P., Vierbuchen, R.C. & Christie-Blick, N. (1985) Structural styles, plate-tectonic settings, and hydrocarbon traps of divergent (transtensional) wrench faults. In: Biddle, K.T. & Christie-Blick, N. (Eds.), Strike-slip deformation, basin formation and sedimentation. Society of Economic Paleontologists and Mineralogists Special Publication, 37, 51-78.

## References

- Harland, W.B. (1971) Tectonic transpression in Caledonian Spitzbergen. *Geological Magazine*, 108, 27-42.
- Harris, C., Franssen, R. & Loosveld, R. (1991) Fractal analysis of fractures in rocks: the Cantors Dust method- comment. *Tectonophysics*, 198, 107-115.
- Haugerud, R.A. & Thoms, E.E. (2004) Geologic Data Assistant (GDA): an ArcPad extension for geologic mapping. *Digital Mapping Techniques 2004, Workshop Proceedings, USGS, Open-File Report 2004-1451*.
- Healy, D., Jones, R.J. & Holdsworth, R.E. (2005) Three-dimensional brittle shear fracturing by tensile crack interaction. *Nature*, in press.
- Henderson, G., Scheiner, E.J., Risum, J.B., Croxton, C.A. & Andersen, B.B. (1981) The West Greenland Basin. In: Kerr, J.W., Fergusson, A.J. (Eds.), *Geology of the North Atlantic Borderlands*. Canadian Society of Petroleum Geologists Memoirs, 7, 399-428.
- Hendriks, B.W.H. (2003) Cooling and denudation of the Norwegian and Barents Sea Margin, Northern Scandinavia. PhD thesis, Vrije Universiteit Amsterdam, 177 pp.
- Hendriks, B.W.H. & Andriessen, P.A.M. (2002) Pattern and timing of the post-Caledonian denudation of Northern Scandinavia constrained by apatite fission-track thermochronology. In: Doré, A.G., Cartwright, J.A., Stoker, M.S., Turner, J.P. & White, N. (Eds.), *Exhumation of the North Atlantic Margin: Timing, Mechanisms and implications for Petroleum exploration*, Geological Society Special Publication 196, 117-137.
- Henkel, H. (1991) Magnetic crustal structures in northern Fennoscandia. *Tectonophysics*, 192, 57-79.
- Henriksen, N., Higgins, A.K., Kalsbeek, F. & Pulvertaft, T.C.R. (2000) Greenland from Archaean to Quaternary. Descriptive text to the geological map of Greenland, 1:2,500,000. *Geology of Greenland Survey Bulletin*, 185, 93 pp.
- Hingham, J.C. (1977) Sedimentology and diagenesis of the red Lower and Middle Devonian sediments in Northern Scotland. Unpublished PhD. Thesis, University of Hull.
- Hippler, S.J. & Knipe, R.J. (1990) The evaluation of cataclastic fault rocks from pre-existing mylonite. In: Knipe, R.J. & Rutter, E.H. (Eds.), *Deformation mechanisms, rheology and tectonics*. Geological Society London Special Publication 54, 71-79.
- Hodgetts, D., Drinkwater, N.J., Hodgson, J., Kavanagh, J., Flint, S.S., Keogh, K.J. & Howell, J.A. (2004) Three dimensional geological models from outcrop data using digital data collection techniques: an example from the Tanqua Karoo depocenter, South Africa. In: Curtis, A. and Wood, R. (Eds.), *Geological Prior Information*. Geological Society Special Publication, 239, 57-75.
- 
- Hodgson, R.A. (1961) Classification of structures on joint surfaces. *American Journal of Science*, 259, 493-502.

## References

- Holdsworth, R.E. (1989) Late brittle deformation in a Caledonian ductile thrust wedge: new evidence for gravitational collapse in the Moine Thrust sheet, Sutherland, Scotland. *Tectonophysics*, 170, 17-28.
- Holdsworth, R.E. & Strachan, R.A. (1996) The Moine Thrust sheet and mylonites on the Faraid Head and Durness regions, Sutherland, Scotland. Abstracts of the Tectonic Studies Group Conference, Birmingham.
- Holdsworth, R.E., Butler, C. A. & Roberts, A. M. (1997) The recognition of reactivation during continental deformation. *Journal of the Geological Society (London)*, 154, 73-78.
- Holdsworth, R.E., Strachan, R.A. & Alsop, G.I. (2001a) Solid geology of the Tongue district, Memoir of the British Geological Survey, Sheet 114E (Scotland).
- Holdsworth, R. E., Stewart, M., Imber, J. & Strachan, R. A. (2001b) The structure and rheological evolution of reactivated continental fault zones: a review and case study. In: Miller, J. A., Holdsworth, R. E., Buick, I. S. & Hand, M. (Eds.), *Continental Reactivation and Reworking*. Geological Society Special Publication 184, 115-137.
- Holm, P.M., Gill, R.C.O., Pedersen, A.K., Larsen, J.G., Hald, N., Nielsen, T.F.D. & Thirlwall, M.F. (1993) The Tertiary picrites of West Greenland; contributions from 'Icelandic' and other sources. *Earth and Planetary Science Letters*, 115, 227-244.
- Houlding, S.W. (1994) 3-D geoscience modelling – computer techniques for geological characterisation. Springer-Verlag, New York. 309 pp.
- Hruska, J. & Burk, C. F. (1971) Computer based storage and retrieval of geoscience information: bibliography 1946-69. Geological Survey of Canada, Ottawa. Its paper 71/40.
- Hutchison, W.W. (1973) GSC computerizing system for map production, analysis. *Northern miner*, 59(37):95.
- Hutchison, W.W. (1974) Introduction to geological field data systems and generalized geological data management systems. In: *Computer-based systems for geological field data*, Canada Geological Survey Paper, 74/63, 1-6
- Hutson, L. (2005) A picture of Britain. *Materials World*, 13/ 7.
- Hutton, D.H.W. (1988) Granite emplacement mechanisms and tectonic controls: inferences from deformation studies. *Transactions of the Royal Society of Edinburgh, Earth Sciences*, 79, 245-255.
- Imber, J., Holdsworth, R. E., Butler, C. A. & Lloyd, G. E. (1997) Fault-zone weakening processes along the reactivated Outer Hebrides Fault Zone, Scotland. *Journal of the Geological Society (London)*, 154, 105-109.

## References

- Imber, J., Holdsworth, R.E., McCaffrey, K.J.W., Wilson, R.W., Jones, R.R., England, R.W. & Gjeldvik, G. (2005) Early Tertiary sinistral transpression and fault reactivation in the western Vøring Basin, Norwegian Sea: implications for hydrocarbon exploration and pre-break-up deformation in ocean margin basins. *American Association of Petroleum Geologists Bulletin*, 89, 1043-1069.
- Jackson, I. & Asch, K. (2002) The status of digital geological mapping in Europe: the results of a census of the digital mapping coverage, approaches and standards of 29 European geological survey organisations in the year 2000. *Computers and Geosciences*, 28, 783-788.
- Jaeger, J.C. & Cook, N.G.W. (1967) *Fundamentals of rock mechanics*. Halstead Press, New York, 585 pp.
- Johnstone, G.S. & Mykura, W. (1989) *British regional geology: the Northern Highlands of Scotland*, 4<sup>th</sup> edition. HMSO, London for the British Geological Survey.
- Johnson, R.J. & Dingwall, R.G. (1981) The Caledonides: their influence on the stratigraphy of the North West European continental shelf. In: Illing, L.V. & Hobson, G.D. (Eds.), *Petroleum Geology of the Continental Shelf of North-West Europe*, Heyden, London, 85-97.
- Johnson, H., Ritchie, J.D., Hitchen, K., McInroy, D.B. & Kimbell, G.S. (2005) The Cenozoic deformation history of the Northeast Faroe–Shetland Basin, Wyville–Thomson ridge and Hatton Bank area. In: A.G. Doré & B.A. Vining (Eds.), *Petroleum Geology: North-West Europe and Global Perspectives: Proceedings from the 6<sup>th</sup> Petroleum Geology Conference*, Geological Society of London, 2, 993-1008.
- Jones, R.M., Boulton, P., Hillis, R.R., Mildren, S.D. & Kaldi, J. (2000) Integrated hydrocarbon seal evaluation in the Penola Trough, Otway Basin. *Australian Petroleum, Production & Exploration Association Journal*, 194-212.
- Jones, R.R. & Tanner, P.W.G. (1995) Strain partitioning in transpression zones. *Journal of Structural Geology*, 17, 793-802.
- Jones, R.R., McCaffrey, K.J.W., Wilson, R.W. & Holdsworth, R.E. (2004) Digital field data acquisition: towards increased quantification of uncertainty during geological mapping. In: Curtis, A. & Wood, R. (Eds.), *Geological Prior Information*, Geological Society of London Special Publication 239, 43-56.
- Jones, R.R., Clegg, P., Holliman, N.S., McCaffrey, K.J.W., Holdsworth, R.E., Imber, J., Waggott, S. & Wilson, R.W. (2006a) Integration of regional to outcrop digital data: 3D visualisation of multi-scale geological models. In: Zanchi, A. et al. (Eds.) *3D GIS and 3D visualisation*. Special issue of *Computers & Geosciences* (based on presentations at the 32<sup>nd</sup> International Geological Congress, Florence, Italy, 2004), in press.
- 
- Jones, R.R., McCaffrey, K.J.W., Healy, D., Imber, J., Holdsworth, R.E., Clegg, P., De Paola, N. & Wilson, R.W. (2006b), Calibration and validation of reservoir models:



## References

- the importance of high resolution, quantitative outcrop analogues. In: Griffiths P. et al. (Eds.), *The future of geological modelling in the hydrocarbon industry*, Geological Society Special Publication, in press.
- Jones, T.A., Hamilton, D.E. & Johnson, C.R. (1986) Contouring geologic surfaces with the computer. van Nostrand Reinhold, New York.
- Japsen, P., Green, P.F. & Chalmers, J.A. (2005) Separation of Palaeogene and Neogene uplift on Nuussuaq, West Greenland. *Journal of the Geological Society (London)*, 162, 299–314.
- Kalsbeek, F., Pidgeon, R.T., & Taylor, P.N. (1987) Nagssugtoqidian mobile belt of West Greenland: cryptic 1850 Ma suture between two Archaean continents – chemical and isotropic evidence. *Earth and Planetary Science Letters*, 85, 365-385.
- Kalsbeek, F., & Nutman, A.P. (1996) Anatomy of the Early Proterozoic Nagssugtoqidian Orogen, West Greenland, explored by reconnaissance SHRIMP U-Pb dating. *Geology*, 24, 515-518.
- Karpuz, M.R., Roberts, D., Olesen, O., Gabrielsen, R.H., & Herrevold, T. (1993) Application of multiple data sets to structural studies on Varanger Peninsula, northern Norway. *International Journal of Remote Sensing*, 14, 979-1003.
- Karpuz, M.R., Roberts, D., Moralev, V.M., & Terekhov, E. (1995) Regional lineaments of eastern Finnmark, Norway, and the western Kola Peninsula, Russia. *Norges Geologiske Undersøkelse Special Publication* 7, 121-135.
- Kimbell, G.S., Ritchie, J.D., Johnson, H. & Gatliff, R.W. (2005) Controls on the structure and evolution of the NE Atlantic margin revealed by regional potential field imaging and 3D modelling. In: Doré, A.G. & Vining, B.A. (Eds.), *Petroleum Geology: North-West Europe and Global Perspectives: Proceedings from the 6<sup>th</sup> Petroleum Geology Conference*, Geological Society of London, 2, 933-945.
- Kinney, P.D., Friend, C.R.L. & Love, G.J. (2005) Proposal for a terrane-based nomenclature for the Lewisian Gneiss Complex of NW Scotland. *Journal of the Geological Society (London)*, 162, 175-186.
- Kirton, S.R. & Hitchen, K. (1987) Timing and style of crustal extension N of the Scottish mainland. In: Coward, M.P., Dewey, J.F. & Hancock, P.L. (Eds.), *Continental Extensional Tectonics*, Geological Society of London Special Publication 28, 501-510.
- Klein, A.C. & Steltenpohl, M.G. (1999) Basement-cover relations and late- to post-Caledonian extension in the Leknes group, west-central Vestvågøy, Lofoten, north Norway. *Norsk Geologisk Tidsskrift*, 79, 19-31.
- Knox-Robinson, C.M. & Gardoll, S.J. (1998) GIS-Stereoplot: an interactive stereonet plotting module for ArcView 3.0 Geographic information system. *Computers and Geosciences*, 24, 243-250.

## References

- Korstgård, J.A., Ryan, B. & Wardle, R. (1987) The boundary between Proterozoic and Archaean crustal blocks in central West Greenland and Northern Labrador. In: Park, R.G. & Tarney, J. (Eds.), *Evolution of Lewisian and comparable Precambrian terranes*. Geological Society of London Special Publication 27, 247-259.
- Kramer, J.H. (2000) Digital mapping systems for field data collection. *Digital Mapping Techniques 2002, Workshop Proceedings, USGS, Open-File Report 00-325*.
- Krantz, R.W. (1988) Multiple fault sets and three-dimensional strain: theory and application. *Journal of Structural Geology*, 10, 225-237.
- Krantz, R.W. (1989) Orthorhombic fault patterns: the odd axis model and slip vector orientations. *Tectonics*, 8, 483-495.
- Laubach, S.E. & Marshak, S. (1987) Fault patterns generated during extensional deformation of crystalline basement, NW Scotland. In: Coward, M.P., Dewey, J.F. & Hancock, P.L. (Eds.), *Continental Extensional Tectonics*, Geological Society of London Special Publication 28, 495-499.
- Lee, M.J. & Hwang, Y.J. (1993) Tectonic evolution and structural styles of the East Shetland Basin. In: Parker, J.R. (Ed.), *Petroleum Geology of Northwest Europe: Proceedings from the 4<sup>th</sup> Conference*, Geological Society London, UK, 1137-1149.
- Le Pichon, X., & Hayes, D.E. (1971) Marginal offsets, fracture zones and the early opening of the South Atlantic. *Journal of Geophysical Research*, 76, 6283-6293.
- Lister, G.S., Etheridge, M.A. & Symonds, P.A. (1986) Detachment faulting and the evolution of passive continental margins. *Geology*, 14, 246-250.
- Lister, G.S., Etheridge, M.A. & Symonds, P.A. (1991) Detachment models for the formation of passive continental margins, *Tectonics*, 10, 1038-1064.
- Lloyd, G. E. & Knipe, R. J. (1992) Deformation mechanisms accommodating faulting of quartzite under upper crustal conditions. *Journal of Structural Geology* 14, 127-143.
- Logan J.M., Dengo C.A., Higgs N.G. & Wang Z.Z. (1992) Fabrics of experimental fault zones: their development and relationship to mechanical behaviour. In: Evans B. & Wong T.F. (Eds.), *Fault mechanics and transport properties of rocks*, Academic Press, London, 33-67.
- Longley, P.A., Goodchild, M.F., Maguire, D.J. & Rhind, D.W. (2001) *Geographic information systems and science*. Wiley, Chichester, 454 pp.
- Lundin, E.R. & Doré, A.G. (1997) A tectonic model for the Norwegian passive margin with implications for the NE Atlantic: early Cretaceous to break-up. *Journal of the Geological Society (London)*, 154, 545-550.
- 
- Lundin, E.R. & Doré, A.G. (2005) NE Atlantic break-up: a re-examination of the Iceland plume model and the Atlantic – Arctic linkage. In: Doré, A.G. & Vining,

## References

- B.A. (Eds.): Petroleum geology of Northwest Europe and Global Perspectives, Proceedings of the 6<sup>th</sup> Conference. Geological Society, London, 2, 739-754.
- Løseth, T. & Tveten, E. (1996) Post-Caledonian structural evolution of the Lofoten and Vesterålen offshore and onshore areas, *Norsk Geologisk Tidsskrift*, 76, 215-230.
- McIntyre et al., (1956) On the Conglomerate of supposed Old Red Sandstone are near Tongue, Sutherland. *Transactions of the Royal Society of Glasgow*, 22, 35-47.
- Maerten, L. (2000) Variation in slip on intersecting normal faults: implications for palaeostress inversion. *Journal of Geophysical Research*, 105, 25553-25565.
- Maerten, L., Pollard, D.D. & Maerten, F. (2001) Digital mapping of three-dimensional structures of the Chimney Rock fault system, central Utah. *Journal of Structural Geology*, 23, 585-592.
- Mallet, J.L. (1992) GOCAD: a computer aided design program for geological applications. In: Turner, A.K. (Ed.) *Three-dimensional modelling with Geoscientific Information Systems*. NATO ASI series C: Mathematical and Physical Sciences, 354, 123-141.
- Mann, P., Hempton, P.R., Bradley, D.C. & Burke, K. (1983) Development of pull-apart basins. *Journal of Geology*, 91, 529-554.
- Marker, M., Mengel, F., van Gool, J. & field party (1995) Evolution of the Palaeoproterozoic Nagssugtoqidian orogen: DLC investigations in West Greenland. *Rapport Grønlands Geologiske Undersøgelse* 165, 100-105.
- Marrett R. & Allmendinger R.W. (1990) Kinematic analysis of fault-slip data. *Journal of Structural Geology*, 12, 973-986.
- Marrett R. & Peacock D. (1999) Strain and stress. *Journal of Structural Geology*, 21, 1057-1063.
- McCaffrey, K.J.W. & Johnston, J.D. (1996) Fractal analysis of a mineralized vein deposit; Curraghinalt gold deposit, County Tyrone. *Mineralium Deposita*, 31, 52-58.
- McCaffrey, K.J.W., Holdsworth, R.E., Clegg, P., Jones, R.R. & Wilson, R.W. (2003a) Using Digital Mapping Tools and 3D visualisation to Improve Undergraduate fieldwork. *PLANET*, 5, 34-37.
- McCaffrey, K.J.W., Sleight, J.M., Pugliese, S. & Holdsworth, R.E. (2003b) Fracture formation and evolution in crystalline rocks: Insights from attribute analysis. In: Petford, N. & McCaffrey, K.J.W. (Eds.), *Hydrocarbons in Crystalline Rocks*, Geological Society Special Publication, 214, 109-124.
- McCaffrey, K.J.W., Jones, R.R., Holdsworth, R.E., Wilson, R.W., Clegg, P., Imber, J., Holliman, N. & Trinks, I. (2005) ~~Unlocking the spatial dimension: digital technologies and the future of geoscience fieldwork.~~ *Journal of the Geological Society (London)*, 162, 927-938.

## References

- McClay, K. (1987) *The Mapping Geological Structures*. Geological Society of London Handbook Series, Open University Press, Milton Keynes.
- McClay, K.R. & White, M. (1995) Analogue models of orthogonal and oblique rifting. *Marine and Petroleum Geology*, 12, 137-151.
- McClay, K.R., Dooley, T., Whitehouse, P. & Mills, M. (2002) 4D evolution of rift systems: insights from scaled physical models, *American Association of Petroleum Geologists Bulletin*, 86, 935-959
- McCoss, A..M.. (1986) Simple constructions for deformation in transpression/transtension zones. *Journal of Structural Geology*, 8, 715-718.
- McGuire, P.C., et al. (2005) Field geology with a wearable computer: first results of the Cyborg Astrobiologist system. *Proceedings of ICINCO 2005, 2<sup>nd</sup> international conference on Informatics in Control, Automation and Robotics*, 14-17 September 2005, Barcelona, Spain.
- McNoleg, O. (1996) The integration of GIS, remote sensing, expert systems and adoptive co-kriging for environmental habitat modelling for the Highland Haggis using object oriented, fuzzy logic and neural network techniques. *Computers and Geosciences*, 22, 585-588.
- Means, W.D. (1976) *Stress and strain: basic concepts of continuum mechanics for geologists*. Springer-Verlag, New York, 339 pp.
- Meisling, K., Cobbold, P.R. & Mount, V.S. (2001) Segmentation of an obliquely rifted margin, Campos and Santos basins, southeastern Brazil. *American Association of Petroleum Geologists Bulletin*, 85, 1903-1924.
- Michael, A.J. (1984) Determination of stress from slip data: faults and folds. *Journal of Geophysical Research*, 89, 11517-11526.
- Mjelde, R., Shimamura, H., Kanazawa, T., Kodaira, S., Raum, T. & Shiobara, H. (2003) Crustal lineaments, distribution of lower crustal intrusives and structural evolution of the Vøring Margin, NE Atlantic; new insight from wide-angle seismic models. *Tectonophysics*, 369, 199-218.
- Mokhtari, M. & Pegrum, R. (1992) Structure and evolution of the Lofoten continental margin, offshore Norway. *Norsk Geologisk Tidsskrift*, 72, 339-355.
- Moody, J. D. & Hill, M. J. (1956) Wrench fault tectonics. *Bulletin of the Geological Society of America*, 67, 1207-1246.
- Morley, C.K., Nelson, R.A., Patton, T.L. & Munn S.G. (1990) Transfer zones in the East African Rift system and their relevance to hydrocarbon exploration in rifts. *American Association of Petroleum Geologists Bulletin*, 74, 1234-1253.
- Morley, C.K. (1999) How successful are analogue models in addressing the influence of pre-existing fabrics on rift structure? *Journal of Structural Geology*, 21, 1267-1274.

## References

- Morley, C.K., Haranya, C., Phoosongsee, W., Pongwapee, S., Kornawan, A. & Wonganan, N. (2004) Activation of rift oblique and parallel pre-existing fabrics during extension and their effect on deformation style: examples from the rifts of Thailand. *Journal of Structural Geology*, 26, 1803-1829.
- Mosar, J. (2003) Scandinavia's North Atlantic passive margin. *Journal of Geophysical Research*, 108 (B8), 2360, doi:10.1029/2002JB002134.
- Mosar, J., Eide, E.A., Osmundsen, P.T., Sommaruga, A. & Torsvik, T.H. (2002) Greenland-Norway separation: A geodynamic model for the North Atlantic. *Norwegian Journal of Geology*, 82, 281-298.
- Muir Wood, R. & Mallard, D.J. (1992) When is a fault 'extinct?' *Journal of the Geological Society (London)*, 149, 251-256.
- Nelson, R.A., Patton, T.L. & Morley, C.K. (1992) Rift-segment interaction and its relation to hydrocarbon exploration in continental rift systems. *American Association of Petroleum Geologists Bulletin*, 76, 1153-1169.
- Nieto-Samaniego, A.F. (1999) Stress, strain and fault patterns. *Journal of Structural Geology*, 21, 1065-1070.
- Nieto-Samaniego, A.F. & Alaniz-Alvarez, S.A. (1995) Influence of the structural framework on the origin of multiple fault patterns. *Journal of Structural Geology*, 17, 1571-1577.
- Nieto-Samaniego, A.F. & Alaniz-Alvarez, S.A. (1997) Origin and tectonic interpretation of multiple fault patterns. *Tectonophysics*, 270, 197-206.
- Norton, M.G., McClay, K.R. & Way, N.A. (1987) Tectonic evolution of Devonian basins in Northern Scotland and Southern Norway. *Norsk Geologisk Tidsskrift*, 67, 323-338.
- O'Driscoll, E.S.T. (1980) The double helix in global tectonics. *Tectonophysics*, 63, 397-417.
- Oertel, G. (1965) The mechanics of faulting in clay experiments, *Tectonophysics*, 2, 343-393.
- Oldow, J.S. (2003) Active transtensional boundary zone between the western Great Basin and the Sierra Nevada block, western U.S. Cordillera. *Geology*, 31, 1033-1036
- O'Leary, D.W., Freidman, J.D. & Pohn, H.A. (1976) Lineaments, linear, lineation: some proposed new names and standards. *Geological Society of America Bulletin*, 87, 1463-1469.
- Olesen, N.Ø. (1984) 1:100 000 scale geological map sheet 67 V.1. Nord, Agto. *Geology of Greenland Survey*.

## References

- Olesen, O., Henkel, H., Kaada, K. & Tveten, E. (1991) Petrophysical properties of a prograde amphibolite-granulite facies transition zone at Sigerfjord, Vesterålen, northern Norway. *Tectonophysics*, 192, 33-39.
- Olesen, O., Torsvik, T.H., Tveten, E., Zwaan, K.B., Løseth, T. & Henningsen, T. (1997) Basement structure of the continental margin in Lofoten-Lopphavet area, northern Norway: constraints from potential field data, on-land structural mapping and palaeomagnetic data. *Norrsk Geologisk Tidsskrift*, 77, 15-30.
- Olesen, O., Lundin, E.R., Nordgulen, O., Osmundsen, P.T., Skilbrei, J.R., Smethurst, M.A., Solli, A., Bugge, T. & Fichler, C. (2002) Bridging the gap between the onshore and offshore geology in Nordland, northern Norway. *Norwegian Journal of Geology*, 82, 243-262.
- Olesen, O., Ebbing, J., Lundin, E., Skilbrei, J.R., Torsvik, T.H., Hansen, E.K., Henningsen, T., Midbøe, P. & Sand, M. (2005) A new tectonic model for the Eocene opening of the Norwegian-Greenland Sea - simplified geology by using modern aeromagnetic data, paper presented at the EGU 2<sup>nd</sup> General Assembly, Vienna, Austria, 24-29 April, EGU05-A-02692
- Olsen, J.C. (2005) The Baffin and Labrador Seas – new tectonic models and exploration opportunities between Greenland and Canada. American Association of Petroleum Geologists annual convention, Calgary, Canada, June 19-22, 2005.
- O'Reilly, K.J. (1983) Composition and age of the conglomerate outliers around the Kyle of Tongue, north Sutherland, Scotland. *Proceedings of the Geologists' Association*, 94, 53-64.
- Ottesen, T.G. (1991) Preliminary seismic study of part of the pre-Palaeocene section offshore southern West Greenland between 66N and 68N. *Grønlands Geologiske Undersøgelse open file series 91/6*.
- Park, R.G. (1991) The Lewisian Complex. In: Craig, G.Y. (Ed.), *Geology of Scotland*, 3<sup>rd</sup> edition, Geological Society London, 25-64.
- Park, R.G. & Tarney, J. (1987) The Lewisian Complex: a typical Precambrian high-grade terrain? In: Park, R.G. & Tarney, J. (Eds.), *Evolution of the Lewisian and Comparable Precambrian High Grade Terrains*, Geological Society of London Special Publication 27, 13-25.
- Paton, D.A. & Underhill, J.R. (2004) Role of crustal anisotropy in modifying the structural and sedimentological evolution of extensional basins: the Gamtoos Basin, South Africa. *Basin Research*, 16, 339-359.
- Peach, B.N., Horne, J., Gunn, W., Clough, C.T. & Hinxman, L.W. (1907) The geological structure of the Northwest Highlands of Scotland. *Memoir of the Geological Survey London, U.K.*, 668 pp.
- Peacock, D.C.P. & Sanderson, D.J. (1992) Effects of layering and isotropy on fault geometry. *Journal of the Geological Society (London)*, 149, 793-802.

## References

- Petit, J.P. (1987) Criteria for the sense of movement on fault surfaces in brittle rocks. *Journal of Structural Geology*, 9, 597–608.
- Piazolo, S., Alsop, G.I., Møller Nielsen, B. & van Gool, J.A.M. (2004) The application of GIS to unravel patterns of deformation in high grade terranes: a case study of indenter tectonics from west Greenland. In: Alsop, G.I., Holdsworth, R.E., McCaffrey, K.J.W., Hand, M. (Eds.), *Flow processes in faults and shear zones*, Geological Society of London Special Publication 224, 63-78.
- Pinheiro, R.V.L. & Holdsworth, R.E. (1997) Reactivation of Archaean strike-slip fault systems, Amazon region, Brazil. *Journal of the Geological Society (London)*, 154, 99-104.
- Planke, S. et al. (Eds.) (2004) *Geophysical Atlas of the West Greenland Basins: integrated seismic, gravity and magnetic interpretation*. VBPR, TGS-Nopec and GEUS.
- Platou, S.W. (1971) An electronic data processing system for geological field and laboratory data, the E.D.P. system AGTO. *Gronlands Geologiske Undersøgelse*. ITS Rapport 39.
- Pollard, D.D., Saltzer, S.D., & Rubin, A.M. (1993) Stress inversion methods: are they based on faulty assumptions? *Journal of Structural Geology*, 15, 1045-1054.
- Pollard D.D., Peacock D., & Marrett R. (1999) Strain and stress; discussion and reply. *Journal of Structural Geology*, 22 (9), 1359-1378.
- Potts, G.J. & Reddy, S.M. (1999) Construction and systematic assessment of relative deformation histories. *Journal of Structural Geology*, 21, 1245-1254.
- Potts, G.J. & Reddy, S.M. (2000) Application of younging tables to the construction of relative deformation histories – 1: Fracture systems. *Journal of Structural Geology*, 22, 1473-1490.
- Pringle, J.K., Westerman, A.R., Clark, J.D., Drinkwater, N.J. & Gardiner, A.R. (2004) 3D high-resolution digital models of outcrop analogue study sites to constrain reservoir model uncertainty: an example from Alport Castles, Derbyshire, UK. *Petroleum Geoscience*, 10, 343-352.
- Pundt, H. & Brinkkotter-Runde, K. (2000) Visualisation of spatial data for field based GIS. *Computers & Geosciences*, 26, 51-56.
- Ramberg, H. (1949) On the petrogenesis of the gneiss complexes between Sukkertoppen and Christianshaab, West Greenland. *Meddelinger Dansk Geologisk Forening*, 11, 312–327.
- Ramsay, J.G. & Huber, M.I. (2002) *The Techniques of Modern Structural Geology*, Volumes 1-2. Academic Press, London, 700 pp.
- Ramsay, J.G. & Lisle, R.J. (2000) Fault slip analysis and stress tensor calculations: Session 32. In: *The Techniques of Modern Structural Geology*. Volume 3:

## References

- Applications of Continuum Mechanics in Structural Geology, Academic Press, London, 785-810.
- Ranalli, G. & Yin, Z.M. (1990) Critical stress difference and orientation of faults in rocks with strength anisotropies: the two dimensional case. *Journal of Structural Geology*, 12, 1067-1071.
- Rasmussen, T.M. & van Gool, J.A.M. (2000) Aeromagnetic survey in southern West Greenland: project Aeromag 1999. *Geology of Greenland Survey Bulletin*, 186, 73-77.
- Redfield, T.F., Osmundsen, P.T. & Hendricks, B.W.H. (2005) The role of fault reactivation and growth in the uplift of western Fennoscandia, *Journal of the Geological Society (London)*, 162, 1013-1030.
- Reches, Z. (1978) Analysis of faulting in a three-dimensional strain field. *Tectonophysics*, 47, 109-129.
- Reches, Z. (1987) Determination of the tectonic stress tensor from slip along faults that obey the Coulomb yield condition. *Tectonics*, 6, 849-861.
- Ren, S., Faleide, J.I., Eldholm, O., Skogseid, J. & Gradstein, F. (2003) Late Cretaceous-Paleocene tectonic development of the NW Vøring Basin. *Mar. Pet. Geol.*, 20, 177-206.
- Rhind, D. W. (1971) The production of a multi-colour geological map by automated means. *Nachrichten aus dem Karten- und Vermessungswesen, Reihe 1*, #52:47-51.
- Rhind, D. W. (1973) Computer mapping of drift lithologies from borehole records. Report of the institute of geological sciences, 73/6, HMSO, London.
- Rhind, D.W. (1992) Spatial data handling in the geosciences. In: Turner, A.K. (Ed.), *Three-dimensional modelling with geographic information systems*. NATO ASI series C, Mathematical and Physical Sciences, Kluwer Academic, Dordrecht 334, 13-27.
- Rives, T., Razack, M., Petit, J.P. & Rawnsley, K.D. (1992) Joint spacing: analogue and numerical simulations, *Journal of Structural Geology*, 14, 925-937.
- Roberts, A.M. & Holdsworth, R.E. (1999) Linking onshore and offshore structures: Mesozoic extension in the Scottish Highlands. *Journal of the Geological Society (London)*, 156, 1061-1064.
- Rock, N.M.S., Gaskarth, J.W., Henney, P.J. & Shand, P. (1988) Late Caledonian dyke swarms of northern Britain; some preliminary petrogenic and tectonic implications of their distributions and chemical variations. *Canadian Mineralogist*, 26, 3-22.
- Roest, W.R. & Stivastava, S.P. (1989) Sea-floor spreading in the Labrador Sea: a new reconstruction. *Geology* 17, 1000-1003.
- Rogers, D. A., Marshall, J. E. A. & Astin, T. R. (1989) *Devonian and Later Movements*



## References

- On the Great Glen Fault System, Scotland. *Journal of the Geological Society (London)*, 146, 369-372.
- Rosenberg, L.I. (2004) Investigating the San Simeon earthquake using ArcPad and GPS. *Digital Mapping Techniques 2004, Workshop Proceedings, USGS, Open-File Report 2004-1451*.
- Rosendahl, B.R. (1987) Architecture of continental rifts with special reference to East Africa. *Annual Review of Earth and Planetary Science*, 15, 445-503.
- Rumph, B., Reaves, C.M., Orange, V.G. & Robinson, D.L. (1993) Structuring and transfer zones in the Faeroe Basin in a regional context. In: Parker, J.R (Ed.), *Petroleum Geology of Northwest Europe: Proceedings from the 4<sup>th</sup> Conference*, Geological Society London, UK, 999-1009.
- Sabins, F.F. (1987) *Remote Sensing; Principals and interpretation*. W.H. Freeman, New York.
- Sagy, A., Reches, Z. & Agnon, A. (2003) Hierarchic three-dimensional structure and slip partitioning in the western Dead sea pull-apart. *Tectonics*, 22, 10.1029/2001TC0013223.
- Sampson, R.J. & Davis, J.C. (1966) FORTRAN II trend-surface program with unrestricted input for the IBM 1620 computer. Special distribution publication 26, Lawrence KS: State Geological Survey.
- Sanderson, D.J. & Marchini, W.R.D. (1984) Transpression. *Journal of Structural Geology* 6, 449-458.
- Schetselaar, E.M. (1995) Computerized field-data capture and GIS analysis for generation of cross sections in 3-D perspective views. *Computers & Geosciences*, 21, 687-701.
- Schreurs, G. & Colletta, B. (1998) Analogue modelling of faulting in zones of continental transpression and transtension. In: Holdsworth, R.E., Strachan, R.A., & Dewey J.F. (Eds.), *Continental Transpressional and Transtensional Tectonics*, Geological Society Special Publication 135, 59-79.
- Schlische R.W., Withjack, M.O., & Eisenstadt, G. (2002) An experimental study of the secondary deformation produced by oblique-slip normal faulting. *American Association of Petroleum Geologists Bulletin*, 86, 885-906.
- Sellevoll, M.A. (1983) The study of the Earth in the island area of Lofoten-Vesterålen, northern Norway. *Norges geologiske undersøkelse*, 380, 235-243.
- Seranne, M. (1992) Devonian extensional tectonics versus Carboniferous inversion in the northern Orcadian basin. *Journal of the Geological Society (London)*, 149, 27-37.
- Serra, S. & Nelson, R.A. (1988) Clay modelling of rift asymmetry and associated structures. *Tectonophysics*, 153, 307-312.

## References

- Shaw, S.H. (1972) Automated geological cartography. Commonwealth Geological Liaison Office, London, report: CGLO LR 116.
- Sherlock, S.C. (2001) Two stage erosion and deposition in a continental margin setting: An  $^{40}\text{Ar}/^{39}\text{Ar}$  laserprobe study of offshore detrital white micas in the Norwegian Sea. *Journal of the Geological Society (London)*, 158, 793-799.
- Sibson, R. H. (1977) Fault rocks and fault mechanisms. *Journal of the Geological Society (London)*, 133, 191-213.
- Sibson R.H. (1985) A note on fault reactivation. *Journal of Structural Geology*, 7, 751-754.
- Sibson, R.H. (1995) Continental fault structure and shallow earthquake source. *Journal of the Geological Society (London)*, 140, 741-767.
- Skogseid, J., T. Pedersen, O. Eldhom, and B.T. Larsen (1992), Tectonism and magmatism during NE Atlantic continental break-up, the Vøring margin. In: Storey, B.C., Alabaster, T. & Pankhurst, R.J. (Eds.), *Magmatism and the cause of continental break-up*, Geological Society Special Publication, 68, 305-320.
- Skogseid, J., Planke, S., Faleide, J.I., Pedersen, T., Eldhom, O. & Neverdal, F. (2000) NE Atlantic continental rifting and volcanic margin formation. In: Nøttvedt, A. (Ed.), *Dynamics of the Norwegian Margin*, Geological Society Special Publication 167, 295-326.
- Sleight, J.M. (2001) Fracture characteristics from two reactivated basement fault zones: Examples from Norway and Scotland, Unpublished PhD thesis, University of Durham, UK, 310 pp.
- Smith, J.V. & Durney, D.W. (1992) Experimental formation of brittle structural assemblages in oblique divergence. *Tectonophysics*, 216, 235-253.
- Smith, M.J. (2005) The Journal of Maps: an electronic journal for presentation and dissemination of map based data. *Journal of Maps*, v2005, 1-6.
- Smith, W. (1815) *A Delineation of the Strata of England and Wales, with Part of Scotland*.
- Snyder, D.B. (1990) The Moine Thrusts in the BIRPS data set. *Journal of the Geological Society (London)*, 147, 81-86.
- Snyder, D.B., England, R.W. & McBride, J.H. (1997) Linkage between mantle and crustal structures and its bearing on inherited structures in northwestern Scotland. *Journal of the Geological Society (London)*, 154, 79-84.
- Sonder, R.A. (1956) *Mechanik der Erde*. E. Schweizerbart'sche Verlagsbuchhandlung, Stuttgart, Germany.
- Song, T., Cawood, P. A. & Middleton, M. (2001) Transfer zones normal and oblique to rift trend: examples from the Perth Basin, Western Australia In: Wilson, R. C. L.,

## *References*

- Whitmarsh, R. B., Taylor, B. & Froitzheim, N. (Eds.), Non-volcanic rifting of continental margins: a comparison of evidence for land and sea. Geological Society Special Publication 187, 475-488.
- Soper, N.J. & Woodcock, N.H. (2003) The lost Lower Old Red Sandstone of England and Wales: a record of post-Iapetan flexure or Early Devonian transtension? *Geological Magazine*, 140, 627-647.
- Sorenson, J.H. & Buchanan, R.C. (1990) Referencing and archiving digitally produced maps at the Kansas Geological Survey. *Geoscience Information Society newsletter*, 126, 9-10.
- Sperner, B., Ratschbacher, L. & Ott, R. (1993) Fault-Striae analysis: a Turbo Pascal program package for graphical presentation and reduced stress tensor calculation. *Computers & Geosciences*, 19, 1361-1388.
- Sperner, B., Müller, B., Heidbach, O., Delvaux, D., Reinecker, J. & Fuchs, K. (2003) Tectonic stress in the Earth's crust: advances in the World stress map project. In: Nieuwland, D.A. (Ed.), *New Insights into Structural Interpretation and Modelling*. Geological Society Special Publication, 212, 101-116.
- Speight, J.M. & Mitchell, J.G. (1979) The Permo-Carboniferous dyke-swarm of northern Argyll and its bearing on dextral displacement on the Great Glen Fault. *Journal of the Geological Society (London)*, 136, 3-11.
- Srivastava, S.P. (1983) Davis Strait: structures, origin and evolution. In: Bott, M.H.P., Saxov, S., Talwani, M., Thiede, J. (Eds.), *Structure and development of the Greenland – Scotland Ridge: new methods and concepts*. Plenum, New York, 159-189.
- Steel, R.J. & Wilson, A.C. (1975) Sedimentation and tectonism (?Permo-Triassic) on the margin of the North Minch Basin, Lewis. *Journal of the Geological Society (London)*, 131, 183-202.
- Stein, A.M. (1988) Basement controls upon basin development in the Caledonian foreland, NW Scotland. *Basin Research*, 1, 107-119.
- Stein, A.M. & Blundell, D.J. (1990) Geological inheritance and crustal dynamics of the northwest Scottish continental shelf. *Tectonophysics*, 173, 455-467.
- Steinitz, C., Parker, P. & Jordan, L. (1976) Hand drawn overlays: their history and perspective uses. *Landscape Architectures*, 66, 444-455.
- Steltenpohl, M.G., Hames, W.E. & Andresen, A. (2004) The Silurian to Permian history of a metamorphic core complex in Lofoten, northern Scandinavian Caledonides. *Tectonics*, 23, TC1002, doi: 10.1029/2003TC001522.
- Stewart I.S. & Hancock P.L. (1994) Neotectonics. In: Hancock P.L. (Ed.), *Continental Deformation*. Pergamon press, Oxford, 370-409.

## References

- Stoker, M.S., Hitchen, K. & Graham, C.C. (1993) The Geology of the Hebrides and West Shetland shelves, and adjacent deep-water areas. United Kingdom offshore regional report. HMSO, London for the British Geological Survey.
- Soller, D.R. (Ed.) Proceedings of a Workshop on Digital Mapping Techniques: Methods for Geologic Map Capture, Management and Publication. USGS, Open File report, 97-269.
- Storey, M., Duncan, R.A., Pedersen, A.K., Larsen, L.M. & Larsen, H.C. (1998)  $^{40}\text{Ar}/^{39}\text{Ar}$  geochronology of the West Greenland Tertiary volcanic province. *Earth and Planetary Science Letters*, 160, 569–586.
- Struik, L.C., Atrens, A. & Haynes, A. (1991) Hand-held computer as a field notebook and its integration with the Ontario Geological Survey's 'FIELDLOG' program. *Geological Survey of Canada, current research, part A*, 91-1A, 279-284.
- Strömberg, A. (1976) A pattern of tectonic zones in the western part of the East European Platform. *Geologiska Föreningens i Stockholm Förhandlingar*, 98, 227-243.
- Sutton, J. & Watson, J. V. (1986) Architecture of the continental lithosphere. *Philosophical Transactions of the Royal Society, London A317*, 5-12.
- Sykes, L.R. (1978) Intraplate seismicity, reactivation of pre-existing zones of weakness, alkaline magmatism and other tectonism post-dating continental fragmentation. *Reviews of Geophysics and Space Physics*, 16, 621-688.
- Sylvester, A.G. (1988) Strike-slip faults. *Bulletin of the Geological Society of America*, 100, 1666-1703.
- Sørensen, K. (1983) Growth and dynamics of the Nordre Strømfjord shear zone. *Journal of Geophysical Research*, 88, 3419-3437.
- Talwani, M. & Eldholm, O. (1977) Evolution of the Norwegian –Greenland Sea. *Geological Society of America Bulletin*, 83, 969-999.
- Taylor, B., Crook, K. & Sinton, J. (1994) Extensional transform zones and oblique spreading centres. *Journal of Geophysical Research*, 99, B10, 19707-19718.
- Teso, R.R., Poe, M.P., Younglove, T., & McCool, P.M. (1996) Use of logistic regression and GIS modelling to predict groundwater vulnerability to pesticides. *Journal of Environmental Quality*, 25, 425-432.
- Teufel, L.W. & Clark, J.A. (1984) Hydraulic fracture propagation in layered rock: experimental studies of fracture containment. *Society of Petroleum Engineers Journal*, 24, 19-32.
- Teysier, C. & Tikoff, B. (1999) Fabric stability in oblique convergence and divergence. *Journal of Structural Geology*, 21, 969-974.

## References

- Thomson, K. & Underhill, J.R. (1993) Development and evolution of structural styles in the Inner Moray Firth. In: Parker, J.R. (Ed.): *Petroleum Geology of North-West Europe: Proceedings of the 4th Conference*, 1167-1178.
- Tikoff, B. & Teyssier, C. (1994) Strain modelling of displacement field partitioning in transpressional orogens, *Journal of Structural Geology*, 16, 1575-1588.
- Tikoff, B. & Wojtal, S.F. (1999) Displacement control of geologic structures. *Journal of Structural Geology*, 21, 959-967.
- Titus, S.J., Fossen, H., Pedersen, R.B., Vigneresse, J.L. & Tikoff, B. (2002) Pull-apart formation and strike-slip partitioning in an obliquely divergent setting, Leka Ophiolite, Norway. *Tectonophysics*, 354, 101-119.
- Tjia, H. D. (1971) Fault movement, reoriented stress field and subsidiary structures. *Pacific Geology*, 5, 49-70.
- Tavarnelli, E., Holdsworth, R.E., Clegg, P., Jones, R.R. & McCaffrey, K.J.W. (2004) The anatomy and evolution of a transpressional imbricate zone, Southern Uplands, Scotland. *Journal of Structural Geology*, 26, 1341-1360.
- Trinks, I., Clegg, P., McCaffrey, K.J.W., Jones, R.R., Hobbs, R., Holdsworth, R.E., Holliman, N., Imber, J., Waggott, S. & Wilson, R.W. (2005) Mapping and analysing virtual outcrops. *Visual Geosciences*, doi: 10.1007/s10069-005-0026-9.
- Tron, V. & Brun, J-P. (1991) Experiments on oblique rifting in brittle-ductile systems. *Tectonophysics*, 188, 71-84.
- Tsikalas, F., Faleide, J.I. & Eldholm, O. (2001) Lateral variations in tectono-magmatic style along the Lofoten-Vesterålen volcanic margin off Norway. *Marine & Petroleum Geology*, 18, 807-832.
- Tull, J.F., Bartley, J.M., Hodges, K.V., Andresen, A., Steltenpohl, M.G., & White, J.M. (1985) The Caledonides in the Ofoten region (68-69N), north Norway: Key aspects of tectonic evolution. In: Gee, D.G. & Sturt, B.A. (Eds.) *The Caledonian Orogen – Scandinavia and related areas*, John Wiley, Hoboken, N.J., 553-569.
- Turner, A.K. (1992) Three-dimensional modelling with Geoscientific Information Systems. NATO ASI series C: Mathematical and Physical Sciences, 354.
- Turner, A.K. (2000) Geoscientific modelling: past, present and future. In: Coburn, T.C., Yarus, J.M. (Eds.), *Geographical information systems in petroleum exploration and development*. American Association of Petroleum Geologists Computer Applications in Geology 4, 27-36.
- Tveten, E. (1978), *Geologisk kart over Norge, berggrunnskart SVOLVÆR 1:250,000, Norges Geologiske Undersøkelse*.
- Tveten, E. & Zwaan, K.B. (1993) *Geology of the coast-region from Lofoten to Loppa, with special emphasis on faults, joints and related structures*. Norges Geologiske Undersøkelse report 93.083,

## References

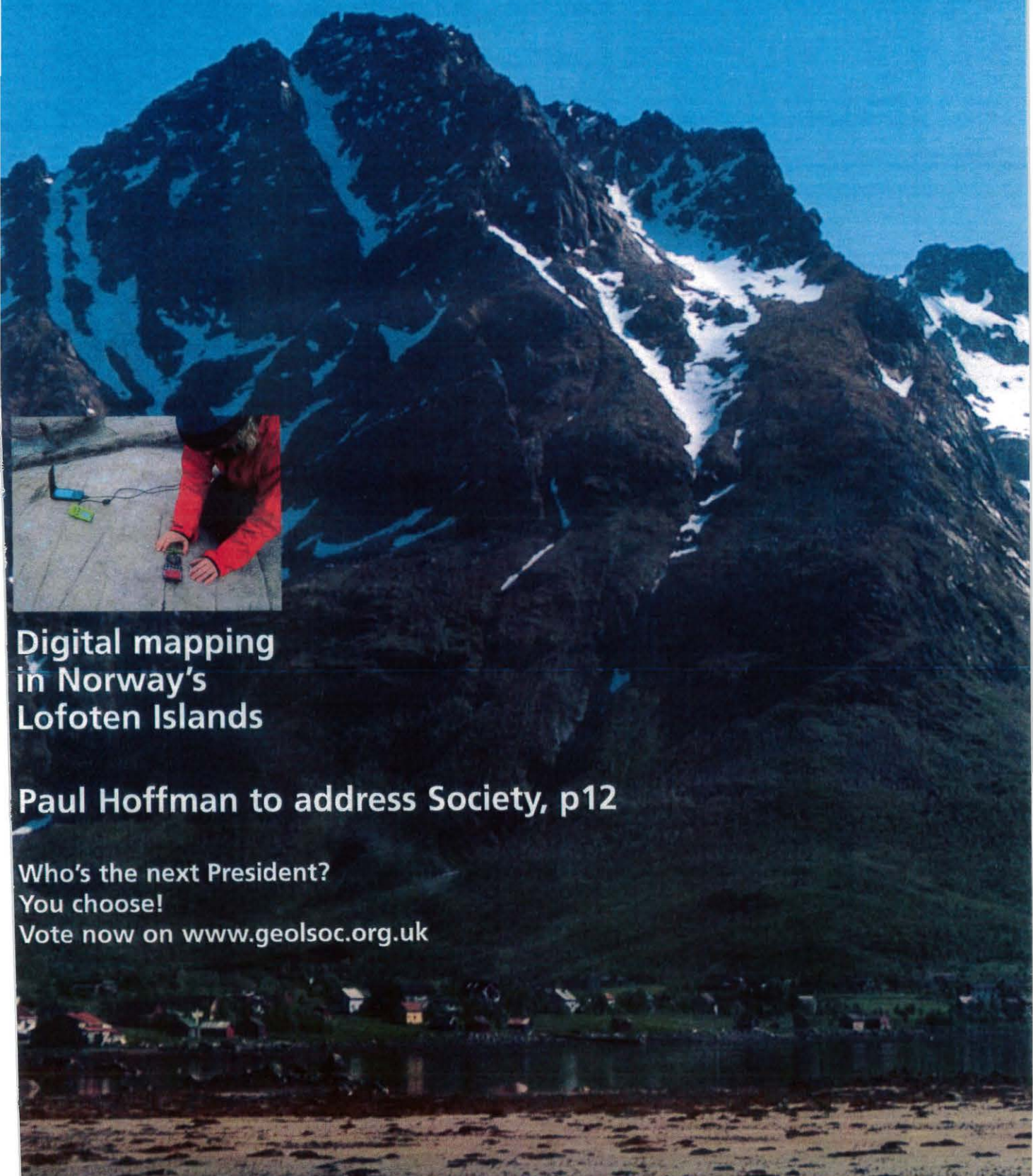
- Twiss, R.J. & Moores, E.M. (1992) *Structural Geology*. W.H. Freeman & Co., New York, 532 pp.
- Twiss, R.J. & Unruh, J.R. (1998) Analysis of fault slip inversions: do they constrain stress or strain rate? *Journal of Geophysical research*, 103, 12,205-12,222.
- van Gool, J., Marker, M., Mengel, F., and field party (1996) The Palaeoproterozoic Nagssugtoqidian orogen in West Greenland: current status of work by the Danish Lithosphere Centre. Report of activities, 1995. *Bulletin Grønlands Geologiske Undersøgelse*, 172, 88-94.
- van Gool, J.A.M., Connelly, J.N., Marker, M. & Mengel, F.C. (2002) The Nagssugtoqidian orogen of West Greenland: tectonic evolution and regional correlations from a West Greenland perspective. *Canadian Journal of Earth Sciences*, 39, 665–686.
- Vaughan, A.P.M. (1996) A tectonomagmatic model for the genesis and emplacement of Caledonian calc-alkaline lamprophyres. *Journal of the Geological Society (London)*, 153, 613-623.
- Waldron, J.W.F (2005) Extensional fault arrays in strike-slip and transtension. *Journal of Structural Geology*, 27, 23-34.
- Wallace, R.E. (1984) Patterns and timing of late Quaternary faulting in the Great Basin Province and relation to some regional tectonic features. *Journal of Geophysical Research*, 89, 5763-5769.
- Watson, J. (1983) Lewisian. In: Craig, G.Y. (Ed.) *Geology of Scotland*. Scottish Academic Press, Edinburgh.
- Wheeler, J. & Butler, R.W.H. (1994) Criteria for identifying structures related to true crustal extension in orogens. *Journal of Structural Geology*, 16, 1023-1027.
- Whittaker, R.C. (1995) A preliminary assessment of the structure, basin development and petroleum potential offshore central West Greenland. *Grønlands Geologisk Undersøgelse Open File Series 95/9*, 33 pp., 6 maps.
- Wilcox, R.E., Harding, T.P. & Seely, D.R. (1973) Basic wrench tectonics. *American Association of Petroleum Geologists Bulletin*, 57, 74-94.
- Wilson, R.C.L. & Williams, C.A. (1979) Oceanic transform structures and the development of Atlantic continental margin sedimentary basins – a review. *Journal of the Geological Society (London)*, 136, 311-320.
- Wilson, R.W., McCaffrey, K.J.W., Holdsworth, R.E., Jones, R.R., Imber, J. & Clegg, P. (2005) Lofoten has its Faults! Detailed fault analysis and 3D digital mapping in Norway's Lofoten Islands. *Geoscientist, Geological Society of London*, 15/2, 4-9.
- Wilson, R.W., Klint, K.E.S., van Gool, J.A.M., McCaffrey, K.J.W., Holdsworth, R.E. & Chalmers, J.A. (2006) Faults and fractures in central West Greenland: onshore

## *References*

- expression of continental break-up and sea-floor spreading in the Labrador-Baffin Bay Sea. Geological survey of Denmark and Greenland Bulletin, x, in press.
- Winchester, S. (2001) The map that changed the world. Viking, Penguin books Ltd., London, 338 pp.
- Withjack, M.O. & Jamison, W.R. (1986) Deformation produced by oblique rifting. *Tectonophysics*, 126, 99-124.
- Withjack, M.O., Schlische, R.W. & Olsen, P.E. (1998) Diachronous rifting, drifting and inversion on the passive margin of Central Eastern North America: an analogue for other passive margins. *American Association of Petroleum Geologists Bulletin*, 82, 817-835.
- Woodcock, N.H., 1986. The role of strike-slip systems at plate boundaries. *Philosophical Transactions of the Royal Society*, London, A317, 13-29.
- Xu, X., Battacharya, J.A., Davis, R.K. & Aiken, C.L.V. (2000) Digital Geological mapping of the Ferron Sandstone, Muddy Creek, Utah, with GPS and reflectorless Laser Rangefinders, *GPS Solutions*, 5, 15-23.
- Xue, Y., Cracknell, A.P. & Guo, H.D. (2002) Telegeoprocessing: the integration of remote sensing, Geographic Information Systems (GIS), Global Positioning System (GPS) and telecommunication. *International Journal of Remote Sensing*, 23, 1851-1893.
- Yamaji, A. (2003) Are the solutions of stress inversion correct? Visualization of their reliability and the separation of stresses from heterogeneous fault-slip data. *Journal of Structural Geology*, 25, 241-252
- Yin Z.M. & Ranalli G. (1992) Critical stress difference, fault orientation and slip direction in anisotropic rocks under non-Andersonian stress systems. *Journal of Structural Geology*, 14, 237-244.
- Youash, Y. (1969) Tension tests in layered rocks. *Geological Society of America Bulletin*, 80, 303-306.

# Geoscientist

the magazine of The Geological Society of London



**Digital mapping  
in Norway's  
Lofoten Islands**

**Paul Hoffman to address Society, p12**

**Who's the next President?  
You choose!  
Vote now on [www.geolsoc.org.uk](http://www.geolsoc.org.uk)**



# Lofoten has its

Detailed fault analysis and 3D digital mapping in the Norway's Lofoten Islands was a field research project funded by the Geological Society's Annie Greenly fund for detailed geological mapping. Robert Wilson, Ken McCaffrey, Richard Jones, Jonny Imber, Phill Clegg and Bob Holdsworth report on their work...

Lofoten does indeed have its faults, and it was these that principally drew us to this windswept archipelago, north of the Arctic Circle, off the west coast of Norway. The sea-approach is spellbinding, dominated by "Lofotenveggen" - the Lofoten Wall (picture) a 160km-long mountain ridge running out into the Norwegian Sea. Lofoten is a series of mountainous islands with many sharp peaks, rising to over 1000m. Late Cenozoic glaciation has shaped these lands into an 'Alpine' landscape, although here the familiar corries and hanging valleys descend straight in to the sea.

But there is more to the Lofoten islands than large mountains and breathtaking scenery. They mark a prominent NE-SW trending ridge, bounded on both sides by deep sedimentary basins (the Vestfjorden and Ribban Basins), which formed during the opening of the North Atlantic. Lofoten, and neighbouring islands in Vesterålen, are comprised of probably the youngest and oldest rocks on mainland Norway. The ridge is dominated by Precambrian basement gneisses (as old as 2.7Ga), while in the north, on the island of Andøya, Norway's only onshore examples of Jurassic and Cretaceous sediments are exposed.

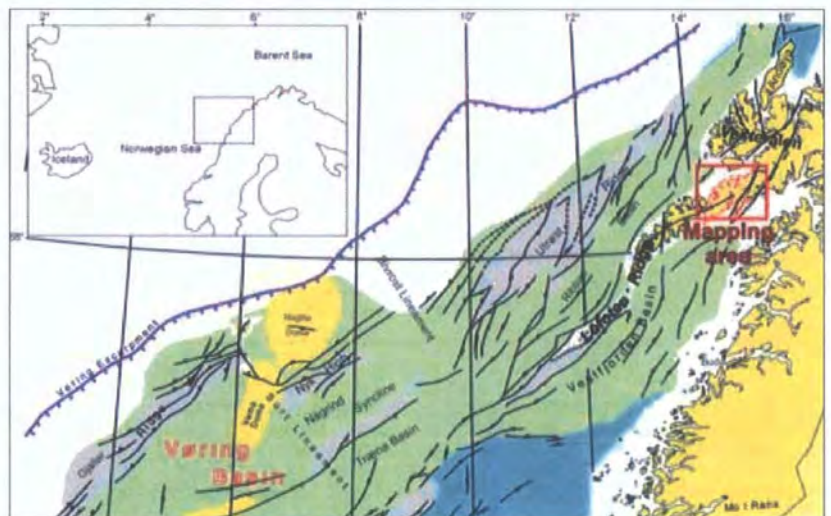


Figure 1. Location of the Lofoten mapping area, and its regional tectonic setting (after Blystad et al. 1995)

## Why go to Lofoten?

It has long been postulated that structures in basement rocks play a key role in the development and evolution of younger offshore basins. In the NE Atlantic margin, for example, where offshore fault patterns have been established from studies of 2D and 3D seismic data, many offshore basin-bounding faults can be traced onshore where their characteristics can be studied in more detail. The Lofotens represent one such area, where subsurface structures from the eastern margin of the Vøring Basin, can be traced onshore (Fig. 1).

Figure 2. Panoramic view of southern Austvågøya and "Lofotenveggen" ("the Lofoten Wall"), from Vesvågøya (looking N)



# faults!

Due to the severe climate, vegetation cover is limited on the islands and, combined with the effects of glaciation and dramatic relief, this provides the geologist with superb levels of outcrop exposure. Fault surfaces are exceptionally well displayed, and almost all show good indicators of fault-slip movement, in the form of striations and slickenfibres. Until now little detailed structural analysis of fault patterns, kinematics and geometries has been carried out on these exposed basin margin structures. In the offshore areas west of the Lofoten archipelago lies one of the last unexplored provinces on the Norwegian continental shelf, and according to the predictions of the Norwegian Petroleum Directorate, more than a quarter of total oil resources on the Norwegian Continental Shelf have yet to be discovered. Thus investigating the geological data recorded onshore could be of vital importance to future exploration offshore.

## Why go digital?

It is becoming increasingly common to see maps presented as digital data in Geographic Information Systems (GIS). Both the Ordnance Survey and the BGS provide their maps in a GIS format, and it is now commonplace to see digital maps used as part of the undergraduate curriculum in universities. Yet the field data that most people collect while making these maps is still largely based on paper maps and notebooks. Recent innovations in the use of handheld computers and Global Positioning Systems (GPS) have provided geologists with a whole new way of collecting their field data. Recent examples of this can be seen in recent past issues of *Geoscientist* – v14, 8 and v15, 1.

*article continues on page 8*

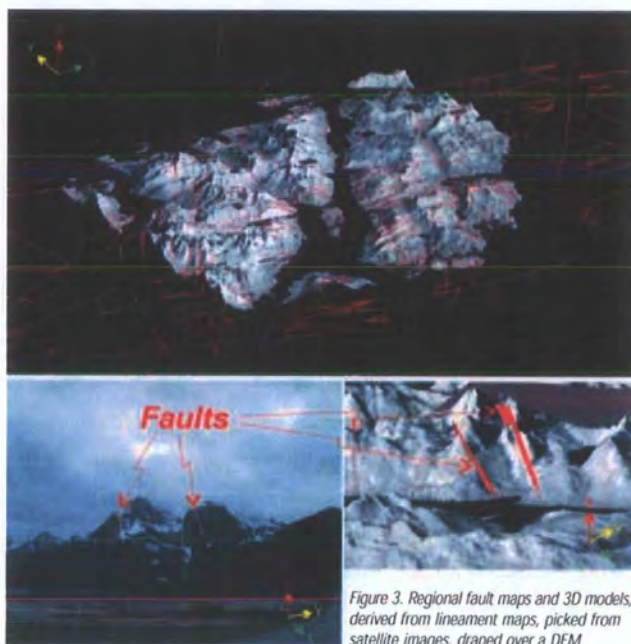


Figure 3. Regional fault maps and 3D models, derived from lineament maps, picked from satellite images, draped over a DEM

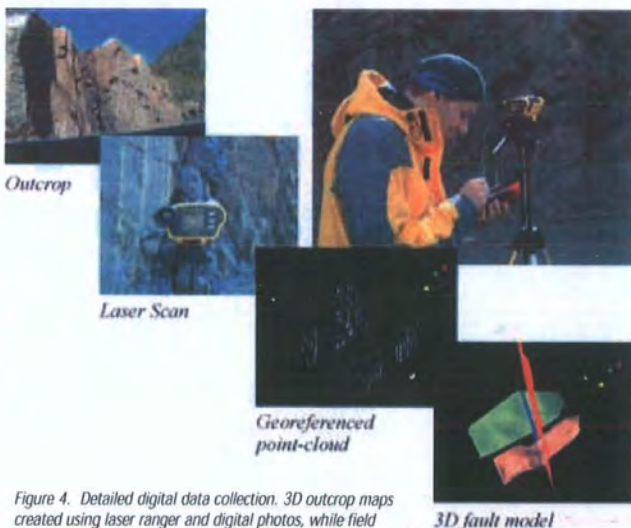


Figure 4. Detailed digital data collection. 3D outcrop maps created using laser ranger and digital photos, while field observations are recorded on a Pocket PC (top right)



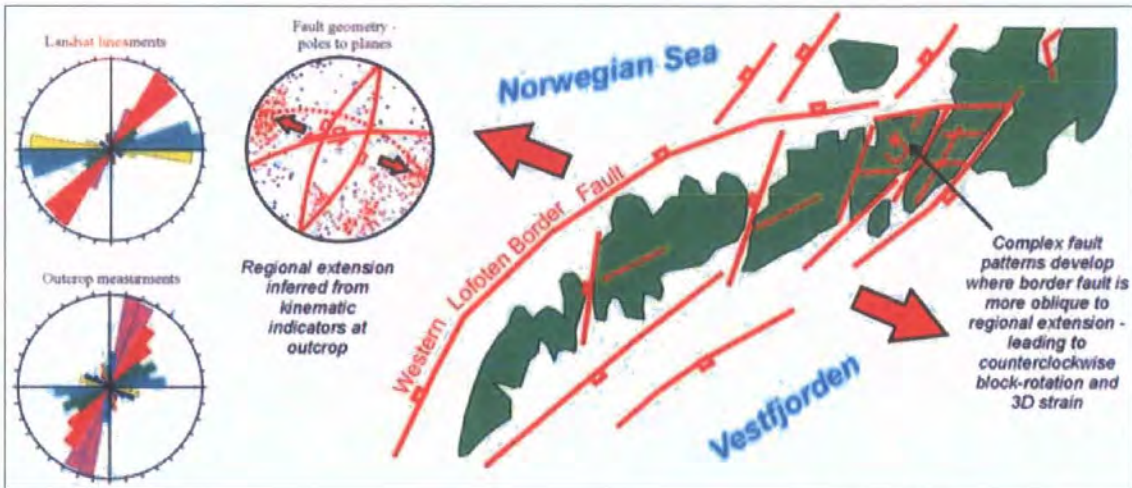


Figure 5. Summary of fault data recorded with overall interpretations

## Digital field mapping on a shoestring!

Many people might be put off trying out these new digital methods, as they seem an expensive alternative to traditional "map, compass and notebook methods". However this is now no longer the case; with the recent increase in popularity of Pocket PCs and GPS systems, prices are becoming more and more affordable. With a little shopping around it is now quite easy to set your self up with the vital equipment needed for digital field mapping with a budget of under £500!



The essential items required for a digital mapping exercise are: **Pocket PC** (from £170), **GPS** (from £75), a **data cable** (connects GPS to Pocket PC, from ~£15), **mapping software** (e.g. ArcPad 6 - £75, educational price, from ESR) and a **digital camera** (from £100). Optional extras include: **Ruggedised PDA case** (the Pocket PC is the most expensive item, therefore protecting it from adverse weather conditions and general wear and tear is advisable, from ~£30), **data storage cards** (for hard back up of data, ~£20). **Total budget: £485.** GIS software is also required on a desktop/ laptop computer for post processing and data analysis.

The Reactivation Research Group in Durham has pioneered a digital mapping system for Earth Scientists known as GAVA (Geospatial Acquisition, Visualisation and Analysis). Digital data acquisition is not a new concept, but it is only recently that the equipment and software have met the range of the field geologist's needs (portability, accuracy, power, versatility and cost). The equipment we used in Lofoten comprised: a pocket PC equipped with mobile GIS software (a digital field notebook and base map all rolled in to one!), a backpack-mounted differential-GPS (high accuracy, not so good on long treks), a handheld GPS (small, lightweight alternative to the DGPS better on long treks!), a laser rangefinder, and a digital camera.

Collecting GPS-located field data in a digital format has many benefits. Field-based GIS mapping tools allow the field data to be recorded both into a database and onto a map simultaneously. This leads to a much faster and efficient workflow from data collection through to analysis and visualisation. So much so that it offers the user real-time analysis of the data, giving the geologist the potential to visualize and analyse both collected data (i.e. outcrop measurements) and stored data (i.e. pre-existing maps and photos) while still standing on the outcrop. An additional advantage for our

Figure 6. Immersive 3D visualisation and analysis of digital data, using Schlumberger's Inside Reality™ software

Lofoten study is that the digital format means that the data are more compatible with interpretations derived from offshore data.

### Data collection and mapping

Lofoten's northernmost island, Austvågøya, was chosen as the main site for field mapping and data analysis. The purpose of the study was to investigate the geometry and kinematics of basement faults exposed in the area, and to produce detailed regional and outcrop 3D "maps" of these structures.

A high-accuracy fault database has been compiled in GIS, using DTMs (digital terrain models), satellite imagery, combined with field data collection using GPS/Laser rangefinder technologies. The field data collected consisted of structural measurements and observations, outcrop-scale maps, photographs, and rock sample data.

Regional lineament maps have been constructed using satellite imagery, and show NE-SW and ENE-WSW preferred orientations. Digital field mapping revealed similar preferred fault orientations at the outcrop scale, although it should be noted that the dominant NE-SW trend at outcrop is oriented ~20° counter-clockwise of that at the regional scale. This comparison however only takes into account fault orientation, and does not reflect the dip or overall geometry of the faults. So, to investigate further the scale invariance of these fault patterns, 3D fault maps have been constructed, using gOcad™ visualisation software, at both the regional and outcrop scales.

Draping our lineament maps over topographic models and fitting "fault planes" through the resulting linear traces can then generate regional models. Our outcrop models on the other hand are derived directly from X,Y,Z point data collected in the field using a laser rangefinder. These models are comparable with 3D fault models produced from geological interpretations of 2D and 3D seismic reflection data, but to a much higher resolution.

### Results and findings

We recorded over 600 fault measurements, and observed a range of fault geometries. Two main fault orientations became apparent - NNE-SSW and ENE-WSW. As mentioned earlier, there is a counter-clockwise trend of smaller faults relative to major structures. This would appear to indicate that extension was oblique to the major bounding structures along the Lofoten ridge. Slickenline analysis and cross-cutting relationships indicate that all fault sets are contemporaneous with one phase of WNW-ESE-orientated oblique extension.

Traditional interpretations of offshore seismic data would generally assume that the Lofoten islands formed as a simple uplift horst during extension orthogonal to the continental margin. The onshore data demonstrate, however, that it forms part of a moderately trans-tensional ridge system, leading to the formation of complex fault and fracture patterns. These small faults and fractures are likely to be present in the regions immediately offshore, but are well below the resolution of industry seismic data with important implications for petroleum plays and fluid flow pathways in the sub-surface. All the data collected here can be integrated with, and compared directly to, offshore data to improve fault and fracture models (which is the next step in this study!)

### Future work

Our first objective is to develop additional 3D models, which will allow us to constrain further our preliminary hypotheses for the fault structure of the Lofoten ridge in an outcrop through to regional scale 3D model. The next step will then be to integrate offshore models derived from seismic data from around the Lofoten Islands, thus creating a fully integrated onshore-offshore fault model. Our onshore 3D model benefits from the observed slip indicators, but the timings of movements are difficult to constrain. Offshore, temporal constraints are easily determined in regions where the sedimentation rate exceeds the fault displacement rate, but fault slip directions are usually inferred. Therefore, comparing onshore and offshore models has many benefits, and data in digital format will help to link them. Finally, we look forward to 'stepping inside' and exploring our 3D models with the installation of a new immersive 3D visualisation system located in the University of Durham e-Science Research Institute.

*This research is part of a NERC Ocean Margins LINK project - 'Quantifying fault zone evolution and basement reactivation in passive margins' co-sponsored by BP and Statoil (UK). Our thanks go to the Annie Greenly Fund of the Geological Society of London, and the AAPG Grants-in-aid program for helping to fund this fieldwork.*

For more information on digital field mapping and Durham's new GAVA facility please visit: [http://www.dur.ac.uk/react.res/RRG\\_web/GAVA.htm](http://www.dur.ac.uk/react.res/RRG_web/GAVA.htm)

## Society Research Funds

To find out more about Geological Society research funds and how to apply for them, visit <http://www.geolsoc.org.uk/template.cfm?name=researchfunds>. The first February, each year is the closing date for applications. So - if you have missed the boat, make a note in your diary now!

### Further Reading

Blystad, P., Brekke, H., Færseth, R.B., Larsen, B.T., Skogseid, J. & Tørudbakken, B., 1995. Structural Elements of the Norwegian continental shelf. Part II. The Norwegian Sea Region. *NPD Bulletin* 8, p. 45

Doré, A.G., Lundin, E.R., Fichler, C. & Olesen, O. 1997. Patterns of basement structure and reactivation along the NE Atlantic margin. *Journal of the Geological Society*, 154, 85-92

Edmondo, G.P. 2002, Digital Geologic Field Mapping Using ArcPad. *Digital Mapping Techniques 2002*, Workshop Proceedings, USGS. <http://pubs.usgs.gov/of/2002/of02-370/edmondo.html>

Jones, R.R., McCaffrey, K.J.W., Wilson, R.W. & Holdsworth, R.E. 2004. Digital field data acquisition: towards increased quantification of uncertainty during geological mapping. In: Curtis, A & Wood, R. (eds.) *Geological Prior Information*. Geological Society Special Publication 239. In Press.

McCaffrey, K.J.W., Holdsworth, R.E., Clegg, P., Jones, R.R. & Wilson, R.W. 2003. Using Digital Mapping Tools and 3D visualisation to Improve Undergraduate fieldwork. *PLANET*, 5, 34-37



## Complex fault patterns, transtension and structural segmentation of the Lofoten Ridge, Norwegian margin: Using digital mapping to link onshore and offshore geology

Robert W. Wilson,<sup>1</sup> Kenneth J. W. McCaffrey,<sup>1</sup> Robert E. Holdsworth,<sup>1</sup> Jonathan Imber,<sup>1</sup> Richard R. Jones,<sup>2,3</sup> Alastair I. F. Welbon,<sup>4</sup> and David Roberts<sup>5</sup>

Received 23 August 2005; revised 27 April 2006; accepted 30 May 2006; published 26 August 2006.

[1] An integrated onshore-offshore study involving regional to outcrop-scale fault analysis is used to develop a self-consistent structural model for transtension along the Lofoten Ridge. The Lofoten-Vesterålen archipelago (LVA) is a segmented basement high showing distinct lateral variations in trend, deformational style, and structural complexity. This study investigates whether segmentation can be linked to differences in the obliquity of preexisting structures relative to plate movement vectors. Regional analysis of fault lineament patterns using Geographic Information Systems (GIS) reveals that the LVA can be subdivided into a series of distinct lineament domains. These domains are closely coincident with changes in ridge trend and variations in structure within offshore models derived from seismic reflection studies. Digital field mapping and spatial analysis of faulting in the north Lofoten reveal that multimodal faulting is dominated by transtensional dip-slip and oblique-slip movements which are comparable to analogue models where the ridge axis is 30° oblique to regional extension. The overall change in fault orientation, fault geometry, and deformation style are consistent with models for transtension where the ridge-bounding structure becomes increasingly oblique to regional extension. Previously identified transfer zones simply reflect segment domain boundaries and are not reactivating basement structures. This model is a possible analogue for other orthogonal and oblique rift structures on the Norwegian and other margins. Citation: Wilson, R. W., K. J. W. McCaffrey, R. E. Holdsworth, J. Imber, R. R. Jones, A. I. F. Welbon, and D. Roberts (2006), Complex fault patterns, transtension and structural segmentation of the Lofoten Ridge, Norwegian margin: Using digital mapping to link onshore and

offshore geology, *Tectonics*, 25, TC4018, doi:10.1029/2005TC001895.

### 1. Introduction

[2] Most passive margins are segmented along strike, giving rise to discrete zones characterized by constancy in structural style [e.g., Francheteau and Le Pichon, 1972; Doré et al., 1997; Clemson et al., 1997; Song et al., 2001]. This segmentation is also seen in continental rifts that are the precursor to these passive margins [e.g., Rosendahl, 1987; Morley et al., 1990]. The boundaries between margin/rift segments are generally believed to exhibit a variety of structural styles ranging from transfer faults [Gibbs, 1984] and accommodation zones [Bosworth et al., 1986] to transform faults. The origins of this segmentation and segment boundary zones are often attributed to the influence of basement structure [e.g., Davison, 1997; Clemson et al., 1997]. One possibility is that such segmentation reflects along-strike changes in the orientation of preexisting structures in the underlying continental basement. A corollary of this model is that if such preexisting structures undergo reactivation then they will often be significantly oblique to the direction of regional extension. This leads to the development of zones of oblique extension or transtension on what would otherwise be a simple extensional margin [Dewey, 2002; Morley et al., 2004].

[3] Transtension may be described as oblique extension which combines coaxial orthogonal extension and noncoaxial deformation zone parallel shear [Sanderson and Marchini, 1984; Dewey, 2002]. Transtensional strain will occur when bulk displacement is at an oblique angle  $\alpha$  to the deformation zone boundary faults (Figure 1a). Pure shear coaxial extension ( $\alpha = 90^\circ$ ) and noncoaxial wrench simple shear ( $\alpha = 0^\circ$ ) represent the end-member strain states for transtension, both of which lead to plane strain (two-dimensional) deformation. Transtension ( $0^\circ < \alpha < 90^\circ$ ) on the other hand results in noncoaxial three-dimensional (3-D) strain [De Paola et al., 2005a]. Transtensional strains are characterized by complex relationships between finite and infinitesimal strain axes that critically depend on the angle  $\alpha$  (Figure 1). In extension-dominated transtension ( $20^\circ < \alpha < 90^\circ$ ) the axes of infinitesimal ( $z$ ) and finite shortening ( $Z$ ) should always be coincident and vertical, which is comparable to the case of orthogonal extension ( $\alpha = 90^\circ$ ) (Figures 1b) [McCoss, 1986; Smith and Durney, 1992; De Paola et al., 2005a]. However, at low angles of divergence ( $\alpha < 20^\circ$ ), the infinitesimal axis  $z$  is

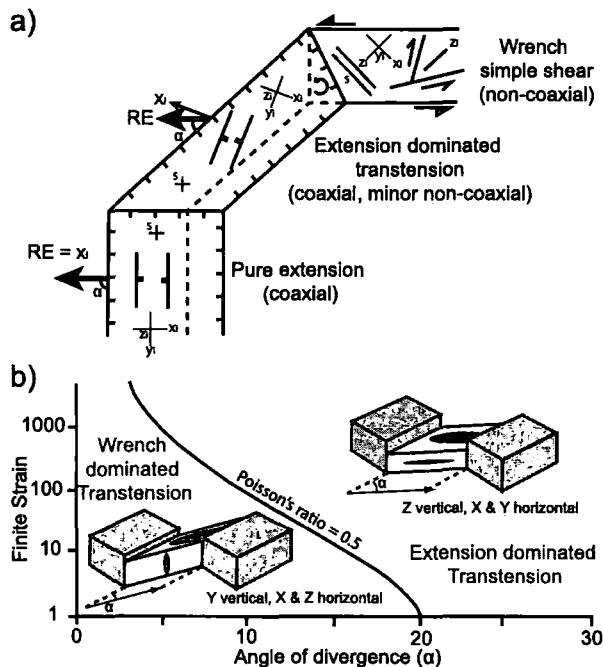
<sup>1</sup>Reactivation Research Group, Department of Earth Sciences, University of Durham, Durham, UK.

<sup>2</sup>Geospatial Research Ltd., Department of Earth Sciences, University of Durham, Durham, UK.

<sup>3</sup>e-Science Research Institute, University of Durham, Durham, UK.

<sup>4</sup>Statoil ASA, Stavanger, Norway.

<sup>5</sup>Geological Survey of Norway, Trondheim, Norway.



**Figure 1.** (a) Schematic plan view diagram showing an example of transtension (in this example extension-dominated transtension) in an increasingly oblique margin [after Dewey, 2002]. RE, regional extension direction. (b) Cartoon graph showing horizontal finite strain versus angle of divergence,  $\alpha$ . Solid curved line highlights the angle  $\alpha_{crit}$  which marks the transition from wrench-dominated to extension-dominated transtension for materials with a Poisson's ratio of 0.5 (modified from Teyssier and Tikoff [1999]).

horizontal, with the finite axis (Z) eventually swapping orientation with the vertical intermediate finite axis Y with increasing amounts of finite strain ("wrench-dominated transtension"; Figure 1b). It is not surprising, therefore, that both field- and laboratory-based studies of deformation styles in oblique and transtensional settings have shown that these zones exhibit more complex fault patterns than those traditionally associated with orthogonal rifting [e.g., Withjack and Jamison, 1986; Schreurs and Colletta, 1998; Clifton et al., 2000; McClay et al., 2002; Dewey, 2002; De Paola et al., 2005a]. Furthermore, the presence of preexisting structures lying at an oblique angle to imposed opening vectors may commonly lead to the partitioning of oblique rifting into contemporaneous domains of wrench- and extension-dominated transtension [Titus et al., 2002; Oldow, 2003; De Paola et al., 2005b].

[4] The Norwegian continental margin is a well documented example of a segmented passive margin [Doré et al., 1997; Tsikalas et al., 2001; Olesen et al., 2002; Mosar, 2003]. This segmentation is generally defined by the presence of a series of approximately NW-SE trending cross-

margin accommodation/transfer zones (Figures 2a and 2b) [Blystad et al., 1995; Olesen et al., 1997, 2002; Brekke, 2000; Tsikalas et al., 2001]. These transfer zones are believed to reflect major basement structures at depth [Strömberg, 1976; Mjelde et al., 2003]. This appears to be true for the largest transfer zones (e.g., Jan Mayen, Bivrost, Senja fracture zones), which we term here first-order transfer zones. However, others are simply inferred across areas of changing fault trend, fault polarity or basin geometry (e.g., Mosken and Jannegga transfer zones) [Tsikalas et al., 2001], and in many cases no attributable basement structure is observed. These we term second-order transfer zones, and they are more comparable to accommodation zones and twist zones [Colletta et al., 1988; Peacock et al., 2000].

[5] In this paper, we shall use integrated regional to outcrop-scale onshore and offshore studies to investigate the variations in fault pattern and structural style across a zone of increasing obliquity relative to the regional extension vector. Furthermore, we investigate the hypothesis that it is the orientation of individual ridge/margin segments, and their bounding faults, relative to regional extension that controls fault complexity and the development of second-order transfer structures.

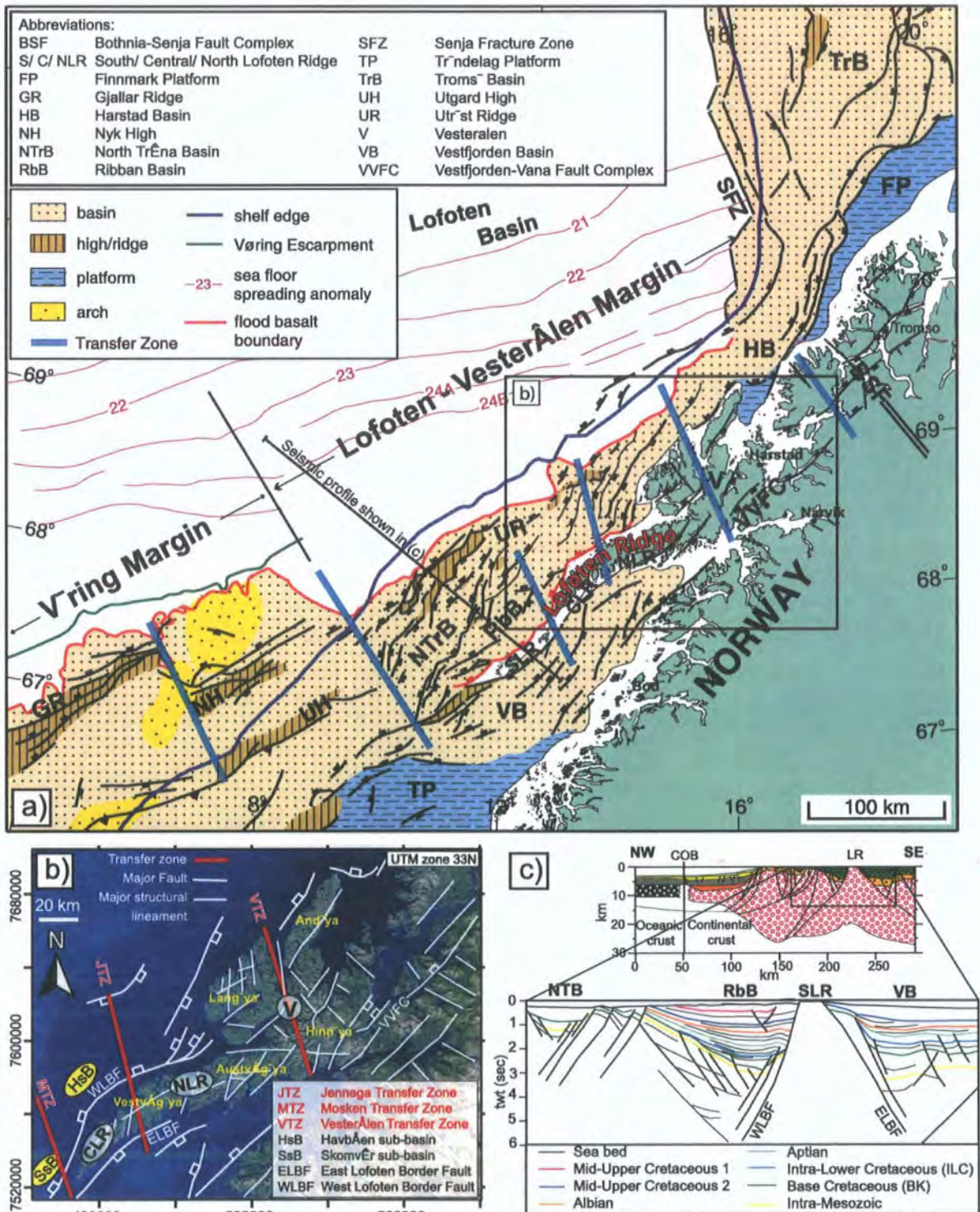
[6] The Lofoten Ridge (Figure 2b) is a basement ridge showing distinct lateral variations in trend, and provides a good opportunity to compare fault architectures found in crystalline basement onshore [Tveten and Zwaan, 1993; Løseth and Tveten, 1996; Olesen et al., 1997; Klein and Steltenpohl, 1999; Steltenpohl et al., 2004], with those developed in sedimentary basins offshore [Mokhtari and Pegrum, 1992; Løseth and Tveten, 1996; Tsikalas et al., 2001]. The Lofoten Ridge has been strongly affected by tectonic activity during the Late Mesozoic extension prior to the separation of Norway and Greenland and, given its curved geometry, is an ideal location to look for evidence of basement-influenced oblique extension. The area is also an excellent analogue for offshore basement fault blocks beneath the Norwegian and other passive margins.

[7] In the present study, we apply new digital mapping workflows [Jones et al., 2004; Wilson et al., 2005; McCaffrey et al., 2005] to construct a structural database for both onshore and offshore structures on the Lofoten-Vesterålen archipelago (LVA; Figure 2c). All data are stored digitally in a Geographic Information System (GIS) database that facilitates the interpretation of multiple/integrated data sets (e.g., seismic data, remote sensing, field mapping [Jones et al., 2004; Piazzolo et al., 2004]). It also provides an ability to analyze structures spatially across a wide range of scales.

## 2. Regional Setting

### 2.1. Lofoten-Vesterålen Margin

[8] Past studies have shown that the Norwegian continental margin can be divided into a series of segments (Møre, Vøring, Lofoten-Vesterålen, and Western Barents Sea margins; Figure 2) [Talwani and Eldholm, 1977; Olesen et al., 1997; Doré et al., 1999; Brekke, 2000; Mosar, 2003]. The Lofoten-Vesterålen Margin segment lies between the



**Figure 2.** (a) Tectonomagmatic map of the Lofoten-Vesterålen margin (modified from Tsikalas et al. [2001]). (b) Landsat image of the Lofoten-Vesterålen archipelago. The transfer zones proposed in past studies are highlighted in red [Olesen et al., 1997, 2002; Tsikalas et al., 2001]. (c) Simplified cross sections across the Lofoten-Vesterålen margin and south Lofoten Ridge (modified from Tsikalas et al. [2001]).

Bivrost and Senja fracture zones (Figure 2) [Eldholm *et al.*, 1979; Tsikalas *et al.*, 2001]. Compared to its neighboring margin segments, the Lofoten-Vesterålen Margin has a relatively narrow continental shelf and steep slope. Seismic and geophysical studies in this segment show a rift complex of margin-parallel basement ridges and shallow Mesozoic basins [Mokhtari and Pegrum, 1992; Løseth and Tveten, 1996; Olesen *et al.*, 1997, 2002; Tsikalas *et al.*, 2001]. Tsikalas *et al.* [2001] further subdivide the margin into a series of intramargin segments based on changes in fault polarity and intensity. These intramargin segments are thought to be separated by transfer zones (Jannegga, Vesterålen; Figure 2a), also identified by Olesen *et al.* [1997, 2002].

[9] The Norwegian margin has a prolonged Paleozoic to Cenozoic history of intermittent extension and basin formation dating from the Devonian postorogenic (i.e., post-Scandian) collapse of the Caledonide mountain belt [Fossen and Dunlap, 1998; Doré *et al.*, 1999; Fossen, 2000]. Regional extension episodes have been documented in the Devonian-Carboniferous, Permian, through the Late Jurassic to Early Cretaceous, and in Late Cretaceous to Early Cenozoic times [Blystad *et al.*, 1995; Lundin and Doré, 1997; Brekke, 2000]. The last extensional event is considered to have culminated in continental breakup and massive igneous activity at the Paleocene-Eocene transition, ~55 Ma [Eldholm *et al.*, 1989; Skogseid *et al.*, 1992, 2000; Eide, 2002; Ren *et al.*, 2003].

[10] Late Jurassic–Early Cretaceous rifting is the dominant tectonic episode that gave rise to the prominent NE-SW trending faults on the margin [Blystad *et al.*, 1995; Doré *et al.*, 1999; Brekke, 2000; Tsikalas *et al.*, 2001; Mosar, 2003]. There are two dominant NE-SW oriented ridges on the Lofoten-Vesterålen Margin: the Lofoten Ridge and the Utrøst Ridge (Figures 2a and 2c). Extensive synrift thickening of Lower Cretaceous sequences is apparent along faults bordering the western flank of the Lofoten Ridge, indicating that tectonism was active until about Hauterivian time, ~130 Ma [Doré *et al.*, 1999; Tsikalas *et al.*, 2001].

## 2.2. Lofoten-Vesterålen Archipelago

[11] The inner Lofoten-Vesterålen margin is dominated by the Lofoten Ridge, which can be split into three sections (north, central, and south) showing variations in trend (Figure 2a). With the exception of a few small islands (e.g., Røst and Værøy), the south Lofoten Ridge lies below sea level (Figure 2a), whereas the central and north Lofoten Ridge make up part of the Lofoten-Vesterålen archipelago (LVA) (Figure 2b). Collectively, the ridge marks a prominent NE-SW trending horst, bound on both sides by deep sedimentary basins (Vestfjorden and Ribban basins) [Mokhtari and Pegrum, 1992; Blystad *et al.*, 1995; Løseth and Tveten, 1996]. The archipelago is composed mainly of high-grade metamorphic Precambrian rocks [Griffin *et al.*, 1978] which have undergone a multistage exhumation history [Griffin *et al.*, 1978; Hendriks, 2003]. The exposed rocks are mainly migmatitic gneisses that were metamorphosed to amphibolite and granulite facies, and extensively

intruded by mangeritic and charnockitic plutons [Griffin *et al.*, 1978; Corfu, 2004a]. U-Pb dating of these plutons suggest that the main phase of emplacement was between 1800 and 1790 Ma [Corfu, 2004a] and make up the bulk of the rocks exposed in north Lofoten (i.e., on Austvågøya and Vestvågøya) [Tveten, 1978; Corfu, 2004a]. Basement fabrics within these rocks are somewhat variable, both in trend and intensity, along the ridge [Tveten, 1978]. Unlike other exposures of the Western Gneiss Region, the Caledonian fabrics are only weakly developed in these basement rocks of the LVA [Griffin *et al.*, 1978; Tull *et al.*, 1985; Steltenpohl *et al.*, 2004]. This has been attributed to the lack of fluids in the dry granulite facies basement in the area [Bartley, 1982; Olesen *et al.*, 1997]. Separating these Precambrian basement terranes from the Caledonian nappe sequences to the east are a series of steeply dipping brittle-ductile to cataclastic faults called the Vestfjorden-Vanna fault complex (Figure 2) [Andresen and Forslund, 1987; Olesen *et al.*, 1997]. This fault zone has been attributed to Late Jurassic–Early Cretaceous movements [Andresen and Forslund, 1987], although older Permian movements have also been suggested [Olesen *et al.*, 1997; Steltenpohl *et al.*, 2004].

[12] The only onshore exposures of nonbasement rocks can be found on Andøya [Dalland, 1981], where Jurassic and Lower Cretaceous sediments outcrop. Similar age sediments have also been documented from within fjords on Vesterålen [e.g., Davidsen *et al.*, 2001].

[13] A large fault defines the western flank of the Lofoten Ridge (the West Lofoten Border Fault, WLBF [Løseth and Tveten, 1996]), and also forms the major bounding fault to the Ribban Basin offshore (Figure 2). This basin is subdivided into the Skomvær and Havbåen subbasins (Figure 2b) [Mokhtari and Pegrum, 1992; Olesen *et al.*, 1997; Tsikalas *et al.*, 2001]. In places, the WLBF has a cumulative throw to the west or NW in excess of 3 km [Tsikalas *et al.*, 2001]. Traced northward, the WLBF changes orientation from a NNE-SSW trend to NE-SW/ENE-WSW trend between Moskenesøya and Vestvågøya (Figure 2b), and this is reflected in the overall trend of the Lofoten Ridge. This change is coincident with an apparent change in fault polarity within the Ribban Basin from dominantly NW dipping in the south to dominantly SE dipping in the north [Tsikalas *et al.*, 2001]. It also coincides with a decrease in throw on the Eastern Lofoten Border Fault (ELBF; Figure 2b) northward. These observations led both Tsikalas *et al.* [2001] and Olesen *et al.* [2002] to infer a transfer zone through the area (Figures 2a and 2b); however, the exact trend and location are still debated.

[14] Another major transfer zone has been inferred to run through Vesterålen [Olesen *et al.*, 1997, 2002; Tsikalas *et al.*, 2001]. However, apart from a few discrete NW-SE trending strike-slip faults running across Vesterålen that may be associated with this transfer structure, no major transverse fault is apparent. The transfer zone is instead characterized by an apparent regional barrier to the propagation of NE-SW faults [Olesen *et al.*, 1997]. This region has been described as a “twist zone” by Olesen *et al.* [1997, 2002], and is comparable to the “transfer zones” or “ac-



commodation zones" described by *Peacock et al.* [2000]. Also spatially coincident with this inferred transfer zone on Vesterålen is a steep magnetic gradient oriented NNW-SSE with a positive anomaly to the west and a negative anomaly to the east. This boundary has been attributed to the prograde metamorphic transition from amphibolite-facies migmatites in the east to granulite-facies rocks in the west [*Griffin et al.*, 1978; *Olesen et al.*, 1991]. However, *Corfu* [2004b] has proposed alternatively that this gradient marks a major Caledonian tectonic boundary on Vesterålen.

[15] All transfer zones that have been inferred in the region (Figure 2) are based on changes in fault polarity and sediment thickness offshore [*Tsikalas et al.*, 2001], and variation in crustal structure onshore [*Løseth and Tveten*, 1996; *Olesen et al.*, 1997, 2002]. All follow a preferred NNW-SSE to NW-SE orientation, which may be linked to the influence of Proterozoic shear zones within basement (e.g., the Bothnian-Senja Fault Zone, Figure 2b) [*Henkel*, 1991; *Lundin and Doré*, 1997; *Olesen et al.*, 1997; *Fichler et al.*, 1999]. These transfers have also been speculatively linked to fracture zones far offshore that supposedly offset early magnetic anomalies generated during seafloor spreading [*Lister et al.*, 1991; *Tsikalas et al.*, 2001], although the results of new aeromagnetic surveys now question the existence of these oceanic fracture zones that coincide with these "second-order" transfers [*Olesen et al.*, 2005].

[16] Apatite fission track (AFT) data, radiometric dating and onshore analysis all suggest that the basement rocks of Lofoten and Vesterålen experienced similar post-Caledonian histories until the Late Paleozoic [*Hames and Anderson*, 1996; *Klein and Steltenpohl*, 1999]. Subsequently, these two areas appear to have undergone differential vertical movements [*Hendriks and Andriessen*, 2002]. Again segmentation is apparent, with different cooling and denudation histories found throughout the archipelago. AFT analysis in central and north Lofoten and Vesterålen suggest that outer Vesterålen (i.e., Langøya) was exhumed (based on cooling ages) in Permo-Triassic times, whereas analyses in north Lofoten (and possibly also inner Vesterålen) suggest Jurassic-Cretaceous denudation ages [*Hendriks and Andriessen*, 2002; *Hendriks*, 2003], at a time when Langøya was subsiding and covered by sediments [*Davidson et al.*, 2001]. Central Lofoten shows evidence for cooling in Mid-Cretaceous times [*Hendriks and Andriessen*, 2002]. *Hendriks and Andriessen* [2002] proposed that the transfer zones have in some way accommodated these differential vertical movements, although the precise mechanism to account for such movements is not explained.

### 3. Methods and Data Acquisition

#### 3.1. GIS Database

[17] In any study where both onshore and offshore fault data are examined at a range of scales it will be advantageous to use a Geographic Information System (GIS). GIS is an information system used to input, store, retrieve, manipulate, analyze and visualize geographically referenced

geospatial data [*Longley et al.*, 2001]. In this study we compiled remote sensing, fieldwork and offshore seismic reflection data sets in a single GIS database using the ArcGIS™ suite. All data are geospatially located in a consistent coordinate system (WGS 84 UTM zone 33). This digital workflow forms part of a new in-house mapping methodology, Geospatial Acquisition, Visualization and Analysis (GAVA) [*Clegg et al.*, 2005; *Wilson et al.*, 2005; *McCaffrey et al.*, 2005] which integrates field- and laboratory-based digital mapping methodologies and allows for continual data analysis and evaluation at every stage in the data gathering process.

#### 3.2. Onshore ("Surface") Data Set

[18] Regional-scale structures have been mapped using remote sensing techniques, particularly lineament analysis, and the digitization of preexisting geological maps. Fault structures at this scale were interpreted from Landsat thematic mapper (TM) data. The application of lineament analysis for the interpretation of geological structures is a well established method that has been widely applied in Norway [e.g., *Gabrielsen and Ramberg*, 1979; *Karpuz et al.*, 1993, 1995; *Gabrielsen et al.*, 2002]. Lineaments were picked from Landsat images along the LVA at a scale of 1:100,000. Attribute data (i.e., trend; length; offset; comments) were also recorded and stored in the GIS database. After interpretation, lineaments were then compared to a digital terrain model (DTM) and refined using GIS analysis. Particular care was taken to avoid the inclusion of basement fabrics in the lineament database. This was confirmed by studying preexisting geological maps during lineament analysis, and was additionally checked during fieldwork.

[19] Outcrop-scale structures were collected using some of the new digital geological techniques outlined by *McCaffrey et al.* [2005]. Digital methods are becoming a common means of field data acquisition [*Maerten et al.*, 2001; *Hodgetts et al.*, 2004; *Jones et al.*, 2004; *Clegg et al.*, 2005]. This is in part because the equipment and software required now meet the needs of the field geologist (e.g., portability, accuracy, versatility, cost, etc. [*Edmondo*, 2002; *Wilson et al.*, 2005]), but also because it is becoming increasingly recognized that having precise geospatially located field data enables efficient 3-D visualization and analysis in ways that are not possible with data collected using traditional paper-based notebook collection methods [*McCaffrey et al.*, 2005]. Gathering outcrop data in digital format (compatible with standard software used in the hydrocarbon industry) is a prerequisite for efficient comparison between onshore and offshore data.

[20] The equipment used for data capture during geological fieldwork in Lofoten comprised the following: (1) a hand-held computer (HP Jornada PDA) equipped with mobile GIS Software; (2) a backpack mounted Differential Global Positioning Satellite receiver (Trimble™ AG122); (3) a laser rangefinder (MDL LaserAce 300); and (4) a digital camera [*Wilson et al.*, 2005]. Field data were recorded in the form of 3-D shape files (containing xyz position), using ArcPad™ (version 6), a mobile GIS software suitable for running on Windows CE devices

[Edmondo, 2002]. Outcrop data (e.g., fault measurements and lithological data) were stored in point shape files, while linear features in map view (e.g., fault trace, traverse line, etc.) were recorded as polylines. These were supplemented by georeferenced outcrop photos and field sketches, both in a digital format. Structures exposed in vertical outcrops (i.e., road cuts) were recorded using a combination of digital photography and 3-D outcrop data capture using a laser ranger (recording xyz point cloud data for outcrop surfaces and fault traces [Xu *et al.*, 2000]).

[21] Field mapping was concentrated on Lofoten's northernmost island, Austvågøya (Figure 2c). This was in part because of the dramatic topography and excellent exposure on Austvågøya.

### 3.3. Offshore ("Subsurface") Data Set

[22] During the development of our regional structural database a number of regional offshore fault maps were digitized, including Mokhtari and Pegrum [1992], Blystad *et al.* [1995], Løseth and Tveten [1996], Olesen *et al.* [1997, 2002], and Tsikalas *et al.* [2001]. However, some inconsistencies were found between these data sets (i.e., trends of faults, fault linkage, etc.) and consequently twenty-four 2-D seismic lines (data coverage approximately 100 km × 75 km) were studied for an area west of the Lofoten Ridge (see Figure 6 in section 4.2.1 for location of survey area).

[23] Seismic interpretation was carried out using GeoFrame IESX™ before exporting fault and horizon data to TrapTester™ to construct a 3-D structural model of the area. Five prominent reflectors were mapped, and have been correlated with the intra-Mesozoic, Base Cretaceous, intra-Lower Cretaceous, Aptian and Albian horizons mapped by Tsikalas *et al.* [2001] in the Ribban Basin. Larger faults have been linked with some confidence based on mapped variations in fault throw, and the resulting fault polygon maps have been exported to GIS for comparison with onshore structures, while geometries have been analyzed in TrapTester.

### 3.4. Building 3-D Models

[24] The 3-D models provide a powerful tool for regional-scale structural investigations. Simple models for the Lofoten Ridge were first constructed in ArcGIS, by overlaying Landsat images for the LVA region onto a DTM (Digital Terrain Model) of the area. These models can be viewed from different vantage points, zoomed to different scales, and simulated "fly through" animations created. This is particularly useful for studying the relationship between structures and topography. Bedrock maps, gravity maps and magnetic maps were also draped onto the DTM for similar studies. These simple models have been described as "2.5-D" representations [Longley *et al.*, 2001; Jones *et al.*, 2004] as they do not provide any direct information about the subsurface geology. For a fully 3-D model (i.e., equivalent to seismic models offshore) structures must be projected into and out of the topographic surface. For this type of analysis, more specific 3-D modeling software is required. Following structural interpretations in GoCAD™, regional 3-D fault models were then reimported into ArcGIS

(ArcScene) for integration with field GIS data and offshore fault and horizon models.

## 4. Regional Structural Analysis

### 4.1. Onshore Surface Analysis

#### 4.1.1. Lineament Populations

[25] Along the Lofoten-Vesterålen archipelago, good exposures in crystalline basement and the strong topographic relief permit the ground truthing of lineaments that were mapped using Landsat TM data. The region appears highly faulted and fractured, as indicated by the dense set of 2000 lineaments identified from the remote sensed data [Gabrielsen *et al.*, 2002; this study]. These regional lineament maps show the Lofoten Ridge to have two dominant lineament trends, NNE-SSW (020°–040°) and ENE-WSW (070°–090°) (Figure 3), with subsidiary NW-SE, NE-SW, and E-W trends. Central Lofoten (i.e., Flakstadøya and Moskenesøya) and outer Vesterålen both show dominant N-S and NNE-SSW oriented lineament suites, while an ENE-WSW trending lineament suite can be seen in north Lofoten (Vestvågøya and Austvågøya) running east toward Ofotfjorden (Figures 3a and 3b). Other systems include a NW-SE trending suite on Vesterålen (Figures 3a and 3b).

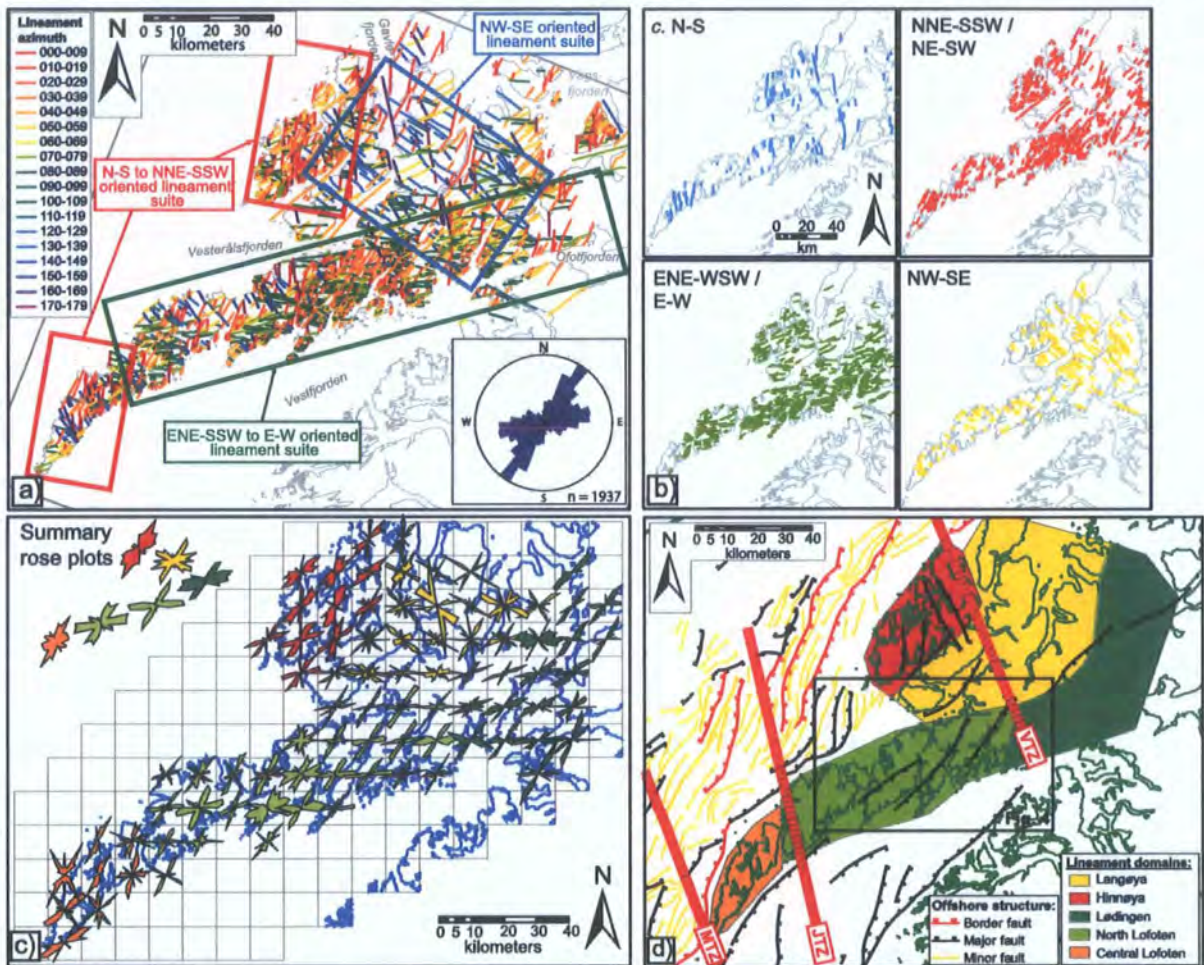
#### 4.1.2. Lineament Domains

[26] Using ArcGIS, lineament density maps were made by counting the total number and total length of lineaments within a moving 1 km<sup>2</sup> search window. These maps highlight the dominant lineament in different parts of the LVA. Directional analysis was also carried out using rose diagram plotting tools in ArcView. Having gridded the area into 10 km × 10 km cells, rose diagrams were plotted for each cell (Figure 3c). These spatial analyses reveal that the LVA can be subdivided into a series of distinct lineament domains: (1) central Lofoten (CLD), (2) north Lofoten (NLD), (3) Lødigen (LøDD), (4) Hinnøya (HinD), and (5) Langøya (LangD); Figure 3d). In all 5 domains, a dominant lineament trend is NNE-SSW to NE-SW, with some domains also showing a second dominant trend: ENE-WSW in north Lofoten, and NW-SE on Hinnøya. These domains are coincident with changes in ridge trend, and with previously documented variations in regional gravity and magnetics (Figures 4b and 4c), but also denudation ages and offshore fault patterns [Tsikalas *et al.*, 2001; Hendriks and Andriessen, 2002; Olesen *et al.*, 2002]. Gravity highs appear to be associated with domains showing a single preferred lineament trend (i.e., central Lofoten and Langøya domains [see Olesen *et al.*, 2002, Figure 10]).

#### 4.1.3. Detailed Lineament Studies on Austvågøya

[27] Figure 4 shows a more detailed view of the multimodal lineament trends seen on Austvågøya (north Lofoten). In this area 4 main lineament systems have been identified: approximately N-S (system 0); NNE-SSW to NE-SW (system 1); ENE-WSW to E-W (system 2); and ESE-WNW to SE-NW (system 3).

[28] System 0 lineaments (S0, Figure 4) are represented by deep, wide valleys and fjords, showing characteristics of classic glacial U-shaped valleys. Compared to other systems, this system has a relatively wide spacing (roughly



**Figure 3.** Regional lineament analysis of satellite data for the LVA. (a) Landsat TM image with structural lineaments mapped at 1:100,000 scale, plus a rose diagram highlighting dominant lineament trends. (b) Lineament maps showing distribution of the four main lineament systems identified in Lofoten (N-S; NNE-SSW/NE-SW; ENE-WSW/E-W; NW-SE). (c) Rose diagram map for lineaments. Map gridded in to 10 × 10 km squares, with corresponding rose diagrams plotted for each square. Plots are colored according to similarities in trend. Plots in top left show summary plots for changes in lineament trend along the ridge. (d) Lineament domains identified from spatial analysis using GIS (i.e., lineament density maps for each lineament trend and rose diagram maps shown in Figure 3c).

every 3–5 km), and as a result there are fewer S0 lineaments to be observed. However, they do form the largest valleys, and also appear to separate the largest islands (i.e., Flakstadøya, Vestvågøya, Austvågøya). Wide N-S valleys (S0) often appear bend, or be offset, in a counterclockwise/left lateral sense. This later deformation may suggest that S0 lineaments are relatively old structures.

[29] System 1 lineaments (S1, Figure 4) are the most common lineament trend along the ridge and are characterized by narrow, deeply incised valleys and fjords, such as Raftsundet (Figure 4c). System 2 lineaments (S2, Figure 4) have a similar geomorphologic style to S1, i.e., represented by arrow, steep sided valleys such as the famous Trollfjord (Figure 4d). A distinct change in trend of S2 lineaments

(from ENE-WSW to E-W) can be seen across Austvågøya (Figure 4). This change appears to roughly match a change in the trend of the overall ridge.

[30] A strong correlation between the change in trend of S2 and the frequency and orientation of S1 lineaments is also apparent. The density of S1 appears higher where S2 lineaments trend E-W, and the mean orientation of S1 lineaments in this same zone also appear to be  $\sim 10^\circ$  clockwise of S1 trends farther to the southwest (Figure 4). Crosscutting relationships observed between S1 and S2 lineaments appear to be quite complex, with good examples of both S2 cutting S1 and vice versa. This mutual crosscutting relationship is likely to suggest that

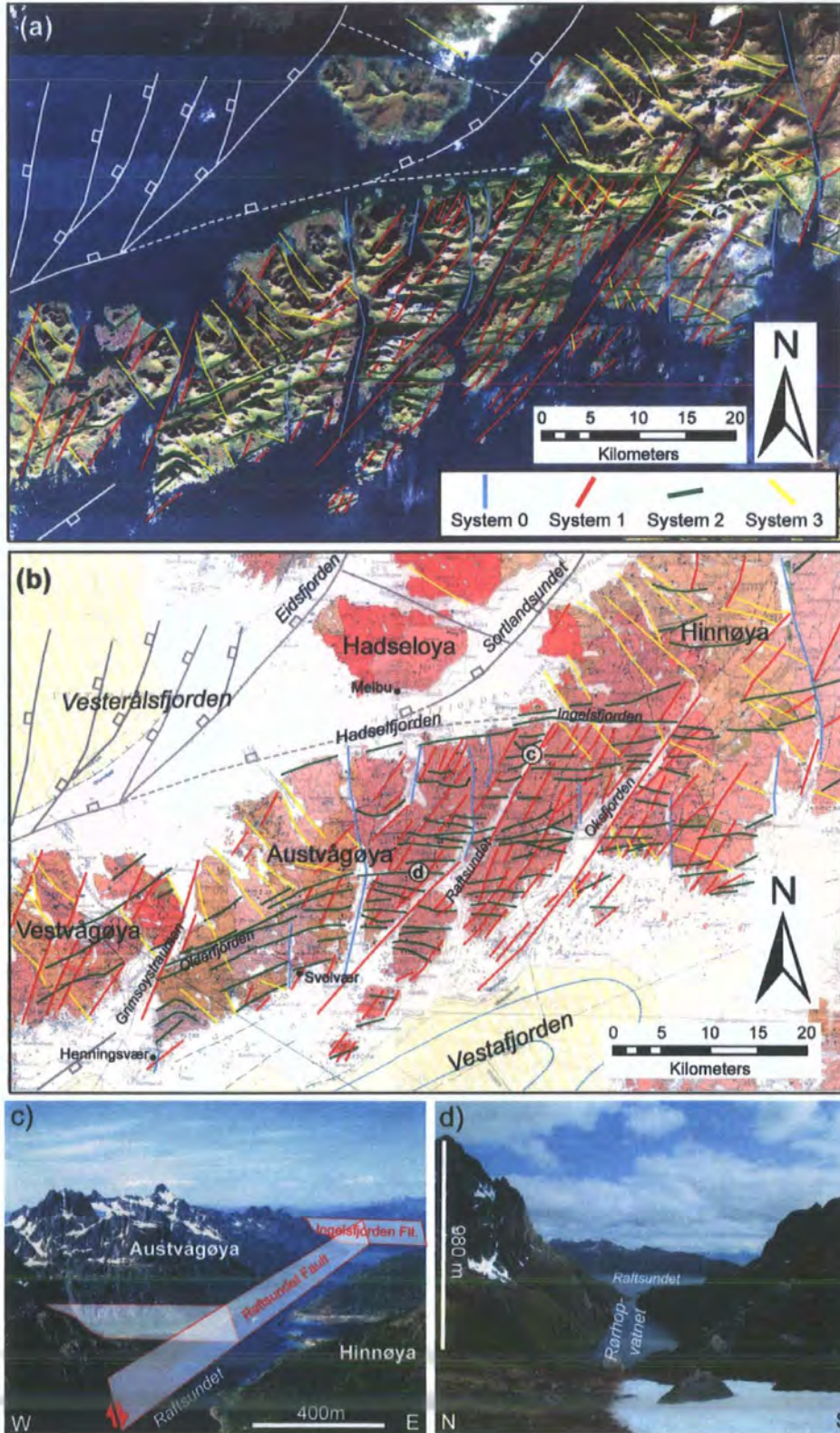


Figure 4

these systems formed, or were active during the same tectonic event.

[31] System 3 (S3, Figure 4) is most pronounced on Vesterålen; however, a number can also be seen cutting the Lofoten Ridge. These lineaments are represented by both narrow and wide valleys. Crosscutting relationships suggest that S3 lineaments are the youngest system as they appear to truncate most other trends, although caution must be taken when interpreting age relationships from lineaments as it is often unclear if truncations represent lineament terminations or true crosscutting older by younger.

#### 4.1.4. Regional Onshore Structural Model

[32] The 3-D fault models have been created for these lineament maps in an attempt to construct onshore models equivalent to those produced from offshore seismic studies. This was done using structural modeling tools in GoCAD™ by overlaying Landsat lineament interpretations (in vector form) over a 50 m DTM; the lineaments then take on a 2.5-D configuration (a curved line in 3-D space). If there is sufficient interaction between topography and the lineament trace (the considerable topographic relief of Lofoten is perfect for this), then best fit surfaces can be constructed along each lineament, thus producing a representative fault plane (see Figure 5). Not only does this method provide a model to help visualize the 3-D structure of the region, but also allows the strike and dip of these regional fault surfaces to be calculated. These faults can then be compared to the equivalent geometries interpreted from offshore seismic data and to field data (Figure 5).

[33] The 3-D fault models were created using this method over a 25 km × 50 km area of north Lofoten (Figures 4 and 5). Like the rest of the NLD, lineament orientations in this area have two distinct preferred orientations, ~035°–215° (S1) and ~080°–260° (S2). The resulting 3-D model for these structures displays a rhombic fault block pattern (Figure 5), while the poles to planes of these regional structures appear to cluster in a bimodal distribution (Figure 5f). Because of the lineament picking method favoring straighter lines (i.e., the picker is nearly always biased toward drawing straighter lines, particularly across areas of uncertainty, such as hillslopes in shadow or less distinct lineament trace), the faults may appear steeper than they really are (because a straighter line equates to a steeper structure), which may account for the apparent clustering around the vertical dip.

## 4.2. Offshore Subsurface Analysis

### 4.2.1. Offshore Central Lofoten and the Havbåen Subbasin

[34] Offshore central Lofoten is characterized by a single major NNE-SSW to NE-SW trending border fault (parallel to the ridge trend) bounding a large depocenter (the Havbåen subbasin; Figures 6a and 6b). Synrift thicken-

ing of Upper Jurassic and Lower Cretaceous sequences is apparent along the West Lofoten Border Fault (WLBF) in this area, while most Middle Cretaceous sediment infilling the Havbåen subbasin appears to be associated with thermal subsidence, thickening toward the center of the basin. Intra-Lower Cretaceous and Middle Cretaceous hanging wall sequences dip away from the WLBF before shallowing to horizontal through a hanging wall syncline (Figure 6a). Overlying strata can be seen to onlap these tilted horizons (see profile F, Figure 6b). This geometry resembles a similar compaction-related geometry discussed by *Thomson and Underhill* [1993] for faulting in the Moray Firth. These structures are interpreted to form in response to differential compaction as a consequence of varying hanging wall and footwall lithologies together with a buttressing effect created by the underlying rigid footwall. Further synrift thickening of Upper Cretaceous sediments appear restricted to the deepest part of the basin (see profile F, Figure 6a).

### 4.2.2. Offshore North Lofoten

[35] Offshore north Lofoten shows a number of contrasting structures and styles compared those observed farther south. First, the throw on the WLBF appears to decrease markedly, which has resulted in a much shallower basin in this area. Furthermore, the WLBF also shows a distinct change in trend in this area, bending round into a NE-SW to ENE-WSW orientation (Figures 6b and 6d). A number of NNE-SSW trending, west dipping normal faults (green faults in Figure 6) appear to bend round and join the WLBF (Figures 6b and 6d). These have been interpreted as a system of en echelon faults splaying off the border fault as it bends round into an ENE-WSW trend. Alternatively they may represent a system of breached relays. Either way, these imply a component of sinistral oblique extension along the WLBF in this area. These splay faults cut Late Jurassic and Base Cretaceous strata. Also characteristic of this area are a number of major NNE-SSW trending, east dipping faults located farther offshore (yellow faults in Figure 6). These show extensive synrift thickening of hanging wall sequences of Late Jurassic to Mid-Cretaceous (Aptian) age (Figure 6a). These faults lie along strike from the prominent WLBF bounding the central Lofoten segment and likely take up much of the extension not seen along the border fault as it is traced northward.

[36] Throws on the WLBF and associated faults are reduced compared to those seen farther south, and more faults can also be seen cutting lower Cretaceous strata. This may suggest that deformation is less focused along the bounding fault in north Lofoten and that strain is more distributed across the basin. Further to this observation is the fact that there is no significant depocenter in this area compared to central Lofoten and there is also significantly less evidence for thermal subsidence and infilling (Figures 6a and 6b). In the northern part of this area,

**Figure 4.** (a) Detailed lineament studies of north Lofoten. Lineaments are colored according to fault/lineament system (S0–S3). Offshore trends are adapted from *Løseth and Tveten* [1996] and results of this study. Dashed lines show inferred link up of faults. (b) Lineament trends plotted on geological map of Lofoten [*Tveten*, 1978]. (c) Oblique aerial photograph of Raftsundet (S1), looking north. (d) Photograph of E-W trending narrow, steep sided valley (S2), truncated by Raftsundet, looking east.

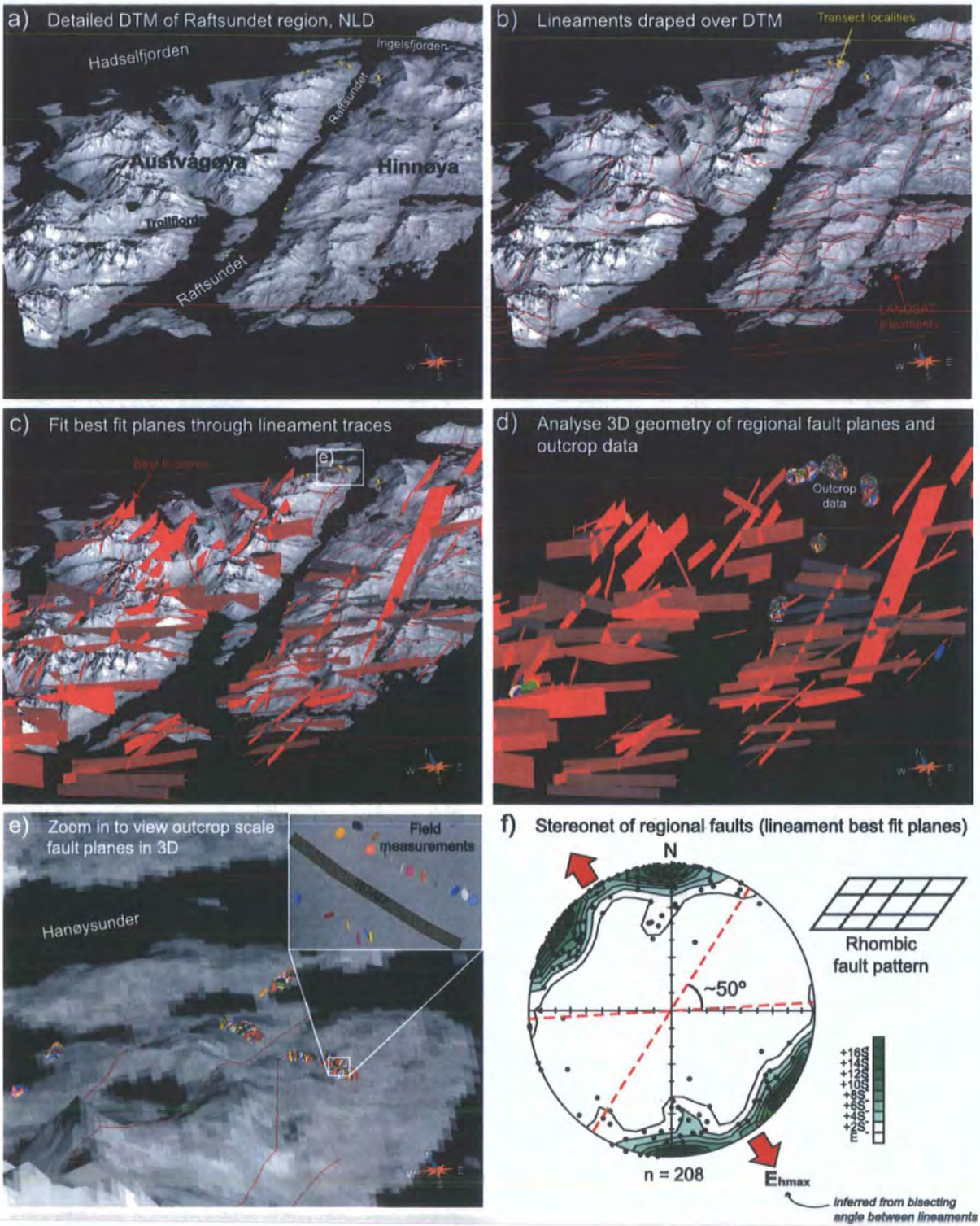


Figure 5

sedimentary sequences appear to have been uplifted and eroded. This is likely to have occurred at the same time as the sediments that covered Vesterålen were eroded away [Dalland, 1981; Løseth and Tveten, 1996].

[37] A NNW-SSE trending transfer zone (Jannegga transfer zone [Tsikalas *et al.*, 2001]) has previously been mapped through the area between these two domains. However, it should be noted that no distinct structures marking the position of this transfer zone can be seen in seismic data (see Figure 6a), and thus this zone simply marks the transition between domains of differing fault polarity and basin location.

## 5. Field Data Analysis

### 5.1. Outcrop Exposures Around Raftsundet

[38] Field reconnaissance mapping in north Lofoten (Austvågøya and Vestvågøya) has confirmed that most lineaments correspond to major fault structures (Figures 4c and 4d). In some cases the structures themselves cannot be directly identified as they lie at the bottom of fjords or vegetated valleys (e.g., Raftsundet; see Figures 4c and 7a). However, the intensity of fracturing in adjacent areas of exposed rock is consistent with their location close to major fault structures. Almost all exposures in the mapping area were in charnockites (orthopyroxene granite) and mangerites (orthopyroxene monzonite) of the Raftsund Pluton (colored pink in Figure 4b). These rocks exhibit a weak E-W trending fabric; however, in many places, basement fabrics were indiscernible. The freshest exposures of fault surfaces were found on road cut sections and shorelines; however, because of the dramatic topography of the area, many faults and fault zones can also be easily traced up mountainsides (Figure 7b). Fault exposures varied from large solitary faults in a relatively undeformed country rock (Figure 7c) to fault zones of highly fractured rock (Figures 7d and 7h). Fault rocks observed were generally semibrittle (slickenlines) to brittle (cataclasite) (Figures 7d and 7e), and little evidence for fluid interaction during deformation was observed (the only example of mineralization was found at a locality in the hanging wall of the Ingelsfjorden fault, in the form of epidotic slickenfibers).

### 5.2. Fault Populations

[39] During fieldwork, 666 mesoscale (centimeter-decimeter scale exposures) faults and fractures and associated slip striae have been measured at over 20 localities across NE Austvågøya. More than 60% of the faults measured exhibit good kinematic indicators, in the form of slickenlines and striated coatings (Figure 7e). Kinematic

indicators such as Riedel shears were used to infer shear direction and shear sense on each fault plane [Petit, 1987].

#### 5.2.1. Steep Brittle Faults

[40] When plotted stereographically, three main brittle fault clusters are apparent (Figure 8a, left), with strike orientations that closely match the data derived from lineament analysis (Figure 5f). These clusters reflect 2 distinct fault geometries: (1) NNE-SSW to NE-SW trending faults, dipping NW and SE (system 1/S1; Figure 8b) and (2) ENE-WSW to E-W trending faults dipping mainly to the north (system 2/S2; Figures 7b and 8c). These fault geometries are matched by similar fracture/joint trends (i.e., surfaces with no clear evidence for shear; Figure 8a, right). Only ENE-WSW and E-W trending surfaces showed plumose markings characteristic of joints (Figure 7g), and these were found in the vicinity of an E-W trending lamprophyre dike at locality LO3 (the margins of which have been reactivated by sinistral strike-slip movements; Figures 9a and 10). A second lamprophyre dike trending NNE-SSW was also observed at Locality LO2 (Figure 9b), in this case the dike was highly deformed and reactivated by both dip-slip and dextral oblique-slip faults. Plots of slip striae (Figure 8a, middle) show that all fault orientations are dominated by dip-slip (i.e., slickenline pitch  $>60^\circ$ ) or oblique-slip (pitch  $30^\circ$ – $60^\circ$ ) normal fault movements. However, a small number of strike-slip (pitch  $<30^\circ$ ) movements were also observed, and some faults also exhibit multiple slip striae. Strike-slip striae on system 1 (NNE-SSW oriented) faults indicate a dextral shear sense; while on system 2 (ENE-WSW oriented) faults show sinistral shear, and may represent a conjugate pair (Figure 8d).

[41] A spatial analysis of fault geometry and slickenline data was carried out in ArcView using an interactive GIS stereoplot program provided by Knox-Robinson and Gardoll [1998]. Figure 10 shows a summary map, and associated stereonets, for fault populations for localities in the area of Raftsundet. No distinct patterns of spatial distribution are apparent across the mapping area; however, it may be noted that fault geometries at outcrop generally reflect local lineament trends. At a number of localities, there also appears to be a strong correlation between the dominant slickenlines orientation and the mean fault intersection (Figure 10).

#### 5.2.2. Low-Angle Normal Faults

[42] A number of low-angle ( $<45^\circ$  dip) normal faults can be found in the vicinity of Raftsundet (e.g., localities LO9, 10 and 11; Figure 10). These generally dip to the west and northwest and have a listric geometry. These faults are characterized by a deformation zone (50–200 cm thick) of ductile (mylonitic) to semibrittle fault rocks (Figure 7f). Similar structures have been described by Heier [1960] and Løseth and Tveten [1996] on Hinnøya and Langøya to the

**Figure 5.** (a) A 2.5-D model of the Raftsundet region, Austvågøya, north Lofoten, comprising a Landsat image draped over DTM. (b) Lineaments (vector data) imported from ArcGIS and draped over DTM. (c) Best fit planes fitted through 3-D lineament traces to produce a 3-D fault model. (d) Regional and outcrop-scale fault planes analyzed in same 3-D model. (e) Fault planes at outcrop. Fault geometries are recorded as point data in the field using digital mapping methods. (f) Equal-area lower hemisphere stereoplot of regional fault planes derived from best fit planes through 3-D lineament traces. All models are constructed using GoCAD.

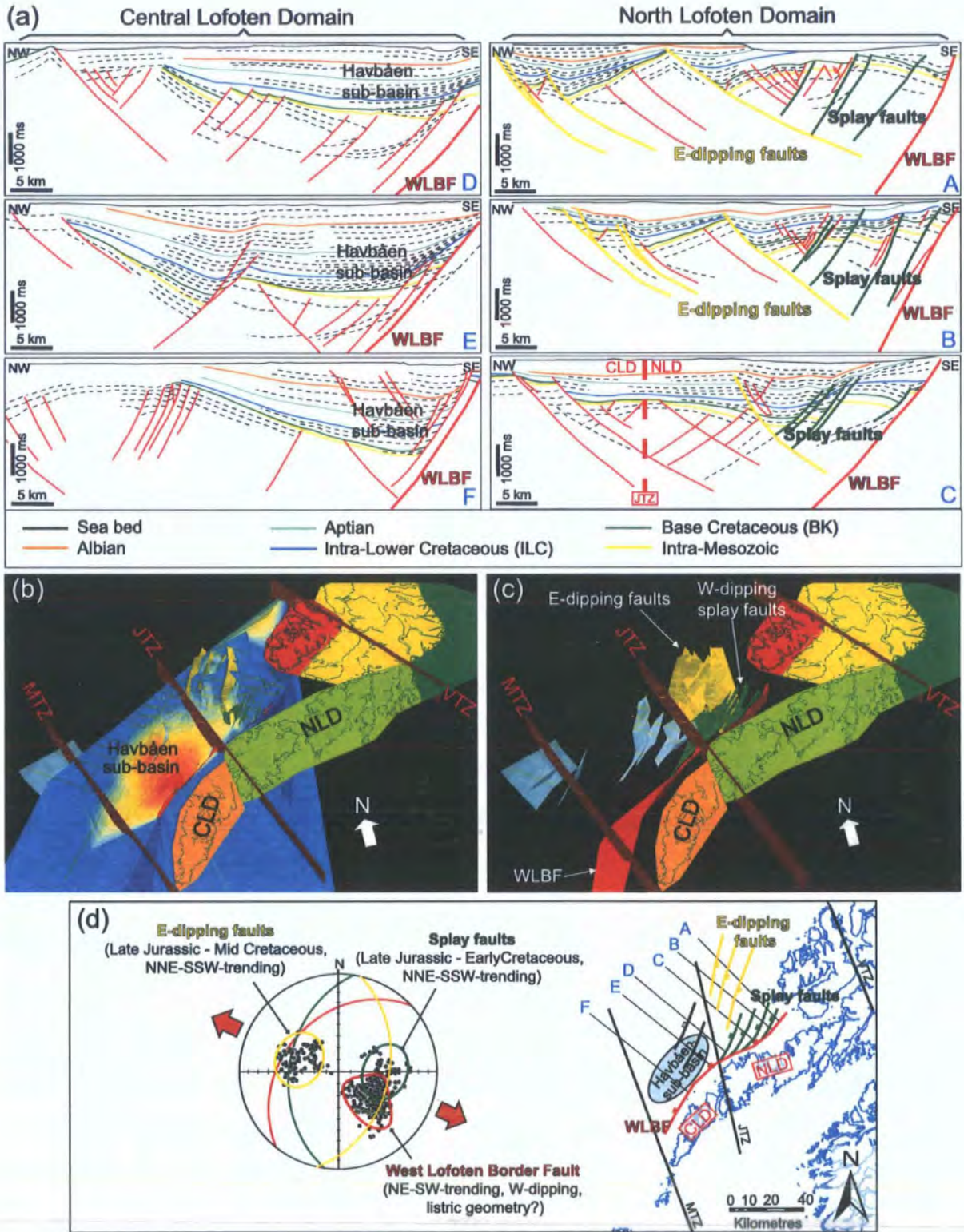


Figure 6



north. These faults are important as they appear to be locally reactivated by later brittle faults described above (Figure 7).

### 5.3. Age Relationships

[43] Both crosscutting fault relationships and overprinting slickenline have been analyzed in an attempt to determine a temporal succession of fault movements. A younging table (Table 1) was constructed using methodology of *Potts and Reddy*, [1999] in order to determine the relative age relationships of each fault set based on the field observations (e.g., crosscutting relationships and overprinting fault striae; Figure 7f). For the interpretation of age relationships faults have been categorized into six distinct systems based on orientation and slip: NNE-SSW (normal); NNE-SSW (strike slip); ENE-WSW (dip slip); ENE-WSW (strike slip); NE-SW (oblique slip); low-angle normal faults.

[44] Only a few conclusive and consistent crosscutting relationships between faults can be identified. Low-angle normal faults are clearly the oldest faults observed, with NNE trending (S1) faults appearing to be next, followed by ENE-WSW (S2) and NE-SW. However, the relationship between S1 and S2 faults appears far more complex with examples of S1 faults crosscutting S2 faults, and vice versa, being seen within any one exposure. This mutual crosscutting relationship therefore likely suggests that these fault systems developed at a similar time or at least were active during the same tectonic event. It should be noted that strike-slip striae appear to postdate dip-slip striae on most NNE-SSW trending (S1) fault surfaces; however, the relationship between dip-slip and strike-slip movements on S2 faults is more unclear. In many cases, multiple slickenlines on a single fault surface can be attributed to fault interaction rather than reactivation (see Figures 9c and 9d and section 5.5).

### 5.4. Kinematic Analysis

[45] Kinematic analysis was carried out using so-called "paleostress analysis" techniques. The analysis of fault slip data yields information concerning the orientation of the strain tensor, and thus the calculated axes are referred to using infinitesimal/finite strain nomenclature rather than principle stresses. The aims of our study here were (1) to determine if all fault movements are compatible with a single strain field and (2) to derive a "paleostress" tensor from the outcrop data that can be compared to kinematics inferred from regional fault patterns developed onshore and offshore. Kinematic inversion techniques have been exten-

sively used by various workers for nearly 40 years (see *Angelier* [1994] and *Ramsay and Lisle* [2000] for an exhaustive review). The assumptions and methods of paleostress have been discussed in detail in many other papers [*Etchecopar et al.*, 1981; *Angelier*, 1984, 1994; *Michael*, 1984; *Reches*, 1987; *Delvaux and Sperner*, 2003] and are not discussed here. It should be noted, however, that this approach is reasonable only in regions where there is little misorientation between finite and infinitesimal strain axis (i.e., in areas where finite noncoaxial strain is low).

#### 5.4.1. Inversion Procedures

[46] In total, 414 faults with good kinematic indicators were recorded (Figure 8a), which can be used for kinematic inversion. My Fault™ stereonet software, produced by Pangaea Scientific Ltd., was used for kinematic analysis.

[47] Two separate procedures for sorting the fault data into populations for inversion analysis have been applied during the present study. The first (procedure 1) simply uses the entire unsorted data set (i.e., all 414 fault and fault striae) while the second (procedure 2) required manual sorting and separate analysis of the data into fault systems.

[48] In procedure 1, after input of the raw data, data files were corrected to ensure that all striae lie perfectly on their respective fault planes (i.e., no angular mismatch). To do this, fault striae were rotated along the common plane containing the striae and the pole of the fault plane. Following this, the bulk fault population data set was inverted. Those faults with high misfit angles (>40°) relative to the inversion result were then rejected and the inversion rerun. This procedure was repeated until a single group of faults with a homogeneous solution could be found. The rejected data were then rerun through the program in an attempt to derive multiple paleostress vectors. A similar iterative approach has been applied by *Titus et al.* [2002]. This procedure was then repeated for various inversion methods [i.e., *Angelier*, 1984; *Michael*, 1984; *Reches*, 1987] to test the consistency of the results.

[49] In procedure 2, a potential risk when analyzing a bulk fault population data set with uncertain age relationships is that the kinematic data being analyzed represent more than one phase of movement. This can result in the derived vectors reflecting a combination of the two or more phases and may not be geologically meaningful [*Delvaux and Sperner*, 2003]. Fault data were separated according to fault geometry (i.e., fault systems 1 and 2; Figures 8b and 8c), and any examples of structures associated with fault interaction were disregarded as this violates the basic assumptions of inversion methods [*Nieto-Samaniego and*

**Figure 6.** (a) A series of interpreted seismic profiles, trending NW-SE, across the Ribban Basin. Profiles highlight changes in basin geometry and fault style between central Lofoten and north Lofoten. (b)–(c) Onshore-offshore 3-D models in ArcGIS (ArcScene). Figure 6b is a base Cretaceous horizon map showing a large depocenter (the Havbåen subbasin) offshore central Lofoten, and no basin apparent in north Lofoten. Figure 6c shows a fault model showing distinct change in geometry from south to north Lofoten (red, WLBF; green, splaying faults; yellow, low-angle east dipping faults; blue, other minor faults). Also shown are onshore lineament domains (colored polygons) and NNW-SSE trending transfer zones (red planes). Figure 6d is a stereonet (poles to planes) of faults picked in seismic (dips calculated using an interval velocity of 3000 m/s; readings taken every 1 km), plus base map showing location of seismic lines, fault trends, and "transfer zones."

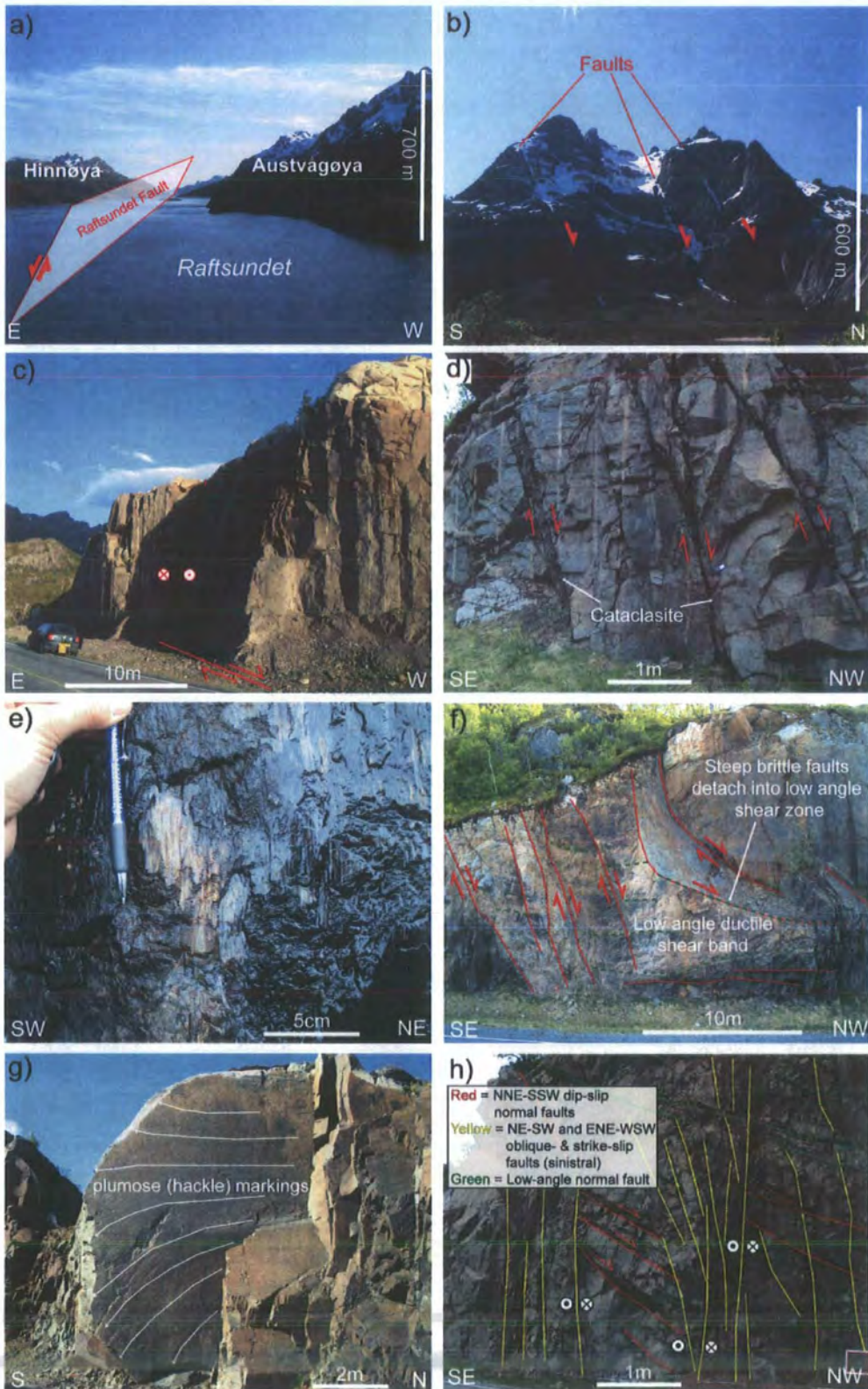


Figure 7

*Alaniz-Alvarez*, 1997]. As the data have already been sorted prior to analysis, the “iterative” sorting approach, used during procedure 1, was only required for the strike-slip fault set.

#### 5.4.2. Inversion Results

[50] Bulk inversion of all fault data (procedure 1) using the inversion method of *Michael* [1984] produced a sub-horizontal maximum infinitesimal extension strain axis ( $x_1 \equiv \sigma_3$ ) of 316/03, and subvertical minimum infinitesimal extension (or shortening) strain axis ( $z_1 \equiv \sigma_1$ ) of 170/86, and thus suggests that maximum horizontal extension ( $E_{hmax}$ ) was oriented NW-SE (Figure 11a). Similarly oriented axes were calculated using all other inversion methods [e.g., *Angelier*, 1984; *Reches*, 1987].

[51] Following procedure 2, three separate sets of paleo-stress axes can be derived, one for each fault system analyzed (i.e., system 1 dip-slip, system 2 dip-slip, and all strike-slip faults; Figures 8b–8d). Analysis of each fault system yield similarly oriented axes (of course, for strike-slip faults the  $y_i$  and  $z_i$  axes are switched; i.e.,  $Z$  is horizontal); although there is a 12° variation in the azimuth of the extensional axes ( $x_i$ ) (Figure 11b). These results are all consistent with a NW-SE maximum horizontal extension ( $E_{hmax}$ ), which is roughly 60° to the trend of the north Lofoten Ridge (i.e., in mapping area ridge trends approximately E-W).

#### 5.5. Fault Interaction: Implications for Stress Inversion

[52] In recent years, a number of studies have examined the limitations of inversion methods [*Pollard et al.*, 1993; *Cashman and Ellis*, 1994; *Nieto-Samaniego and Alaniz-Alvarez*, 1997; *Maerten*, 2000]. Slickenlines are kinematic indicators (slip vectors), and when these are used to interpret the regional stress field a number of assumptions have to be made. One of the most important assumptions is that the slickenlines are produced by the general stress tensor, implying that faults do not interact and that the stress field is not significantly perturbed after fault slip. *Pollard et al.* [1993] discuss how interaction between preexisting planes can lead to stress field perturbations of up to 40° in orientation when the density of fault planes is high. Interacting fault movements on preexisting planes can lead to multiple slickenline sets forming under a single regional stress field [e.g., *Cashman and Ellis*, 1994].

[53] In some areas of north Lofoten there is strong evidence to suggest that fault interaction has played a

significant role in the development of faults. As there are multiple fault orientations, and the spacing between faults is small (generally <2 m) some interaction between structures is likely. The mean slickenline orientations at many outcrops appear to coincide with the mean intersection between faults (e.g., Figure 10), which is consistent with the interacting block model of *Nieto-Samaniego and Alaniz-Alvarez* [1997]. Several examples of exactly this type of fault interaction have been recognized at outcrop (e.g., Figure 9c). Another example of interaction between faults is shown in Figure 9d. Here we see a continuous set of slickenlines that can be traced round a 90° bend, from an approximately N-S trending fault plane to one trending approximately E-W. The intersection between these planes appears well rounded, thus suggesting shear along these planes was directly linked. Fault movements suggest a counterclockwise rotation about a subvertical axis (note fault intersection plunges steeply toward the NE; Figure 9d), and are consistent with NW-SE extension with potentially a component wrench simple shear.

[54] *Nieto-Samaniego and Alaniz-Alvarez* [1997] have suggested that fault systems controlled by fault block interaction may not be suitable for paleostress analysis as a number of basic assumptions of these methods are violated. However, given the large number of data collected in the present study and the seeming consistency of the paleostress analysis results, we feel that in this case, a valid result has been obtained. One reason for this is that using a GIS for data management allowed efficient, quantitative filtering of all data points that do not meet certain geospatial or geological criteria. For example, all faults showing outcrop evidence for “fault interaction” were removed from the analysis.

[55] Furthermore, detailed analysis of fault movements associated with these examples of fault interaction indicate that kinematics appear consistent with stress axis interpreted using paleostress analysis described above (Figure 9).

## 6. Discussion

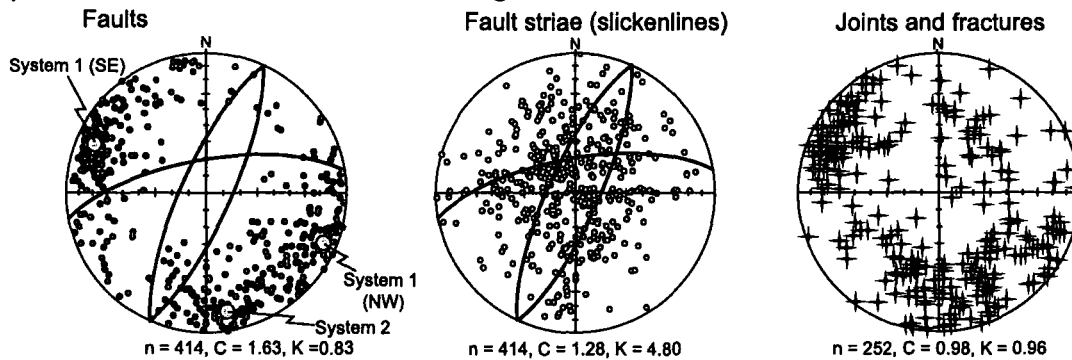
### 6.1. Structural Variations Along the Lofoten Ridges

#### 6.1.1. Variations Between Onshore and Offshore Structures

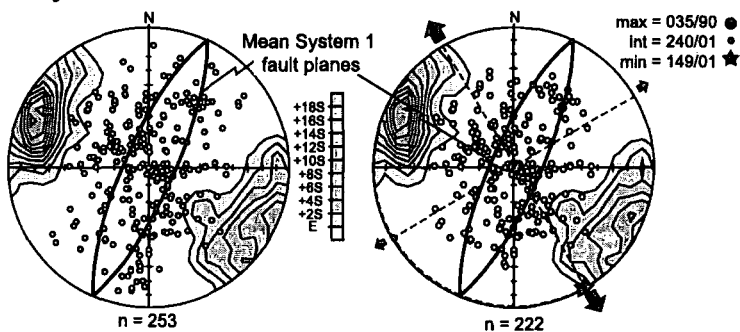
[56] Detailed onshore lineament studies have revealed that the LVA can be divided into a series of distinct lineament domains (Figure 3). These variations are coinci-

**Figure 7.** Photographs showing regional to outcrop-scale structures seen in Lofoten. (a) Raftsundet, believed to mark the trace of a major SE dipping fault (based on topographic contrasts either side of fjord, and also dominant dip direction of outcrop-scale faults; see Figure 8). (b) Lineaments picked from Landsat images are easily identifiable in the field, faults shown are S2 lineaments. (c) Good example of fault exposure seen in field, example shown is a N-S trending dextral oblique slip/strike-slip fault. (d) NW dipping system 1 faults containing cataclasite fracture bands, associated slip striae show dip-slip and dextral oblique-slip movements. (e) Dip-slip extensional slickenlines (striae) on system 1 faults. (f) Low-angle ductile shear zone showing mylonite shear bands dipping to NW, similar to Devonian detachments described by *Heier* [1960] and *Løseth and Tveten* [1996] farther north in Vesterålen. Brittle faults appear to locally reactivate/detach into these shear bands. (g) E-W trending joint with ornamentations that closely resemble plumose markings [*Hodgson*, 1961]. (h) Complex fault exposures near Raftsundet, from which crosscutting relationships may be observed (in this case, S2 cutting S1).

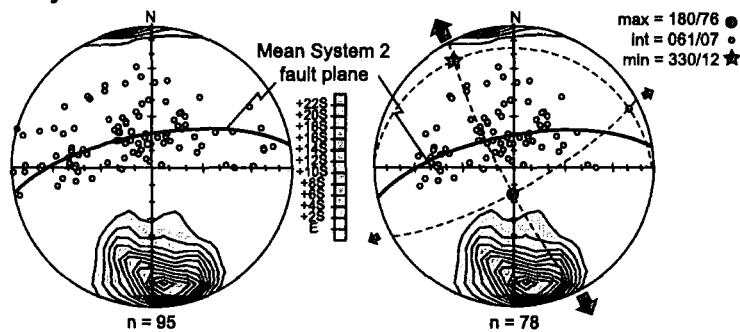
## a) Structural data collected during fieldwork



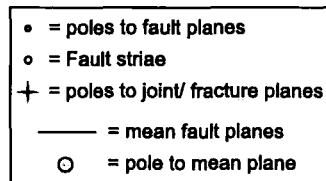
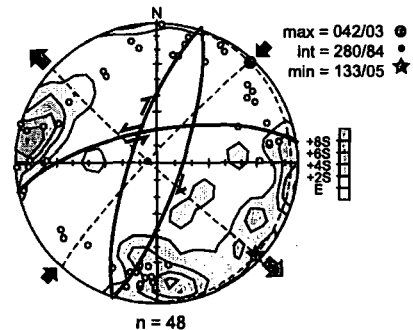
## b) System 1 faults



## c) System 2 faults



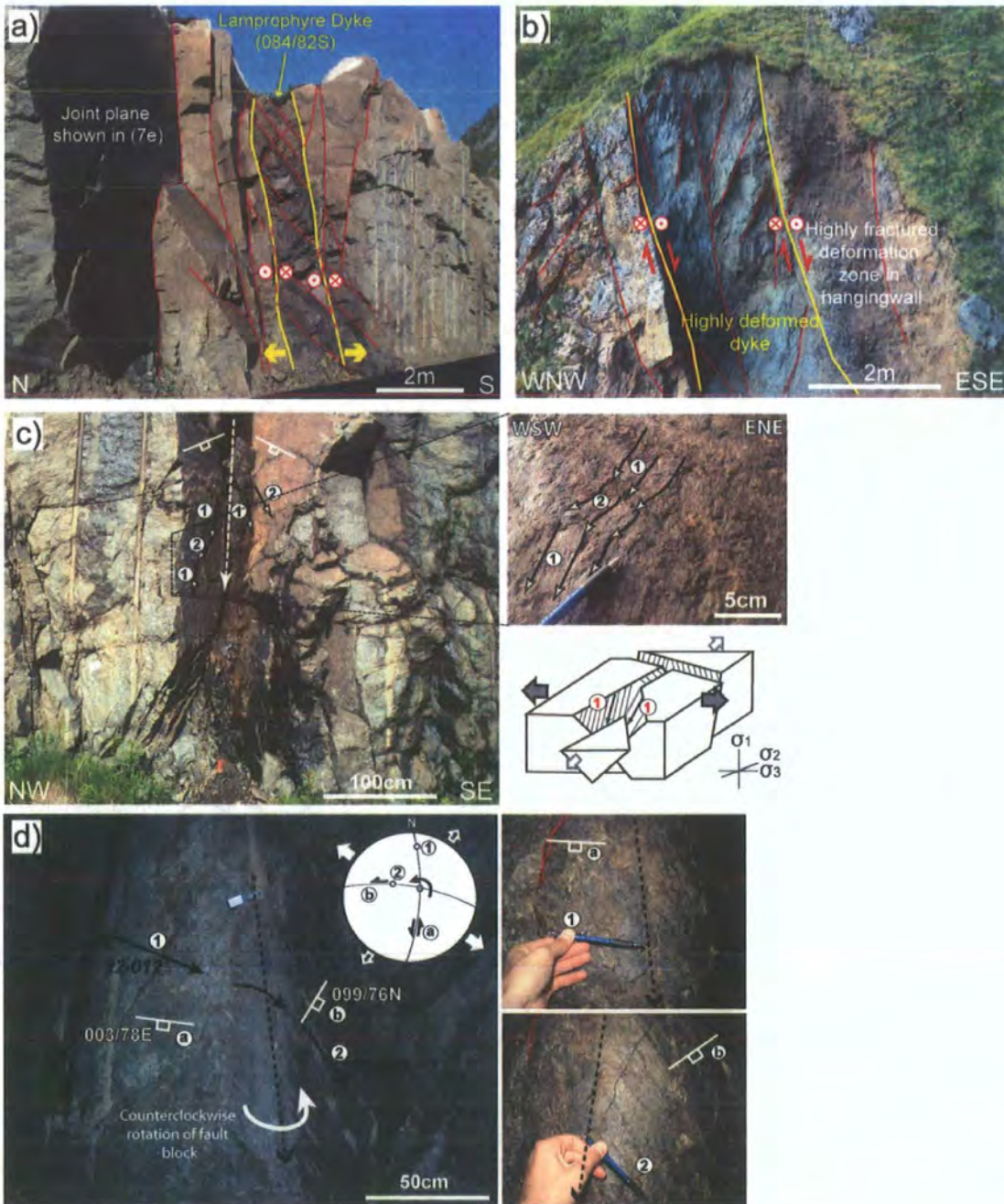
## d) Strike-slip faults



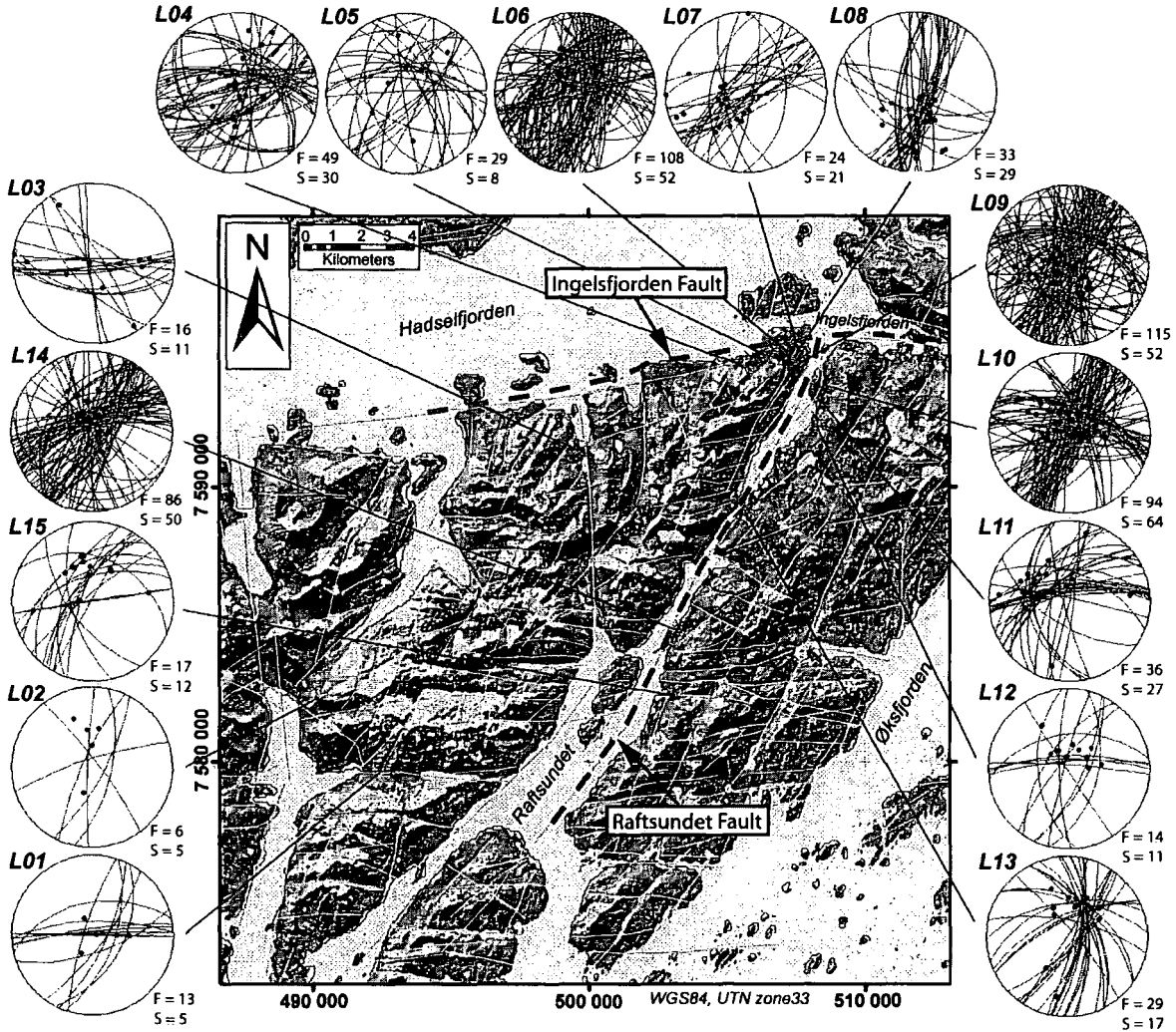
**Figure 8.** Equal-area lower hemisphere stereonets of structural data from Austvågøya, north Lofoten. (a) (left) poles to planes for all faults recorded in the field, (middle) slickenline lineations on these faults, and (right) poles to planes for joints and fractures. (b) Stereonets for system 1 faults (NNE-SSW/NE-SW trending) showing (left) contours of poles to planes, plus all associated slickenlines (points), and (right) dip-slip slickenlines, plus paleostress axes (calculated using procedure 2). (c) Stereonets for system 2 faults (ENE-WSW trending) showing (left) contours of poles to planes, plus all associated slickenlines (points) and (right) dip-slip and oblique-slip slickenlines, plus paleostress axes (calculated using procedure 2). (d) Combined strike-slip slickenlines for systems 1 and 2, plus paleostress axes (calculated using procedure 2). Data included on each plot are number of data (n) and eigenvector ratios reflecting “strength” (C) and “shape” (K) of preferred orientation.

dent with changes in ridge trend and physiography (i.e., landscape, topography, etc). In central Lofoten (CLD) the trend of the ridge is NNE-SSW, whereas in north Lofoten (NLD) the trend of the ridge is closer to ENE-WSW and is

also much broader. In this northern segment the lineament patterns appear more complex than those to the south. These changes onshore are consistent with important structural changes offshore. The WLB bounding the central Lofoten



**Figure 9.** (a) Lamprophyre dike at locality LO3 (see Figure 10 for locality map) trending parallel to system 2 faults and joints shown in Figure 7g. Dike margins reactivated by sinistral strike-slip faults movements. (b) Second dike exposure (locality LO2, Figure 10) trending NNE-SSW, again reactivated by later fault movements. (c) Outcrop photo showing a good example of fault interaction between intersecting faults (locality L06; Figure 10). Note stepwise trend of slickenlines, with a set running parallel to fault intersection line, which is comparable to the interacting block model of *Nieto-Samaniego and Alaniz-Alvarez* [1997]. (d) Second example of complex fault interaction (also locality L06), showing a continuous set of slickenlines that can be traced round a 90° bend, from an approximately N-S trending fault to an approximately E-W fault. Fault movements suggest a counterclockwise rotation about a subvertical axis and are consistent with NW-SE extension associated with a component wrench simple shear.

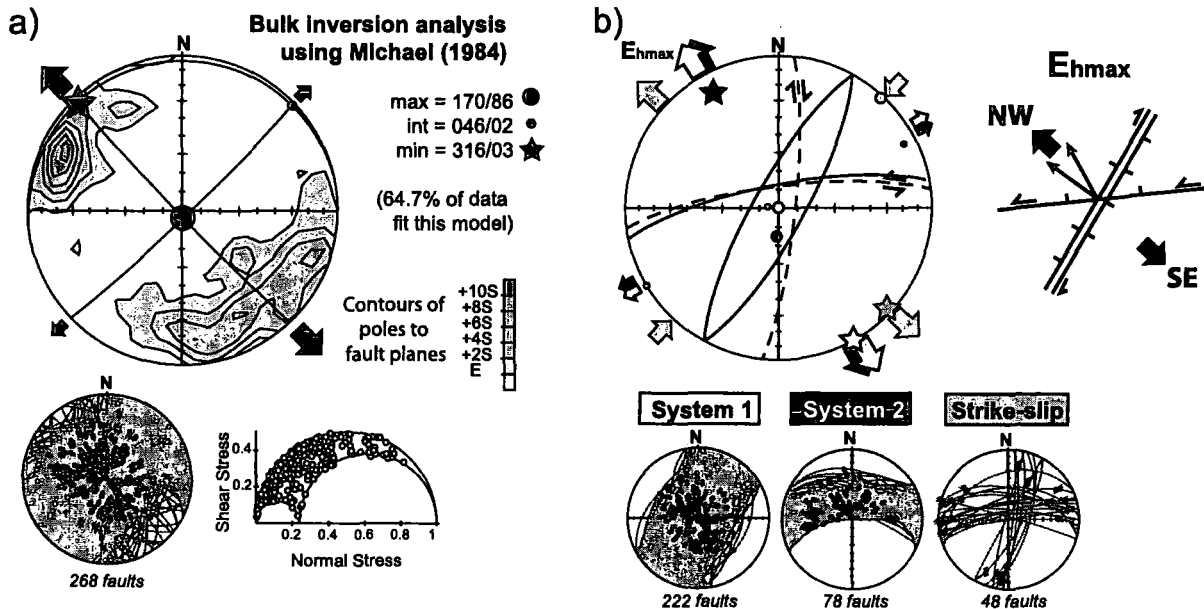


**Figure 10.** ArcGIS map showing location of fault populations and traverse sites, surrounded by individual stereonets for each locality. Stereonets plotted using GIS Stereoplot [Knox-Robinson and Gardoll, 1998] for ArcView 3.x.

**Table 1.** Matrix of Age Relationships Between Faults (Based on Outcrop Observations) Constructed Using Methods of Potts and Reddy [1999]<sup>a</sup>

Older	Younger					
	NE-SW (Oblique Slip)	ENE-WSW (Strike Slip)	ENE-WSW (Dip Slip)	NNE-SSW (Strike Slip)	NNE-SSW (Normal)	Low-Angle Normal Faults
NE-SW (oblique slip)		✓ (1)	✓ (3)	(not seen)	(not seen)	(not seen)
ENE-WSW (strike slip)	(not seen)		✓ (2)	✓ (2)	(not seen)	(not seen)
ENE-WSW (dip slip)	✓ (2)	✓ (4)		✓ (5)	✓ (4)	(not seen)
NNE-SSW (strike slip)	(not seen)	✓ (4)	✓ (1)		✓ (2)	✓ (1 - reactivated)
NNE-SSW (normal)	✓ (12)	(not seen)	✓ (5)	✓ (7)		(possible?)
Low-angle normal faults	✓ (2)	(not seen)	✓ (3)	✓ (5)	✓ (10)	

<sup>a</sup>Each cell in the matrix represents a possible relative age for the six fault sets/movements identified. Note that relative ages are determined through crosscutting and overprinting (reactivation) relationships; however, kinematics and fault interaction are not taken into account. Values in parentheses refer to number of observations made.



**Figure 11.** Kinematic inversion analysis. (a) Stereonet showing results of inversion analysis for bulk data (after 6 iterations) using *Michael's* [1984] method, plus stereonet of raw data and corresponding three-dimensional Mohr circle. (b) Stereonet showing results of inversion analysis for system 1 (dip slip) faults, system 2 (dip slip) faults, and strike-slip faults, using *Michael's* [1984] method. Arrows show horizontal stresses. All results suggest a NW-SE maximum horizontal extension (i.e.,  $E_{hmax}$  range from  $318^\circ$  to  $330^\circ$ ).

Ridge is a single, major, NNE-SSW trending fault with  $\sim 3$  km throw (Figure 6a), whereas offshore north Lofoten the WLBF is much less prominent, and appears to bend round into a NE-SW or ENE-WSW trend (i.e., trend similar to the ridge) with a series of NNE-SSW trending, west dipping, splay faults, with lesser throw (Figure 6). There is also a change in fault polarity farther offshore, with east dipping normal faults appearing to accommodate much of the extensional strain seen farther south on the WLBF.

[57] Both onshore and offshore north Lofoten fault patterns appear complex; however, slight differences can be seen between these areas (i.e., compare stereonets in Figures 5 and 6). This is likely to be due to the onshore and offshore study areas being located on slightly different parts of the ridge (i.e., offshore data is from west of Vestvågøya and southern Austvågøya, whereas onshore data is from northern Austvågøya) and thus slightly different ridge trends (approximately ENE-WSW and approximately E-W, respectively). A further explanation may also be that onshore we are looking at deformation within basement rocks in the footwall to the border fault; while offshore it is deformation within cover rocks of the hanging wall. However, onshore lineament trends on Vestvågøya appear similar to those offshore; therefore the former explanation appears more likely.

#### 6.1.2. Regional Versus Field Measurements of Onshore Faults

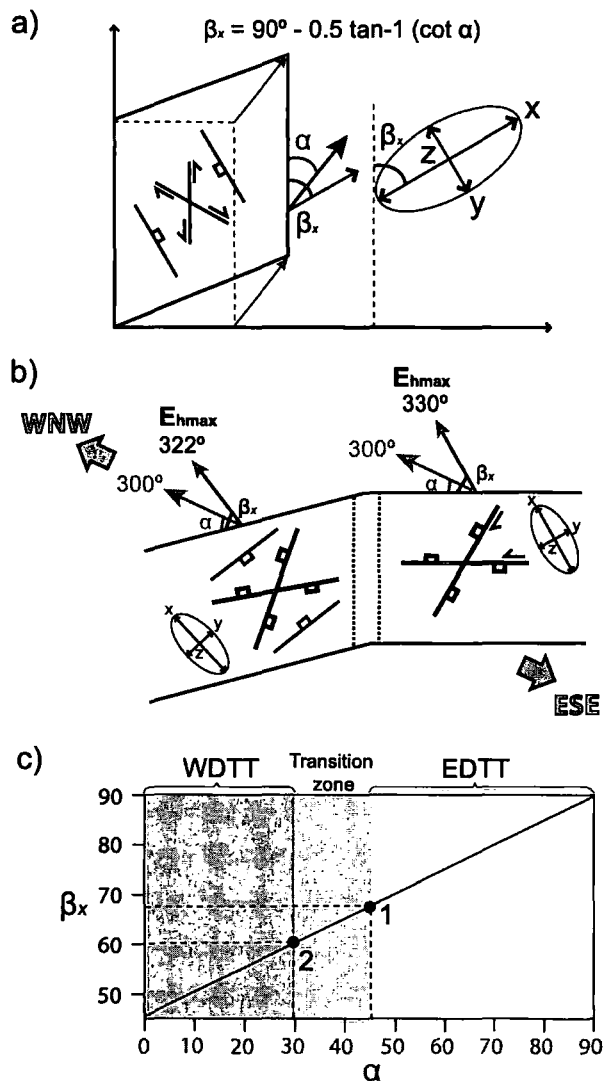
[58] Regional fault models derived from lineament analysis for the NLD show a rhombic fault block pattern

(Figure 5), with the poles to planes of these regional faults clustering in a bimodal distribution (i.e., near vertical dips; Figure 5f). However, field observations suggest that many of these regional faults have a shallower dip than those suggested by our 3-D model. For example, Figure 7b shows 3 large fault traces identified in the field which dip at  $\sim 60$ – $65^\circ$  north. These faults were also recognized from lineaments on the Landsat image and in the GoCAD™ model; however, these planes appear to dip at  $>80^\circ$ . Therefore it would appear that a limitation of this method of fitting best fit planes through lineament traces can lead to an oversteepening of the fault plane by  $\sim 10$ – $15^\circ$ . Hence any regional fault dipping at  $>75^\circ$  is likely to appear near vertical in this model. Consequently, we interpret the derived lineament data as masking a multimodal fracture distribution which we relate to 3-D deformation, rather than 2-D plane strain (see below and *Oertel* [1965], *Reches* [1978], and *Krantz* [1989]).

## 6.2. Oblique Extension and Transtension in North Lofoten

### 6.2.1. Multimodal Faulting in North Lofoten: Polyphase Deformation or 3-D Strain?

[59] Rift systems that undergo extension oblique to the basin bounding faults commonly show complex multimodal fault patterns [e.g., *Withjack and Jamison*, 1986; *Clifton et al.*, 2000; *Dewey*, 2002; *De Paola et al.*, 2005a, 2005b]. As the extension directions calculated in north Lofoten appear moderately oblique to the trend of the ridge, it is likely that



**Figure 12.** (a) Simplified box model summarizing relationship between  $\alpha$  and  $\beta_x$  and the relative to the deformation boundary. (b) Cartoon diagram summarizing corrections due to obliquity between  $E_{hmax}$  and local ridge trend in order to estimate true regional extension (i.e., use equation (1) to calculate  $\alpha$  (angle between regional extension vector and trend of ridge) from  $\beta_x$  (angle between  $E_{hmax}$  and trend of ridge)). (c) An  $\alpha$  versus  $\beta_x$  plot corresponding to solution of equation (1) [from *De Paola et al.*, 2005a]. Points 1 and 2 correspond to  $\alpha$  and  $\beta_x$  angles for north Lofoten Ridge segments shown in Figure 12b. Results suggest fault patterns developed under oblique WNW-ESE extension.

this area has undergone transtensional deformation. Both regional and outcrop studies in north Lofoten have revealed an apparent multimodal fault geometry, i.e., fault patterns dominated by more than two distinct fault sets (Figure 8a). Multiple fault orientations are common in many geological

settings [e.g., *Krantz*, 1988, 1989; *Nieto-Samaniego and Alaniz-Alvarez*, 1997; *Sagy et al.*, 2003]. *Nieto-Samaniego and Alaniz-Alvarez* [1997] proposed four main mechanisms to develop such multimodal fault patterns are (1) polyphase deformation (i.e., two or more sets of faults, developed due to two or more deformation events, assuming Andersonian fault models); (2) reactivation of noninteracting faults according to the *Bott* [1959] model; (3) faulting associated with 3-D strain (e.g., orthorhombic faulting [*Reches*, 1978; *Krantz*, 1989]); and (4) interacting block model [*Nieto-Samaniego and Alaniz-Alvarez*, 1997]. As transtensional deformation is a combination of extension and strike-slip deformation [*Sanderson and Marchini*, 1984; *Dewey*, 2002], fault patterns associated with 3-D strain are also likely to develop [*Reches*, 1978; *De Paola et al.*, 2005a]. Therefore, during a bulk homogeneous transtensional deformation, case 3 seems to be the most likely kinematic solution which will govern the development of faulting patterns under infinitesimal strain fields. As finite strains accumulate, however, case 2 and particularly case 4 could increasingly become important [*Nieto-Samaniego and Alaniz-Alvarez*, 1997; *De Paola*, 2005]. This appears to be the case in north Lofoten where we see a regional set of multimodal faults not dissimilar to orthorhombic patterns of *Reches* [1978], with strong evidence for fault interaction in areas of highest fracture density (i.e., near major faults such as the Raftsundet Fault).

[60] An alternative model to transtension in north Lofoten is that each fault system developed independently (i.e., as suggested by *S. G. Berge et al.* (The Lofoten-Vesterålen continental margin: A multiphase Mesozoic-Palaeogene rifted shelf as shown by offshore-onshore brittle fracture analysis, submitted to *Norwegian Journal of Geology*, 2006, hereinafter referred to as *Berge et al.*, submitted manuscript, 2006) during slightly different regional stress. Although some degree of polyphase deformation is apparent from observations made in this study (i.e., multiple slikenines and crosscutting relationships), mutual crosscutting relationships between S1 and S2 faults suggest they are likely to be contemporaneous. Thus we suggest that much of the apparent polyphase deformation seen in Lofoten is the result of fault interaction and localized variations in stress during a prolonged phase of deformation. This model is also favored by the fact that kinematic indicators on almost all faults correspond to a similar NW-SE extension. However, without better age constraints for individual fault movements, distinguishing which of these contrasting models is more likely is somewhat difficult.

#### 6.2.2. Corrections Because of Oblique Extension

[61] Up to this point we have been discussing NW-SE extension axes based on observations in north Lofoten. However, in section 6.2.1 we suggest that the fault patterns in this area likely developed in transtension, and that maximum horizontal extension is oblique to the trend of the ridge. *Withjack and Jamison* [1986] show that during oblique rifting the orientation of maximum horizontal extension-strain ( $E_{hmax}$ ) is controlled by  $\alpha$ , the angle between the rift trend and the direction of displacement. This is defined by the relationship between the angles  $\alpha$  and



**Table 2.** Summary of the Predicted Orientations of Faults On the Basis of Fault Models of *Withjack and Jamison* [1986] for Segmented Transtension Model for the Lofoten Ridge<sup>a</sup>

Deformation Zone (and Trend)	Deformation Type	$\alpha/\beta$	Faults Predicted by <i>Withjack and Jamison</i> [1986]		
			Fault Type	Trend Relative to the Deformation Zone Boundary	Apparent Strain Axis
A (030)	pure extension	90/90	normal	0 (030)	290
B (075)	wrench/extension-dominated transtension	45/67	sinistral SS, dextral SS, normal	0° Counterclockwise (075), 60° Counterclockwise (015), 30° Counterclockwise (045)	322
C (090)	wrench-dominated transtension	30/60	sinistral SS, dextral SS	8° Counterclockwise (082), 68° Counterclockwise (012)	330

<sup>a</sup>See Figure 13. Regional extension is taken to be 300–120 (i.e., normal to mean trend of normal faults, which also matches results of applying equation (1) to mean “paleostress” vector determined through kinematic analysis in deformation zone C.

$\beta$ , which correspond to the acute angles of the regional extension vector, and the maximum horizontal extension strain ( $E_{hmax}$ ), respectively, measured relative to the deformation zone boundary (Figure 12a) according to (shown graphically in Figure 12c)

$$\beta_x = 90^\circ - 0.5 \tan^{-1}(\cot \alpha) \quad (1)$$

which may be rewritten more simply as [McCoss, 1986]

$$90^\circ - \beta_x = \frac{1}{2}(90^\circ - \alpha) \quad (2)$$

In north Lofoten,  $E_{hmax}$  ( $330^\circ$ – $150^\circ$ ) inferred from lineament trends, and calculated from paleostress inversion, appears to be moderately oblique ( $\beta_x \approx 60^\circ$ ) to the trend of the ridge (trend  $090^\circ$ – $270^\circ$ ). By applying equation (1), we see that this  $\beta_x$  angle corresponds to an  $\alpha$  value of  $30^\circ$ , and thus implies a regional extension closer to WNW-ESE ( $300^\circ$ ; Figure 12b and Table 2).

### 6.2.3. Orthogonal and Oblique Ridge Segments

[62] Ridge segment orientations relative to the direction of plate motion appear to play a critical role in determining the structural architecture of a particular ridge segment [see also *Taylor et al.*, 1994; *Clifton and Schlische*, 2003]. Onshore, variations in the dominant lineament/fracture trends along the Lofoten Ridge can be explained using a model for oblique extension/transtension along the LVA that develops due to the changing trend of the deforming zone boundary structures (i.e., border faults to the ridge) with respect to the regional extension vector (Figure 13). In this model there are three distinct deformation zones. In central Lofoten, there is a zone of orthogonal extension ( $\alpha = 90^\circ$ ) (zone A), passing northward into two zones of transtension (B and C). Zone B corresponds to an angle  $\alpha$  of  $\sim 45^\circ$ , which is close to the transition between extension-dominated and wrench-dominated transtension (shown as  $20^\circ$  in Figure 1, but it generally ranges from  $30^\circ$  to  $40^\circ$  for most rocks, Figure 12c; see *De Paola et al.* [2005a]) while zone C lies just within the wrench-dominated field (horizontal  $z$  axis) with an  $\alpha$  value of  $30^\circ$  (Figure 13).

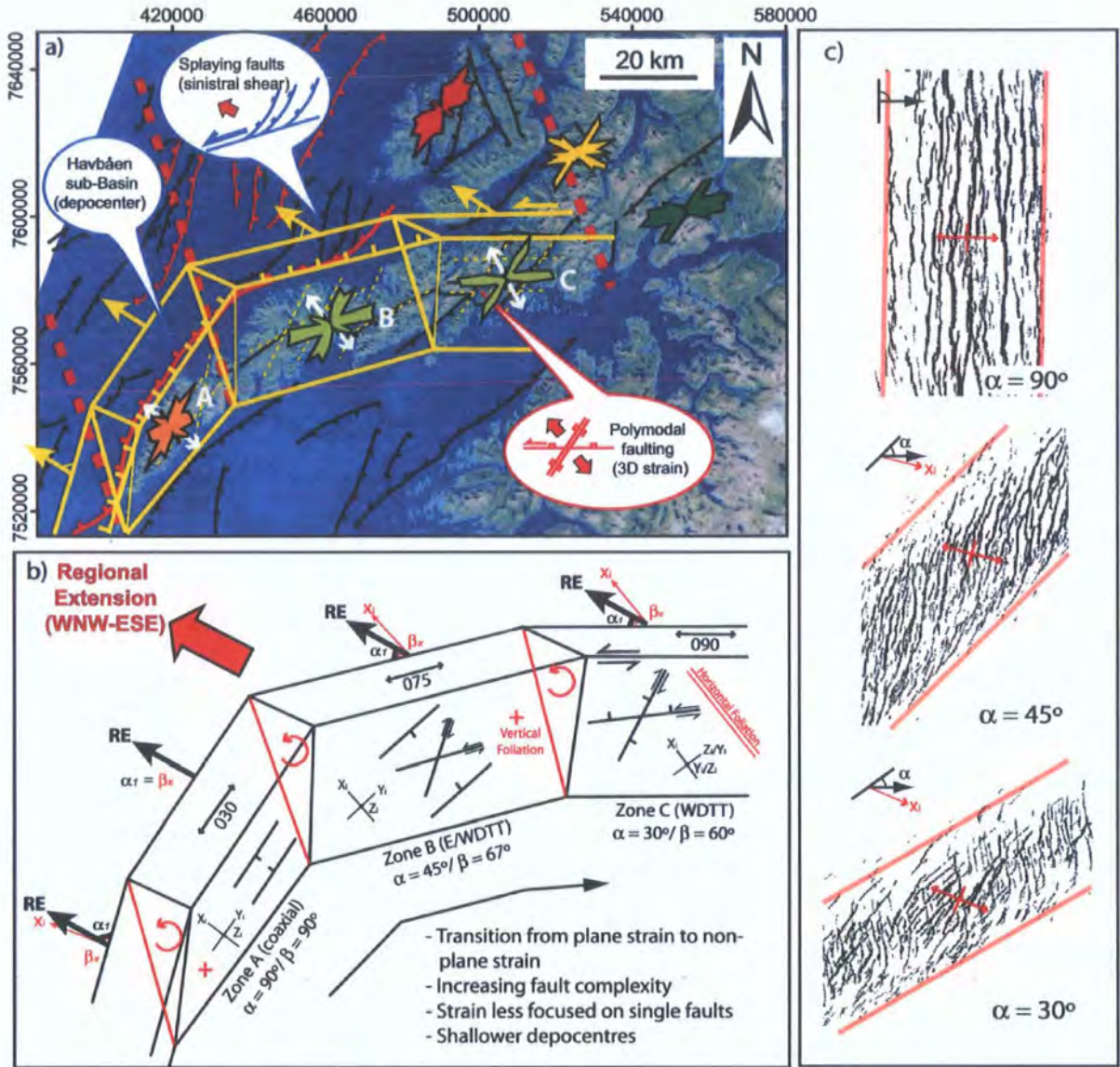
[63] The model for increasingly oblique transtension northward along the Lofoten Ridge is also consistent with offshore structural changes. Each zone is predicted to exhibit different faulting patterns and degrees of vertical shortening. In zone A, the shortening axis is vertical

predicting a significant amount of vertical thinning and rift-related subsidence. In zones B and C smaller amounts of vertical thinning and rift-related subsidence are predicted. Our observations offshore suggest that in the central Lofoten domain the WLBF has a large throw, with a deep sedimentary basin developed in its hanging wall. Along strike in the region offshore from the NLD, the fault throws are reduced and the basins are markedly shallower or even absent.

[64] In our model, the boundaries between each domain may have started off trending roughly N-S (perhaps controlled by preexisting Permian extensional structures (Figure 14) [*Steltenpohl et al.*, 2004]) and highly oblique to the regional extension. As extension continued these boundaries are likely to have rotated counterclockwise to lie parallel to the NNW-SSE trending transfer zones inferred by *Tsikalas et al.* [2001] (Figures 2 and 13).

### 6.2.4. Comparisons With Experimental Models and Other Field Analogues

[65] Experimental clay models for oblique rifting show that fault orientation will change with respect to the angle of obliquity,  $\alpha$  (Figure 13c and Table 2) [*Withjack and Jamison*, 1986; *Clifton et al.*, 2000]. The fracture patterns predicted by these models show similar trends to those observed in lineament patterns for each domain along the Lofoten Ridge (Figure 3 and 13a). Significantly, the complex multimodal fault patterns and orientation of faults relative to the ridge bounding fault seen in north Lofoten (i.e., Austvågøya and Vestvågøya) resemble models for  $20^\circ$ – $30^\circ$  oblique divergence (Figure 13c) [*Withjack and Jamison*, 1986; *Clifton et al.*, 2000]. This model for oblique extension also appears valid for offshore fault patterns which show an en echelon style set of faults splaying off the WLBF, and suggest a component of sinistral shear along the border fault (note that this may also explain the significant decrease in throw along the WLBF in this area). The kinematic inversion analysis of outcrop-scale faults within north Lofoten suggests a NW-SE extension. If we use the ridge trend in this domain (approximately E-W) to define regional-scale orientation of the deformation zone boundary faults, then  $\beta = 60^\circ$  for the NLD. By applying equation (1), we obtain an angle  $\alpha = 30^\circ$ , and a regional extension vector (RE) oriented  $300^\circ$  (for exact values see Figure 12 and Table 2). Importantly, this WNW-ESE

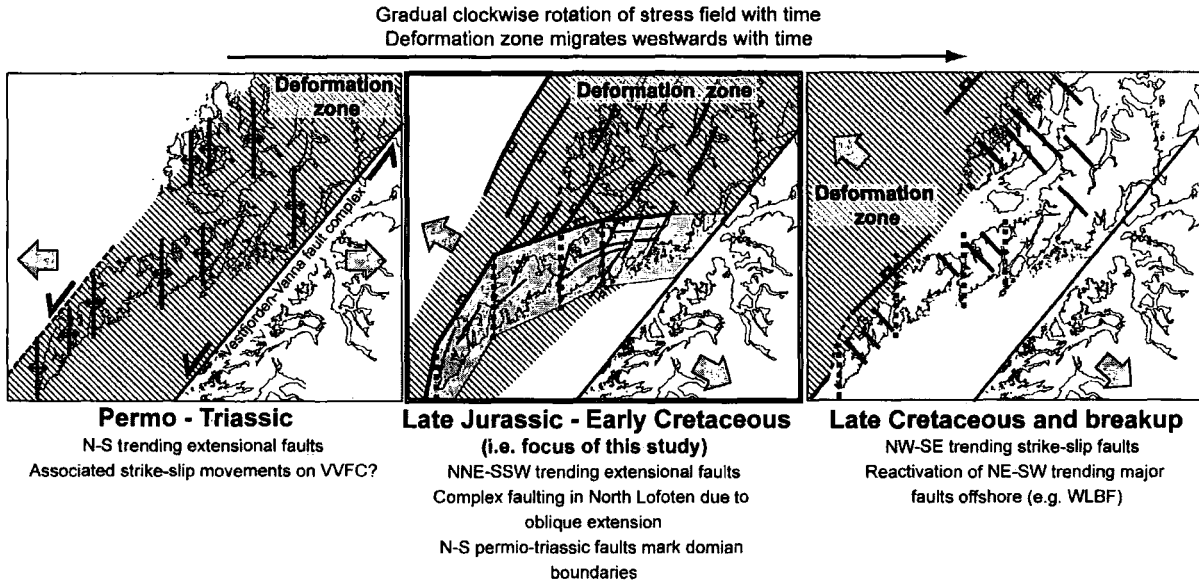


**Figure 13.** (a) Summary map showing variations in fault patterns and structural style along the Lofoten Ridge. A, B, C refer to deformation zones described in Table 2. Rose diagrams show summary of lineament trends for each lineament domain outlined in Figure 3. Offshore faults adapted from *Tsikalas et al.* [2001]. (b) Predicted deformation patterns and the effects of increasing obliquity along the Lofoten Ridge (based on models of *Withjack and Jamison* [1986] and *Dewey* [2002]) (see also Table 2). (c) Fault trace maps for various angles of divergence, highlighting the effects of increasing obliquity (i.e., decreasing  $\alpha$ ) on fault patterns; taken from results of experimental clay models by *Clifton et al.* [2000].

extension direction corresponds well with extension directions documented along other parts of the Norwegian margin during the Early Cretaceous [e.g., *Mosar et al.*, 2002].

[66] Similar fault patterns to those seen in north Lofoten have also been observed on the Reykjanes Peninsula, SW Iceland, where plate motion is roughly  $30^\circ$  oblique to the plate boundary in a left lateral sense [*Taylor et al.*, 1994;

*Clifton and Schlische*, 2003]. In this example multimodal fault patterns are again apparent, with a combination of both strike-slip and dip-slip fault kinematics [*Clifton and Schlische*, 2003]. Recent studies have shown that these faults developed under a variable stress history, with alternating phases of extension-dominated and wrench-dominated deformation, over short geological timescales (i.e., less than 1000 years) [*Kattenhorn and Clifton*, 2005]. These



**Figure 14.** Possible model for the structural evolution of the Lofoten Ridge from Permian through to Eocene. Main structures discussed in this study correspond to Late Jurassic–Early Cretaceous extension.

variations in deformation style have been attributed to the influence of oscillatory magmatic events on local stress field, and have led to complex crosscutting, overprinting and fault reactivation, during what may be described as a single tectonic event [Holdsworth *et al.*, 1997]. A similar explanation may be applicable for the complex crosscutting relationships and overprinting of strike-slip and dip-slip slickenlines seen in the Lofoten as a relatively young Lamprophyre dike (compared to those described by Griffin *et al.* [1978]) was seen trending parallel to (084/82S), and reactivated by, system 2 faults (Figure 9a). A prominent set of tensile fractures/joints, were also seen trending parallel to this dike (Figure 7e). A second more highly deformed dike was also seen trending parallel to S1 faults (Figure 9b). The age of these dikes is unknown, but we suggest that they may have been emplaced synchronous with extensional faults and joint formation in these basement rocks (i.e., similar to the model of Kattenhorn and Clifton [2005]). However, as this model is based on the observation of just two Lamprophyre dikes, further field research is required.

[67] A further similarity between the observations made in this study and those described from the Reykjanes Ridge is the occurrence of complex fault interaction, particularly at the “inside corners” of fault/ridge segments [Clifton *et al.*, 2005]. As shown in Figure 9c, d a number of good examples of fault interaction have been observed in this study, all of which were found at the inside (i.e., footwall) corner between the intersecting Raftsundet and Ingelsfjorden Faults (i.e., localities LO6, LO8, and LO9; Figure 10).

### 6.3. Margin Segmentation and Evolution

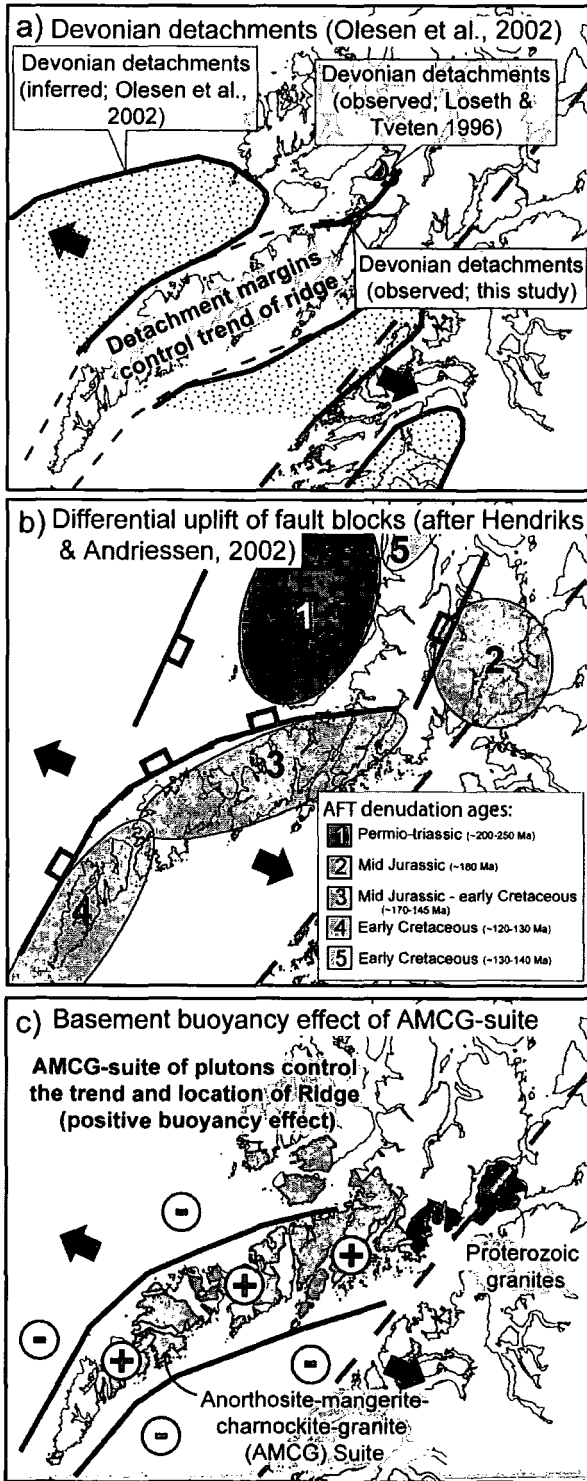
#### 6.3.1. Ridge Development and Fault Evolution

[68] A number of different fault/fracture trends have been identified from lineament studies (S0–S3; Figures 3 and 4).

However, only two of these trends are accounted for in our model for oblique extension during the Late Jurassic and Early Cretaceous (i.e., S1 and S2). Age relationships interpreted from apparent crosscutting relationships identified during remote sensing and visualization of 2.5-D and 3-D models suggested that S0 lineaments are likely to be older and S3 lineaments younger, than S1/S2 structures. We therefore tentatively suggest a model for the development of these structures as follows: the progressive development of S0 faults/fractures during E-W extension, followed by S1/S2 faults developing during WNW-ESE oblique extension, and finally S3 strike-slip faults during NW-SE extension (Figure 14). Consistent with observations made by Lundin and Doré [1997] and Olesen *et al.* [1997] there is likely to have been a westward shift in deformation with time from the east Lofoten and the Vestafjorden-Vana fault complex during the Permian, through to offshore west Lofoten in the Cretaceous (Figure 14). This model is similar to the multistage model proposed by Berge *et al.* (submitted manuscript, 2006), the only exception being in our model S1 and S2 faults are active contemporaneously due to oblique extension. This suggested evolution is consistent with plate reconstructions of the Norwegian-Greenland margins which show E-W extension during Permian to Jurassic times, rotating progressively through WNW-ESE during Late Jurassic to Early Cretaceous, to NW-SE extension during Late Cretaceous and Paleogene, and ending with NW-SE seafloor spreading in the Eocene [Doré *et al.*, 1999; Mosar *et al.*, 2002].

#### 6.3.2. Segmentation of the LVA: Transfer Zones and Segment Boundaries

[69] Most maps of both the Norwegian and Lofoten-Vesterålen margins show that they are segmented by a series of NW-SE transfer zones [Lundin and Doré, 1997;



Olesen et al., 1997, 2002; Brekke, 2000; Tsikalas et al., 2001]. This inferred segmentation of the Lofoten-Vesterålen region is based on changes in fault polarity and sediment thickness offshore, and crustal structure (derived from potential field data) onshore [Olesen et al., 1997, 2002; Tsikalas et al., 2001]. Hendriks and Andriessen [2002] have also shown that separate ridge segments appear to show different denudation histories. A number of rift segments and transfer zones have been proposed (see Figure 2), but there are disagreements concerning the exact position and orientation of these structures [e.g., Tsikalas et al., 2001; Olesen et al., 2002]. A key reason for this indecision on the location of these structures is the fact that no distinct lineaments representing these transfer zones can be identified.

[70] The Bivrost, Vesterålen and Senja transfer zones have been attributed to the influence of deep seated basement structures at depth [Olesen et al., 2002; Mjelde et al., 2003]. Known examples of such structures may include the Bothnian-Kvænangen and the Bothnian-Senja fault complexes (Figure 2). It is somewhat difficult, however, to link other transfer zones on the LVA (e.g., the Mosken, Jennegga transfer zones) to such basement shear zones. Instead, these transfer zone boundaries appear to be zones of “soft linkage” (or accommodation zones [Peacock et al., 2000]) between margin segments characterized by different basin and fault geometries. Furthermore, the structure of these differing margin segments appears to correspond to variations in the divergence angle between the ridge (or margin) bounding faults and the regional extension vector (Figure 13). Similar observations have also been made along the Brazilian margin of the South Atlantic [Davison, 1997] where the width of the margin may also be linked to obliquity.

**6.3.3. Origins of Oblique Ridge Segments**

[71] As our model for margin segmentation is based on the influence of oblique margin segments, we must therefore assess the origins of margin obliquity. Oblique extension is generally associated with the reactivation or control of preexisting structures [Holdsworth et al., 1997]. No distinct fabrics (e.g., shear zones, strong foliation, etc.)

**Figure 15.** Possible controls on the development of the obliquely trending north Lofoten Ridge segment. (a) Reactivation of “spoon-shaped” Devonian detachment faults that may have controlled the trend of the northern part of the Lofoten Ridge [Olesen et al., 2002]. However, only localized reactivation of Devonian low-angle faults has been observed in this study. (b) Differential uplift of fault blocks from Permian to Cretaceous that may effect the development of fault trends in neighboring blocks (i.e., older fault blocks in result in outer Vesterålen Block, block 1, may have acted as a barrier to later faults developing during the uplift of the main Lofoten Ridge, blocks 2, 3, and 4). Denudation ages from AFT studies by Hendriks [2003]. (c) A basement buoyancy effect caused by the AMCG suite (anorthosite-mangerite-charnockite-granite) underlying much of North Lofoten that may have led to the preferential uplift of an oblique trending ridge block, i.e., similar to effect of granites under Mid-North Sea High [Donato et al., 1983].

were observed within the basement rocks studied that could directly account for the oblique trend of the north Lofoten Ridge. A few discreet E-W trending joints and dikes were recorded that appear to be reactivated by faults at outcrop; however, the age of these is unclear (i.e., they may be synchronous with faulting), and they are not intense enough to account for the overall change in ridge trend. Figure 15 shows three possible origins for this obliquity; however, research is required to investigate these further.

[72] *Olesen et al.* [2002] proposed a model in which the border faults to the north Lofoten Ridge reactivate “spoon-shaped” Devonian detachments (Figure 15a; also see Figure 16 of *Olesen et al.* [2002]). Field observations of these low-angle, Devonian, detachment structures have been made in Hinnøya [*Løseth and Tveten*, 1996] and northern Austvågøya (this study). However, such low-angle structures are only likely to have a limited effect on the location and orientation of steeply dipping Mesozoic basin bounding extensional structures, and therefore further structural influence is required. Geophysical studies [*Sellevoll*, 1983; *Olesen et al.*, 1997, 2002] in central and northern Norway show the Lofoten Ridge to be associated with strong magnetic and gravimetric anomalies. A positive gravity anomaly beneath the south and central Lofoten Ridge are believed to reflect a shallow Moho discontinuity and uplifted high-grade rocks of intermediate density [*Sellevoll*, 1983; *Olesen et al.*, 2002]. This exhumation of rocks from the deep crust has led some authors to describe Lofoten as a “core complex” [*Hames and Anderson*, 1996] which may have developed as far back as the Devonian.

[73] Recent Apatite fission track (AFT) studies suggest that the LVA has undergone differential block uplift in post-Caledonian times (Figure 15b). *Hendriks and Andriessen* [2002] document various AFT ages along the LVA indicating differential vertical movements across the area. The oldest cooling/denudation ages were observed on Langøya, which indicate uplift/exhumation during the Permian/Triassic. North Lofoten on the other hand shows evidence for cooling/denudation from Mid-Jurassic to Early Cretaceous. It is possible that the earlier exhumed Langøya block acted as a barrier to the developing WLBF, thus leading to it deflecting eastward toward the already established Vestfjorden-Vanna fault complex [*Olesen et al.*, 1997]. As the WLBF changes in trend, strain is also accommodated by east dipping faults farther offshore, and to the west of the Langøya Block, thus leading to a Jurassic/Cretaceous basin bound on three sides on Vesterålen (Figure 15b) [*Dalland*, 1981; *Davidsen et al.*, 2001].

[74] A third model is one of basement buoyancy similar to the models proposed by *Bott* [1967] and *Donato et al.* [1983] for parts of the North Sea. The rocks of the north Lofoten Ridge are dominated by an anorthosite-mangerite-charnockite-granite (AMCG) suite of plutons (Figure 15c) [*Griffin et al.*, 1978; *Corfu*, 2004a] dating from ~1.8 Ga. The basement rocks on south Lofoten on the other hand are dominantly older Archaean/Paleoproterozoic gneisses [*Tveten*, 1978; *Corfu*, 2004a]. These granites typically have a slightly lower density than the surrounding basement rocks, which may lead to a slight buoyancy effect of the

granites as they move toward equilibrium with the surrounding basement [*Bott*, 1967]. This basement buoyancy effect has been used to explain the tectonic stability and/or uplift of areas underlain by granites [*Bott*, 1967; *Donato et al.*, 1983]. In addition, it has been suggested that this stability is most effective during times of extension [*Bott et al.*, 1978]. It is possible that the AMCG suite may have controlled the trend and development of the north Lofoten Ridge in this manner (Figure 15c). However, as these granites are of Precambrian age, it is likely that they reached equilibrium with surrounding rocks long before the Cretaceous, although it is possible that this buoyancy effect may have influenced the development of the Devonian detachments described above [*Olesen et al.*, 2002]. This may also explain the apparent elevated nature of the Lofoten Ridge through time [*Sherlock*, 2001]. Although each of the models presented in Figure 15 are presented as mutually exclusive hypotheses, they may all play a role in the development of the ridge and could be applicable in combination.

## 7. Conclusions and Implications for Future Exploration on the Norwegian Margin

[75] Through an integrated onshore, offshore and regional to outcrop-scale fault study we present a self-consistent structural model for transtension and structural segmentation along the Lofoten Ridge. Segment orientations relative to the direction of regional extension appear to play a critical role in determining the structural architecture of each particular ridge segment [see also *Taylor et al.*, 1994; *Clifton and Schlische*, 2003].

[76] The Lofoten-Vesterålen archipelago can be divided into a series of distinct structural domains reflecting varying fault patterns. These domains are concurrent with changes in trend of the Lofoten Ridge; therefore we attribute these variations in fault/fracture pattern to changes in  $\alpha$  (the angle between the trend of the ridge and the regional extension vector; Figures 1, 12, and 13). Analysis of lineament trends and kinematic analysis of field data (including paleostress inversion) suggest a maximum horizontal extension ( $E_{hmax}$ ) direction of ~320° to 325° in north Lofoten. This corresponds to a  $\beta_x$  value of ~60° and thus an  $\alpha$  of ~30°. Therefore regional extension associated with this deformation is WNW-ESE. This model for oblique extension is supported by offshore variations depocenter location and fault geometry, with deep basins and simple faulting typical of areas where the ridge/border fault is orthogonal to extension, and complex faulting and less subsidence in more oblique settings. The changes in fault orientation, fault geometry and inferred extension directions for each domain in the Lofoten are consistent with analogue studies and experimental clay models of where the boundary conditions become increasingly oblique to extension (Figure 12) [*Withjack and Jamison*, 1986; *Clifton et al.*, 2000; *Clifton and Schlische*, 2003; *Dewey*, 2002].

[77] No major basement structures (e.g., shear zones) have been identified either onshore or offshore separating segment domains, and are thus instead interpreted as zones of soft linkage or accommodation zones. Therefore previ-

ously identified transfer zones segmenting the Lofoten Ridge, such as the Mosken and Jennegga transfer zones (Figure 2) [Tsikalas et al., 2001] may thus be attributed to changes in deformation style between margin segments of differing obliquity (i.e., second-order transfer zones) rather than reactivation of basement structures as proposed for other transfer zones on the margin (e.g., Bivrost and Vesterålen transfer zones; first-order transfer zones).

[78] Our results highlight that zones of oblique extension generally exhibit complex fault patterns characteristic of 3-D strain, and also less localized deformation compared to areas of orthogonal extension. These variations in structural style and depocenter location seen along the Lofoten Ridge may have important implications when assessing the likelihood of hydrocarbon plays and reservoir potential along other orthogonal and oblique rift segments of the Norwegian, and other, passive margins (e.g., Nordland Ridge, Utrøst Ridge and Gjallar Ridge [Mosar, 2003]). A number of recent studies of basement ridge structures on the Norwegian margin have shown that ridge trend relative to the regional shortening/extension vector plays an important role in the complexity of basins and potential reservoir plays [e.g., Gernigon et al., 2003;

Ren et al., 2003; Imber et al., 2005]. Many of these studies attribute these complex reservoirs to later reactivation of rift systems [e.g., Imber et al., 2005]. Our study broadly confirms this suggestion and additionally illustrates that these zones of complexity can form early in the development of rifted margin due to variations in initial rift trend that may be themselves controlled by features originating in the deeper basement.

[79] **Acknowledgments.** This paper has resulted from a NERC Ocean Margins LINK project (NER/T/S/2000/01018) cofunded by BP and Statoil (UK) Ltd. and associated tied studentship (NER/S/S/2001/06740). The fieldwork carried out in this paper was funded by an AAPG grants-in-aid award and by the Geological Society's Annie Greenly fund for detailed geological mapping. C. Morley, M. Daignieres, and an anonymous reviewer are thanked for their reviews and comments that helped to improve this paper significantly. Thanks to Schlumberger and Badley Geoscience Ltd. for kindly providing seismic interpretation software (GeoFrame® and Trapt Tester) and T. Henningsen for releasing the seismic data used in this study. R.W.W. would like to thank B. Hendriks, J. Dehls, N. De Paola, and P. Clegg for their help and advice at various stages of this study and to S. Berge for his discussions and debate on the development of faults in Lofoten. The authors would also like to thank A. Doré for his continued support and encouragement to the Reactivation Research Group at Durham.

## References

- Andresen, A., and T. Forslund (1987), Post-Caledonian brittle faults in Troms: Geometry, age and tectonic significance, paper presented at the Caledonian and Related Geology of Scandinavia Conference, Dep. of Geol., Univ. Coll., Cardiff, U.K., 22–23 Sept.
- Angelier, J. (1984), Tectonic stress analysis of fault slip data sets, *J. Geophys. Res.*, **89**, 5835–5848.
- Angelier, J. (1994), Fault slip analysis and palaeostress reconstruction, in *Continental Deformation*, edited by P. L. Hancock, pp. 53–101, Elsevier, New York.
- Bartley, J. M. (1982), Limited basement involvement in Caledonian deformation, Hinnøy, north Norway, and tectonic implications, *Tectonophysics*, **83**, 185–203.
- Blystad, P., H. Brække, R. B. Færseth, B. T. Larsen, J. Skogseid, and B. Tørudbakken (1995), Structural elements of the Norwegian continental shelf II: The Norwegian Sea region, *NPD Bull.*, **8**, Norw. Pet. Dir., Stavanger.
- Bosworth, W., G. S. Lister, M. A. Etheridge, and P. A. Symonds (1986), Comment and reply on 'Detachment faulting and the evolution of passive continental margins', *Geology*, **14**, 890–892.
- Bott, M. H. P. (1959), The mechanics of oblique slip faulting, *Geol. Mag.*, **96**, 109–117.
- Bott, M. H. P. (1967), Geophysical investigations of the northern Pennine basement rocks, *Proc. Yorkshire Geol. Soc.*, **36**, 139–168.
- Bott, M. H. P., J. Robinson, and M. M. Kohnstamm (1978), Granite beneath Market Weighton, east Yorkshire, *J. Geol. Soc. London*, **135**, 535–543.
- Brekke, H. (2000), The tectonic evolution of the Norwegian Sea continental margin with emphasis on the Vøring and Møre basins, in *Dynamics of the Norwegian Margin*, edited by A. Nøttvedt, *Geol. Soc. Spec. Publ.*, **167**, 327–378.
- Cashman, P. H., and M. A. Ellis (1994), Fault interaction may generate multiple slip vectors on a single fault surface, *Geology*, **22**, 1123–1126.
- Clegg, P., I. Trinks, K. J. W. McCaffrey, R. E. Holdsworth, R. R. Jones, R. Hobbs, and S. Waggott (2005), Towards the virtual outcrop, *Geoscientist*, **15**(1), 8–9.
- Clemson, J., J. Cartwright, and J. Booth (1997), Structural segmentation and the influence of basement structure on the Namibian passive margin, *J. Geol. Soc. London*, **154**, 477–482.
- Clifton, A. E., and R. W. Schlische (2003), Fracture populations on the Reykjanes Peninsula, Iceland: Comparison with experimental clay models of oblique rifting, *J. Geophys. Res.*, **108**(B2), 2074, doi:10.1029/2001JB000635.
- Clifton, A. E., R. W. Schlische, M. O. Withjack, and R. V. Ackermann (2000), Influence on rift obliquity on fault-population systematics: Results of experimental clay models, *J. Struct. Geol.*, **22**, 1491–1509.
- Clifton, A. E., S. A. Kattenhorn, and L. Fernandes (2005), Structural architecture of a highly oblique divergent plate boundary, *Geophys. Res. Abstr.*, **7**, Abstract 03398.
- Colletta, B., P. Le Quellec, J. Letouzey, and I. Moretti (1988), Longitudinal evolution of the Suez rift structure (Egypt), *Tectonophysics*, **153**, 221–233.
- Corfu, F. (2004a), U-Pb age, setting and tectonic significance of the Anorthosite-Mangerite-Charnockite-Granite Suite, Lofoten-Vesterålen, Norway, *J. Petrol.*, **45**, 1799–1819.
- Corfu, F. (2004b), U-Pb geochronology of the Leknes Group: An exotic Early Caledonian metasedimentary assemblage stranded on Lofoten basement, northern Norway, *J. Geol. Soc. London*, **161**, 619–629.
- Dalland, A. (1981), Mesozoic sedimentary succession at Andøy, northern Norway, and relation to the structural development of the North Atlantic area, *Can. Soc. Pet. Geol. Mem.*, **7**, 563–584.
- Davidson, B., M. Smelov, and D. Ottesen (2001), Et nyoppdaget Mesozoisk basseng i Sortlandsundet, Vesterålen, in *XVII Vinterkonferanse, Abstracts Volume*, pp. 42–43, Norsk Geol. Forening, Trondheim, Norway.
- Davison, I. (1997), Wide and narrow margins of the Brazilian South Atlantic, *J. Geol. Soc. London*, **154**, 471–476.
- Delvaux, D., and B. Spermer (2003), New aspects of tectonic stress inversion with reference to the TENSOR program, in *New Insights Into Structural Interpretation and Modelling*, edited by D. A. Nieuwland, *Geol. Soc. Spec. Publ.*, **212**, 75–100.
- De Paola, N. (2005), The structural evolution of trans-tensional basins and rifted margin, Ph.D. thesis, Univ. of Durham, Durham, U.K.
- De Paola, N., R. E. Holdsworth, and K. J. W. McCaffrey (2005a), The influence of lithology and pre-existing structures on reservoir-scale faulting patterns in trans-tensional rift zones, *J. Geol. Soc. London*, **162**, 471–480.
- De Paola, N., R. E. Holdsworth, K. J. W. McCaffrey, and M. R. Barchi (2005b), Partitioned transtension: An alternative to basin inversion models, *J. Struct. Geol.*, **27**, 607–625.
- Dewey, J. F. (2002), Transtension in arcs and orogens, *Int. Geol. Rev.*, **44**, 402–439.
- Donato, J. A., W. Martindale, and M. C. Tully (1983), Buried granites within the mid North Sea High, *J. Geol. Soc. London*, **140**, 825–837.
- Doré, A. G., E. R. Lundin, C. Fichler, and O. Olesen (1997), Patterns of basement structure and reactivation along the NE Atlantic margin, *J. Geol. Soc. London*, **154**, 85–92.
- Doré, A. G., E. R. Lundin, L. N. Jensen, Ø. Birkeland, P. E. Eliassen, and C. Fichler (1999), Principal tectonic events in the evolution of the northwest European Atlantic margin, in *Petroleum Geology of Northwest Europe: Proceedings of the Fifth Conference*, edited by A. J. Fleet and S. A. R. Boldy, pp. 41–61, Geol. Soc. London, London.
- Edmondo, G. P. (2002), Digital geologic field mapping using ArcPad, digital mapping techniques 2002, workshop proceedings, *U.S. Geol. Surv. Open File Rep.*, **02-370**, 129–134.
- Eide, E. A. (Coord.) (2002), BATLAS—Mid Norway plate reconstruction atlas with global and Atlantic perspectives, 75 pp., Geol. Surv. of Norw., Oslo.
- Eldholm, O., E. Sundvor, and A. Myhre (1979), Continental margin off Lofoten-Vesterålen, northern Norway, *Mar. Geophys. Res.*, **4**, 3–35.

- Eldholm, O., J. Thiede, and E. Taylor (1989), Evolution of the Vøring volcanic margin, *Proc. Ocean Drill. Program Sci. Results*, 104, 1033–1065.
- Eisbacher, A. G., Vasseur, and M. Daignieres (1981), An inverse problem in microtectonics for the determination of stress tensors from fault striation analysis, *J. Struct. Geol.*, 3, 51–65.
- Fichler, C., E. Rundhøvd, O. Olesen, B. M. Sæther, H. Rueslåtten, E. R. Lundin, and A. G. Doré (1999), Regional tectonic interpretation of image enhanced gravity and magnetic data covering the mid-Norwegian Shelf and adjacent mainland, *Tectonophysics*, 306, 183–197.
- Fossen, H. (2000), Extensional tectonics in the Caledonides: Synorogenic or postorogenic?, *Tectonics*, 19, 213–224.
- Fossen, H., and W. J. Dunlap (1998), Timing and kinematics of Caledonian thrusting and extensional collapse, southern Norway: Evidence from  $^{40}\text{Ar}/^{39}\text{Ar}$  thermochronology, *J. Struct. Geol.*, 20, 765–781.
- Francheteau, J., and X. Le Pichon (1972), Marginal fracture zones as structural framework of continental margins in South Atlantic Ocean, *AAPG Bull.*, 56, 991–1007.
- Gabrielsen, R. H., and I. B. Rønberg (1979), Fracture patterns in Norway from Landsat imagery: Results and potential use, in *Proceedings of the Norwegian Sea Symposium*, pp. 1–28, Norw. Pet. Soc., Tromsø, Norway.
- Gabrielsen, R. H., A. Braathen, J. Dehls, and D. Roberts (2002), Tectonic lineaments of Norway, *Norw. J. Geol.*, 82, 153–174.
- Gernigon, L., J. C. Ringenbach, S. Planke, B. Le Gall, and H. Jonquet-Kolsto (2003), Extension, crustal structure and magmatism at the outer Vøring Basin, Norwegian margin, *J. Geol. Soc. London*, 160, 197–208.
- Gibbs, A. D. (1984), Structural evolution of extensional basin margins, *J. Geol. Soc. London*, 141, 609–620.
- Griffin, W. L., P. N. Taylor, J. W. Hakkinen, K. S. Heier, I. K. Iden, E. J. Krogh, O. Malin, K. I. Olsen, D. E. Ormason, and E. Tveten (1978), Archean and Proterozoic crustal evolution in Lofoten-Vesterfjorden, N Norway, *J. Geol. Soc. London*, 135, 629–647.
- Hames, W. E., and A. Anderson (1996), Timing of Palaeozoic orogeny and extension in the continental shelf of north-central Norway as indicated by laser  $^{40}\text{Ar}/^{39}\text{Ar}$  muscovite dating, *Geology*, 24, 1005–1008.
- Heier, K. S. (1960), Petrology and geochemistry of high-grade metamorphic and igneous rocks on Langøya, northern Norway, *Norg. Geol. Undersøkelser*, 207, 246 pp.
- Hendriks, B. W. H. (2003), Cooling and denudation of the Norwegian and Barents Sea Margin, northern Scandinavia, Ph.D. thesis, 177 pp., Vrije Univ., Amsterdam.
- Hendriks, B. W. H., and P. A. M. Andriessen (2002), Pattern and timing of the post-Caledonian denudation of northern Scandinavia constrained by apatite fission-track thermochronology, in *Exhumation of the North Atlantic Margin: Timing, Mechanisms and Implications for Petroleum Exploration*, edited by A. G. Doré et al., *Geol. Soc. Spec. Publ.*, 196, 117–137.
- Henkel, H. (1991), Magmatic crustal structures in northern Fennoscandia, *Tectonophysics*, 192, 57–79.
- Hodgetts, D., N. J. Drinkwater, J. Hodgson, J. Kavanagh, S. S. Flint, K. J. Keogh, and J. A. Howell (2004), Three dimensional geological models from outcrop data using digital data collection techniques: An example from the Tanqua Karoo depocenter, South Africa, in *Geological Prior Information*, edited by A. Curtis and R. Wood, *Geol. Soc. Spec. Publ.*, 239, 57–75.
- Hodgson, R. A. (1961), Classification of structures on joint surfaces, *Am. J. Sci.*, 259, 493–502.
- Holdsworth, R. E., C. A. Butler, and A. M. Roberts (1997), The recognition of reactivation during continental deformation, *J. Geol. Soc. London*, 154, 73–78.
- Imber, J., R. E. Holdsworth, K. J. W. McCaffrey, R. W. Wilson, R. R. Jones, R. W. England, and G. Gjeldvik (2005), Early Tertiary sinistral transpression and fault reactivation in the western Vøring Basin, Norwegian Sea: Implications for hydrocarbon exploration and pre-break-up deformation in ocean margin basins, *AAPG Bull.*, 89, 1043–1069.
- Jones, R. R., K. J. W. McCaffrey, R. W. Wilson, and R. E. Holdsworth (2004), Digital field data acquisition: Towards increased quantification of uncertainty during geological mapping, in *Geological Prior Information*, edited by A. Curtis and R. Wood, *Geol. Soc. Spec. Publ.*, 239, 43–56.
- Karpuz, M. R., D. Roberts, O. Olesen, R. H. Gabrielsen, and T. Herrevoeld (1993), Application of multiple data sets to structural studies on Varanger Peninsula, northern Norway, *Int. J. Remote Sens.*, 14, 979–1003.
- Karpuz, M. R., D. Roberts, V. M. Moralev, and E. Terekhov (1995), Regional lineaments of eastern Finnmark, Norway, and the western Kola Peninsula, Russia, *Geol. Undersøkelser Spec. Publ.*, 7, 121–135.
- Kattenhorn, S. A., and A. E. Clifton (2005), Time-variable faulting behaviour at an oblique spreading centre, southwest Iceland, *Geol. Soc. Am. Abstr. Programs*, 37(7), 421.
- Klein, A. C., and M. G. Steltenpohl (1999), Basement-cover relations and late- to post-Caledonian extension in the Leknes group, west-central Vestfjorden, Lofoten, north Norway, *Nor. Geol. Tidsskr.*, 79, 19–31.
- Knox-Robinson, C. M., and S. J. Gardoll (1998), GIS-stereonet: An interactive stereonet plotting module for ArcView 3.0 geographic information system, *Comput. Geosci.*, 24, 243–250.
- Krantz, R. W. (1988), Multiple fault sets and three-dimensional strain: Theory and application, *J. Struct. Geol.*, 10, 225–237.
- Krantz, R. W. (1989), Orthorhombic fault patterns: The odd axis model and slip vector orientations, *Tectonics*, 8, 483–495.
- Lister, G. S., M. A. Etheridge, and P. A. Symonds (1991), Detachment models for the formation of passive continental margins, *Tectonics*, 10, 1038–1064.
- Longley, P. A., M. F. Goodchild, D. J. Maguire, and D. W. Rhind (2001), *Geographic Information Systems and Science*, 454 pp., John Wiley, Hoboken, N. J.
- Leseth, T., and E. Tveten (1996), Post-Caledonian structural evolution of the Lofoten and Vesterfjorden offshore and onshore areas, *Nor. Geol. Tidsskr.*, 76, 215–230.
- Lundin, E. R., and A. G. Doré (1997), A tectonic model for the Norwegian passive margin with implications for the NE Atlantic: Early Cretaceous to break-up, *J. Geol. Soc. London*, 154, 545–550.
- Maerten, L. (2000), Variation in slip on intersecting normal faults: Implications for paleostress inversion, *J. Geophys. Res.*, 105, 25,553–25,565.
- Maerten, L., D. D. Pollard, and F. Maerten (2001), Digital mapping of three-dimensional structures of the Chimney Rock fault system, central Utah, *J. Struct. Geol.*, 23, 585–592.
- McCaffrey, K. J. W., R. R. Jones, R. E. Holdsworth, R. W. Wilson, P. Clegg, J. Imber, N. Holliman, and I. Trinks (2005), Unlocking the spatial dimension: Digital technologies and the future of geoscience fieldwork, *J. Geol. Soc. London*, 162, 927–938.
- McClay, K. R., T. Dooley, P. Whitehouse, and M. Mills (2002), 4D evolution of rift systems: Insights from scaled physical models, *AAPG Bull.*, 86, 935–959.
- McCoss, A. M. (1986), Simple constructions for deformation in transpression/transension zones, *J. Struct. Geol.*, 8, 715–718.
- Michael, A. J. (1984), Determination of stress from slip data: Faults and folds, *J. Geophys. Res.*, 89, 11,517–11,526.
- Mjelde, R., H. Shimamura, T. Kanazawa, S. Kodaira, T. Raum, and H. Shiobara (2003), Crustal lineaments, distribution of lower crustal intrusives and structural evolution of the Vøring Margin, NE Atlantic: New insight from wide-angle seismic models, *Tectonophysics*, 369, 199–218.
- Mokhtari, M., and R. Pegrum (1992), Structure and evolution of the Lofoten continental margin, offshore Norway, *Nor. Geol. Tidsskr.*, 72, 339–355.
- Morley, C. K., R. A. Nelson, T. L. Patton, and S. G. Munn (1990), Transfer zones in the East African Rift system and their relevance to hydrocarbon exploration in rifts, *AAPG Bull.*, 74, 1234–1253.
- Morley, C. K., C. Haranya, W. Phoosongsee, S. Pongwapee, A. Kornawan, and N. Wonganai (2004), Activation of rift oblique and parallel pre-existing fabrics during extension and their effect on deformation style: Examples from the rifts of Thailand, *J. Struct. Geol.*, 26, 1803–1829.
- Mosar, J. (2003), Scandinavia's North Atlantic passive margin, *J. Geophys. Res.*, 108(B8), 2360, doi:10.1029/2002JB002134.
- Mosar, J., E. A. Eide, P. T. Osmundsen, A. Sommaruga, and T. H. Torsvik (2002), Greenland-Norway separation: A geodynamic model for the North Atlantic, *Norw. J. Geol.*, 82, 281–298.
- Nieto-Samaniego, A. F., and S. A. Alaniz-Alvarez (1997), Origin and tectonic interpretation of multiple fault patterns, *Tectonophysics*, 270, 197–206.
- Oertel, G. (1965), The mechanics of faulting in clay experiments, *Tectonophysics*, 2, 343–393.
- Oldow, J. S. (2003), Active transensional boundary zone between the western Great Basin and the Sierra Nevada block, western U.S. Cordillera, *Geology*, 31, 1033–1036.
- Olesen, O., H. Henkel, K. Kaada, and E. Tveten (1991), Petrophysical properties of a prograde amphibolite-granulite facies transition zone at Sigerfjord, Vesterfjorden, northern Norway, *Tectonophysics*, 192, 33–39.
- Olesen, O., T. H. Torsvik, E. Tveten, K. B. Zwaan, T. Leseth, and T. Henningsen (1997), Basement structure of the continental margin in Lofoten-Lopphavet area, northern Norway: Constraints from potential field data, on-land structural mapping and paleomagnetic data, *Nor. Geol. Tidsskr.*, 77, 15–30.
- Olesen, O., E. R. Lundin, O. Nordgulen, P. T. Osmundsen, J. R. Skilbrei, M. A. Smethurst, A. Solli, T. Bugge, and C. Fichler (2002), Bridging the gap between the onshore and offshore geology in Nordland, northern Norway, *Norw. J. Geol.*, 82, 243–262.
- Olesen, O., J. Ebbing, E. Lundin, J. R. Skilbrei, T. H. Torsvik, E. K. Hansen, T. Henningsen, P. Midbøe, and M. Sand (2005), A new tectonic model for the Eocene opening of the Norwegian-Greenland Sea - simplified geology by using modern aeromagnetic data, paper EGU05-A-02692 presented at the EGU 2nd General Assembly, Vienna, Austria, 24–29 April.
- Peacock, D. C. P., R. J. Knipe, and D. J. Sanderson (2000), Glossary of normal faults, *J. Struct. Geol.*, 22, 291–305.
- Petit, J. P. (1987), Criteria for the sense of movement on fault surfaces in brittle rocks, *J. Struct. Geol.*, 9, 597–608.
- Piazolo, S., G. I. Alsop, B. Müller Nielsen, and J. A. M. van Gool (2004), The application of GIS to unravel patterns of deformation in high grade terranes: A case study of indentor tectonics from west Greenland, in *Flow Processes in Faults and Shear Zones*, edited by G. I. Alsop et al., *Geol. Soc. Spec. Publ.*, 224, 63–78.
- Pollard, D. D., S. D. Saltzer, and A. M. Rubin (1993), Stress inversion methods: Are they based on faulty assumptions?, *J. Struct. Geol.*, 15, 1045–1054.
- Potts, G. J., and S. M. Reddy (1999), Construction and systematic assessment of relative deformation histories, *J. Struct. Geol.*, 21, 1245–1254.
- Ramsay, J. G., and R. J. Lisle (2000), *The Techniques of Modern Structural Geology*, vol. 3, *Applications of Continuum Mechanics in Structural Geology*, pp. 785–810, Elsevier, New York.

- Reches, Z. (1978), Analysis of faulting in a three-dimensional strain field, *Tectonophysics*, 47, 109–129.
- Reches, Z. (1987), Determination of the tectonic stress tensor from slip along faults that obey the Coulomb yield condition, *Tectonics*, 6, 849–861.
- Ren, S., J. I. Faleide, O. Eldholm, J. Skogseid, and F. Gradstein (2003), Late Cretaceous–Paleocene tectonic development of the NW Vøring Basin, *Mar. Pet. Geol.*, 20, 177–206.
- Rosendahl, B. R. (1987), Architecture of continental rifts with special reference to East Africa, *Annu. Rev. Earth Planet. Sci.*, 15, 445–503.
- Sagy, A., Z. Reches, and A. Agnon (2003), Hierarchic three-dimensional structure and slip partitioning in the western Dead Sea pull-apart, *Tectonics*, 22(1), 1004, doi:10.1029/2001TC001323.
- Sanderson, D. J., and W. R. D. Marchini (1984), Transpression, *J. Struct. Geol.*, 6, 449–458.
- Schreurs, G., and B. Colletta (1998), Analogue modelling of faulting in zones of continental transpression and transtension, in *Continental Transpressional and Transtensional Tectonics*, edited by R. E. Holdsworth, R. A. Strachan, and J. F. Dewey, *Geol. Soc. Spec. Publ.*, 135, 59–79.
- Sellevoll, M. A. (1983), The study of the Earth in the island area of Lofoten–Vesterålen, northern Norway, *Norg. Geol. Undersøkelser*, 380, 235–243.
- Sherlock, S. C. (2001), Two stage erosion and deposition in a continental margin setting: An  $^{40}\text{Ar}/^{39}\text{Ar}$  laserprobe study of offshore detrital white micas in the Norwegian Sea, *J. Geol. Soc. London*, 158, 793–799.
- Skogseid, J., T. Pedersen, O. Eldhom, and B. T. Larsen (1992), Tectonism and magmatism during NE Atlantic continental break-up, the Vøring margin, in *Magmatism and the Cause of Continental Break-up*, edited by B. C. Storey, T. Alabaster, and R. J. Pankhurst, *Geol. Soc. Spec. Publ.*, 68, 305–320.
- Skogseid, J., S. Planke, J. I. Faleide, J. T. Pedersen, O. Eldhom, and F. Noverdal (2000), NE Atlantic continental rifting and volcanic margin formation in *Dynamics of the Norwegian Margin*, edited by A. Nottvedt, *Geol. Soc. Spec. Publ.*, 167, 295–326.
- Smith, J. V., and D. W. Durney (1992), Experimental formation of brittle structural assemblages in oblique divergence, *Tectonophysics*, 216, 235–253.
- Song, T., P. A. Cawood, and M. Middleton (2001), Transfer zones normal and oblique to rift trend: Examples from the Perth Basin, Western Australia, in *Non-volcanic Rifting of Continental Margins: A Comparison of Evidence for Land and Sea*, edited by R. C. L. Wilson et al., *Geol. Soc. Spec. Publ.*, 187, 475–488.
- Steltenpohl, M. G., W. E. Hames, and A. Andresen (2004), The Silurian to Permian history of a metamorphic core complex in Lofoten, northern Scandinavian Caledonides, *Tectonics*, 23, TC1002, doi:10.1029/2003TC001522.
- Strömberg, A. (1976), A pattern of tectonic zones in the western part of the East European Platform, *Geol. Foeren. Stockholm Foerh.*, 98, 227–243.
- Talwani, M., and O. Eldholm (1977), Evolution of the Norwegian–Greenland Sea, *Geol. Soc. Am. Bull.*, 83, 969–999.
- Taylor, B., K. Crook, and J. Sinton (1994), Extensional transform zones and oblique spreading centres, *J. Geophys. Res.*, 99, 19,707–19,718.
- Teyssier, C., and B. Tikoff (1999), Fabric stability in oblique convergence and divergence, *J. Struct. Geol.*, 21, 969–974.
- Thomson, K., and J. R. Underhill (1993), Development and evolution of structural styles in the Inner Moray Firth, in *Petroleum Geology of North-west Europe: Proceedings of the 4th Conference*, edited by J. R. Parker, pp. 1167–1178, *Geol. Soc., London*.
- Titus, S. J., H. Fossen, R. B. Pedersen, J. L. Vigneresse, and B. Tikoff (2002), Pull-apart formation and strike-slip partitioning in an obliquely divergent setting, Leka Ophiolite, Norway, *Tectonophysics*, 354, 101–119.
- Tsikalas, F., J. I. Faleide, and O. Eldholm (2001), Lateral variations in tectono-magmatic style along the Lofoten–Vesterålen volcanic margin off Norway, *Mar. Pet. Geol.*, 18, 807–832.
- Tull, J. F., J. M. Bartley, K. V. Hodges, A. Andresen, M. G. Steltenpohl, and J. M. White (1985), The Caledonides in the Ofoten region (68–69N), north Norway: Key aspects of tectonic evolution, in *The Caledonian Orogen–Scandinavia and Related Areas*, edited by D. G. Gee and B. A. Sturt, pp. 553–569, John Wiley, Hoboken, N. J.
- Tveten, E. (1978), Geologisk kart over Norge, Berggrunnskart SVOLVÆR 1:250,000, *Norg. Geol. Undersøkelser*, Oslo.
- Tveten, E., and K. B. Zwaan (1993), Geology of the coast-region from Lofoten to Loppa, with special emphasis on faults, joints and related structures, *Norg. Geol. Undersøkelser Rep.*, 93.083.
- Wilson, R. W., K. J. W. McCaffrey, R. E. Holdsworth, R. R. Jones, J. Imber, and P. Clegg (2005), Lofoten has its faults! Detailed fault analysis and 3D digital mapping in Norway's Lofoten Islands, *Geoscientist*, 15(2), 1–9.
- Withjack, M. O., and W. R. Jamison (1986), Deformation produced by oblique rifting, *Tectonophysics*, 126, 99–124.
- Xu, X., J. A. Battacharya, R. K. Davis, and C. L. V. Aiken (2000), Digital geological mapping of the Ferron Sandstone, Muddy Creek, Utah, with GPS and reflectorless laser rangefinders, *GPS Solutions*, 5, 15–23.
- R. E. Holdsworth, J. Imber, K. J. W. McCaffrey, and R. W. Wilson, Reactivation Research Group, Department of Earth Sciences, University of Durham, Durham DH1 3LE, UK. (r.e.holdsworth@durham.ac.uk; robert.wilson@durham.ac.uk)
- R. R. Jones, Geospatial Research Ltd., Department of Earth Sciences, University of Durham, Durham DH1 3LE, UK.
- D. Roberts, Geological Survey of Norway, N-7491 Trondheim, Norway.
- A. I. F. Welbon, Statoil ASA, Forshagen, Grenseveien 21, N-4035 Stavanger, Norway.

